A Study of the Importance of Secondary Reactions in Char Formation and Pyrolysis

A dissertation presented in partial fulfilment of the requirements for the degree of

Doctor of Philosophy
in
Process Engineering

at Massey University, Manawatū,
New Zealand.

Georg Dietrich Ripberger

2016

Abstract

Anthropogenic climate change, caused primarily by excessive emissions of carbon dioxide, has led to a renewed interest in char, the solid product of pyrolysis. When applied to soil as biochar it can both sequester carbon and improve soil function. To make its manufacture environmentally friendly and economically viable it is important to maximise char yield, which can be done by promoting secondary reactions.

This research shows that secondary reactions, which are enhanced by prolonged vapour-phase residence time and concentration, not only increase the char yield but are the source of the majority of the char formed. All four biomass constituents (extractives, cellulose, hemicellulose and lignin) undergo secondary reactions concurrent with primary reactions over the entire pyrolysis range ≈ 140 to 500 °C, which makes it practically impossible to separate them. Secondary char formation was confirmed to be exothermic which affects the overall heat of pyrolysis. Impregnating the feedstock with the elements K, Mg and P, which are plant macro-nutrients naturally present in biomass, resulted in the catalysis of secondary char formation. The results reveal that a first order reaction model does not describe pyrolysis accurately when char formation is enhanced by catalysis and secondary reactions.

Secondary char can be enhanced by increasing the particle size but there is a limit due to increased cracking and fracturing of the pyrolysing solid. This limitation is overcome by pyrolysis in an enclosed vessel, termed autogenous pressure pyrolysis, which was discovered to cause significant changes in the volatile pyrolysis products; indicating the co-production of a high quality liquid. This process, however, negatively affects the char properties relevant for biochar like the surface area, similar to self-charring and co-carbonisation of condensed volatile pyrolysis products. To increase research capabilities a unique high temperature/ high pressure reactor (600 °C at 20 MPa) was designed to allow the detailed characterisation of all three pyrolysis product classes under extreme pyrolysis conditions. This was demonstrated to be invaluable for understanding the underlying pyrolysis mechanism and physical processes at play.

Acknowledgements

Doing research is a bit like a quest into the unknown. Over the past few years I embarked on my own journey to discover the unknown, and shed some light onto it. There are a few people who helped me along the way, who I would sincerely like to thank:

My principal supervisor Professor Jim Jones and co-supervisor Professor Tony Paterson whose guidance and mentorship throughout this journey has been invaluable. They helped me to conquer the seemingly ever-increasing mountain of research questions and provided me with many opportunities to further my knowledge and gain experience for the tasks ahead. I am grateful for their continuous support, ideas, and encouragement.

The fourth year students Fatima Bashir, Uchena Evanson, Craig Kirwan, Hani Mohd-Hanif, Saleh Alyami and Nadeem Caco who contributed with their final year research projects to the outcome of this quest.

John McDonald-Wharry from the University of Waikato, who I would like to thank for taking SEM images, doing Raman analysis, and the helpful discussions and comments about char chemistry and the nanostructural development.

Associate Professor Marta Camps, Roberto Calvelo Pereira, Tao Wang, Laura Munoz and everyone from the New Zealand Biochar Research Centre for assisting me with experiments, and helping me to understand the complexities of biochar and its intricate interplay with soil.

Professor Peter Buurman, Barry Scott and Bruce Fraser for their help with Py/ GC-MS, and the team from DKSH New Zealand for their support with elemental analysis.

Rhonda Bridges for her help with experiments during her Masters, and for being a friend and running partner; keeping me physically fit for the challenges of this journey.

Clive Bardell, Bruce Collins, Ian Thomas, Anthony Wade, and all the workshop team from the School of Engineering and Advanced Technology that provided the specialised equipment needed for my PhD endeavour. Special thanks goes also to the

team from Worley Parsons New Zealand and Fitzroy Engineering Ltd for their expertise in designing the high temperature/ high pressure reactor.

The academic staff, in particular Professor John Bronlund, Professor Robert McLachlan, and Colin Brown for their assistance with modelling; Mike Bretherton, Ian Furkert, John Sykes, and all the technical staff that helped with the analytical equipment and its maintenance. A special thank you goes to John Edwards for always making time, organising all the bits-and-pieces, and for giving me ideas on how to tackle the problems encountered; Ann-Marie Jackson, the Lab Manager; Nick Look and Michael Lusby for IT support; Glenda Rosoman, Gayle Leader and all the administrative staff that were part of making this project possible.

I would also like to acknowledge my fellow explorers Eli, Grace, Ian, Julawit, Sadia, Shakti, Sureewan, Tawan, Tiyaporn and all the others in the postgraduate office not named here, who offered their friendship and company while embarking on their own journey.

Last but not least, many special thanks go to my family back in Germany and my New Zealand family. Their support and backing seems to have no boundaries, and they are the best cheerleaders one could ever ask for. Especially, I would like to thank my wife Amber Rose for being so understanding about the commitment such a task takes and sacrificing her personal time with me so I could immerse myself into the world of research.

Like an expedition into the wild, this journey was not a single person's effort. One can only be as good as the team that supports them; imparting their knowledge, wisdom, and insight along the way. Thus, journeys are not defined by reaching the finish line, but rather by the experiences we gain, the people we meet, and the friendships we develop. I have been privileged to be part of a great team that made this journey possible to whom I am greatly indebted.

Statement of Contribution to Doctoral Thesis Containing Publications

List of Publications

Report:

Ripberger, G. D. (2012). *Biochar pyrolysis engineering* [PhD Confirmation Report]. Massey University, Palmerston North, New Zealand.

[PhD Confirmation Report]

Conference presentations:

Ripberger, G. D., Jones, J. R., Paterson, A. H. J., & Holt, R. (2015, September/October). *Is it possible to produce biochar at different highest treatment temperatures in the pyrolysis range?—The exothermic nature of pyrolysis*. Paper presented at the APCChE 2015 Congress incorporating Chemeca 2015, Melbourne, Australia.

[Conference Oral Presentation & Peer Reviewed Paper; Speaker: Georg Ripberger]

Ripberger, G. D., Jones, J. R., Paterson, A. H. J., & Holt, R. (2013, September). *Temperature regime of secondary char forming reactions in the pyrolysis of radiata pine*. Paper presented at the Chemeca 2013: Challenging Tomorrow conference, Brisbane, Australia. Paper retrieved from http://www.conference.net.au/chemeca2013/papers/25402.pdf

[Conference Oral Presentation & Peer Reviewed Paper; Speaker: Georg Ripberger]

Ripberger, G. D., Kirwan, C., Jones, J. R., & Paterson, A. H. J. (2014, October). The intricate relationship between vapour phase residence time and biochar/biofuel yield properties. In R. Craggs (Chair), *Next generation liquid biofuels and co-products science symposium: Session three*. Symposium conducted at the meeting of the Advanced Biofuels Research Network (ABRN), Rotorua, New Zealand.

[Conference Oral Presentation; Speaker: Georg Ripberger]

Ripberger, G. D., Kirwan, C., Jones, J. R., & Paterson, A. H. J. (2014, September). The intricate relationship between vapour phase residence time and biochar/biofuel yield properties. In D. Elliott (Chair), *Symposium on thermal and catalytic sciences for biofuels and biobased products: Pyrolysis session 3*. Symposium conducted at the TCS2014 conference, Denver, CO.

[Conference Oral Presentation; Speaker: Georg Ripberger]

Ripberger, G. D., Jones, J. R., & Paterson, A. H. J. (2014, May). The science of producing biochar effectively. In H. Ohtani (Chair), *Presentation Session 5: Applied Pyrolysis*. Symposium conducted at the Pyro2014 20th International Symposium on Analytical and Applied Pyrolysis, Birmingham, United Kingdom.

[Conference Oral Presentation; Speaker: Georg Ripberger]

McDonald-Wharry, J., Ripberger, G. D., Manley-Harris, M., & Pickering, K. (2013, July). Studying carbonisation with raman spectroscopy. In R. Calvelo Pereira (Chair), *Session 2: Formation, characterisation and monitoring of biochars*. Symposium conducted at the New Zealand 2013 Biochar Workshop, Palmerston North, New Zealand.

[Conference Oral Presentation; Speaker: J. McDonald-Wharry]

Ripberger, G. D., Jones, J. R., & Paterson, A. H. J. (2013, July). Secondary char formation. Part 1. It's role, potential and limitations in the manufacture of biochar. In R. Calvelo Pereira (Chair), *Session 2: Formation, characterisation and monitoring of biochars*. Symposium conducted at the New Zealand 2013 Biochar Workshop, Palmerston North, New Zealand.

[Conference Oral Presentation; Speaker: Georg Ripberger]

Ripberger, G. D., Jones, J. R., & Paterson, A. H. J. (2013, July). Secondary char formation. Part 2. Questions to be answered. In R. Calvelo Pereira (Chair), *Session 2: Formation, characterisation and monitoring of biochars*. Symposium conducted at the New Zealand 2013 Biochar Workshop, Palmerston North, New Zealand.

[Conference Oral Presentation; Speaker: Georg Ripberger]

Ripberger, G. D., Jones, J. R., & Paterson, A. H. J. (2012, February). The necessity for a char formation model, In *Session 3: Production Technology*. Symposium conducted at the New Zealand 2012 Biochar Workshop, Palmerston North, New Zealand.

[Conference Oral Presentation; Speaker: Georg Ripberger]

Conference posters:

Ripberger, G. D., Jones, J. R., & Paterson, A. H. J. (2015, November). *Designing a pyrolysis reactor that creates new research capabilities*. Poster presented at tcbiomass2015: Technology for the Bioeconomy, Chicago, IL.

[Conference Poster; Presented by Georg Ripberger]

Ripberger, G. D., Jones, J. R., & Paterson, A. H. J. (2015, September/October). *Designing a pyrolysis reactor that creates new research capabilities*. Poster presented at the APCChE 2015 Congress incorporating Chemeca 2015, Melbourne, Australia.

[Conference Poster; Presented by Georg Ripberger]

Ripberger, G. D., Kirwan, C., Jones, J. R., & Paterson, A. H. J. (2014, September/October). *Effect of autogeneous pressure on volatile pyrolysis products*. Poster presented at Chemeca 2014: Processing excellence; Powering our future, Perth, Australia.

[Conference Poster; Presented by Georg Ripberger]

Ripberger, G. D., Kirwan, C., Jones, J. R., & Paterson, A. H. J. (2014, May). *Effect of autogeneous pressure on volatile pyrolysis products*. Poster presented at the Pyro2014 20th International Symposium on Analytical and Applied Pyrolysis, Birmingham, United Kingdom.

[Conference Poster; Presented by Georg Ripberger]

Ripberger, G. D., Jones, J. R., Paterson, A. H. J., & Holt, R. (2014, May). *The role of secondary char formation in the manufacture of biochar*. Poster presented at the Pyro2014 20th International Symposium on Analytical and Applied Pyrolysis, Birmingham, United Kingdom.

[Conference Poster; Presented by Georg Ripberger]

Ripberger, G. D., Jones, J. R., Paterson, A. H. J., & Holt, R. (2014, May). *Temperature regime of secondary char forming reactions in the pyrolysis of radiata pine*. Poster presented at the Pyro2014 20th International Symposium on Analytical and Applied Pyrolysis, Birmingham, United Kingdom.

[Conference Poster; Presented by Georg Ripberger]

Bridges, R. P., Jones, J. R., Ripberger, G. D., & Paterson, A. H. J. (2014, May). *Design and characterisation of a distributed biochar reactor*. Poster presented at the Pyro2014 20th International Symposium on Analytical and Applied Pyrolysis, Birmingham, United Kingdom.

[Conference Poster; Presented by Georg Ripberger]

Ripberger, G. D., Jones, J. R., & Paterson, A. H. J. (2012, September). *Modelling secondary char formation reactions — Implication for the manufacture of biochar*. Poster presented at Chemeca 2012: Quality of life through chemical engineering, Wellington, New Zealand.

[Conference Poster; Presented by Georg Ripberger]

Seminars:

Ripberger, G. D., Jones, J. R., & Paterson, A. H. J. (2014, June). *Die Wissenschaft von einer effektiven Herstellung von Biokohle (The science of producing biochar effectively)*. Oral presentation presented at the Leibniz-Institut für Agrartechnik Potsdam-Bornim e.V., Potsdam, Germany.

[Oral Presentation; Speaker Georg Ripberger]

Ripberger, G. D., Jones, J. R., & Paterson, A. H. J. (2014, May). *The science of producing biochar effectively*. Oral presentation presented at the UK Biochar Research Centre, Edinburgh, Scotland, United Kingdom.

[Oral Presentation; Speaker Georg Ripberger]

Ripberger, G. D., Jones, J. R., Paterson, A. H. J., & Holt, R. (2013, September). *Wood pyrolysis – Why size matters*. Oral presentation presented at Callaghan Innovation, Wellington, New Zealand.

[Oral Presentation; Speaker Georg Ripberger]

Ripberger, G. D. (2012, May). *Biochar pyrolysis engineering*. PhD confirmation seminar presented at Massey University, Palmerston North, New Zealand.

[Oral Presentation; Speaker Georg Ripberger]

Statement of Contribution

These outputs were distributed over the time of Georg Ripberger's PhD study. They represent the state of knowledge at the time. The final opinions are contained in the thesis which, in some cases, are different to those expressed in the publications and presentations. In other words, the work has evolved over time. Georg had ownership of his PhD project and the work contained is entirely his. The role of the supervisors, Jim Jones and Tony Paterson, was to mentor him. A number of honours research projects were conducted alongside the PhD; these were supervised by Georg Ripberger and Jim Jones. We discussed many of the ideas presented in the publications, but emphasise that they are the work of Georg. Percentages are hard to ascribe, but as supervisors, we can only attribute ourselves a small percentage commensurate with mentoring.

Signed

Jim Jones, Principal Supervisor

Table of Contents

List of Figures

List of Tables

Chapter 1 Project Overview

1.1 Introduction

This research fits within the array of methods aimed at minimising global climate change and its impact on *flora* and *fauna*, and ultimately humanity by sequestering carbon as biochar into soil and concurrently enhancing soil properties. The following sections provide an overview and introduce the reader to the concept of biochar. In the last part of this chapter the research required to make biochar a viable tool to combat climate change is discussed, and the specific tasks for this study are outlined.

1.1.1 Climate Change and Carbon Balance

Global warming, caused by the anthropogenic or enhanced greenhouse effect, has gained increased publicity over the last decades, not only on a local but also a global scale. More recently, it is referred to as climate change, due to the fact that it is likely to be the source of extreme events such as droughts, floods, cyclones and many more (Ministry for the Environment - Manatū Mō Te Taiao, n.d.). These phenomena are attributed, *inter alia*, to amplified atmospheric greenhouse gas concentrations triggered by human activities, like the combustion of fossil fuels (Forster et al., 2007). In the IPCC, Intergovernmental Panel on Climate Change, Fourth Assessment Report Forster et al. (2007) report that carbon dioxide has the largest positive radiative forcing, that is, it has the highest potential to increase the energy of the Earth's atmosphere and thus the Earth's surface temperature.

The Earth, including its atmosphere, can be regarded as a closed carbon system. This is a valid assumption as the exchange with the outer space is negligible (Macías & Camps-Arbestain, 2010). Thus, the amount of carbon within the boundary area is conserved and the first law of thermodynamics is applicable (Houghton, 2007). The observed variations in the quantity of carbon in the different geochemical compartments, lithosphere, pedosphere, hydrosphere, biosphere, and atmosphere, are balanced (Houghton, 2007; Macías & Camps-Arbestain, 2010; New Zealand Biochar Research Centre, n.d.). Variations occur due to the natural carbon cycle, and more recently due to human activities (Denman et al., 2007; Macías & Camps-Arbestain, 2010; New Zealand Biochar Research Centre, n.d.). Activities like the combustion of fossil fuels, the production of cement, and land-use changes shift the natural balance to a raised concentration of carbon in the atmosphere (Denman et al., 2007; Forster et al., 2007). The concentration of carbon dioxide in the atmosphere has risen from its pre-

industrialisation value of 280 ±5 ppmv in 1750 (Neftel, Moor, Oeschger, & Stauffer, 1985) to 397.08 ppmv in September 2015 (Thomas Conway & Pieter Tans, 2012). The present rate of increase is ≈ 2 ppm/year (T. Conway & P. Tans, 2012; Hansen et al., 2008). Hansen et al. (2008) suggest a target atmospheric CO_2 concentration of at least 350 ppmv or below to preserve the climate on Earth as we know it.

1.1.2 Biochar and its Potential

The above outline gives substance to the idea to reverse the process of increasing carbon dioxide concentration in the atmosphere by sequestering it into the other geochemical compartments (Macías & Camps-Arbestain, 2010; New Zealand Biochar Research Centre, n.d.). Biochar has great potential towards achieving this goal. It offers a way of interrupting the atmospheric and terrestrial carbon cycle by forming a long-term carbon sink (Lehmann, 2007; New Zealand Biochar Research Centre, n.d.). While the exact stability, i.e., the longevity of biochar is still debated (Lehmann, 2007), the mean residence time of black carbon ranges from several years (Nguyen et al., 2008) to several thousand years (Lehmann et al., 2008) with the bulk of the evidence leaning towards the longer time frame (Lehmann, Czimczik, Laird, & Sohi, 2009). This is supported by the great age of charcoal found in soil, for example Glaser, Haumaier, Guggenberger, and Zech (2001) radiocarbon dated the age of charcoal pieces and black carbon, taken from a depth of about 60 cm from a clayey Terra Preta soil near Santarém, Brazil, to be 1,775 ± 325 years BP. Terra Preta soil belongs to the Amazonian dark earths, which are believed to be formed by humans, that is, anthropic or anthropogenic, as reviewed by C.J Barrow (2012), who states that these soils are characterized by a high sustainable fertility compared to the surrounding, nutrient-poor, Oxisols. Most of the Amazonian dark earth soil sites have an age of 500 to 2,500 years BP (Neves, Petersen, Bartone, & Silva, 2003); their very existence was the impulse for much of the early biochar research.

Keeping the variation in the longevity of char in soil in mind, the definition used for biochar in this study is that of Verheijen, Jeffery, Bastos, van der Velde, and Diafas (2009):

> charcoal (biomass that has been pyrolysed in a zero or low oxygen environment) for which, owing to its inherent properties, scientific consensus exists that application to soil at a specific site is expected to sustainably sequester carbon and concurrently improve soil functions (under current and future management), while avoiding short- and long-term detrimental effects to the wider environment as well as human and animal health. (p. 5)

Thus, only stable charcoal is regarded as biochar in this study because it can store carbon in the soil for a sufficient time to count as a carbon sink, for reducing the atmospheric CO_2 concentration.

Apart from sequestering carbon, biochar is believed to have a variety of other potential benefits. These were reviewed by C. J. Barrow (2012) and are summarised in Table A-1 in Appendix A.1.

In addition to biochar, charcoal can be utilised in many other ways:

- as a reductant in the iron and steel industry (Antal et al., 1996; Wang et al., 2011);
- as cooking fuel (Antal et al., 1996; Antal & Grønli, 2003);
- as fuel for heat in general (Lehmann & Joseph, 2009);
- as filter (Lehmann & Joseph, 2009);
- as activated carbon (Antal et al., 1996; Cao, Darmstadt, & Roy, 2001);
- as colouring agent (Antal & Grønli, 2003; Lehmann & Joseph, 2009);
- for the manufacture of chemicals such as carbon disulfide and silicon carbide (Antal et al., 1996);
- for the production of fireworks (Antal et al., 1996);
- for deodorisation in the livestock industry (Okimori, Ogawa, & Takahashi, 2003);
- for controlling humidity in houses (Okimori et al., 2003);
- as decolourant (Okimori et al., 2003);
- for water purification (Okimori et al., 2003); or

- as a method for disposing hazardous materials such as wood waste treated with chromated copper arsenic (Ratte, Marias, Vaxelaire, & Bernada, 2009).

However, these uses are not the subject of this research because the literature clearly states that the *sine qua non* for the charcoal to be called biochar is its application to soil (Krull, Baldock, Skjemstad, & Smernik, 2009; Lehmann & Joseph, 2009; UK Biochar Research Centre, n.d.). Nevertheless, some of these methods can contribute as carbon sinks, e.g. the use of charcoal in construction, or fulfil other tasks to achieve a sustainable future (Lehmann, Gaunt, & Rondon, 2006; Okimori et al., 2003).

1.2 Problem Definition

Despite the overwhelming potential of biochar, as discussed above, there are also many criticisms. Biofuelwatch (2011) published a report that outlines their concerns about biochar, which are summarised in Table A-2 in Appendix A.1.

A more balanced review is given by Verheijen et al. (2009). However, both studies reveal that more research needs to be undertaken to ensure that biochar does not suffer the same fate as biofuel of the so-called first-generation (Glover, 2009); that is, rushed application without researching its wider impact on land-use changes, deforestation and food prices. Among other things, this resulted in social concerns and increasingly negative public opinion (Fairley, 2011; Fargione, Hill, Tilman, Polasky, & Hawthorne, 2008; Harvey & Pilgrim, 2011; Potters, van Goethem, & Schutte, 2010; Righelato & Spracklen, 2007; Searchinger et al., 2008; Stoeglehner & Narodoslawsky, 2009; Worldwatch Institute, 2011). C. J. Barrow (2012) warns in his review on biochar that a lack of research could result in the same pitfall leading to discouragement of biochar application. Therefore, to use the biochar concept as a tool to solve crucial future challenges like carbon sequestration, food security, energy security, and waste management, it has to be ascertained that it is applied in a sustainable way and that its limitations are known and understood. The manufacture of biochar plays an important role, for which understanding is still developing (Brown, 2009); to name an example, the formation of polycyclic aromatic hydrocarbons, PAH, is dependent on the pyrolysis conditions (Hilber, Blum, Leifeld, Schmidt, & Bucheli, 2012), and thus critical for the application of biochar.

The research presented in this thesis is aimed at the manufacture of biochar, which is the solid product of pyrolysis, in order to develop a mechanistic understanding of the char formation processes. Special attention will be drawn to the reactions that promote formation of secondary char and how they affect the yield and quality. Such knowledge will be new to the field. When char is the desired product, promoting secondary char formation has the potential to improve pyrolysis efficiency and biochar economics. While the focus of this work is the solid char and the kinetics of its formation, this work will also review the formation of the volatile pyrolysis products, which has a considerable body of research, particularly from those interested in fast pyrolysis. Here, however, the focus of this review is on those pyrolysis products

formed during slow pyrolysis both in ambient and pressurised conditions where producing a high value liquid product alongside biochar could provide an economic advantage. The common biochar manufacturing practices involve producing either a high temperature or a low temperature biochar under varying and scarcely controlled pyrolysis conditions in the so-called slow pyrolysis regime without paying much attention to secondary char formation and its possible implications. Thus, the objective of this study is:

> *maximising the yield of biochar in the slow pyrolysis regime by understanding how secondary reactions affect the yield and pyrolysis process.*

The reason that the main focus of this research is on the char formation and the char yield rather than on the characteristics required for soil application, is that there is a conundrum between sequestration, which requires a high yield and non-labile carbon, and the properties for biochar in soil, which require a high yield and accessible carbon along with the presence of functional groups. Thus, yield is crucial for the economic and sustainable manufacture of char, and understanding its formation will not only aid in optimizing the manufacture of char but also provide the basis for understanding how char characteristics are affected by the manufacturing conditions. Overall, the research outcomes will assist in accomplishing the goals, outlined by Brown (2009), for advanced biochar production, that is, to improve energy efficiency, process economics, biochar yields and properties by process control, and to reduce pollution emissions. Thus, knowledge in this area significantly contributes to making biochar production feasible and sustainable on a large scale.

1.3 Concise Statement of Research Tasks and Questions

Table 1-1 summarises the research tasks and questions, which have been developed from the literature review.

Table 1-1. Concise statement of research tasks and questions.

Tasks	Questions
Part 1: Develop a mechanistic understanding of pyrolysis of wood; in particular secondary reactions that lead to char formation	
1. Establish the role and extent of secondary char formation over the whole biochar production range (300 to 700 °C)	• Is there a difference between intraparticle and extraparticle secondary char formation? • What is the temperature regime of secondary reactions? • What is their impact on the yield of charcoal?
2. Understand the transport processes occurring during pyrolysis of wood	• What conditions cause transfer limitations? • To what extent do fractures and shrinkage affect secondary char forming reactions?
3. Investigate the catalytic action of inorganics during pyrolysis	• Do they catalyse primary, secondary or both reactions?
4. Determine the heat of pyrolysis	• What impacts have secondary reactions on the heat of pyrolysis?
5. Analyse the volatiles involved in secondary reactions	• How do secondary reactions affect the composition of the liquid pyrolysis product? • Is it possible to draw conclusions about the underlying reaction mechanism? • Can a high yield charcoal and high quality liquid product be co-produced?
6. Investigate the effect secondary reactions have on the structure and properties of the char	• What is the effect of secondary reactions on the morphology and physical properties of char? • Are secondary reactions desired in the manufacture of biochar?
Part 2: Design experimental kit and methods based on the findings in part 1 that allows the simulation of a wide range of pyrolysis conditions, with emphasis on conditions maximising secondary reactions for char formation, that offers new research capabilities to quantify the relationship between pyrolysis conditions and product properties, in particular with respect to char.	

1.4 References

Antal, M. J., Croiset, E., Dai, X., DeAlmeida, C., Mok, W. S.-L., Norberg, N., . . . Al Majthoub, M. (1996). High-yield biomass charcoal. *Energy & Fuels, 10*(3), 652-658. doi:10.1021/ef9501859

Antal, M. J., & Grønli, M. G. (2003). The art, science, and technology of charcoal production. *Industrial & Engineering Chemistry Research, 42*(8), 1619-1640. doi:10.1021/ie0207919

Barrow, C. J. (2012). Biochar: Potential for countering land degradation and for improving agriculture. *Applied Geography, 34*, 21-28. doi:10.1016/j.apgeog.2011.09.008

Barrow, C. J. (2012). Biochar: Potential for countering land degradation and for improving agriculture. *Applied Geography, 34*(0), 21-28. doi:10.1016/j.apgeog.2011.09.008

Biofuelwatch. (2011). *Biochar: A critical review of science and policy*. Retrieved from Biofuelwatch website: http://www.biofuelwatch.org.uk/wp-content/uploads/Biochar-Report3.pdf

Brown, R. C. (2009). Biochar production technology. In J. Lehmann & S. Joseph (Eds.), *Biochar for environmental management: Science and technology* (pp. 127-146). London, England, United Kingdom: Earthscan.

Cao, N., Darmstadt, H., & Roy, C. (2001). Activated carbon produced from charcoal obtained by vacuum pyrolysis of softwood bark residues. *Energy & Fuels, 15*(5), 1263-1269. doi:10.1021/ef0100698

Conway, T., & Tans, P. (2012). *Recent global CO_2.* Retrieved December 2, 2015, from http://www.esrl.noaa.gov/gmd/ccgg/trends/global.html

Conway, T., & Tans, P. (2012). *Annual mean global carbon dioxide growth rates.* Retrieved October 8, 2015, from http://www.esrl.noaa.gov/gmd/ccgg/trends/global.html

Denman, K. L., Brasseur, G., Chidthaisong, A., Ciais, P., Cox, P. M., Dickinson, R. E., . . . Zhang, X. (2007). Couplings between changes in the climate system and biogeochemistry. In S. Solomon, D. Qin, M. Manning, Z. Chen, M. Marquis, K. B. Averyt, M. Tignor, & H. L. Miller (Eds.), *Climate change 2007: The physical science basis. Contribution of working group I to the fourth assessment report of the Intergovernmental Panel on Climate Change*. Cambridge, United Kingdom and New York, NY: Cambridge University Press.

Fairley, P. (2011). Introduction: Next generation biofuels. *Nature, 474*(7352), S2-S5. doi:10.1038/474S02a

Fargione, J., Hill, J., Tilman, D., Polasky, S., & Hawthorne, P. (2008). Land clearing and the biofuel carbon debt. *Science, 319*(5867), 1235-1238. doi:10.1126/science.1152747

Forster, P., Ramaswamy, V., Artaxo, P., Berntsen, T., Betts, R., Fahey, D. W., . . . Van Dorland, R. (2007). Changes in atmospheric constituents and in radiative forcing. In S. Solomon, D. Qin, M. Manning, Z. Chen, M. Marquis, K. B. Averyt, M. Tignor, & H. L. Miller (Eds.), *Climate change 2007: The physical science basis. Contribution of working group I to the fourth assessment report of the Intergovernmental Panel on Climate Change*. Cambridge, United Kingdom and New York, NY: Cambridge University Press.

Glaser, B., Haumaier, L., Guggenberger, G., & Zech, W. (2001). The 'Terra Preta' phenomenon: A model for sustainable agriculture in the humid tropics. *Naturwissenschaften, 88*(1), 37-41. doi:10.1007/s001140000193

Glover, M. (2009). Taking Biochar to market: Some essential concepts for commercial success. In J. Lehmann & S. Joseph (Eds.), *Biochar for environmental management: Science and technology* (pp. 375-392). London, England, United Kingdom: Earthscan.

Hansen, J., Sato, M., Kharecha, P., Beerling, D., Berner, R., Masson-Delmotte, V., . . . Zachos, J. C. (2008). Target atmospheric CO_2: Where should humanity aim? *The Open Atmospheric Science Journal, 2*(1), 217-231. doi:10.2174/1874282300802010217

Harvey, M., & Pilgrim, S. (2011). The new competition for land: Food, energy, and climate change. *Food Policy, 36, Supplement 1*(0), S40-S51. doi:10.1016/j.foodpol.2010.11.009

Hilber, I., Blum, F., Leifeld, J., Schmidt, H.-P., & Bucheli, T. D. (2012). Quantitative determination of PAHs in biochar: A prerequisite to ensure its quality and safe application. *Journal of Agricultural and Food Chemistry*. doi:10.1021/jf205278v

Houghton, R. A. (2007). Balancing the global carbon budget. *Annual Review of Earth and Planetary Sciences, 35*, 313-347. doi:10.1146/annurev.earth.35.031306.140057

Krull, E. S., Baldock, J. A., Skjemstad, J. O., & Smernik, R. J. (2009). Characteristics of biochar: Organo-chemical properties. In J. Lehmann & S. Joseph (Eds.), *Biochar for environmental management: Science and technology* (pp. 53-66). London, England, United Kingdom: Earthscan.

Lehmann, J. (2007). A handful of carbon. *Nature, 447*, 143-144. doi:10.1038/447143a

Lehmann, J., Czimczik, C., Laird, D., & Sohi, S. (2009). Stability of biochar in the soil. In J. Lehmann & S. Joseph (Eds.), *Biochar for environmental management: Science and technology* (pp. 183-205). London, England, United Kingdom: Earthscan.

Lehmann, J., Gaunt, J., & Rondon, M. (2006). Bio-char sequestration in terrestrial ecosystems – A review. *Mitigation and Adaptation Strategies for Global Change, 11*(2), 395-419. doi:10.1007/s11027-005-9006-5

Lehmann, J., & Joseph, S. (2009). Biochar for environmental management: An introduction. In J. Lehmann & S. Joseph (Eds.), *Biochar for environmental management: Science and technology* (pp. 1-12). London, England, United Kingdom: Earthscan.

Lehmann, J., Skjemstad, J., Sohi, S., Carter, J., Barson, M., Falloon, P., . . . Krull, E. (2008). Australian climate-carbon cycle feedback reduced by soil black carbon. *Nature Geoscience, 1*(12), 832-835. doi:10.1038/ngeo358

Macías, F., & Camps-Arbestain, M. (2010). Soil carbon sequestration in a changing global environment. *Mitigation and Adaptation Strategies for Global Change, 15*(6), 511-529. doi:10.1007/s11027-010-9231-4

Ministry for the Environment - Manatū Mō Te Taiao. (n.d.). *What is climate change?* Retrieved May 23, 2011, from http://www.climatechange.govt.nz/science/what-is-climate-change.html

Neftel, A., Moor, E., Oeschger, H., & Stauffer, B. (1985). Evidence from polar ice cores for the increase in atmospheric CO_2 in the past two centuries. *Nature, 315*(6014), 45-47. Retrieved from

http://www.scopus.com/inward/record.url?eid=2-s2.0-0021890538&partnerID=40&md5=11a62dd15c2b473164fe2eaf4407626f

Neves, E. G., Petersen, J. B., Bartone, R. N., & Silva, C. A. D. (2003). Historical and socio-cultural origins of Amazonian dark earths. In J. Lehmann, D. C. Kern, B. Glaser, & W. I. Woods (Eds.), *Amazonian dark earths: Origin, properties, management* (pp. 29-50). Dordrecht, Netherlands: Kluwer Academic.

New Zealand Biochar Research Centre. (n.d.). *Why Biochar?* Retrieved May 23, 2011, from http://www.biochar.co.nz/why.html

Nguyen, B., Lehmann, J., Kinyangi, J., Smernik, R., Riha, S., & Engelhard, M. (2008). Long-term black carbon dynamics in cultivated soil. *Biogeochemistry, 89*(3), 295-308. doi:10.1007/s10533-008-9220-9

Okimori, Y., Ogawa, M., & Takahashi, F. (2003). Potential of CO_2 emission reductions by carbonizing biomass waste from industrial tree plantation in South Sumatra, Indonesia *Mitigation and Adaptation Strategies for Global Change, 8*(3), 261-280. doi:10.1023/B:MITI.0000005643.79908.5a

Potters, G., van Goethem, D., & Schutte, F. (2010). Promising biofuel resources: Lignocellulose and algae. *Nature Education, 3*(9), 14. Retrieved from http://www.nature.com/scitable/topicpage/promising-biofuel-resources-lignocellulose-and-algae-14255919

Ratte, J., Marias, F., Vaxelaire, J., & Bernada, P. (2009). Mathematical modelling of slow pyrolysis of a particle of treated wood waste. *Journal of Hazardous Materials, 170*(2-3), 1023-1040. doi:10.1016/j.jhazmat.2009.05.077

Righelato, R., & Spracklen, D. V. (2007). Carbon mitigation by biofuels or by saving and restoring forests? *Science, 317*(5840). doi:10.1126/science.1141361

Searchinger, T., Heimlich, R., Houghton, R. A., Dong, F., Elobeid, A., Fabiosa, J., . . . Yu, T.-H. (2008). Use of U.S. croplands for biofuels increases greenhouse gases through emissions from land-use change. *Science, 319*(5867), 1238-1240. doi:10.1126/science.1151861

Stoeglehner, G., & Narodoslawsky, M. (2009). How sustainable are biofuels? Answers and further questions arising from an ecological footprint perspective. *Bioresource Technology, 100*(16), 3825-3830. doi:10.1016/j.biortech.2009.01.059

UK Biochar Research Centre. (n.d.). *What is Biochar?* Retrieved May 17, 2011, from http://www.biochar.org.uk/what_is_biochar.php

Verheijen, F., Jeffery, S. L., Bastos, A. C., van der Velde, M., & Diafas, I. (2009). *Biochar application to soils - A critical scientific review of effects on soil properties, processes and functions* (EUR 24099 EN) [JRC Scientific and Technical Reports (EUR collection)]. Retrieved from http://publications.jrc.ec.europa.eu/repository/handle/111111111/13558

Wang, L., Trninic, M., Skreiberg, Ø., Grønli, M. G., Considine, R., & Antal, M. J. (2011). Is elevated pressure required to achieve a high fixed-carbon yield of charcoal from biomass? Part 1: Round-robin results for three different corncob materials. *Energy & Fuels, 25*(7), 3251-3265. doi:10.1021/ef200450h

Worldwatch Institute. (2011). *Worldwatch perspective: Nothing is simple, not even biofuels.* Retrieved March 18, 2012, from http://www.worldwatch.org/node/5319

Chapter 2 Literature Review: Pyrolysis

2.1 Introduction

Pyrolysis is the process by which biochar is produced, as outlined in chapter 1. To economically manufacture biochar with defined properties and low variability it is essential to understand the whole concept of biomass pyrolysis; that is, the effect feedstock composition and properties, reactor design and pyrolysis conditions have on the chemical and physical processes at play (Antal & Grønli, 2003; Babu, 2008; Bridgwater, Meier, & Radlein, 1999; Di Blasi, 2008; Grieco & Baldi, 2011; Laird, Brown, Amonette, & Lehmann, 2009; Maschio, Koufopanos, & Lucchesi, 1992). This indicates the complexity of pyrolysis and its dependence on a multitude of parameters, which are partly interconnected and not well understood (Babu & Chaurasia, 2003b; R. C. Brown, 2009; Rao & Sharma, 1998).

The aim of this chapter is to provide a review of the literature regarding these aspects and to gain a mechanistic understanding of biomass pyrolysis. Special emphasis is drawn to the char, which is the solid product of pyrolysis, and the role of secondary reactions.

2.2 What is Pyrolysis?

Pyrolysis, the first step in combustion (Babu & Chaurasia, 2003a, 2003b), has been part of human life since the first fire was lit. In this manner it has significantly contributed to the development of modern humans. This section provides a definition for the term pyrolysis, and provides an overview of its processes.

2.2.1 Definition

Pyrolysis is a thermochemical conversion process (Babu, 2008; Goyal, Seal, & Saxena, 2008) that takes place in an environment free of an oxidant (Babu, 2008; Boutin, Ferrer, & Lédé, 2002; Bridgwater, 2003; Goyal et al., 2008; Laird et al., 2009; Maschio et al., 1992; Mohan, Pittman, & Steele, 2006). In this manner it distinguishes itself from combustion (total oxidation), and gasification (partial oxidation), where it is an initial process (Babu & Chaurasia, 2003a, 2003b; Bridgwater, 2003; Maschio et al., 1992; Rao & Sharma, 1998). The reported characteristic temperature range for pyrolysis to produce biochar varies in the literature. According to the definition by Emrich (1985), Goyal et al. (2008), Lehmann and Joseph (2009a) and the International Biochar Initiative (2012) the relevant pyrolysis temperature range for the manufacture of biochar is 300 to 700 °C. The products of pyrolysis exist in the three states, solid, liquid and gaseous, and are discussed in more detail in section 2.3.

2.2.2 Overview of Processes Involved

Pyrolysis involves physical processes and chemical reactions, which can be regarded as a series of steps based on phenomena mentioned in several articles (Babu, 2008; Babu & Chaurasia, 2003b; Czernik, Johnson, & Black, 1994, as cited in Fox, 2010; Sinha, Jhalani, Ravi, & Ray, 2000, as cited in Mohan et al., 2006; Neves, Thunman, Matos, Tarelho, & Gómez-Barea, 2011). These are depicted in Figure 2-1, which is a modified version of a figure developed by Neves et al. (2011).

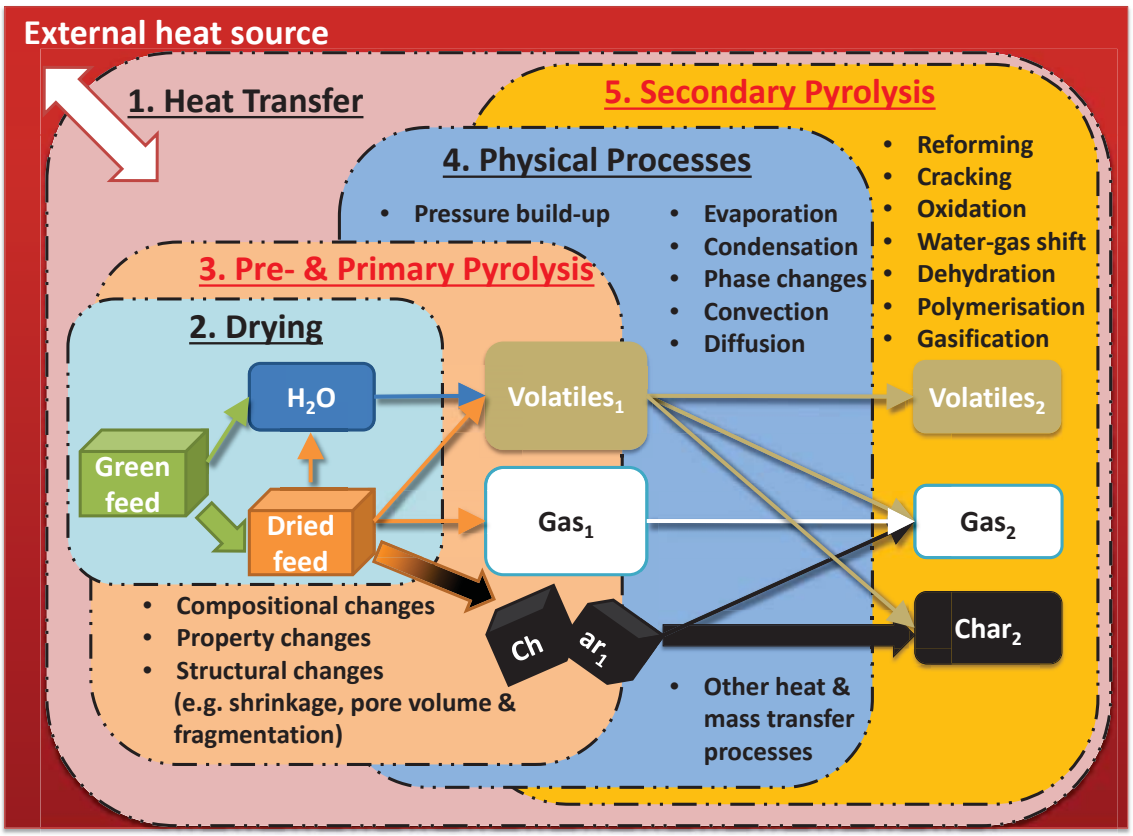

Figure 2-1. Biomass pyrolysis steps and their interactions. The coloured boxes with the dashed boundaries represent the physical (black headings) and chemical (red headings) processes. Overlapping boxes illustrate their interactions. The scheme with the arrows in the lower centre of the figure, apart from the drying step, is a simplified mechanism for the main product formation paths as proposed by Shafizadeh and Chin (1977) and modified by Thurner and Mann (1981) and Di Blasi (1996a). The solid phase has been depicted by thick arrows as this is the product of interest in this research. The points listed in step 3 refer to the pyrolysing material and are illustrations of effects that interactions between all steps have on the solid material. The remarks made in step 4 are examples of these processes and the ones in step 5 display secondary reactions. The figure is adapted from Neves et al. (2011). Modifications have been made on basis of several articles (Babu, 2008; Babu & Chaurasia, 2003b; Czernik, Johnson, & Black, 1994, as cited in Fox, 2010; Haseli, Van Oijen, & De Goey, 2011; Maschio et al., 1992; Sinha, Jhalani, Ravi, & Ray, 2000, as cited in Mohan et al., 2006; Park, Atreya, & Baum, 2010).

Figure 2-1 shows that the first step always involves a form of heat transfer from the reactor system to the sample, which results in an increase in the feedstock temperature (Babu & Chaurasia, 2003b). The heat transfer, depending on the reactor design, will be mainly by radiation and convection. In the sample itself conduction in the cell wall is the main mode of heat transfer. Temperature gradients will exist in the sample if the internal resistance to heat transfer is relatively large compared to the external resistance to heat transfer. For conduction problems with surface convection effects this is described by the Biot number, Bi:

$$Bi \equiv \frac{hl_{ch}}{\lambda} = \frac{l_{ch}/(\lambda A)}{1/(hA)} = \frac{R_{t,cond}}{R_{t,conv}}, \qquad (2.1)$$

where h is the convection heat transfer coefficient in W/(m^2·K), l_{ch} the characteristic length in m, λ the thermal conductivity in W/(m·K), A the area in m^2, and $R_{t,cond}$ and $R_{t,conv}$ are the conductive and convective thermal resistance in K/W respectively (T. L. Bergman, Lavine, Incropera, & Dewitt, 2011). Typically, if the Biot number is smaller than 0.1 internal transfer limitations are negligible (*ibid*). In a rough approximation, using the thermal conductivity of softwood $\lambda = 0.12\ W/(m \cdot K)$ at 300 K and a minimum heat transfer coefficient of $25\ W/(m^2 \cdot K)$ characteristic for forced convection of gases (T. L. Bergman et al., 2011), a maximum characteristic length of 480 µm is required to achieve negligible internal heat transfer resistance. This shows that even when dealing with sawdust (particle thickness > 1 mm) transfer limitations are to be expected. In more general terms it illustrates that the sample and reactor size/geometry, the reactor design and the feedstock properties (e.g. λ) are important parameters that affect the heat transfer required for pyrolysis to take place.

As the sample is "heated", heat is also transferred to the water in the sample (step 2 in Figure 2-1). That is, the temperature of the water increases, and thus its vapour pressure; meaning that the rate of evaporation rises. Consequently, more water molecules transition to the gas-phase where a concentration gradient forms between the site of evaporation and the outside atmosphere (typically pyrolysis is performed in nitrogen). The evaporation of water is an endothermic process, which is explained by the kinetic gas theory by the reduced kinetic energy of the liquid phase when the high energetic water molecules leave into the gaseous phase (latent heat). Thus, a considerable temperature lag can result between the sample inside and the outside affecting the evaporation rate and subsequent pyrolysis processes. Here it is important to point out that wood not only contains free water but also bound water, which is chemically bound by hydrogen bonding to the cellulose molecule (at the hydroxyl locations) (Di Blasi, 1998). Due to the extra bonding more energy is required for its evaporation (desorption and evaporation) compared to free water. Thus free water is removed first followed by bound water (Di Blasi, 1998; Ratte, Marias, Vaxelaire, & Bernada, 2009). The moisture content from which on only bound water is present is referred to as fibre saturation point, FSP, and discussed in more detail in 2.5.3. Both bound and free water are in equilibrium with the water vapour (Ratte et al., 2009). Once bound water is being removed there forms also a moisture gradient in the solid phase of the wood.

Similar to the above discussed heat transfer, the moisture transport can be subject to transfer limitations, which in the case of sample surface convection and internal mass transfer by diffusion can be described analogue to equation (2.1) by a mass transfer Biot number, Bi_m:

$$Bi_m \equiv \frac{h_m l_{ch}}{D_{AB}} = \frac{l_{ch}/(D_{AB}A)}{1/(h_m A)} = \frac{R_{m,diff}}{R_{m,conv}}, \tag{2.2}$$

where h_m is the convection mass transfer coefficient in m/s, D_{AB} the binary mass diffusivity in m^2/s, $R_{m,diff}$ and $R_{m,conv}$ are the internal and boundary layer species transfer resistance in s/m^3 by diffusion and convection respectively (T. L. Bergman et al., 2011). For diffusion both the water vapour in the cell lumen and the bound water in the cell wall substance have to be regarded (free/capillary water transport occurs by convection) (Di Blasi, 1998; Ratte et al., 2009). That is, intergas diffusion and bound water diffusion respectively (Siau, 1984). If the diffusion coefficient of water vapour in bulk air is converted to the basis of moisture concentration in the cell wall substance, which is in equilibrium with the air, it can be shown that the bound water diffusion coefficient is smaller than the water vapour diffusion in the air in the cell lumen (*ibid*). This is to be expected due to the additional bonding in the case of bound water, and thus more energy is required to move the molecules in the cell wall compared to the air (but less than is required for desorption). Both diffusion coefficients are a function of temperature and moisture content (see 2.5.3). Additionally, the bound water diffusion coefficient is dependent on the direction (Siau, 1984), because of the anisotropic structure of wood (see section 2.5). This is also the case for conduction; both values are larger in longitudinal direction. Hence, the diffusion of water is highly dependent on the feedstock properties and structure like porosity. Another structural effect is capillary condensation, which occurs due to the presence of small capillaries in the cell wall.

In the case that the diffusion of water vapour (from the inside to the outside) is slower than the rate of evaporation, which increases with rising temperature (heat transfer in opposite direction to mass transfer), the pressure inside the wood increases resulting in the development of a pressure gradient. Consequently, mass transport occurs additionally by advection, which is dependent on the permeability of the wood. The permeability itself is a function of the feedstock type and the structural component of the wood (Siau, 1984). For softwood the permeability decreases during drying due to

the aspiration of bordered pits, see section 2.5.1, (*ibid*). In the case of gas advection Knudson diffusion has to be considered as well, as the dimensions of the capillaries in wood are in the order of the mean free path of the gas molecules, causing a slip flow leading to a higher specific gas permeability (*ibid*). This illustrates the intricate relationship between the physical processes and the structural properties and changes that take place when wood is dried. The most recognised structural changes that are associated with wood drying are shrinkage and swelling, which occur when moisture is removed or absorbed below the FSP respectively (see 2.5.3). This adds to the complexity of processes occurring during wood drying and subsequent pyrolysis. The overlapping nature of the different processes is illustrated in Figure 2-1 by the dashed boundary lines.

An often neglected transport process is thermal-diffusion, that is water is transported in the presence of a temperature gradient in the direction of decreasing temperature (Peralta & Skaar, 2007; Siau, 1984). This can even take place, when a moisture gradient is present in opposite direction to the temperature gradient (*ibid*). Therefore, in samples with fast heating rates, heat transfer and mass transfer can occur in the same direction. However, eventually the water is transported out of the sample (from the centre to the surface) so that the overall heat and mass transfer are in opposing directions.

It is important to note that the actual drying process is more complex than outlined here due to the interaction of the different processes and their varying dynamics. For more detailed information the reader is referred to the modelling studies of Di Blasi (1998) and Ratte et al. (2009).

The actual pyrolysis (thermal decomposition) reactions, step 3 in Figure 2-1, take place increasingly with rising temperature, which is generally described by the Arrhenius equation (Biagini & Tognotti, 2014; Fantozzi, Colantoni, Bartocci, & Desideri, 2007; Flynn, 1997; Flynn & Wall, 1966; Grønli, Várhegyi, & Di Blasi, 2002; Sun, Huang, Gong, & Cao, 2006; X. Y. Wang, Wan, Chen, & Wang, 2012; White, Catallo, & Legendre, 2011):

$$k_i(T) = A_i e^{\left(-\frac{E_i}{R_g T}\right)} , \tag{2.3}$$

where k_i is the decomposition rate constant of component i in 1/s, R_g the universal gas constant (0.008314 kJ/(mol·K)), T the temperature in K, and A_i and E_i are the pre-

exponential and exponential factor of component *i* in 1/s and kJ/mol respectively. It is important to note that the parameters here given are for a first order reaction, which is not necessarily the case. Equation (2.3) shows that the decomposition rate increases not only with a temperature rise but also a decrease in the activation energy. The latter one is caused by the presence of catalyst, which are naturally present in the wood at various concentrations depending on the feedstock type (see 2.5.2).

The decomposition reactions are lumped into three classes in Figure 2-1 leading to the formation of primary volatiles, gas and char (denoted by subscript "1" in Figure 2-1). In this study the definitions of gas and volatiles are substances that are non-condensable and condensable at room temperature, respectively. Each of the aforementioned reactions has a heat of reaction, which consequently affects the temperature distribution and therefore the reaction rate (feedback loop). Similar to the drying step the generated volatiles are transferred by diffusion and advection in opposite direction to the overall heat transfer, and again the mass transfer is dependent on the structural properties of the wood, which change due to the decomposition of the wood. For example further shrinkage occurs as cell wall components are volatilised, which in turn further impacts the porosity and permeability of the wood. If the volatiles are generated faster than they are transported away (low permeability) the resulting pressure gradients can result in cracking of the wood, increasing its permeability (this can already occur during drying). It is important to note that pressure profiles also affect the boiling points of liquid substances including water (feedback loop).

The above described "primary pyrolysis stage" (Neves et al., 2011, p. 613) can be according to Maschio et al. (1992) sub-divided into pre-pyrolysis and main pyrolysis. They state that pre-pyrolysis takes place in the temperature range 120 to 200 °C. During this period only a slight mass-loss occurs (Koufopanos, Lucchesi, & Maschio, 1989, as cited in Maschio et al., 1992) but it is associated with interior structural rearrangements like bond breakage and formation of functional groups such as carboxyl and carbonyl groups (Shafizadeh, 1982, as cited in Maschio et al., 1992). Maschio and his co-workers report that these structural changes affect the product yields of pyrolysis, which gives pre-pyrolysis a significant role within the overall pyrolysis process. The subsequent main pyrolysis, which is also referred to as "primary pyrolysis" or "devolatilisation" (Commandré, Lahmidi, Salvador, & Dupassieux, 2011) is the region where the major mass loss happens (L. Zhang, Xu, & Champagne, 2010). Maschio et al. report that substantial decomposition rates are obtained in the temperature range 300

to 600 °C. This zone is also called "active pyrolysis zone" (Karaosmanoglu, Çift, & Işigigür-Ergüdenler, 2001, p. 771). The range can vary depending on the experimental conditions and the feedstock used (White et al., 2011). For example Fisher, Hajaligol, Waymack, and Kellogg (2002) report that most of the decomposition studies in literature suggest the region from 200 to 400 °C as the main primary pyrolysis sector, where 95 % of the overall decomposition occurs. On the other hand, Neves et al. (2011) suggest 200 to 600 °C. After the majority of mass is lost, only slight devolatilisation occurs, which Maschio et al. attribute to continuing C-H and C-O bond scission. This is often classified as a separate stage, since it is mainly characterised by aromatisation and not decomposition (Downie, Crosky, & Munroe, 2009; Fisher et al., 2002; Maschio et al., 1992).

As the gas and volatiles leave their place of origin, they contribute to the heat transfer, for example they can condense in cooler regions (Babu & Chaurasia, 2003b). These processes in combination with the above outlined mass transfer processes are summarised as physical processes in step 4 of Figure 2-1.

The fifth and last step in Figure 2-1 refers to secondary pyrolysis, which is a consequence of mass transfer limitations. It encompasses homogenous and heterogeneous reactions of the primary pyrolysis products. Examples are homogeneous and heterogeneous tar cracking reactions, auto-catalytic reactions and gasification reactions with carbon dioxide and water (Babu & Chaurasia, 2003b; Boroson, Howard, Longwell, & Peters, 1989; Neves et al., 2011), and others as noted in step 5 in Figure 2-1. The products are again generalised as volatiles, gas and char but this time denoted by the subscript "2". They complicate the overall pyrolysis process further as they themselves have a rate and heat of reaction, which differ from the primary reactions.

Overall, there is an intricate interdependence between chemical and physical processes, which becomes evident when observing the structural changes (step 3 in Figure 2-1) of the pyrolysing material (Di Blasi, 2008) that affect the transport processes (mass, heat and momentum transfer) and reaction kinetics, which again influence the chemical reactions (Kanury, 1972; Roberts, 1970, as cited in Di Blasi, 1993). An example where structure affects secondary reactions both positively and negatively is that an increase in porosity provides additional reaction sites for heterogeneous vapour solid reactions (Anthony & Howard, 1976, as cited in Babu, 2008) but contrary shrinkage decreases vapour residence time, which leaves less time for the reactions to occur (Di Blasi, 1996a).

It is clear that the above mentioned five idealised steps are not separate entities but complex processes which are interconnected and partly occur in parallel or in series. The reaction mechanism illustrated in Figure 2-1, proposed by Shafizadeh and Chin (1977) and modified by Thurner and Mann (1981) and Di Blasi (1996a), represents the one most commonly used in the literature. However, the actual mechanism is not yet understood (R. C. Brown, 2009; White et al., 2011). A variety of alternative pyrolysis mechanisms proposed in the literature are reviewed in subsection 2.7.

To sum it up, biomass pyrolysis is an intrinsic complicated process that is not yet completely deciphered despite its long history (Antal & Grønli, 2003; R. C. Brown, 2009; Di Blasi, 1993). For this reason further research is required, especially in the field of secondary reactions and particularly concerning their role in char formation.

2.3 Products

In this section a brief overview of the pyrolysis products, solid, liquid and gaseous, is given. Their characteristics and application depend on the feedstock composition and the operating conditions (R. C. Brown, 2009; K. Y. Chan & Xu, 2009; Mohan et al., 2006; Neves et al., 2011), which are discussed in sections 2.5 and 2.6 respectively.

2.3.1 Solid

The solid product of pyrolysis is the product of main interest in this research. In its most general case it is called char, but is also called charcoal when in lump form and more recently biochar when sourced sustainably and applied to soil. Since biochar is a relatively new term (its origin is discussed in the supplementary information of Woolf, Amonette, Street-Perrott, Lehmann, and Joseph (2010)) the terms char and charcoal are more frequently used throughout this study. Indeed, charcoal has a long history. In their review on charcoal production, Antal and Grønli (2003) state that char is one of the oldest products produced by humankind, in excess of 30,000 years (Bard, 2001), produced specifically for charcoal drawings. More recently its applications are wide ranging, as listed in 1.1.2. A picture of a typical charcoal is shown in Figure 2-2.

Figure 2-2. Charcoal produced in a retort kiln.

Despite there being a visual association with the product in Figure 2-2, charcoal is not a defined chemical substance (as indicated in Table A-2 in Appendix A, and mentioned by Antal et al. (2000) and L. Wang et al. (2011)). This becomes evident when looking at the somewhat untidy stoichiometric equations developed for the formation of charcoal from cellulose (Klason et al., 1909, as cited in L. Wang et al., 2011):

$$C_6H_{10}O_5 \rightarrow 3.75CH_{0.60}O_{0.13} + 2.88H_2O + 0.5CO_2 + 0.25CO + C_{1.5}H_{1.25}O_{0.38}\ , \quad (2.4)$$

and wood pyrolysis (Klason et al., 1908, Klar, 1925, as cited in Antal & Grønli, 2003):

$$2C_{42}H_{60}O_{28} \rightarrow 3C_{16}H_{10}O_2 + 28H_2O + 5CO_2 + 3CO + C_{28}H_{34}O_9 \quad (2.5)$$

at 400 °C respectively. The first and last products in both reactions represent the char and the residual tar. Because the tar accounts for a large amount of carbon loss (Antal & Grønli, 2003), an opportunity for increased char production exists by minimising the formation of tar, as shown in Figure 2-1. This relationship is a harbinger of the varying char yields that have been observed in the literature, as reviewed by Antal and Grønli (2003).

The efficiency of char production directly relates to the economics of the manufacture of biochar and its environmental impact. It is determined on a solely quantitative basis as char yield, y_{char}:

$$y_{\text{char}} = \frac{m_{\text{char}}}{m_{\text{feed}}}, \quad (2.6)$$

where m_{char} and m_{feed} are the mass of dry charcoal and dry feedstock respectively (Antal et al., 2000; L. Wang et al., 2011). According to equation (2.6) the yield of char in reaction (2.4) is 34.0 % (wt/wt) with a carbon content of 81.7 % (wt/wt) and in reaction (2.5) 34.7 % (wt/wt) with a carbon content of 82.0 % (wt/wt). However, equations (2.4) and (2.5) depend on the pyrolysis conditions, as indicated above. In 2.6.2 it is discussed that with increasing pyrolysis temperature the char yield decreases whereas the carbon content increases. This reveals that the yield of biochar alone is not sufficient for characterising a biochar manufacturing process, as it is easy to obtain high yields of residue under conditions of incomplete pyrolysis (Mok, Antal, Szabo, Varhegyi, & Zelei, 1992; L. Wang et al., 2011).

An alternative to y_{char} is the fixed carbon yield, y_{FC}:

$$y_{\text{FC}} = y_{\text{char}}\left(\frac{\%\,FC}{100 - \%\,feed\ ash}\right), \quad (2.7)$$

which describes the conversion efficiency of biomass carbon into char carbon, relevant when using the char as reductant in the iron and steel industry, (Antal et al., 2000; Antal & Grønli, 2003; L. Wang et al., 2011). In equation (2.7) % *FC* is the percentage of fixed carbon in the charcoal and % *feed ash* is the percentage of ash in the feedstock on

a dry basis (L. Wang et al., 2011). Nonetheless, this information is not sufficient for the manufacture of biochar. More soil relevant information is required such as "Basic Utility Properties", "Toxicant Assessment" and "Advanced Analysis and Soil Enhancement Properties", as proposed in the "Standardized product definition and product testing guidelines for biochar that is used in soil" by the International Biochar Initiative (2014) (IBI guidelines). This information defines the interaction of the biochar with soil (Lehmann & Joseph, 2009b). It is important to note that the major alternative to these guidelines is the European Biochar Certificate (European Biochar Foundation, 2012) (EBC), which has similar requirements (ref: see http://www.biochar-international.org/sites/default/files/IBI-EBC_comparison_Oct2014.pdf). Standards like this ensure that the production and application of biochar is sustainable and has no negative effects on the soil and the subsequent food chain, such as due to the presence of PAHs (Hilber, Blum, Leifeld, Schmidt, & Bucheli, 2012).

To benchmark the achieved yield, it is desirable to know the maximum theoretical yield. This is rather difficult due to the complexity of biomass (Mok et al., 1992). Easier to determine is the hypothetical yield of carbon from cellulose pyrolysis from the stoichiometric equation:

$$C_6H_{10}O_5 \rightarrow 6C + 5H_2O \qquad (2.8)$$

which is 44.4 % (wt/wt) (Antal et al., 1996; Mok et al., 1992). Antal et al. (1996) assumed a fixed carbon content of 82 % (wt/wt) for a high-quality charcoal, which agrees with the carbon content of cellulose and wood char produced at 400 °C (see (2.4) and (2.5)), and thus calculated a theoretical yield of 54 % (wt/wt). Using equation (2.5) the dry wood carbon content is 49.8 % (wt/wt), the dry char carbon content is 82.0 % (wt/wt) and the carbon yield is 57.1 % (wt/wt). Table 2-1 compares the theoretical yields to those attained in poor and good industrial operations. The large differences warrant further research into secondary char forming reactions.

Table 2-1. Charcoal yields for conventional pyrolysis.

Biomass pyrolysis	Charcoal yield in % (wt/wt)
Theoretical predicted yield	44 to 55[a]
Traditional kiln	Can be below 10[b]
Modern slow pyrolysis at ~500 °C & long vapour phase residence times, ~5-30 min	35[c]

[a]Antal, DeAlmeida, Mok, and Sinha (1991, as cited in Mok et al., 1992). [b]Antal and Grønli (2003). [c]R. C. Brown (2009).

L. Wang et al. (2011) observed similar variations in the fixed carbon yield of corncobs. They predict theoretical fixed carbon yields for corncobs in the range of 32.4 to 36.5 % (wt/wt) at 950 °C and discovered that about 90 % of the theoretical yield are achievable under pressure compared to only 49 to 54 % of the theoretical value using standard proximate analysis at atmospheric pressure with short volatile residence time and small samples. The effect of these operating conditions is discussed in more detail in 2.6 but generally the differences are attributed to secondary reactions that comprise "vapor-phase" or "nascent vapor-phase species" (L. Wang et al., 2011, p. 3263). These results, in combination with earlier findings, reveal the significant effect of secondary reactions on char formation (Antal et al., 2000; Antal et al., 1996; Mok et al., 1992; L. Wang et al., 2011).

Biochar quality defined by either the aforementioned IBI or EBC guidelines is known to affect the interaction of the biochar with soil. For example Joseph et al. (2012) mentioned that organic molecules like phenols, diols, triols, alcohols and other complex organic molecules can influence microbial growth and thus nutrient uptake. These labile organic compounds are mainly present in low temperature biochars (E. Graber, 2011, as cited in Joseph et al., 2012). Additionally research indicates that small amounts of toxic organic molecules can cause hermetic responses and systemic resistance, that is, stimulate the plants inherent defence mechanism (Joseph et al., 2012; Lehmann et al., 2011). High temperature biochars contain benzene, toluene, ethylbenzene, and xylenes, BTEX, (E. Graber, 2011, as cited in Joseph et al., 2012). Next to these chemical differences exist a variety of structural dissimilarities, like surface area and porosity (Downie et al., 2009). Downie et al. (2009) show in their review that the surface area is an essential soil property as it effects fertility, aeration, water and nutrient retention, as well as microbial activity. The surface area usually increases with highest treatment temperature, *HTT*, at least in the range of biochar manufacture, 300 to 700 °C, (R. A. Brown, Kercher, Nguyen, Nagle, & Ball, 2006;

Downie et al., 2009). Thus, it might be beneficial to mix a low temperature biochar with a high temperature biochar.

While secondary char forming reactions increase yield and make the manufacture of biochar more economical, the mechanism by which this occurs is unclear. Also unclear is the impact that secondary char has on biochar quality. Both aspects will be studied in this work.

2.3.2 Liquid

The liquid product of pyrolysis is the fraction of the volatiles that are condensable at room temperature, as mentioned in sub-section 2.2.2. Similar to the solid product of pyrolysis the use of tars have a long history. Lédé (2012) mentions for example their use for corpse embalming in Egyptian Pharaon civilisation. It is often more loosely referred to as bio-oil, pyrolysis oil, bio-crude, pyroligneous tar, and liquid smoke (Bridgwater, 2003; Laird et al., 2009; McCarl, Peacocke, Chrisman, Kung, & Sands, 2009). It consist of several phases, for instance water, light pyrolysis oils, insoluble tars, and pyroligneous acid (R. C. Brown, 2009; Lédé, 2012), indicating that its composition is very complex. Czernik and Bridgwater (2004) state that it contains more than three hundred compounds. Di Blasi (1996a) mention levoglucosan and furfural, furan derivatives, and phenolic compounds as typical products of the biomass constituents cellulose, hemicellulose and lignin respectively. However, similar to the char, it is not a well-defined chemical substance as its composition varies depending on the pyrolysis conditions (Klason, 1914). Bridgwater (2003) states that it is generally obtained by rapid quenching and can be viewed as a micro-emulsion consisting of an aqueous solution of holocellulose pyrolysis products, the continuous phase, stabilising the pyrolytic lignin macromolecules.

Bio-oil generally has a relatively high energy density (Laird et al., 2009). The higher heating value, *HHV*, is typically 17.0 MJ/kg or 22.5 MJ/kg on a wet and dry basis respectively (Bridgwater et al., 1999). Its potential use comprises transport fuel or fuel in general (Bridgwater & Peacocke, 2000; Czernik & Bridgwater, 2004), gasification feedstock (McCarl et al., 2009), which can be even in combination with char (Henrich & Weirich, 2004), or raw material for the production of chemicals like fertiliser, resins or liquid smoke (Czernik & Bridgwater, 2004; McCarl et al., 2009). In particular its potential use as a liquid fuel has led to increased research in its

manufacture since the oil crisis in the 1970s (Czernik & Bridgwater, 2004; Oasmaa & Czernik, 1999), and more recently it is driven by climate change and the finite nature of fossil fuels (Bridgwater, 2006; Mohan et al., 2006). It is usually characterised by a high oxygen content (typically 35 to 40 % (wt/wt) (Czernik & Bridgwater, 2004)) that gives the bio-oil undesirable properties like low heating value, low energy density compared to fossil fuels, immiscibility with hydrocarbon fuels, and instability (Bridgwater et al., 1999; Czernik & Bridgwater, 2004; Kantarelis, Yang, and Blasiak, 2013 as cited in Kantarelis, Yang, & Blasiak, 2013). The oxygen derives from water initially present in the biomass and reaction water (Bridgwater et al., 1999). Its efficient removal is the main challenge for processing bio-oil in petroleum refineries (Kantarelis et al., 2013). Bio-oils also have a high corrosiveness due to the large presence of organic acids (Czernik & Bridgwater, 2004).

The liquid product is of interest to this study as it is the reactant in secondary reactions, and could possibly be a high value by-product.

2.3.3 Gas

The gas is also referred to as syngas, synthetic gas, permanent gas or simply pyrolysis gas. It is the fraction of the volatile pyrolysis products that are non-condensable at room temperature (Boateng, Jung, & Adler, 2006; Di Blasi, 2008; McCarl et al., 2009). Generally, the produced gases have a relatively low heating value (*HHV* of approximately 6 MJ/kg (González, Román, Encinar, & Martínez, 2009; Laird et al., 2009)) and consist mainly of CO, CO_2, CH_4, H_2 and small amounts of non-condensable light hydrocarbons, C_1 to C_5 species (Di Blasi, 1996a; Goyal et al., 2008; Grieco & Baldi, 2011; McCarl et al., 2009; Neves et al., 2011). As for the solid and liquid products, the actual gas composition is dependent on the operating conditions and the stage of pyrolysis (Antal et al., 1996).

The gaseous product can be used as syngas for producing fuels or chemicals (Bridgwater & Peacocke, 2000; Kamm & Kamm, 2004; Lange, 2007; Spath & Dayton, 2003), or simply combusted to generate heat or electricity (Laird et al., 2009; Lange, 2007). In the case of the manufacture of biochar it is a by-product that has to comply with emission regulations, and may be integrated into the heat supply of the pyrolysis reactor.

2.4 Pyrolysis Types/ Modes

Generally, pyrolysis is classified according to the feedstock heating rate, *ß*, which is also referred to as fuel heating rate. It is dependent on a variety of parameters such as reactor design and feedstock properties (Di Blasi, 1996b), and is typically divided into slow, intermediate and fast pyrolysis (Bridgwater, 2006; International Energy Agency, 2006), Table 2-2.

Table 2-2. Common pyrolysis classification.

Type	***HTT* in °C**	**$t_{volatiles}$ in s**	**Yields in % (wt/wt)**		
			Char	**Gas**	**Liquid**
Slow	~ 400 °C	≥ 10…20	35	35	30
Intermediate	~ 500 °C	10…20	20	30	50
Fast	~ 500 °C	≈ 1	12	13	75

Note. The yields in this table refer to a dry wood basis. *HTT* = highest treatment temperature; $t_{volatiles}$ = residence time of volatile pyrolysis products. Adapted from International Energy Agency (2006) and Bridgwater (2006).

However, the classification in Table 2-2 is not universal and can vary in the literature (in range and naming). For instance Babu (2008) distinguishes between conventional, fast, and flash pyrolysis. Again, the differences are in the heating rate, *HTT*, and solid residence time, but additionally particle size, which is interrelated with the heating rate. The principle behind the differentiation is the same, that is, heating the biomass at slow heating rates under conditions of prolonged vapour-phase residence times leads to higher char and gas yields while heating small samples of biomass at very high heating rates and short vapour-phase residence time leads to high liquid yields, Table 2-2. The reasons are believed to be; (a), increased re-arrangement reactions during slow pyrolysis at low temperatures favouring char formation (Collard & Blin, 2014) (addressed under pre-pyrolysis in 2.2.2); and (b), increased secondary reactions at long vapour-phase residence times (see Figure 2-1). Since the influencing parameters can be adjusted over the range of interest continuously the classification of pyrolysis in separate modes is somewhat arbitrary, and explains why they are not universal in the literature.

It is important to add that pyrolysis can also be classified according to other process parameters like the atmosphere under which it is carried out, for instance steam

pyrolysis (Antal & Grønli, 2003; Pütün, Apaydın, & Pütün, 2004) or hydropyrolysis (Dilcio Rocha, Luengo, & Snape, 1999), which are performed in the presence of steam or hydrogen respectively. Some of those alternative processes and their remarkable results are discussed in 2.8. The manufacture of biochar is mainly by slow conventional pyrolysis as it is fairly well understood and the reactors are less complicated requiring less investment costs and operational skill. Although, more recently the production of hydrochar by hydrothermal carbonisation with its potential use as biochar is being investigated (Libra et al., 2011), see 2.8.6.

Table 2-2 shows that slow pyrolysis is the desired mode of operation for the manufacture of biochar. As the heating rate limits were the values of Babu (2008) for conventional pyrolysis, 0.1 to 1 K/s, selected. The char yield of 35 % is at the upper end of the practically achievable range. Nevertheless, it is significantly smaller than the theoretical yields shown in Table 2-1, which supports the hypothesis that by optimising secondary char formation processes, further gains can be made in char yield and pyrolysis process efficiency. While understanding the mechanism of secondary char formation is the focus of this study, it is important to understand the feedstock and how it behaves during thermal degradation.

2.5 Feedstock

The feedstock plays an important role in pyrolysis, as it is not only the source for pyrolysis but also affects the properties of the biochar product (Lehmann, 2007a). For example the nutrient composition of biochars as well as the presence of heavy metals depends on the feedstock used as reviewed by K. Y. Chan and Xu (2009). Furthermore, the feed organic composition along with its mineral matter content has been found to affect the product distribution and properties (Raveendran, Ganesh, & Khilar, 1995, 1996). Typically the structure of biochar resembles the morphology of the feedstock (Joseph et al., 2010) so therefore, when studying pyrolysis, one has to be aware of the feedstock composition, properties and structure.

In this research only one feedstock, New Zealand radiata pine (*Pinus radiata*), is used to investigate the effects of pyrolysis conditions and secondary reactions on biochar. Thus, this section deals mainly with softwood in general and radiata pine in particular.

2.5.1 Structure of Softwood/ Radiata Pine

As indicated above New Zealand radiata pine belongs to the softwood genera, *gymnospermae* (Bowyer, Shmulsky, & Haygreen, 2007). A thorough description of the structure of wood in general is given by Bowyer et al. (2007). The following is a summary from their book regarding the structure of softwood with additional information from other sources as cited:

The focus of this review has been on the trunk, as the wood used in this research comes from the stem of a single radiata pine tree. The bark is not discussed in detail here, as it is not subject to this research. A part of a softwood trunk with subsequent magnifications is shown Figure 2-3.

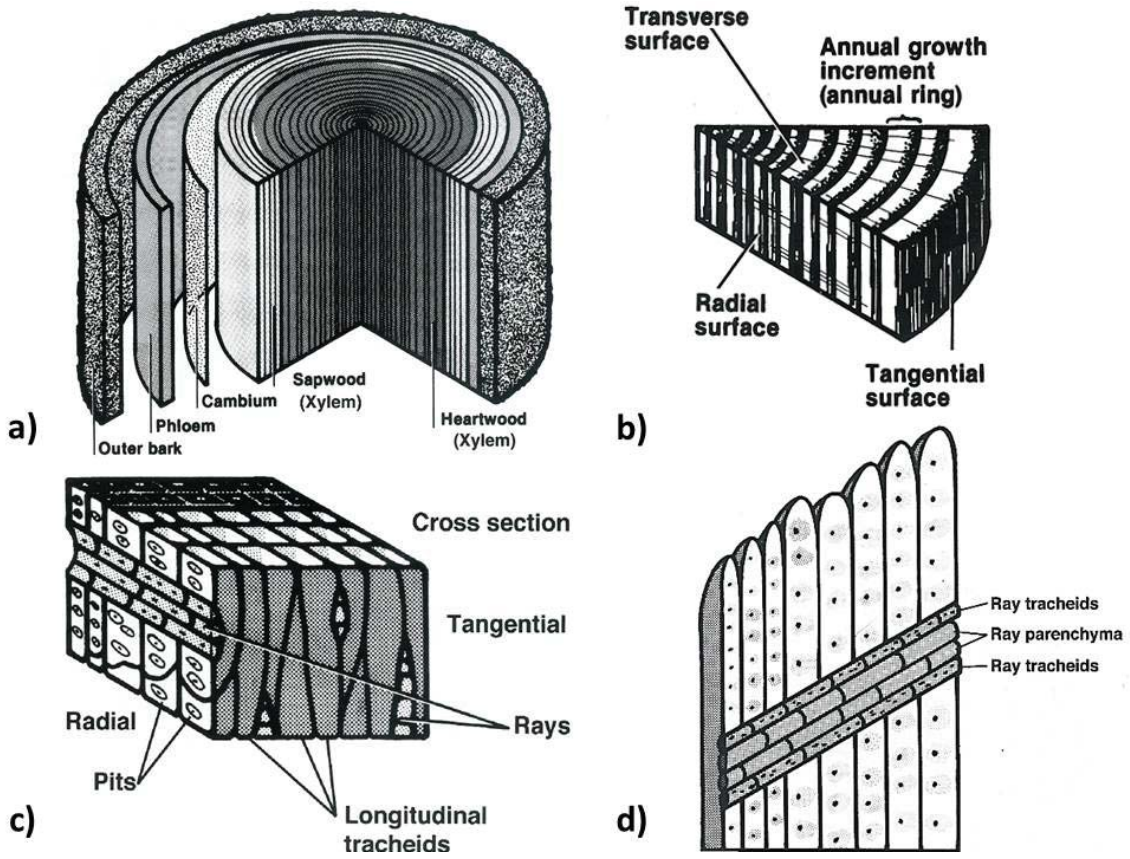

Figure 2-3. Structure of softwood. a) Mature tree trunk with characteristic layers. b) Slice of a softwood trunk with its three characteristic surfaces. c) Magnified block of white fir—unmagnified size is about 1/50,000 cm^3. d) Tracheids with ray cells. From *Forest products & wood science: An introduction* (p. 11, 26, 9, and 75 respectively), by J. L. Bowyer, R. Shmulsky and J. G. Haygreen with drawings by K. Lilley, 2007, Ames, IA: Blackwell. Copyright 2007 by Blackwell.

Starting on the left-hand side of Figure 2-3 a) we see that a wood trunk consists of an outer layer called the outer bark. This is a protective layer to shelter the softer inner bark, phloem, from environmental influences like extensive water loss by evaporation, or mechanical damage caused for example by animals (Wiedenhoeft & Miller, 2005). The inner bark together with the outer bark is referred to as bark. The phloem transports sugars, formed in the leaves, required for new wood, xylem, production down the tree. The next layer referred to as cambium or vascular cambium is very thin (Bowyer et al., 2007; Wiedenhoeft & Miller, 2005). From it, new phloem and xylem are formed. In temperate zones growth occurs rapidly in early spring, slows down towards the end of summer, and stops in autumn. The cells formed in early spring are generally characterised by a large diameter and thin walls compared to cells with a short radial diameter and thick cell walls at the end of the growing season. The former cells form the earlywood and the latter the latewood, which are illustrated in detail in Figure 2-4 b) and c) and Table 2-3.

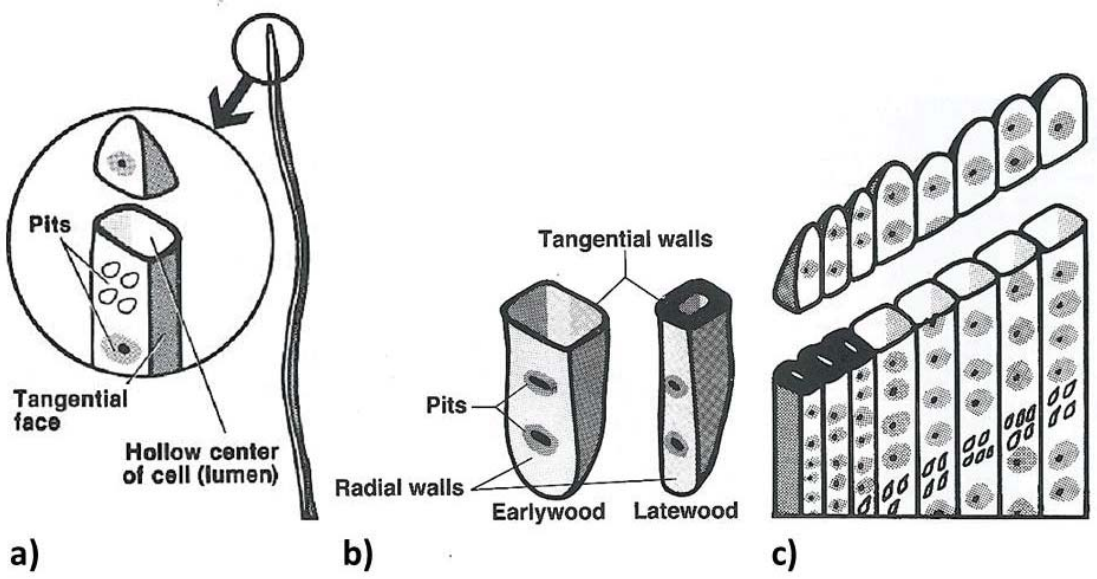

Figure 2-4. Tracheids. a) Longitudinal tracheid. b) Earlywood and latewood tracheid ends. c) Tracheids of one year growth—earlywood right top and latewood bottom left. From *Forest products & wood science: An introduction* (p. 68, 28, and 69 respectively), by J. L. Bowyer, R. Shmulsky and J. G. Haygreen with drawings by K. Lilley, 2007, Ames, IA: Blackwell. Copyright 2007 by Blackwell.

Latewood appears darker and has a higher density. This results in the appearance of visible growth rings, Figure 2-3 b).

Figure 2-3 a) shows that the xylem is divided into sapwood and heartwood. It is important to note, that most of the cells in a mature tree are dead (Wiedenhoeft & Miller, 2005). The sapwood is the part of the wood that contains living metabolically active parenchyma cells (*ibid*). The name sap itself refers to a solution of water, sugars, growth regulators and various other substances. Sapwood has the task to transport mineral-rich water from the roots upwards, and to store and synthesise biochemicals (Bowyer et al., 2007; Wiedenhoeft & Miller, 2005). The heartwood chemicals, formed in the living parenchyma cells at the boundary to the heartwood, are responsible for the heartwood formation (Hillis, 1996, as cited in Wiedenhoeft & Miller, 2005), which is generally darker wood towards the centre of the trunk (Wiedenhoeft & Miller, 2005). It has the same basic cell structure as sapwood but all the cells are dead and is characterised by the presence of the above mentioned heartwood chemicals, which are often called extractives (Wiedenhoeft & Miller, 2005). They are discussed in more detail in sub-section 2.5.2. The long-term storage of these chemicals is the main task of heartwood (Wiedenhoeft & Miller, 2005). Not shown in Figure 2-3 a) is the pith, which is located in the centre of the tree, and is the residue from its early development (Wiedenhoeft & Miller, 2005).

Figure 2-3 b), shows a slice of a wood trunk with its three characteristic surfaces. It is important to be familiar with the names transverse, radial and tangential, as they are often used when dealing with wood to describe its anisotropy. The first magnification, Figure 2-3 c), displays the major constituents of softwood. Ray cells form horizontal rays in the wood and are responsible for the transport of sap in the respective direction, as well as for storing carbohydrates. They are usually one cell wide, uniseriate, but several cells high. Figure 2-3 d) illustrates that there exist two types of ray cells, ray tracheids and ray parenchyma. In general, tracheids are mainly responsible for transport and their thick secondary walls deliver mechanical support. In contrast, the main function of parenchyma cells is storage and transport. Rays can either be homogeneous, entirely made of ray parenchyma or ray tracheids, or heterogeneous (made of both) Figure 2-5 7 to 7a, and 11 to 15.

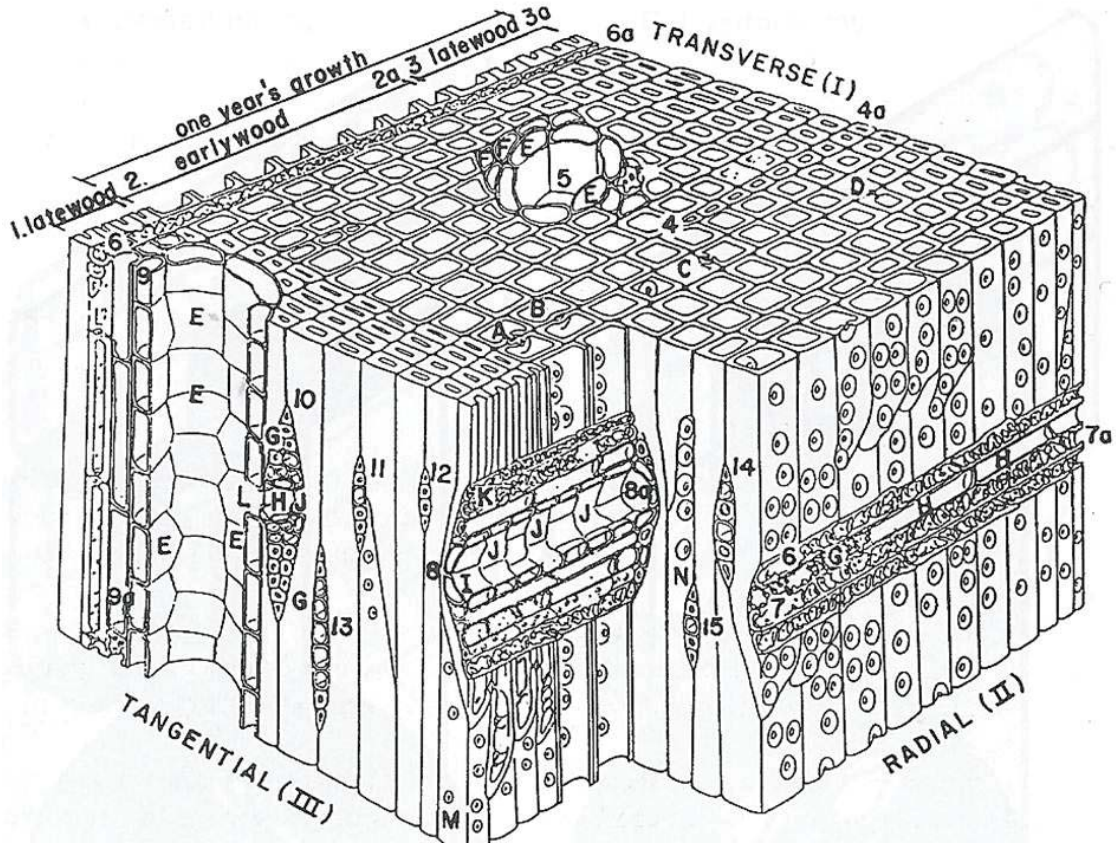

Figure 2-5. Detailed three dimensional softwood section of southern pine. The section shows two latewood rings, 1 and 3 to 3a. The latter one with earlywood tracheids from 2 to 2a forms one annual growth ring. The transition from earlywood to latewood is relatively abrupt. 4 to 4a = tracheids formed by anticlinal division of a fusiform initial; 5 = resin canal; 6 to 6a = transversely sectioned ray tracheids; 7 to 7a = longitudinal section of uniseriate heterogeneous ray; 8 to 8a = sectioned fusiform ray; 9 to 9a = septated longitudinal parenchyma cell; 10 = fusiform ray; 11 = uniseriate heterogeneous ray; 12 = homogeneous tracheid ray; 13, 14 and 15 = uniseriate heterogeneous ray; A, B, C and D = transversely sectioned bordered pits; E = epithelial cells; F = longitudinal parenchyma, thin-walled; G = ray tracheids; H = ray parenchyma; I = resin canal; J = short, bricklike epithelial cells; K = unsectioned ray tracheid; L = opening connecting transverse and longitudinal resin canals; M = pitting in latewood tracheids; N = pitting in earlywood tracheids. From *Forest products & wood science: An introduction* (p. 78), by J. L. Bowyer, R. Shmulsky and J. G. Haygreen with drawings by K. Lilley, 2007, Ames, IA: Blackwell. Copyright 2007 by Blackwell.

In some softwoods, like radiata pine, a resin canal exists in some (1 out of 20) rays, which is then called a fusiform ray. This ray is not uniseriate and consists next to epithelial cells, which form the resin canal, generally of ray tracheids and ray parenchyma. Such a fusiform ray is depicted in Figure 2-5 8 to 8a. Next to these horizontal resin canals exist longitudinal ones, Figure 2-5 5. The resin is secreted into the canal by the surrounding epithelial cells (E in Figure 2-5). Ray cells are interconnected by pits. There are simple, bordered and half-bordered pit pairs (Figure 2-6) (Grønli, 1996).

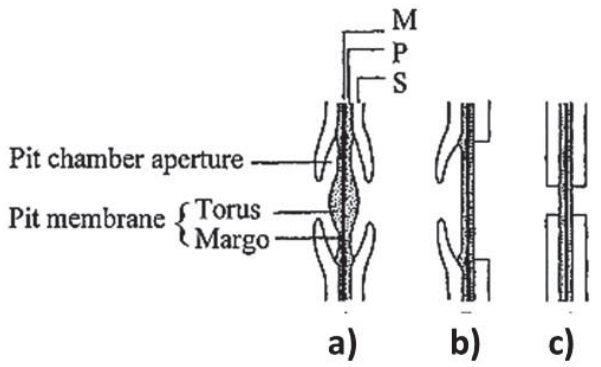

Figure 2-6. Types of pit pairs. a) Bordered pit pair. b) Half-bordered pit pair. c) Simple pit pair. M = middle lamella; P = primary wall; S = secondary wall. From *A theoretical and experimental study of the thermal degradation of biomass* (p. 13), by M. G. Grønli, 1996, Trondheim, Norway. Retrieved from http://ntnu.diva-portal.org/smash/record.jsf?pid=diva2:321540.

Bordered, half-bordered and simple types link generally tracheid–tracheid, tracheid–parenchyma, and parenchyma–parenchyma cells, respectively. Pits are typically present in pairs as can be seen in Figure 2-6. It also shows that in pits the secondary wall is missing (Bowyer et al., 2007; Harris, 1991). In the case of simple pits, Figure 2-6 c), the cell lumens of adjacent cells are only separated by the respective primary walls with a thin intercellular layer in between. This assembly is referred to as the pit membrane. The pit membranes are holopermeable, that is fully, and therefore are avenues for transport of water and other dissolved substances (Bowyer et al., 2007; Harris, 1991). The other main types of pits are bordered pits, Figure 2-6 a). They are called bordered pits because the secondary wall forms a dome-shaped cover over the pit with an opening in the centre (Bowyer et al., 2007; Harris, 1991). Their pit membrane is different to the other two types in Figure 2-6 in that a torus is formed by accumulation of microfibrils, as the bordered pit develops (Figure 2-6 a), and Figure 2-7 a) and d)). Microfibrils are a threaded-like assembly of cellulose molecules, which have a high tensile strength (Wiedenhoeft, 2010).

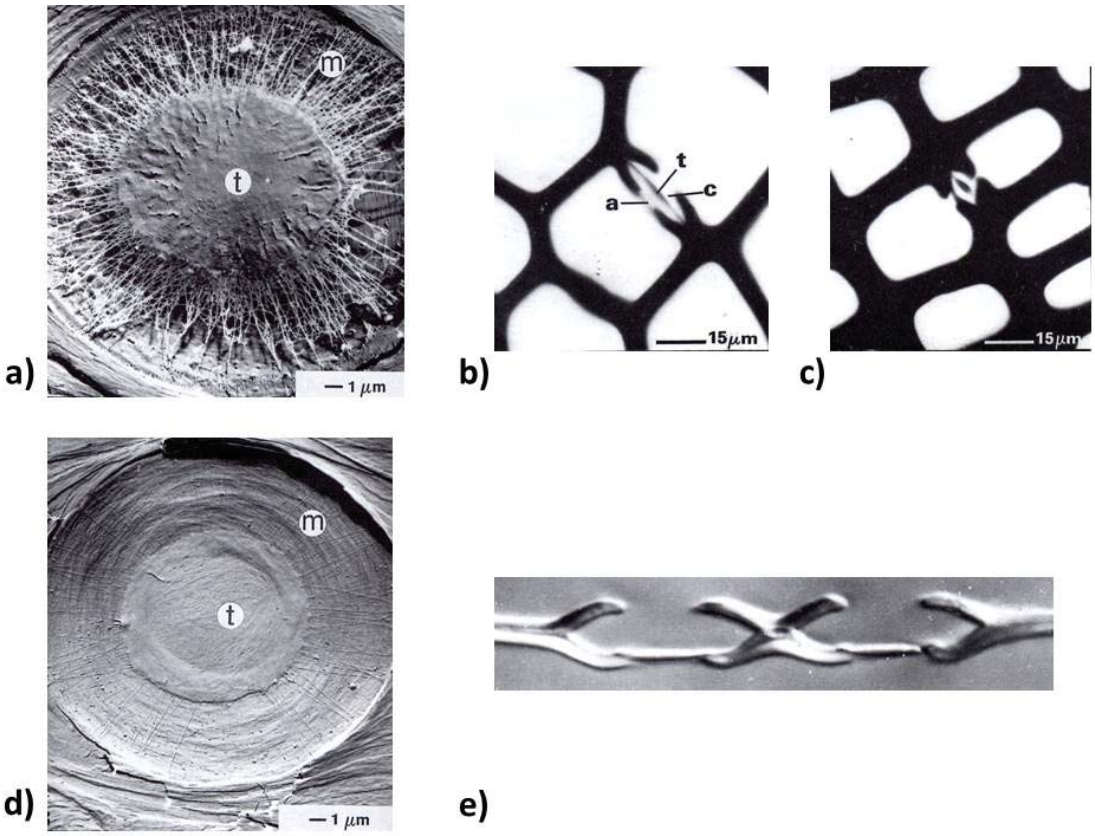

Figure 2-7. Bordered pits in radiata pine. a) Direct replica of bordered pit membrane in the earlywood tracheids of undried sapwood. b) Section through earlywood bordered pit pair. c) Section through latewood bordered pit pair. d) Direct replica of aspirated bordered pit membrane in the earlywood tracheids of sapwood. e) Aspirated earlywood pit pairs. a = pit aperture; c = pit chamber; m = margo; t = torus. Adapted from Structure of wood and bark. In J. A. Kininmonth & L. J. Whitehouse (Eds.), *Properties and uses of New Zealand radiata pine: Volume one – wood properties* (p. 2-9 & 2-10), by J. Maddern Harris, 1991, Rotorua, New Zealand: Ministry of Forestry, Forest Research Institute, with financial support from the New Zealand Lottery Grants Board. Copyright 1991 by Forest Research Institute.

Another difference to simple pits is the margo, radiating strands of microfibrils with free spaces (formed by enzymatic decomposition of the pectin-rich compound middle lamella) in between, which attaches the torus to the circumference of the pit (Figure 2-7 a). Figure 2-7 b) and c) reveal that there is difference between earlywood and latewood bordered pits. The function of earlywood bordered pits is to stop gas bubbles from spreading, and thus damaging the water conduction system by interrupting the water columns in the stem (Harris, 1991). Harris (1991) state, that this is achieved by aspiration of the bordered pits; that is the torus is pulled against the pit aperture due to surface tension caused by the gas-water interface (Figure 2-7 d) and e)). They also report that aspiration is a practically irreversible process that occurs during drying and the formation of heartwood. In contrast, in latewood, aspiration cannot take place due to the ratio of margo strands to pit chamber volume (Harris, 1961, as cited in Harris,

1991). The half-bordered pit type is a mix between the simple and bordered pits where the pit membrane is the same as in the simple type (Figure 2-6).

Returning to the ray cells, Figure 2-3 c) and d) shows that they are embedded by longitudinal tracheids. Tracheids are the most common cells, 90 to 95 % (vol/vol), in softwood. The magnified image in Figure 2-4 shows that they are hollow, referred to as cell lumen, and have a rectangular cross-section. The tracheids have an average diameter of 25 to 45 µm and a length of 3 to 4 mm. However, the exact dimensions depend on whether they are formed early in the growing season or at the end, as well as where they are located in the trunk; that is the corewood or outerwood, as shown in Table 2-3 (Harris & Cown, 1991).

Table 2-3. Radiata pine tracheid dimensions.

Wood type	Length in mm	Diameter in µm	Wall thickness in µm
Corewood			
Earlywood	2.0	30.0	3.0
Latewood	2.5	20.0	4.0
Outerwood			
Earlywood	3.5	40.0	4.0
Latewood	4.0	30.0	5.0

Note. The dimensions in this table represent typical values of radiata pine. Adapted from Basic wood properties. In J. A. Kininmonth & L. J. Whitehouse (Eds.), *Properties and uses of New Zealand radiata pine: Volume one – wood properties* (p. 6-10), by J. Maddern Harris and D. J. Cown, 1991, Rotorua, New Zealand: Ministry of Forestry, Forest Research Institute, with financial support from the New Zealand Lottery Grants Board. Copyright 1991 by Forest Research Institute.

Figure 2-4 shows that the ends of tracheids are closed and the cell wall is perforated by pits, which serve as linkages between cells. Pits that connect a longitudinal tracheid with a ray parenchyma cell are of the half-bordered type and called crossfield pits. Their apertures can have varying shapes, lemon drop, cat's eye, extended slit or a windowlike form. Pits in lemon drop shape can be seen in Figure 2-4 a) and c). However, the majority of pits in longitudinal tracheid cells are bordered pits connecting two tracheids.

Having discussed the structure of wood and the different cell types in softwood, attention is now drawn to the assembly of the cell wall. In the majority of cases the cell wall in wood is decisive for the function of the cell, as most of the cells in wood are dead, that is have no protoplasm, except the parenchyma cells in sapwood (Wiedenhoeft

& Miller, 2005). The assembly of a typical wood cell wall is illustrated in Figure 2-8 a) (Wiedenhoeft & Miller, 2005).

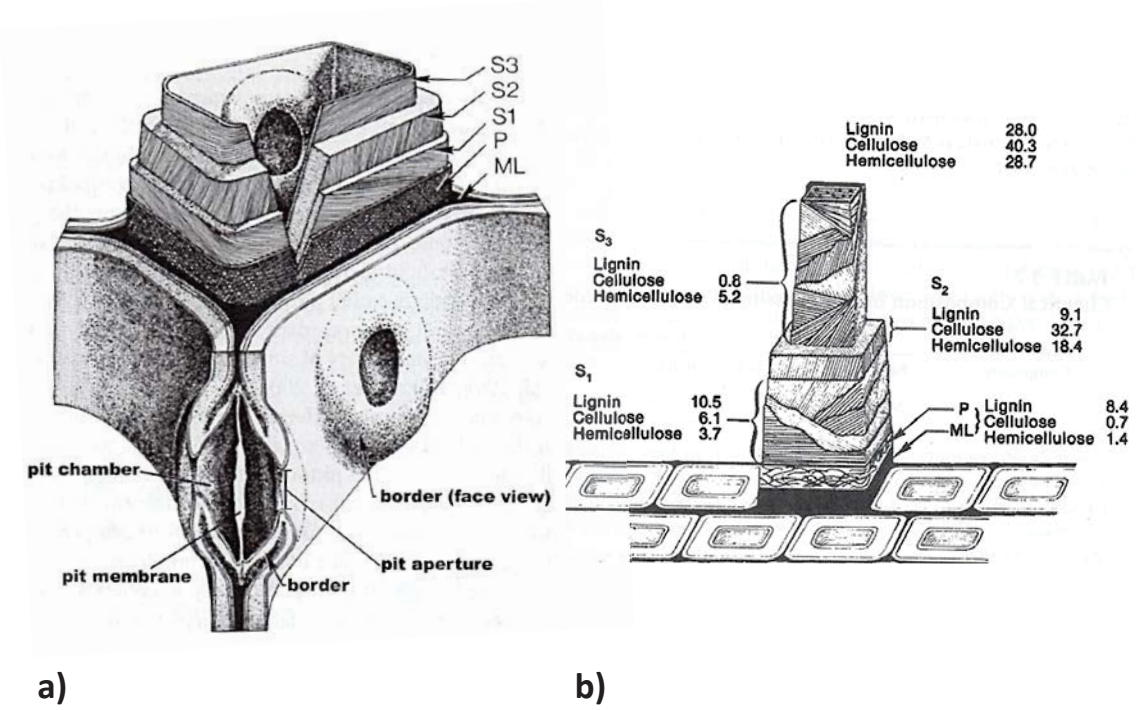

Figure 2-8. Cell wall structure. a) Layers of a mature cell wall. The thickness of the layers is proportional to their real dimensions. From Structure and function of wood. In R. M. Rowell (Ed.), Handbook of wood chemistry and wood composites (p. 19), by A. C. Wiedenhoeft and R. B. Miller, 2005, Boca Raton, FL: CRC Press. Copyright 2005 by CRC press. b) Cell wall of scots pine showing its chemical composition. From Cell wall chemistry. In R. M. Rowell (Ed.), Handbook of wood chemistry and wood composites (p. 51), by R. M. Rowell, R. Pettersen, J. S. Han, J. S. Rowell and M. A. Tshabalala, 2005, Boca Raton, FL: CRC Press. Copyright 2005 by CRC press. ML = middle lamella; P = primary wall; S1, S2, and S3 = three layers of the secondary wall numbered according to their formation order.

Figure 2-8 shows that the cell wall consists of a middle lamella, a primary wall and three layers of secondary wall. Their composition is revealed in Figure 2-8 b) (Rowell, Pettersen, & Tshabalala, 2013). They all consist in varying concentrations of cellulose, hemicellulose and lignin, which are also dependent on the tree species and the location in the tree and wood (Harris, 1991; Rowell et al., 2013; Wiedenhoeft & Miller, 2005). Figure 2-8 b) shows that the highest lignin concentration is found in the middle lamella and primary wall, 80 %, and is lowest in the S3 layer to allow transpiration as lignin is hydrophobic (Wiedenhoeft & Miller, 2005). Even though the highest concentration of lignin is found in the middle lamella, the majority of the lignin is present in the secondary wall which is much thicker than the middle lamella as shown in Table 2-4. Hemicelluloses and the other carbohydrates apart from cellulose form an amorphous matrix (Harris, 1991). Harris (1991) state that this matrix is “reinforced” (p. 2-6) by

cellulose microfibrils and at the end of the cell development "permeated and encrusted with lignin" (p. 2-6) to give it rigidity. The external layer of each cell is the middle lamella, which also separates the two neighbouring cells (Harris, 1991; Wiedenhoeft & Miller, 2005). Wiedenhoeft and Miller (2005) report that the adjacent layer, the primary wall, is very thin and thus very difficult to distinguish from the middle lamella. Therefore, the name "compound middle lamella" was introduced, which is defined as the middle lamella in conjunction with the primary walls of the neighbouring cells (Wiedenhoeft & Miller, 2005). A characteristic difference between the primary wall and the three subsequent layers of the secondary wall is the orientation of the cellulose microfibrils, Figure 2-8 a). It is important to note that the angle of the microfibrils does not change abruptly; rather, the layers are made up of sublayers called lamellae. They have a uniform thickness and the angle of the microfibrils within them changes gradually from layer to layer. The microfibril angle in the respective cell wall parts is summarised in Table 2-4.

Table 2-4. Cellulose microfibril orientation and microfibril angle.

	Primary wall	**Secondary wall**		
	P	**S1**	**S2**	**S3**
Microfibril orientation (microfibril angle[a)]	Largely random orientation (0 to 90°)[b]	positioned in a helical manner[b]; large angle (79 to 113°)[c]	Low angle (1 to 59°)[c]	Similar to S1[b] (50 to 113°)[c]
thickness	Very thin[b]	4 to 6 layers of clustered microfibrils, or lamellae[d] (equivalent to 0.1 µm in earlywood cell)[e]	30 to 40 lamellae in earlywood or 150 and more in latewood[d] (equivalent to 0.6 µm in earlywood cell)[e]	4 to 6 layers of clustered microfibrils, or lamellae[d] (equivalent to 0.1 µm in earlywood cell)[e]

Note. P = primary wall; S1, S2, and S3 = three layers of the secondary wall, Figure 2-8 a).
[a]Relative to long axis of cell. [b]Wiedenhoeft and Miller (2005). [c]Measured for radiate pine by Donaldson and Xu (2005). [d](Kollmann and Côté, 1968, 26, as cited in Bowyer et al., 2007). [e]Bowyer et al. (2007).

Table 2-4 also gives the thickness of the respective cell wall layers. The difference between earlywood and latewood thickness results mainly from the number of lamellae present in the S2 layer as illustrated in Table 2-4 (Harris, 1991). The warty layer

completes the description of the cell wall. It is the rough coating on the innermost cell wall layer (Harris, 1991).

The above discussed structure reveals that wood is highly anisotropic, which affects its transport properties discussed in more detail in 2.5.3. Also structural elements like the bordered pits play a central role as they can aspirate during drying minimising the permeability. The structure of the cell wall is moreover relevant from a chemical reaction point of view, as it reveals that the wood components hemicellulose, cellulose and lignin are intrinsically interwoven (Figure 2-8). This enables interaction and reactions between the wood components, and the wood components and their decomposition products; ultimately permitting secondary reactions.

2.5.2 Wood Composition

Rowell et al. (2013) define wood as a "three-dimensional biopolymer composite composed of an interconnected network of cellulose, hemicelluloses, and lignin with minor amounts of extractives and inorganics" (p. 34). Generally, water is the largest component in a living tree (Bowyer et al., 2007; Rowell et al., 2013). The moisture content, *MC*, in percent is defined as (Bowyer et al., 2007):

$$MC = \frac{m_{\text{water}}}{m_{\text{OD}}} \cdot 100 \ , \tag{2.9}$$

where m_{water} is the mass of water in kg and m_{OD} the oven-dry mass in kg (dried at 105 °C). Harris and Cown (1991) state, that the moisture content depends on the density of wood and varies between sapwood and heartwood, which is illustrated in Table 2-5.

Table 2-5. Average moisture content in radiata pine sapwood and heartwood.

Wood type	**Moisture content in % (wt/wt)**
sapwood	150 (can vary between 100 to over 200)
heartwood	45 (relatively constant)

Note. The data in this table has been obtained from Harris and Cown (1991).

The dry-weight main constituents of wood are carbohydrates, 65 to 75 %, and lignin, 18 to 35 % (Rowell et al., 2013). The approximate composition of radiata pine sapwood and mature bark is given in Table 2-6 (Uprichard, 1991).

Table 2-6. Chemical composition of radiata pine sapwood and mature bark.

Component	% Composition	
	Wood	**Bark**
Cellulose	40	12
Hemicelluloses + other compounds	31	6
Lignin	27	15
Extractives		
Non-polar	2	3
Lower molecular weight phenols	(0.1)	4
Condensed tannins	-	18
Tannins/phenolic acids	-	40
Subtotal	2	65
Ash	(0.2)	2

Note. The data in this table is based on oven-dry weight. Adapted from Chemistry of wood and bark. In J. A. Kininmonth & L. J. Whitehouse (Eds.), *Properties and uses of New Zealand radiata pine: Volume one – wood properties* (p. 4-2), by J. M. Uprichard, 1991, Rotorua, New Zealand: Ministry of Forestry, Forest Research Institute, with financial support from the New Zealand Lottery Grants Board. Copyright 1991 by Forest Research Institute.

The following paragraphs describe the wood components given in Table 2-6. Except where otherwise cited, the source of the description is Rowell et al. (2013).

Cellulose is a glucan polymer, and accounts typically for 40 to 45 % (wt/wt) of dry wood. The glucan polymer consists of D-glucopyranose units joined together by β-linkages, that is, β-(1→4)-glucosidic bonds (Bowyer et al., 2007; Rowell et al., 2013). Two connected sugars form cellobiose, which is the actual building block of cellulose, Figure 2-9 from overpage. The degree of polymerization, *DP*, of cellulose can be as high as 15,000 but is on average around 10,000 (Bowyer et al., 2007; R. C. Brown, 2009; Rowell et al., 2013). This approximates to a 5 μm long linear chain. Bowyer et al. (2007) state that the diameter of a cellulose molecule is about 8 Å. According to its *DP*, the molecular weight varies from 10,000 to 150,000. The cellulose in wood is classified into crystalline, amorphous, accessible and non-accessible. The crystalline portion increases with packing density and can be up to 65 % for wood-derived cellulose. The crystallinity is a result of the parallel alignment of neighbouring cellulose molecules, due to the formation of hydrogen bonds, both intra- and intermolecular (Figure 2-10 a)), as well as the stacking of the so formed layers due to

van der Waal's forces (Figure 2-10 b). In amorphous cellulose, the molecules are orientated in a random manner as a result of the reduced packing density. The accessibility describes the availability of cellulose to water and microorganisms. For example crystalline cellulose, except for its surface, is non-accessible for water compared to accessible amorphous cellulose, which can be non-accessible too, if it is enclosed by hemicellulose and lignin.

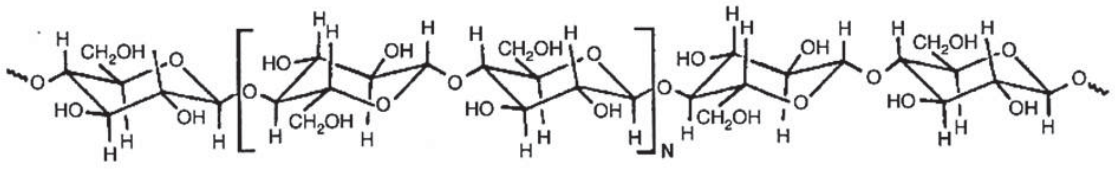

Figure 2-9. Partial structure of cellulose. The disaccharide in the brackets is cellobiose, which is N times repeated to form the polysaccharide cellulose. From Cell wall chemistry. In R. M. Rowell (Ed.), *Handbook of wood chemistry and wood composites* (p. 38), by R. M. Rowell, R. Pettersen, J. S. Han, J. S. Rowell and M. A. Tshabalala, 2005, Boca Raton, FL: CRC Press. Copyright 2005 by CRC press.

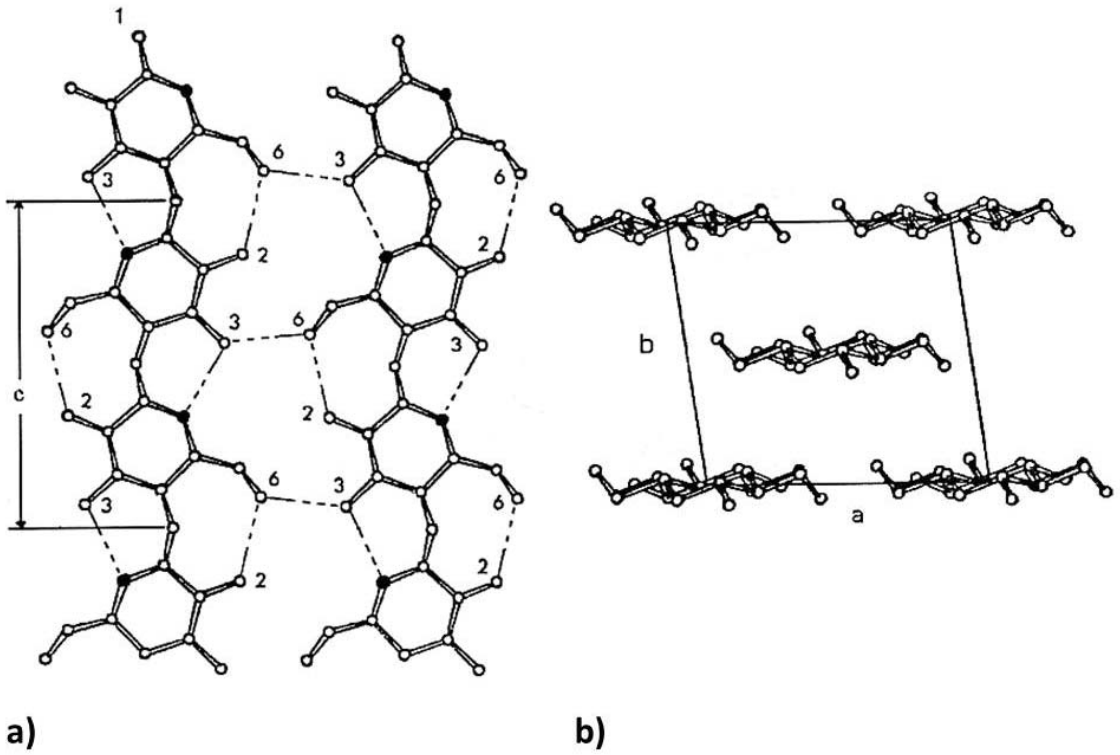

Figure 2-10. Formation of crystalline structure. a) Parallel alignment of cellulose molecules—planar projection of crystal structure. Dashed lines represent intra and intermolecular hydrogen bonds. c = distance of one cellobiose unit, 10.38 Å (Gardner & Blackwell, 1974). b) Axial projection of crystal structure with a = 16.34 Å and b = 15.72 Å (Gardner & Blackwell, 1974). From Cell wall chemistry. In R. M. Rowell (Ed.), *Handbook of wood chemistry and wood composites* (p. 38-39), by R. M. Rowell, R. Pettersen, J. S. Han, J. S. Rowell and M. A. Tshabalala, 2005, Boca Raton, FL: CRC Press. Copyright 2005 by CRC press.

Hemicellulose is made up of a variety of polysaccharides that have, compared to cellulose, lower molecular weight (Bowyer et al., 2007; Rowell et al., 2013). The average *DP* is between 100 to 200. Its main components are D-xylopyranose, D-glucopyranose, D-galactopyranose, L-arabinofuranose, D-mannopyranose, D-glucopyranosyluronic acid, D-galactopyranosyluronic acid, as well as other sugars in marginal quantities. A compilation of the major hemicelluloses in softwood is given in Table 2-7 (Rowell et al., 2013). Characteristic for the structure of hemicelluloses are short side-chains (Figure 2-11) which are the reason for the amorphous nature of hemicelluloses.

Table 2-7. Major hemicelluloses in softwood.

Hemicellulose Type (*DP*)	Percent in wood	Units	Molar ratio	Linkage
Galactoglucomannan (100)	5–8	β-D-Man*p*	3	1→4
		β-D-Glu*p*	1	1→4
		α-D-Gal*p*	1	1→6
Galactoglucomannan (100)	10–15	β-D-Man*p*	4	1→4
		β-D-Glu*p*	1	1→4
		α-D-Gal*p*	0.1	1→6
		Acetyl	1	
Arabinoglucuronoxylan (100)	7–10	β-D-Xyl*p*	10	1→4
		4-*O*-Me-α-D-Glu*p*A	2	1→2
		α-L-Ara*f*	1.3	1→2
Arabinogalactan (200)—Larch wood	5–35	β-D-Gal*p*	6	1→4 1→6
		α-L-Ara*f*	2–3	1→6
		β-D-Ara*p*	1–3	1→3
		β-D-Glu*p*A	trace	1→6

Note. D and L = standard configurations for the two optical isomers of glyceraldehyde; α and β = configuration of the OH-group on C–1; A = acid; Ara = arabinose; *DP* = degree of polymerization; f = furanose; Gal = galactose; Glu = glucose; Man = mannose; Me = methyl; *p* = pyranose; Xyl = xylose. Adapted from Cell wall chemistry. In R. M. Rowell (Ed.), *Handbook of wood chemistry and wood composites* (p. 42), by R. M. Rowell, R. Pettersen, J. S. Han, J. S. Rowell and M. A. Tshabalala, 2005, Boca Raton, FL: CRC Press.

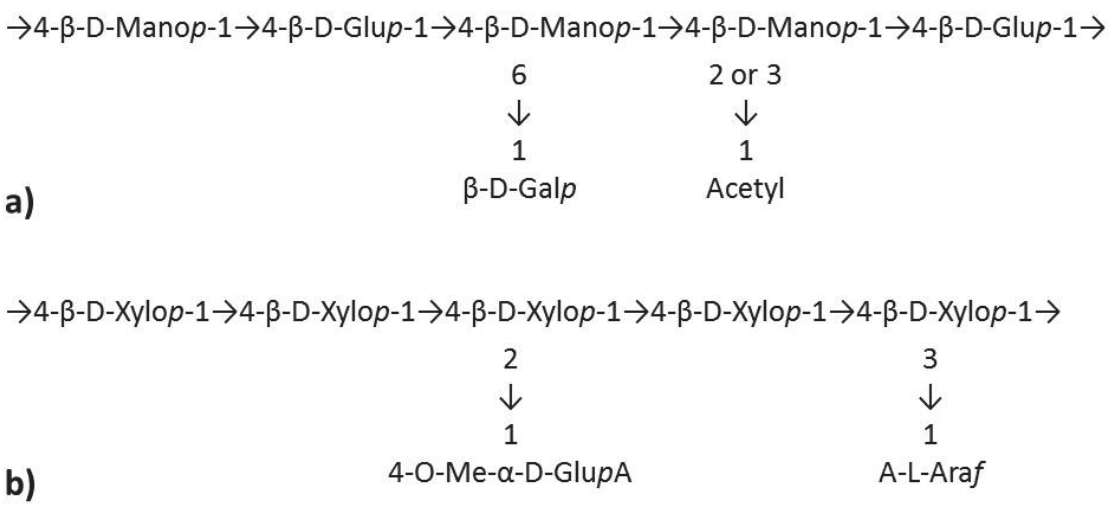

Figure 2-11. Partial structure of the two main softwood hemicelluloses. a) *O*-acetyl-galacto-glucomannan. The backbone polymer consists of glucose and mannose, and the side-chain of galactose. Table 2-7 shows that there exist two fractions of these polymers. The units in the backbone are linked by β-(1→4) bonds and D-galactopyranose is attached as a single-unit by α-(1→6) bonds. Acetyl groups are substituted on the C–2 and C–3 positions of the backbone polymer—approximately every third to fourth hexose unit. b) arabino 4-*O*-methylglucuronoxylan. The backbone polymer is made of β-(1→4) linked xylopyranose units to which D-glucopyranosyluronic acid—approximately every 2 to 10 xylose units—and L-arabinofuranose—approximately every 1.3rd xylose unit—is linked by α-(1→2) and α-(1→3) bonds respectively. Adapted from Cell wall chemistry. In R. M. Rowell (Ed.), *Handbook of wood chemistry and wood composites* (p. 42-43), by R. M. Rowell, R. Pettersen, J. S. Han, J. S. Rowell and M. A. Tshabalala, 2005, Boca Raton, FL: CRC Press. Copyright 2005 by CRC press.

In addition to the two major carbohydrates, cellulose and hemicellulose, there are **other minor polysaccharides** like pectins and starch, as well as proteins. Pectin consists of D-galacturonic-acid units, which are linked by α-(1→4) bonds. It is part of the bordered pits, and middle lamella. Pectin is also found in the inner bark, where it is present in the parenchyma cell walls. Starch is the major reserve polysaccharide, which exists in two forms, amylose and amylopectin. Amylose is made of D-glucopyranose units that are connected by α-(1→4) bonds. Amylopectin has additionally on approximately every 25th glucopyranosyl unit branches attached by α-(1→6) linkages. The two forms are depicted in Figure 2-12 (Schröder, 2010). Starch is mainly present in the form of granules.

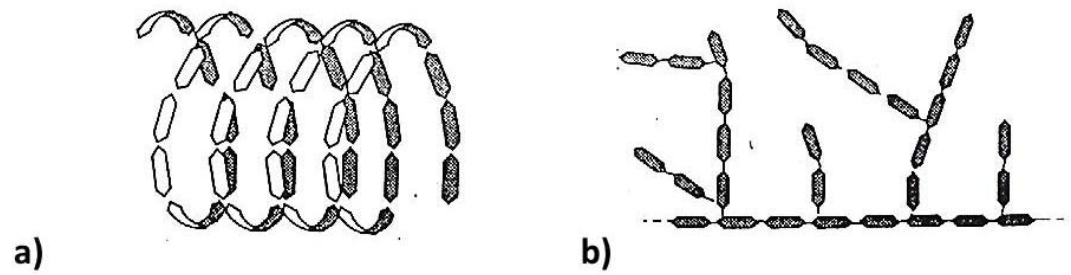

Figure 2-12. Structure of starch. a) Amylose with its typical helix structure caused by the α-configuration. b) Amylopectin with its typical branched structure. From *Verarbeitung nachwachsender Rohstoffe* [Lecture notes] (2.3 Stärke p. 8), by H.-W. Schröder, 2010, Freiberg: Germany.

Lignin is the second largest dry-weight fraction in wood. It is not a carbohydrate as indicated above (Antal et al., 2000; Bowyer et al., 2007; Sjostrom, 1993, as cited in R. C. Brown, 2009; Rowell et al., 2013). R. C. Brown (2009) states that it is formed from the monomers coniferyl alcohol, sinapyl alcohol and coumaryl alcohol as shown in Figure 2-13, where each monomer consists of an aromatic ring and various substituents. A section of a typical softwood lignin structure is illustrated in Figure 2-14 (Adler, 1977).

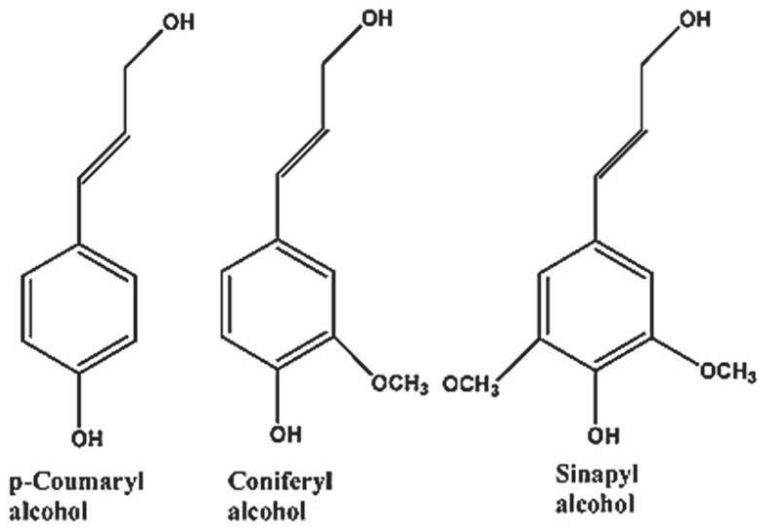

Figure 2-13. Monomers that form lignin. From "Pyrolysis of wood/biomass for bio-oil: A critical review," by D. Mohan, C. U. Pittman and P. H. Steele, 2006, Energy & Fuels, 20, p. 853. Copyright 2006 by American Chemical Society.

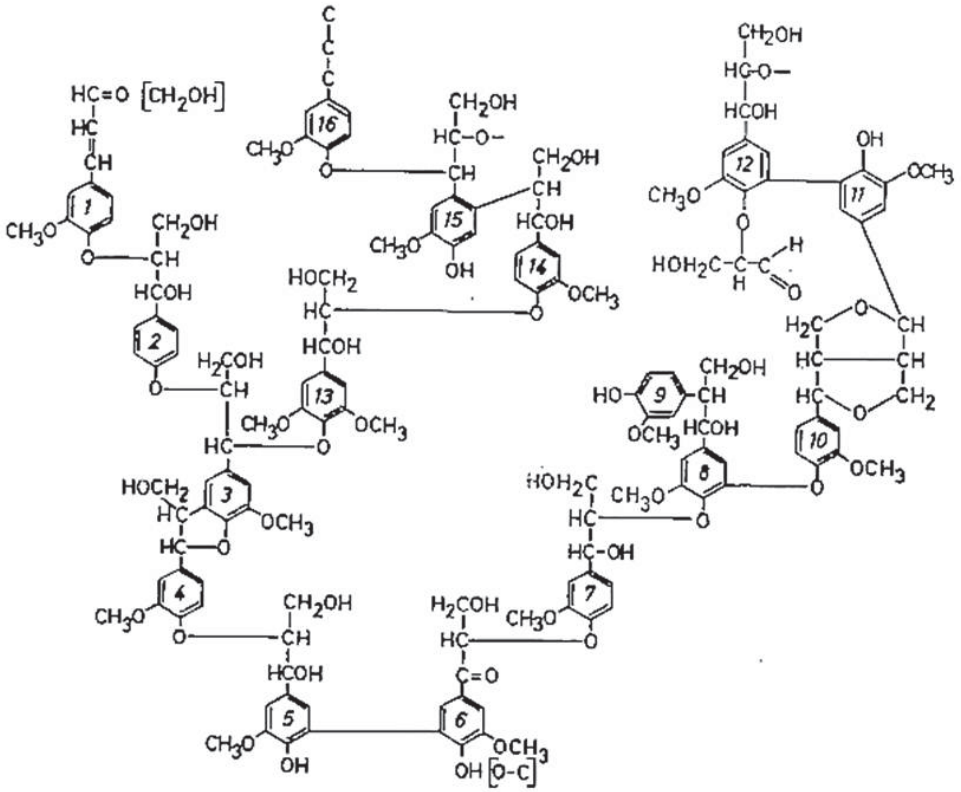

Figure 2-14. Section of a typical softwood lignin structure. From "Lignin chemistry—past, present and future," by E. Adler, 1977, Wood Science and Technology, 11, p. 203. Copyright 1977 by Springer-Verlag.

Figure 2-14 reveals that lignin has a complex structure and is amorphous (R. C. Brown, 2009; Rowell et al., 2013). The difference between softwood and hardwood lignin is that softwood lignin is mainly made of coniferyl phenylpropane units (Figure 2-13),

whereas hardwood lignin consist of coniferyl and sinapyl phenylpropane units (Figure 2-13) (R. C. Brown, 2009; Rowell et al., 2013). The former one is also referred to as guaiacyl lignin and the latter one as guaiacyl-syringyl lignin (R. C. Brown, 2009; Rowell et al., 2013). Both wood type lignins contain minor amounts of p-coumaryl alcohol (Rowell et al., 2013). Lignin-lignin and lignin-polysaccharide bonds are mainly ether and covalent bonds respectively (R. C. Brown, 2009). Rowell et al. (2013) report that methoxyl content in softwood lignin is approximately 15 to 16 %, and that substitutions of phenylpropane can occur at α, β, or γ positions (Sakakibara, 1991, as cited in Rowell et al., 2013). It is however important to note that the configuration of lignin in wood is not yet completely understood (Bowyer et al., 2007). In summary, lignin is a complex, amorphous, mainly aromatic, high molecular weight polymer made of phenylpropane units: (a) p-hydroxyphenyl, (b) guaicyl and (c) syringyl, which vary in their proportions depending on the lignocellulosic species (Bowyer et al., 2007; Collard & Blin, 2014; Rowell et al., 2013).

Extractives are components that can be extracted with solvents (Rowell et al., 2013) and are present in small concentrations in wood (R. C. Brown, 2009). R. C. Brown (2009) state that their influence on the char formation process is believed to be negligible due to their low concentrations but that they can impact the gaseous pyrolysis emission profile. Usually, extractives are classified according to their solubility (R. C. Brown, 2009; Rowell et al., 2013). There are hydrophilic, water-soluble, and lipophilic, soluble in organic solvents, extractives (R. C. Brown, 2009). The latter ones are often described as resins apart from phenolic substances (R. C. Brown, 2009). The class of extractives comprises hundreds of organic compounds, and their exact function is not always understood (Rowe, 1989, as cited in R. C. Brown, 2009). For instance, functions can range from wound response and resisting insect attacks to precursors for other chemicals (Rowell et al., 2013). Extractives include for example resins, fats, fatty acids, fatty alcohols, phenolics, terpenes, steroids, rosin, waxes, phytosterols, etc. (R. C. Brown, 2009; Rowell et al., 2013). These cell wall chemicals can occur as monomers, dimers, and polymers, and are mainly located in the heartwood, where they contribute to the distinct colour, smell and durability (Rowell et al., 2013). Their concentration is generally higher in softwoods (*ibid*).

Wood also contains a range of **inorganic** components (Bowyer et al., 2007; R. C. Brown, 2009). They are very important from the viewpoint of pyrolysis as they have a catalytic effect, which is outlined in a review by White et al. (2011). Similar results

were found in a review of literature by Couhert, Commandre, and Salvador (2009), who state that with increasing mineral content in biomass the degradation rate, the char yield and the total gas yield increases, whereas the liquid yield decreases. For example, the alkali metals potassium, sodium, magnesium and calcium have been identified as catalysts, which favour char formation and influence the degradation process (Fahmi et al., 2007; Jensen, Dam-Johansen, Wójtowicz, & Serio, 1998; Nik-Azar, Hajaligol, Sohrabi, & Dabir, 1997). The inorganic content in wood can vary but is mostly less than 0.5 % (Browning, 1967, as cited in Rowell et al., 2013). It is also often called ash, which describes the inorganic matter and mineral salts that are retained after high temperature combustion (R. C. Brown, 2009; Rowell et al., 2013). The majority of the ash, up to 80 %, is Ca, Mg and K (Rowell et al., 2013). It also includes alkali earth metals, transition metals and various trace elements (R. C. Brown, 2009). The elemental nutrients N and P form part of the inorganic content of biomass as well (R. C. Brown, 2009), and impact the nutrient properties of biochar (K. Y. Chan & Xu, 2009). The literature shows that the inorganic content in wood varies not only between and within species but also depending on the age of the tree and the location inside the tree as reviewed by Rowell et al. (2013) and Uprichard (1991).

2.5.3 Transport Properties of Wood

The transport properties of wood relevant for heat and mass transfer like conductivity and permeability were shown to be important parameters affecting the course of pyrolysis in 2.2.2. That is, the quantity and quality of the pyrolysis products, including biochar, is directly related to these feedstock properties, which themselves are dependent on the complex and anisotropic microscopic structure of the wood (see 2.5.1). Following the transport properties and their directional dependency is illustrated.

Crucial to the heat transfer in wood is its thermal conductivity, which is defined as the rate of heat flow (Q in W) across a material with unit surface area (A in m^2) and of unit thickness (l in m) exposed to a temperature difference (ΔT) of 1 °C (R. Bergman et al., 2010; Gu & Zink-Sharp, 2005; Siau, 1984):

$$\lambda = \frac{Q \cdot l}{A \cdot \Delta T} \ . \tag{2.10}$$

Wood has a fairly low thermal conductivity; for example at room temperature $\lambda = 0.1254$ W/(m·K) for wood perpendicular to the fibre axis that has a specific gravity, G, of 0.45 and a MC of 12 % (Siau, 1984). This shows that wood can be regarded as an insulator and that its thermal conductivity depends on a range of parameters (*ibid*). With respect to the direction the thermal conductivity is 2.25 to 2.75 times greater in the longitudinal direction than in the transverse direction as reviewed by Gu and Zink-Sharp (2005). In the transverse plane there is a difference between conduction in the radial and tangential direction, with the conductivity in the radial direction being 5 to 10 % higher compared to the tangential direction (Griffiths & Kaye, 1923; Gu & Zink-Sharp, 2005). This is due to the fact that heat transfer in wood occurs primarily by conduction through the cell walls (Gu & Zink-Sharp, 2005), as the air in the lumens has a lower thermal conductivity (e.g. 0.024 W/(m·K) at room temperature (Siau, 1984)). The reduced conductivity perpendicular to the fibre axis can be explained by increased contact resistances as a result of the large length to diameter ratios (50 to 200 in Table 2-3) of the wood cells. Gu and Zink-Sharp (2005) show that the difference in the tangential to the radial direction lies mainly in the positioning of the cells. In Figure 2-5 it can be seen that the cells are perfectly aligned in the radial direction and are out of phase in the tangential direction. This explains the slightly faster heat transfer in the radial direction (Gu & Zink-Sharp, 2005). This effect is enhanced by the radial alignment of the ray cells, which is more pronounced in hardwoods compared to softwoods (Steinhagen, 1977, as cited in Gu & Zink-Sharp, 2005). Gu and Zink-Sharp further mention that the concentration of latewood has a significant impact on the transverse thermal conductivities, which is intuitive as the main heat transfer occurs by conduction in the cell walls, which are thicker in latewood (see 2.5.1).

The specific gravity of wood:

$$G = \frac{m_{OD}}{V_{moist} \cdot \rho_{water}} , \tag{2.11}$$

where m_{OD} is the mass of oven-dry wood in kg, V_{moist} the moist volume of the wood in m^3 and ρ_{water} the normal density of water at 4 °C (1000 kg/m^3) (Siau, 1984), is another parameter that was stated above with the thermal conductivity. This is because the thermal conductivity of wood increases with increasing density and moisture content (R. Bergman et al., 2010). In equation (2.11) V_{moist} becomes larger due to swelling of wood with a rise in bound moisture content that leads to a decrease in specific gravity

(Siau, 1984). It is important to note that wood only swells till it reaches its fibre saturation point, FSP. The FSP is the moisture content where the cell walls are saturated with moisture (maximum bound water is present) but no liquid water, that is free water, is present (Rowell, 2013). Alternatively, it can be defined as the moisture content where abrupt changes in the physical properties of the wood occur, which can be observed for most woods from temperate zones at a MC of 30 % (Siau, 1984). At the FSP the specific gravity has a minimum and remains constant at higher MC's as the volume of the wood does not increase any further (Siau, 1984). However, the density of wood:

$$\rho_{wood} = \frac{m_{moist}}{V_{moist}} \tag{2.12}$$

keeps increasing (*ibid*). In equation (2.12) m_{moist} is the moist wood mass, which is defined as (Siau, 1984):

$$m_{moist} = m_{OD}(1 + 0.01MC)\,. \tag{2.13}$$

A rise in MC increases m_{moist} faster than V_{moist} leading to a density increase, which is even faster above the FSP as V_{moist} remains constant (*ibid*). Equations (2.11), (2.12) and (2.13) can be combined to obtain ρ_{wood} as a function of G and MC. This shows that ultimately changes in the moisture content are responsible for the changes in the thermal conductivity. The reason is that water has a higher thermal conductivity (0.606 W/(m·K) at 22 °C (T. L. Bergman et al., 2011)) than the cell wall substance (hemicellulose, cellulose and lignin). Generally, below the FSP the thermal conductivity of wood can be described by a linear function of the MC and G (R. Bergman et al., 2010; Gu & Zink-Sharp, 2005). Above the FSP Gu and Zink-Sharp (2005) found with their model that the thermal conductivity increases significantly and nonlinearly in tangential and radial direction due to the relative high thermal conductivity of the present free liquid water. This leads to the disappearance of structural differences on the thermal conductivities, that is, ratio of radial thermal conductivity to tangential thermal conductivity is close to 1 (*ibid*).

Compared to the above discussed parameters the effect of temperature on the thermal conductivity of wood is relatively minor (2 to 3 % per 10 °C) (R. Bergman et al., 2010). Other factors affecting the thermal conductivity are extractives content, structural irregularities, and fibril angle (*ibid*).

Another important thermal property is the heat capacity, which is the energy required to increase the temperature of a unit mass by 1 K (R. Bergman et al., 2010). It is dependent on the moisture content and the temperature and fairly independent of the wood species (*ibid*). For example the heat capacity of oven-dry wood at room temperature is 1.2 kJ/(kg·K) and increases with temperature according to the following equation (*ibid*):

$$c_{p,OD} = 0.1031 + 0.003867T\,, \tag{2.14}$$

where $c_{p,OD}$ is the heat capacity in kJ/(kg·K) and T is the temperature in K. The heat capacity of wood increases with the moisture content as water has a relatively high heat capacity (4.18 kJ/(kg·K) at room temperature). Below the FSP it consists of the heat capacity of dry wood, water, and an additional factor accounting for the energy of the wood-water bond (R. Bergman et al., 2010). Above the FSP the contribution of water to the heat capacity is by the rule of mixtures (*ibid*).

Forming the ratio of the above discussed thermal conductivity to the product of heat capacity and density, the thermal diffusivity, α_T in m^2/s, is obtained (T. L. Bergman et al., 2011):

$$\alpha_T = \frac{k}{\rho_{wood} \cdot c_{p,wood}}\,. \tag{2.15}$$

The resulting rate is a measure of the materials ability to conduct thermal energy compared to storing it (*ibid*). Since wood has a relatively low thermal conductivity but moderately high density and heat capacity its thermal diffusivity is relatively low (T. L. Bergman et al., 2011). For the above stated example of wood ($\lambda = 0.1254$ W/(m·K), $G = 0.45$, $MC = 12$ %) the thermal diffusivity is $2.3 \cdot 10^{-7} m^2/s$. As the moisture content in wood increases its thermal conductivity increases but so does its heat capacity leading to a smaller thermal diffusivity at higher moisture contents revealing that wood samples with high moisture contents will experience a delayed temperature rise (Di Blasi, 1998).

The mass transfer properties of wood most relevant for pyrolysis were identified to be the diffusion coefficient and the permeability in 2.2.2. Analogue to Fourier's law Fick's first law describes the relationship in steady state between diffusion flux and concentration gradient (Siau, 1984). Thus the diffusion coefficient D in m^2/s is defined similar to equation (2.10):

$$D = \frac{\dot{m} \cdot l}{A \cdot \Delta\rho} \,, \tag{2.16}$$

where $\dot{m}$ is the mass flow in kg/s and $\Delta\rho$ the concentration gradient in kg/m^3 (*ibid*). Equation (2.16) reveals that with increasing diffusion coefficient the diffusion flux increases. Generally, the magnitude of the diffusion coefficient varies with the type of the continuous phase (solid < polymers and glasses < liquid < gas) and temperature (Green & Perry, 2008). In 2.2.2 it was reported that the diffusion coefficient of bound water (D_B) is lower than of water vapour in the air in the lumens (D_V), which is the result of the lower mobility of the bound water molecules. The bound water diffusivity is also a function of the MC, and increases with it, which can be explained by reduced bonding energies that approach zero as the FSP is attained; after that water is present as free water and only held by capillary forces (Siau, 1984). Similarly to the thermal conductivity, the bound water diffusion coefficient is directionally dependent (longitudinal ≈ 3 x tangential, radial ≈ 1/2 longitudinal) (Stamm, 1964, as cited in Siau, 1984). The temperature dependence can be described by an Arrhenius equation as reviewed by Siau (1984). Values of D_B in the transverse direction compared to D_V are given in Figure 2-15 as a function of moisture content and temperature.

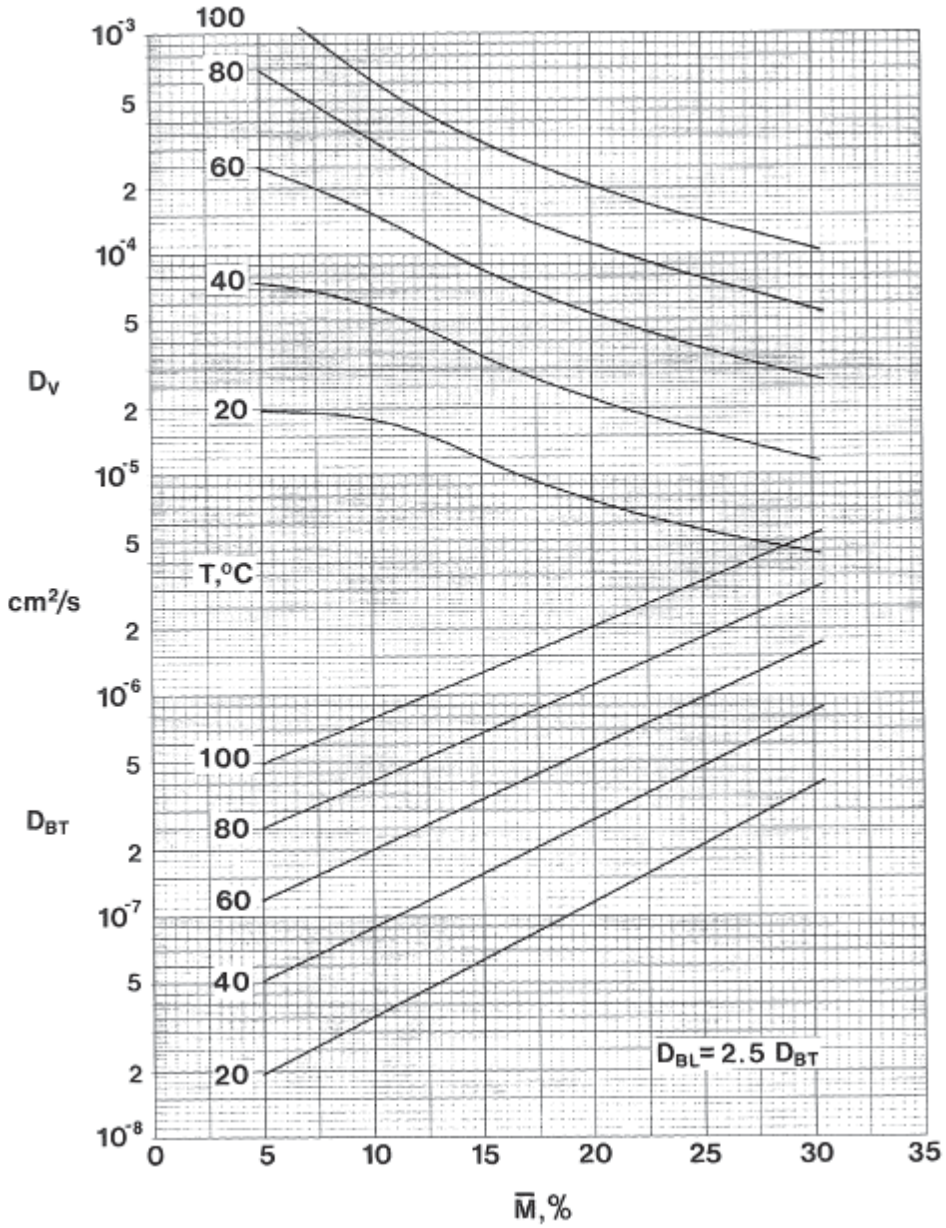

Figure 2-15. Values of the bound water diffusivity in the transverse direction (D_{BT}) compared to the water vapour diffusion coefficient in air in the lumens (D_V) as a function of the average moisture content ($\bar{M}$) and temperature T. From *Transport processes in wood* (p. 158), by J. F. Siau, 1984, Berlin, Germany: Springer Verlag. Copyright 1984 by Springer Verlag.

The values in Figure 2-15 can be combined to determine the overall transverse diffusion coefficient (D_T) of wood considering the alternating sequence of lumen and cell wall (Figure 2-5). For more detail the reader is referred to the original source Siau (1984), where also a moisture diffusion model for the longitudinal direction is described.

Similar to the diffusion of water vapour there is also a diffusion coefficient for the various volatile pyrolysis products. Their determination is complicated as the composition of the volatile mixture in the lumens is changing during pyrolysis. Simplifications can be made by assuming that the gas mainly consists of nitrogen and

considering a binary diffusion (Ratte et al., 2009). When determining an effective diffusion coefficient (D_{eff}) for the bulk diffusion in pores the interaction with the wood fibres has to be considered, which can be done by the introduction of the tortuosity (τ):

$$D_{eff} = \frac{\varepsilon \cdot D_{AB}}{\tau} \,, \tag{2.17}$$

where ε is the void fraction available for gas flow and D_{AB} the binary diffusion coefficient (Green & Perry, 2008; Ratte et al., 2009). Other factors that have to be considered are Knudson diffusion and surface diffusion.

The property that determines the magnitude of bulk flow in a porous media in the presence of a pressure gradient is the permeability K in $m^3/(m \cdot Pa \cdot s)$ (Siau, 1984). It is analogue to D and λ the proportionality constant that relates flux to the gradient:

$$K = \frac{\dot{V} \cdot l}{A \cdot \Delta P} \,, \tag{2.18}$$

where $\dot{V}$ is the volume flow in m^3/s (*ibid*). Equation (2.18) applies to liquids but can be written in differential form for gases to account for the gas expansion (*ibid*). It is further modified in the case of wood drying and pyrolysis by the introduction of the relative permeability to consider the interaction between the different phases (Di Blasi, 1998; Ratte et al., 2009). From equation (2.18) it is obvious that the flow rate is proportional to the pressure differential revealing that Darcy's law is only applicable to laminar flow (turbulent flow: $\Delta p \sim \dot{V}^2$) (Siau, 1984). Other limitations of Darcy's law are discussed in more detail by Siau (1984), where also equations are presented that adjust for non-linear flow and slip-flow/Knudsen diffusion. In summary the permeability is a measure of the interconnectedness of the pores, which in the case of softwood is created by the pit pairs described in 2.5.1 (*ibid*). Thus pit aspiration, encrusting or occlusion of the pit membranes can greatly reduce its value, which varies with grain direction (ratio of parallel to perpendicular permeability can vary between 10,000 and 40,000) due to its structural dependence (*ibid*).

Shrinkage and swelling, which are a function of the moisture content and the structure of the wood (Rowell, 2013), can affect the transport processes as well. The shrinkage and distortion of a wood cross section dried below the FSP is shown in Figure 2-16. Before looking at Figure 2-16 in detail the reader is reminded that there is no change in wood volume occurring when drying above the FSP (Rowell, 2013).

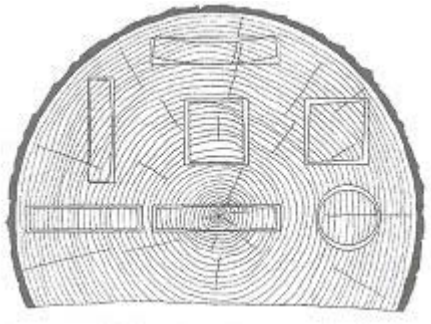

Figure 2-16. Shrinkage and distortion of wood when dried below the FSP. FSP = fibre saturation point. Adapted from Moisture properties. In R. M. Rowell (Ed.), *Handbook of wood chemistry and wood composites* (2nd ed., p. 77), by R. M. Rowell, 2013, Boca Raton, FL: CRC Press. Copyright 2013 by CRC press.

Figure 2-16, illustrating the shrinkage in wood, reveals that the varying wood cuts distort differently, which is a result of the anisotropic nature of wood (*ibid*). Rowell states that shrinkage in the longitudinal direction is usually negligible and shrinkage in the tangential direction (generally less than 10 %) is the largest, being about twice as much as in the radial direction (generally below 6 %). The low microfibril angle in the thick S2 layer (see Table 2-4) in Figure 2-8 is the reason for the reduced swelling and shrinking of wood in the longitudinal direction (0.1 to 0.3 %) (Rowell et al., 2013). The reason that wood shrinks less in radial direction than in tangential direction is partially due to the presence of ray cells (Bowyer et al., 2007), which are relatively uniformly distributed due to their formation mechanism and prevent shrinkage along the longest dimension of the cell similar to tracheid cells. Bowyer et al. (2007) states that they also present "planes of weakness" (p. 37), which is the reason why wood is often observed to split along ray cells during drying (*ibid*). The process of shrinkage is reversible, that is, dry wood can swell when water enters the cell wall (by mass flow and/ or diffusion) (Rowell, 2013). It is important to note that other factors like specific gravity, sample size and the rate of drying also affect the extent of shrinkage (*ibid*).

The example of the ray cells revealed that the anisotropic nature of wood affects mechanical properties like strength and stiffness too. Again, the thick S2 layer in Figure 2-8 is believed to have the biggest impact on these properties (Panshin and deZeeuw, 1980, as cited in Wiedenhoeft & Miller, 2005). For example the increased thickness of the S2 layer in the latewood is the reason for the two to three times increased strength and stiffness of latewood compared to earlywood (Bowyer et al., 2007). In general the strength and stiffness is largest in the longitudinal direction followed by the radial direction, which is ten to twenty times less, and is minimal in the tangential direction, which is more than twenty times less; again, these result from the

aforementioned structural differences (U.S. Department of Agriculture, 1974, as cited in Walford, 1991). The strength is an important parameter as it determines the maximum pressure that can be generated inside the wood affecting the transport processes as well as the contact between the reagents and reactants in the pyrolysis stage.

Further Bowyer et al. mention that heartwood can have a slightly higher density, darker colour, distinct odour, decay- and insect resistance. However, these properties are not of interest to this study. Contrary, more interesting is the fact that heartwood has a lower hygroscopicity, a reduced fibre saturation point and that there is no difference between the strength of heartwood and sapwood (Bowyer et al., 2007).

2.5.4 Decomposition Behaviour of Wood Components

Because the properties of wood are a function of its structure, it is to be expected that the thermal decomposition behaviour of wood is a function of the chemical structure of its constituents. To give a state of the art review on the pyrolysis behaviour of each of the wood components is beyond the scope of this research and the reader is referred to more detailed reviews in the literature such as the one by Collard and Blin (2014). Since the subject of this research is the pyrolysis of wood in its entirety, the aim here is to provide the reader an awareness of the different pyrolysis mechanisms of the biomass constituents of cellulose, hemicellulose, lignin and extractives. Interaction between these during pyrolysis has been reported negligible but their proportions do affect the product distribution (Koufopanos, Lucchesi, & Maschio, 1989; Raveendran et al., 1996; Shen, Gu, & Bridgwater, 2010; Yang et al., 2006). However, there are also studies that show an interaction. For instance, Couhert et al. (2009) demonstrated that it is impossible to predict the gas yields from biomass pyrolysis by its constituent composition, and state as explanations that (a) the components interact with each other and (b) the pyrolysis reactions are influenced by the minerals present. The findings are supported by Jensen et al. (1998) who found, in a study of straw pyrolysis, that the interaction between the biomass components is influenced by the mineral matter content. Further evidence of component interaction is given by Hosoya, Kawamoto, and Saka (2009), who discovered solid/ liquid and vapour-phase interactions between cellulose and lignin. These results agree with the earlier finding of Hosoya, Kawamoto, and Saka (2007). However, this study also showed that the interaction between cellulose and hemicellulose is insignificant (*ibid*). In the case of inorganics, the literature widely agrees that they affect the pyrolysis characteristics and product composition as demonstrated by Raveendran et al. (1996), and mentioned in 2.5.2. A more detailed review of interactions is given by Collard and Blin (2014) giving support to the approach taken in this study to research biomass pyrolysis rather than component pyrolysis.

The decomposition of lignin is reported to have the largest degradation temperature range (≈ 160 to 900 °C), and the decomposition of the holocellulose occurs in parallel to lignin with hemicellulose having the lowest temperature range (≈ 220 to 315 °C) followed by cellulose (≈ 315 to 400 °C) (Yang, Yan, Chen, Lee, & Zheng, 2007). The reason for the increased thermal stability of cellulose compared to hemicellulose is its crystalline microfibril arrangement (R. C. Brown, 2009).

Yang et al. (2007) report differences in the heat of pyrolysis with cellulose being endothermic in the main weight-loss region, whereas hemicellulose and lignin are exothermic in the range 150 to 500 °C. This effect could be related to char formation, which has been reported to be exothermic (Ball, McIntosh, & Brindley, 2004), because hemicellulose and lignin form more char than cellulose (Yang et al., 2007). Char formation occurs, as reviewed by Collard and Blin (2014), due to intra- and intermolecular rearrangement reactions leading to the formation of a thermally stable polycyclic aromatic structure. Above 500 °C the aforementioned trends seem to change with cellulose becoming exothermic and lignin and hemicellulose endothermic (Yang et al., 2007). The observed differences in char formation of the biomass constituents indicate differences in their susceptibility to secondary char formation.

One of the more interesting observations is that melting phenomena have been reported for the pyrolysis of individual and physically mixed pyrolysis constituents (Collard & Blin, 2014). For instance Sharma et al. (2004) observed the formation of liquid melt at 250 °C during fast pyrolysis of lignin, which resulted in the formation of a fused particle mass with vesicles originating from the internal gas release. Similarly Lédé, Blanchard, and Boutin (2002) report the formation of a short lifetime "intermediate liquid compound", ILC, during radiant flash pyrolysis of cellulose from which the solid, liquid and gaseous pyrolysis products were formed. They report the formation of chars at lower absorbed heat flux densities while its formation is absent at very high absorbed heat flux densities. The ILC is solid at room temperature, which distinguishes it from conventional bio-oil that is liquid at room temperature (see 2.3.2), and it is not melted cellulose as it is soluble in water (*ibid*). The presence of primary intermediate species like ILC along with phase change phenomena have been discussed controversially in the literature, as reviewed by Lédé (2012) for cellulose. He concludes: "it is well agreed that phase change phenomena occur during the reaction, producing several types of intermediate structures: from high viscosity plastic material until liquids, depending on reaction temperature" (p.29). He then argues that these phenomena are already known from the other biomass constituents (hemicellulose and lignin), as well as from wood, coal and polymeric plastics. The difference in the viscosity of the ILC at fast (low viscosity) and slow (high viscosity) heating can explain why char from cellulose loses its initial structure under high heating conditions but maintains it under slow heating (*ibid*). Thus, the knowledge of the occurrence of ILC during biomass pyrolysis is important for the manufacture of biochar as it can affect

structural properties (e.g. surface area, porosity) along with impacting the heat and mass transfer processes and chemical reactions during the pyrolysis process affecting the overall product distribution and properties as a function of the pyrolysis conditions (Collard & Blin, 2014; Lédé, 2012; Sharma et al., 2004).

To conclude, there are interactions between the pyrolysis behaviour of cellulose, hemicellulose and lignin, which affect the overall pyrolysis outcome, and warrant the research on wood itself rather than on model compounds. This discussion also shows that there is close interaction between pyrolysis chemistry and operating conditions, which is the topic of the next section.

2.6 Effect of Pyrolysis Conditions

The classification of pyrolysis into different modes in 2.4 revealed that the pyrolysis outcome is dependent on the pyrolysis conditions, which is further elaborated upon in this section. While the main focus of this research is on wood pyrolysis, single component pyrolysis has also been reviewed (see previous section), as wood is made of cellulose, hemicellulose and lignin (2.5.2). Often cellulose is regarded as representative for biomass pyrolysis as it is generally the largest fraction in the biomass. The following subsections discuss each of the earlier identified conditions that affect pyrolysis: the heating rate, the highest treatment temperature, soak time, the influence of vapour-phase pressure, atmosphere, and thermal pre-treatment.

2.6.1 Heating Rate

The heating rate has been recognised to influence pyrolysis as early as 1875 by Gruner (as cited in Lédé, 2012), who found that with increasing heating rate the volatile fraction increases while the solid fraction decreases. A difference in the physical structure of the char was reported as well (*ibid*). Klason (1914) state that the quantity and composition of the char is dependent on the presence of two types of char, that is, primary char and secondary tar-coke. Primary char is defined as char deriving directly from the wood, called $char_1$ in Figure 2-1, and secondary tar-coke as char deriving from the volatile pyrolysis products, called $char_2$ in Figure 2-1. To prevent confusion from here on, the term char is used to refer to any solid decomposition product encountered as a result of pyrolysis; however formed. Generally, the char can be divided into charcoal, coke and soot. Charcoal and soot are defined according to Evans and Milne (1987) as solid that retains the morphology of the feedstock and solid that is "formed from homogeneous nucleation of high-temperature decomposition products of hydrocarbons from the vapor phase" (p.136) respectively. Coke is defined in this study as char formed from volatiles or a liquid. This is a simplistic definition, as it is generally also related to the graphitisability of the char (Nic, Jirat, & Kosata, 2014); however, this is outside of the scope of this research and so has not been reviewed. The formation of the above mentioned secondary tar-coke is favoured under slow heating rates and explains the difference in the observed char yield from 39.44 % (wt/wt) dry ash free (daf) at slow charring velocities compared to 25.51 % (wt/wt) daf at high charring velocities in the study of Klason (1914). He further reported that with increasing tar-coke proportion the

char appears to be firmer, and that at 500 °C the difference in the determined atom ratio of carbon to available hydrogen between coke and primary char observed at 400 °C disappears. This reveals that the heating rate, by impacting the char yield and composition, affects the char properties but also that temperature has an effect on the char composition and properties, which is discussed in more detail 2.6.2. Another observation made by Klason was that with decreasing charring velocity pyrolysis becomes more exothermic, which he attributed to the decomposition of tar to coke, water, and lighter volatiles.

In their review on charcoal production, Antal and Grønli (2003) report that the effect of heating rate on the yield of char predates Klason (1914) to work by Violette in 1851, who made similar findings to Klason, that is, the charcoal yield and its carbon content increases, and the char becomes more hard, dense and heavy with decreasing heating rate. However, this does not mean that the charcoal yield can be continuously increased with a reduction in the heating rate as this will result in the asymptotic attainment of a maximum char yield (Antal, Mok, Varhegyi, & Szekely, 1990). On the opposite end of the spectrum, Antal and Grønli (2003) report the work of Lédé and co-workers (e.g. Lédé et al. (2002)), who observed no char formation from cellulose at high heat flux densities.

The structure of char is also affected by plastic deformation (Cetin, Moghtaderi, Gupta, & Wall, 2004) where, at very high heating rates (500 °C/s), the char was observed to have smoother surfaces, spherical cavities, and primarily consists of macro pores. The feedstock analysed was *pinus radiata*, *eucalyptus maculata* and sugar cane bagasse (*ibid*). These phenomena were already mentioned in the previous section (see 2.5.4).

2.6.2 Highest Treatment Temperature

The highest treatment temperature (*HTT*) is the peak temperature that is attained during pyrolysis. As described above, Klason (1914) showed that the *HTT*, impacts the distribution of pyrolysis products, char, liquid and gas. In 2.2.2 it was reported that the temperature dependence of the thermal decomposition is generally described by the Arrhenius equation (equation (2.3)). Thus, increasing *T* decreases the solid yield while the proportion of volatile products increases. This leads to a change in the elemental composition of the solid product with *HTT* as reported by Klason (1914) and

demonstrated in the more recent review by Neves et al. (2011). Therefore, it can be hypothesised that the change in the carbon content with increasing *HTT* might be an alternative means of determining a char formation rate as opposed to the traditional method of gravimetric studies as reported by W.-C. R. Chan, Kelbon, and Krieger (1985), Di Blasi and Branca (2001), Thurner and Mann (1981) and Wagenaar, Prins, and van Swaaij (1993). This hypothesis is supported by the findings of Klason (1914) who also discovered that the carbon content of the char appears to increase with heating rate (2.6.1) and pressure (2.6.4), as a consequence of enhanced secondary reactions. By tracking the change in elemental carbon content and yield for different heating rates, *HTT* and pressure, it is hypothesised that it will be possible to distinguish between primary and secondary char formation rates.

HTT also affects the chemical, mechanical, electrical, and structural properties of the char as reviewed by Antal and Grønli (2003). For instance chemical properties that change are the elemental composition as mentioned above, as well as the volatile matter content (Keiluweit, Nico, Johnson, & Kleber, 2010), the pH (Lehmann, 2007a), and the surface functional groups (Antal & Grønli, 2003). Examples for mechanical and electrical properties are mechanical strength (Downie et al., 2009) and electrical conductivity (Rhim et al., 2010). Structural properties that are altered with pyrolysis peak temperature are pore structure and surface area (Antal & Grønli, 2003; Keiluweit et al., 2010). These changes are a consequence of the structural rearrangement that occurs in the solid with increasing charring intensity (Keiluweit et al., 2010), and considerably affect biochar-soil interactions by modifying the biochar properties as reviewed in the book “Biochar for Environmental Management” (Lehmann & Joseph, 2009b).

Downie et al. (2009) state that the *HTT* is most likely the most important control parameter for the biochar structure, because the underlying fundamental processes like depolymerisation and volatilisation are temperature dependent. However, as discussed in 2.6.1 and 2.6.4 pyrolysis becomes increasingly exothermic with increasing extent of secondary reactions that ultimately can impact the controllability of the *HTT* as reviewed by Antal et al. (1990).

It is important to add that the *HTT* has also been used in the literature to define secondary reactions. For instance Khelfa, Bensakhria, and Weber (2013) define secondary reactions as reactions occurring above 400 °C, and primary reactions as reactions below 400 °C. However, this is different to the definition in Figure 2-1, where

secondary reactions are defined on the basis of the further reaction of the volatile pyrolysis products. It is believed that Khelfa et al. (2013) refer with secondary reactions to the aromatisation process that occurs in the solid product after the majority of thermal decomposition reactions (dehydration and depolymerisation) are completed, which is a separation made by Fisher et al. (2002), and was described in 2.2.2. Thus, caution must be exercised when reading literature about secondary reactions, as the definitions can differ. Other studies also report that secondary reactions of volatile primary pyrolysis products occur only above a temperature threshold. For instance in the review of F. L. Brown (1958), 280 °C is reported as temperature where secondary reactions start to occur, which can be catalysed by the formed charcoal itself (Pattanotai, Watanabe, & Okazaki, 2013) and/or its mineral matter content (L. Wang et al., 2011). Pattanotai et al. (2013) report that secondary char formation takes place between 380 to 400 °C. Due to the uncertainty in these results, it is important to establish the exact temperature range over which the secondary volatile reactions take place and form secondary tar-coke.

2.6.3 Soak Time

The soak time is the time that the charring material is held at the *HTT*. This is an important parameter as the reaction rate changes with temperature (equation (2.3)). Thus the time required for completion of the reactions varies with temperature.

2.6.4 Pressure and Vapour-phase Concentration

An excellent review on the effect of pressure on pyrolysis is given by Antal and Grønli (2003) in their review on charcoal production. The main studies mentioned in their review are discussed in the following paragraphs.

Klason (1914) discovered that vacuum impacts pyrolysis. He observed that tar yields under vacuum were greatly enhanced (43.66 % (wt/wt) daf) compared to tar yields at atmospheric pressures under slow heating conditions (1.8 % (wt/wt) daf). At the same time the char yield increased from 19.38 % (wt/wt) daf to 39.44 % (wt/wt) daf, which was associated with changes in the elemental composition of the char and tar (*ibid*), where the vacuum tar distinguishes itself from the atmospheric tar in the way that it is more translucent, has a firmer consistency, as well as higher oxygen content. Klason also discovered that the decomposition of tar with increasing pressure to char,

water and light volatiles is an exothermic process; indicating that pressure affects pyrolysis and its products in multiple ways.

The effect of elevated pressure in relation to atmospheric pressure on pyrolysis was already observed as early as 1853 by Violette. Antal and Grønli (2003) comment that his "observations are intriguing, and his experiments remain novel even today" (Antal & Grønli, 2003, p. 1628). One of his novel experiments was the pyrolysis of wood in sealed glass tubes. Some of them broke due to the high pressure caused by the evolving pyrolysis gases, but others were analysed and had a charcoal yield and carbon content of 79.1 % (wt/wt) and 77.1 % respectively (*ibid*). Antal and Grønli note that the magnitude of these values is implausibly high but the experiments are seminal.

A more subtle increase in charcoal yield with rising pressure was reported by Palmer (1914). He investigated hardwood distillation in an autoclave at 0, 60 and 120/150 psi (0, 0.4 and 0.8/1.0 MPa) pressure. The pressure was set by controlling the gas outlet (*ibid*), that is, the pressure was caused by the evolving pyrolysis gases, which is from here on referred to as autogenous pressure. The final temperature in Palmers experiments was limited to about 335 °C. He stated that with increasing pressure the point of destructive distillation occurs at higher temperatures. Palmer also discovered that the yield of charcoal from birch chips increased from 36.61 to 40.48 % (wt/wt) when pressure was raised from 0 psi (0 MPa) to 120 psi (0.8 MPa). Balancing this, the yields of tar, acetic acid and pyroligneous liquor decreased whereas the yield of gas increased. Palmer also noted that in a moderate pressure range the yield of alcohol increases slightly with elevated pressure. In fact, Palmer pointed out that above 60 psi (0.4 MPa) pressure has less effect on the product yields. Also he found that pressure has the most significant effect on tar. Palmer attempted to carry out experiments at 450 psi (3.1 MPa) but the experiments had to be stopped, because of the high intensity of the exothermic reaction, which supports the finding of Klason (1914) that pressure affects the heat of pyrolysis.

The effect of autogenous pressure was also studied by Frolich, Spalding, and Bacon (1928), who applied a maximum pressure of 300 atm (30.4 MPa) and a maximum *HTT* of 500 °C in their experiments. However, no direct comparison between the char yields at different pressures was possible, because the temperature was changed between runs. Only at a temperature of 372 °C was a comparison possible between a run at atmospheric pressure and 90 atm (9.1 MPa). In this run the organic residue increased with pressure from 42 to 44 g on a basis of 100 g of dry wood, which

equates to an increase in char yield of about 5 %, which is less than that found by Palmer (1914), mentioned above. However, Frolich et al. frequently tapped the liquid products in this run, which allowed the release of some of the gases, and could have had an impact on the formation of char. Despite this, the overall char yields of Frolich et al. were higher, 42 % (wt/wt), than those observed by Palmer, 36.6 to 38.9 % (wt/wt), at atmospheric pressure, and could be a result of the higher pressure or due to compositional differences (see 2.5). Frolich et al. also studied the effect of hydrogen pressure under gas flow rates but their data did not allow the determination of a relationship between pressure and char yield. Antal and Grønli (2003) argue that it is possible that the whole extent of pressure was unnoticed by Frolich et al. due to the application of high gas flow rates and low *HTT's*. Nevertheless, Frolich et al. suggest that pressure inhibits tar volatilisation, which thus forms char and gases.

The effect of absolute pressure on cellulose pyrolysis was studied by Mok and Antal (1983a, 1983b). In their studies the pressure was regulated by a carrier gas rather than by autogenous pressure generation. By using steam as the carrier gas Mok and Antal (1983a) discovered that the yield of char and CO_2 increased with pressure whereas the amount of CO and hydrocarbons decreased. For measuring the heat of pyrolysis Mok and Antal (1983b) applied argon as carrier gas and found that the heat of pyrolysis declines (becomes less endothermic) with increasing pressure. To demonstrate that the vapour-phase residence is a major factor Mok and Antal (1983b) varied the volumetric gas flow rates. In the case of the lowest flow rate applied, they recorded an increase in char yield from about 12 % (wt/wt) at 1 atm (0.1 MPa) to about 18.5 % (wt/wt) at 10 atm (1 MPa) pressure respectively. The yield increased even further to 22 % (wt/wt) at a pressure of 25 atm (2.5 MPa). While these increases are significantly higher than found by Palmer (1914) and Frolich et al. (1928), these values cannot be compared directly, as the effect of pressure on pure cellulose pyrolysis is expected to be different from wood due to the compositional dissimilarities. Much more radical (at the time) is the conclusion of Antal and Varhegyi (1995), who argue that the formation of char from cellulose is only a result of secondary vapour-solid interactions ranging from 0 to 40 % (wt/wt) for cellulose char. Returning to the work of Mok and Antal (1983b), when volumetric carrier gas flowrates were higher, char yield was lowered and heat of pyrolysis was raised (more endothermic). The heat of pyrolysis became even more endothermic under vacuum (*ibid*).

The intricacies of the relationship between pressure and product composition were investigated in more detail by Mok et al. (1992), who carried out experiments in sealed reactors. The autogenous pressures were changed by varying the sample loading of cellulose, and ranged from 3 to 14 MPa at 450 °C. They discovered that with increasing autogenous pressure the reaction becomes more exothermic and the yield of char increased, whereas the onset temperature of the reaction decreased. The latter point contradicts Palmer (1914) who found that destructive distillation occurs at higher temperatures when pressure is increased. A possible explanation for this is that Palmer based the destructive distillation point on the occurrence of tar formation—percent total distillate as a function of temperature—whereas Mok et al. obtained the onset temperature from the analysis of the Differential Scanning Calorimetry, DSC, curves. Thus, in Palmers data a lag is included between the collection of the tar product and the starting point of the actual reaction. Furthermore, the DSC data includes any reaction, not only tar formation reactions. As Mok et al. pointed out, the effect of pressure is evident when the yields obtained in the sealed reactors, 36 to 40 % (wt/wt), are compared to the yield of a cellulose sample, 22 % (wt/wt), that was pyrolysed in an open crucible, exposed to argon, at 1 atm (0.1 MPa) pressure. When the argon sweep gas flowrate was increased the yield of char even decreased further to 6 % (wt/wt). To see what role the vapour-phase concentration and absolute system pressure play, Mok et al. (1992) then carried out an experiment, where they added dry ice to increase the total pressure independently of the concentration of the released volatiles apart from CO_2. They found that the increased pressure, due to the addition of CO_2, at comparable mass loadings caused a decrease in the exothermic reaction heat, and the charcoal yield from cellulose was reduced by circa 10 %. However, this yield is still substantially higher than under atmospheric conditions. They concluded that the vapour-phase concentration has a stronger impact on the yield of char and the heat of reaction than the absolute pressure. Mok et al. (1992) also carried out experiments for hemicellulose and lignin, which are briefly mentioned in 2.6.5. Lastly, they further performed sealed reactor experiments for six woody and three herbaceous biomass samples. All samples produced very high charcoal yields close to theoretical yields, 40 % (wt/wt) for cellulose and 48 % (wt/wt) for *Eucalyptus gummifera* (*cf.* the proposed theoretical yields in Table 2-1).

Antal et al. (1996) tried to investigate at what pressures high yields can be obtained. They discovered that high char yields of 40.5 % (wt/wt) from Macadamia nut

shells are already achievable at 0.4 MPa in a stagnant gas environment (autogenous pressure). Their results also showed that the yield increases further with pressure to 51 % (wt/wt) at a pressure of 3.3 MPa. However, they mention that this increase is partly a result of the higher volatile matter content of their high pressure chars and would have been less if the sample was heated longer. Antal et al. further note that the pressure enhances the heat transfer in the reactor leading to a more constant product, while decreasing the heating time.

The findings of Antal et al. (1996) were confirmed by Antal et al. (2000), who discovered that near theoretical fixed carbon yields can be obtained by pyrolysis in a stagnant gas environment at elevated pressure (autogenous pressure). They also showed that their method reduced the commonly experienced pyrolysis time of oak wood in Missouri kilns from about 10,000 min (≈ 7 days) to approximately 70 min, which can provide economic incentives as discussed by Antal and Grønli (2003).

This work has so far only looked at the effect of pressure on the yield of char and not on its quality as measured by its properties as defined by the International Biochar Initiative (2014) (IBI) or European Biochar Foundation (2012) (EBF). Unfortunately, many studies did not report fixed carbon contents or other char properties due to the small amount of sample available for analysis, for example in the study of Mok et al. (1992). In the low temperature experiments of Palmer (1914) and Frolich et al. (1928) it is possible that the produced char was of inferior quality than the one produced by Mok et al. (1992). The properties of char will vary not only with degree of pyrolysis, as outlined in 2.3.1 and 2.6.2, but also expected with the mechanism by which it is formed; that is, primary or secondary char (see 2.6.1). In the work of Violette (1853, as cited in Antal & Grønli, 2003) the char formed under high pressure from wood in sealed glass tubes was reported to be “shiny and brittle and had undergone fusion similar to coking coal” (p. 1628). Mok and Antal (1983b) report the secondary char from cellulose pyrolysis as being “soft and fluffy” (p. 182), whereas they describe the primary char as resembling the feed. Mok et al. (1992) used Fourier transform infrared spectroscopy, FTIR, to analyse the formation of charcoal from cellulose in sealed and open reactors. They compared spectra obtained at different stages of carbonisation and found hardly any difference between runs in sealed and open reactors. Chemical changes they analysed were dehydration, carbonyl group formation and elimination, pyranose ring opening, decomposition of aliphatic char units and formation of aromatic char units. They cross-checked their results with literature

data on atmospheric cellulose pyrolysis and found it to be consistent. Thus, they concluded that the chars produced in sealed and open reactors are chemically identical. Mok et al. (1992) also state that their spectra were similar to the one obtained by Pakdel et al. (1989, as cited in Mok et al., 1992) for the char of *Populus deltoids* produced by vacuum pyrolysis, apart from the fact that the carbonyl content seemed to be higher. This again indicates that there is little difference chemically between primary and secondary char from cellulose pyrolysis. These findings are contrary to the physically observed difference by Mok and Antal (1983b). When comparing the appearance of char formed at atmospheric pressure to that formed at elevated pressure, either autogenously or with a regulated hydrogen environment, Frolich et al. (1928) found that the physical appearance varied only as a function of the pressure and not by the mode of pressure application.

Performing a more morphology detailed char analysis Cetin et al. (2004) discovered that chars produced at increasing pressures have bigger cavities, thinner cell walls, slightly decreased surface areas, are generally bigger, and have a perforated surface. They also report that the effect of disappearing cell wall structures with high heating rates, as discussed in 2.6.1, is enhanced at elevated pressures. Cetin et al. mention that these effects were less pronounced in bagasse compared to the soft and hardwood species indicating some compositional effects. They observed that particles pyrolysed at atmospheric pressure at high heating rates undergo the following steps: (a) swell, (b) melt, (c) form a droplet, and (d) rupture due to the evolving volatiles. In contrast, at high pressure they report that step (a) is not evident and the rupturing of step (d) is missing. This is more likely to be as the high system pressure means the gradient across the particles is reduced. This results in the formation of bubbles, which explain the larger cavities formed under pressure (Cetin et al., 2004). This reveals that pressure increases the resistance or reduces the gradient for mass transfer and so becomes a major factor in determining the physical properties of the char. This is supported by the findings of L. Wang et al. (2011) and L. Wang, Skreiberg, Grønli, Specht, and Antal (2013).

Two mechanisms have to be distinguished when it comes to the effect of pressure. There is; a), autogenous pressure, which produces long vapour-phase residence times and high concentrations of the primary volatile pyrolysis products while concurrently providing intimate contact with the pyrolysing solid; and b), absolute pressure, which produces similarly long residence times but at lower vapour pressure of

tarry compounds due to the presence of carrier gas (Antal & Grønli, 2003). Thus, both mechanisms result in increased secondary reactions (see Figure 2-1) with associated increased char yield and reaction exothermicity. Further, Antal and Grønli (2003) outline in their review that under both conditions, a) and b), char can act as a catalyst (see also 2.6.2) due to the close contact between volatiles and the charring solid, water, vapour or chemisorbed moisture, can have an autocatalytic effect (2.6.6), as well as the presence of early pyrolysis products, formic acid and acetic acid, in combination with water can change the reaction chemistry of the holocellulose to acid catalysed hydrolysis, which creates a unique high pressure pyrolysis chemistry. Autogenous pressure will produce higher yields than achieving the same absolute pressure with a carrier gas, because the tarry vapour and catalyst molecules are in closer proximity.

2.6.5 Vapour-phase Residence Time, Particle Size and Sample Loading

The results in 2.6.4 showed that increased vapour-phase residence time of the volatile pyrolysis products in the pyrolysing solid enhances secondary reactions and produces higher char yields.

This relationship was further investigated in a recent study by L. Wang et al. (2011). They used corncobs prepared in different ways and found that samples pyrolysed by conventional pyrolysis, that is proximate analysis according to ASTM E 871 and 872, resulted in fixed carbon yields of only 49 to 54 % of the theoretical value. Higher yields were obtained when corncob powders were pyrolysed in deep crucibles that prolonged the vapour-phase residence time by limiting the access of the nitrogen purge gas. These yields were further increased when the crucibles were closed with a lid that had a small pin hole. Compared to the powder, single particles with similar weights had higher yields, which are believed to be partly due to compositional differences and changed sample dimensions that affected the internal pressure profiles. In agreement with the powder experiments the yield increased with increasing sample size/ mass. The next highest yields were obtained by pyrolysing whole corncobs in closed crucibles in a muffle furnace purged with nitrogen or when pyrolysing corncob cross-sections in a micro-TGA. The highest yields of fixed carbon, 70 to 85 % of the theoretical value at 950 °C, were obtained at elevated pressure, 0.8 MPa, in a flash carbonisation reactor. These findings illustrate the close relationship between pressure, vapour phase residence time, sample mass and sample dimension.

That is, any method that increases the vapour-phase residence time of the volatile pyrolysis products inside or on the surface of the pyrolysing solid (e.g. bed of particles, large sample size or mass, low gas flow rates and high pressure) increases the fixed carbon yield by enhancing secondary reactions. Interestingly L. Wang et al. (2011) observed the highest yields at pressure even when employing an air atmosphere compared to nitrogen experiments at atmospheric pressure revealing the potential of pressure during pyrolysis. These results were confirmed for wood by L. Wang et al. (2013), who concluded that any pyrolysis condition that enhances secondary reactions, by prolonging the vapour-phase residence time, might be more important than the heating rate for the charcoal yield.

In the studies of L. Wang et al. above, pressure was found to be the main parameter for obtaining near theoretical yields, and in 2.6.4 it was proposed that the vapour-phase concentration is more important than the absolute pressure. Thus, it is expected that the char yield is also a function of the sample loading, which is the amount of sample relative to the volume of the reactor and directly impacts on the achievable autogenous pressure. Mok et al. (1992) investigated sample loading and found that the exothermic reaction heat and the yield of char increased with loading while at the same time the onset temperature of the reaction decreased and the reaction kinetics were faster. In the case of cellulose, the char yield increased from 36 to 40 % (wt/wt) with increasing mass loading, corresponding to an autogenous pressure change from 3 to 14 MPa. They observed similar trends for hemicellulose pyrolysis but for lignin no trends could be observed due to the fact that its decomposition occurs over a wide temperature range (2.5.4).

2.6.6 Moisture

Antal et al. (1996) state that “there is a long history of confusing and contradictory results concerning the influence of moisture content and steam on the pyrolysis chemistry of biomass materials” (p. 655), which they outline in their short review. Antal et al. argue that these seemingly contradictory results might be a consequence of the fact that water affects pyrolysis only in a stagnant environment at elevated pressure, that is, under autogenous pressure conditions. One of the main studies supporting this hypothesis is the work of Mok et al. (1992), where they discovered that the addition of water, 6.6 % to 27.3 %, in sealed crucibles with a cellulose loading of ≈ 67 mg/ml

improved the charcoal yield from 36 to 40 % (wt/wt) on a dry basis and decreased the pyrolysis onset temperature from above 275 °C to 250 °C. No correlation was found by them between moisture and the reaction heat. Mok et al. state that similar trends were discovered for hemicellulose but for lignin no trends could be observed due to the fact that lignin decomposition occurs over a wide temperature range, as mentioned in 2.6.5. Thus, water can act as an autocatalyst during pyrolysis (Mok et al., 1992). These findings are supported by research in the field of the geological formation of fossil fuels (Pennisi, 1993), which is discussed in more detail in 2.8.3, although some uncertainties remain (see 2.8.4). A more recent review on the effect of water is given by Antal and Grønli (2003), who come to the same conclusion that autogenous pressure is the critical parameter, but also state that the underlying mechanisms are not resolved yet.

Few studies are available on the impact of moisture on the structure of the char, except that steam pyrolysis removes labile carbon that blocks the internal pore structure (Antal & Grønli, 2003), and thus is used to produce activated carbon (Downie et al., 2009). Also Kantarelis et al. (2013) showed that steam affects the quantity and quality of all the pyrolysis products, and that it even causes reduced oxygen content, which is one of the major problems associated with bio-oil as discussed in 2.3.2, in the liquid product.

2.6.7 Atmosphere

The impact of different atmospheres (N_2, CO_2, CO, CH_4 and H_2) during fast pyrolysis on the bio-oil was investigated by H. Zhang et al. (2011). They found that the different atmospheres affect the composition and yields of the products showing that the highest yields of char were obtained in a CH_4 atmosphere and the lowest yields in CO_2. The char yields in a CO and H_2 atmosphere were similar to the char yield in N_2 supporting the earlier mentioned findings of L. Wang et al. (2011) that a reactive atmosphere not necessarily means a reduction in char yield. However, as their focus was on the liquid product no properties of the char were reported. Pyrolysis in a hydrogen atmosphere under pressure is discussed briefly in 2.8.5.

These different atmospheres are all present to some extent during autogenous pressure pyrolysis, which makes it an interesting field of research.

2.6.8 Thermal Pre-treatment

Mok and Antal (1983b) investigated the effect of thermal pre-treatment on cellulose pyrolysis. They discovered that preheating the samples is of advantage when char is the desired product. Mok and Antal state that the char yield increases along with a decrease in the heat of pyrolysis as the pre-treatment time is prolonged from 2 to 2.5 h and the temperature increased from 240 to 270 °C. They found that this effect was more pronounced at lower sweep gas flow rates, where the heat of pyrolysis even changed from endothermic to exothermic. In their study this is attributed to cellulose dehydration, which is preferred at lower temperatures and results in anhydrocellulose and subsequent competitive reactions (see reaction 3 and 4 in Figure 2-22).

In their review Antal and Grønli (2003) state that "there is no doubt that a thermal pre-treatment can augment the char yield from cellulose" (p. 1623) but also report that its effect is limited when it comes to lignocellulosic biomass (Antal et al., 1990; Varhegyi, Antal, Szekely, Till, & Jakab, 1988; Varhegyi, Antal, Szekely, Till, Jakab, et al., 1988).

The thermal pre-treatment is also referred to as torrefaction and mainly applied in the field of gasification and fast pyrolysis to improve the energy efficiency, and the syngas and liquid oil quality respectively (Chen, Peng, & Bi, 2015; Wigley, Pang, & Yip, 2014). There it is defined as mild pyrolysis, which takes place in the temperature range 230 to 300 °C (Prins, Ptasinski, & Janssen, 2006). In this temperature range primarily hemicellulose is converted and dehydration reactions occur in cellulose (Collard & Blin, 2014; Prins et al., 2006), as illustrated in the mechanism in Figure 2-22 discussed above. Wigley et al. (2014) report that with increasing torrefaction temperature the char yield increases, and that this occurs above 240 °C at the expense of the gas yield. However, this is in contradiction with the above mentioned results of Antal and his team, and needs to be investigated further.

2.6.9 Summary

Section 2.6 demonstrates that all environmental and physical properties affect the product distribution and properties of the char. The main finding is that they are caused by secondary reactions, which occur after primary pyrolysis and the extent of which are controlled by all of the above mentioned parameters. Autogenous pressure was

identified as the parameter with the highest potential to increase the extent of secondary reactions.

2.7 Proposed Pyrolysis Mechanism

A range of pyrolysis mechanisms have been developed over the years to describe the pyrolysis of lignocellulosic biomass or its constituents. It is important to point out here that the terms "mechanism" and "model" are commonly used synonymously in the pyrolysis literature when referring to the kinetic rate equation (Galwey, 2004; White et al., 2011). However, White et al. (2011) advise to preserve the traditional definition of "mechanism" to describe "the detailed sequence of physicochemical steps" (p.14). The latter definition is the subject of this section.

The aim is to give a brief overview of the proposed pyrolysis mechanism available in the literature starting with easier schemes applicable for modelling, followed by more detailed mechanisms that are too complex for modelling, and finally arriving at the "black box" description, highlighting the unresolved nature of pyrolysis, as mentioned in 2.2.2 and outlined in 2.5.4.

2.7.1 Simple Schemes Applicable for Modelling

In this section a scheme is presented for each of the most common biomass pyrolysis kinetic model classes; these are single-step global models, semi-global models, and multi-step models (White et al., 2011).

The simplest models are **one-step global models**. They describe the devolatilisation of the feedstock or its degradation into volatiles and char (Grønli, 1996), and are represented by the scheme in Figure 2-17.

Figure 2-17. One-step global scheme. Subscripts s and g are referring to the state of matter of the component, which are solid and gaseous respectively. k is the reaction rate constant. Adapted from Grønli (1996).

Grønli (1996) states its disadvantages as not being able to distinguish the volatile fraction into gases and tar unless a constant distribution is assumed *a priori*, and the yield of the volatiles and char are not a function of the operating conditions. The latter prevents extrapolation to conditions for which they have not been determined, and thus makes them unsuitable for simulating pyrolysis processes (Di Blasi, 1996a).

Intuitively, the scheme in Figure 2-17 can be extended to visualise a **multi-component model** by describing wood pyrolysis as the independent decomposition of its main constituents hemicellulose, cellulose and lignin (Grønli, 1996). This is illustrated in Figure 2-18.

Figure 2-18. Reaction scheme of a multi-component one-step model. Subscripts s and g are referring to the state of matter of the component, which are solid and gaseous respectively. k is the reaction rate constant. Subscript i stands for the component i, which for wood is primarily hemicellulose, cellulose and lignin. Adapted from Grønli (1996).

The disadvantages of the one-step global model remain valid for the multi-component model, except that this time more coefficients have to be determined *a priori* (Grønli, 1996). Also it is assumed that the components decompose independently, which does not reflect the reality, as there are for instance interactions with the ash fraction (see 2.5.2 and 2.5.4).

The next class of models are **semi-global models**, which assume that the products of pyrolysis can be lumped into gas, tar and char (White et al., 2011). The most common semi-global reaction model is based on the scheme of Shafizadeh and Chin (1977) depicted in Figure 2-19.

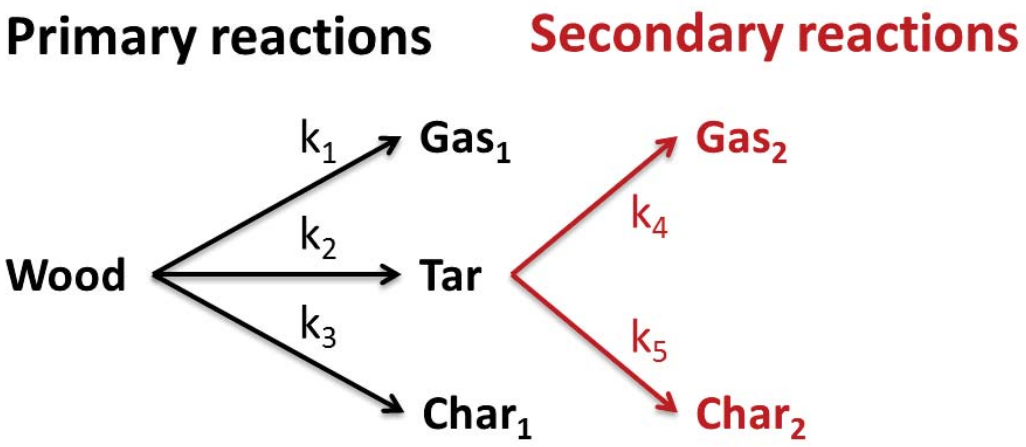

Figure 2-19. Commonly applied pyrolysis mechanism based on Shafizadeh and Chin (1977) and modified by Thurner and Mann (1981) and Di Blasi (1996a). Char is an unspecific term referring to charcoal, coke or soot. The subscript on the pyrolysis products refers to primary (1) and secondary (2) reactions respectively. The primary reactions, depicted in black, are representative of a one-stage semi-global model, and the primary and secondary reactions combined represent a two-stage-semi-global model. k_1 to k_5 are reaction rates.

In Figure 2-19 the primary reactions, illustrated in black, represent a one-stage semi-global model, and the primary and secondary reactions combined form a two-stage semi-global model respectively. Both the one-stage semi-global model and the two-stage semi-global model have been applied in the literature for modelling pyrolysis successfully (for instance Ratte et al. (2009) and Fantozzi et al. (2007) respectively). The advantage of semi-global models is that they can be coupled with transport phenomena (Di Blasi, 1996a; Ratte et al., 2009; White et al., 2011). The most preferred is the two-stage semi-global model as it is able to account for the important effect of vapour-phase residence time (see 2.6). The disadvantage of the semi-global models is that the kinetic data cannot be extrapolated to other conditions outside their experimental ranges (Nunn, Howard, Longwell, & Peters, 1985; White et al., 2011). Similarly to the one-step global model, the semi-global model can be turned into a multi-component model, in particular the one-stage semi-global model.

The third major category form **multiple-step models**, which aim is to accurately model pyrolysis under varying process conditions (White et al., 2011). A simple multi-step model is represented by the scheme of Bradbury, Sakai, and Shafizadeh (1979) for cellulose (also known as the Broido-Shafizadeh model (A. L. Brown, Dayton, & Daily, 2001)), which has been extended to include tar cracking in Figure 2-20 (Di Blasi, 2008).

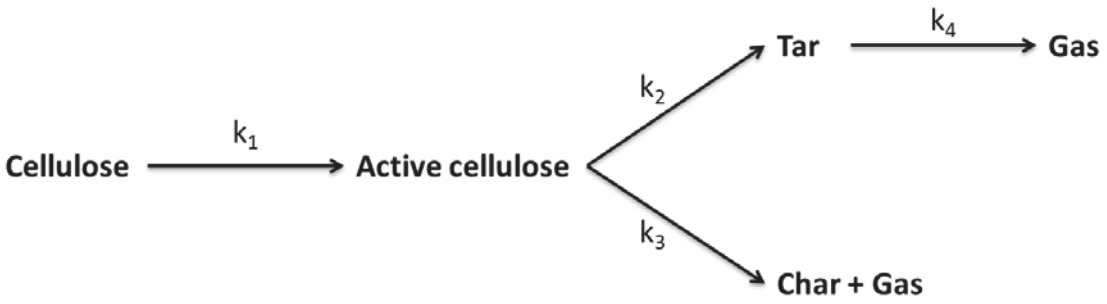

Figure 2-20. Reaction scheme proposed by Bradbury et al. (1979) for cellulose with added tar cracking step by Di Blasi (2008). k is the reaction rate constant. Adapted from Di Blasi (2008).

A more detailed model was proposed by Diebold (1994), which is illustrated in Figure 2-21.

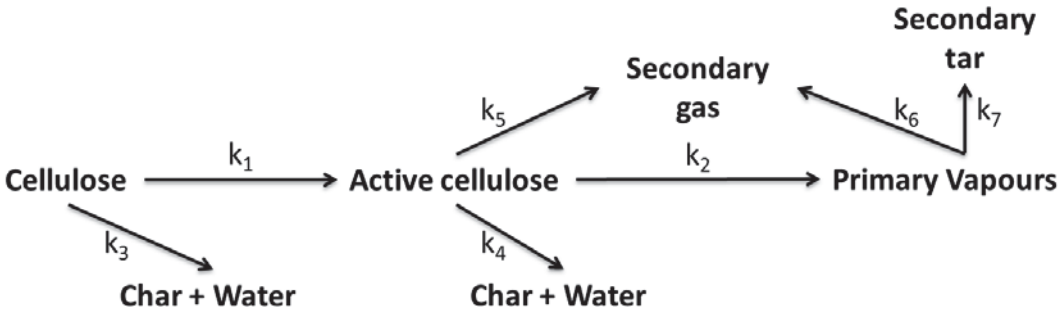

Figure 2-21. Seven-step global reaction scheme proposed by Diebold (1994) for cellulose. k is the reaction rate constant. Adapted from Di Blasi (2008).

The presence of active cellulose is discussed controversially in the literature (Antal & Varhegyi, 1995; A. L. Brown et al., 2001; Lédé, 2012; Varhegyi, Jakab, & Antal, 1994). Nevertheless, the model illustrated in Figure 2-21 is able to accurately predict slow and fast pyrolysis processes (A. L. Brown et al., 2001; Diebold, 1994; White et al., 2011). However, White et al. (2011) state that except for a few simple cases the use of these models remains limited because of the large number of reactions that need to be considered, the incomplete identification of the pyrolysis tar and its intermediate species, as well as the interdependency of serial reactions. In particular, the latter point can lead to model inaccuracies by magnifying small errors in the early part of the serial reaction system (A. L. Brown et al., 2001).

It is important to note that there are other models available like biomass deactivation models and distributed activation energy models. However, since this section is focused on the mechanism and not modelling they are only mentioned here,

and for more detail the reader is referred to the reviews of Di Blasi (2008) and White et al. (2011).

2.7.2 Complex Multistep Pyrolysis Mechanism

A classic complex multistep pyrolysis mechanism is the one proposed by Mok and Antal (1983b) for cellulose, Figure 2-22.

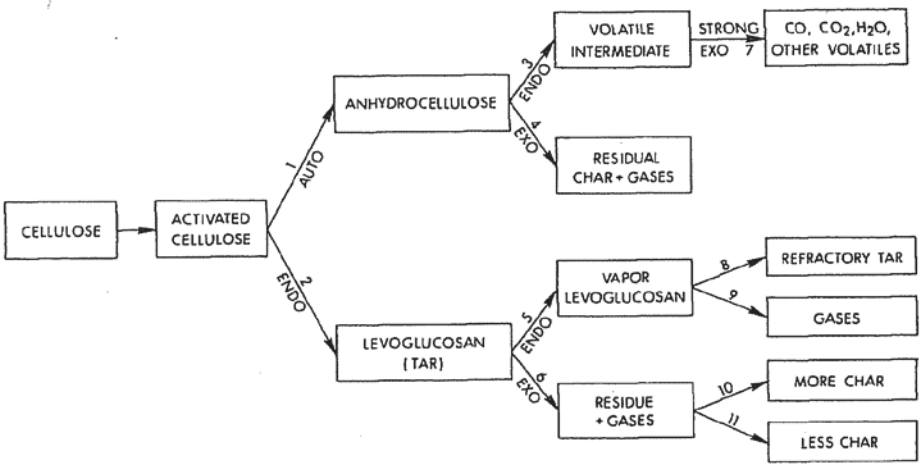

Figure 2-22. Cellulose pyrolysis mechanism proposed by Mok and Antal (1983b). The numbers above the arrows denote the respective reaction step, and "ENDO" and "EXO" designate the endothermic or exothermic nature of the reaction step respectively. Taken from Mok and Antal (1983b).

The scheme in Figure 2-22 was developed by Mok and Antal to particularly take into account the effects of sweep gas flow rate and pressure on the pyrolysis of cellulose. It also considers the reaction heat effects as discussed earlier in 2.6.

Figure 2-22, similarly to Figure 2-20 and Figure 2-21, includes active cellulose as an intermediate product, which subsequently can produce either anhydrocellulose or levoglucosan. The dehydration path, 1, to form anhydrocellulose is preferred at lower temperatures (*ibid*). Mok and Antal call the char produced from anhydrocellulose by reaction 4 primary char, which resembles the feed and is the main char formed. In contrast, char formed by reaction 6, is "soft and fluffy" (Mok & Antal, 1983b, p. 182) and results either from liquid or gaseous volatiles, which they call secondary char (Mok & Antal, 1983b). Mok and Antal explain that high pressure and a low flow rate of sweep gas limits mass transfer and thus inhibits the evaporation of levoglucosan, reaction 5, leading to more secondary char (reaction 6). This is in accordance with the suggestion made by Frolich et al. (1928), that pressure prevents volatilisation. High

pressure and low sweep gas flow favours reaction 4 over 3 (Mok & Antal, 1983b) and results in a decrease in the heat of pyrolysis, i.e., increased exothermicity (see also 2.6), which is due to the suppression of the endothermic reactions 3 and 5 (Mok & Antal, 1983b). However, at low flow rates reaction 7 is actually enhanced making the combination of reaction 3 and 7 more exothermic than reaction 4, as stated by Mok and Antal. Thus, one would anticipate an increase in the overall heat of pyrolysis (increasing endothermicity) due to the absence of the strong exothermic reaction 7 at low flow rates but Mok and Antal argue that the major effect comes from the enhanced role of reaction 6 over 5, and that the contribution of low flow on the exothermicity by reaction 7 with increasing pressure reduces due to the decreased production of volatiles with pressure (reaction 3). Applying the same reasoning, the high heat of pyrolysis (endothermicity) detected during vacuum experiments (see 2.6.4) is attributed to the enhanced evaporation of levoglucosan (reaction 5) and the increased production of intermediate volatiles (reaction 3). In this case reaction 7 plays no role due to the low concentration of the gas molecules and their short residence time (*ibid*). Mok and Antal state that the effect of pressure and flow rate (see 2.6) is only due to vapour reactions and not due to reactions in the solid phase (reactions 1 and 2). Mok and Antal (1983b) also mention that high heating rates favour the decomposition path that leads to the formation of levoglucosan (reactions 2 and 5), which explains why higher char yields are observed at lower heating rates (see Table 2-2).

Despite being able to explain the complete effect of pressure and sweep gas rate on the reaction pathway, this mechanism contains the controversial active cellulose step, mentioned in 2.7.1, and the presented scheme is not suitable as a kinetic model due to its complexity (Antal & Grønli, 2003). Pyrolysis of wood is even more complex, because of the presence of the other biomass constituents, leading to more uncertainties and more mechanism “including radical and/or ionic reactions” (Lédé, 2012, p. 28), adding to the complexity.

2.7.3 Empirical Approach

Considering the complexity of pyrolysis with the associated large number of uncertainties, it almost feels natural to treat pyrolysis as a "black box", Figure 2-23.

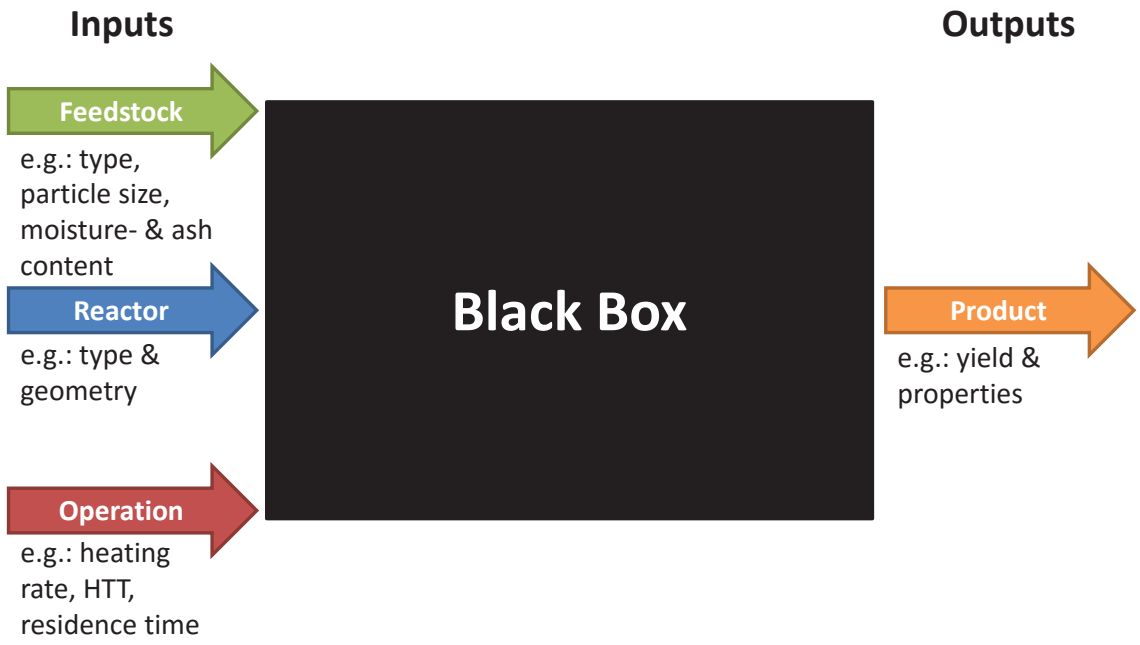

Figure 2-23. "Black box" approach. HTT = highest treatment temperature. Adapted from Jones (2011).

In Figure 2-23 the pyrolysis mechanism is treated as unknown, that is as a "black box", and thus outputs are merely observed as a function of inputs. That these outputs can be described by empirical relationships was demonstrated by Neves et al. (2011), who, in a comprehensive survey of the literature, were able to predict the yield of tar simply as a function of input parameters (feedstock elemental composition, dry-ash free char yield, and the reactor temperature).

2.7.4 Summary and Conclusion

The array of approaches to describe pyrolysis reiterate the earlier mentioned fact that pyrolysis is not yet understood. They show that the process of pyrolysis can be described by varying degrees of complexity, where the most appropriate should relate to its end-use (Jones, 2011). With respect to the manufacture of biochar it is important to predict the yield of char and its properties, which are dependent on the reaction pathway or more generally speaking on the extent of secondary reactions. Such predictions are, to the best knowledge of the author, currently not possible, and require detailed product characterisation studies as a function of variable extents of secondary reactions.

2.8 Pyrolysis Processes Involving or Closely Related to Autogenous Pressure Pyrolysis

In 2.6 it was found that the main parameters for increasing secondary reactions and in particular secondary char formation are increased vapour-phase residence time and –concentration, which are best attained under autogenous pressure. Therefore, in this section is a selection of pyrolysis processes involving or closely related to autogenous pressure pyrolysis reviewed.

2.8.1 Improved Batch Reactor for Charcoal Production

US Patent No. 5,551,958 (1996) from Antal describes a batch pyrolysis process that provides: (a) increased batch turnaround time (≤ 2 h), (b) improved charcoal yields (35 to 50 % (wt/wt)), (c) reduced char volatile matter content (< 25 %), and (d) a char heat value of about 13,000 BTU/lb (30,238 kJ/kg) compared to a conventional atmospheric process that (a) comprises an 8 day batch cycle, (b) a char yield of typically 25 % (wt/wt) rarely exceeding 35 % (wt/wt), and (c) a char volatile matter content equal or smaller than 35 % (wt/wt). This patent pyrolyses the material in an enclosed container at *HTT's* ≥ 350 °C and ≤ 550 °C in the pressure range 15 to 150 psig (1 to 10 bar). It is specifically stated that this can be achieved with feedstock's having high moisture contents (15 to 50 % (wt/wt)). Overall, this patented reactor is based on the principle of autogenous pressure pyrolysis and the fact that water can act as an autocatalytic agent as discussed in 2.6.

2.8.2 Deoxy-liquefaction

Deoxy-liquefaction is according to Lu, Guo, Zhang, and Wang (2013) "a similar miniature of the underground evolution from biomass to petroleum and coals during hundred thousands of years" (p. 2157). With the aim of optimum oil production, it involves heating a feedstock in a closed vessel (sample loading 0.51 to 0.64 g/ml) in the presence of 15 to 20 % water as medium at relatively slow heating rates, 10 to 80 K/min, to a *HTT* of 350 to 420 °C with a subsequent soak time of 15 min up to several hours resulting in autogenous pressures of 60 to130 bar (Lu et al., 2013; C. Wang, Du, Pan, Li, & Yang, 2007). The resulting oil, obtained by subsequent distillation of the residue, has a fairly low yield, 10 to 17 % (wt/wt), but is characterised by a high heating value (≥ 40 MJ/kg) and consisting mainly of benzenes, phenols and

long chain alkanes, which distinguishes it from conventional fast pyrolysis oils and hydrothermal liquefaction (Lu et al., 2013; C. Wang et al., 2007). Since the main focus of the deoxy-liquefaction is the manufacture of liquid oil, only limited information is available on the produced char. The char has been reported to have a H/C and O/C ratio similar to coal, and typical char yields are above 30 % (wt/wt) containing about 50 % (wt/wt) of the feedstock carbon (Lu et al., 2013). Intriguingly the combined effect of primary and secondary reactions, which are enhanced under autogenous pressure, lead to oxygen removal both in the solid and liquid phase. Thus, the question arises: Can high-value solid and liquid products be co-produced?

Before discussing other technical processes, it is useful to understand the natural process of fossil fuel formation. Let us assume the proven reserves of fossil fuels as gas, liquid and solid are proportional to what is theoretically possible. The proportions of oil, coal and natural gas from the proven reserves (BP, 2014) have been calculated as 18.7, 69.9, and 11.4 % (wt/wt) respectively. Interestingly, Antal et al. (1996) estimated the theoretical yield for charcoal from most biomass feeds in the range 55 to 71 % (wt/wt). The former one was for corn cobs (45 % carbon content) and the latter one for Macadamia nut shells (58 % carbon content) (Antal et al., 1996). However, those numbers are not directly comparable, as the composition/ quality of the product classes differ (e.g. natural gas vs. pyrolysis gas), and it is important to note that petroleum derives mainly from type I (algal) and II (liptinitic) kerogen while coal derives primarily from type III (humic) kerogen (Schobert, 2013), which reflects the earlier mentioned impact feedstock has on pyrolysis. Nevertheless, it shows that the formation of petroleum (a high quality liquid product) is associated with the formation of a much larger proportion of coal from type III kerogen, which in turn agrees with the deoxy-liquefaction results. This nurtures the idea of co-producing a liquid and solid product from biomass, which will be kept in mind during this research. It is important to add here that it might be possible to change the yield distribution by adding catalyst (Borgund & Barth, 1999; Lu et al., 2013; Wu, Guo, Wang, & Yang, 2008), which was suggested in 2.5.2 but which requires further research.

2.8.3 Hydrous Pyrolysis

Hydrous pyrolysis, applied in the field of organic geochemistry, is used to simulate petroleum generation from an organic-rich source rock (prehydrocarbon generation stage of diagenesis (Lewan, Winters, & McDonald, 1979)). It involves heating the feedstock with liquid water to subcritical water temperatures in a closed pressure vessel (void volume often filled with helium), for a period of a few days resulting in a product close to natural crude oil that is present as liquid layer on the water and sorbed film on the solid residue (Barth, 1999; Barth, Borgund, & Hopland, 1989; Lewan, 1983; Lewan et al., 1985; Lewan et al., 1979; Pennisi, 1993; Winters, Williams, & Lewan, 1983). According to its definition the critical parameter is the presence of liquid water excluding supercritical water or water vapour (Lewan, 1993a, as cited in Lewan, 1997). The higher temperatures used in the hydrous pyrolysis experiments (300 to < 374 °C) compared to the natural system offset the longer time period required during geological formation (Arrhenius relationship equation (2.3)) without affecting much the oil-quality (Lewan, 1983; Lewan et al., 1979; Winters et al., 1983).

Apart from being used to estimate the petroleum potential of oil source rocks (Funke & Ziegler, 2010; Lewan et al., 1985; Lewan et al., 1979) it has also been used to study the coalification of solid organic residue (Behar, Lewan, Lorant, & Vandenbroucke, 2003; Funke & Ziegler, 2010; Mansuy & Landais, 1995; Monthioux, Landais, & Monin, 1985), but this is discussed in more detail in 2.8.6 under hydrothermal carbonisation, HTC.

The beneficial effects of using high-temperature pressurised liquid water have been reviewed by Sealock, Elliott, Baker, and Butner (1993). They conclude that "because of its reactivity and special chemical and physical properties, high-temperature pressurised liquid water is an excellent reaction medium for conducting synthesis and conversion of organic compounds" (p.1540), and thus has significant potential for future developments. Barth (1999) proposes that the knowledge gained during geochemical applications of pyrolysis could aid in converting biomass into petroleum-like liquid fuel. In her study, she applied hydrous pyrolysis to marine macro-algae biomass and compared it with hydrous pyrolysis of Kimmeridge clay (immature oil source rock) and brown coal. She concluded that there is a considerable potential for converting biomasses into petroleum compatible fuels despite the limitation of lower carbon and higher oxygen content in the biomass. The high oxygen content leads to carbon loss by the formation of low molecular weight substances like CO_2 and carboxylic acid (Barth,

1999), but also to the loss of hydrogen by the formation H_2O (Lu et al., 2013). Lu et al. (2013) suggest that higher liquid yields could be obtained by choosing the right catalyst to avoid the formation of H_2O and promote the combination of C and H. Another option, suggested by Barth (1999), would be a pre-treatment step similar to diagenesis.

The production of a petroleum-like liquid fuel appears to be the outstanding characteristic of hydrous pyrolysis and deoxy-liquefaction compared to the commonly used fast or flash pyrolysis (fast heating rates, moderate temperatures, and short vapour-phase residence time (Bridgwater et al., 1999)). Fast pyrolysis leads to the formation of a high yield liquid product, up to 80 % (wt/wt) including water (usually no separate phase, i.e. miscible (Bridgwater, 2003; Peterson et al., 2008)) on a dry feed basis (Bridgwater et al., 1999). It has a high oxygen content and is incompatible with petroleum products (Barth, 1999). The high oxygen content (typically 35 to 40 % (wt/wt) (Czernik & Bridgwater, 2004)) gives the bio-oil undesirable properties like low heating value, immiscibility with hydrocarbon fuels, and instability (Czernik & Bridgwater, 2004; Kantarelis, Yang, and Blasiak, 2013 as cited in Kantarelis et al., 2013). Thus, the efficient removal of oxygen from the fast pyrolysis bio-oils has been regarded as the main challenge for their processing in petroleum refineries by Kantarelis et al. (2013). In particular, phenol with its low reactivity and high stability makes it the key limiting substance for deoxygenation of pyrolysis oil (Bu et al., 2012; Collard & Blin, 2014). Interestingly, it appears that oxygen (even from phenol) is removed under autogenous pressure pyrolysis (Lu et al., 2013) without the addition of extra catalyst. Oxygen removal by catalyst addition is necessary for the two most common bio-oil upgrading processes: (a) hydrotreating, and (b) catalytic vapour cracking (Bu et al., 2012; Czernik & Bridgwater, 2004). However, the oxygen removal during autogenous pressure pyrolysis needs further investigation, in particular by analysing the high molecular weight fraction of the liquid product.

2.8.4 Confined Medium Pyrolysis without the Addition of Water

The simulation of the natural maturation process (fossil fuel formation) discussed in the previous section is also possible in a confined system without the addition of water. Behar, Kressmann, Rudkiewicz, and Vandenbroucke (1992), Michels, Landais, Torkelson, and Philp (1995) and Monthioux et al. (1985) achieved this by using gold tubes. In particular Monthioux et al. (1985) studied the artificial maturation of oxygen-

rich type III (humic) kerogen by confined-medium pyrolysis (without free volume, and in the absence of a diluting inert gas) to *HTT's* in the range of 250 to 550 °C (heating rate of 25 °C/min and soak time of 24 hr) by comparing the elemental changes occurring in the feedstock to those in a homologous natural coal series. A hydrostatic pressure range of 0.5 (minimum pressure required to prevent bursting of the sealed gold tube due to gas formation) to 4 kb was applied. They found that the artificial maturation for the solid residue agrees with the natural path in the van Krevelen diagram. Also, the petroleum potential, quantities, and timing of hydrocarbon and non-hydrocarbon product formation were qualitatively similar to natural maturation. Monthioux et al. also compared their results with open-medium pyrolysis and closed-medium pyrolysis in sealed glass ampoules from the literature. The results differed significantly, but that the sealed-medium experiments gave a better simulation, which was very close to the confined medium pyrolysis (natural maturation), if the glass capsules were initially evacuated. Monthioux et al. attribute this to the fact that in the evacuated capsules the pressure is caused solely by the pyrolysis products and their concentration is not diluted by an inert gas (e.g. N_2). Thus, the critical factor is a high partial pressure (concentration) of the pyrolysis products, which explains the poor results of the open-medium pyrolysis, and agrees with the findings of Mok et al. (1992) discussed in 2.6. They further report that the differences observed with degree of confinement (partial pressure of pyrolysis products) are related to the loss mechanism of hydrogen and oxygen (Monin et al., 1980, Tissot and Vandenbroucke, 1983, as cited in Monthioux et al., 1985). That is, at low partial pressures oxygen is lost by dehydration reactions, which leads to an early loss of hydrogen whereas at higher partial pressures oxygen loss occurs by the formation of CO_2 with hydrogen loss being delayed to higher temperatures (Monthioux et al., 1985). This agrees with the findings of the deoxy-liquefaction studies mentioned in 2.8.2. Monthioux et al. explain that the presence of water is not required in their confined-medium pyrolysis experiments as the released hydrocarbons, which remain in close contact with the pyrolysing solid, provide the same pressure inducing effect as water does in hydrous pyrolysis. Importantly, the released hydrocarbons act as a hydrogen donor by quenching the free radicals (Durand et al., 1977, as cited in Monthioux et al., 1985). This results in an increased yield of the extractable hydrocarbons (e.g. Lewan et al. (1979)), and a reduced olefin content (by hydrogenation) in the extract (e.g. Lewan et al. (1979)). The role of the produced

hydrocarbons as a solvating fluid that promotes hydrogen transfer has also been shown by Mansuy, Landais, and Ruau (1995).

In summary, the local availability of donatable hydrogen, with its free radical quenching ability, plays a decisive role during the course of pyrolysis, and can for example explain the differences observed in organic residue maturation between open and confined medium pyrolysis.

2.8.5 Hydropyrolysis

Having established the important role of hydrogen in 2.8.4 it comes as no surprise that hydropyrolysis (pyrolysis under hydrogen pressures up to 15 MPa, not autogenous) has also been applied to produce bio-oils with reduced oxygen contents compared to conventional fast pyrolysis (Dilcio Rocha et al., 1999; Rocha, Brown, Love, & Snape, 1997). However, due to the need for hydrogen, which for a sustainable process has to be acquired from a renewable source (expensive), and a two stage reactor with catalyst for subsequent hydrotreating (Dilcio Rocha et al., 1999) to obtain fuels that have comparable oxygen contents to deoxy-liquefaction, this process is not further investigated.

2.8.6 Hydrothermal Processes

The hydrothermal processes of hydrothermal liquefaction and hydrothermal gasification are essentially hydrous pyrolysis at elevated temperature and pressure (Libra et al., 2011). They are discussed below.

Hydrothermal liquefaction typically takes place at temperatures ranging from 300 to 350 °C, and at pressures of 150 to 200 bar (Kruse, Funke, & Titirici, 2013). Although Peterson et al. (2008) widens the range from 280 to 380 °C and 70 to 300 bar. Common to all processes is the presence of liquid water and a catalyst to improve liquid hydrocarbon formation (Kruse et al., 2013; Libra et al., 2011; Peterson et al., 2008). Reducing gases, such as CO and H_2, can also be applied, and the residence times can range from 10 to 60 min (Peterson et al., 2008). As the name suggests, the product of interest is the liquid. Its yield and composition along with that of the char and the gas depend on the operating conditions of temperature, particle size, feedstock, heating rate, solvent density, solvent properties, pressure, residence time, and presence of a reducing gas/ hydrogen donors, as reviewed by Akhtar and Amin (2011). The liquid product

consists of the same two phases as reported for hydrous pyrolysis, a biocrude and an aqueous solution containing dissolved organics (where research is aimed at favouring biocrude formation) (Kruse et al., 2013). The viscous biocrude is generally characterised by a heating value of 30 to 36 MJ/kg, and an oxygen content of 10 to 20 % (wt/wt) (Peterson et al., 2008), which makes it better than fast pyrolysis bio-oil but inferior to the above discussed bio-petroleum from deoxy-liquefaction. The biocrude yield is typically between that for oils of deoxy-liquefaction and fast pyrolysis. Thus, as a rule of thumb, increases in oil quality come at the expense of yield. In order to co-process the hydrothermal biocrude with conventional fossil fuel petroleum the oxygen content needs to be reduced further (oxygen content $\leq 1\%$ (Aitani, 2004, as cited in Peterson et al., 2008)) by applying similar processes as used for fast pyrolysis, but generally they are slightly more straight forward for biocrude. There is a large amount of research on liquefaction with organic solvents (Akhtar & Amin, 2011; Behrendt, Neubauer, Oevermann, Wilmes, & Zobel, 2008; Libra et al., 2011). However, Behrendt et al. (2008) point out that it is currently not economic due to the required removal of oxygen, but that a two-step approach with the addition of hydrogen and catalyst at pressure may be technically feasible for the production of liquid transportation fuels. Information about the char product is generally limited, as it has not been the motivation of researchers working on hydrothermal liquefaction.

When the focus is shifted from the liquid to the gaseous product, primarily methane or hydrogen, the process is called **hydrothermal gasification** (Kruse et al., 2013). There are three types (a) aqueous phase reforming, (b) near-critical catalytic gasification, and (c) supercritical water gasification, which are reviewed by Kruse et al. (2013). Only the latter two are directly applicable to biomass (*ibid*), but are not at primary interest to this study because of the low char and liquid yield.

With the recent renewed interest in the char product, hydrous pyrolysis/ hydrothermal liquefaction has gained new momentum. It is also variously called **hydrothermal carbonisation (HTC)** or **wet pyrolysis** (Funke & Ziegler, 2010; Libra et al., 2011). While this process has been in use for over a century, it has received less attention due to the traditionally higher interest in the manufacture of liquid fuels. Funke and Ziegler (2010) attribute this to the fact that "coal as an energy carrier is inferior to liquid or gaseous fuels" (p. 161). This sentiment has changed since the discovery of biochar and the development of functionalised carbonaceous materials

(Funke & Ziegler, 2010; Hu, Yu, Wang, Liu, & Xu, 2008; Libra et al., 2011). The char produced from HTC is generally termed hydrochar to distinguish it from biochar.

Funke and Ziegler (2010) state that there is not an exact definition of HTC, and instead outline an operational envelope in their review. It appears that the main difference to hydrous pyrolysis (2.8.3) is the focus on the solid product, and lower treatment temperatures, 180 to 250 °C (*ibid*). In their review on wet and dry pyrolysis, Libra et al. (2011) report that one of the main benefits of HTC over dry pyrolysis is the ability to convert wet feedstock without drying into a high yield char termed hydrochar. They report that wet pyrolysis can operate on "water contents" above 75 to 90 %, but is not likely to have economic advantages over dry pyrolysis at water contents below 40 %. For comparison they estimated the maximum water content for economic operation of dry pyrolysis to be between 50 to 70 %. Libra et al. found that generally theoretical char yields are not obtained during HTC either, but that their yields are typically higher compared to dry pyrolysis. Most intriguing was their observation that hydrochar yield seemed to approach its theoretical yield with increasing residence time, which they attributed to the further reaction of the intermediates to char. This is very similar to dry pyrolysis and indicates parallels between the secondary reactions of both processes and supports the findings of Monthioux et al. (1985) discussed in 2.8.4. However, more research is required as Libra et al. state that there are large variations in the char yields reported. It is possible that the concentration of solids could play a role too. In general, caution has to be exercised when comparing yields, because high yields of poor quality char can be obtained at low temperature, as was discussed earlier in 2.3.1. A more meaningful parameter for comparison, in particular for carbon sequestration, is the carbon conversion efficiency (Libra et al., 2011). For hydrochar they report this to be in the range of 60 to 84 % compared to commonly 50 % in dry pyrolysis (Lehmann, 2007b) but even with this much greater conversion efficiency, the efficiency of the char (e.g. for application in soil) depends on its properties. Unfortunately, there are few studies on this aspect. Libra et al. (2011) compare wet and dry pyrolysis char in their review, focusing on material properties and possible applications. They observed clear differences between both types of char but note that "better quantification, reporting and standardization of char characteristics and production conditions are required in order to understand the wide variability found in experimental investigations" (p.116). This especially is true for biochar. With respect to the application of hydrochar as biochar they found that it may have soil ameliorating

properties (large number of hydroxyl groups) but has reduced stability and internal surface area compared to dry pyrolysis biochar. Thus, it is likely to have varying effects in soil than dry pyrolysis biochar but, due to the limited research available, no final conclusion can be drawn about its behaviour in soil (Libra et al., 2011). The differences in the composition and properties of hydrochar compared to dry pyrolysis char originate from the varying underlying reactions, which have been reviewed by Libra et al. The relevant points are highlighted here, and for more detail the reader is referred to Libra et al. page 94 to 96 and the original sources within their review:

- the initial step in HTC is hydrolysis due to its low activation energy resulting in reduced decomposition temperatures of the biomass constituents;
- hydrochar is more similar to natural coal than dry pyrolysis char, i.e. chemical bonds and elemental composition (higher H/C ratio), implying a higher decarboxylation to dehydration ratio for HTC;
- aromatic structures in hydrochar are arranged differently compared to dry pyrolysis char, to mention are characteristic carbon spheres that have been observed for the case of HTC of glucose, which are believed to have an aromatic core made up of cross-linked aromatic furans having aldehydic and carboxy functional end groups;
- subcritical hot water favours ionic reactions over radical reactions;
- hydrolysis can cause complete disintegration of the physical feedstock structure; and
- liquid HTC media contains nearly all produced fragments and, due to their low mobility in this phase, a confined environment is created which enables and favours re-condensation reactions leading to the formation of a large proportion of coke.

Kruse et al. (2013), who reviewed the reactions forming hydrochar, concluded that hydrochar is essentially made up of different fractions encompassing the above mentioned coke as well as the “traditional” char (referred to in this study as primary char or charcoal) from solid state reactions. However, the exact mechanism of hydrochar formation is not yet resolved, that is, the proportion of spherical particles (coke) to primary char (Funke, Reebs, & Kruse, 2013). It is believed that dry pyrolysis

with significant secondary char forming reactions produces a char similar to hydrochar due to the increased fraction of coke. This is particular true when pyrolysis is carried out under autogenous pressure; as evaporation is inhibited, more char (i.e. coke) is formed from the liquid phase, as discussed in 2.6. It is important to note here that water is a product of pyrolysis (Figure 2-1), and thus hydrolysis reactions can also occur during dry pyrolysis under autogenous pressure conditions.

2.8.7 Summary

The review above demonstrates that autogenous pressure creates a unique pyrolysis chemistry that produces high yield char and good quality bio-oil with a reduced oxygen content. Water can have an important role in this process, but it is not completely understood yet (Pennisi, 1993). The reviewed processes are depicted in Figure 2-24 superimposed on the phase diagram of water.

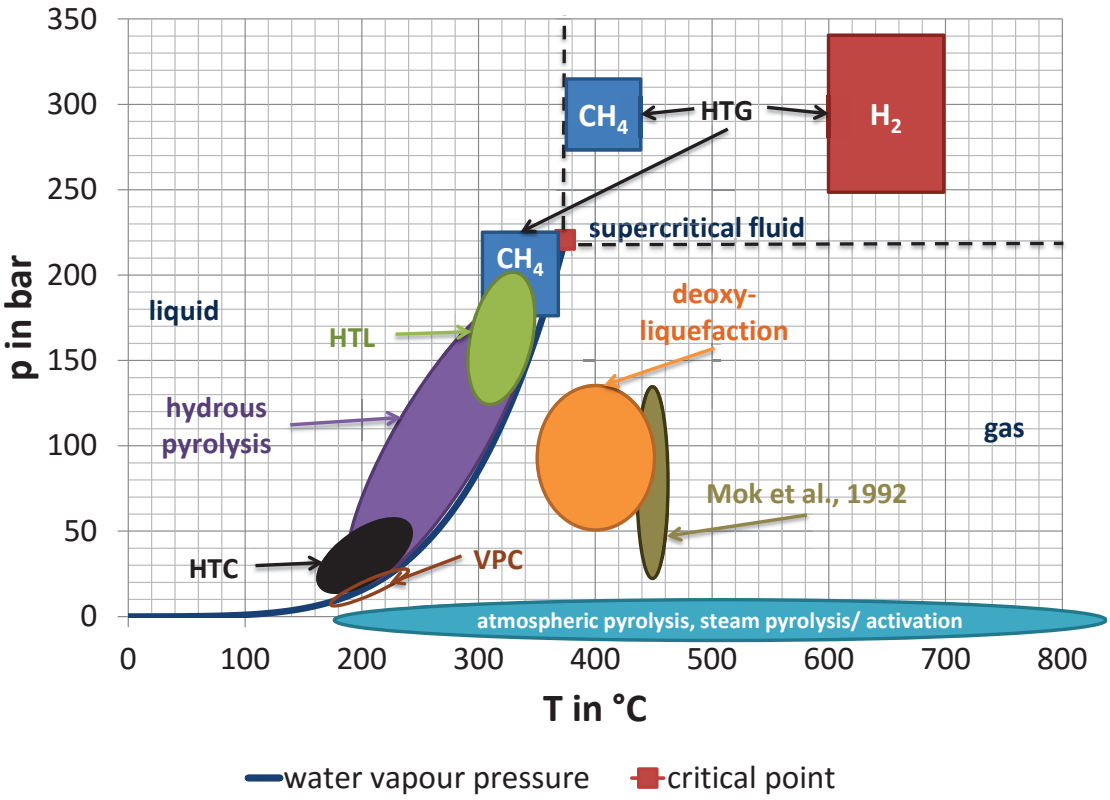

Figure 2-24. Phase diagram of water including the operating ranges of the different pyrolysis processes containing water as reviewed in 2.8. The vapour pressure curve has been calculated according to the Wagner equation as given by Poling, Prausnitz, and O'Connell (2001). HTC = Hydrothermal carbonisation; HTG = Hydrothermal gasification; HTL = Hydrothermal liquefaction; Mok et al., 1992 = Mok, Antal, Szabo, Varhegyi, and Zelei (1992); p = pressure; T = temperature; VTC = Vapothermal carbonisation. Adapted from Kruse, Funke, and Titirici (2013).

Also included are steam pyrolysis, vapothermal carbonisation (VTC) and the operating regime of the experiments of Mok et al. (1992), which were discussed in 2.6. Steam pyrolysis is added as it has been shown to affect the product yields and composition of the solid, liquid and gaseous products as well (Kantarelis et al., 2013). Steam reduces the oxygen content in the liquid product due to favoured decarbonylation and decarboxylation reactions (*ibid*). It is also commonly applied to produce activated carbon (Downie et al., 2009). The important role of water in the gas phase is further illustrated by the operational envelope of the experiments of Mok et al. (1992), which reveals that their observed catalytic effect of water on char formation and pyrolysis in general (see 2.6) is associated with water in the gas phase. However, it is important to note that they employed slow heating rates (5 to 25 °C/min), which means water was present at lower temperatures in liquid form. The same is true for the deoxy-liquefaction experiments. The process of VTC is another method that utilises the reactivity of gaseous water. It is similar to HTC except that saturated steam is used

instead of liquid water, which allows for a higher solid content (Funke et al., 2013). Funke et al. (2013) compared this process to HTC, and to closed and open torrefaction. They found that the carbon content of the solid product decreases in the following order HTC > VPC > closed torrefaction > open torrefaction revealing again the effect water has in its different states on carbonisation. They further showed that VPC has a higher process efficiency due to the reduced loss of carbon in the liquid phase, and the fact that less water needs to be heated. Generally Funke et al. found that dewatering is beneficial for both HTC and VPC, and that torrefaction is less efficient for moist biomasses, illustrating that the choice of optimum process depends on the feedstock.

While the influencing factors of autogenous pressure and the presence of water most affect the product quantity and distribution, there is a lack of a detailed understanding of the underlying relationship and fundamental processes. Such understanding is important for biochar-soil interactions. Often, only the *HTT* is stated when biochar is added to soil without the exact knowledge of biochar properties or production history, which could be a reason why there are sometimes positive and negative effects observed upon biochar addition to soil (Table A-2 in Appendix A.1). Libra et al. (2011) have called for better communication between users and producers so that the pyrolysis processes can be adjusted to produce a char that meets the needs of a specific target soil. They point out that this will be an iterative process as still more knowledge has to be gained about biochar-soil interactions in order to establish what biochar characteristics are required to cause a positive soil effect. Pyrolysis processes need to be economical. This review shows that the manufacture of biochar is more than just heating a feedstock in the absence of oxygen to varying temperatures. Also important are complete product life cycle assessments of **all** pyrolysis products to evaluate environmental impact of the various pyrolysis processes (Libra et al., 2011), which are often not clearly distinguishable. It would be beneficial if a by-product could be converted into a high value commodity. But so far, as outlined above, it seems that research on thermochemical conversion processes and their product applications is highly specialised and compartmentalised to gas, liquid or solid product, which is related to the complexity of pyrolysis. This can lead to missed opportunities as discussed by Morgan and Kandiyoti (2014) for coal and biomass pyrolysis. For example there is the common perception in the field of oil production that char is a pure waste product, and vice versa in the field of biochar manufacture where bio-oil is

merely to supply heat. This view needs to be challenged because this literature study indicates that it might be possible to co-produce a high value liquid and solid product.

In order to overcome this compartmentalisation a reactor is required that allows studying the effect of a range of pyrolysis processes and conditions on the pyrolysis products gas, liquid, and solid. Ideally, it is able to cover the processes outlined in Figure 2-24 except for the supercritical processes, which are not relevant for the manufacture of char due to the low yield. For instance being able to optimise the application of water would have economic benefits, as for example deoxy-liquefaction utilises less water than HTC (Lu et al., 2013), which means less water needs to be heated in the case of a dry feedstock. Of interest is also the possible role of water in controlling the reaction temperature (Bergius, 1928) by buffering the exothermic heat release of secondary pyrolysis reactions (see 2.6).

Reviewing the literature for a suitable reactor resulted in the observation that, to the best knowledge of the author, currently no laboratory reactor kit is available that is flexible enough to study pyrolysis, in particular autogenous pressure pyrolysis under such a wide range of pyrolysis conditions, while ensuring that enough products for characterisation are obtainable. However, such a reactor is a *sine qua non* for addressing the knowledge gap that exists in order to explain the relationship between char production, char properties and char application. It is important to produce char under a range of well-defined reproducible conditions, so that physical properties can be matched to production conditions, and so that the mechanisms of char formation can be elucidated. If this can be done, the functions and interactions of biochar in soil can be properly studied. Also important are energetic analyses to compare the different pyrolysis modes/ processes. This will aid in making economic predictions along with the investigation of co-producing a high value liquid product.

2.9 Conclusion

Despite pyrolysis being one of the oldest processes applied by human kind (Antal & Grønli, 2003)—in excess of 30,000 years (Bard, 2001), and the vast amount of research that has been done since the ground-breaking work of Violette (1853, as cited in Antal & Grønli, 2003) the actual pyrolysis mechanism remains unknown. Reasons are believed to be the complexity of pyrolysis as well as the compartmentalisation of pyrolysis research into separate fields (e.g. pyrolysis for bio-oil production, pyrolysis for char production as a reductant for the manufacture of silicon, geological formation of fossil fuels, etc.), and the limited availability of suitable reactors that allow the thorough investigation of secondary reactions along with their effects on pyrolysis products over the widest possible range of pyrolysis conditions. This is thought to be the reason that so far, to the best knowledge of the author, there is no model that can predict the pyrolysis product yields and properties. However, such a model is necessary for soil scientist to engineer biochar to the requirements of a specific target soil, and might be able to contribute in explaining the partly contradictory plant responses currently observed in the literature after biochar application in soil.

The following research detailed in this thesis tries to overcome the compartmentalisation, and establish the role of secondary reactions in char formation and during pyrolysis. By understanding the role and inferring the kinetics alongside on understanding of the influence of heat and mass transfer limitation, this work will contribute to the development of a pyrolysis model that can be used to predict product properties and yields. As part of this a sub aim is to develop an experimental kit that provides new research capabilities to investigate pyrolysis mechanisms.

2.10 References

Adler, E. (1977). Lignin chemistry—past, present and future. *Wood Science and Technology, 11*(3), 169-218. doi:10.1007/bf00365615

Akhtar, J., & Amin, N. A. S. (2011). A review on process conditions for optimum bio-oil yield in hydrothermal liquefaction of biomass. *Renewable and Sustainable Energy Reviews, 15*(3), 1615-1624. doi:10.1016/j.rser.2010.11.054

Antal, M. J. (1996). *US Patent No. 5,551,958*. Washington, DC: U.S. Patent and Trademark Office.

Antal, M. J., Allen, S. G., Dai, X., Shimizu, B., Tam, M. S., & Grønli, M. G. (2000). Attainment of the theoretical yield of carbon from biomass. *Industrial & Engineering Chemistry Research, 39*(11), 4024-4031. doi:10.1021/ie000511u

Antal, M. J., Croiset, E., Dai, X., DeAlmeida, C., Mok, W. S.-L., Norberg, N., . . . Al Majthoub, M. (1996). High-yield biomass charcoal. *Energy & Fuels, 10*(3), 652-658. doi:10.1021/ef9501859

Antal, M. J., & Grønli, M. G. (2003). The art, science, and technology of charcoal production. *Industrial & Engineering Chemistry Research, 42*(8), 1619-1640. doi:10.1021/ie0207919

Antal, M. J., Mok, W. S.-L., Varhegyi, G., & Szekely, T. (1990). Review of methods for improving the yield of charcoal from biomass. *Energy & Fuels, 4*(3), 221-225. Retrieved from http://www.scopus.com/inward/record.url?eid=2-s2.0-0025434090&partnerID=40&md5=e397506586bcbfac82518a387556e697

Antal, M. J., & Varhegyi, G. (1995). Cellulose pyrolysis kinetics: The current state of knowledge. *Industrial & Engineering Chemistry Research, 34*(3), 703-717. doi:10.1021/ie00042a001

Babu, B. V. (2008). Biomass pyrolysis: A state-of-the-art review. *Biofuels, Bioproducts and Biorefining, 2*(5), 393-414. doi:10.1002/bbb.92

Babu, B. V., & Chaurasia, A. S. (2003a). Modeling for pyrolysis of solid particle: Kinetics and heat transfer effects. *Energy Conversion and Management, 44*(14), 2251-2275. doi:10.1016/S0196-8904(02)00252-2

Babu, B. V., & Chaurasia, A. S. (2003b). Modeling, simulation and estimation of optimum parameters in pyrolysis of biomass. *Energy Conversion and Management, 44*(13), 2135-2158. doi:10.1016/S0196-8904(02)00237-6

Ball, R., McIntosh, A. C., & Brindley, J. (2004). Feedback processes in cellulose thermal decomposition: Implications for fire-retarding strategies and treatments. *Combustion Theory and Modelling, 8*(2), 281-291. doi:10.1088/1364-7830/8/2/005

Bard, E. (2001, June). Extending the calibrated radiocarbon record. *Science, 292*(5526), 2443-2444. Retrieved from http://www.sciencemag.org/content/292/5526/2443.short

Barth, T. (1999). Similarities and differences in hydrous pyrolysis of biomass and source rocks. *Organic Geochemistry, 30*(12), 1495-1507. doi:10.1016/S0146-6380(99)00121-7

Barth, T., Borgund, A. E., & Hopland, A. L. (1989). Generation of organic compounds by hydrous pyrolysis of Kimmeridge oil shale—Bulk results and activation energy calculations. *Organic Geochemistry, 14*(1), 69-76. doi:10.1016/0146-6380(89)90020-X

Behar, F., Kressmann, S., Rudkiewicz, J. L., & Vandenbroucke, M. (1992). Experimental simulation in a confined system and kinetic modelling of kerogen

and oil cracking. *Organic Geochemistry, 19*(1–3), 173-189. doi:10.1016/0146-6380(92)90035-V

Behar, F., Lewan, M. D., Lorant, F., & Vandenbroucke, M. (2003). Comparison of artificial maturation of lignite in hydrous and nonhydrous conditions. *Organic Geochemistry, 34*(4), 575-600. doi:10.1016/S0146-6380(02)00241-3

Behrendt, F., Neubauer, Y., Oevermann, M., Wilmes, B., & Zobel, N. (2008). Direct liquefaction of biomass. *Chemical Engineering & Technology, 31*(5), 667-677. doi:10.1002/ceat.200800077

Bergius, F. (1928). Beiträge zur Theorie der Kohleentstehung. *Naturwissenschaften, 16*(1), 1-10. doi:10.1007/bf01504496

Bergman, R., Cai, Z., Carll, C. G., Clausen, C. A., Dietenberger, M. A., Falk, R. H., . . . Zelinka, S. L. (2010). *Wood handbook - Wood as an engineering material* (General Technical Report FPL-GTR-190). Retrieved from Forest Products Laboratory website: http://www.fpl.fs.fed.us/documnts/fplgtr/fpl_gtr190.pdf

Bergman, T. L., Lavine, A. S., Incropera, F. P., & Dewitt, D. P. (2011). *Fundamentals of heat and mass transfer* (7th ed.). Hoboken, NJ: Wiley.

Biagini, E., & Tognotti, L. (2014). A generalized procedure for the devolatilization of biomass fuels based on the chemical components. *Energy & Fuels, 28*(1), 614-623. doi:10.1021/ef402139v

Boateng, A. A., Jung, H. G., & Adler, P. R. (2006). Pyrolysis of energy crops including alfalfa stems, reed canarygrass, and eastern gamagrass. *Fuel, 85*(17-18), 2450-2457. doi:10.1016/j.fuel.2006.04.025

Borgund, A. E., & Barth, T. (1999). Effects of base catalysis on the product distribution from pyrolysis of woody biomass in the presence of water. *Organic Geochemistry, 30*(12), 1517-1526. doi:10.1016/S0146-6380(99)00123-0

Boroson, M. L., Howard, J. B., Longwell, J. P., & Peters, W. A. (1989). Heterogeneous cracking of wood pyrolysis tars over fresh wood char surfaces. *Energy & Fuels, 3*(6), 735-740. doi:10.1021/ef00018a014

Boutin, O., Ferrer, M., & Lédé, J. (2002). Flash pyrolysis of cellulose pellets submitted to a concentrated radiation: Experiments and modelling. *Chemical Engineering Science, 57*(1), 15-25. doi:10.1016/s0009-2509(01)00360-8

Bowyer, J. L., Shmulsky, R., & Haygreen, J. G. (2007). *Forest products and wood science: An introduction* (5th ed.). Ames, IA: Blackwell.

BP. (2014). *BP statistical review of world energy 2014* [Statistical review]. Retrieved from http://www.bp.com/content/dam/bp/pdf/Energy-economics/statistical-review-2014/BP-statistical-review-of-world-energy-2014-full-report.pdf

Bradbury, A. G. W., Sakai, Y., & Shafizadeh, F. (1979). Kinetic model for pyrolysis of cellulose. *J Appl Polym Sci, 23*(11), 3271-3280. doi:10.1002/app.1979.070231112

Bridgwater, A. V. (2003). Renewable fuels and chemicals by thermal processing of biomass. *Chemical Engineering Journal, 91*(2-3), 87-102. doi:10.1016/S1385-8947(02)00142-0

Bridgwater, A. V. (2006). Biomass for energy. *Journal of the Science of Food and Agriculture, 86*(12), 1755-1768. doi:10.1002/jsfa.2605

Bridgwater, A. V., Meier, D., & Radlein, D. (1999). An overview of fast pyrolysis of biomass. *Organic Geochemistry, 30*(12), 1479-1493. doi:10.1016/s0146-6380(99)00120-5

Bridgwater, A. V., & Peacocke, G. V. C. (2000). Fast pyrolysis processes for biomass. *Renewable and Sustainable Energy Reviews, 4*(1), 1-73. doi:10.1016/s1364-0321(99)00007-6

Brown, A. L., Dayton, D. C., & Daily, J. W. (2001). A study of cellulose pyrolysis chemistry and global kinetics at high heating rates. *Energy & Fuels, 15*(5), 1286-1294. doi:10.1021/ef010084c

Brown, F. L. (1958). *Theories of the combustion of wood and its control. A survey of the literature* (Report No. 2136). Retrieved from Forest Products Laboratory website: http://www.fpl.fs.fed.us/documnts/fplr/fplr2136.pdf

Brown, R. A., Kercher, A. K., Nguyen, T. H., Nagle, D. C., & Ball, W. P. (2006). Production and characterization of synthetic wood chars for use as surrogates for natural sorbents. *Organic Geochemistry, 37*(3), 321-333. doi:10.1016/j.orggeochem.2005.10.008

Brown, R. C. (2009). Biochar production technology. In J. Lehmann & S. Joseph (Eds.), *Biochar for environmental management: Science and technology* (pp. 127-146). London, England, United Kingdom: Earthscan.

Bu, Q., Lei, H., Zacher, A. H., Wang, L., Ren, S., Liang, J., . . . Ruan, R. (2012). A review of catalytic hydrodeoxygenation of lignin-derived phenols from biomass pyrolysis. *Bioresource Technology, 124*, 470-477. doi:10.1016/j.biortech.2012.08.089

Cetin, E., Moghtaderi, B., Gupta, R., & Wall, T. F. (2004). Influence of pyrolysis conditions on the structure and gasification reactivity of biomass chars. *Fuel, 83*(16), 2139-2150. doi:10.1016/j.fuel.2004.05.008

Chan, K. Y., & Xu, Z. (2009). Biochar: Nutrient properties and their enhancement. In J. Lehmann & S. Joseph (Eds.), *Biochar for environmental management: Science and technology* (pp. 67-84). London, England, United Kingdom: Earthscan.

Chan, W.-C. R., Kelbon, M., & Krieger, B. B. (1985). Modelling and experimental verification of physical and chemical processes during pyrolysis of a large biomass particle. *Fuel, 64*(11), 1505-1513. doi:10.1016/0016-2361(85)90364-3

Chen, W.-H., Peng, J., & Bi, X. T. (2015). A state-of-the-art review of biomass torrefaction, densification and applications. *Renewable and Sustainable Energy Reviews, 44*, 847-866. doi:10.1016/j.rser.2014.12.039

Collard, F.-X., & Blin, J. (2014). A review on pyrolysis of biomass constituents: Mechanisms and composition of the products obtained from the conversion of cellulose, hemicelluloses and lignin. *Renewable and Sustainable Energy Reviews, 38*, 594-608. doi:10.1016/j.rser.2014.06.013

Commandré, J. M., Lahmidi, H., Salvador, S., & Dupassieux, N. (2011). Pyrolysis of wood at high temperature: The influence of experimental parameters on gaseous products. *Fuel Processing Technology, 92*(5), 837-844. doi:10.1016/j.fuproc.2010.07.009

Couhert, C., Commandre, J. M., & Salvador, S. (2009). Is it possible to predict gas yields of any biomass after rapid pyrolysis at high temperature from its composition in cellulose, hemicellulose and lignin? *Fuel, 88*(3), 408-417. doi:10.1016/j.fuel.2008.09.019

Czernik, S., & Bridgwater, A. V. (2004). Overview of applications of biomass fast pyrolysis oil. *Energy & Fuels, 18*(2), 590-598. doi:10.1021/ef034067u

Di Blasi, C. (1993). Analysis of convection and secondary reaction effects within porous solid fuels undergoing pyrolysis. *Combustion Science and Technology, 90*(5), 315 - 340. doi:10.1080/00102209308907620

Di Blasi, C. (1996a). Heat, momentum and mass transport through a shrinking biomass particle exposed to thermal radiation. *Chemical Engineering Science, 51*(7), 1121-1132. doi:10.1016/S0009-2509(96)80011-X

Di Blasi, C. (1996b). Kinetic and heat transfer control in the slow and flash pyrolysis of solids. *Industrial & Engineering Chemistry Research, 35*(1), 37-46. doi:10.1021/ie950243d

Di Blasi, C. (1998). Multi-phase moisture transfer in the high-temperature drying of wood particles. *Chemical Engineering Science, 53*(2), 353-366. doi:10.1016/S0009-2509(97)00197-8

Di Blasi, C. (2008). Modeling chemical and physical processes of wood and biomass pyrolysis. *Progress in Energy and Combustion Science, 34*(1), 47-90. doi:10.1016/j.pecs.2006.12.001

Di Blasi, C., & Branca, C. (2001). Kinetics of primary product formation from wood pyrolysis. *Industrial & Engineering Chemistry Research, 40*(23), 5547-5556. doi:10.1021/ie000997e

Diebold, J. P. (1994). A unified, global-model for the pyrolysis of cellulose. *Biomass & Bioenergy, 7*(1-6), 75-85. doi:10.1016/0961-9534(94)00039-v

Dilcio Rocha, J., Luengo, C. A., & Snape, C. E. (1999). The scope for generating bio-oils with relatively low oxygen contents via hydropyrolysis. *Organic Geochemistry, 30*(12), 1527-1534. doi:10.1016/s0146-6380(99)00124-2

Donaldson, L., & Xu, P. (2005). Microfibril orientation across the secondary cell wall of radiata pine tracheids. *Trees - Structure and Function, 19*(6), 644-653. doi:10.1007/s00468-005-0428-1

Downie, A., Crosky, A., & Munroe, P. (2009). Physical properties of biochar. In J. Lehmann & S. Joseph (Eds.), *Biochar for environmental management: Science and technology* (pp. 13-32). London, England, United Kingdom: Earthscan.

Emrich, W. (1985). *Handbook of charcoal making: The traditional and industrial methods*. Dordrecht, The Netherlands: Reidel.

European Biochar Foundation. (2012). *European biochar certificate - Guidelines for a sustainable production of biochar*. Retrieved from European Biochar Foundation website: http://www.european-biochar.org/biochar/media/doc/ebc-guidelines.pdf

Evans, R. J., & Milne, T. A. (1987). Molecular characterization of the pyrolysis of biomass. 1. Fundamentals. *Energy & Fuels, 1*(2), 123-137. doi:10.1021/ef00002a001

Fahmi, R., Bridgwater, A. V., Darvell, L. I., Jones, J. M., Yates, N., Thain, S., & Donnison, I. S. (2007). The effect of alkali metals on combustion and pyrolysis of Lolium and Festuca grasses, switchgrass and willow. *Fuel, 86*(10–11), 1560-1569. doi:10.1016/j.fuel.2006.11.030

Fantozzi, F., Colantoni, S., Bartocci, P., & Desideri, U. (2007). Rotary kiln slow pyrolysis for syngas and char production from biomass and waste - Part II: Introducing product yields in the energy balance. *Journal of Engineering for Gas Turbines and Power, 129*(4), 908-913. doi:10.1115/1.2720539

Fisher, T., Hajaligol, M., Waymack, B., & Kellogg, D. (2002). Pyrolysis behavior and kinetics of biomass derived materials. *Journal of Analytical and Applied Pyrolysis, 62*(2), 331-349. doi:10.1016/S0165-2370(01)00129-2

Flynn, J. H. (1997). The 'Temperature Integral' — Its use and abuse. *Thermochimica Acta, 300*(1–2), 83-92. doi:10.1016/S0040-6031(97)00046-4

Flynn, J. H., & Wall, L. A. (1966). General treatment of the thermogravimetry of polymers. *Journal of Research of the National Bureau of Standards—A. Physics and Chemistry, 70A*, 487-523. Retrieved from file:///C:/Users/gdripber/Downloads/1286.pdf

Fox, M. (2010). *Design of biochar pyrolysis unit* (Unpublished final year project report). Massey University, Palmerston North, New Zealand. The report can be accessed by contacting J.R.Jones@massey.ac.nz

Frolich, P. K., Spalding, H. B., & Bacon, T. S. (1928). Destructive distillation of wood and cellulose under pressure. *Industrial & Engineering Chemistry, 20*(1), 36-40. doi:10.1021/ie50217a019

Funke, A., Reebs, F., & Kruse, A. (2013). Experimental comparison of hydrothermal and vapothermal carbonization. *Fuel Processing Technology, 115*, 261-269. doi:10.1016/j.fuproc.2013.04.020

Funke, A., & Ziegler, F. (2010). Hydrothermal carbonization of biomass: A summary and discussion of chemical mechanisms for process engineering. *Biofuels, Bioproducts and Biorefining, 4*(2), 160-177. doi:10.1002/bbb.198

Galwey, A. K. (2004). Is the science of thermal analysis kinetics based on solid foundations?: A literature appraisal. *Thermochimica Acta, 413*(1–2), 139-183. doi:10.1016/j.tca.2003.10.013

Gardner, K. H., & Blackwell, J. (1974). The hydrogen bonding in native cellulose. *Biochimica et Biophysica Acta (BBA) - General Subjects, 343*(1), 232-237. doi:10.1016/0304-4165(74)90256-6

González, J. F., Román, S., Encinar, J. M., & Martínez, G. (2009). Pyrolysis of various biomass residues and char utilization for the production of activated carbons. *Journal of Analytical and Applied Pyrolysis, 85*(1–2), 134-141. doi:10.1016/j.jaap.2008.11.035

Goyal, H. B., Seal, D., & Saxena, R. C. (2008). Bio-fuels from thermochemical conversion of renewable resources: A review. *Renewable and Sustainable Energy Reviews, 12*(2), 504-517. doi:10.1016/j.rser.2006.07.014

Green, D. W., & Perry, R. H. (Eds.). (2008). *Perry's chemical engineers' handbook* (8th ed.). New York, NY: McGraw-Hill.

Grieco, E., & Baldi, G. (2011). Analysis and modelling of wood pyrolysis. *Chemical Engineering Science, 66*(4), 650-660. doi:10.1016/j.ces.2010.11.018

Griffiths, E., & Kaye, G. W. C. (1923). The measurement of thermal conductivity. *Proceedings of the Royal Society London Series A*, 71-98. Retrieved from http://rspa.royalsocietypublishing.org/content/104/724/71.full.pdf

Grønli, M. G. (1996). *A theoretical and experimental study of the thermal degradation of biomass* (Doctoral thesis, Norwegian University of Science and Technology, Trondheim, Norway). Retrieved from http://ntnu.diva-portal.org/smash/record.jsf?pid=diva2:321540

Grønli, M. G., Várhegyi, G., & Di Blasi, C. (2002). Thermogravimetric analysis and devolatilization kinetics of wood. *Industrial & Engineering Chemistry Research, 41*(17), 4201-4208. doi:10.1021/ie0201157

Gu, H., & Zink-Sharp, A. (2005). Geometric model for softwood transverse thermal conductivity. Part I. *Wood and fiber science, 37*(4), 699-711. Retrieved from http://www.fpl.fs.fed.us/documnts/pdf2005/fpl_2005_gu002.pdf

Harris, J. M. (1991). Structure of wood and bark. In J. A. Kininmonth & L. J. Whitehouse (Eds.), *Properties and uses of New Zealand radiata pine: Volume one - wood properties* (Vol. 1, pp. 2-1 - 2-18). Rotorua, New Zealand: Ministry of Forestry, Forest Research Institute, with financial support from the New Zealand Lottery Grants Board.

Harris, J. M., & Cown, D. J. (1991). Basic wood properties. In J. A. Kininmonth & L. J. Whitehouse (Eds.), *Properties and uses of New Zealand radiata pine: Volume one - wood properties* (Vol. 1, pp. 6-1 - 6-28). Rotorua, New Zealand: Ministry

of Forestry, Forest Research Institute, with financial support from the New Zealand Lottery Grants Board.

Haseli, Y., Van Oijen, J. A., & De Goey, L. P. H. (2011). Modeling biomass particle pyrolysis with temperature-dependent heat of reactions. *Journal of Analytical and Applied Pyrolysis, 90*(2), 140-154. doi:10.1016/j.jaap.2010.11.006

Henrich, E., & Weirich, F. (2004). Pressurized entrained flow gasifiers for biomass. *Environmental Engineering Science, 21*(1), 53-64. doi:10.1089/109287504322746758.

Hilber, I., Blum, F., Leifeld, J., Schmidt, H.-P., & Bucheli, T. D. (2012). Quantitative determination of PAHs in biochar: A prerequisite to ensure its quality and safe application. *Journal of Agricultural and Food Chemistry*. doi:10.1021/jf205278v

Hosoya, T., Kawamoto, H., & Saka, S. (2007). Cellulose-hemicellulose and cellulose-lignin interactions in wood pyrolysis at gasification temperature. *Journal of Analytical and Applied Pyrolysis, 80*(1), 118-125. doi:10.1016/j.jaap.2007.01.006

Hosoya, T., Kawamoto, H., & Saka, S. (2009). Solid/liquid- and vapor-phase interactions between cellulose- and lignin-derived pyrolysis products. *Journal of Analytical and Applied Pyrolysis, 85*(1-2), 237-246. doi:10.1016/j.jaap.2008.11.028

Hu, B., Yu, S.-H., Wang, K., Liu, L., & Xu, X.-W. (2008). Functional carbonaceous materials from hydrothermal carbonization of biomass: an effective chemical process. *Dalton Transactions*(40), 5414-5423. doi:10.1039/b804644c

International Biochar Initiative. (2012). *Frequently Asked Questions about Biochar.* Retrieved March 27, 2012, from http://www.biochar-international.org/biochar/faqs#question1

International Biochar Initiative. (2014). *Standardized product definition and product testing guidelines for biochar that is used in soil* (Document Reference Code: IBI-STD-2.0) [Product Definition and Specification Standards]. Retrieved from International Biochar Initiative website: http://www.biochar-international.org/sites/default/files/IBI_Biochar_Standards_V2%200_final_2014.pdf

International Energy Agency. (2006). *Annual report 2006: IEA Bioenergy*. Retrieved from IEA Bioenergy website: http://www.ieabioenergy.com/DocSet.aspx?id=5566&ret=lib

Jensen, A., Dam-Johansen, K., Wójtowicz, M. A., & Serio, M. A. (1998). TG-FTIR study of the influence of potassium chloride on wheat straw pyrolysis. *Energy & Fuels, 12*(5), 929-938. doi:10.1021/ef980008i

Jones, J. R. (2011, September). *Mechanisms of pyrolysis*. Paper presented at the ANZBRN Regional Meeting, Melbourne, Australia. Powerpoint retrieved from http://www.anzbiochar.org/2011%20Regional%20Meeting%20Presentations/JR Jones%20-%20Mechanisms%20of%20Pyrolysis%20-%20Melb%2029%20Sept%202011.pdf

Joseph, S., Camps-Arbestain, M., Lin, Y., Munroe, P., Chia, C. H., Hook, J., . . . Amonette, J. E. (2010). An investigation into the reactions of biochar in soil. *Soil Research, 48*(7), 501-515. doi:10.1071/SR10009

Joseph, S., Camps-Arbestain, M., Lin, Y., Munroe, P., Hook, J., Chia, C., . . . Thomas, P. (2012, February). *Labile organic molecules in biochar; Their role in plant health and nutrition; More questions than answers.* Paper presented at New Zealand Biochar Workshop 2012, Palmerston North, New Zealand.

Kamm, B., & Kamm, M. (2004). Principles of biorefineries. *Applied Microbiology and Biotechnology, 64*(2), 137-145. doi:10.1007/s00253-003-1537-7

Kantarelis, E., Yang, W., & Blasiak, W. (2013). Production of liquid feedstock from biomass via steam pyrolysis in a fluidized bed reactor. *Energy & Fuels, 27*(8), 4748-4759. doi:10.1021/ef400580x

Karaosmanoglu, F., Çift, B. D., & Işigigür-Ergüdenler, A. (2001). Determination of reaction kinetics of straw and stalk of rapeseed using thermogravimetric analysis. *Energy Sources, 23*(8), 767-774. doi:10.1080/009083101316862525

Keiluweit, M., Nico, P. S., Johnson, M. G., & Kleber, M. (2010). Dynamic molecular structure of plant biomass-derived black carbon (biochar). *Environmental Science & Technology, 44*(4), 1247-1253. doi:10.1021/es9031419

Khelfa, A., Bensakhria, A., & Weber, J. V. (2013). Investigations into the pyrolytic behaviour of birch wood and its main components: Primary degradation mechanisms, additivity and metallic salt effects. *Journal of Analytical and Applied Pyrolysis, 101*, 111-121. doi:10.1016/j.jaap.2013.02.004

Klason, P. (1914). Versuch einer Theorie der Trockendestillation von Holz. I. *Journal für Praktische Chemie, 90*(1), 413-447. doi:10.1002/prac.19140900127

Koufopanos, C. A., Lucchesi, A., & Maschio, G. (1989). Kinetic modelling of the pyrolysis of biomass and biomass components. *The Canadian Journal of Chemical Engineering, 67*(1), 75-84. doi:10.1002/cjce.5450670111

Kruse, A., Funke, A., & Titirici, M.-M. (2013). Hydrothermal conversion of biomass to fuels and energetic materials. *Current Opinion in Chemical Biology, 17*(3), 515-521. doi:10.1016/j.cbpa.2013.05.004

Laird, D. A., Brown, R. C., Amonette, J. E., & Lehmann, J. (2009). Review of the pyrolysis platform for coproducing bio-oil and biochar. *Biofuels, Bioproducts and Biorefining, 3*(5), 547-562. doi:10.1002/bbb.169

Lange, J.-P. (2007). Lignocellulose conversion: An introduction to chemistry, process and economics. *Biofuels, Bioproducts and Biorefining, 1*(1), 39-48. doi:10.1002/bbb.7

Lédé, J. (2012). Cellulose pyrolysis kinetics: An historical review on the existence and role of intermediate active cellulose. *Journal of Analytical and Applied Pyrolysis, 94*, 17-32. doi:10.1016/j.jaap.2011.12.019

Lédé, J., Blanchard, F., & Boutin, O. (2002). Radiant flash pyrolysis of cellulose pellets: Products and mechanisms involved in transient and steady state conditions. *Fuel, 81*(10), 1269-1279. doi:10.1016/S0016-2361(02)00039-X

Lehmann, J. (2007a). Bio-energy in the black. *Frontiers in Ecology and the Environment, 5*(7), 381-387. Retrieved from http://www.jstor.org/stable/20440704

Lehmann, J. (2007b). A handful of carbon. *Nature, 447*, 143-144. doi:10.1038/447143a

Lehmann, J., & Joseph, S. (2009a). Biochar for environmental management: An introduction. In J. Lehmann & S. Joseph (Eds.), *Biochar for environmental management: Science and technology* (pp. 1-12). London, England, United Kingdom: Earthscan.

Lehmann, J., & Joseph, S. (Eds.). (2009b). *Biochar for environmental management: Science and technology*. London, England, United Kingdom: Earthscan.

Lehmann, J., Rillig, M. C., Thies, J., Masiello, C. A., Hockaday, W. C., & Crowley, D. (2011). Biochar effects on soil biota – A review. *Soil Biology and Biochemistry, 43*(9), 1812-1836. doi:10.1016/j.soilbio.2011.04.022

Lewan, M. D. (1983). Effects of thermal maturation on stable organic carbon isotopes as determined by hydrous pyrolysis of Woodford Shale. *Geochimica et Cosmochimica Acta, 47*(8), 1471-1479. doi:10.1016/0016-7037(83)90306-X

Lewan, M. D. (1997). Experiments on the role of water in petroleum formation. *Geochimica et Cosmochimica Acta, 61*(17), 3691-3723. doi:10.1016/S0016-7037(97)00176-2

Lewan, M. D., Spiro, B., Illich, H., Raiswell, R., Mackenzie, A. S., Durand, B., . . . De Leeuw, J. W. (1985). Evaluation of petroleum generation by hydrous pyrolysis experimentation [and discussion]. *Philosophical Transactions of the Royal Society of London. Series A, Mathematical and Physical Sciences, 315*(1531), 123-134. Retrieved from http://rsta.royalsocietypublishing.org/content/roypta/315/1531/123.full.pdf

Lewan, M. D., Winters, J. C., & McDonald, J. H. (1979). Generation of oil-like pyrolyzates from organic-rich shales. *Science, 203*(4383), 897-899. doi:10.1126/science.203.4383.897

Libra, J. A., Ro, K. S., Kammann, C., Funke, A., Berge, N. D., Neubauer, Y., . . . Kern, J. (2011). Hydrothermal carbonization of biomass residuals: A comparative review of the chemistry, processes and applications of wet and dry pyrolysis. *Biofuels, 2*(1), 71-106. doi:10.4155/bfs.10.81

Lu, W., Guo, Y., Zhang, B., & Wang, C. (2013). Comprehensive analysis on elements, energy recovery, and oil compositions of biomass deoxy-liquefaction. *Energy and Fuels, 27*(4), 2157-2166. doi:10.1021/ef400157e

Mansuy, L., & Landais, P. (1995). Importance of the reacting medium in artificial maturation of a coal by confined pyrolysis. 2. Water and polar compounds. *Energy & Fuels, 9*(5), 809-821. doi:10.1021/ef00053a012

Mansuy, L., Landais, P., & Ruau, O. (1995). Importance of the reacting medium in artificial maturation of a coal by confined pyrolysis. 1. Hydrocarbons and polar compounds. *Energy & Fuels, 9*(4), 691-703. doi:10.1021/ef00052a018

Maschio, G., Koufopanos, C., & Lucchesi, A. (1992). Pyrolysis, a promising route for biomass utilization. *Bioresource Technology, 42*(3), 219-231. doi:10.1016/0960-8524(92)90025-S

McCarl, B. A., Peacocke, C., Chrisman, R., Kung, C.-C., & Sands, R. D. (2009). Economics of biochar production, utilization and greenhouse gas offsets. In J. Lehmann & S. Joseph (Eds.), *Biochar for environmental management: Science and technology* (pp. 341-357). London, England, United Kingdom: Earthscan.

Michels, R., Landais, P., Torkelson, B. E., & Philp, R. P. (1995). Effects of effluents and water pressure on oil generation during confined pyrolysis and high-pressure hydrous pyrolysis. *Geochimica et Cosmochimica Acta, 59*(8), 1589-1604. doi:10.1016/0016-7037(95)00065-8

Mohan, D., Pittman, C. U., & Steele, P. H. (2006). Pyrolysis of wood/biomass for bio-oil: A critical review. *Energy & Fuels, 20*(3), 848-889. doi:10.1021/ef0502397

Mok, W. S.-L., & Antal, M. J. (1983a). Effects of pressure on biomass pyrolysis. I. Cellulose pyrolysis products. *Thermochimica Acta, 68*(2-3), 155-164. doi:10.1016/0040-6031(83)80221-4

Mok, W. S.-L., & Antal, M. J. (1983b). Effects of pressure on biomass pyrolysis. II. Heats of reaction of cellulose pyrolysis. *Thermochimica Acta, 68*(2-3), 165-186. doi:10.1016/0040-6031(83)80222-6

Mok, W. S.-L., Antal, M. J., Szabo, P., Varhegyi, G., & Zelei, B. (1992). Formation of charcoal from biomass in a sealed reactor. *Industrial & Engineering Chemistry Research, 31*(4), 1162-1166. doi:10.1021/ie00004a027

Monthioux, M., Landais, P., & Monin, J.-C. (1985). Comparison between natural and artificial maturation series of humic coals from the Mahakam delta, Indonesia. *Organic Geochemistry, 8*(4), 275-292. doi:10.1016/0146-6380(85)90006-3

Morgan, T. J., & Kandiyoti, R. (2014). Pyrolysis of coals and biomass: Analysis of thermal breakdown and its products. *Chemical Reviews, 114*(3), 1547–1607. doi:10.1021/cr400194p

Neves, D., Thunman, H., Matos, A., Tarelho, L., & Gómez-Barea, A. (2011). Characterization and prediction of biomass pyrolysis products. *Progress in Energy and Combustion Science, 37*(5), 611-630. doi:10.1016/j.pecs.2011.01.001

Nic, M., Jirat, J., & Kosata, B. (2014). *IUPAC compendium of chemical terminology - The Gold Book.* Retrieved from http://goldbook.iupac.org

Nik-Azar, M., Hajaligol, M. R., Sohrabi, M., & Dabir, B. (1997). Mineral matter effects in rapid pyrolysis of beech wood. *Fuel Processing Technology, 51*(1–2), 7-17. doi:10.1016/s0378-3820(96)01074-0

Nunn, T. R., Howard, J. B., Longwell, J. P., & Peters, W. A. (1985). Product compositions and kinetics in the rapid pyrolysis of sweet gum hardwood. *Industrial & Engineering Chemistry Process Design and Development, 24*(3), 836-844. doi:10.1021/i200030a053

Oasmaa, A., & Czernik, S. (1999). Fuel oil quality of biomass pyrolysis oils - State of the art for the end users. *Energy & Fuels, 13*(4), 914-921. doi:10.1021/ef980272b

Palmer, R. C. (1914). Effect of pressure on yields of products in the destructive distillation of hardwood. *Journal of Industrial & Engineering Chemistry, 6*(11), 890-893. doi:10.1021/ie50071a004

Park, W. C., Atreya, A., & Baum, H. R. (2010). Experimental and theoretical investigation of heat and mass transfer processes during wood pyrolysis. *Combustion and Flame, 157*(3), 481-494. doi:10.1016/j.combustflame.2009.10.006

Pattanotai, T., Watanabe, H., & Okazaki, K. (2013). Experimental investigation of intraparticle secondary reactions of tar during wood pyrolysis. *Fuel, 104*(0), 468-475. doi:10.1016/j.fuel.2012.08.047

Pennisi, E. (1993, February 20). Surreptitiously converting dead matter into oil and coal. *Science News.* Retrieved from http://www.thefreelibrary.com/Surreptitiously+converting+dead+matter+into+oil+and+coal.-a013528247

Peralta, P. N., & Skaar, C. (2007). Experiments on steady-state nonisothermal moisture movement in wood. *Wood and fiber science, 25*(2), 124-135.

Peterson, A. A., Vogel, F., Lachance, R. P., Fröling, M., Antal, M. J., & Tester, J. W. (2008). Thermochemical biofuel production in hydrothermal media: A review of sub-and supercritical water technologies. *Energy & Environmental Science, 1*(1), 32-65. doi:10.1039/B810100K

Poling, B. E., Prausnitz, J. M., & O'Connell, J. P. (2001). *The properties of gases and liquids* (5th ed.). New York, NY: McGraw-Hill.

Prins, M. J., Ptasinski, K. J., & Janssen, F. J. J. G. (2006). More efficient biomass gasification via torrefaction. *Energy, 31*(15), 3458-3470. doi:10.1016/j.energy.2006.03.008

Pütün, A. E., Apaydın, E., & Pütün, E. (2004). Rice straw as a bio-oil source via pyrolysis and steam pyrolysis. *Energy, 29*(12–15), 2171-2180. doi:10.1016/j.energy.2004.03.020

Rao, T. R., & Sharma, A. (1998). Pyrolysis rates of biomass materials. *Energy, 23*(11), 973-978. doi:10.1016/s0360-5442(98)00037-1

Ratte, J., Marias, F., Vaxelaire, J., & Bernada, P. (2009). Mathematical modelling of slow pyrolysis of a particle of treated wood waste. *Journal of Hazardous Materials, 170*(2-3), 1023-1040. doi:10.1016/j.jhazmat.2009.05.077

Raveendran, K., Ganesh, A., & Khilar, K. C. (1995). Influence of mineral matter on biomass pyrolysis characteristics. *Fuel, 74*(12), 1812-1822. doi:10.1016/0016-2361(95)80013-8

Raveendran, K., Ganesh, A., & Khilar, K. C. (1996). Pyrolysis characteristics of biomass and biomass components. *Fuel, 75*(8), 987-998. doi:10.1016/0016-2361(96)00030-0

Rhim, Y.-R., Zhang, D., Fairbrother, D. H., Wepasnick, K. A., Livi, K. J., Bodnar, R. J., & Nagle, D. C. (2010). Changes in electrical and microstructural properties of microcrystalline cellulose as function of carbonization temperature. *Carbon, 48*(4), 1012-1024. doi:10.1016/j.carbon.2009.11.020

Rocha, J. D., Brown, S. D., Love, G. D., & Snape, C. E. (1997). Hydropyrolysis: A versatile technique for solid fuel liquefaction, sulphur speciation and biomarker release. *Journal of Analytical and Applied Pyrolysis, 40–41*, 91-103. doi:10.1016/S0165-2370(97)00041-7

Rowell, R. M. (2013). Moisture properties. In R. M. Rowell (Ed.), *Handbook of wood chemistry and wood composites* (2nd ed., pp. 75-98). Boca Raton, FL: CRC Press.

Rowell, R. M., Pettersen, R., & Tshabalala, M. A. (2013). Cell wall chemistry. In R. M. Rowell (Ed.), *Handbook of wood chemistry and wood composites*. Boca Raton, FL: CRC Press.

Schobert, H. (2013). *Chemistry of fossil fuels and biofuels*. Cambridge, United Kingdom: Cambridge University Press.

Schröder, H.-W. (2010). *Verarbeitung nachwachsender Rohstoffe* [Lecture notes]. Freiberg, Germany: Technische Universität Bergakademie Freiberg.

Sealock, L. J., Elliott, D. C., Baker, E. G., & Butner, R. S. (1993). Chemical processing in high-pressure aqueous environments. 1. Historical perspective and continuing developments. *Industrial & Engineering Chemistry Research, 32*(8), 1535-1541. doi:10.1021/ie00020a001

Shafizadeh, F., & Chin, P. P. S. (1977). Thermal deterioration of wood. In I. S. Goldstein (Ed.), *Wood Technology: Chemical Aspects* (Vol. 43, pp. 57-81). doi:10.1021/bk-1977-0043.ch005

Sharma, R. K., Wooten, J. B., Baliga, V. L., Lin, X., Chan, W. G., & Hajaligol, M. R. (2004). Characterization of chars from pyrolysis of lignin. *Fuel, 83*(11–12), 1469-1482. doi:10.1016/j.fuel.2003.11.015

Shen, D. K., Gu, S., & Bridgwater, A. V. (2010). The thermal performance of the polysaccharides extracted from hardwood: Cellulose and hemicellulose. *Carbohydrate Polymers, 82*(1), 39-45. doi:10.1016/j.carbpol.2010.04.018

Siau, J. F. (1984). *Transport processes in wood*. Berlin: Springer-Verlag.

Spath, P. L., & Dayton, D. C. (2003). *Preliminary screening-technical and economic assessment of synthesis gas to fuels and chemicals with emphasis on the potential for biomass-derived syngas* (NREL/TP-510-34929). Retrieved from http://www.nrel.gov/docs/fy04osti/34929.pdf

Sun, J. T., Huang, Y. D., Gong, G. F., & Cao, H. L. (2006). Thermal degradation kinetics of poly(methylphenylsiloxane) containing methacryloyl groups.

Polymer Degradation and Stability, 91(2), 339-346. doi:10.1016/j.polymdegradstab.2005.04.037

Thurner, F., & Mann, U. (1981). Kinetic investigation of wood pyrolysis. *Industrial & Engineering Chemistry Process Design and Development, 20*(3), 482-488. doi:10.1021/i200014a015

Uprichard, J. M. (1991). Chemistry of wood and bark. In J. A. Kininmonth & L. J. Whitehouse (Eds.), *Properties and uses of New Zealand radiata pine: Volume one - wood properties* (Vol. 1, pp. 4-1 - 4-46). Rotorua, New Zealand: Ministry of Forestry, Forest Research Institute, with financial support from the New Zealand Lottery Grants Board.

Varhegyi, G., Antal, M. J., Szekely, T., Till, F., & Jakab, E. (1988). Simultaneous thermogravimetric-mass spectrometric studies of the thermal decomposition of biopolymers. 1. Avicel cellulose in the presence and absence of catalysts. *Energy & Fuels, 2*(3), 267-272. doi:10.1021/ef00009a007

Varhegyi, G., Antal, M. J., Szekely, T., Till, F., Jakab, E., & Szabo, P. (1988). Simultaneous thermogravimetric-mass spectrometric studies of the thermal decomposition of biopolymers. 2. Sugarcane bagasse in the presence and absence of catalysts. *Energy & Fuels, 2*(3), 273-277. doi:10.1021/ef00009a008

Varhegyi, G., Jakab, E., & Antal, M. J. (1994). Is the Broido-Shafizadeh Model for cellulose pyrolysis true? *Energy & Fuels, 8*(6), 1345-1352. doi:10.1021/ef00048a025

Wagenaar, B. M., Prins, W., & van Swaaij, W. P. M. (1993). Flash pyrolysis kinetics of pine wood. *Fuel Processing Technology, 36*(1-3), 291-298. doi:10.1016/0378-3820(93)90039-7

Walford, G. B. (1991). Mechanical properties. In J. A. Kininmonth & L. J. Whitehouse (Eds.), *Properties and uses of New Zealand radiata pine: Volume one - wood properties* (Vol. 1, pp. 8-1 - 8-21). Rotorua, New Zealand: Ministry of Forestry, Forest Research Institute, with financial support from the New Zealand Lottery Grants Board.

Wang, C., Du, Z., Pan, J., Li, J., & Yang, Z. (2007). Direct conversion of biomass to bio-petroleum at low temperature. *Journal of Analytical and Applied Pyrolysis, 78*(2), 438-444. doi:10.1016/j.jaap.2006.10.016

Wang, L., Skreiberg, Ø., Grønli, M. G., Specht, G. P., & Antal, M. J. (2013). Is elevated pressure required to achieve a high fixed-carbon yield of charcoal from biomass? Part 2: The importance of particle size. *Energy & Fuels, 27*(4), 2146-2156. doi:10.1021/ef400041h

Wang, L., Trninic, M., Skreiberg, Ø., Grønli, M. G., Considine, R., & Antal, M. J. (2011). Is elevated pressure required to achieve a high fixed-carbon yield of charcoal from biomass? Part 1: Round-robin results for three different corncob materials. *Energy & Fuels, 25*(7), 3251-3265. doi:10.1021/ef200450h

Wang, X. Y., Wan, X. J., Chen, M. Q., & Wang, J. (2012). Kinetic model of biomass pyrolysis based on three-component independent parallel first-order reactions. *Guocheng Gongcheng Xuebao/The Chinese Journal of Process Engineering, 12*(6), 1020-1024. Retrieved from http://www.scopus.com/inward/record.url?eid=2-s2.0-84872227037&partnerID=40&md5=db7f9f47b41717d346ac4ce828d9edbf

White, J. E., Catallo, W. J., & Legendre, B. L. (2011). Biomass pyrolysis kinetics: A comparative critical review with relevant agricultural residue case studies. *Journal of Analytical and Applied Pyrolysis, 91*(1), 1-33. doi:10.1016/j.jaap.2011.01.004

Wiedenhoeft, A. C. (2010). *Wood handbook, chapter 03: Structure and function of wood* (General Technical Report FPL-GTR-190). Retrieved from U.S. Department of Agriculture, Forest Service, Research and Development, Forest Products Laboratory website: http://www.fpl.fs.fed.us/documnts/fplgtr/fplgtr190/chapter_03.pdf

Wiedenhoeft, A. C., & Miller, R. C. (2005). Structure and function of wood. In R. M. Rowell (Ed.), *Handbook of wood chemistry and wood composites* (pp. 9-34). Boca Raton, FL: CRC Press.

Wigley, T., Pang, S., & Yip, A. (2014). *Development of the fast pyrolysis process to produce a high quality liquid fuel from woody biomass.* Paper presented at Pyro2014 20th International Symposium on Analytical and Applied Pyrolysis, Birmingham, United Kingdom.

Winters, J. C., Williams, J. A., & Lewan, M. D. (1983). A laboratory study of petroleum generation by hydrous pyrolysis. In M. Bjorøy (Ed.), *Advances in organic geochemistry 1981* (pp. 524-533). Chichester, United Kingdom: John Wiley and Sons.

Woolf, D., Amonette, J. E., Street-Perrott, F. A., Lehmann, J., & Joseph, S. (2010). Sustainable biochar to mitigate global climate change. *Nature Communications, 1*(5), 56. doi:10.1038/ncomms1053

Wu, L., Guo, S., Wang, C., & Yang, Z. (2008). Direct deoxy-liquefaction of poplar leaves to biopetroleum with two kinds of catalysts. *Industrial & Engineering Chemistry Research, 47*(23), 9248-9255. doi:10.1021/ie801129b

Yang, H., Yan, R., Chen, H., Lee, D. H., & Zheng, C. (2007). Characteristics of hemicellulose, cellulose and lignin pyrolysis. *Fuel, 86*(12-13), 1781-1788. doi:10.1016/j.fuel.2006.12.013

Yang, H., Yan, R., Chen, H., Zheng, C., Lee, D. H., & Liang, D. T. (2006). In-depth investigation of biomass pyrolysis based on three major components: Hemicellulose, cellulose and lignin. *Energy & Fuels, 20*(1), 388-393. doi:10.1021/ef0580117

Zhang, H., Xiao, R., Wang, D., He, G., Shao, S., Zhang, J., & Zhong, Z. (2011). Biomass fast pyrolysis in a fluidized bed reactor under N_2, CO_2, CO, CH_4 and H_2 atmospheres. *Bioresource Technology, 102*(5), 4258-4264. doi:10.1016/j.biortech.2010.12.075

Zhang, L., Xu, C., & Champagne, P. (2010). Overview of recent advances in thermo-chemical conversion of biomass. *Energy Conversion and Management, 51*(5), 969-982. doi:10.1016/j.enconman.2009.11.038

Chapter 3 Role of Secondary Char Formation in the Manufacture of Biochar

3.1 Introduction

This chapter deals first with the characterisation of the feedstock which is essential to any pyrolysis operation. It then investigates the role of secondary reactions in the char formation process and in general during pyrolysis. This is achieved by investigating pyrolysis in a laboratory scale thermogravimetric analyser, TGA, and a Macro-TGA to cover a large range of sizes, extending from thin slices to large cylindrical specimens in the micrometre and centimetre ranges respectively. Secondary reactions are divided into intraparticle and extraparticle reactions to differentiate between the case of a single particle and a "bed" of particles. Also discussed are the structural changes and transfer limitations that occur during pyrolysis, as they directly impact the ongoing reactions. Finally, the temperature regime of secondary reactions is established and interpreted with respect to the constituents present in the feedstock. Torrefaction as a thermal pre-treatment step is also investigated, as it is reported to increase rearrangement reactions (primary char forming reactions) to give a comparison between char yield enhancement by secondary and primary reactions.

3.2 Materials and Methods

3.2.1 Feedstock

3.2.1.1 Origin

New Zealand Radiata Pine, *Pinus Radiata*, purchased from Pacific Pine Industries Ltd (Putaruru, New Zealand) is used throughout this study. It was chosen due to its commercial plantation in New Zealand and the manufacture of biochar offers a unique opportunity to manage the unused residues. To keep variability at a minimum, a single log (tree trunk from one tree), sufficient for all the experiments, was obtained. The trunk was delivered debarked in five beams, 0.3 x 0.3 x 1.1 m. The centre of the beam coincides with the centre of the trunk (pith); containing heartwood in the centre and sapwood towards the outside. The beams were cut by Foxton Sawmilling Co. Ltd (Foxton, New Zealand) to manageable sizes. A range of sample shapes and sizes were produced by planing, sawing, and turning. Turning was done by Woodturners Manawatu Ltd (Rongotea, New Zealand). Sawdust was produced with the help of an electric plane that was moved across the grain of the entire cross section, 0.3 x 0.3 m, and subsequently sieved to obtain a particle size < 1 mm. All the samples were air-dried unless stated otherwise, that is, the sample is in equilibrium with the ambient air.

3.2.1.2 Composition

Sawdust samples representing the average trunk composition were sent to Veritec (Rotorua, New Zealand) for extractive, carbohydrate and lignin analysis, as listed in Table 3-1.

Table 3-1. Extractive, carbohydrate and lignin analysis.

Sample	ID	% (wt/wt) od	% (wt/wt) extracted od							
		DCM extractives	Lignin		Natural carbohydrates					Total[a]
			Acid-insoluble (Klason)	Acid-soluble	Arab	Galac	Gluc	Xyl	Man	
1	1	2.69	31.50	0.66	1.50	3.76	39.44	4.63	9.56	91.05
	2	2.60	31.71	0.63	1.49	3.81	39.54	4.64	9.10	90.92
	μ	2.65	31.61	0.65	1.50	3.79	39.49	4.64	9.33	90.99
2	1	8.13	31.10	0.59	1.61	3.70	43.03	4.54	11.22	95.79
	2	7.77	30.76	0.59	1.62	3.69	43.00	4.53	10.61	94.80
	μ	7.95	30.93	0.59	1.62	3.70	43.02	4.54	10.92	95.30
	μ	5.30	31.27	0.62	1.56	3.74	41.25	4.59	10.12	93.14
	σ	3.07	0.42	0.03	0.07	0.06	2.04	0.06	0.97	2.52
	CV	0.579	0.014	0.055	0.045	0.015	0.049	0.013	0.096	0.027

Note. Extractive, carbohydrate and lignin analysis was carried out by Veritec (Rotorua, New Zealand). Sugars are reported as anhydrosugar units.

Method: Samples are extracted using DCM solvent on a Soxtec apparatus, boiling time 1 hour, rinse time 1 hour. Acid insoluble lignin in wood and pulp, modified method based on TAPPI Standards Method, T 222 om 88. Acid soluble lignin in wood and pulp, TAPPI Useful Method UM 250. Wood sugar analysis by Anion Chromatography, Pettersen, R. C., & Schwandt, V. H. (1991). Wood sugar analysis by anion chromatography. *Journal of Wood Chemistry and Technology, 11*(4), 495-501. doi: 10.1080/02773819108051089.

Arab = Arabinan; *CV* = coefficient of variation; DCM = Dichloromethane; Galac = Galactan; Gluc = Glucan; Man = Mannan; od = oven-dry; Xyl = Xylan; μ = average; σ = standard deviation in pp.

[a]sum of the sugar and lignin values.

The cellulose and hemicellulose content was calculated from Table 3-1 according to Newman, Hemmingson, and Suckling (1993):

$$Cellulose = Glucose - 0.27\ Mannose\ , \tag{3.1}$$

$$Hemicellulose = 1.27\ Mannose + Galactose + 1.18\ Xylose + Arabinose\ . \tag{3.2}$$

The results are shown in Table 3-2 combined with the lignin content.

Table 3-2. Cellulose, hemicellulose, and lignin content of radiata pine.

% (wt/wt) extracted od			
Cellulose	**Hemicellulose**	**Lignin[a]**	∑
38.52	23.56	31.89	93.97

Note. The cellulose and hemicellulose content have been determined from Table 3-1 according to Newman et al. (1993) (equation (3.1) and (3.2)). od = oven-dry.

[a]sum of acid-insoluble and acid-soluble lignin from Table 3-1.

The values in Table 3-2 are similar to those reported in literature (Butt, 2006; Kininmonth & Whitehouse, 1991; Z. Wang, Cao, & Wang, 2009). It is important to note that a range of literature sources use the method of Robertson and Van Soest (1981) to determine the biomass components cellulose, hemicellulose, and lignin (Calvelo Pereira et al., 2011; González, Román, Encinar, & Martínez, 2009; Lu, Guo, Zhang, & Wang, 2013; Shen, Gu, Jin, & Fang, 2011; Wu, Guo, Wang, & Yang, 2009; Yu, Wang, Wang, & Yang, 2011). However, this method is not appropriate for wood, as it was developed for analysing forages for ruminant animals, and later has been extended to some degree for human foods (P. J. Harris, personal communication, August 6, 2013). Applying the Van Soest method for the radiata pine wood used in these experiments (Bridges, 2013) results in too high a cellulose content, too low hemicellulose and lignin contents, as well as too low a yield of the sum of the three components (C. Altaner, personal communication, August 1, 2013). The same trend is apparent in the work of Shen et al. (2011). For this reason it is advised to use the methods in Table 3-1 and Table 3-2. A yield of 94 % (wt/wt) in Table 3-2 is typical for radiata pine, and is caused by the presence of other minor constituents like acetyl groups and uronosyl units on the hemicelluloses, proteins and extractives, which were not part

of the analysis by Veritec, as well as analytical errors like method biases and variability (I. Suckling, personal communication, November 10, 2014).

Looking at Table 3-1 it becomes evident that there is a relatively large variation in the extractives content between the two different samples. Both sawdust samples were prepared from the same tree but were analysed at different times, and so had different exposure times to the ambient environment (sample 2 was analysed first). Possible reasons for the variation are evaporation of extractive compounds due to their vapour pressure (Arshadi & Gref, 2005), different proportions of heartwood and sapwood in the two samples (heartwood has generally a higher extractives content (Rowell, Pettersen, & Tshabalala, 2013)) arising from the natural heterogeneity of wood. Another factor is that the extractive presence and composition can be changed by microbiological (Martínez-Iñigo, Immerzeel, Gutierrez, del Río, & Sierra-Alvarez, 1999) and auto-oxidative chemical reactions (Hemingway et al., 1971, as cited in Arshadi & Gref, 2005).

3.2.1.3 Ultimate Analysis

An Elementar Analysensysteme GmbH (Hanau, Germany) vario MACRO cube elemental analyser was used for ultimate analysis. The analyser was operated in CHNS mode. Sawdust, dried for 24 h at 105 °C and subsequently stored over silica gel to ensure completely dry samples, was used for analysis. The samples were mixed with tungsten trioxide (WO_3) powder, a combustion aid, in the weight ratio 1:2 and wrapped in tin boats for analysis. Results are given in Table 3-3, and agree with literature (Cetin, Gupta, & Moghtaderi, 2005; Chen, Charpenay, Jensen, Wójtowicz, & Serio, 1998; Huang, Kudo, Masek, Norinaga, & Hayashi, 2012; Lapuerta, Hernández, & Rodríguez, 2007).

Table 3-3. Ultimate analysis of radiata pine on a dry (dry ash free) basis.

	μ	σ	*CV*
	% (wt/wt)	**pp**	
C	51.32 (51.48)	0.256	0.005
H	7.014 (7.035)	0.207	0.029
O	41.22[a] (41.35)		
N	0.139 (0.140)	0.017	0.119
S	0[b]		

Note. The results represent averages of 9 samples except nitrogen which was averaged over 7 samples as two samples were under ranging the calibrated range. μ = average; σ = standard deviation; *CV* = coefficient of variation.

[a]determined by difference using the ash value in Table 3-7. [b]values were below the detection limit.

The oxygen content, O, in Table 3-3 was calculated by difference using the ash content in Table 3-7 according to the following equation:

$$O = 100 - C - H - N - S - Ash\,, \tag{3.3}$$

where O, C, H, N, S and Ash are in % (wt/wt). Therefore, O represents the organic oxygen content. Assuming the complete ash content in Table 3-7 is made up of CaO, which was found to be the largest ash compound by Cetin et al. (2005), deriving from $CaCO_3$ the maximum theoretical inorganic carbon has been calculated to be 0.06 % (wt/wt). This is below the standard deviation of carbon in Table 3-3. Thus, it can be safely stated that the carbon content in Table 3-3 represents the organic carbon content in radiata pine.

The empirical formula of radiata pine wood, Table 3-4, was calculated from Table 3-3.

Table 3-4. Empirical formula and molar *H/C* and *O/C* ratio of radiata pine wood.

Empirical formula	**Molar *H/C* ratio**	**Molar *O/C* ratio**
$CH_{1.628}N_{0.002}O_{0.603}$	1.628	0.603

3.2.1.4 Proximate Analysis

Proximate analysis was carried out in a laboratory simultaneous thermogravimetric analyser (TGA) and differential scanning calorimeter (DSC), SDT Q600 from TA Instruments (Melbourne, Australia). Air-dried sawdust, 6-12 mg, was heated in an Alumina, Al_2O_3, crucible with a diameter of 5 mm and height of 4 mm according to the

procedure in Table 3-5. Analysis runs were done with and without a lid as both methods have been used in literature (Hayward, 2011; L. Wang, Skreiberg, Grønli, Specht, & Antal, 2013).

Table 3-5. TGA procedure for proximate analysis.

Step	Atmosphere[a]	Temperature in °C	Heating rate in °C/min	Hold time at final temperature in min
1	N_2	Room temperature→25	5	30
2	N_2	25→900	5	0
3	Air	900	Isothermal	≥30
4	N_2	25		

Note. The procedure is the one typically used by the New Zealand Biochar Research Centre (Calvelo Pereira et al., 2011; Hayward, 2011).

[a]applied gas flow rate is 20 ml/min.

The equipment was calibrated with respect to three variables (a) weight (reference and sample beam have been calibrated from room temperature, RT, to 1250 °C with known weights), (b) temperature (calibration against pure metals (Sn, Pb, Zn, Al) with known melting points), and (c) heat flow (calibrated against sapphire standard) for a heating rate of 5 °C/min (M. Bretherton, personal communication, March 27, 2013). A heating rate of 5 °C/min was applied throughout this research as it represents slow pyrolysis for the manufacture of biochar.

Typically the water contained in the sample is defined as weight-loss till 107 °C (Hayward, 2011) or 110 °C (Calvelo Pereira et al., 2011; Narayan & Antal, 1996). However, looking at the derivative weight-loss curves in Figure 3-1 reveals that this temperature did not coincide with the end of the peak that is associated with water loss (1st peak in Figure 3-1).

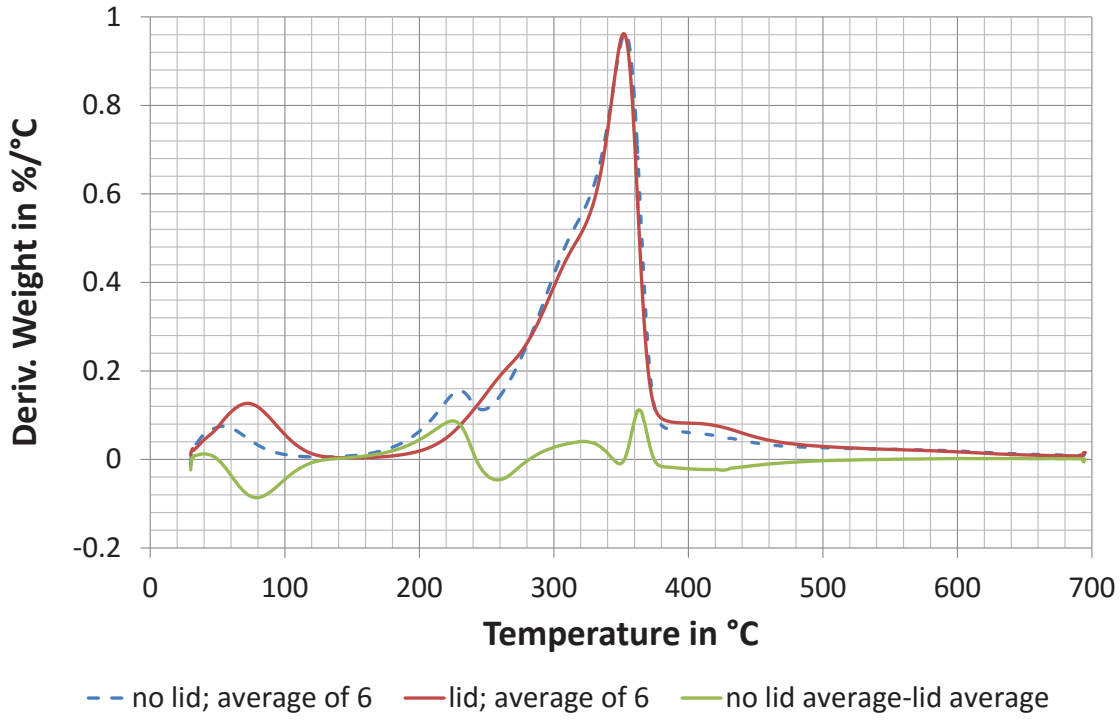

Figure 3-1. Average derivative weight curve of the proximate analysis experiments with and without a lid. It is important to note that each curve includes an extra pyrolysis run till 700 °C for which reason this graph is only plotted till 700 °C and not 900 °C. The "no lid average-lid average curve" illustrates the difference between the two cases lid and no lid.

The minima between the first two peaks in Figure 3-1 were determined as the temperature where drying is completed. They are 152 and 126 °C for the runs with and without a lid respectively. The moisture peak for the run with a lid is shifted to the right compared to the run without a lid. This indicates that the drying step is prolonged in the case of a lid due to reduced mass transfer and/or increased thermal lag. In contrast, the good overlap of the pyrolysis peaks indicates that the pyrolysis step is not affected by the aforementioned processes. Transfer limitations are discussed in more detail in 3.3.5.

The amount of water (moisture), M, in % (wt/wt) present in the sample was then calculated according to:

$$M = \frac{(m_{in} - m_d)}{m_{in}} \cdot 100 \ , \tag{3.4}$$

where m_{in} is the initial feedstock weight in kg at RT, and m_d the weight of the dried feedstock in kg at 152 and 126 °C in kg for the case lid and no lid respectively. It is important to note that M in equation (3.4) is different to the moisture content in equation (2.6) in section 2.5.2, which is divided by the oven-dry sample weight.

The volatile matter, VM, in % (wt/wt) is determined accordingly as the weight-loss from the dried sample to the introduction of air at 900 °C (Table 3-5) and expressed by equation (3.5):

$$VM = \frac{(m_d - m_{air})}{m_{in}} \cdot 100 \ . \tag{3.5}$$

In equation (3.5) m_{air} is the weight of the sample in kg just before the introduction of air at 900 °C.

The fixed carbon, FC, in % (wt/wt) is defined as the difference in weight between the introduction of air till no more weight-loss occurs:

$$FC = \frac{(m_{air} - m_r)}{m_{in}} \cdot 100 \ , \tag{3.6}$$

where m_r is the weight of the residue in kg.

The results of proximate analysis with and without a lid are shown in Table 3-6 and Table 3-7 respectively.

Table 3-6. Proximate analysis with lid of air-dried radiata pine in % (wt/wt) on an air-dry basis.

	Moisture	**Volatile matter**	**Fixed carbon**	**Ash**
μ in % (wt/wt)	9.409	72.438	17.879	0.274[a]
σ in pp	0.384	0.569	0.319	0.019
CV	0.041	0.008	0.018	0.063

Note. The results represent averages of 5 samples except ash which was averaged over 9 samples. *CV* = coefficient of variation; μ = average; σ = standard deviation.

[a]determined by Residue on Ignition with and according to Bridges (2013).

Table 3-7. Proximate analysis without lid of air-dried radiata pine in % (wt/wt) on an air-dry basis.

	Moisture	**Volatile matter**	**Fixed carbon**	**Ash**
μ in % (wt/wt)	9.307	77.229	13.190	0.274[a]
σ in pp	0.206	0.355	0.492	0.019
CV	0.022	0.005	0.037	0.063

Note. The results represent averages of 5 samples except ash which was averaged over 9 samples. *CV* = coefficient of variation; μ = average; σ = standard deviation.

[a]determined by Residue on Ignition with and according to Bridges (2013).

It was important to check the validity of the moisture determination method, set as 152 and 126 °C for the TGA analysis for the trials 'with' and 'without' a lid, respectively. To do this, wood samples (cut wood rods of varying length with a diameter of 20 mm) were placed in a Series 5 Contherm Digital Series Oven (Contherm Scientific, Upper Hutt, New Zealand) at 105 °C till no more weight change occurred, Table 3-8.

Table 3-8. Moisture contained in air-dried radiata pine in % (wt/wt) on an air-dry basis as determined by oven-drying.

	Weight-loss when dried at 105 °C[a]	**Weight-loss when dried at 110 °C[b]**
μ in % (wt/wt)	9.434	10.535
σ in pp	0.536	0.386
CV	0.057	0.037

Note. The results represent averages of 6 samples. *CV* = coefficient of variation; μ = average; σ = standard deviation.

[a]determined till no more weight-loss occurred. [b]weight-loss when dried at 110 °C for 114.6 h

Table 3-8 shows that the moisture determined at the commonly used drying temperature of 105 °C agrees with the values obtained by proximate analysis in Table 3-6 and Table

3-7, confirming the applied method. The weight-loss for drying wood at 110 °C for a long period of time (114.6 h) has been included to illustrate that this results in an increased weight-loss indicating that some drying still takes place above 105 °C.

The results in Table 3-7 agree with Cetin, Moghtaderi, Gupta, and Wall (2004), who also conducted proximate analysis on radiate pine wood. Comparing the proximate analysis results done without a lid (Table 3-7) to the results employing a lid in Table 3-6 it becomes evident that this small change has a relatively large impact on the proximate analysis results. That is, in the case of a lid, the *VM* decreases and the *FC* increases, which agrees with the findings of L. Wang et al. (2013). This reveals that the "property", in this case the *VM* and *FC* content, is dependent on the measurement method, which is a harbinger of the intrinsic difficulty of separating primary and secondary reactions during pyrolysis (Morgan & Kandiyoti, 2013).

It is important to note that the proximate analysis results in Table 3-6 and Table 3-7 have been adjusted for the ash content determined by Residue on Ignition, ROI, according to Bridges (2013), which uses large samples (~1-5 g). This method was necessary as there was a large scatter in the ash content determined by the TGA, where the coefficient of variation (CV) was 2.720 and 1.974 for the proximate analysis experiments with and without a lid respectively (see Appendix B.1 for the original TGA proximate analysis data). The large TGA ash *CV*s occur both because the ash content is very small (~0.3 %) and due to the compounding of errors in M, VM, and FC. Dependencies of ash contents on analysis methods have also been reported in literature (L. Wang et al., 2013).

3.2.1.5 Higher Heating Value

The higher heating value (*HHV*), a major fuel property (Channiwala & Parikh, 2002; Sheng & Azevedo, 2005), was determined experimentally and compared to estimated values in Table 3-9.

Table 3-9. Higher heating value of radiata pine wood in MJ/kg measured and estimated.

	Measured	**Ultimate analysis**		**Proximate analysis open crucible**		**Proximate analysis closed crucible**	
HHV	19.450[a]	20.806	20.964	17.600	19.633	18.424	19.832
σ	0.919						
CV	0.047						
Ref	NL[b]	(Demirbas, 1997; Demirbas, Gullu, Çaglar, & Akdeniz, 1997)	(Sheng & Azevedo, 2005)	(Demirbas, 1997)	(Sheng & Azevedo, 2005)	(Demirbas, 1997)	(Sheng & Azevedo, 2005)

Note. For the equations the reader is referred to the original sources. Ultimate analysis uses the elemental carbon and hydrogen contents. Proximate analysis uses the volatile matter and fixed carbon contents. *CV* = coefficient of variation; *HHV* = higher heating value; NL = Nutrition Laboratory; Ref = reference; σ = standard deviation in MJ/kg.

[a]average of 2 samples. [b]determined by Nutrition Laboratory of the Institute of Food, Nutrition and Human Health (Massey University, Palmerston North, New Zealand).

Table 3-9 shows that the *HHV* can be estimated from a range of basic analysis data (Sheng & Azevedo, 2005). It is important to note that it can also be determined from the biomass constituents cellulose, hemicellulose, and lignin, but Sheng and Azevedo (2005) state that this is not reliable due to the variation of the components properties, and so has been disregarded here. Instead, they regard ultimate analysis as the most accurate estimation method for *HHV*, which is better than proximate analysis predictions. The lower accuracy of the latter one has been attributed to the fact that proximate analysis "provides only the empirical composition of biomass" (*ibid*, p. 506). This work agrees that proximate analysis is not a suitable method for determining properties as it is strongly dependent on the employed method (e.g. lid or no lid, Table 3-9) or the equipment/crucible design (how easy it is for volatile pyrolysis products to escape) due to the action of secondary reactions (L. Wang et al., 2013). Thus, using proximate analysis does not fulfil the earlier mentioned requirement that the measurement of a property has to be independent of its method (Morgan & Kandiyoti, 2013). For this reason, it is disregarded even though it seems to be closer to the measured value in Table 3-9 than the estimate by ultimate analysis. However, the measured value of 19.450 MJ/kg is lower than the typical range for softwood, 20 to 22 MJ/kg, as reviewed by Demirbas et al. (1997), which could be due to measurement error as only 2 samples were done, 18.8 and 20.1 MJ/kg respectively. The relatively

large variation between the two measured values indicates that the ultimate analysis predictions might be more accurate.

Overall Table 3-9 highlights that secondary reactions play a considerable (unwanted) role when it comes to laboratory analysis techniques. This indicates that they will have an even bigger role in large scale pyrolysis, as is the case in the manufacture of biochar. The effect of particle size will be further discussed in sections 3.2.2 and 3.2.3.

3.2.1.6 Density and Porosity

The basic density (oven-dry weight divided by green volume (Kininmonth & Whitehouse, 1991)) of rods of radiata pine wood (containing both earlywood and latewood) having a diameter of 2 cm and various length (0.9 to 2.3 cm) were determined with a GeoPyc 1360 Envelope Density Analyser from Micromeritics (Norcross, GA, USA). Before each run, a blank run was performed to obtain the volume of the embedding material called DryFlo. The consolidation force was 51 N, and 5 cycles were applied to determine the volume; before the 5 cycles were 3 preparation cycles carried out to assure the optimum arrangement of DryFlo grains around the sample. The results are shown in Table 3-10.

Table 3-10. Porosity, basic and apparent density of radiata pine wood.

	Basic density in kg/m^3	**Apparent density in kg/m^3**	**Porosity**
μ	450.12[a]	1450.5[b]	0.690
σ	25.52	3.6	
CV	0.057	0.002	

Note. *CV* = coefficient of variation; μ = average; σ = standard deviation.
[a]average of 9 samples. [b]average of 10 cycles.

The basic density in Table 3-10 conforms with the average of the basic density of earlywood and latewood of radiata pine wood, which is 350 and 550 kg/m^3, respectively, as reported by Kininmonth and Whitehouse (1991). Table 3-10 also includes the apparent density (skeletal density) of the wood, which was determined by Micromeritics Analytical Services (Norcross, GA, USA) with a Micromeritics (Norcross, GA, USA) AccuPyc II 1340 FoamPyc V1.06 using Helium as analysis gas in a 35 cm^3 chamber. The value of 1450.5 kg/m^3 compares to the 1500 kg/m^3 used in

literature for modelling pyrolysis of wood (Ratte, Marias, Vaxelaire, & Bernada, 2009). The porosity, ε, was subsequently calculated from both values, basic (ρ_{basic}) and apparent ($\rho_{apparent}$) density according to the following equation:

$$\varepsilon = \left(1 - \frac{\rho_{basic}}{\rho_{apparent}}\right) \cdot 100 \ . \tag{3.7}$$

3.2.2 Laboratory Scale Thermogravimetric Analysis

Lab scale TGA was performed with the equipment described in 3.2.1.4. It consists of a horizontal furnace that surrounds the horizontal dual beam balance mechanism measuring the weight of the sample and reference pan. Heat transfer occurs by conduction (through the gas), and convection as a purge gas flow is applied through the centre of the furnace surrounding the balance beams to transport the decomposition products away. Radiation plays an increasing role at higher temperatures. The temperature of the sample and the reference crucible are measured by a thermocouple that is positioned directly underneath each crucible within the ceramic beam, allowing differential temperature measurements. The temperature profile of the samples is controlled by the sample thermocouple (S. Shamis, personal communication, November 13, 2016)

After the proximate analysis discussed above, a large number of further TGA experiments were carried out with different particle characteristics in order to study intra- and extra-particle char formation. It is these trials which are presented below. All experiments were carried out at a heating rate of 5 °C/min to a highest treatment temperature, *HTT*, of 700 °C as this is typically the maximum temperature applied in the manufacture of biochar. The *HTT* was later adjusted to 750 °C due to the fact that the final set temperature was never achieved in the TGA. The temperature programme is given in Table 3-11.

Table 3-11. Temperature programme of pyrolysis experiments in the laboratory scale TGA.

Step	Atmosphere[a]	Temperature in °C	Heating rate in °C/min	Hold time at final temperature in min
1	N_2	Room temperature→25	5	30
2	N_2	25→700 (750)[b]	5	0

Note. TGA = thermogravimetric analyser.

[a]applied gas flow rate is 20 ml/min. [b]temperature was later adjusted to 750 °C as the final set temperature was never achieved in the TGA.

The TGA was operated at atmospheric pressure, and as indicated in Table 3-11, a nitrogen purge gas flow of 20 ml/min was applied to ensure an inert atmosphere. The initial holding time at 25 °C also guaranteed that all the air was purged out of the system before pyrolysis started. In some cases, once the pyrolysed sample was cooled back to RT, a proximate analysis was carried out on the char (according to the method given in Table 3-5). Again the results were adjusted for the ash content determined by ROI discussed in 3.2.1.4. Depending on whether experiments were 'with' or 'without' a lid, the subsequent proximate analysis was also carried out 'with' or 'without' the lid. This, however, had no impact on the results as shown in chapter 7, which deals with the analysis of the char.

To investigate intraparticle secondary char formation a range of different sample sizes and shapes were pyrolysed in crucibles without a lid. These were thin shavings, cuboid and cylindrical samples of *pinus radiata*. The manufacture and properties of these samples have been discussed in 3.2.1. Thin slices, produced by hand planing (in the grain direction) and cut with the help of a scalpel, were positioned in the crucible so that the grain direction was horizontal. Originally, pine shavings of various thicknesses were planned as stripes of length 20 to 30 mm which naturally rolled themselves up. These had a width of approximately 4 mm to fit in the crucibles of the lab scale TGA (see 3.2.1.4) as shown in Figure 3-2 a.

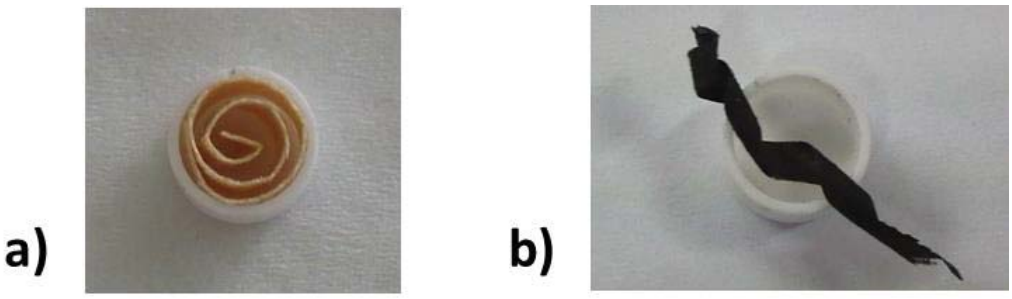

Figure 3-2. Original positioning of cut pine shavings. a) before and b) after pyrolysis to 700 °C. The crucible is an Alumina crucible with a diameter of 5 mm and height of 4 mm.

However, during pyrolysis the sample shrunk and the internal tension caused the "curl" to extend like a spring, Figure 3-2 b), which made weighing inaccurate as it touched the reference crucible. Therefore, small strips were cut to a length of approximately 5 to 10 mm, Figure 3-3 a), and positioned next to each other, Figure 3-3 b).

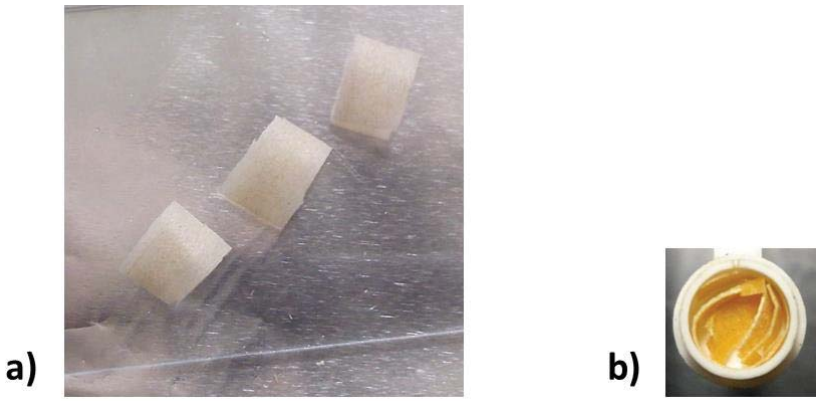

Figure 3-3. Final positioning of cut pine shavings. a) Small strips of radiata pine with a length of approximately 5 to 10 mm and a width/height of ≈ 4 mm. b) Positioning of shavings in crucible. The crucible is an Alumina crucible with a diameter of 5 mm and height of 4 mm.

Cuboid samples are essentially thicker slices, and are positioned according to the slices in the crucible with the grain direction being horizontal. The characteristic dimension for the slices and cuboid samples was chosen as their thickness orthogonal to the grain, because heat and mass transfer is reduced in this direction as discussed in chapter 2. As far as it was practically possible the samples were prepared to have a length to characteristic dimension ratio larger than 4 in order to reduce end effects (Alves and Figueiredo, 1989, as cited in Grieco & Baldi, 2011). The cylindrical samples, with the grain direction along its axis, could only be placed vertically in the crucible, and the characteristic dimension is their diameter. The dimensions of the samples were measured with a Carrera Precision calliper (resolution 0.01 mm). The thickness of the slices and cuboid samples was averaged over their entire length.

For investigating the impact of extractives on pyrolysis, shavings were produced from the heartwood by planing, and subsequently the sections containing the resin cut out with a scalpel, as shown in Figure 3-4.

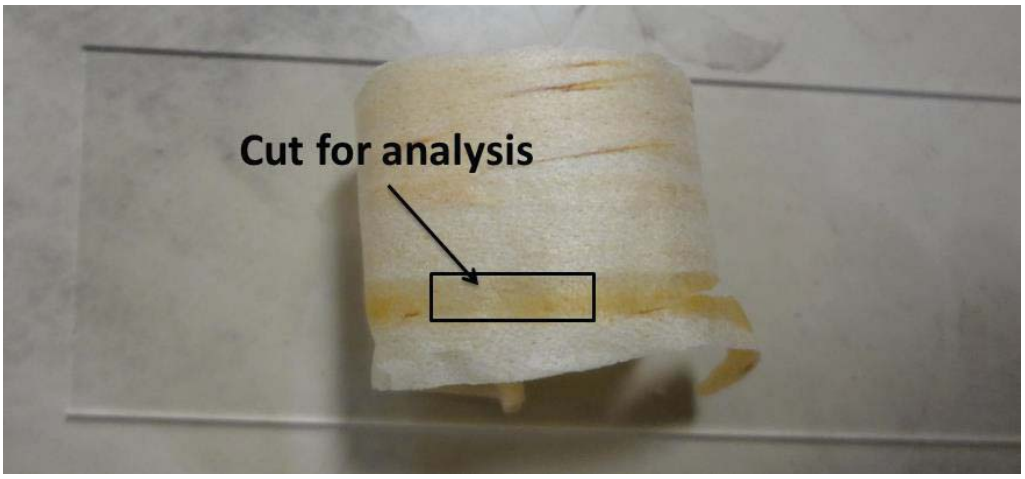

Figure 3-4. Preparation of heartwood stripes containing resin.

The TGA data of several runs was averaged to establish the difference between runs 'with' and 'without' a lid. To do this, data corresponding to a common temperature had to be selected, as generally the temperatures at which data were recorded never coincide due to fluctuating starting temperatures and floating point arithmetic. Thus, a Matlab (MathWorks, Natick, MA, USA) program (Matlab version R2011b) was written that selects the closest data set corresponding to a temperature in the desired range 30 to 700 °C at 0.5 °C increments, which then could be used to determine the average. The lower temperature was chosen as 30 °C as at this temperature no pyrolysis occurs and it is common to all pyrolysis experiments, Table 3-11. All the air-dry yields reported in this research are based on the initial weight at 30 °C. The Matlab code is given in Appendix B.2. It is important to note that the raw data output by the TGA was subsequently smoothed with the TGA software TA Universal Analysis 2000 (TA Instruments, New Castle, Delaware) using a least square average. The applied smoothing region width was 10 °C.

Additionally, pyrolysis experiments employing a torrefaction step were carried out in the laboratory TGA in crucibles without a lid filled with sawdust. The settings were the same as in the experiments above except that the temperature was held for 60 min at the torrefaction temperatures of 200, 250, and 300 °C before they were further heated at 5 °C/min to the *HTT*. The holding time at the torrefaction temperature is

based on the work of Wigley, Pang, and Yip (2014), who suggested a minimum torrefaction time of 20 min.

3.2.3 Macro-Thermogravimetric Analysis

Macro-TGA was carried out in a custom made Binder Burner (see Appendix B.3.1, Figure B-1) at Callaghan Innovation (Lower Hutt, New Zealand), which was modified to accommodate the pyrolysis experiments in this research as follows. A stainless steel crucible (see Appendix B.3.1, Figure B-2) with a diameter of 130 mm and a height of 75 mm was built in the Massey University workshop (Palmerston North, New Zealand) to facilitate large cylindrical samples (d = 120 mm, h = 60 mm). The sidewall of the crucible was slotted to allow the escape of decomposition products. Furthermore, a condenser (see Appendix B.3.1, Figure B-3) was built in the Massey University workshop to eliminate the tars from the pyrolysis off-gases, along with an exhaust burner (see Appendix B.3.1, Figure B-4) to avoid the accumulation of flammable/explosive gases before releasing them into the ventilation system. The condenser and exhaust burner have both been designed to cope with samples having the maximum dimensions that the Macro-TGA can accommodate. A special feature of the exhaust burner is, that if it fails to combust the pyrolysis gases, it dilutes them to below 50 % of the lower flammability limit of LPG, in air, which is 1.81 % (vol/vol) (Mishra & Rahman, 2003). To achieve this it consists of an inner pipe, the combustion pipe, and an outer pipe, the dilution pipe. The combustion pipe has a liquefied petroleum gas, LPG, pilot burner as well as a spark plug, which continuously creates a spark, to light the gases. The combustion pipe supplies the air necessary for complete combustion, as well as some excess air. Cooling the flue gases to about 75 °C is the task of the outer air supply. It can also provide additional air to the flame if required, and as indicated before in case the pilot flame and spark plug fail to light the pyrolysis gases, the dilution pipe carries enough air to dilute the flammable pyrolysis gases to a safe concentration.

The pyrolysis experiments were run up to 700 °C at 5 °C/min in a nitrogen atmosphere (flow rate 150 ml/min) at atmospheric pressure. However, it was discovered that the actual heating rate in the Macro-TGA was slightly higher at 5.5 °C/min. Heating occurs by a resistive heater positioned in the sidewall of the cylindrical furnace (see Appendix B.3.1, Figure B-2). A single thermocouple in central position on the lateral surface controlled the furnace temperature (T_s in Figure 3-5).

Before each experiment commenced, the Macro-TGA pyrolysis chamber was twice evacuated and refilled with nitrogen in order to ensure that an inert atmosphere was present. This was necessary because the Pyrolyser chamber lay within a much larger volume of the bell-jar that sealed the binder burner unit (see Appendix B.3.1, Figure B-1).

Similarly to the lab scale TGA experiments, the wood cylinders, with grain direction along their axis, could only be placed on their flat surface, resulting in a vertical grain direction during pyrolysis.

In addition to the weight-loss experiments, thermocouple runs were performed; that is, up to four type K thermocouples (1.5 x 500 mm from Labfacility Ltd, Sheffield, UK) were evenly distributed across the radius of the wood cylinder depending on the size of the cylinder. In Figure 3-5 a schematic diagram is given, illustrating the distribution of two thermocouples over the radius with the other two used to record the temperature in the crucible.

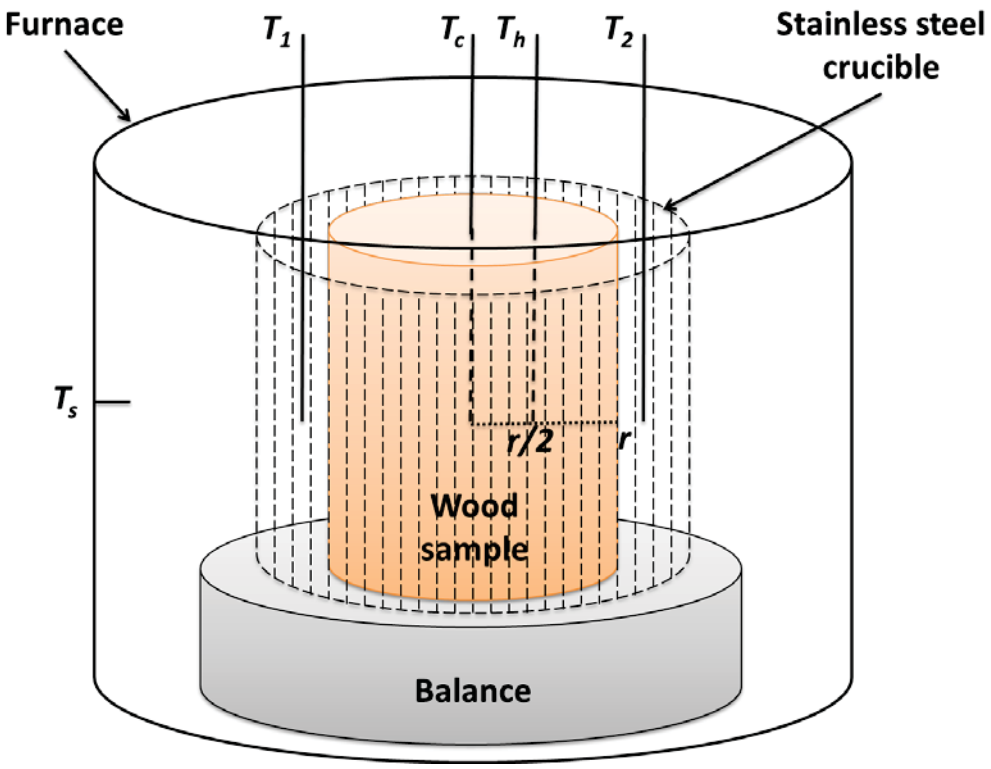

Figure 3-5. Scheme of Macro-TGA with loaded sample. r = radius; T_c = centre temperature; T_h = temperature halfway between centre and surface; T_s = surface temperature used for controlling heat input; T_1 and T_2 additional thermocouples to record more temperatures along the radius in large samples or to record the temperature in the crucible in case of small samples.

All the samples had a height of 60 mm and varying diameters of 20, 30 and 74 mm. The thermocouple holes were drilled 35 mm deep and provided a snug fit, as shown in Figure 3-6 a).

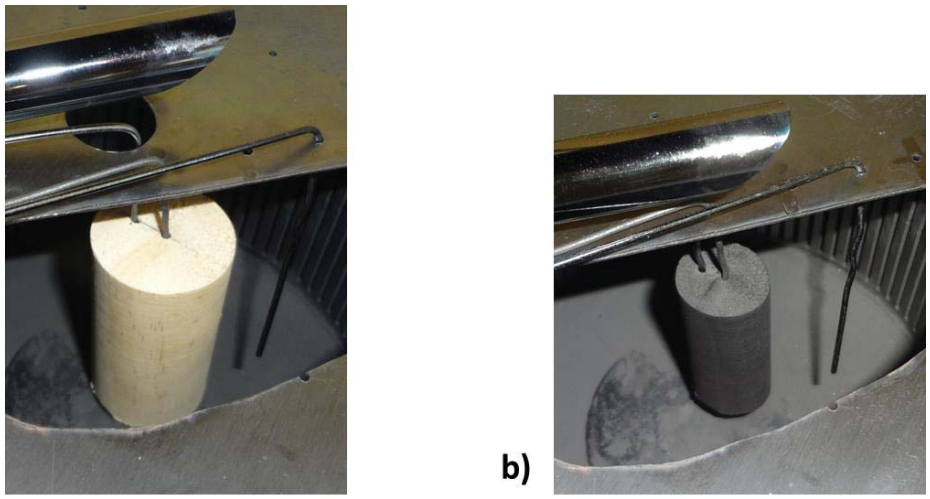

Figure 3-6. Thermocouple positioning. a) Before and b) after pyrolysis to 700 °C. Initially the sample had a diameter of 30 mm and a height of 60 mm. After pyrolysis the sample had a diameter of 21 mm and a height of 47 mm.

During pyrolysis the sample shrank onto the thermocouples to give a tight fit and, as they shrank, samples were lifted away from the weigh scales, which is why gravimetric and thermocouple runs had to be done separately. The temperature readings were smoothed by fitting a polynomial equation to the heater temperature with time to eliminate noise in the signals, which was important for plotting derivatives.

The extended operating procedure applied at Callaghan Innovation is attached in Appendix B.3.2.

The shrinkage (Figure 3-6 b)) in % of the samples used in the Macro-TGA was calculated according to:

$$Shrinkage = \frac{(dim_{in} - dim_{char})}{dim_{in}} \cdot 100 \ , \qquad (3.8)$$

where dim_{in} is the dimension of interest of the initial feedstock in mm, and dim_{char} is the respective dimension of the charred sample in mm. For measuring the characteristic dimensions, that is diameter in radial and tangential direction and sample height, the Carrera Precision calliper mentioned in 3.2.2 was used. The diameter in radial and tangential direction was determined over the length of the sample at three positions (top, middle, and bottom). The height was measured at four opposing point's perpendicular to each other to get a representative measurement, that is two in tangential and two in radial direction of the growth rings. Subsequently the volume shrinkage was calculated

by substituting the volume of the feedstock and char for dim_{in} and dim_{char} respectively.

3.2.4 Drum Pyrolyser

A supervised 4th year engineering project was carried out to investigate macroscopic structural changes during pyrolysis with the title "Fracturing of Wood During Pyrolysis" (Bashir, 2012). For this study a lab scale gas-fired drum pyrolyser was used (see Appendix B.4.1, Figure B-5), which had to be modified to meet the requirements of this research (see Appendix B.4.2). Small beams of radiata pine with a length of approximately 175 mm and three different cross-sections (15 x 15 mm, 32 x 32 mm, and 67 x 67 mm) were pyrolysed (see Appendix B.4.1, Figure B-6). The samples were cut in two different ways to obtain beams with grain direction parallel and perpendicular to the length of the beam named "grain" and "against grain" respectively, as shown in Figure 3-7.

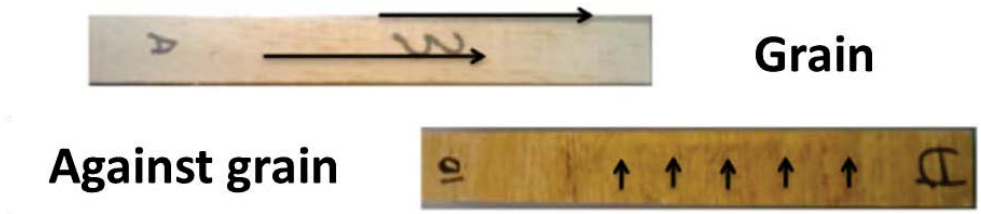

Figure 3-7. Cutting direction of sample beams. 'Grain' means the sample beams were cut to have the grain direction parallel to the beam and 'against grain' means the grain direction is perpendicular to the length of the beam. Picture taken from Bashir (2012).

The samples were either oven-dried at 105 °C for approximately 24 h or soaked in water till no more weight change occurred (approximately 1 week). It was aimed to pyrolyse them at three different *HTT's*, that is 300, 500, and 700 °C. However, it was difficult to control this temperature for two reasons; (i), as the control thermocouple was situated inside the sample holder (see Figure B-6 in Appendix B.4.1) and thus was shielded from the hot drum wall; and (ii), the fact that pyrolysis is exothermic, which is discussed in more detail in chapter 5. Nevertheless, the temperature trend was still maintained, that is the sample was exposed to a low, medium, or high *HTT*.

3.2.5 Hot Stage Experiments

Hot stage experiments were carried out as a subproject of this PhD in a supervised 4th year engineering project titled "Hot Stage for Pyrolysis" (Mohd-Hanif, 2013) to visualise the changes occurring during pyrolysis. An HCS621V precision heating/cooling stage with a MK1000 temperature controller, WinTemp software, and a C300W-U water chiller from Instec (CO, USA) were used. The hot stage was installed on a BH microscope (Olympus, Japan), and pictures were taken with a charge-coupled device (CCD) camera MITO2-2MC (Instec, CO, USA) attached to the microscope, and operated with WinDV software from Instec. The samples analysed were slices (approximately 70 μm thick) of radiata pine wood (sapwood and heartwood) obtained by planing along the grain of radiata pine boards. All samples were air-dried. Pyrolysis was viewed at 4x magnification. Experiments were done under nitrogen atmosphere and vacuum (-60 kPa). In the case of nitrogen a purge flow of 5 l/min was applied to provide an inert atmosphere and prevent clouding of the viewing area by the volatile pyrolysis products. The wood was heated from room temperature to 500 °C at 5, 10, and 20 °C/min. The change in pore area and width was measured with ImageJ (National Institutes of Health, MD, USA). Three closed pores that remained intact till the end of pyrolysis were chosen for pore area analysis per sample.

3.2.6 Evolved Gas Analysis

Evolved Gas Analysis, EGA, was carried out with a Frontier Laboratories Ltd (Fukushima, Japan) Multi-Shot Pyrolyser Model EGA/PY-3030D with Auto-shot sampler Model AS-1020E connected to a Shimadzu (Kyoto, Japan) Gas Chromatograph Mass Spectrometer GCMS-QP2010 Ultra. The Gas Chromatograph, GC, and Mass Spectrometer, MS, parameters are given in Table 3-12.

Table 3-12. Py-GC/MS parameters for EGA.

Py parameters	**GC parameters**	**MS parameters**
Initial Temp.: 40 °C	Column Oven Temp.: 300 °C (Isothermal)	Ionization Mode: EI at 70 eV
Initial Hold Time: 0 min	Injection Temp.: 300 °C	Ion Source Temp.: 230 °C
Heating Rate: 5 °C/min	Injection Mode: Split	Interface Temp.: 300 °C
Final Temp.: 700 °C	Flow Control Mode: Linear velocity	Solvent Cut Time: 0 min
Final Hold Time: 1 min	Pressure: 69.2 kPa	Micro Scan Width: 0 u
Interface Temp.: 300 °C (Auto[a])	Total Flow: 135.1 ml/min	Start Time: 0 min
	Column flow: 0.73 ml/min	End Time: 140 min[b]
	Linear Velocity: 117.8 cm/s	Acq. Mode: Scan
	Purge Flow: 3.0 ml/min	Event Time: 0.5 s
	Split Ratio: 180	Scan Speed: 1111
		Start *m/z*: 2
		End *m/z*: 500

Note. EGA = Evolved Gas Analysis; EI = Electron Ionization; GC = Gas Chromatograph; MS = Mass Spectrometer; *m/z* = mass-to-charge ratio; Py = Pyrolysis.

[a]Auto means that the interface temperature is set automatically 100 °C above the furnace temperature but 300 °C is the maximum temperature. [b]based on Py-program.

The samples were placed in deactivated stainless steel crucibles, Eco-cup LF (*d*=4 mm; *h*=8 mm), which were flame cleaned with a torch for 1-2 seconds, that is until the cup was slightly red glowing. After the sample cup was cooled to room temperature it was filled with 6.0 ± 0.1 mg air-dried pine sawdust and gravity fed into the pyrolyser furnace. In the furnace the sample was heated at 5 °C/min from 40 to 700 °C, where it was held for one minute. A continuous Helium flow was applied to provide an inert pyrolysis atmosphere and to carry the volatile pyrolysis products to the splitter, where they were split according to the split ratio shown in Table 3-12. A portion was vented through the split vent and the rest carried through the GC column to the MS detector. GC/MS analysis commenced immediately with the heating profile of the pyrolyser furnace. A deactivated Ultra ALLOY-DTM-2.5N EGA column (l = 2.5 m; ID = 0.15 mm; no stationary phase) from Frontier Lab was employed for the EGA experiments. More detail about the Py-GC/MS is given in chapter 6.

3.2.7 Summary of Experimental Plan

In Table 3-13 is the experimental plan summarised to give an overview.

Table 3-13. Experimental plan.

Objective	Experimental plan	Measurements performed
Establish the role and extent of secondary char formation		
• Induced by external means	• Pyrolyse sawdust and planed heartwood slices with varying initial weights in the labscale TGA in crucibles with and without a lid	• Proximate analysis of wood • Weight loss with temperature/time • Heat flow (discussed in chapter 5)
• Induced internally	• Pyrolyse particles of varying size/weight and shape of earlywood and/or latewood in the labscale TGA and Macro-TGA	• Weight loss with temperature/time • Heat flow of laboratory TGA experiments (discussed in chapter 5)
Establish relationship between char yield and fixed carbon yield	• Perform proximate analysis on the previously obtained char of selected labscale TGA and Macro-TGA experiments	• Proximate analysis on the char

(continued)

Objective	Experimental plan	Measurements performed
Analyse structural changes during pyrolysis	• Observe the macroscopic structural changes as a function of sample size in the Macro-TGA experiments • 4th year engineering project into cracking and fracturing during pyrolysis of wood as a function of sample size, HTT, grain direction and moisture content • 4th year engineering project into the microscopic structural changes	• Qualitatively and quantitatively analyse cracks and fractures • Measure shrinkage in longitudinal, tangential and radial direction • Analyse microscopic structural changes in a microscopic hot stage
Investigate relationship between derivative weight loss curves and internal sample temperature to draw conclusions about transfer limitations and thermal lag	• Repeat Macro TGA pyrolysis experiments but this time measure instead of the weight loss the internal temperature	• Measure the sample centre temperature and the temperature at half radius of the cylindrical samples (h=60 mm; d=20, 30 and 74 mm) used in the Macro TGA weight loss experiments
Investigate the role of time-temperature history and torrefaction on char formation	• Pyrolyse sawdust in crucibles without a lid in the lab TGA according to conditions in the previous experiments except this time include an isothermal step for 60 min at varying temperatures (200, 250 and 300 °C) after which the normal temperature programme recommences	• Weight loss with temperature/time

3.3 Results and Discussion

3.3.1 Extraparticle Secondary Char Formation

Literature shows that employing a lid restricts the escape of the volatile pyrolysis products from the pyrolysis zone leading to secondary char formation (L. Wang et al., 2013; L. Wang et al., 2011). In this study, this process is referred to as extraparticle secondary char formation due to the fact that the vapour-phase residence time is increased by external means, i.e. a lid. This section deals with the further analysis of the proximate analysis results to establish the role and extent of these extraparticle secondary char forming reactions over the whole pyrolysis range to a maximum temperature of 700 °C.

Figure 3-1 shown at the beginning of the chapter reveals that more char results in thermogravimetric analysis (TGA) experiments when the sample crucible was capped with a lid. The weight loss difference is evident right from the beginning of pyrolysis to about 500 °C. This indicates that secondary reactions are present over the entire pyrolysis range associated with the majority of the weight-loss.

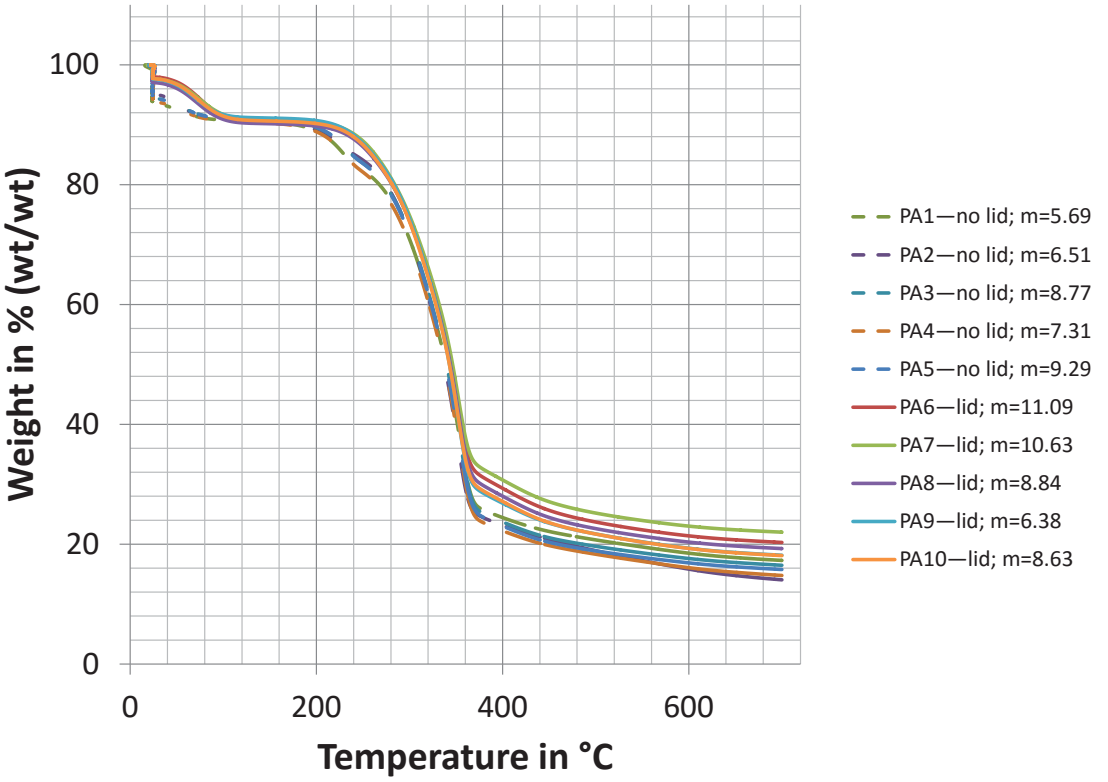

Figure 3-8. Weight-loss curves of the proximate analysis runs in section 3.2.1.4. Legend: Run number—lid or no lid; dry weight in mg. m = dry weight in mg determined for lid and no lid at 152 and 126 °C respectively; PA = proximate analysis.

Similarly to Figure 3-1, containing averaged results, the individual results of Figure 3-8 show a weight loss difference over the whole pyrolysis range, extending from approximately 150 to 700 °C. In both figures, it appears that the char forming secondary reactions are completed below 500 °C, and the difference above 380 °C in Figure 3-8 is a mere result of them having taken place. Apart from this, Figure 3-8 reveals that there is considerable scatter within each set of experiments. The scatter could be due to the heterogeneity of the starting material or the varying amounts of starting material, which has also been reported to affect the char yield (L. Wang et al., 2013; L. Wang et al., 2011). To eliminate quantity as a variable, Figure 3-9 shows pyrolysis experiments which heated approximately the same amount of feedstock with and without a lid to 700 °C.

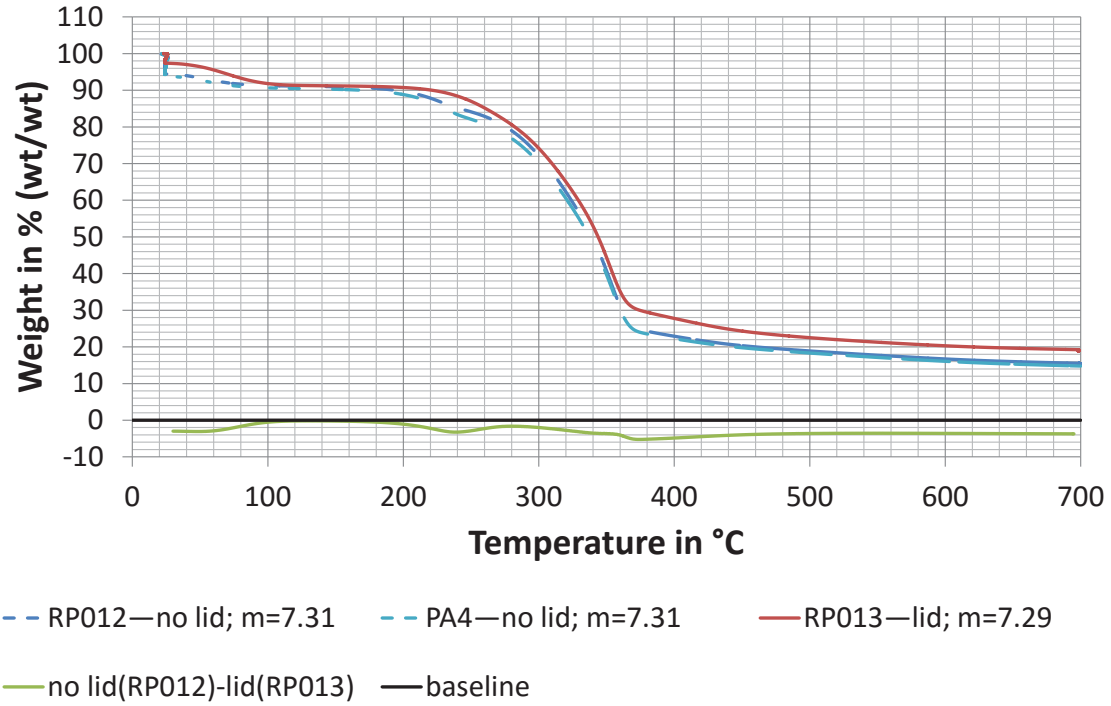

Figure 3-9. Weight-loss curve of pyrolysis experiments to 700 °C with and without a lid having approximately the same initial sample weight. The "no lid-lid curve" illustrates the difference between the two cases lid and no lid. Legend: Run number—lid or no lid; dry weight in mg. m = dry weight in mg determined for lid and no lid at 152 and 126 °C respectively.

Figure 3-9 indicates that the above observed difference is indeed caused by the presence or absence of the lid and not just by varying sample amounts. To get an idea of the repeatability and the influence of sample heterogeneity the proximate analysis run "PA4" without a lid has been included in Figure 3-9, which had the identical initial sample weight to run "RP012" without a lid, showing that this seems to have a minor effect. The difference curve in Figure 3-9 illustrates the difference in a more comprehendible way. Below 100 °C there is a difference, which is associated with the removal of moisture, indicating possible transfer limitations or increased thermal lag in the samples with a lid. It disappears above 100 °C once drying is completed and the samples attained the same pre-pyrolysis weight fraction. At temperatures larger than 150 °C a difference re-emerges, extending to the end of the pyrolysis experiments. That the magnitude of the difference is similar below 100 °C and above 400 °C is coincidence. Analogous results are obtained when comparing runs in Figure 3-8 having similar initial weights (see Appendix B.5.1 Figure B-7 and Figure B-8). Consequently, the proximate analysis experiments in Figure 3-8, and the two additional runs in Figure 3-9 were averaged to obtain the averaged curves shown in Figure 3-1 and Figure 3-10.

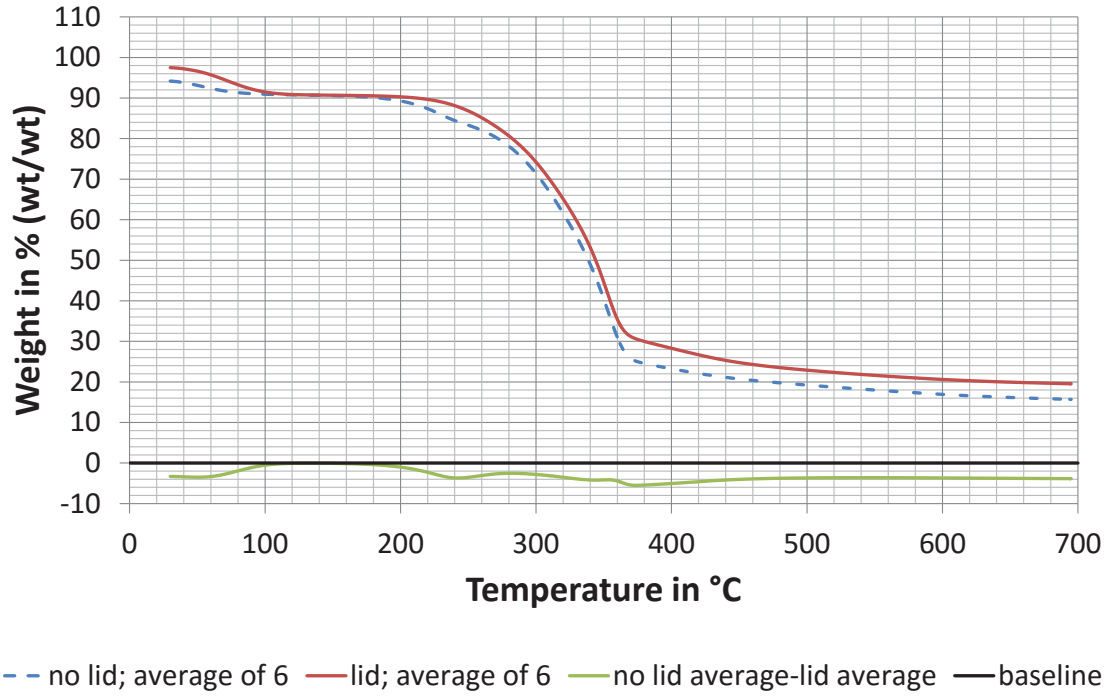

Figure 3-10. Average weight-loss curve of pyrolysis experiments with and without a lid to 700 °C. The "no lid-lid curve" illustrates the difference between the two cases lid and no lid.

To attain a better understanding of the relationship between initial sample mass and the presence or absence of a lid on the char yield a simple correlation analysis was done on the char yield at 695 °C. The temperature of 695 °C was chosen as not all the experiments attained 700 °C as mentioned in 3.2.2. The raw data is given in Appendix B.5.2 Table B-3. It is important to note that this data contains additional values from extra sets of experiments not previously discussed. They were not included for obtaining the average curves in Figure 3-1 and Figure 3-10, due to the fact that the data was slightly different in the temperature range 150 to 250 °C, which is associated to the second peak of the no lid curve shown in Figure 3-1. The difference and their cause is discussed further below. Despite this they showed the same trends and similar yields (see Appendix B.5.1 Figure B-9 and Figure B-10) for which reason they were included in the statistical analysis to obtain a more meaningful representation. The results of the correlation analysis are given in Table 3-14.

Table 3-14. Correlation analysis.

	Char yield	Lid/no lid	Dry sample weight[a]
Char yield	1		
Lid/no lid	0.605	1	
Dry sample weight[a]	0.244	0.014	1

Note. The analysis was performed with Microsoft Excel (Microsoft, Redmond, WA, USA).
[a]Dry weight was determined for lid and no lid at 152 and 126 °C respectively.

Table 3-14 confirms the previous findings that there is a greater correlation between the yield of char and the presence and absence of a lid than the initial dry sample mass. But it also shows that the yield of char is positively correlated with the initial dry sample mass, as shown in Figure 3-11.

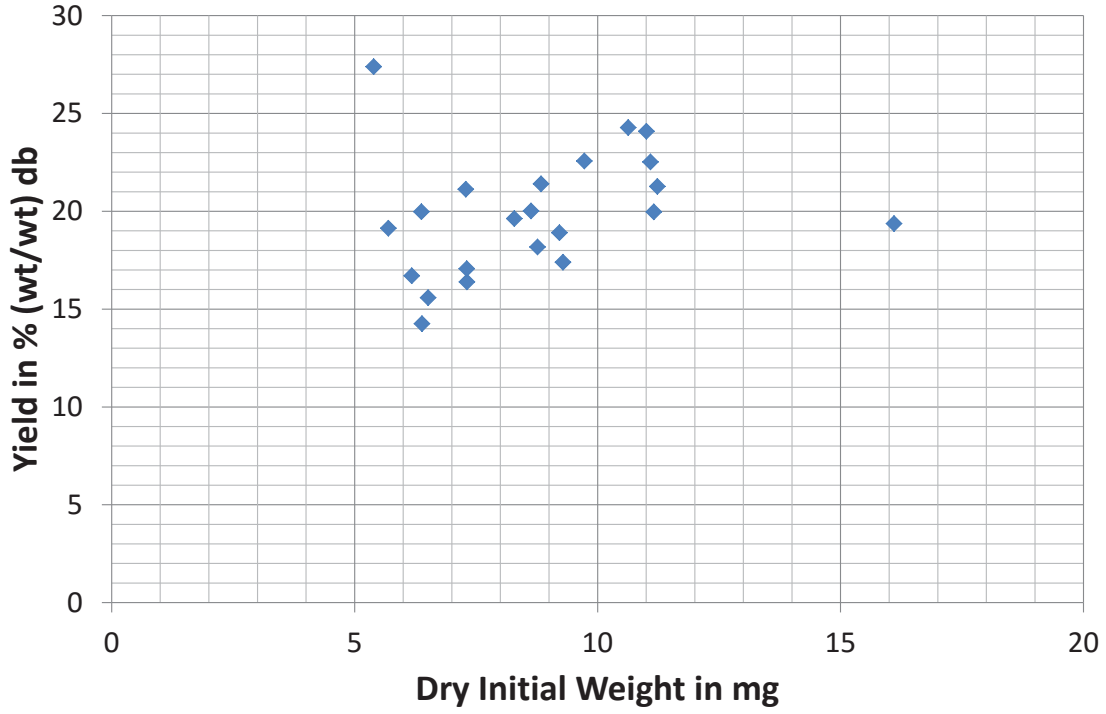

Figure 3-11. Correlation plot between char yield at 695 °C and the initial dry sample mass. The dry weight was determined for lid and no lid experiments at 152 and 126 °C respectively. db = dry basis.

Figure 3-11 shows the presence of two possible outliers; their relevance will be returned to later. Based on these findings a multiple regression analysis was carried out on the data in Appendix B.5.2 Table B-3 with Microsoft Excel (Microsoft, Redmond, WA, USA). The results are shown in Table 3-15, Table 3-16, and Table 3-17.

Table 3-15. Regression statistics.

Multiple R	R^2	Adjusted R^2	Standard Error	Observations
0.6488	0.4209	0.3600	2.4973	22

Note. The analysis was performed with Microsoft Excel (Microsoft, Redmond, WA, USA). R = correlation coefficient; R^2 = coefficient of determination.

The important value in Table 3-15 is the adjusted coefficient of determination, R^2, as the analysis was based on two variables (initial dry mass and lid/no lid). The value is relatively low stating that the model explains only 36 % of the variation in the yield of char. However, moving on to the analysis of variance in Table 3-16 the P-value of the F-test shows that the model is significant, as it is below the pre-selected significance level of 0.05.

Table 3-16. Analysis of variance.

	df	SS	MS	F	Significance F[a]
Regression	2	86.1170	43.0585	6.9043	0.0056
Residual	19	118.4923	6.2364		
Total	21	204.6093			

Note. The analysis was performed with Microsoft Excel (Microsoft, Redmond, WA, USA). The significance level was set to 0.05. df = degrees of freedom; F = F-test for null hypothesis; MS = Mean sum of squares; SS = sum of squares.

[a]P-value.

Table 3-17. Coefficient analysis.

	Coefficients[a]	Standard error[b]	t Stat	P-value	Lower 95%	Upper 95%
Intercept	15.4687	2.0413	7.5777	3.71E-07	11.1962	19.7413
Lid/no lid	3.6668	1.0650	3.4432	0.0027	1.4378	5.8958
$m_{start,dry}$	0.2936	0.2178	1.3482	0.1935	-0.1622	0.7495

Note. The analysis was performed with Microsoft Excel (Microsoft, Redmond, WA, USA). The significance level was set to 0.05. Stat = statistics.

[a]least squares estimate. [b]least squares estimate of standard error.

The coefficient analysis in Table 3-17 reveals that only the intercept and the presence and absence of the lid are significant (P-value is 3.71E-07 and 0.0027 respectively). However, if the two outliers in Figure 3-11 are removed, the adjusted R^2 would increase to 0.60, the P-value of the F-test decrease to 0.0002, and both variables (initial dry weight and lid/no lid) were significant with the initial weight having the lower P-value

0.002 compared to 0.013 for lid/no lid. Again, the presence or absence of the lid would have a bigger impact on the model than the starting weight, as is the case in Table 3-17. Therefore, taking this into account along with literature, which suggests an impact of sample mass, it was decided to keep the sample mass as an important factor. The relationship between both factors is illustrated in Figure 3-12.

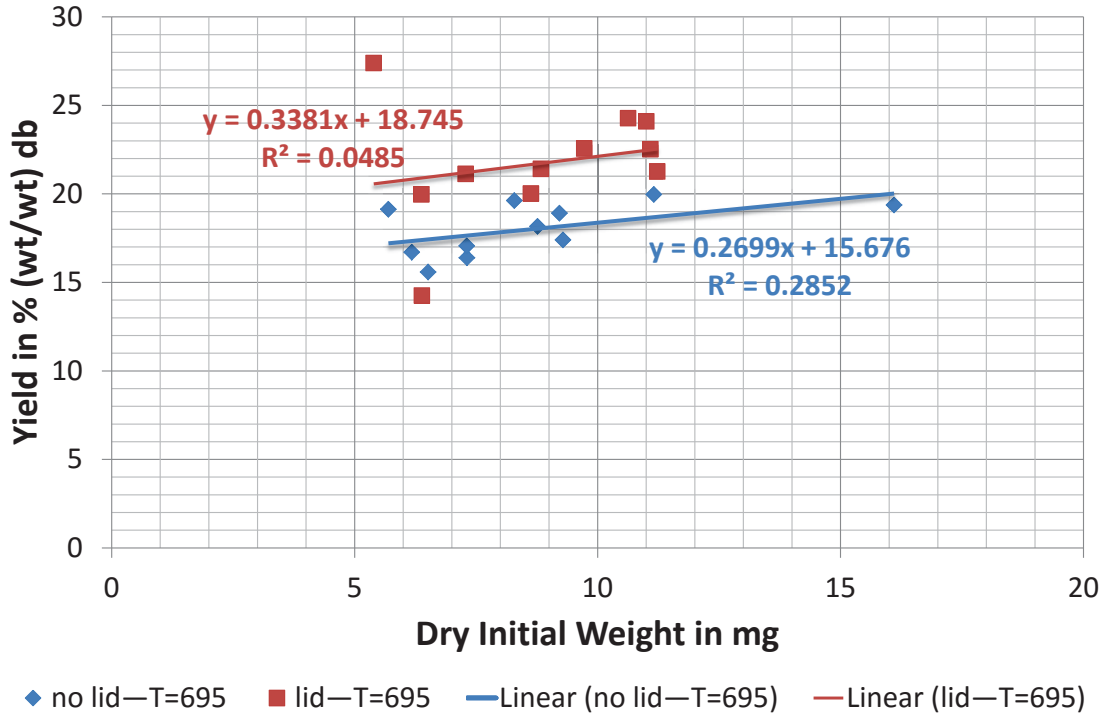

Figure 3-12. Char yield at 695 °C of pyrolysis experiments with and without a lid as a function of the initial dry sample weight. The dry weight was determined for lid and no lid experiments at 152 and 126 °C respectively. db = dry basis; R^2 = coefficient of determination.

The outliers have not been removed in Figure 3-12, as the cause is unknown and the investigated weight range was only small due to the limited capacity of the laboratory TGA. A possible reason could be sample heterogeneity, whose impact is elevated when using such small sample weights, as well as particle size distribution (effect of particle size is discussed in 3.3.2). Despite this, Figure 3-12 shows that the yield increases with the presence of a lid and sample mass, which is attributed in literature to increased secondary char formation (e.g. L. Wang et al. (2011)) but could also be due to more reactions that take place at lower temperatures for the larger samples as they increase the thermal lag. The increase in yield with increasing amount of feedstock could also indicate that secondary reactions are not only a function of vapour-phase residence time but also of concentration as proposed by Mok, Antal, Szabo, Varhegyi, and Zelei (1992).

The correlation between yield increase and sample size is further analysed by comparing the difference in the derivative weight curves of samples with high and low sample mass corresponding to high and low char yields respectively with the difference in the derivative weight curves between runs with and without a lid, Figure 3-1. An example for the case with and without a lid is depicted in Figure 3-13 and Figure 3-14 respectively.

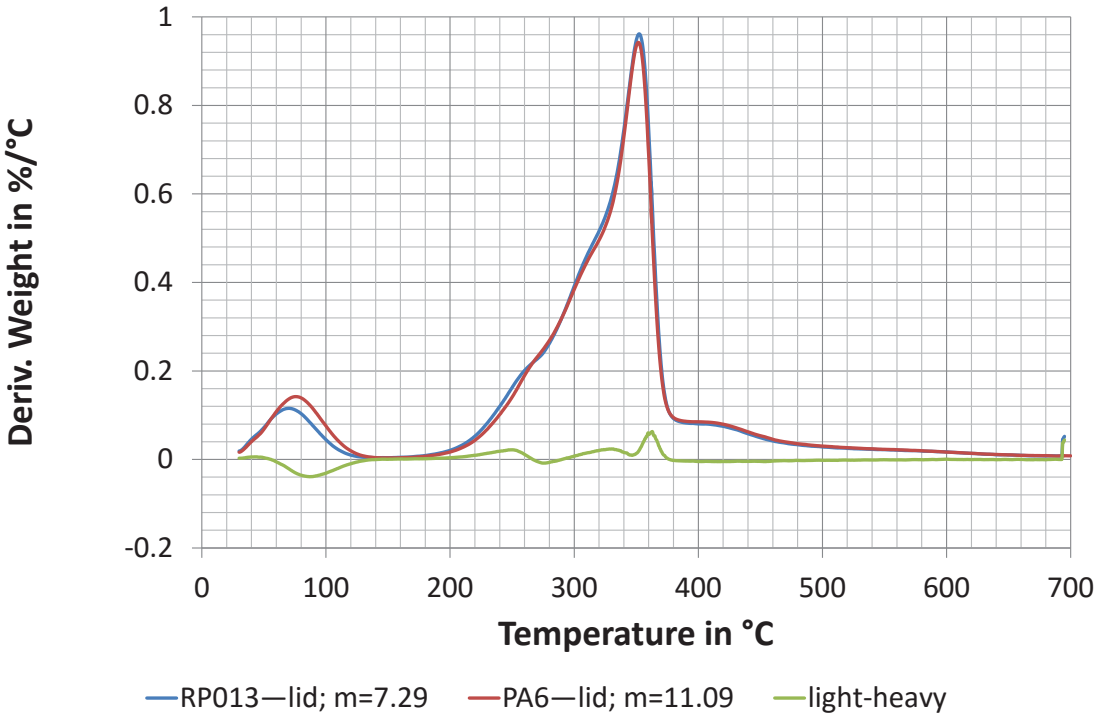

Figure 3-13. Difference between derivative weight curves of pyrolysis experiments with a lid that have differing initial sample weights correlating to yield differences caused by the varying feedstock weight. The "light-heavy" curve illustrates the difference between the two pyrolysis runs with differing initial weights corresponding to the difference curve "no lid-lid" in Figure 3-1. Legend: Run number—lid or no lid; dry weight in mg. m = dry weight in mg determined at 152 °C.

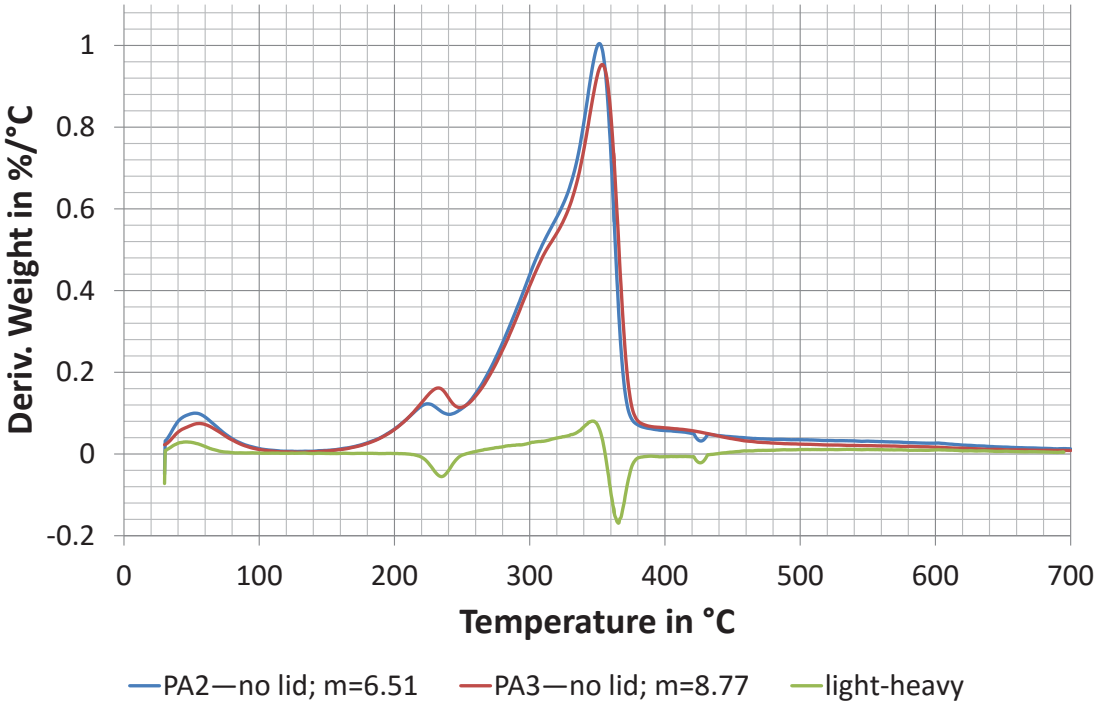

Figure 3-14. Difference between derivative weight curves of pyrolysis experiments without a lid that have differing initial sample weights correlating to yield differences caused by the varying feedstock weight. The "light-heavy" curve illustrates the difference between the two pyrolysis runs with differing initial weights corresponding to the difference curve "no lid-lid" in Figure 3-1. Legend: Run number—lid or no lid; dry weight in mg. m = dry weight in mg determined at 126 °C.

Figure 3-13 shows, similar to Figure 3-1, a shift of the moisture peak to higher temperatures for the heavier sample, which in this case is believed to be mainly due to increased thermal lag caused by the larger absolute mass of water as the maximum vapour pressure is limited by the lid to an overpressure of 61.4 Pa. However, such a peak shift towards higher temperatures is not present for the main weight loss region (140 to 500 °C) indicating that thermal lag plays a minor role at this stage. Contrary, in Figure 3-14, where no lid was present a slight shift in the main pyrolysis peak is visible but this was not detected in the other runs (see Figure B-18 to Figure B-20 Appendix B.5.3) and could be due to sample inhomogeneity. Thus it is believed that vapour phase residence time plays a more important role than thermal lag. It is important to note that the small jump around 700 °C in the derivative weight curve in Figure 3-13 is caused by the isothermal hold at the *HTT* for at least 30 min. The more subtle effects in the experiments without a lid (see Appendix B.5.3) corroborate the importance of vapour phase residence time as in this scenario the volatile pyrolysis products can relatively easily escape. Furthermore in the no lid experiments the shift in the moisture peak appears smaller than in the lid experiments highlighting the presence of transfer limitations and their effect on the weight loss curve. The reduced effect in the open lid experiments is confirmed by the lower slope of the linear regression model in Figure 3-12 for the no lid experiments compared to the lid experiments

To investigate the effect of sample heterogeneity planed slices of heartwood containing resin were pyrolysed in crucibles with and without a lid and compared to the respective pyrolysis runs employing sawdust, which is representative of the whole wood composition. The derivative weight curves for the cases no lid and lid are depicted in Figure 3-15 and Figure 3-16 respectively.

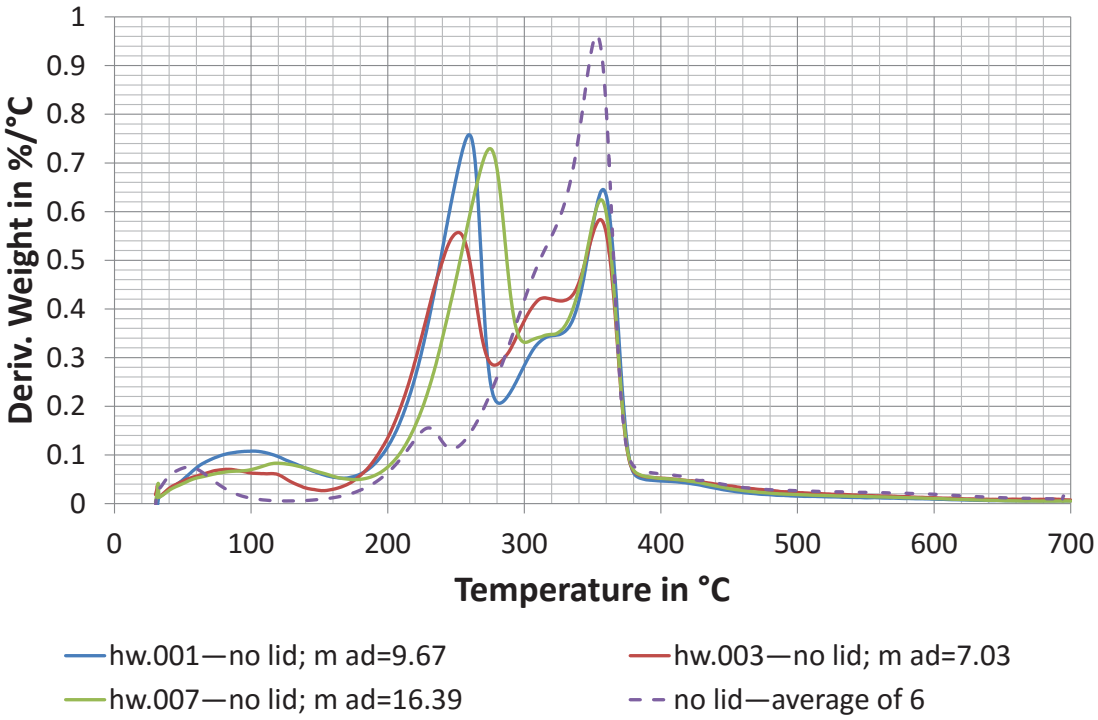

Figure 3-15. Comparison of derivative weight curves of planed heartwood strips containing resin with sawdust representative of the whole wood composition during pyrolysis without a lid. Legend: Run number—lid or no lid; air-dry weight in mg. m ad = air-dry weight in mg determined at 30 °C.

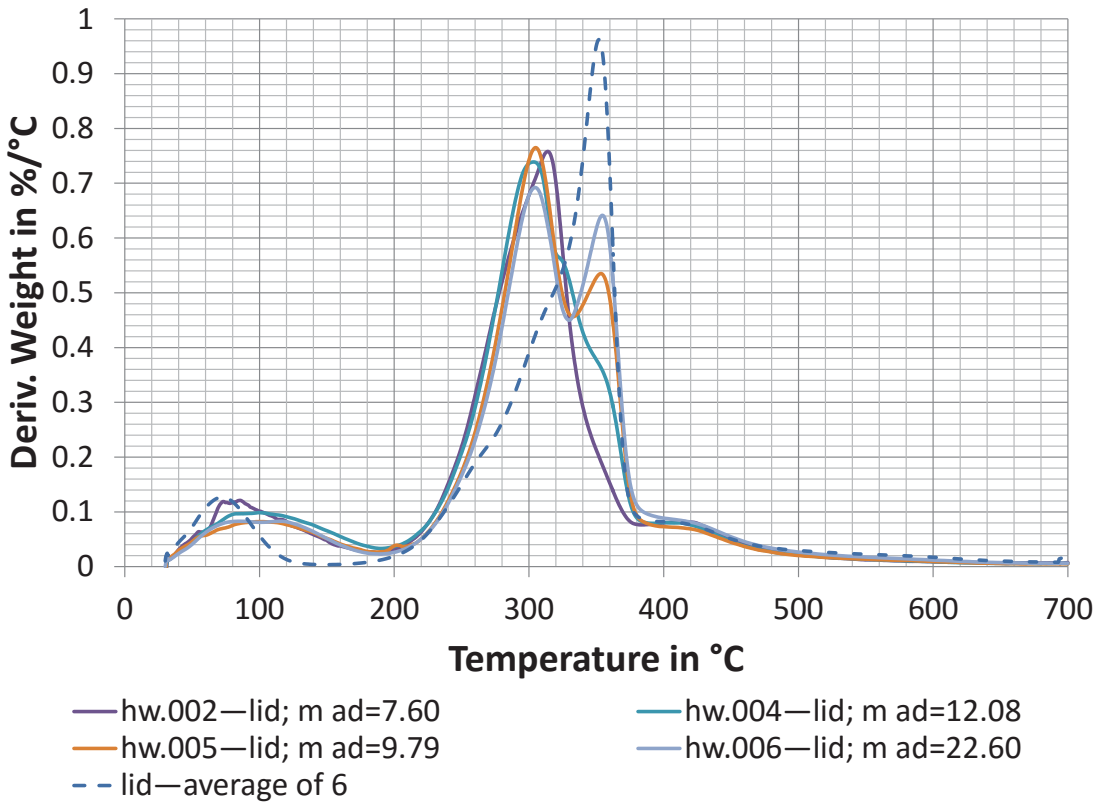

Figure 3-16. Comparison of derivative weight curves of heartwood strips containing resin with sawdust representative of the whole wood composition during pyrolysis with a lid. Legend: Run number—lid or no lid; air-dry weight in mg. m ad = air-dry weight in mg determined at 30 °C.

The open crucible trials in Figure 3-15 reveal a second peak around 230 °C, which is also observed in Figure 3-1, that is related to the extractives present in heartwood. This explains why there were differences existing in this peak between the first sawdust samples pyrolysed to 700 °C in Figure 3-1 compared to the additional experiments in Appendix B.5.1 Figure B-10, which were done approximately a year later; that is, during storage the extractives slowly volatilised and disappeared, as essentially everything that has a partial pressure will evaporate if sufficient time is provided. Thus, this peak was smaller for the runs in Figure B-10. This also agrees with the difference in the observed extractives content in Table 3-1 as discussed in 3.2.1.2, and shows that the extractives are prone to evaporation. Figure 3-15 also shows that there is a relatively large variation between runs, more than previously observed for sawdust (Appendix B.5.1 Figure B-11 and Figure B-12), indicating that sampling variability is higher in small slices planed from wood than for blended sawdust, which is to be expected. Interesting to note is that the extractives peak is subject to thermal lag (peak shifts to higher temperatures with increasing samples mass) in Figure 3-15. This is not apparent in the case when a lid is applied, Figure 3-16. Figure 3-16 shows that the onset

of pyrolysis is delayed when a lid is applied and the extractives peak is less distinguished, agreeing with the results in Figure 3-1. Fairly large differences are observed between repeat runs, especially for the peak around 350 °C associated with cellulose pyrolysis, representing the compositional differences in heartwood, and the inherent variability in collecting heartwood shavings. Figure 3-17 shows the yields of the heartwood pyrolysis runs as a function of the initial dry weight.

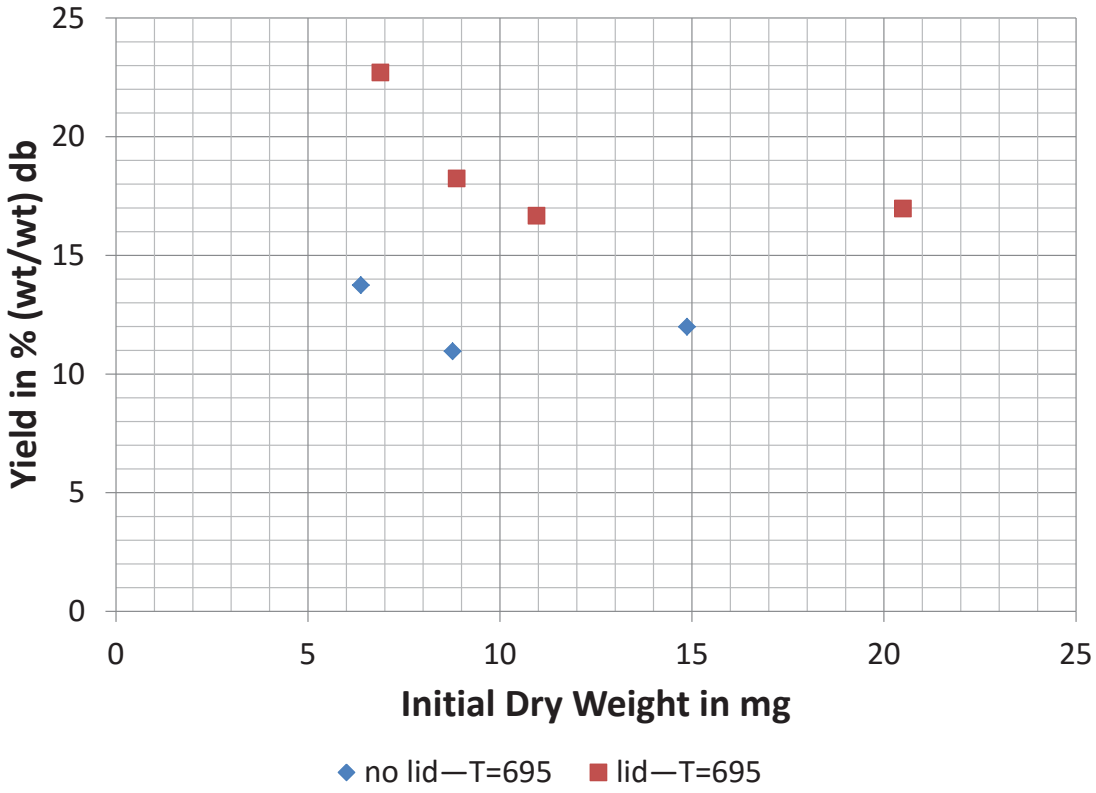

Figure 3-17. Char yield on a dry basis at 695 °C of pyrolysis experiments with and without a lid employing heartwood slices containing extractives as a function of the initial dry sample weight. The moisture content of the samples was estimated based on the proximate analysis results in 3.2.1.4 as the region of moisture evaporation was not distinguishable from the onset of pyrolysis in these samples.

It is important to note that for the yield and initial weight in Figure 3-17 the moisture content was estimated based on the proximate analysis results in 3.2.1.4, as the region of moisture evaporation was not distinguishable from the onset of pyrolysis in these samples (see Figure 3-15 and Figure 3-16; or Appendix B.5.1 Figure B-13). A correlation with sample mass is not visible in Figure 3-17, which could be related to the limited number of experiments or the fact that single particles were pyrolysed compared to sawdust in Figure 3-12 allowing less intimate contact between the volatile pyrolysis products and the solid. The difference in yield between runs with and without a lid in Figure 3-17 was tested for significance. A preliminary test for the equality of variances,

one tail F-test, with a significance level of 0.05 was performed revealing equal variance, Table 3-18.

Table 3-18. F-test for equality of variances.

	Lid	**No lid**
Mean	18.6419	12.2327
Variance	7.7760	1.9806
Observations	4	3
df	3	2
F	3.9260	
P(F<=f) one-tail	0.2096	
F Critical one-tail	19.1643	

Note. The analysis was performed with Microsoft Excel (Microsoft, Redmond, WA, USA). The significance level was set to 0.05. df = degrees of freedom; F = F-test for null hypothesis; P(F<=f) one-tail = P-value for one tail F-test.

Therefore, a t-test assuming equal variances was done, Table 3-19.

Table 3-19. t-test for equality of means assuming equal variances.

	Lid	**No lid**
Mean	18.6419	12.2327
Variance	7.7760	1.98062
Observations	4	3
Pooled Variance	5.4578	
Hypothesized Mean Difference	0	
df	5	
t Stat	3.5920	
P(T<=t) one-tail	0.0078	
t Critical one-tail	2.0150	
P(T<=t) two-tail	0.0157	
t Critical two-tail	2.5706	

Note. The analysis was performed with Microsoft Excel (Microsoft, Redmond, WA, USA). The significance level was set to 0.05. df = degrees of freedom; P(T<=t) one-tail = P-value for one tail t-test; P(T<=t) two-tail = P-value for two tail t-test; t Stat = t-statistics.

Table 3-19 shows that the null hypothesis of equal means was rejected (two tail t-test) with 98.4 % confidence (P-value of 0.016), indicating that secondary char is formed from extractives, which is contrary to what was suggested in the literature review in chapter 2. This is supported by the three distinguishable peaks of the feedstock

components, hemicellulose, cellulose, and lignin, seen in Figure 3-18 (and Figure B-14 in Appendix B.5.1) obtained by plotting the differences in the weight-loss and derivative weight curves of the runs with and without a lid.

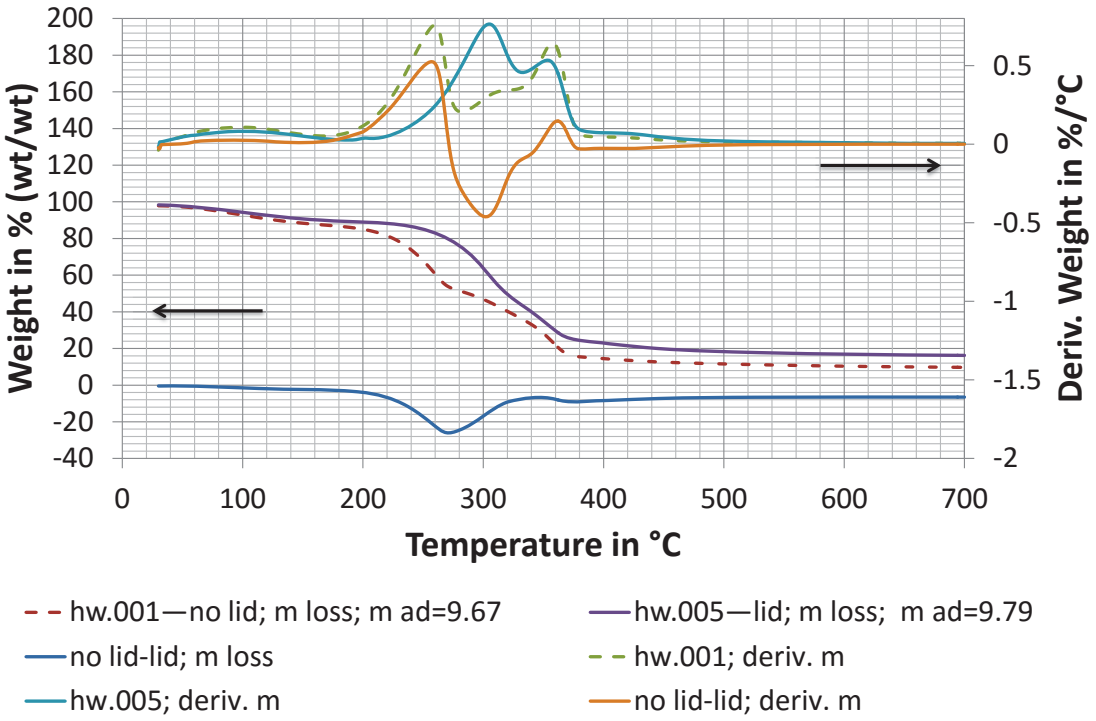

Figure 3-18. Differences between weight-loss and derivative weight curves of heartwood strips containing resin during pyrolysis with and without a lid. The "no lid-lid" curve illustrates the difference between the two cases lid and no lid. Legend: Run number—lid or no lid; weight-loss or derivative weight curve; air-dry weight in mg. m ad = air-dry weight in mg determined at 30 °C; deriv. m = deriv. weight; m loss = weight-loss.

It is important to note here that the plotted experiments were chosen on the basis of having similar initial weights. Similarly to Figure 3-1 and Figure 3-10, the differences occur over the whole pyrolysis range. Also interesting is the large difference in weight around 270 °C indicating that some mass transfer limitations are present that are associated with the extractives. This effect was present but not so pronounced when the extractives content was lower, as observed for the sawdust samples in Figure 3-10 and in Figure B-9 in Appendix B.5.1. Transfer limitations are discussed further in 3.3.5. Overall, these results reveal that the increased thermal lag caused by the presence of increased amount of extractives (Figure 3-15) has no effect on the char yield (Figure 3-17) but the presence of a lid has, as it enables secondary reactions. The increased partial pressure of the volatiles indeed causes secondary reactions by changing the volatile composition as confirmed in chapter 6 by Py-GC/MS.

3.3.2 Intraparticle Secondary Char Formation

The above section showed that extraparticle factors can enhance secondary reactions. This section focusses on the intraparticle factors that affect the extent of secondary char formation. This was studied by pyrolysing earlywood and latewood particles of varying size and shape under the same conditions, as shown in Figure 3-19.

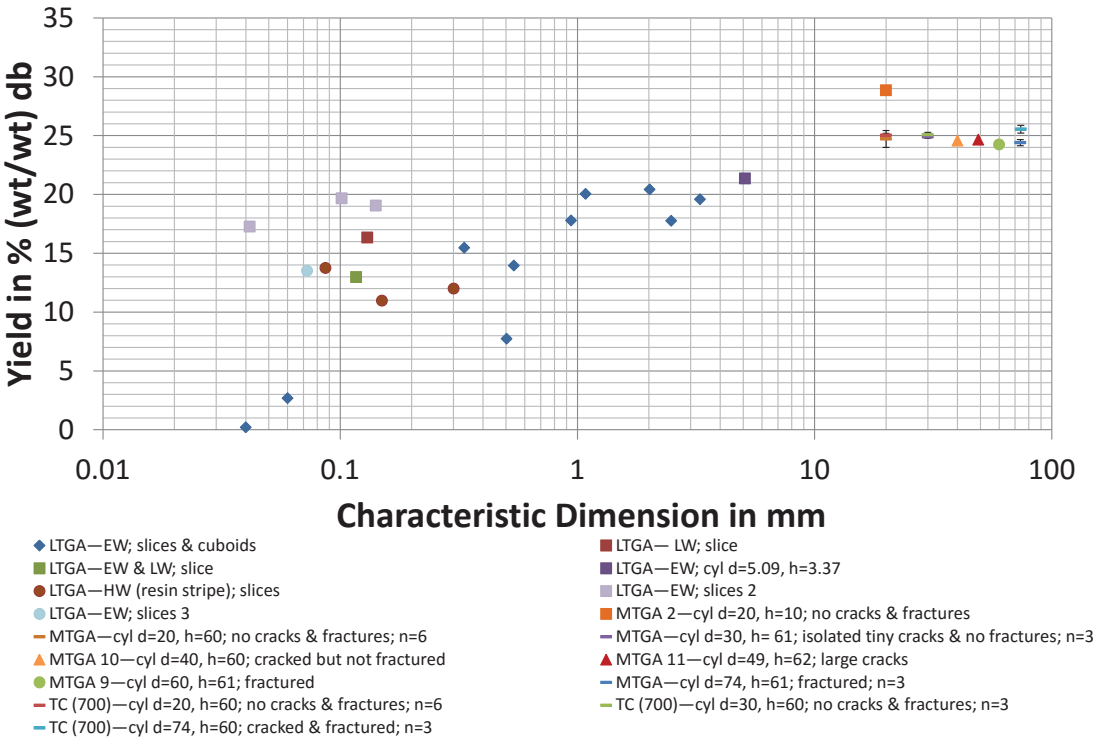

Figure 3-19. Yield of char at 695 °C as a function of sample size. The graph contains data of three sets of experiments a) laboratory scale thermogravimetric analysis (LTGA), b) Macro-TGA, and c) thermocouple runs (TC) to give a broad range of sample size distribution and shapes. The characteristic dimension for the slices and cuboid samples is their thickness perpendicular to the grain and for the cylindrical samples, their diameter. The standard deviation is shown where values have been averaged. The dry weight was taken at a temperature of 152 °C except for the heartwood slices and the Macro-TGA samples, where a "dry temperature" could not be determined due to the presence of low volatile components or heat and mass transfer limitations respectively. In those cases the moisture content was estimated based on the proximate analysis of the air-dried wood. Legend: a) type of experiment—wood type; sample geometry_run number (if several have been done), b) type of experiment_experiment number—sample geometry; structural information; number of runs that have been averaged, and c) type of experiment (*HTT*)—sample geometry; structural information; number of runs that have been averaged. Cracking means the samples are still in one piece at the end of the run and fracturing means the sample broke into separate pieces. The *HTT* is stated in the TC runs as this refers to the temperature at which the yield was determined (the weight at 695 °C could not be recorded as the presence of the thermocouples made this impossible). Unless stated otherwise the samples of the slices and cuboids were prepared from sapwood. The large cylindrical samples $d \geq 20$ mm have been partly from sapwood and heartwood combined. Cyl = cylinder; d = diameter in mm; db = dry basis; EW = earlywood; h = height in mm; HW = heartwood; *HTT* = highest treatment temperature; LTGA = laboratory TGA; LW = latewood; MTGA = Macro-TGA; n = number of samples pyrolysed; TC = thermocouple runs.

Figure 3-19 appears to show a decreasing trend in char yield with decreasing sample size. However, large scatter is present below a characteristic sample dimension of

0.30 mm. The diamond shape data points ("LTGA—EW; slices & cuboids") were a series of experiments that were made in a close time interval in an attempt to remove temporal effects. They consist of cuboid samples and slices. In the case of the cuboid samples only one was placed in the crucible for a single run. For slices, one, two or three were placed next to each other to obtain a higher weight for better measurement accuracy, Figure 3-20.

Figure 3-20. Example of placement of slices in "LTGA—EW; slices & cuboids" experiments in Figure 3-19. In this example three slices were placed next to each other having an average thickness of 0.06 mm. The crucible is an Alumina crucible with a diameter of 5 mm and height of 4 mm.

The results of section 3.3.1 suggest that stacking slices close to each other could have an effect on the yield due to enhanced contact between the volatile pyrolysis products and the pyrolysing solid. This was confirmed by doing the "LTGA—EW; slices 2" experiments, where more slices were stacked next to each other, Figure 3-21.

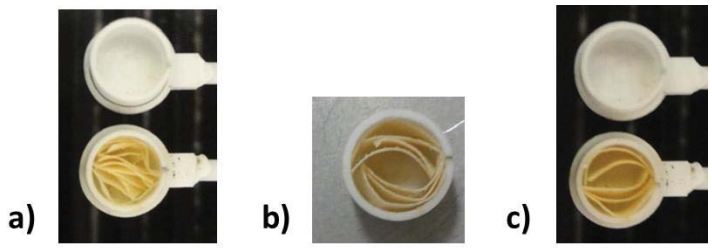

Figure 3-21. Placement of slices in experiments "LTGA—EW; slices 2" in Figure 3-19. The slices had an average thickness of a) 0.04 mm, b) 0.10 mm, and c) 0.14 mm. The crucible is an Alumina crucible with a diameter of 5 mm and height of 4 mm.

The closer stacking of slices in Figure 3-21 explains why higher yields were observed in Figure 3-19 for this series compared to those with a single slice or cuboid, in experiments "LTGA—EW; slices & cuboids". Also, the decreasing amount of stacking from Figure 3-21 a) to c) is the reason that the yield varies slightly between those runs. A higher "stacking density" was also applied for the trial "LTGA—LW; slice" which could explain the higher observed yield, along with it being latewood, which is characterised by cells with a shorter diameter and thicker wall compared to earlywood

(see chapter 2). This is supported by the earlywood and latewood containing slice "LTGA—EW & LW; slice" which fits closer to the trend of the "LTGA—EW; slices & cuboids" experiments, but it is important to note that its "stacking density" was reduced, being very similar to the "LTGA—EW; slices & cuboids" experiments. The yields of the heartwood slices containing resin "LTGA—HW (resin stripe); slices" is somewhat in-between the aforementioned results, which could be due to its markedly different composition or the stacking density, which was denser than in the experiments "LTGA—EW; slices & cuboids".

In order to obtain more samples below 0.2 mm additional experiments were done with earlywood strips from sapwood, and only one slice per run was employed to avoid any effect due to a high "stacking density". Of the three experiments carried out with a sample thickness of 0.03, 0.07, and 0.11 mm, only one is displayed in Figure 3-19; that is, the one with a sample thickness of 0.07 mm ("LTGA—EW; slices 3"), which has a higher char yield than expected. The others are not displayed as they had a negative yield of -59.84 and -9.64 % (wt/wt) for a thickness of 0.03 and 0.11 mm respectively. These negative yields were influenced by the low initial sample weight of these experiments of 0.246 and 0.627 mg respectively compared to 1.401 mg for the sample with the thickness 0.07 mm. According to the supplier the balance has a sensitivity of 0.1 µg meaning that the residual mass after pyrolysis may well be less than the resolution. Nevertheless, this does not explain the larger of the negative results. Therefore, it was speculated that some sample may have fallen out of the crucible during pyrolysis, which indeed occurred in experiment "sliceew.003—EW s 0.03" where no char was visible in the crucible after the pyrolysis run. However, here the weight-loss graphs in Figure 3-22 showed that these trials match the curves of the other runs, thereby ruling out sample loss from the crucible. Indeed, in the most negative trial, experiment "sliceew.004—EW s 0.11", char was visible in the crucible after pyrolysis.

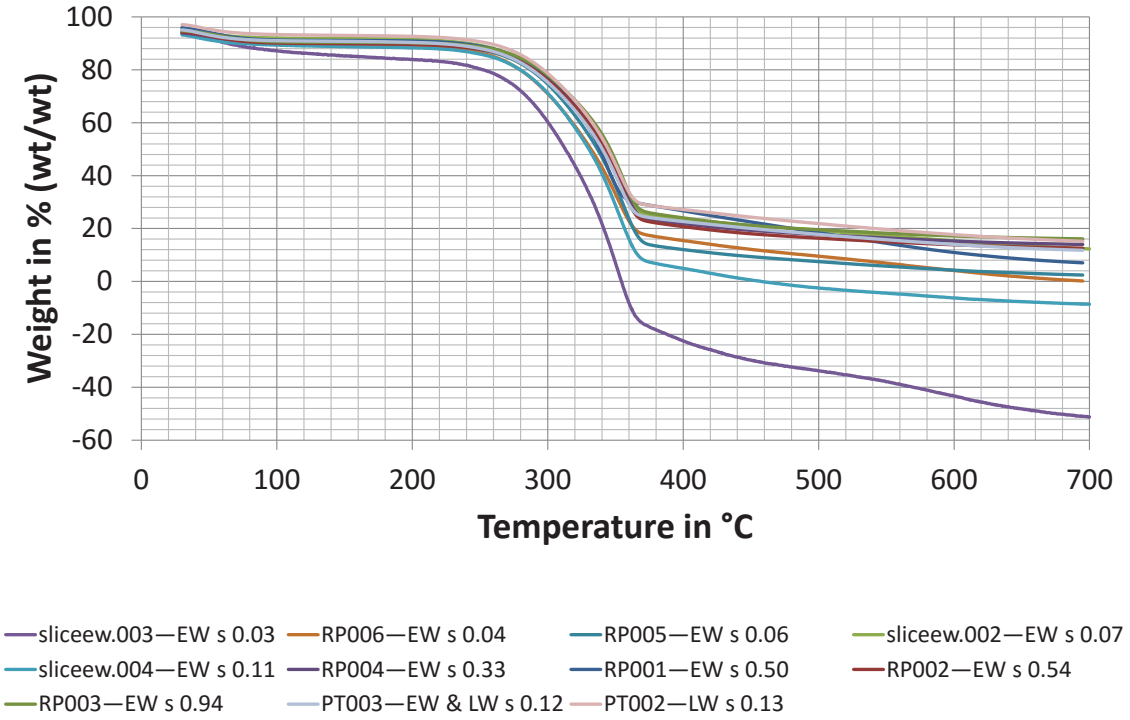

Figure 3-22. Weight-loss curves of the slices in Figure 3-19 that employed a low stacking density. Legend: Run number—wood type_shape_thickness in mm. EW = earlywood; LW = latewood; s = slice.

Furthermore, when converting the mass loss curves in Figure 3-22 to derivative weight curves in Figure 3-23, the two runs with negative yield have too large a peak area and are characterised by relatively large noise despite being smoothed. Viewed together, these factors indicate that errors occur at the limit of the resolution of the equipment, which is supported by the earlier mentioned problem of determining the ash yield accurately with the TGA equipment.

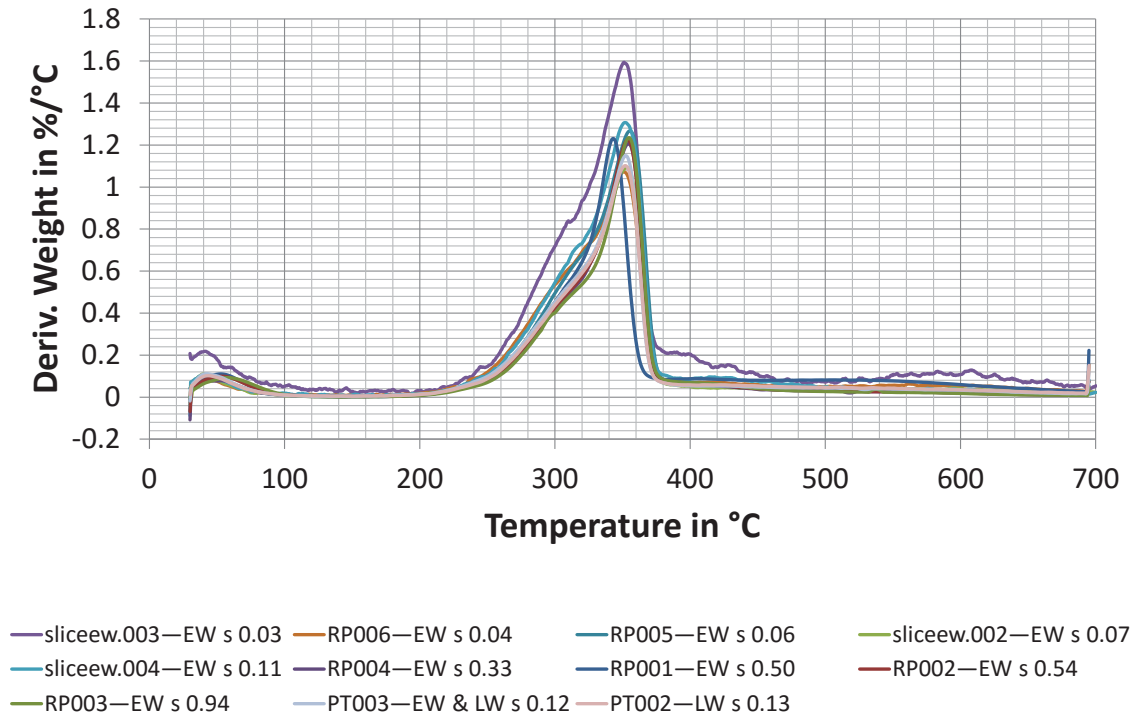

Figure 3-23. Derivative weight curves of the slices in Figure 3-19 that employed a low stacking density. Legend: Run number—wood type_shape_thickness in mm. EW = earlywood; LW = latewood; s = slice.

The above discussion first and foremost outlines the inherent difficulty in studying primary char formation, that is (a) very thin samples are required which in turn exaggerate the sample heterogeneity, and (b) vapour-solid contact needs to be minimised, which means a low "stacking density" is desired. Both points mean results are affected by the resolution limits of the TGA. Nevertheless, the graph in Figure 3-19 shows that the sample yield decreases with sample size and in some cases can be close to zero. It is believed that the yield differences are caused by the varying vapour-phase solid-phase contact times as highlighted by the effect of stacking density. Thus secondary char forming reactions play an important role in the overall char formation process. These conclusions agree with literature, for example Antal and Varhegyi (1995) conclude in their article that "vapour-solid interactions (secondary reactions) are effectively the only source of char formed during the pyrolysis of a pure cellulose" (p. 715), and that "these heterogeneous reactions alone can increase the cellulosic char yield from 0% to more than 40%" (p.715). Of course, wood also contains 32 % (wt/wt) lignin compared to 40 % (wt/wt) cellulose (see Table 3-2). The lignin naturally forms more char due to its high proportion of aromatic rings, underlining its importance in char formation. To study primary char formation and to find out whether or not a char yield of zero is obtained for very small wood samples it is necessary to carry out further

investigation with more precise equipment. A possibility is a wire mesh reactor as proposed by Kandiyoti (2002) and Morgan and Kandiyoti (2013), who recognised the observed interactions as limitations of the TGA apparatus. Here, it is important to note that a characteristic dimension of 0.04 mm in Figure 3-19 corresponds to the diameter of a tracheid cell in the outer wood of radiata pine as discussed in chapter 2. Practically, however, from the viewpoint of the manufacture of biochar it will never be of interest to pyrolyse such small samples and to single those secondary reactions out to such a degree as high char yields are desired, that is secondary char formation is of interest as long as it does not interfere with the macroscopic structure as discussed in chapter 7. Therefore, this has not been investigated further in this research. The main aim here was to establish the role of intraparticle secondary char formation for the overall yield, and Figure 3-19 shows, in accordance with literature (L. Wang et al., 2013; L. Wang et al., 2011), that secondary char formation is responsible for a large portion, if not the majority, of the char yield.

Larger particle size should enhance secondary reactions in the same way that constraining the pyrolysis environment did when using a lid or a larger bed of particles in the earlier trials shown in Figure 3-13 and Figure 3-14. Figure 3-24 shows that this indeed occurs. Because wood is porous and volatiles must transport through these pores, continuous interaction between the volatile pyrolysis products and the pyrolysing solid occur enabling the same secondary reactions as observed in 3.3.1. More graphs corresponding to Figure 3-24 are depicted in Appendix B.6.1, Figure B-23 to Figure B-25 showing similar results.

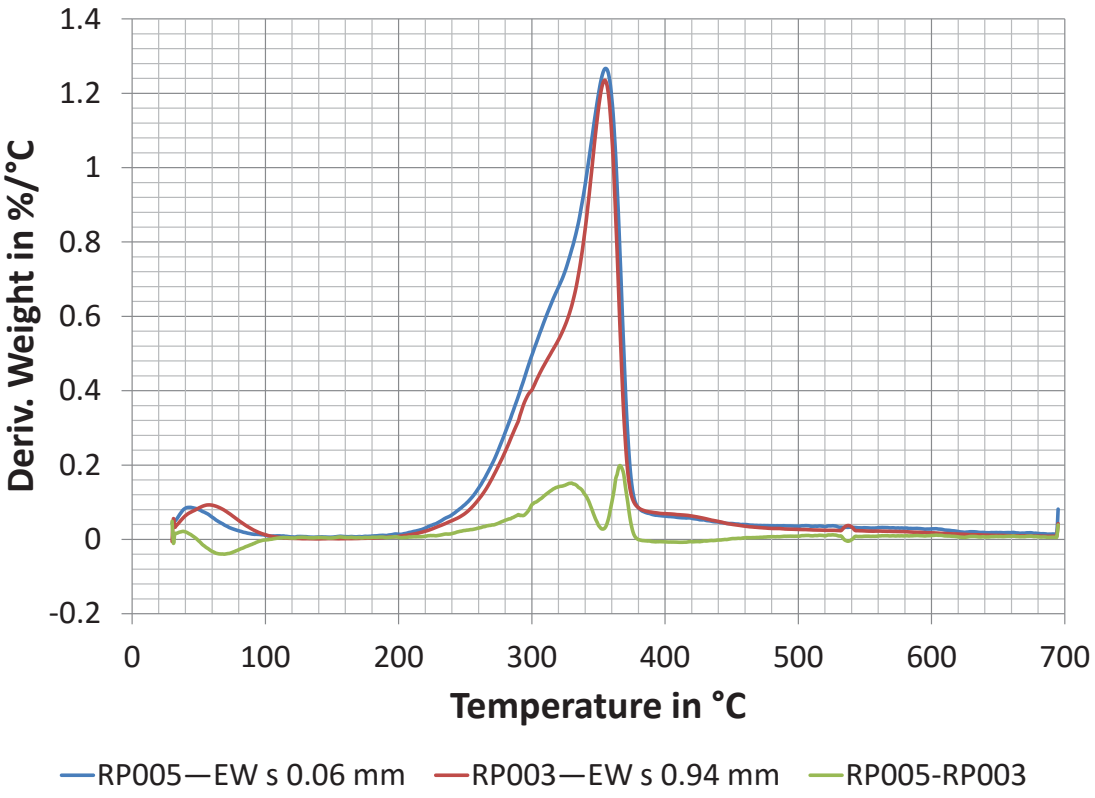

Figure 3-24. Difference between derivative weight curves of a sample with small sample size compared to a sample with larger size showing a corresponding yield increase with size. The "small-large" curve illustrates the difference between the two pyrolysis runs with differing initial sample size corresponding to the difference curve "no lid-lid" in Figure 3-1. Legend: Run number—wood type_shape_thickness in mm. EW = earlywood; s = slice.

Examining Figure 3-24 in further detail shows an absence of the shoulder peak around 230 to 240 °C shown in Figure 3-13, Figure 3-14, and Figure 3-1. This is because the samples in these experiments (Figure 3-24) were obtained from sapwood with minimal extractives content (see chapter 2). Again the moisture peak displays thermal lag but not the main pyrolysis peak.

Returning to Figure 3-19, a macro-TGA was used to obtain yields for very large samples. It is apparent that above a critical sample size no more yield increase occurs with increasing sample size. The yield plateaus at 25.02 ± 0.90 % (wt/wt) on a dry basis, which is attained for cylinders with a diameter of 20 mm. This yield compares to values obtained in literature for the pyrolysis of single pellets ($d = 13.5$ mm, $h = 60$ mm) of pine at a heating rate of 3 °C/min to 700 °C, which has been reported as 26.5 % (wt/wt) (Grieco & Baldi, 2011). It is important to note that the stagnation of the yield happens in parallel with the occurrence of cracks and later fractures, which are discussed in 3.3.4 (Figure 3-28).

3.3.3 Char Yield versus Fixed Carbon Yield

In chapter 2 the importance of introducing the fixed carbon yield to describe how efficiently biomass is turned into pure carbon was discussed, as biochars of high yields could be merely obtained on the basis of incomplete pyrolysis. However, the fixed carbon yield could not be obtained for all the TGA experiments in this research as the residual char yield was often too low for proximate analysis resulting in large scatter in the proximate analysis results due to the limits of the applied TGA, as discussed in 3.3.2. The experiments that were carried out with a subsequent proximate analysis on the produced char showed that the fixed carbon yield was positively correlated with the char yield, as plotted in Figure 3-25.

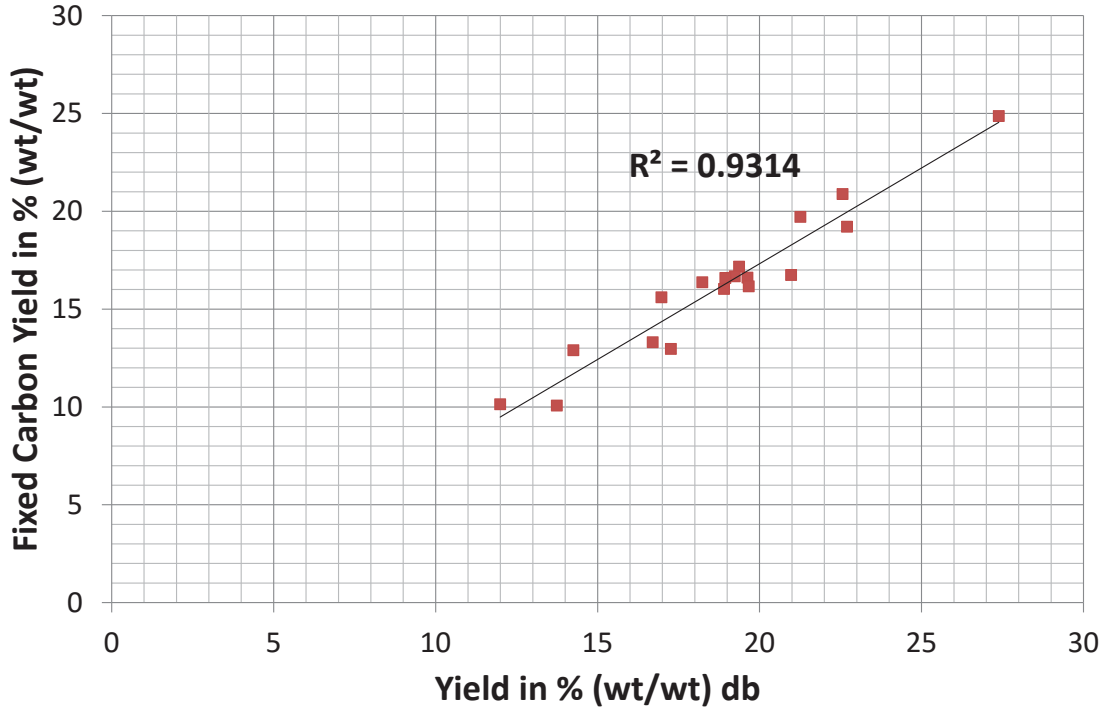

Figure 3-25. Fixed carbon yield at 745 °C as a function of the char yield at 695 °C of lab scale TGA pyrolysis experiments. The fixed carbon yield was determined at 745 °C as this was the maximum pyrolysis temperature to which the char proximate analysis corresponds. db = dry basis; TGA = thermogravimetric analysis.

The linear relationship in Figure 3-25 was anticipated as the fixed carbon yield is a function of the char yield, equation (2.7) in 2.3.1. As all the pyrolysis experiments in this research were done under the same conditions it can be safely assumed that the reported yield relationships in this research reflect the respective trends in the fixed carbon yields.

The fixed carbon yields of some of the Macro-TGA experiments are depicted in Figure 3-26.

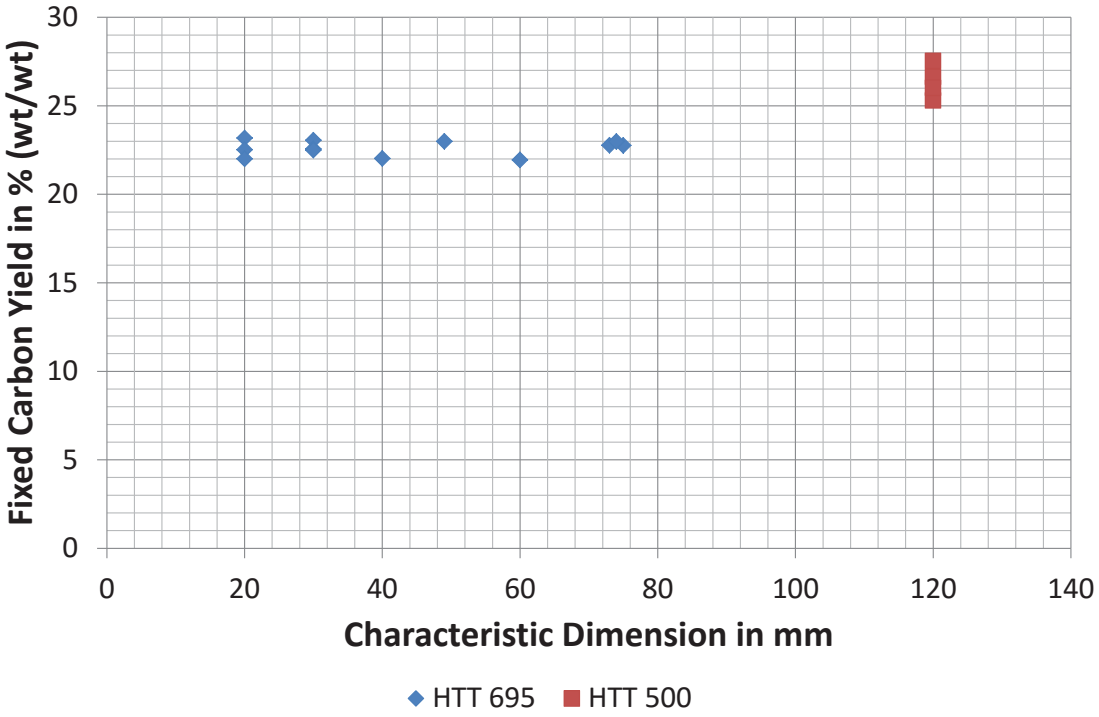

Figure 3-26. Fixed carbon yield of Macro-TGA experiments. The experiments with a *HTT* of 695 °C were carried out at a heating rate of 5.5 °C/min whereas the experiments with a *HTT* of 500 °C were carried out at a heating rate of ≈ 1 °C/min. *HTT* = highest treatment temperature; TGA = thermogravimetric analysis.

Figure 3-26 shows, in accordance to Figure 3-19, that the fixed carbon yield stagnates above a characteristic dimension of 20 mm. Also included are the fixed carbon yields of cylinders with a diameter of 120 mm that have been heated at a heating rate of ≈ 1 °C/min to 500 °C as part of the research in chapter 5. This shows that when the *HTT* is lower, the fixed carbon yield is higher, but that the char has a lower fixed carbon content as shown in Figure 3-27.

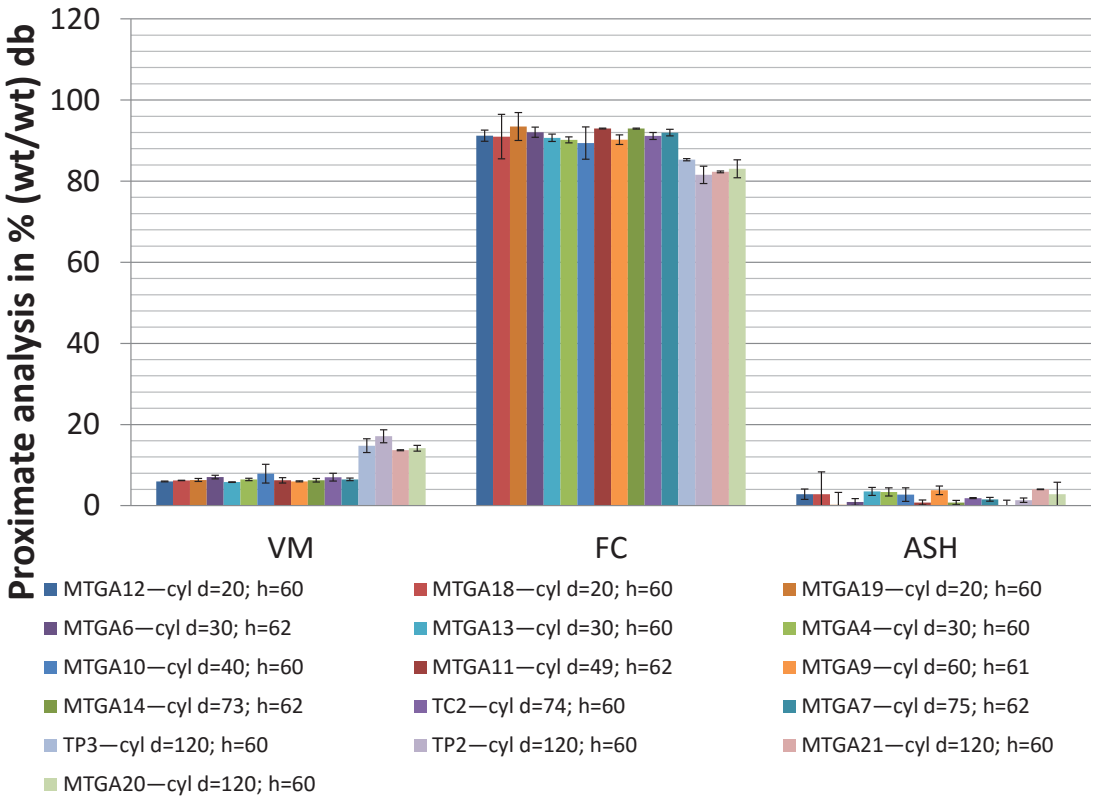

Figure 3-27. Proximate analysis results of the Macro-TGA experiments in Figure 3-26. The error bars represent the standard deviation of two proximate analyses. The samples with a diameter ≤ 120 mm have been heated to a *HTT* of 700 °C at 5.5 °C/min whereas the samples with a diameter of 120 mm were heated to a *HTT* of 500 °C at ≈ 1 °C/min. Legend: Experiment—sample dimensions in mm. cyl = cylinder; d = diameter in mm; db = dry basis; FC =fixed carbon; h = height in mm; TGA = thermogravimetric analysis; VM = volatile matter.

Figure 3-27 shows the typically large error observed in the ash content as discussed in 3.2.1.4.

The variation in the char yield and fixed carbon yield with temperature has to be regarded during the manufacture of biochar, as it directly impacts on how much carbon can be sequestered, and thus the economics. However, for the manufacture of biochar, other properties like porosity are important as well because these are the parameters that affect its soil interaction, which is further discussed in chapter 7.

3.3.4 Structural Changes

In section 3.3.2 it was observed that the yield stagnation in Figure 3-19 (above a characteristic sample dimension of 20 mm) goes along with the increased formation of cracks and fractures as the sample size further increases, which is demonstrated in Figure 3-28.

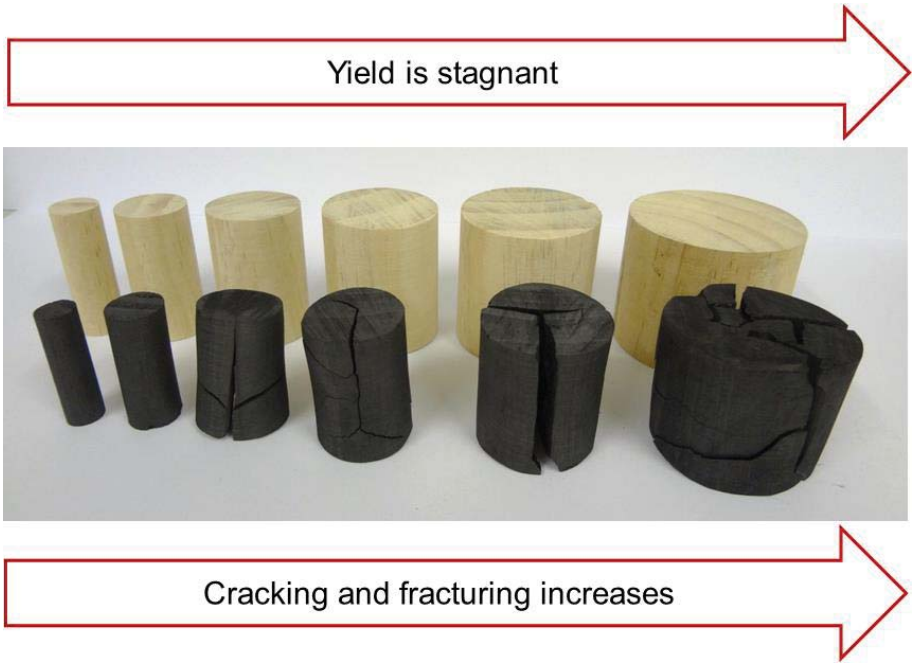

Figure 3-28. Extent of cracking and fracturing in samples with increasing size. All samples had a height of 60 mm and the diameter from left to right is 20, 30, 40, 50, 60 and 74 mm. Cracking means the samples are still in one piece at the end of the run and fracturing means the sample broke into separate pieces.

The cracking and fracturing in Figure 3-28 is a consequence of a combination of processes that occur with increasing decomposition/temperature. These are (a) increased internal pressure gradients, (b) shrinkage, and (c) increased brittleness of the solid. Cracking and fracturing limit secondary char forming reactions due to the reduction of the tortuous path length of escaping volatiles and consequently reduces the residence time of contact between vapour and char. The result is that yield remains constant with increasing sample size. This means that larger yield increases are only possible by external means, i.e., by creating a bed of particles or pyrolysis in an enclosed system. The study of cracking and fracturing was extended in a supervised 4th year engineering project as a subproject of this research (Bashir, 2012). Similar findings were made in that cracking and fracturing increases with particles size, Figure 3-29.

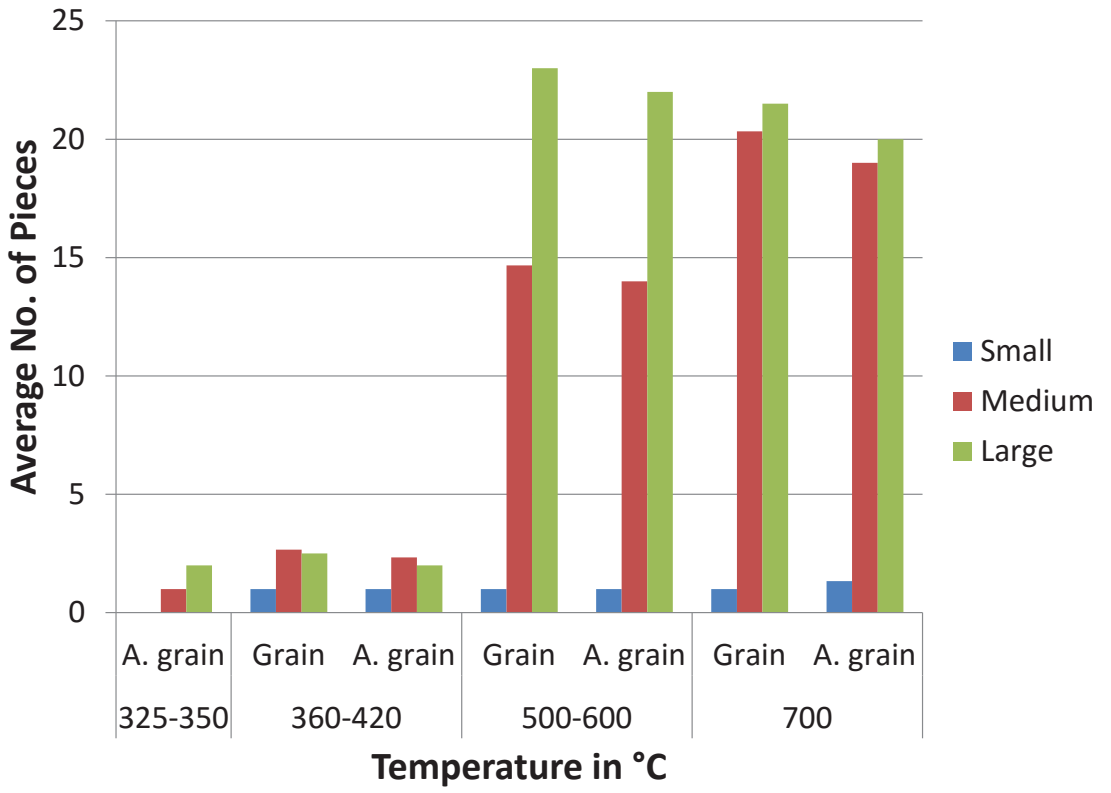

Figure 3-29. Fracturing as a function of sample size, grain direction, and *HTT*. Small, medium, and large refer to cuboid sample beams with a length of approximately 175 mm and a cross section of 15 x 15 mm, 32 x 32 mm, and 67 x 67 mm respectively. A number of 1 piece means the sample did not fracture. A. grain = against grain meaning the grain direction was perpendicular to the length of the beam; grain = means the grain direction was parallel to the length of the beam; *HTT* = highest treatment temperature; No = number. Adapted from Bashir (2012).

Figure 3-29 shows that fracturing is also dependent on *HTT* and grain direction. The overall trend is that fracturing increases with *HTT* and is larger when the grain direction is in parallel to the length of the sample beams. This is to be expected, because increasing temperature, causes more shrinkage and brittleness which increases stress leading to the rupture of the solid matrix. Fracturing is consistently less when the grain direction is perpendicular to the length of the sample beam, which is due to the short path distance travelled by the volatiles as they generally move in the grain direction (see chapter 2). It was also discovered that moisture present in the wood causes more cracking and fracturing, as shown in Figure 3-30, and that the cracks and fractures form generally along ray cells or knots, which represent structural weak points, as shown in Figure 3-31.

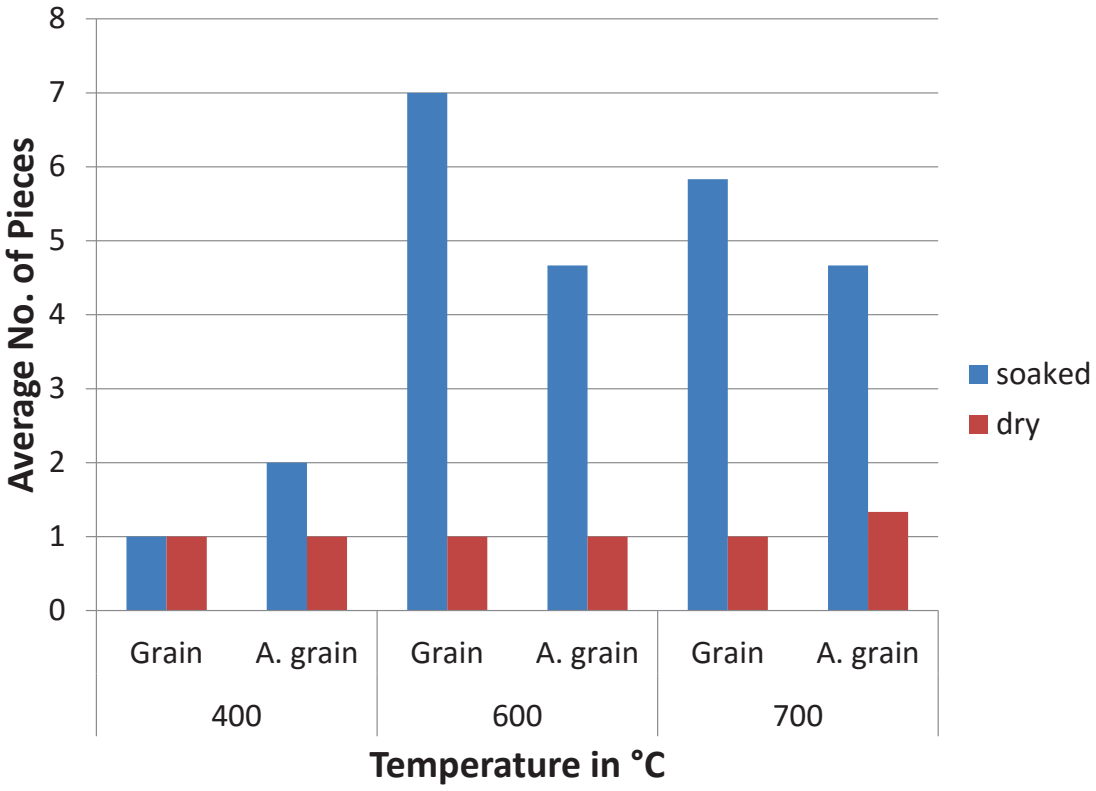

Figure 3-30. Comparison of fracturing between saturated and dried samples. The samples analysed were cuboid sample beams with a length of approximately 175 mm and a cross section of 15 x 15 mm. A number of 1 piece means the sample did not fracture. A. grain = against grain meaning the grain direction was perpendicular to the length of the beam; grain = means the grain direction was parallel to the length of the beam; No = number. Adapted from Bashir (2012).

Figure 3-31. Cracks and fractures in a cuboid sample beam with a length of approximately 175 mm and a cross section of 67 x 67 mm pyrolysed to ≈ 400 °C. Picture taken from Bashir (2012).

The presence of moisture in Figure 3-30 leads to the formation of fractures while they are absent in the dried samples. This is because a large volume of steam is formed due to the evaporation of water, which is subsequently accumulated in the wood as the temperature further increases because of the initially relatively low porosity of the wood inhibiting mass transfer. This causes the wood to eventually rupture as a critical internal pressure gradient is exceeded. In addition, Figure 3-31 shows that a large portion of the cracks appear to originate from the earlywood. This could be associated

with the aspirated bordered pits in the earlywood, which inhibit mass transfer compared to the open bordered pits in latewood as discussed in chapter 2. Another possible explanation is the formation of moisture gradients during the drying process of the soaked samples, which cause an uneven shrinkage resulting in stress and consequently the fracturing of wood.

Shrinkage, it can be argued, may both limit or enhance secondary reactions. On the one hand, shrinkage reduces the tortuous path length for escaping volatiles and, on the other, shrinkage reduces the pore size thus increases the resistance to transport and the intimacy of contact between vapours and the char matrix. Larfeldt, Leckner, and Melaaen (2000) state that shrinkage and cracking combined "will compensate for the reduced thermal diffusivity of charcoal" (p.1641). This illustrates the importance of including shrinkage and cracking/fracturing into a pyrolysis model. However, in the case of cracking and fracturing it is sufficient to introduce a factor for cracking as the study of the cracks and fractures (in the work by Bashir (2012) supervised as part of this PhD) showed that, depending on the material strength, cracks and fractures will occur at regular intervals. That is, whenever the critical pressure gradient is exceeded. The shrinkage has been determined for the samples in Figure 3-19 pyrolysed in the Macro-TGA, and is depicted in Figure 3-32.

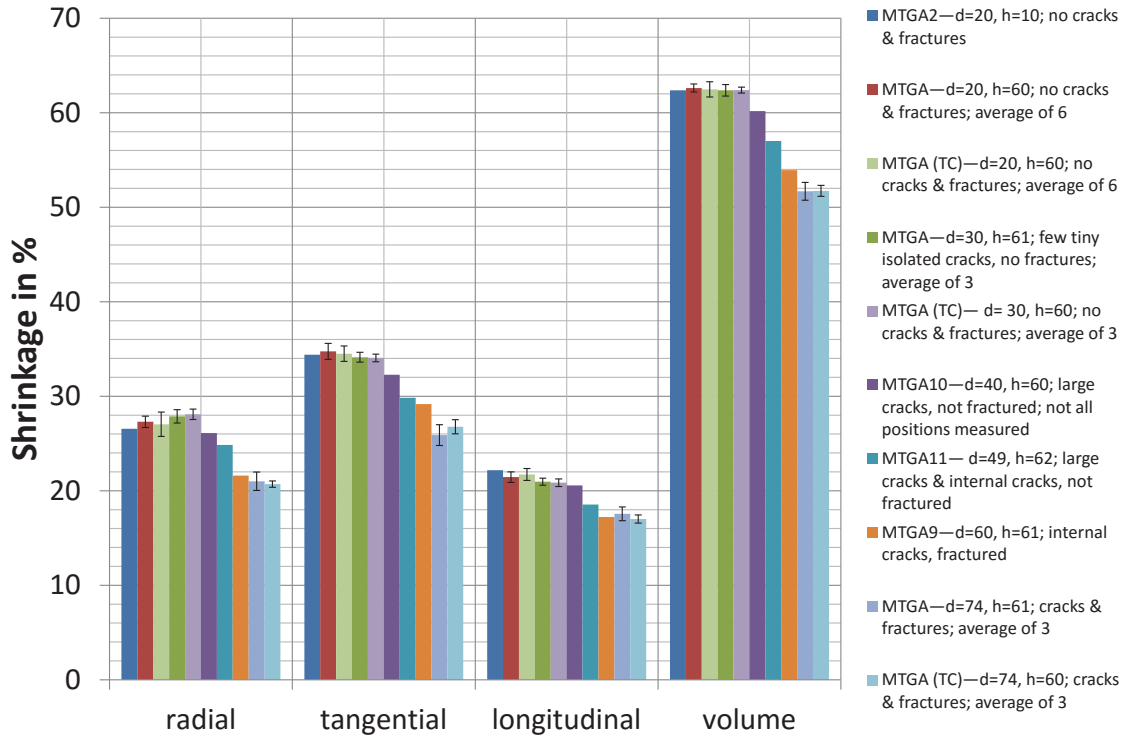

Figure 3-32. Shrinkage of samples pyrolysed to 700 °C. Error bars representing the standard deviation are included for the cases where more than one sample has been analysed. Legend: Experiment—sample geometry; structural information; number of runs that have been averaged for the case several samples were analysed. "Not all positions measured" means not all dimensions outlined in 3.2.3 could be analysed due to the cracks and fractures present. d = diameter in mm; h = height in mm; MTGA = Macro-TGA; TC = thermocouple experiment measuring the internal sample temperature.

Figure 3-32 shows that shrinkage of wood decreases in the following order tangential > radial > longitudinal. This agrees with literature, where Kininmonth and Whitehouse (1991) report that wood typically shrinks about twice as much in the tangential direction compared to the radial direction, and that shrinkage in both of these directions is larger than the longitudinal direction. Interesting is that the shrinkage appears to decrease with increasing sample size for cylinders with a diameter ≥ 40 mm. This is believed to be due to the increased formation of internal cracks as illustrated in Figure 3-28, which counteract the effect of shrinkage. For measuring the dimensions of the fractured samples the pieces were held together and a perfect fit was not always achievable. In general Figure 3-32 reveals that shrinkage is considerable, which becomes obvious when looking at the volume shrinkage that is 62.44 ± 0.66 % in the samples without cracks and fractures. The variation in-between the runs without cracks and fractures can be explained by the sample heterogeneity, that is distribution of earlywood and latewood in the samples as typically earlywood shrinks less than latewood in the radial and tangential directions, and more in the longitudinal direction

(Kininmonth & Whitehouse, 1991). Obviously the shrinkage is dependent on the pyrolysis temperature, which is demonstrated in Figure 3-33.

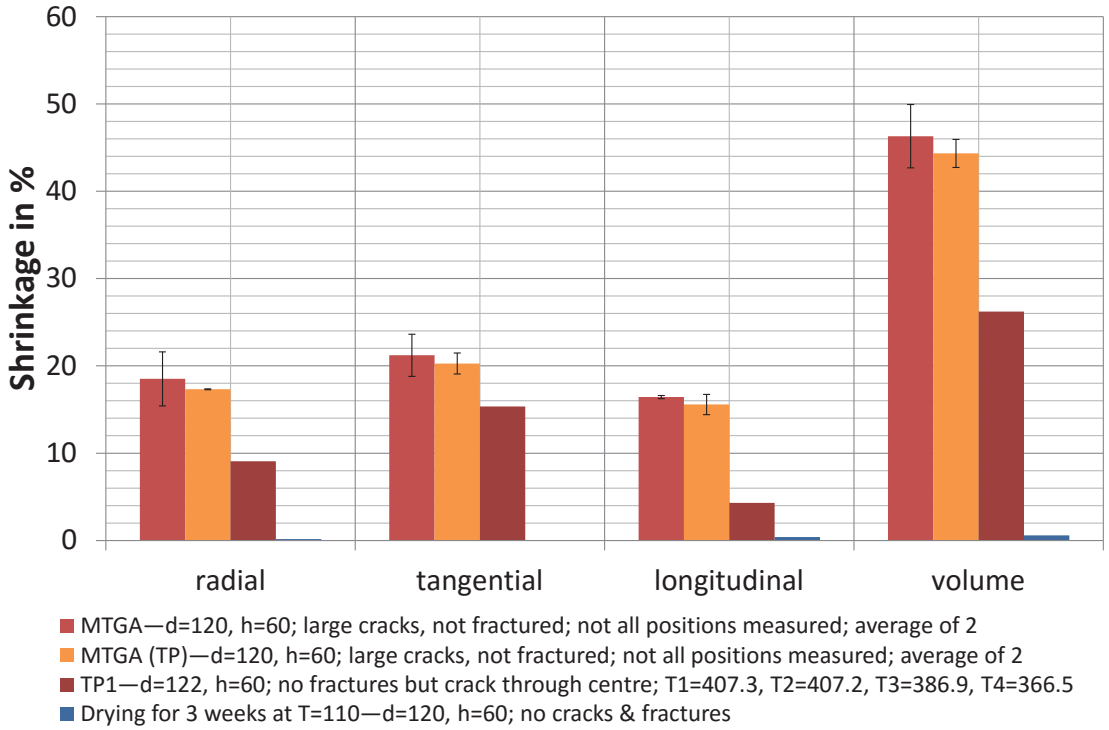

Figure 3-33. Shrinkage of samples after drying, and pyrolysis to between 367 to 407 °C and 500 °C. The samples depicted in this graph were part of the experiments in chapter 5, and were pyrolysed at a heating rate of ≈ 0.85 °C/min to 500 °C unless stated otherwise. Error bars representing the standard deviation are included for the cases where more than one sample has been analysed. Legend: Experiment—sample geometry; structural information; number of runs that have been averaged for the case several samples were analysed. "Not all positions measured" means not all dimensions outlined in 3.2.3 could be analysed due to the cracks present (to note is that the diameters for this sample size have been generally only determined at the top and bottom of the sample). d = diameter in mm; h = height in mm; MTGA = Macro-TGA; T = temperature in °C; T1 to T4 are the recorded sample temperatures in °C from the centre towards the sample surface, being distributed evenly over the radius as depicted in Figure 3-5; TP = temperature profile experiments analysing internal heat generation.

Figure 3-33 shows that the shrinkage is lower when pyrolysed to 500 °C than 700 °C, although it is important to note that the sample was considerably larger, and thus internal cracks will have had an impact as discussed above. However, due to the lower applied heating rate cracking was reduced and fracturing absent, which is different to the runs in Figure 3-32. The role temperature plays is underlined by the run "TP1", which had to be aborted before reaching the set *HTT* of 500 °C due to time constraints. The internal temperatures were recorded in this run at $r = 0$ mm, $r = 15$ mm, $r = 30$ mm, and $r = 45$ mm as 407.3, 407.2, 386.9, and 366.5 °C respectively. This experiment shows that shrinkage was considerably decreased at temperatures around the maximum of the derivative weight peak indicating that shrinkage develops more at

higher temperatures. This conclusion is also supported by the sample that has been dried in an electric furnace for three weeks at 110 °C, which shows a negligible shrinkage compared to the pyrolysis experiments.

To get a more detailed insight into shrinkage and structural changes in general thin slices of radiata pine wood were pyrolysed in a microscopic hot stage. This was done as a subproject of this PhD in a supervised 4th year engineering project titled "Hot Stage for Pyrolysis" (Mohd-Hanif, 2013). This technique of hot stage pyrolysis allowed in situ visualisation of the changes occurring in the pine wood samples undergoing pyrolysis. It was found that the onset of shrinkage coincides with the increase in relative pore area at approximately 300 °C, Figure 3-34.

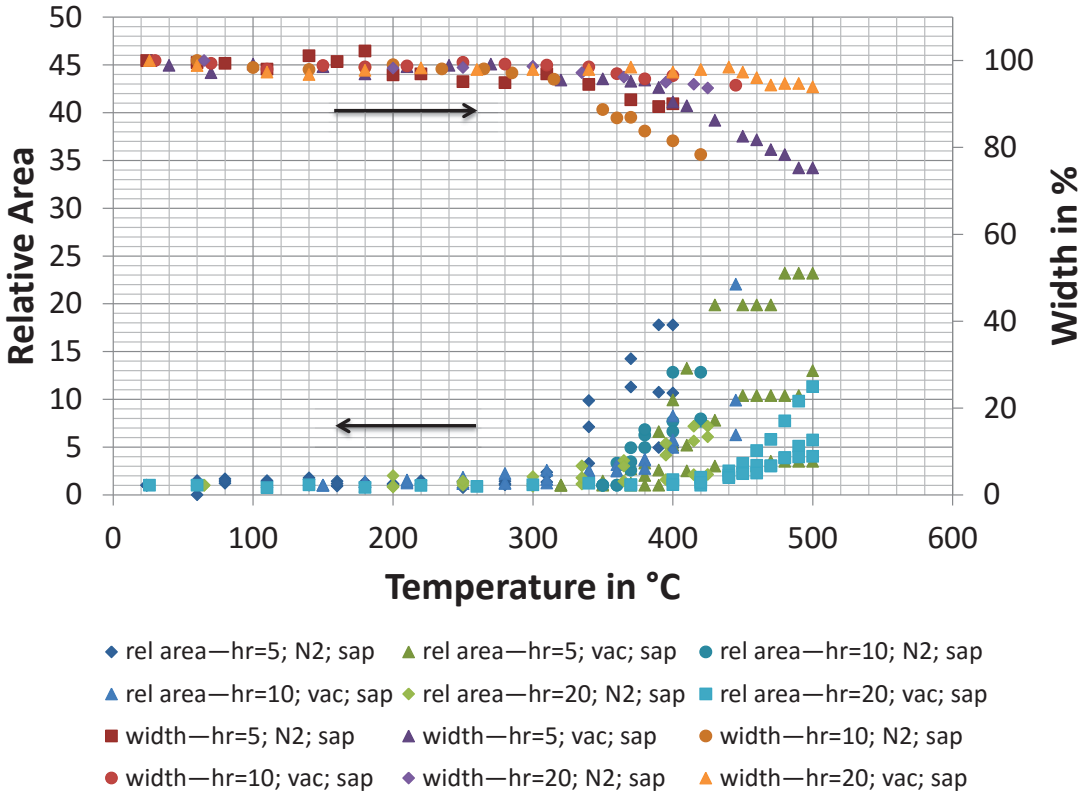

Figure 3-34. Change in relative pore area and sample width during pyrolysis as observed in a microscopic hot stage. The samples were viewed perpendicular to the grain direction, that is, the width change represents the change in tangential or radial dimension. The relative area refers to the ratio of measured area to initial area as determined by ImageJ. Legend: Parameter measured—heating rate in °C/min; atmosphere; sample origin. d = diameter in mm; hr = heating rate in °C/min; N2 = nitrogen purge gas; rel = relative; sap = sapwood; vac = vacuum. Adapted from Mohd-Hanif (2013).

The coincidental increase of relative pore area and shrinkage in Figure 3-34 seems at first contradictory but can be explained by the progressing occurrence of fissures and cracks in the cell walls that lead to joining of neighbouring cell lumen while smaller

ones disappear due to shrinkage and the out flux of pyrolysis products, as was first shown by Haas, Nimlos, and Donohoe (2009), who viewed poplar pyrolysis on a hot stage. Overall this leads to an increase in porosity with temperature although the number of visible smaller pores decreases. The increase in pore area and shrinkage at 300 °C is almost exponential and starts to slow down at temperatures above 400 to 500 °C, where fewer volatiles are released (Figure 3-1), which again agrees with the work of Haas et al. (2009). The shrinkage measured in Figure 3-34 represents the shrinkage in the tangential or the radial direction, which explains some of the observed scatter. Nevertheless, the shrinkage between 400 and 500 °C in Figure 3-34 is similar to the values in Figure 3-33, confirming the results. Thus, shrinkage takes place during the main weight-loss region (Figure 3-1). During this period the cell walls of the pyrolysing material are flexible and malleable without showing any apparent fluidity, and only rupture towards the end of pyrolysis. This is the reason why the charred material retains the structure of the parent material and there are no macroscopic cracks and fractures present for the samples with a diameter ≤ 30 mm in Figure 3-28 and Figure 3-32. This behaviour is explained by Mamleev, Bourbigot, Le Bras, and Yvon (2009) by the cell wall being like a porous viscous suspension consisting of "gas, liquid (or weakly cross-linked gel), and an infusible solid presenting undecomposed material" (p.9) in which the forces of adhesion between the liquid and the solid prevent the collapse of the charring material. These forces allow the shrinkage of the sample as pyrolysis advances, that is, the liquid evaporates or decomposes and the cell wall material degrades (*ibid*). Thus, they make a case for the existence of a liquid phase during slow pyrolysis. The existence of a liquid or molten phase as a consequence of fusion during slow pyrolysis has been discussed controversially in literature as stated in 2.5.4 as it is not directly observable by eye, even at a microscopic scale as done with the hot stage experiments. Mamleev et al. discuss this controversy in their paper. They argue their point with literature and by the method of 'proof by contradiction' on the example of the shrinkage of a sample of *Populus*, which shrinks isotropically compared to *Pinus radiata* used in this study, which shrinks anisotropically due to its fibrous nature. They point out that the cell walls (a) cannot be uniform and contain pores, (b) cannot be a porous system consisting of an incompressible solid, and (c) cannot be likened to a swollen gel otherwise shrinkage could not occur and one could not explain why oxygen and other chemicals are not uniformly distributed. This lead to their above mentioned conclusion that the cell wall is a porous viscous suspension (for more details

the reader is referred to the original publication). The hypothesis that shrinkage indicates the presence of a plastic state was made earlier by Evans and Milne (1987) but they had not the experimental means to verify this. The presence of a liquid phase is further supported by the work of Zhu, Zhu, Xiao, and Yi (2012), who studied cellulose pyrolysis in a sealed glass capsule by in situ visualisation with a microscopic hot stage. They found that the cellulose sample started to deform at 230 °C, and at 240 °C they observed water and an orange oily liquid, which disappeared at 260 °C due to evaporation and further decomposition. This supports the two-phase model described by Mamleev et al. (2009) for cellulose pyrolysis; that is, first a liquid forms due to depolymerisation (transglycosylation), which then attains a quasi-stationary equilibrium between formation and disappearance (decomposition, polymerisation, and evaporation). That water and oily phases are visible in the experiment by Zhu et al. (2012), conducted in sealed capillary tubes, while being absent under atmospheric conditions is due to a delayed evaporation (transfer limited) caused by an increasing (autogenous) pressure in the sealed system. This mechanism also explains the observation of char showing evidence of having gone through molten phase under pressure pyrolysis (L. Wang et al., 2013). Furthermore, a liquid leaving the cell wall during pyrolysis has been reported by Haas et al. (2009). However, this was not actually observable on their video footage. The hot stage experiments conducted in this research neither confirmed nor disproved these arguments apart from detecting liquids associated with the extractives (resin) in the heartwood, as shown in Figure 3-35.

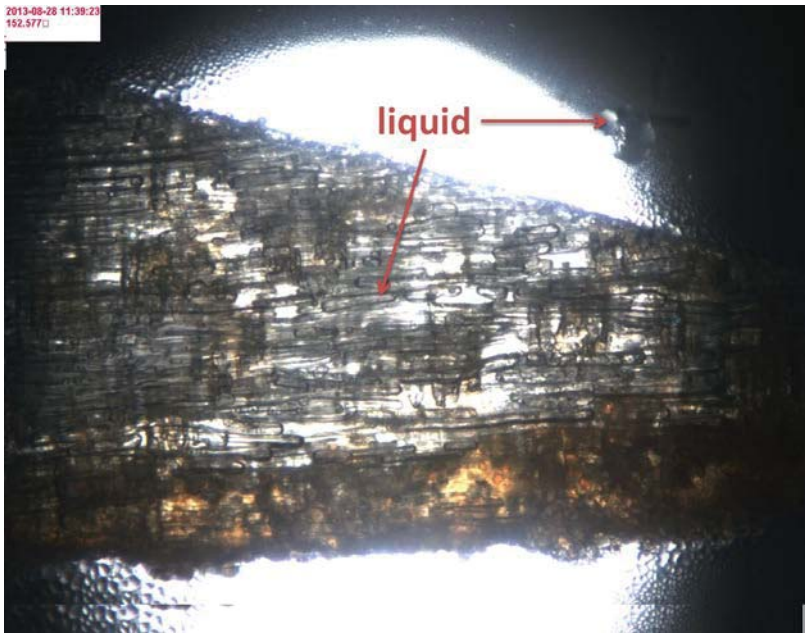

Figure 3-35. Light microscope micrograph of heartwood pyrolysed in nitrogen at a heating rate of 5 °C/min taken at 153 °C.

In Figure 3-35 liquid water is present as condensate on the cover glass of the hot stage. Liquid is also evident in the sample, which was absent for the sapwood samples. Thus, it is believed to derive from the extractives and explains why the extractives peak show evidence of thermal lag in Figure 3-15 (latent heat of evaporation). Evidence of a molten phase during pyrolysis has been provided by Haas et al. in the form of transmission electron micrographs, which show that after pyrolysis subcellular differentiation into middle lamella, primary cell wall and secondary cell wall is not possible anymore, and in some cases material appearing to originate from the middle lamella was observed to have erupted into the cell lumen. The most convincing evidence thus far for the presence of a liquid phase during slow pyrolysis is given by Dufour, Castro-Diaz, Brosse, Bouroukba, and Snape (2012), who investigated molecular mobility during pyrolysis by in situ ^{1}H NMR spectroscopy. Depending on whether the protons are in solid or liquid structures their NMR signals vary (Gaussian-like and Lorentzian-like distribution functions for rigid and mobile structures respectively). They discovered molecular mobility for the first time in cellulose at a low heating rate, and outline that their results are in agreement with the intermediate liquid compounds, ILC, theory (chapter 2.5.4), and with mechanisms that suggest intraparticular liquid tar formation (for details the reader is referred to their publication). Their results further show that lignin exhibits the highest fluid phase (100 % fluid H), followed by xylan (61 % fluid H) and cellulose (35 % fluid H) at their temperatures of

maximum fluidity, which are 225, 275 and 325 °C respectively. Dufour et al further explain that there exist interactions between these cell wall polymers, and additionally also with the mineral content (in particular for cellulose), which affect their mobility during pyrolysis. These interactions explain for example why lignin is observed to melt earlier when it is isolated (Dufour et al., 2012; Sharma et al., 2004).

Knowing whether or not a liquid phase is present during pyrolysis is important for several reasons (Dufour et al., 2012) (a) for identifying the underlying reaction mechanisms, e.g. homolytic versus heterolytic, (Hosoya, Kawamoto, & Saka, 2009; Mamleev et al., 2009), (b) softening can considerably impact pyrolysis product composition and properties (Dufour et al., 2012), (c) affects transfer processes (Dufour, Ouartassi, Bounaceur, & Zoulalian, 2011; Fisher, Hajaligol, Waymack, & Kellogg, 2002; Haas et al., 2009; Jarvis et al., 2011) and thus (d) impacts the selectivity of possible thermochemical processes (Dufour et al., 2011). With respect to secondary reactions in sections 3.3.1 and 3.3.2 this means the increased char yield is caused by either vapour-solid interactions, vapour-liquid interactions, or both combined (chapter 6). The circumstantial evidence presented here leans strongly towards a vapour-liquid interaction for the holocellulose components (Mamleev et al., 2009).

3.3.5 Transfer Limitations

When studying pyrolysis it is important to know when heat and mass transfer limitations start to occur, as it is essential to differentiate between the role of time-temperature history and secondary reactions on the yield of char, or to determine how the limitation affect pyrolysis kinetics. This information can be inferred from TGA data. A selection of derivative weight curves of the runs in Figure 3-19 has been plotted in Figure 3-36 for wood cylinders up to 73 mm diameter.

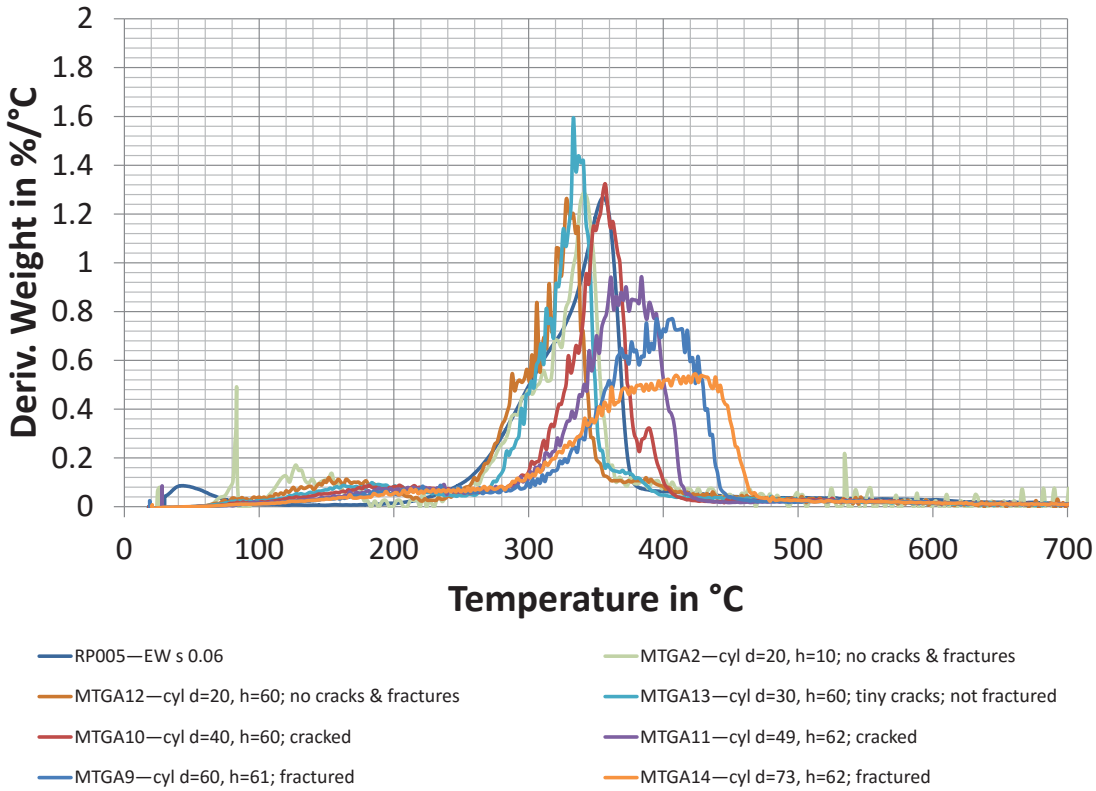

Figure 3-36. Derivative weight curves of a selection of experiments in Figure 3-19. Legend: Experiment/run number—sample description. Cracking means the samples are still in one piece at the end of the run and fracturing means the sample broke into separate pieces. cyl = cylinder; d = diameter in mm; h = height in mm; EW = earlywood; s = slice (the number after s refers to the thickness of the slice in mm).

Figure 3-36 shows that with increasing sample size the main peak of the derivative weight curves widens, the peak height decreases, and the peak maximum shifts to a higher temperature, which is caused by the increased occurrence of transfer limitations (Lin, Cho, Tompsett, Westmoreland, & Huber, 2009). That is, the sample centre temperature increasingly lags behind the sample surface temperature and heater temperature. To infer the onset of transfer limitations, the peak temperature of the derivative weight curves in Figure 3-19 have been plotted as a function of the characteristic dimension in Figure 3-37.

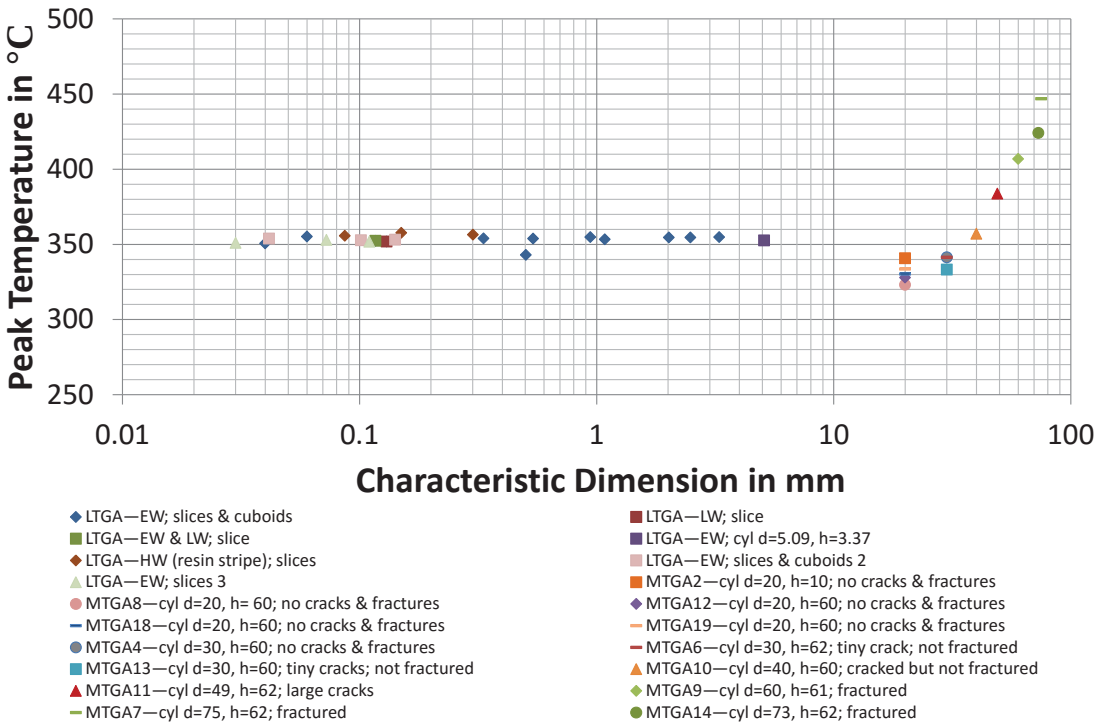

Figure 3-37. Peak temperature of the derivative weight curves of the runs in Figure 3-19 as a function of their characteristic dimension. The graph contains data of two sets of experiments a) laboratory scale thermogravimetric analysis (LTGA), and b) Macro-TGA. The characteristic dimension for the slices and cuboid samples is their thickness perpendicular to the grain and for the cylindrical samples their diameter. Legend: a) type of experiment—wood type; sample geometry_run number (if several have been done), and b) type of experiment including experiment number—sample geometry; structural information. Cracking means the samples are still in one piece at the end of the run and fracturing means the sample broke into separate pieces. Unless stated otherwise the samples of the slices and cuboids were prepared from sapwood. The large cylindrical samples $d \geq 20$ mm have been partly from sapwood and heartwood combined. cyl = cylinder; d = diameter in mm; EW = earlywood; h = height in mm; HW = heartwood; LTGA = laboratory TGA; LW = latewood; MTGA = Macro-TGA.

For small samples, Figure 3-37 shows that the peak temperatures of the derivative weight curves of the runs carried out in the laboratory TGA remained constant at a temperature of approximately 353 °C, which agrees with the peak temperature in Figure 3-1 and Figure B-10 in Appendix B.5.1. For large samples, the Macro-TGA results show a sudden increase in the peak temperature for the specimen with a diameter larger than 30 mm. This is caused by the progressing transfer limitations discussed above. The initially lower peak temperature for the smaller samples analysed in the Macro-TGA is believed to be a consequence of the different design and sample sizes employed in the two TGA's; such effect have already been noted by Morgan and Kandiyoti (2013) who showed that the equipment design affects the analysis. This also explains why in Figure 3-36 the peak of "RP005—EW s 0.06" is at a higher temperature than the ones of the cylinders with a diameter of 20 mm. It is important to note that despite the different peak temperature both, the thin slice and the cylinders with a diameter of

20 mm have a similar onset temperature of pyrolysis, which is to be expected when the same heating rate is applied and the thermal lag is similar between the heater and the sample.

Peak width also varies, if the plots of Figure 3-23 and 3-36 are compared, noting that the actual heating rate in the Macro-TGA was slightly faster than in the lab scale-TGA. The lab-scale TGA results show very similar peak width indicating an absence of transfer limitations. In contrast, the Macro-TGA results gave a range of peak widths, with the smallest 20 mm diameter cylinder having a narrower peak width than the lab-scale results, which is not believed to be due to the slightly higher heating rate in the Macro TGA as this would cause a peak widening due to the increased thermal lag. Thus, the question arises 'What is the cause of this peak narrowing?' A harbinger is given by the lid and no lid experiments in Figure 3-1 and Figure B-10 in Appendix B.5.1, which show a peak narrowing for the cases with a lid. This was confirmed by doing a t-test on the peak temperatures of the experiments with and without a lid in Figure 3-1 and Figure B-10 in Appendix B.5.1. A preliminary F-test indicated equal variance, Table 3-20.

Table 3-20. F-test for equality of variances.

	No lid	**Lid**
Mean	353.26	352.38
Variance	0.48	0.33
Observations	11	11
df	10	10
F	1.45	
P(F<=f) one-tail	0.28	
F Critical one-tail	2.98	

Note. The analysis was performed with Microsoft Excel (Microsoft, Redmond, WA, USA). The significance level was set to 0.05. df = degrees of freedom; F = F-test for null hypothesis; P(F<=f) one-tail = P-value for one tail F-test.

Thus, a t-test assuming equal variances was carried out with a significance level of 0.05, Table 3-21.

Table 3-21. t-test for equality of means assuming equal variances.

	No lid	**Lid**
Mean	353.26	352.38
Variance	0.48	0.33
Observations	11	11
Pooled Variance	0.40	
Hypothesized Mean Difference	0	
df	20	
t Stat	3.26	
P(T<=t) one-tail	0.00196	
t Critical one-tail	1.72	
P(T<=t) two-tail	0.0039	
t Critical two-tail	2.09	

Note. The analysis was performed with Microsoft Excel (Microsoft, Redmond, WA, USA). The significance level was set to 0.05. df = degrees of freedom; P(T<=t) one-tail = P-value for one tail t-test; P(T<=t) two-tail = P-value for two tail t-test; t Stat = t-statistics.

Table 3-21 shows that the null hypothesis of equal means was rejected (two tail t-test) with 99.6 % confidence (P-value of 0.004), revealing that the application of a lid decreases the peak temperature, which agrees with literature (Varhegyi, Antal, Szekely, Till, & Jakab, 1988). This confirms the above mentioned peak narrowing for the cases with lid (believed to be due to enhanced secondary reactions). These findings are further supported by Figure 3-13 and Figure 3-14 (see also Figures in Appendix B.5.3), and Figure 3-24 (see also Figure B-23 to Figure B-25 in Appendix B.6.1) showing that heavier/larger samples lead to an earlier completion of pyrolysis. Thus, the peak narrowing with increased sample size before the onset of the apparent transfer limitations in Figure 3-36 is ascribed to increased secondary reactions. Therefore, Figure 3-37 indicates that transfer limitations are negligible for samples with a characteristic dimension ≤ 20 mm. However, this is in conflict with the calculated characteristic length of 480 μm for a Biot number of 0.1 (negligible internal transfer limitations) in section 2.2.2. The question arises of what is preventing the existing transfer limitations from being detected in the TGA curves? Before exploring this further it is important to mention here that three Macro-TGA experiments have been omitted in Figure 3-37 as they were shifted, which is believed to be due to balance issues experienced during this time. After maintaining the equipment (removing deposited highly viscous tar) this was not observed anymore.

To investigate transfer limitations further the so-called 'thermocouple experiments', discussed in 3.2.3 (Figure 3-5), were carried out. Typical results of those experiments for cylinders with a diameter of 20, 30, and 74 mm are depicted in Figure 3-38, Figure 3-39, and Figure 3-40 respectively.

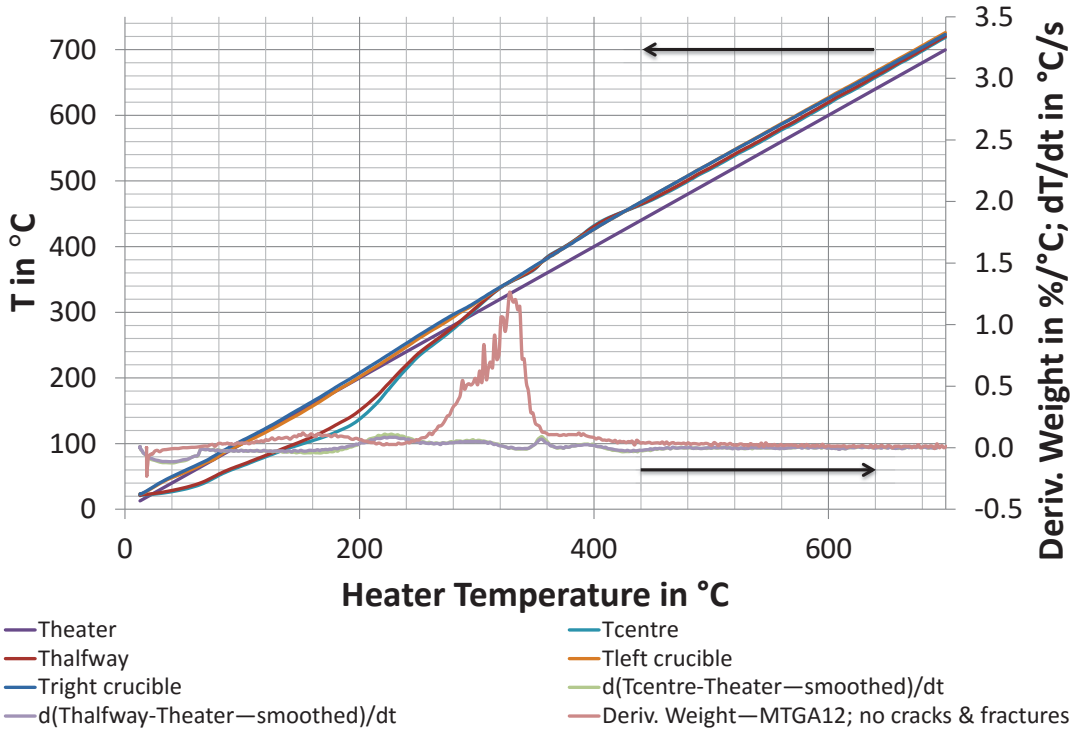

Figure 3-38. Results of thermocouple run 10 employing a cylinder with a diameter of 20 mm and a height of 60 mm. The sample showed no cracks and fractures at the end of the run. Cracking means the samples are still in one piece at the end of the run and fracturing means the sample broke into separate pieces. The derivative weight curve of experiment MTGA12 is included to illustrate the relationship between temperature and weight-loss events. "Tleft crucible" and "Tright crucible" are thermocouples T_1 and T_2 in Figure 3-5 respectively.

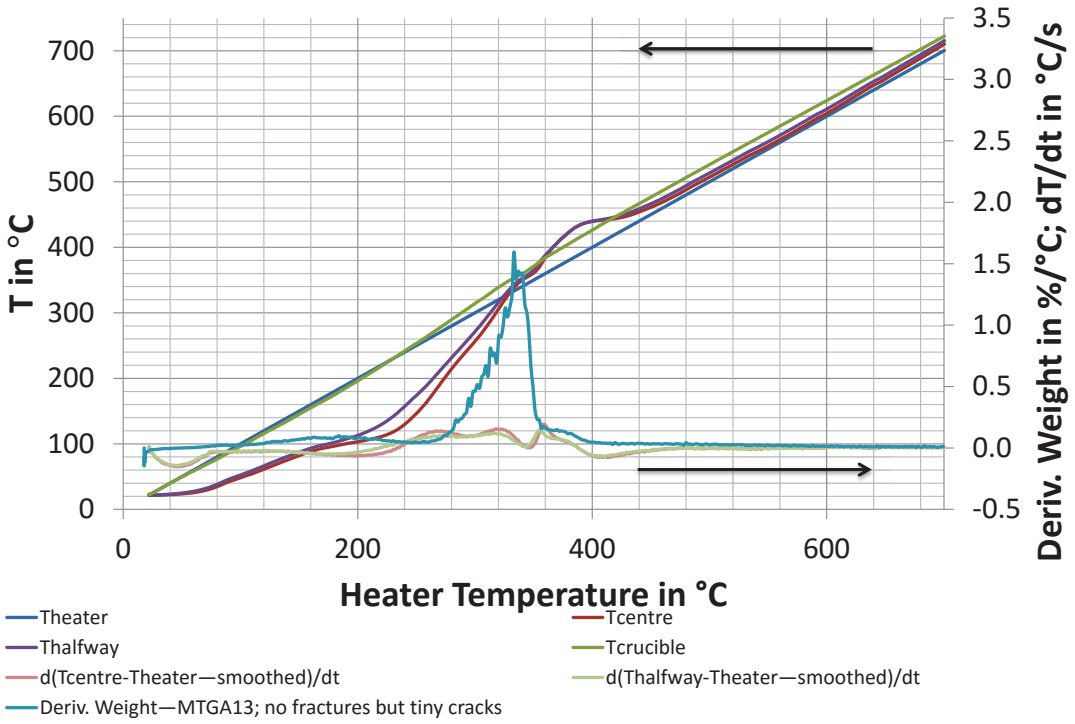

Figure 3-39. Results of thermocouple run 3 employing a cylinder with a diameter of 30 mm and a height of 60 mm. The sample showed no cracks and fractures at the end of the run. Cracking means the sample is still in one piece at the end of the run and fracturing means the sample broke into separate pieces. The derivative weight curve of experiment MTGA13 is included to illustrate the relationship between temperature and weight-loss events.

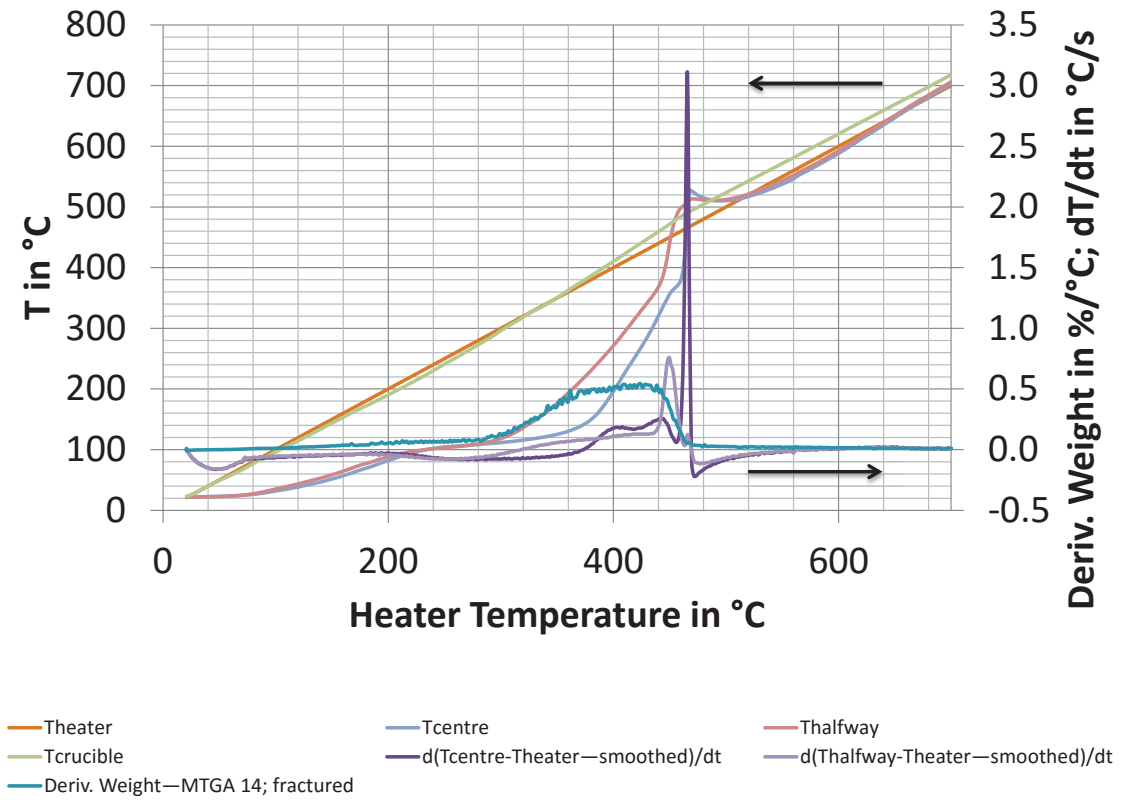

Figure 3-40. Results of thermocouple run 6 employing a cylinder with a diameter of 74 mm and a height of 60 mm. The sample had cracks but no fractures at the end of the run. Cracking means the sample is still in one piece at the end of the run and fracturing means the sample broke into separate pieces. The derivative weight curve of experiment MTGA14 is included to illustrate the relationship between temperature and weight-loss events.

Repeat runs of the experiments in Figure 3-38, Figure 3-39, and Figure 3-40 can be found in Appendix B.6.2. The repeatability of the respective derivative weight curves is illustrated in Appendix B.6.3. Figure 3-38 to Figure 3-40 show, in the first instance, that the heater temperature and the actual temperatures in the sample do not match due to thermal lag, The thermal lag increases with sample size caused by the increasing absolute moisture mass and increasing transfer limitations in the wood (Figure 3-36). The latter one is expressed by the increasing temperature difference between the centre and half radius temperature of the samples with growing sample size. It is important to note that the temperature gradient is much larger between the sample surface and the half radius temperature. In fact the surface temperature will be very close to the heater temperature, which is revealed by the similar pyrolysis onset temperatures in Figure 3-36 despite there being still a large temperature difference between the heater temperature and the sample centre temperature in Figure 3-38. Thus, there is definitely a temperature gradient present in the samples with a diameter of 20 mm, and the reason that there is no temperature lag visible in the pyrolysis peak of this sample is due to the

increasing exothermicity of the pyrolysis reaction with size as revealed by the increasingly faster internal heating rate in Figure 3-38 to Figure 3-40. This is illustrated in Figure 3-38 to Figure 3-40, and in Appendix B.6.2 by the time derivative of the temperature difference between the thermocouples mounted in the sample and the heater thermocouple. A differential temperature decrease is coupled to endothermic processes/reactions and accordingly a differential temperature rise to exothermic processes/reactions (heat of pyrolysis is discussed in more detail in chapter 5). These curves illustrate that the internal sample heating rate is faster than the heater during the main pyrolysis region, and that this internal heating rate is greater with larger samples. Thus , plotting the derivative weight curve of run MTGA12 in Figure 3-36, which had no apparent transfer limitation, as a function of the actual sample centre temperature and not the heater temperature should result in a derivative weight curve matching the one of run RP005 in Figure 3-36, which is depicted in Figure 3-41. It is also noticeable in Figure 3-38 to Figure 3-40 that in all the experiments the measured crucible temperature is higher than the heater temperature from above 200 °C, which was found to be an inherent equipment characteristic. While the exact reason is unknown, it is possibly linked to the positioning of the heater thermocouple in the reactor wall (T_s in Figure 3-5), which caused it to have a reduced view factor.

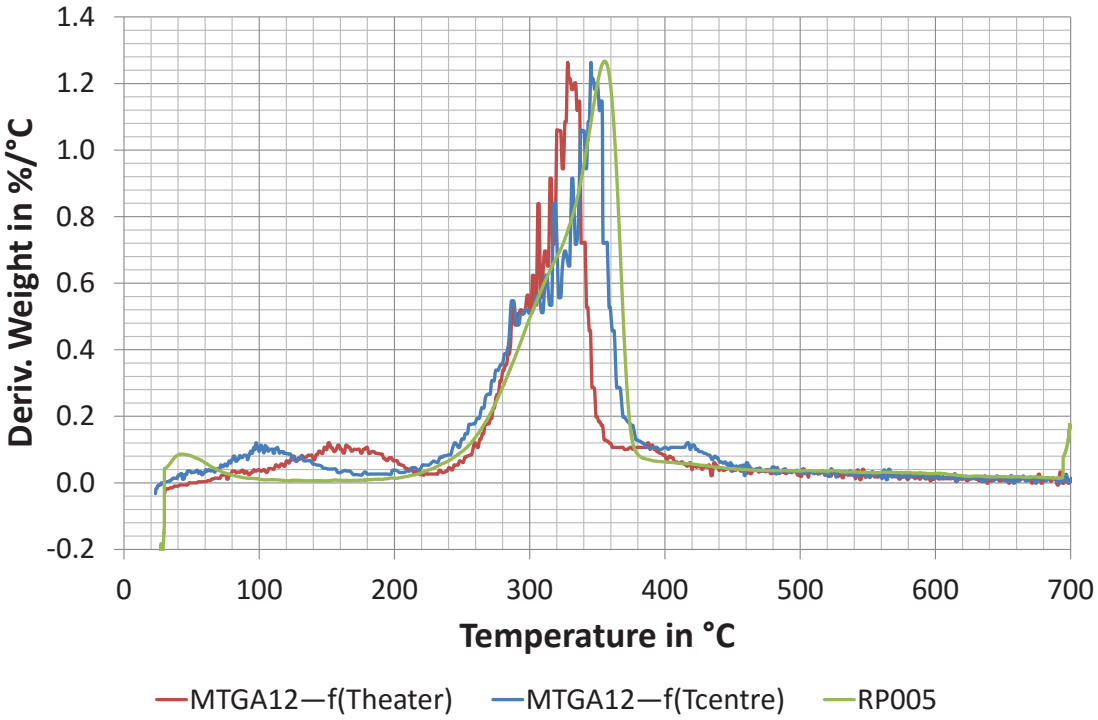

Figure 3-41. Difference between plotting the derivative weight curve of the Macro-TGA experiments as a function of the heater temperature compared to the actual sample temperature. The run RP005 of Figure 3-36 has been included to demonstrate that this is the cause of the different peak temperature in Figure 3-37. Theater = Heater temperature; Tcentre = centre temperature of the pyrolysed sample.

Figure 3-41 confirms the above reasoning and shows that this is the reason for the observed shift in peak temperatures in Figure 3-37. That the corrected curve is still completed at a slightly lower temperature than the labscale TGA run RP005 is due to the fact that the conduction caused by the relatively thick metal sheath of the thermocouples used in the experiments is non-negligible. That is, the actual sample temperature in case of exothermic reactions is higher and for endothermic reactions lower.

These findings reveal that in samples with no apparent transfer limitations (<20 mm in Figure 3-37), that is, the main weight loss does not extend past a heater temperature of 380 °C, the actual pyrolysis time is slightly reduced when a lid (see Table 3-21) or larger/heavier samples are pyrolysed as the main weight loss is completed at lower heater temperatures, which is a function of time. Thus the main weight loss occurs in this regime in increasingly shorter times in samples with a lid or increasing mass/size, meaning the overall heating rate for this period increases. This indicates that the char yield increase is caused by secondary reactions and not the time temperature history as it is a well-established fact that the char yield decreases with heating rate (Antal & Grønli, 2003; Di Blasi, 1996; Grieco & Baldi, 2011; Lin et al.,

2009; McCarl, Peacocke, Chrisman, Kung, & Sands, 2009; Williams & Besler, 1996) (but here the opposite trend; that is, an increase in yield with sample size, is seen in Figure 3-19) unless the extended time period below the onset of pyrolysis caused more char forming reactions, which is explored in the next section. In favour of secondary reactions is also the observation that in the transfer limited samples that cause a widening of the pyrolysis peak to higher heater temperatures (samples with a characteristic length >20 mm in Figure 3-37) due to the significant thermal insulation in these samples do not yield more char although higher yields should be attainable. More char would be expected if the overall slower heating rate in the larger samples would cause the yield increase but instead we observe a constant char yield along with the formation of cracks and fractures supporting the important role of secondary vapour interactions. Interesting is that the overshoot in Figure 3-38, Figure 3-39, and Figure 3-40 occurs at the end of the weight loss region indicating possible exothermic rearrangement reactions.

In general moisture causes always a thermal lag due to its high enthalpy of evaporation. This can be said for any liquid that is undergoing a phase change and thus transfer limitations are expected to be visible in the TGA curve for the extractives fraction, which was shown in 3.3.4 to form a liquid phase. A shift in the extractive peak is present in runs with a lid compared to runs without a lid, as shown in Figure 3-1 and Figure B-10 in Appendix B.5.1. Also, Figure 3-42 shows that as the sample mass increases, transfer limitations cause an increase in the extractive peak temperature, for the no lid case presented earlier in Figure 3-1.

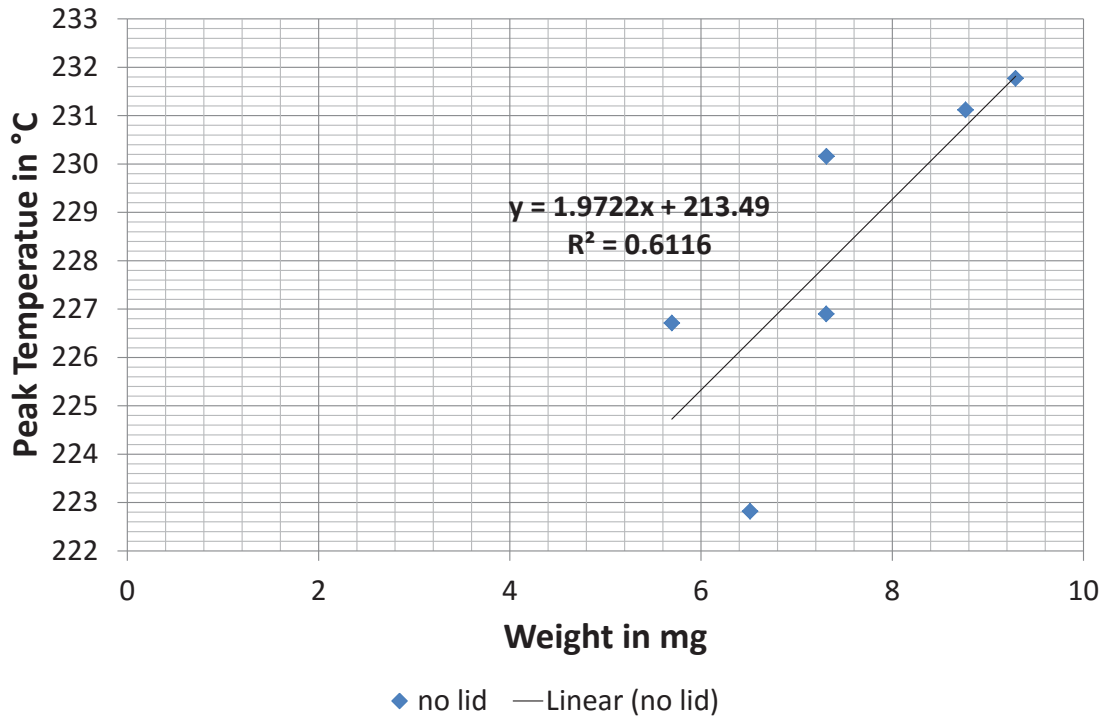

Figure 3-42. Peak temperature of the extractive peaks in Figure 3-1 of the experimental runs without a lid. R^2 = coefficient of determination.

The presence of transfer limitations is further supported by the difference curve "no lid-lid; m loss" in Figure 3-18, which shows a minima at approximately 270 °C indicating that some products are just released later when a lid is used, as mentioned in 3.3.1. Such a peak minima is also observed in Figure 3-1 and in Figure B-9 in Appendix B.5.1 but decreases respective to the reduced extractive content, as reported in 3.3.1. This reveals that the transfer limitations decrease with lower extractives content. An interesting observation from Figure 3-15 and Figure 3-16 is the relatively large delay and widening of the moisture peak, which is not in proportion to the change in Figure 3-23, Figure 3-24, Figure B-11 and Figure B-12 in Appendix B.5.1, the Figures in Appendix B.5.3, and Figure B-22 to Figure B-25 in Appendix B.6.1, indicating that other light volatile substances are present and that the moisture transfer is hindered more in heartwood than in the sapwood samples, a phenomena which could be related to the fact that the bordered pits are aspirated right from the beginning of pyrolysis and so minimise moisture transport. This goes alongside with the observation of increased cracks and fractures in the earlywood, as discussed in 3.3.4. However, as discussed above the position of the main pyrolysis peak is not affected by transfer limitations for the experiments carried out in the laboratory TGA. Contributing to this is also the fact that the porosity increases and the sample shrinks with pyrolysis temperature (section

3.3.4). One further point is that the Macro-TGA experiments shown in Figure 3-36 have wide and flat profiles and do not appear to have extractives peaks, when compared to the lab-TGA runs in Figure 3-1. This is due to the differential heating conditions across the larger samples leading to the release of the lighter pyrolysis products at the same time as extractives.

Another method applied in literature to determine the regime when internal transfer limitations are negligible compared to external, is by reducing the sample size until the solid residue becomes constant. This supposition is based on the principle that the primary char yield is dependent on the reaction temperature and the intraparticle residence time of the volatiles (Di Blasi & Branca, 2001). However, in section 3.3.2 it was shown that a separation of primary and secondary reactions was not possible, and that it is in fact likely that the majority of the char yield derives from secondary char formation.

3.3.6 Torrefaction and Its Impact on Primary Char Formation

Above it was outlined that it is possible that the char yield increases merely due to the fact that the sample spends longer at lower temperature. Thus the char yield increase with sample size/presence of a lid could after all be due to primary reactions. Primary char forming reactions are according to the definition in chapter 2 rearrangement reactions that happen in the solid matrix and lead to a higher char yield. As reviewed by Collard and Blin (2014), these type of reactions (intra- and intermolecular) increase the reticulation and thermal stability of the solid before the onset of depolymerisation, and thus cause an increase in the char yield. In particular dehydration reactions are highly correlated with the char yield especially in the case of cellulose (Collard & Blin, 2014). Collard and Blin elucidate in their review that these rearrangement reactions are favoured under slow pyrolysis conditions explaining the higher observed char yield at lower heating rates. These reactions can also be enhanced by torrefaction. Torrefaction is defined as mild pyrolysis, and was already discussed in 2.6.8. There it was mentioned that with increasing torrefaction temperature the char yield increases but that this was in contradiction with findings of Antal and his team (see 2.6.8). Therefore, the aim of this section is to investigate if the extent of primary char formation under the studied conditions can be influenced by torrefaction and how this compares to the discussion above.

The weight-loss and temperature profile of the three torrefaction experiments carried out in this research are depicted in Figure 3-43.

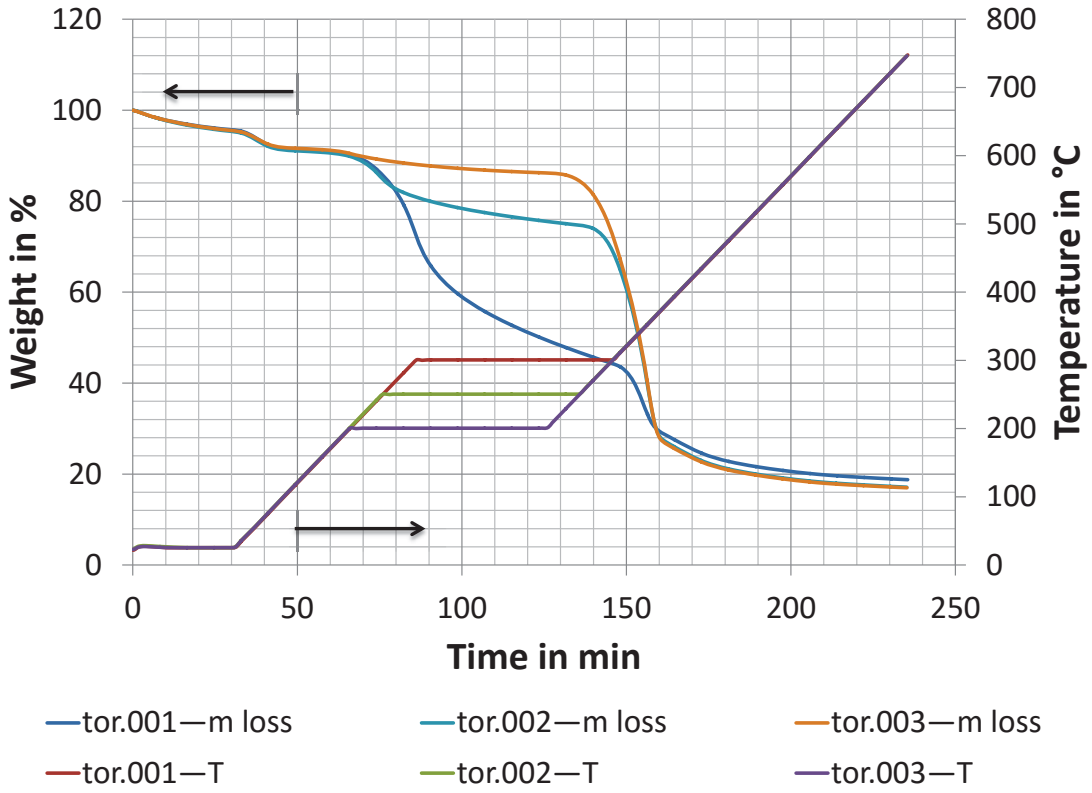

Figure 3-43. Weight-loss and temperature profile of torrefaction experiments. Legend: experiment—parameter displayed. m = weight; T = temperature; tor = torrefaction.

It is important to note that the experiment "tor.003" in Figure 3-43 employed a temperature of 200 °C, which is below the typical torrefaction range discussed in 2.6.8. The reason that such a low temperature was chosen is that at this temperature changes in the extractives content already occur (Figure 3-1, and Figure B-10 in Appendix B.5.1). Figure 3-43 shows that during the holding period weight-loss continues to take place, which is larger for higher torrefaction temperatures. This is due to the above discussed exothermic nature of pyrolysis as illustrated in Figure 3-38 to Figure 3-40, and is discussed in more detail in chapter 5. This reveals that the actual sample temperature does not agree with the set temperature of the TGA, and indicates that it is impossible to hold the sample temperature at a constant value inside the pyrolysis temperature range if no means of quenching is available (for more details see chapter 5). This effect will be exaggerated if a "bed" of particles is applied. Looking at the final weight after the torrefaction step in Figure 3-43 not much difference between the runs is visible, which is particularly true for "tor.002" and "tor.003", which agree with the curve in Figure B-9

in Appendix B.5.1 depicted in Appendix B.8 in Figure B-38. Plotting the yields of the torrefaction results into the graph of Figure 3-12 it is evident that it follows the trend of the no lid experiments, Figure 3-44.

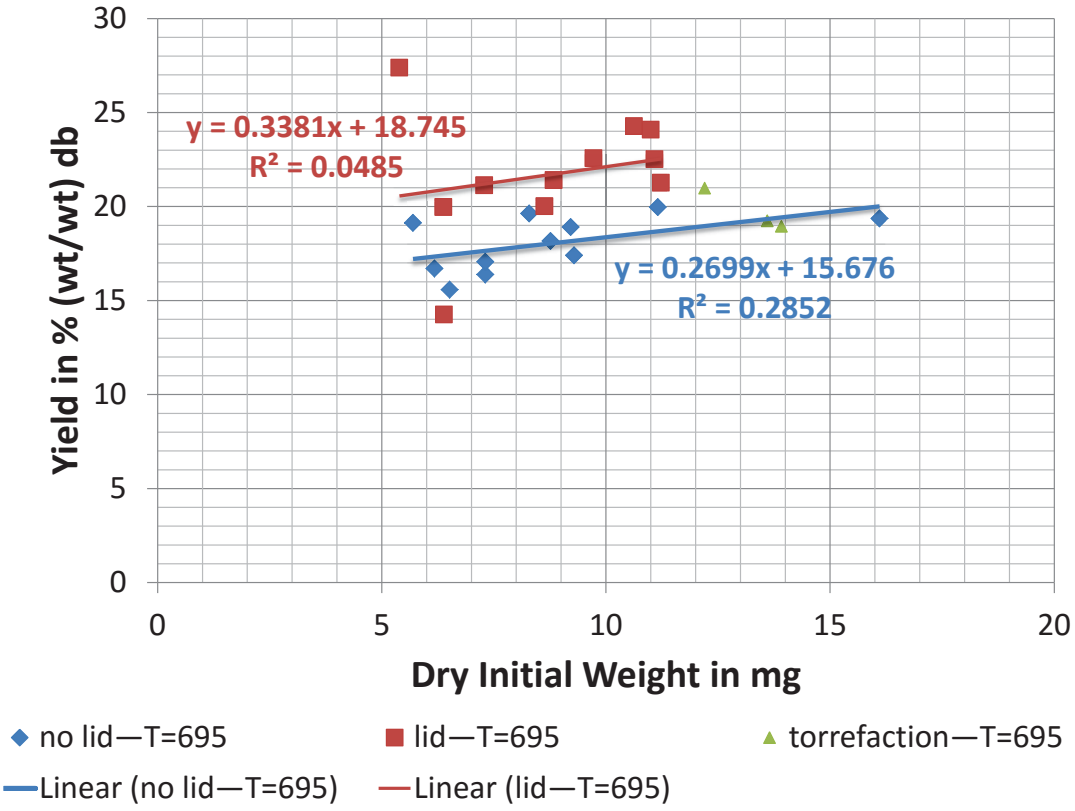

Figure 3-44. Char yield at 695 °C on a dry basis of pyrolysis experiments including a torrefaction step compared to pyrolysis without a torrefaction step with and without a lid as a function of the initial dry sample weight. The torrefaction experiments did not employ a lid. The dry weight was determined for lid and no lid experiments at 152 and 126 °C respectively. db = dry basis; R^2 = coefficient of determination.

Figure 3-44 shows that a torrefaction step has no impact on the charcoal yield. This becomes clearer when plotting the fixed carbon yield, Figure B-39 in Appendix B.8. Thus, the primary reactions are not enhanced by a thermal pre-treatment step in the slow pyrolysis regime and the lower heating rate cannot explain the increasing char yield with larger sample size or mass as argued above. This highlights the importance of secondary reactions involving an enhanced vapour-phase residence time, and agrees with literature (Antal, Mok, Varhegyi, & Szekely, 1990; Varhegyi, Antal, Szekely, Till, & Jakab, 1988; Varhegyi, Antal, Szekely, Till, Jakab, et al., 1988).

3.3.7 Temperature Regime of Secondary Char Forming Reactions

The findings above revealed that extraparticle and intraparticle secondary char formation are essentially the same and that transfer limitations do not affect the main pyrolysis peak in the laboratory scale experiments. This is also the case for the experiments employing sawdust as evidenced by their similar peak temperature, as shown in Table 3-21, to the ones in Figure 3-37. This is further illustrated in Figure B-33 in Appendix B.6.4. Therefore, to demonstrate the temperature regime of secondary reactions the results of the crucible experiments with and without a lid in Figure 3-1 are taken as representative and re-plotted in Figure 3-45 together with the average total ion chromatogram, TIC, from three evolved gas analyses.

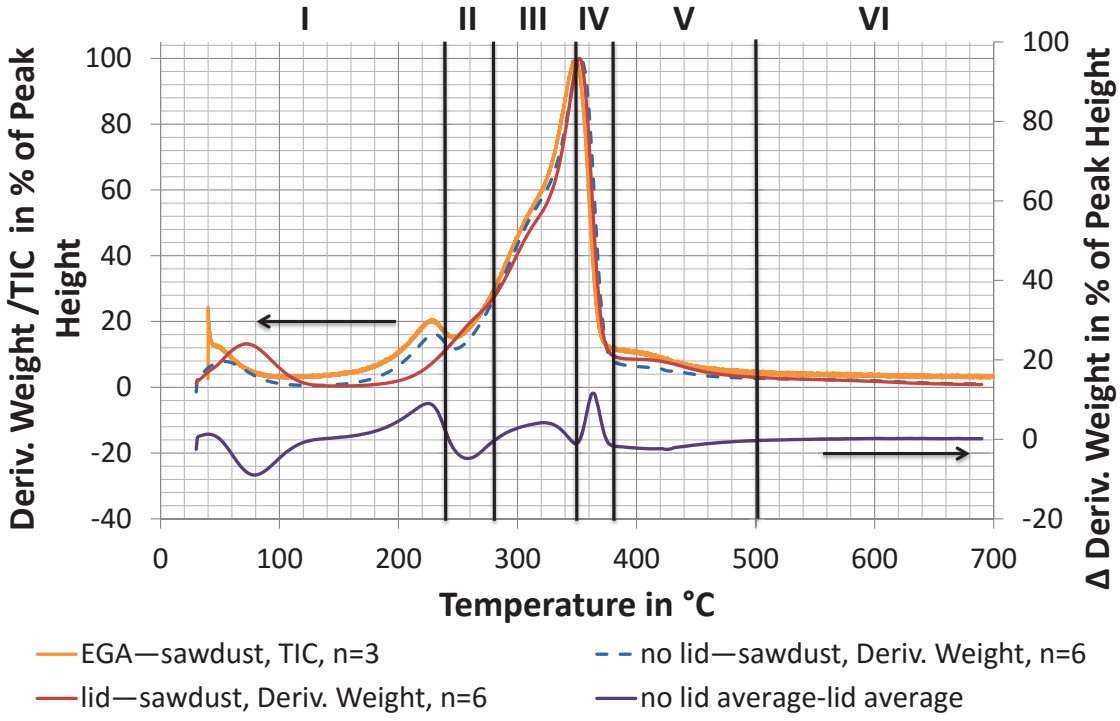

Figure 3-45. Derivative weight-loss of radiata pine in crucibles with and without lid compared to EGA of radiata pine. The derivative weight-loss and the Total Ion Chromatogram, TIC, were plotted as percent of their respective maximum peak height to make them directly comparable. The difference curve of TGA runs with and without lid illustrate the regions were secondary reactions take place apart from the difference caused by the evaporation of water. This curve was used to establish the temperature ranges, separated by the vertical black lines and numbered by Roman numerals, which are relevant for analysis of secondary reactions. EGA = Evolved Gas Analysis; n = number of runs over which was averaged; TIC = Total Ion Chromatogram; TGA = Thermogravimetric analysis.

The EGA results in Figure 3-45 are similar to the open crucible experiments. This is expected as the EGA directly detects the volatile pyrolysis products while the TGA measures the weight which changes according to the release of volatile pyrolysis products. The good agreement verifies that both methods are valid for studying

pyrolysis as the result is independent of the analysis method (Morgan & Kandiyoti, 2013). The difference curve between experiments with and without a lid gives an indication of the temperature regions relevant for studying secondary reactions; i.e., when the difference is unequal to zero. Thus, each point it attains zero was selected as the boundary of a pyrolysis temperature range where secondary reactions occur apart from the region associated with the evaporation of water (below 140 °C). These boundaries are shown in Figure 3-45 by the vertical black lines separating the entire pyrolysis range into six zones giving boundary temperatures: 240 °C, 280 °C, 350 °C, 380 °C, 500 °C, and 700 °C. The Py-GC/MS study in chapter 6 has been based on these target temperatures, and confirms the findings of Figure 3-45 that secondary reactions take place over the entire pyrolysis range, zone I to V. Volatiles are primarily characteristic of depolymerisation reactions taking place in zone III to IV (Collard & Blin, 2014). In zone VI alone no secondary reactions can be detected as the amount of volatiles released is greatly reduced (see chapter 6 for details). This region and zone V are referred to as the charring regions characterised mainly by the organisation of the benzene rings in the solid into a polycyclic structure (*ibid*).

Figure 3-47 overlays on the same plot, differential temperature data from the Macro-TGA trials for the wooden cylinders of diameter 20 mm and height 60 mm as shown in 3.3.5 the differential mass loss curves are similar to the lab-TGA results. Interestingly, the same zones I-VI appear for the Macro-TGA sample, when the internal to external temperature difference is plotted, Tcentre – Theater (position shown in Figure 3-5), displaying the close relationship between pyrolysis reaction energetics and secondary reactions. This confirms that secondary reactions play a major role in pyrolysis, in particular for char formation. The time derivative further shows that pyrolysis is completed at 500 °C.

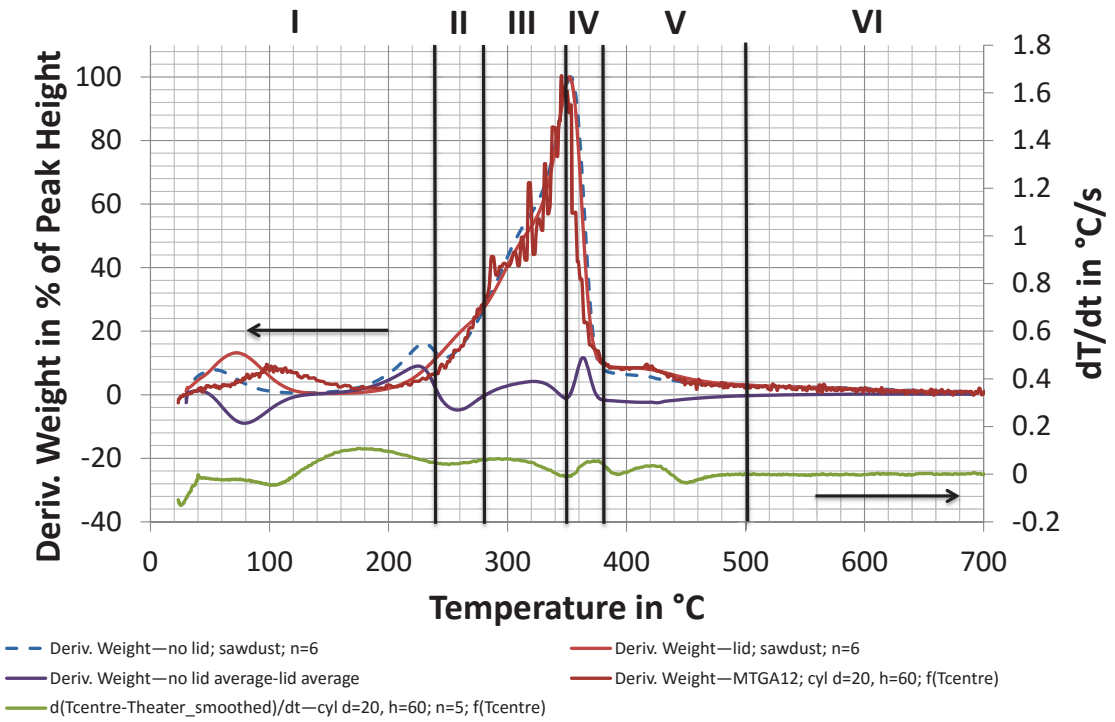

Figure 3-46. Comparison between the difference in the derivative weight of sawdust pyrolysed in crucibles with and without lid in a laboratory TGA to the average time derivative of the temperature difference between the centre and heater temperature observed during the pyrolysis of cylinders with a diameter of 20 mm and a height of 60 mm in a Macro-TGA. The derivative weight curves were plotted as percent of their respective maximum peak height to make them directly comparable. The vertical black lines separate the different regions where secondary reactions take place, which are numbered by roman numerals. cyl = cylinder; d = diameter in mm; Deriv. = derivative; f(Tcentre) = plotted as a function of the measured centre temperature of the sample; h = height in mm; n = number of runs over which was averaged; TGA = Thermogravimetric analysis.

To sum it up Figure 3-45 and Figure 3-46 show that secondary reactions take place over the whole pyrolysis range, that is ≈ 140 to 500 °C, which is lower than previous suggestions that begin from 280 °C (F. L. Brown, 1958) to above 380 °C (Pattanotai, Watanabe, & Okazaki, 2013). A slightly later onset of secondary reactions than 140 °C in literature could be due to the absence of extractives which, in this research, would lead to an onset temperature of pyrolysis and thus secondary reactions of 200 °C, Figure 3-24. The reported temperature of 380 °C by Pattanotai et al. (2013) seems a bit high as the derivative weight curves in Figure 3-45 and Figure 3-46 indicate that the majority of pyrolysis is already completed at this stage, and not much more volatiles are produced which could contribute to secondary reactions. It is believed that the effect of secondary reactions below 380 °C was not observed in the study of Pattanotai et al. as it was hidden by the rapid pyrolysis decomposition reactions taking place at lower temperatures. This is evidenced in Figure 3-10, which shows that the rapid weight loss below 380 °C conceals the difference between both scenarios (lid and

no lid) in the weight-loss curve. This would have been exaggerated by Pattanotai et al. as they employed a higher heating rate of 0.5 K/s affirming the findings of this study.

3.3.8 Biomass Components and their Behaviour during Primary and Secondary Pyrolysis Reactions

In 3.2.1.2 it was outlined that radiata pine in particular and biomass in general consists of four main organic fractions (a) extractives, (b) hemicellulose, (c) cellulose, and (d) lignin. These components have been applied in literature to model pyrolysis based on chemical composition (Biagini & Tognotti, 2014; Grønli, Várhegyi, & Di Blasi, 2002; Koufopanos, Lucchesi, & Maschio, 1989; Orfão, Antunes, & Figueiredo, 1999; Raveendran, Ganesh, & Khilar, 1996; X. Y. Wang, Wan, Chen, & Wang, 2012). The majority of the reported work has been done on a three component mechanism without extractives but due to the relatively high amount of extractives present in the feedstock used, Table 3-1, the extractives are included in this work similar to Biagini and Tognotti (2014). It is important to note here that the aim of this section is not to provide another set of kinetic parameters, which vary widely in literature and are subject to ongoing debate to the point that the underlying principles of solid state reaction theory are questioned including the applicability of the Arrhenius expression (M. E. Brown, 1988; Di Blasi, 2008; White, Catallo, & Legendre, 2011). For detailed information the reader is referred to the excellent review of White et al. (2011). Rather, the goal is to identify the char yield of each of the four so-called pseudo-components, named pseudo because they are not really separable (Branca, Albano, & Di Blasi, 2005; Di Blasi, 2008), and investigate how this is affected by secondary reactions. This was done by fitting a first-order reaction model (Biagini & Tognotti, 2014; Grønli et al., 2002; X. Y. Wang et al., 2012) to the conversion curves of the TGA runs with and without a lid in section 3.3.1, and assuming that in both cases only primary reactions take place. In this model the devolatilisation, as indicated above, is described by four independent parallel reactions representing the four biomass components. That is, it is assumed that the interaction between the pseudo-components is negligible (Biagini & Tognotti, 2014; Cozzani, Lucchesi, Stoppato, & Maschio, 1997; Raveendran et al., 1996; X. Y. Wang et al., 2012). The decomposition scheme is depicted in Figure 2-18 in 2.7.1. Corresponding to Figure 2-18 the mass loss rate of biomass is defined as (Grønli et al., 2002; X. Y. Wang et al., 2012):

$$-\frac{dm_b}{dt} = \sum_{i=1}^{4} x_i \frac{d\alpha_i}{dt} \ , \tag{3.9}$$

where m_b is the biomass weight in % (wt/wt), t the time in s, x_i the fraction of component i that constitutes the overall weight-loss, and α_i the degree of decomposition/conversion of component i in % (wt/wt). The degree of conversion can be calculated by (Sun, Huang, Gong, & Cao, 2006; X. Y. Wang et al., 2012):

$$\alpha_i = \frac{m_{in,i} - m_i}{m_{in,i} - m_{char,i}} \ , \tag{3.10}$$

where $m_{in,i}$, m_i, and $m_{char,i}$ are the initial, actual and final sample weight of component i in kg respectively. It is important to know that the initial sample weight was chosen as the dry sample weight, that is, at 126 and 152 °C for the cases no lid and lid respectively. Generally, the kinetic process is described by the following equation (Cagnon, Py, Guillot, Stoeckli, & Chambat, 2009; Sun et al., 2006; White et al., 2011):

$$\frac{d\alpha_i}{dt} = k_i(T) \cdot f(\alpha_i) \ , \tag{3.11}$$

where k_i is the decomposition rate constant of component i, which is commonly described by the Arrhenius equation (equation (2.3) in 2.2.2). Inserting equation (2.3) into equation (3.11) and assuming, as mentioned above, a first-order reaction model (Biagini & Tognotti, 2014; Grønli et al., 2002; X. Y. Wang et al., 2012) equation (3.12) is obtained:

$$\frac{d\alpha_i}{dt} = A_i e^{\left(-\frac{E_i}{R_g T}\right)} \ (1 - \alpha_i) \ . \tag{3.12}$$

In the case of the application of a constant heating rate, β, in K/min:

$$\beta = \frac{dT}{dt} \tag{3.13}$$

one obtains upon rearrangement, substitution into equation (3.12), separation of variables and integration (Flynn, 1997; Flynn & Wall, 1966; Sun et al., 2006; Tang, Liu, Zhang, & Wang, 2003; X. Y. Wang et al., 2012):

$$\int_0^{\alpha_i} \frac{d\alpha_i}{(1-\alpha_i)} = -\ln(1-\alpha_i) = \frac{A_i}{\beta}\int_{T_0}^{T} e^{\left(-\frac{E_i}{R_g T}\right)} dT \,. \tag{3.14}$$

The lower limit of integration, T_0, in the right hand side of equation (3.14) can be assumed to be 0 if no reaction has taken place between 0 and T_0 (Flynn, 1997), which is valid for the case considered here (starting temperature of 152 and 126 °C for the case with and without a lid respectively is below the onset of pyrolysis, see Figure 3-1). Thus equation (3.14) becomes:

$$\int_0^{\alpha_i} \frac{d\alpha_i}{(1-\alpha_i)} = -\ln(1-\alpha_i) = \frac{A_i}{\beta}\int_0^{T} e^{\left(-\frac{E_i}{R_g T}\right)} dT = \frac{A_i E_i}{\beta R_g}\cdot p(u) \,. \tag{3.15}$$

In equation (3.15) $p(u)$ is the Arrhenius temperature integral with:

$$u = E_i / R_g T \ , \tag{3.16}$$

which cannot be analytically integrated (Flynn, 1997; Sun et al., 2006; Tang et al., 2003). It can be solved numerically or by approximations (Biagini & Tognotti, 2014; Flynn, 1997; Flynn & Wall, 1966; Tang et al., 2003; X. Y. Wang et al., 2012). Depending on the applied method the results can vary as discussed by Flynn (1997).

Here it was decided to use numerical integration in which the ordinary differential equation (3.12) is solved in Matlab R2011b (MathWorks, Natick, MA, USA) with the inbuilt solver ode15s. The stiff solver ode15s had to be used as in the flat end zone, when the conversion is completed, small errors result in oscillations leading to unexpected results (Caballero & Conesa, 2005). These errors made it impossible to fit the derivative curves for which reason the integrals were used for fitting, although the derivative curve is preferred as it represents the devolatilisation mechanism in more detail (Biagini & Tognotti, 2014). Fitting was done with the nonlinear least-squares solver "lsqnonlin" in Matlab. In order to perform fitting a subset of 200 equally spaced points along the arc length of the curve was selected from the raw data as described by Caballero and Conesa (2005). For the fitting procedure itself it is important that the parameters to be optimized (A_i, E_i, and x_i) are well scaled, which is particularly important for TG analysis as parameters can have different orders of magnitude as demonstrated in Table 3-22. Ideally the scaled values should be around 1 (*ibid*). In this study the scaling method outlined by Caballero and Conesa (2005) is

used. That is, E_i is scaled by dividing by 100 kJ/mol and A_i is scaled by introducing a reference rate, $k_{i,ref}$:

$$k_{i,ref}(T) = A_i e^{\left(-\frac{E_i}{R_g T_{i,ref}}\right)} , \tag{3.17}$$

where $T_{i,ref}$, is selected as the predicted maximum temperature of the decomposition of component i. The selected values are based on the case of pyrolysis without a lid, and are 230, 320, 353.26 and 400 °C for the extractives, hemicellulose, cellulose and lignin peak respectively. The values are selected from Figure 3-1 and Table 3-21, where the allocation of the reactions to the peaks was made based on the findings of this research and the work of Biagini and Tognotti (2014). Dividing the Arrhenius equation (equation (2.3) in section 2.2.2) by equation (3.17) results in the alternative form of the Arrhenius equation:

$$k_i = k_{i,ref} e^{\frac{E_i}{R_g}\left(\frac{1}{T_{i,ref}} - \frac{1}{T}\right)} . \tag{3.18}$$

Equation (3.18) is used instead of the Arrhenius expression in equation (3.12) for numerical integration and curve fitting of the parameters $k_{i,ref}$, E_i, and the fraction x_i. Subsequently A_i is obtained by rearranging equation (3.17). It is important to note that lower and upper bounds were introduced for x_i:

$$0 \leq x_i \leq x_{i,max} , \tag{3.19}$$

where $x_{i,max}$ is defined as:

$$x_{i,max} = \frac{m_{i,in}}{\Delta m_b} . \tag{3.20}$$

In equation (3.20) $m_{i,in}$ is the initial mass of component *i* present in the feedstock on a dry basis in kg and Δm_b is the absolute weight-loss of the dry biomass over the pyrolysis range in kg. The initial values for A_i and E_i are taken from Grønli et al. (2002), and the initial values of x_i are based on the feedstock composition in Table 3-1 and Table 3-2. It is important to note that the values in Table 3-2 were converted to an oven-dry basis, and that it is assumed that the decomposition is entirely due to the four pseudo-components, that is, the unidentified residual fraction in Table 3-2 was

disregarded and the pseudo-component composition adjusted to match 100 % (wt/wt). The initial values are summarised in Table 3-22.

Table 3-22. Initial values for A_i, E_i and x_i.

Components	A_i	E_i	x_i
	1/min	**kJ/mol**	
Extractives	2.03E+12	127	0.056
Hemicellulose	1.28E+08	100	0.237
Cellulose	1.37E+19	236	0.387
Lignin	238.86	46	0.320

Note. A_i = pre-exponential factor in Arrhenius equation for component i; E_i = exponential factor in Arrhenius equation for component i; x_i = fraction of component i initially present in the feedstock.

The Matlab code for the numerical integration and curve fitting procedure can be found in Appendix B.7.1.

The fitting was performed on runs “RP012” and “RP013” in Figure 3-9 as they employed the same initial weight and are representative of the cases no lid and lid respectively. The fit is illustrated visually in Figure 3-47 and Figure 3-48 for “RP012” and “RP013” respectively.

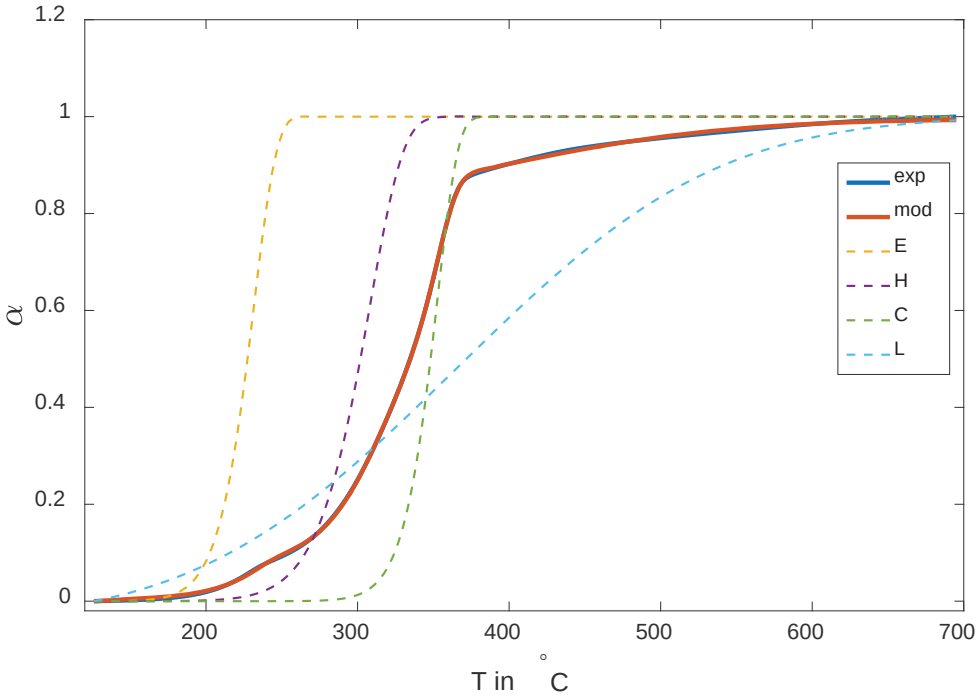

Figure 3-47. Conversion curves of the experimental and modelled data of run RP012 representing pyrolysis experiments without a lid. The thinner dashed lines represent the conversion curves of the four biomass constituents extractives, hemicellulose, cellulose and lignin. exp = experimental data; E = extractives; C = cellulose; H = hemicellulose; L = lignin; mod = modelled data; T = temperature; α = degree of conversion.

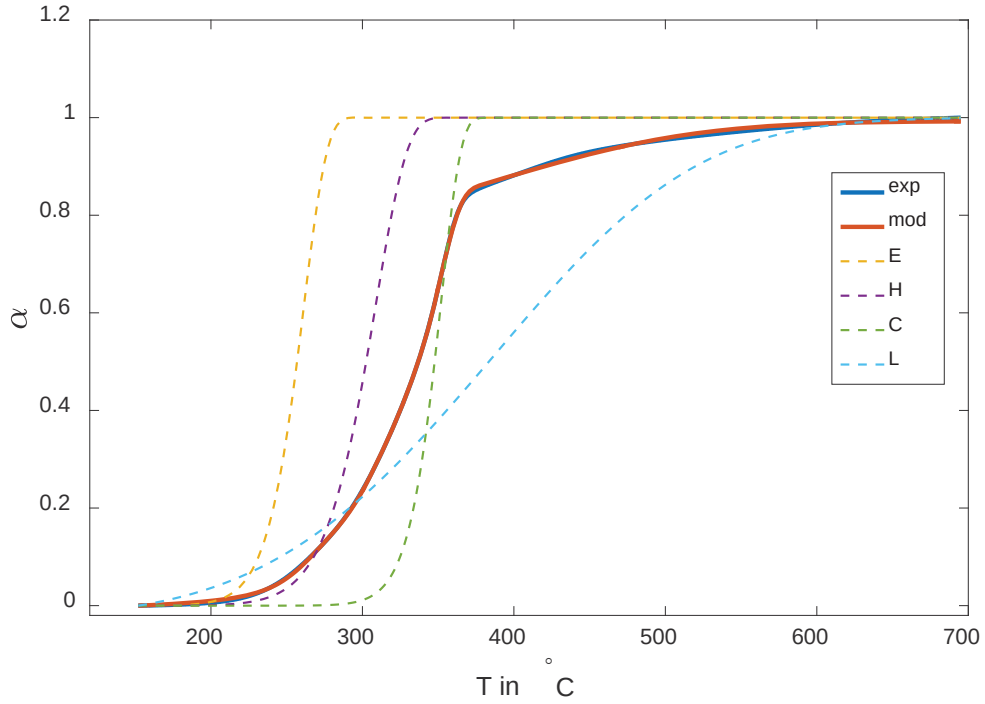

Figure 3-48. Conversion curves of the experimental and modelled data of run RP013 representing pyrolysis experiments with a lid. The thinner dashed lines represent the conversion curves of the four biomass constituents extractives, hemicellulose, cellulose and lignin. exp = experimental data; E = extractives; C = cellulose; H = hemicellulose; L = lignin; mod = modelled data; T = temperature; α = degree of conversion.

Figure 3-47 and Figure 3-48 show a relatively good fit. The average difference, Da, between the experimental and modelled data was calculated according to Biagini and Tognotti (2014):

$$Da = \frac{\sum_n |\alpha_{exp} - \alpha_{mod}|}{n}, \tag{3.21}$$

where α_{exp} and α_{mod} are the degree of conversion of the experimental and modelled data respectively, and n is the number of data points. The average difference of α in percent was calculated to be 0.18 % and 0.22 % for "RP012" and "RP013" respectively. The fitted parameters, the char yield of the corresponding biomass components and the char composition are given in Table 3-23 and Table 3-24 for the optimisations in Figure 3-47 and Figure 3-48 respectively.

Table 3-23. Fitted parameters, char yield of the biomass constituents and char composition of run RP012 representing pyrolysis without a lid.

Components	A_i	E_i	x_i	**Char yield**	**Char composition**	**Tstart**	**Tend**
	1/min	**kJ/mol**		**% (wt/wt)**	**%**	**°C**	**°C**
Extractives	2.37E+14	143.34	0.05	27.75	8.92	175.00	147.32
Hemicellulose	3.95E+10	125.05	0.28	2.11	2.86	226.24	339.34
Cellulose	1.41E+19	234.52	0.44	4.81	10.63	297.13	392.48
Lignin	1.23	19.83	0.22	42.35	77.59	140.48	646.22

Note. The parameters were fitted in the temperature range 126 to 695 °C to capture the actual pyrolysis step without the removal of moisture. Tstart and Tend are the start and end temperature of the decomposition range of component i, which have been determined at $\alpha_i = 0.01$ and $\alpha_i = 0.98$ respectively. A_i = pre-exponential factor in Arrhenius equation for component i; E_i = exponential factor in Arrhenius equation for component i; x_i = fraction of component i that constitutes the overall weight-loss.

Table 3-24. Fitted parameters, char yield of the biomass constituents and char composition of run RP013 representing pyrolysis with a lid.

Components	A_i	E_i	x_i	**Char yield**	**Char composition**	**Tstart**	**Tend**
	1/min	**kJ/mol**		**% (wt/wt)**	**%**	**°C**	**°C**
Extractives	7.73E+14	157.10	0.06	69.87	19.43	203.00	214.40
Hemicellulose	1.70E+11	131.93	0.26	0.00	14.78	229.94	337.13
Cellulose	1.17E+20	244.99	0.43	15.26	12.69	298.65	305.12
Lignin	4.91	26.76	0.25	36.46	38.11	169.14	598.74

Note. The parameters were fitted in the temperature range 152 to 695 °C to capture the actual pyrolysis step without the removal of moisture. Tstart and Tend are the start and end temperature of the decomposition range of component i, which have been determined at $\alpha_i = 0.01$ and $\alpha_i = 0.98$ respectively. A_i = pre-exponential factor in Arrhenius equation for component i; E_i = exponential factor in Arrhenius equation for component i; x_i = fraction of component i that constitutes the overall weight-loss.

Comparing Table 3-23 and Table 3-24, assuming that the differences are solely caused by secondary reactions, reveals that secondary reactions increase the char yield in decreasing order of extractives and cellulose while they decrease the char yield of lignin and hemicellulose. The very low char yield of hemicellulose, which even disappears in the case with a lid, was not expected, as according to the review of Collard and Blin (2014) hemicellulose generally achieves higher char yields than cellulose. This has partly been attributed to the higher mineral content in hemicellulose compared to cellulose, which catalyses char formation (Cagnon et al., 2009; Collard & Blin, 2014; Couhert, Commandre, & Salvador, 2009; Jensen, Dam-Johansen, Wójtowicz, & Serio,

1998). See also chapter 4 for the catalysing effect of minerals. However, even for demineralised glucomannan (Glucomannans are the principal hemicellulose in softwood hemicelluloses (Eronen, Österberg, Heikkinen, Tenkanen, & Laine, 2011; Rowell et al., 2013)) the char yield has been reported to be three times that of cellulose (Hosoya, Kawamoto, & Saka, 2007). The reason is thought to be the amorphous nature of hemicellulose (Alén, Kuoppala, & Oesch, 1996), which allows rearrangement reactions to take place forming a more reticulated solid matrix leading to a higher char yield as reviewed by Collard and Blin (2014). However, the analysis method used here cannot confirm this. The surprising result of hemicellulose producing no char in the model applied here is partly related to errors in the fitted Arrhenius parameters caused *inter alia* by the compensation effect; that is, different sets of A_i and E_i fit the same weight-loss curve (Di Blasi, 2008). As starting values the parameters of Grønli et al. (2002) were taken, which were only evaluated at a low heating rate of 5 K/min. White et al. (2011) recommend evaluation of the parameters at several heating rates to avoid this issue. Applying the parameters (E_i and A_i) of Branca et al. (2005) for hemicellulose, cellulose and lignin, who fitted the data at low and high heating rates, as initial values for the solver improved the situation in that char from hemicellulose is obtained, which is even higher than for cellulose (see Table B-4 and Table B-5 in Appendix B.7.2). The char yield increased for all the components in the case a lid was applied except for cellulose. These results appear more sensible but the overall curve fit is worse for the case that no lid is applied (average difference is 1.16 %) compared to the fitting in Figure 3-47. It is important to note though that the fit was slightly better in the case of a lid (average difference is 0.21 %). The fitted curves are shown in Figure B-36) and Figure B-37 in Appendix B.7.2 for the case of no lid and lid respectively. First and foremost this demonstrates quite clearly that a range of different Arrhenius parameters can be fitted to the same experimental curves, and caution has to be taken when interpreting their meaning. The reason for this is the above mentioned compensation effect, which highlights the importance of evaluating the kinetic parameters at a range of heating rates. This was not done in this research due to the limited time available. The aim here, as outlined above, was not to determine kinetics but to see whether or not this commonly used model could give some indication about what constituents form more char in the case a lid is applied. However, the here presented results show that this is not a valid approach as the fitting is sensitive to the starting values and the results do not agree with the findings from literature. Thus, caution has to be executed when

using the outlined fitting procedure as a method to determine the chemical composition of lignocellulosic materials as done by Biagini and Tognotti (2014). This agrees with the findings in 3.2.1, where it was discussed that secondary reactions can affect the analysis result. It also reveals that small changes in the weight loss curve affect the kinetic parameters (compare Table 3-23 and Table 3-24), and one has to be careful in their interpretation as they can, as argued in this chapter, derive from secondary reactions and transfer limitations associated with the presence of a liquid phase as was detected for the extractives in this study (section 3.3.4). Thus, it is likely that the actual reaction mechanism cannot be accurately represented by a first order reaction. This highlights the fundamental problem encountered in the field of biomass pyrolysis kinetics and solid state kinetics in general that, using simplified mechanisms in a system containing a multitude of reactions (including heterogeneous reactions), the reaction rate is not just dependent on temperature and degree of conversion as suggested by equation (3.11)._ENREF_4

To sum it up, although the weight loss/conversion of the wood can be fitted with a first-order reaction model it does not represent the true reaction mechanism as interactions between the wood components and pyrolysis products are anticipated. More detail about possible reaction mechanisms is given in chapter 6.

3.4 Conclusions

Minor conclusions derived from the feedstock characterisation are (a) the Van Soest method is not appropriate for determination of the wood constituents as it results in too high a cellulose content, too low hemicellulose and lignin contents, as well as too low a yield of the sum of the three components, and (b) methods employing pyrolysis for determination of biomass product properties and composition are not reliable as they are dependent on the method and equipment geometry due to the action of secondary reactions.

The last point in the paragraph above preludes the main conclusions. It was discovered that the yield of char and respectively the fixed carbon yield can be enhanced by keeping the volatile pyrolysis products in close contact with the pyrolysing material. This can be achieved by external means, that is, employing a lid (performing pyrolysis at elevated pressures or under conditions that limit the egress of volatiles) or performing pyrolysis in a bed of particles. In both cases the volatiles are forced to remain in contact with the pyrolysing solid by either inhibiting their escape or prolonging the contact time respectively. The effect is greater when a lid is employed and continues to increase with higher sample mass indicating that not just the vapour-phase residence time is decisive but also the vapour-phase concentration/partial pressure. Both parameters, lid or no lid and sample mass of sawdust in the crucible, have the same effect on the derivative weight-loss curve and the weight-loss curve, revealing that the yield increase is caused by the same mechanism. Identical trends were also found to occur in single particles, that is, with increasing char yield the derivative weight-loss peak narrows and the peak temperature decreases slightly before the onset of apparent mass transfer limitations are detected in the TGA. This occurs for single particles with a characteristic dimension > 20 mm. Thermocouple experiments recording the internal temperature profile in single wood cylinders revealed that this peak narrowing in the derivative weight-loss curve is caused by the exothermic nature of pyrolysis, which increases with higher char yields. The exothermic nature of these reactions explains why the effect of transfer limitations becomes visible in the differential weight loss curves only at a sample size >20 mm (although they are present for much smaller samples) at a heating rate of 5 °C/min. The reason is that below this sample size the internal heating in combination with the low thermal diffusivity of wood

negates the shift of the derivative weight loss peak to higher temperatures that is characteristic for transfer limitations. Due to the internal heating associated with char formation, samples with a characteristic sample size lower than 20 mm experience pyrolysis in slightly shorter time frames with increasing char yield indicating that the char yield increase is due to secondary reactions and not the different time-temperature history. This was confirmed by torrefaction experiments that included an isothermal step for 60 min that did not result in higher char yields. Thus, the yield increase is identified to be caused by exothermic secondary char formation. This shows that intraparticle and extraparticle secondary char formation are essentially the same, which is anticipated as wood is a porous medium enabling continuous interaction between the volatile pyrolysis products and the pyrolysing solid. In accordance, the yield of char was found to decrease with decreasing particle size despite a relatively large scatter observed in the data caused by the limitations of the applied TGA and the intrinsic difficulty in separating primary and secondary char formation. Nevertheless, the results show that secondary char formation is responsible for a large portion, if not the majority, of the char yield. Thus, the yield of char can be increased by increasing the particle size and size reduction steps should be avoided if a high char yield is desired. But there is a limit to the increase due to shrinkage, and the formation of cracks and fractures in large particles (> 30 mm), which reduce the reaction pathway and thus limit the vapour contact/ residence time and therefore the extent of secondary reactions. The maximum yield obtainable by intraparticle secondary char formation was found to be 25.02 ± 0.90 % (wt/wt) on a dry basis at 695 °C and a heating rate of 5 °C/min, which is attained for cylinders with a diameter of 20 mm. Larger yield increases are only possible by external means, i.e. pyrolysis in an enclosed system. Regarding shrinkage, it significantly proceeds at approximately 300 °C along with the expansion of macro pores; both increase almost exponentially in nature with increasing temperature until it starts to slow down at temperatures above 400 to 500 °C due to a sharp decrease in volatile product formation. Shrinkage was observed to increase in the following direction longitudinal < radial < tangential, and the volume of shrinkage was measured at 700 °C as 62.44 ± 0.66 % in the samples without cracks and fractures. In large cylindrical samples, d > 30 mm, shrinkage appears to be reduced due to the formation of internal cracks. Cracks generally start to form at structural weak points like ray cells and knots. Wood samples do not crack and fracture while they decompose and shrink till a particle size > 30 mm, which is due to the flexibility and malleability of the cell

wall during pyrolysis. This, in combination with the absence of an apparent fluidity of the cell walls, explains why the macroscopic parent structure is generally retained after pyrolysis, and indicates that the cell wall is a porous viscous suspension giving support to the hypothesis that secondary char formation is caused by vapour-liquid interactions.

The results of the lab-scale TGA were confirmed by EGA, and it was revealed that secondary pyrolysis reactions take place over the entire pyrolysis range, that is ≈ 140 to 500 °C, which extends lower than previously suggested. The onset temperature maybe delayed to 200 °C if no extractives are present. That is, extractives have the potential to form char at low temperatures, which is believed to be associated with the large portion of cyclic carbohydrates that constitute the extractives (for more detail see chapter 6). Based on the derivative weight-loss difference curve between the cases with and without a lid the temperature range of secondary reactions was divided in six zones: RT to 240 °C, 240 to 280 °C, 280 to 350 °C, 350 to 380 °C, 380 to 500 °C, and 500 to 700 °C.

The EGA or derivative weight-loss curves can be described by the overlapping decomposition of extractives, hemicellulose, cellulose and lignin applying a first-order reaction model. However, comparing the two scenarios of pyrolysis with and without a lid and evaluating the char yield of each component it becomes clear that such a model does not represent reality, which, as argued in this chapter, is due to secondary reactions and highlights that a first order reaction model even though it provides a good fit is not a true representation of the underlying mechanism.

The six zones above, determined from the lab-TGA and EGA trials, were mirrored in the results of the macro-TGA trials when plotting the time derivative of the temperature difference between the centre of the heated cylinder and the chamber. This underlines the close relationship between pyrolysis reaction energetics and secondary reactions, which confirms that secondary reactions play a major role in pyrolysis, in particular for char formation.

Having established the important role of secondary reactions for char formation, the next chapters look at investigating their role with respect to catalytic char formation, the heat of pyrolysis, the volatiles involved in secondary reactions, and the study of their impact on the properties of char/biochar.

3.5 References

Alén, R., Kuoppala, E., & Oesch, P. (1996). Formation of the main degradation compound groups from wood and its components during pyrolysis. *Journal of Analytical and Applied Pyrolysis, 36*(2), 137-148. doi:10.1016/0165-2370(96)00932-1

Antal, M. J., & Grønli, M. G. (2003). The art, science, and technology of charcoal production. *Industrial & Engineering Chemistry Research, 42*(8), 1619-1640. doi:10.1021/ie0207919

Antal, M. J., Mok, W. S.-L., Varhegyi, G., & Szekely, T. (1990). Review of methods for improving the yield of charcoal from biomass. *Energy & Fuels, 4*(3), 221-225. Retrieved from http://www.scopus.com/inward/record.url?eid=2-s2.0-0025434090&partnerID=40&md5=e397506586bcbfac82518a387556e697

Antal, M. J., & Varhegyi, G. (1995). Cellulose pyrolysis kinetics: The current state of knowledge. *Industrial & Engineering Chemistry Research, 34*(3), 703-717. doi:10.1021/ie00042a001

Arshadi, M., & Gref, R. (2005). Emission of volatile organic compounds from softwood pellets during storage. *Forest Products Journal, 55*(12), 132-135. Retrieved from http://ezproxy.massey.ac.nz/login?url=http://search.ebscohost.com/login.aspx?direct=true&AuthType=ip,cookie,url,uid&db=bth&AN=19324033&site=ehost-live&scope=site

Bashir, F. (2012). *Fracturing of wood during pyrolysis* (Unpublished final year project report). Massey University, Palmerston North, New Zealand. The report can be accessed by contacting J.R.Jones@massey.ac.nz

Biagini, E., & Tognotti, L. (2014). A generalized procedure for the devolatilization of biomass fuels based on the chemical components. *Energy & Fuels, 28*(1), 614-623. doi:10.1021/ef402139v

Branca, C., Albano, A., & Di Blasi, C. (2005). Critical evaluation of global mechanisms of wood devolatilization. *Thermochimica Acta, 429*(2), 133-141. doi:10.1016/j.tca.2005.02.030

Bridges, R. (2013). *Design and characterisation of an 'open source' pyrolyser for biochar production* (Master's thesis, Massey University, Palmerston North, New Zealand). Retrieved from http://mro.massey.ac.nz/handle/10179/5864

Brown, F. L. (1958). *Theories of the combustion of wood and its control. A survey of the literature* (Report No. 2136). Retrieved from Forest Products Laboratory website: http://www.fpl.fs.fed.us/documnts/fplr/fplr2136.pdf

Brown, M. E. (1988). *Introduction to thermal analysis: Techniques and applications*. London, United Kingdom: Chapman and Hall.

Butt, D. A. E. (2006). Formation of phenols from the low-temperature fast pyrolysis of Radiata pine (Pinus radiata): Part I. Influence of molecular oxygen. *Journal of Analytical and Applied Pyrolysis, 76*(1–2), 38-47. doi:10.1016/j.jaap.2005.07.003

Caballero, J. A., & Conesa, J. A. (2005). Mathematical considerations for nonisothermal kinetics in thermal decomposition. *Journal of Analytical and Applied Pyrolysis, 73*(1), 85-100. doi:http://dx.doi.org/10.1016/j.jaap.2004.12.003

Cagnon, B., Py, X., Guillot, A., Stoeckli, F., & Chambat, G. (2009). Contributions of hemicellulose, cellulose and lignin to the mass and the porous properties of

chars and steam activated carbons from various lignocellulosic precursors. *Bioresource Technology, 100*(1), 292-298. doi:10.1016/j.biortech.2008.06.009

Calvelo Pereira, R., Kaal, J., Camps-Arbestain, M., Pardo Lorenzo, R., Aitkenhead, W., Hedley, M., . . . Maciá-Agulló, J. A. (2011). Contribution to characterisation of biochar to estimate the labile fraction of carbon. *Organic Geochemistry, 42*(11), 1331-1342. doi:10.1016/j.orggeochem.2011.09.002

Cetin, E., Gupta, R., & Moghtaderi, B. (2005). Effect of pyrolysis pressure and heating rate on radiata pine char structure and apparent gasification reactivity. *Fuel, 84*(10), 1328-1334. doi:10.1016/j.fuel.2004.07.016

Cetin, E., Moghtaderi, B., Gupta, R., & Wall, T. F. (2004). Influence of pyrolysis conditions on the structure and gasification reactivity of biomass chars. *Fuel, 83*(16), 2139-2150. doi:10.1016/j.fuel.2004.05.008

Channiwala, S. A., & Parikh, P. P. (2002). A unified correlation for estimating HHV of solid, liquid and gaseous fuels. *Fuel, 81*(8), 1051-1063. doi:10.1016/S0016-2361(01)00131-4

Chen, Y., Charpenay, S., Jensen, A., Wójtowicz, M. A., & Serio, M. A. (1998). Modeling of biomass pyrolysis kinetics. *Symposium (International) on Combustion, 27*(1), 1327-1334. doi:10.1016/s0082-0784(98)80537-7

Collard, F.-X., & Blin, J. (2014). A review on pyrolysis of biomass constituents: Mechanisms and composition of the products obtained from the conversion of cellulose, hemicelluloses and lignin. *Renewable and Sustainable Energy Reviews, 38*, 594-608. doi:10.1016/j.rser.2014.06.013

Couhert, C., Commandre, J. M., & Salvador, S. (2009). Is it possible to predict gas yields of any biomass after rapid pyrolysis at high temperature from its composition in cellulose, hemicellulose and lignin? *Fuel, 88*(3), 408-417. doi:10.1016/j.fuel.2008.09.019

Cozzani, V., Lucchesi, A., Stoppato, G., & Maschio, G. (1997). A new method to determine the composition of biomass by thermogravimetric analysis. *The Canadian Journal of Chemical Engineering, 75*(1), 127-133. doi:10.1002/cjce.5450750120

Demirbas, A. (1997). Calculation of higher heating values of biomass fuels. *Fuel, 76*(5), 431-434. doi:10.1016/S0016-2361(97)85520-2

Demirbas, A., Gullu, D., Çaglar, A., & Akdeniz, F. (1997). Estimation of calorific values of fuels from lignocellulosics. *Energy Sources, 19*(8), 765-770. doi:10.1080/00908319708908888

Di Blasi, C. (1996). Heat, momentum and mass transport through a shrinking biomass particle exposed to thermal radiation. *Chemical Engineering Science, 51*(7), 1121-1132. doi:10.1016/S0009-2509(96)80011-X

Di Blasi, C. (2008). Modeling chemical and physical processes of wood and biomass pyrolysis. *Progress in Energy and Combustion Science, 34*(1), 47-90. doi:10.1016/j.pecs.2006.12.001

Di Blasi, C., & Branca, C. (2001). Kinetics of primary product formation from wood pyrolysis. *Industrial & Engineering Chemistry Research, 40*(23), 5547-5556. doi:10.1021/ie000997e

Dufour, A., Castro-Diaz, M., Brosse, N., Bouroukba, M., & Snape, C. (2012). The origin of molecular mobility during biomass pyrolysis as revealed by in situ ^{1}H NMR spectroscopy. *ChemSusChem, 5*(7), 1258-1265. doi:10.1002/cssc.201100442

Dufour, A., Ouartassi, B., Bounaceur, R., & Zoulalian, A. (2011). Modelling intra-particle phenomena of biomass pyrolysis. *Chemical Engineering Research and Design, 89*(10), 2136-2146. doi:10.1016/j.cherd.2011.01.005

Eronen, P., Österberg, M., Heikkinen, S., Tenkanen, M., & Laine, J. (2011). Interactions of structurally different hemicelluloses with nanofibrillar cellulose. *Carbohydrate Polymers, 86*(3), 1281-1290. doi:10.1016/j.carbpol.2011.06.031

Evans, R. J., & Milne, T. A. (1987). Molecular characterization of the pyrolysis of biomass. 1. Fundamentals. *Energy & Fuels, 1*(2), 123-137. doi:10.1021/ef00002a001

Fisher, T., Hajaligol, M., Waymack, B., & Kellogg, D. (2002). Pyrolysis behavior and kinetics of biomass derived materials. *Journal of Analytical and Applied Pyrolysis, 62*(2), 331-349. doi:10.1016/S0165-2370(01)00129-2

Flynn, J. H. (1997). The 'Temperature Integral' — Its use and abuse. *Thermochimica Acta, 300*(1–2), 83-92. doi:10.1016/S0040-6031(97)00046-4

Flynn, J. H., & Wall, L. A. (1966). General treatment of the thermogravimetry of polymers. *Journal of Research of the National Bureau of Standards—A. Physics and Chemistry, 70A*, 487-523. Retrieved from file:///C:/Users/gdripber/Downloads/1286.pdf

González, J. F., Román, S., Encinar, J. M., & Martínez, G. (2009). Pyrolysis of various biomass residues and char utilization for the production of activated carbons. *Journal of Analytical and Applied Pyrolysis, 85*(1–2), 134-141. doi:10.1016/j.jaap.2008.11.035

Grieco, E., & Baldi, G. (2011). Analysis and modelling of wood pyrolysis. *Chemical Engineering Science, 66*(4), 650-660. doi:10.1016/j.ces.2010.11.018

Grønli, M. G., Várhegyi, G., & Di Blasi, C. (2002). Thermogravimetric analysis and devolatilization kinetics of wood. *Industrial & Engineering Chemistry Research, 41*(17), 4201-4208. doi:10.1021/ie0201157

Haas, T. J., Nimlos, M. R., & Donohoe, B. S. (2009). Real-Time and post-reaction microscopic structural analysis of biomass undergoing pyrolysis. *Energy & Fuels, 23*(7), 3810-3817. doi:10.1021/ef900201b

Hayward, M. (2011). *Biochar formulation and application to soil opportunities: NZ context* (Project report). Massey University, Palmerston North, New Zealand. The report can be accessed by contacting J.R.Jones@massey.ac.nz

Hosoya, T., Kawamoto, H., & Saka, S. (2007). Pyrolysis behaviors of wood and its constituent polymers at gasification temperature. *Journal of Analytical and Applied Pyrolysis, 78*(2), 328-336. doi:10.1016/j.jaap.2006.08.008

Hosoya, T., Kawamoto, H., & Saka, S. (2009). Solid/liquid- and vapor-phase interactions between cellulose- and lignin-derived pyrolysis products. *Journal of Analytical and Applied Pyrolysis, 85*(1-2), 237-246. doi:10.1016/j.jaap.2008.11.028

Huang, Y., Kudo, S., Masek, O., Norinaga, K., & Hayashi, J.-i. (2012). Simultaneous maximization of the char yield and volatility of oil from biomass pyrolysis. *Energy & Fuels, 27*(1), 247-254. doi:10.1021/ef301366x

Jarvis, M. W., Haas, T. J., Donohoe, B. S., Daily, J. W., Gaston, K. R., Frederick, W. J., & Nimlos, M. R. (2011). Elucidation of biomass pyrolysis products using a laminar entrained flow reactor and char particle imaging. *Energy & Fuels, 25*(1), 324-336. doi:10.1021/ef100832d

Jensen, A., Dam-Johansen, K., Wójtowicz, M. A., & Serio, M. A. (1998). TG-FTIR study of the influence of potassium chloride on wheat straw pyrolysis. *Energy & Fuels, 12*(5), 929-938. doi:10.1021/ef980008i

Kandiyoti, R. (2002). Reply to Letter to the Editor by Sun et al. [FUEL/2001/0120 (Letter)]: "The synergistic effect between macerals during pyrolysis". *Fuel, 81*(7), 975. doi:10.1016/S0016-2361(01)00206-X

Kininmonth, J. A., & Whitehouse, L. J. (Eds.). (1991). *Properties and uses of New Zealand radiata pine: Volume one - wood properties* (Vol. 1). Rotorua, New Zealand: Ministry of Forestry, Forest Research Institute, with financial support from the New Zealand Lottery Grants Board.

Koufopanos, C. A., Lucchesi, A., & Maschio, G. (1989). Kinetic modelling of the pyrolysis of biomass and biomass components. *The Canadian Journal of Chemical Engineering, 67*(1), 75-84. doi:10.1002/cjce.5450670111

Lapuerta, M., Hernández, J. J., & Rodríguez, J. (2007). Comparison between the kinetics of devolatilisation of forestry and agricultural wastes from the middle-south regions of Spain. *Biomass and Bioenergy, 31*(1), 13-19. doi:10.1016/j.biombioe.2006.05.003

Larfeldt, J., Leckner, B., & Melaaen, M. C. (2000). Modelling and measurements of the pyrolysis of large wood particles. *Fuel, 79*(13), 1637-1643. doi:10.1016/s0016-2361(00)00007-7

Lin, Y.-C., Cho, J., Tompsett, G. A., Westmoreland, P. R., & Huber, G. W. (2009). Kinetics and mechanism of cellulose pyrolysis. *The Journal of Physical Chemistry C, 113*(46), 20097-20107. doi:10.1021/jp906702p

Lu, W., Guo, Y., Zhang, B., & Wang, C. (2013). Comprehensive analysis on elements, energy recovery, and oil compositions of biomass deoxy-liquefaction. *Energy and Fuels, 27*(4), 2157-2166. doi:10.1021/ef400157e

Mamleev, V., Bourbigot, S., Le Bras, M., & Yvon, J. (2009). The facts and hypotheses relating to the phenomenological model of cellulose pyrolysis: Interdependence of the steps. *Journal of Analytical and Applied Pyrolysis, 84*(1), 1-17. doi:10.1016/j.jaap.2008.10.014

Martínez-Iñigo, M. J., Immerzeel, P., Gutierrez, A., del Río, J. C., & Sierra-Alvarez, R. (1999). Biodegradability of extractives in sapwood and heartwood from Scots pine by sapstain and white-rot fungi. *Holzforschung, 53*(3), 247-252. doi:10.1515/HF.1999.042

McCarl, B. A., Peacocke, C., Chrisman, R., Kung, C.-C., & Sands, R. D. (2009). Economics of biochar production, utilization and greenhouse gas offsets. In J. Lehmann & S. Joseph (Eds.), *Biochar for environmental management: Science and technology* (pp. 341-357). London, England, United Kingdom: Earthscan.

Mishra, D. P., & Rahman, A. (2003). An experimental study of flammability limits of LPG/air mixtures. *Fuel, 82*(7), 863-866. doi:10.1016/s0016-2361(02)00325-3

Mohd-Hanif, H. (2013). *Hot stage for pyrolysis* (Unpublished final year project report). Massey University, Palmerston North, New Zealand. The report can be accessed by contacting J.R.Jones@massey.ac.nz

Mok, W. S.-L., Antal, M. J., Szabo, P., Varhegyi, G., & Zelei, B. (1992). Formation of charcoal from biomass in a sealed reactor. *Industrial & Engineering Chemistry Research, 31*(4), 1162-1166. doi:10.1021/ie00004a027

Morgan, T. J., & Kandiyoti, R. (2013). Pyrolysis of coals and biomass: Analysis of thermal breakdown and its products. *Chemical Reviews*. doi:10.1021/cr400194p

Narayan, R., & Antal, M. J. (1996). Thermal lag, fusion, and the compensation effect during biomass pyrolysis. *Industrial & Engineering Chemistry Research, 35*(5), 1711-1721. doi:10.1021/ie950368i

Newman, R. H., Hemmingson, J. A., & Suckling, I. D. (1993). Carbon-13 nuclear magnetic resonance studies of kraft pulping. *Holzforschung - International*

Journal of the Biology, Chemistry, Physics and Technology of Wood, 47(3), 234. doi:10.1515/hfsg.1993.47.3.234

Orfão, J. J. M., Antunes, F. J. A., & Figueiredo, J. L. (1999). Pyrolysis kinetics of lignocellulosic materials - three independent reactions model. *Fuel, 78*(3), 349-358. doi:10.1016/s0016-2361(98)00156-2

Pattanotai, T., Watanabe, H., & Okazaki, K. (2013). Experimental investigation of intraparticle secondary reactions of tar during wood pyrolysis. *Fuel, 104*(0), 468-475. doi:10.1016/j.fuel.2012.08.047

Ratte, J., Marias, F., Vaxelaire, J., & Bernada, P. (2009). Mathematical modelling of slow pyrolysis of a particle of treated wood waste. *Journal of Hazardous Materials, 170*(2-3), 1023-1040. doi:10.1016/j.jhazmat.2009.05.077

Raveendran, K., Ganesh, A., & Khilar, K. C. (1996). Pyrolysis characteristics of biomass and biomass components. *Fuel, 75*(8), 987-998. doi:10.1016/0016-2361(96)00030-0

Robertson, J. B., & Van Soest, P. J. (1981). The detergent system of analysis and its application to human foods. In W. P. T. James & O. Theander (Eds.), *The analysis of dietary fiber in food* (Vol. 3, pp. 123-158). New York, NY: Marcel Dekker.

Rowell, R. M., Pettersen, R., & Tshabalala, M. A. (2013). Cell wall chemistry. In R. M. Rowell (Ed.), *Handbook of wood chemistry and wood composites*. Boca Raton, FL: CRC Press.

Sharma, R. K., Wooten, J. B., Baliga, V. L., Lin, X., Chan, W. G., & Hajaligol, M. R. (2004). Characterization of chars from pyrolysis of lignin. *Fuel, 83*(11–12), 1469-1482. doi:10.1016/j.fuel.2003.11.015

Shen, D. K., Gu, S., Jin, B., & Fang, M. X. (2011). Thermal degradation mechanisms of wood under inert and oxidative environments using DAEM methods. *Bioresource Technology, 102*(2), 2047-2052. doi:10.1016/j.biortech.2010.09.081

Sheng, C., & Azevedo, J. L. T. (2005). Estimating the higher heating value of biomass fuels from basic analysis data. *Biomass and Bioenergy, 28*(5), 499-507. doi:10.1016/j.biombioe.2004.11.008

Sun, J. T., Huang, Y. D., Gong, G. F., & Cao, H. L. (2006). Thermal degradation kinetics of poly(methylphenylsiloxane) containing methacryloyl groups. *Polymer Degradation and Stability, 91*(2), 339-346. doi:10.1016/j.polymdegradstab.2005.04.037

Tang, W., Liu, Y., Zhang, H., & Wang, C. (2003). New approximate formula for Arrhenius temperature integral. *Thermochimica Acta, 408*(1–2), 39-43. doi:10.1016/S0040-6031(03)00310-1

Varhegyi, G., Antal, M. J., Szekely, T., Till, F., & Jakab, E. (1988). Simultaneous thermogravimetric-mass spectrometric studies of the thermal decomposition of biopolymers. 1. Avicel cellulose in the presence and absence of catalysts. *Energy & Fuels, 2*(3), 267-272. doi:10.1021/ef00009a007

Varhegyi, G., Antal, M. J., Szekely, T., Till, F., Jakab, E., & Szabo, P. (1988). Simultaneous thermogravimetric-mass spectrometric studies of the thermal decomposition of biopolymers. 2. Sugarcane bagasse in the presence and absence of catalysts. *Energy & Fuels, 2*(3), 273-277. doi:10.1021/ef00009a008

Wang, L., Skreiberg, Ø., Grønli, M. G., Specht, G. P., & Antal, M. J. (2013). Is elevated pressure required to achieve a high fixed-carbon yield of charcoal from biomass? Part 2: The importance of particle size. *Energy & Fuels, 27*(4), 2146-2156. doi:10.1021/ef400041h

Wang, L., Trninic, M., Skreiberg, Ø., Grønli, M. G., Considine, R., & Antal, M. J. (2011). Is elevated pressure required to achieve a high fixed-carbon yield of charcoal from biomass? Part 1: Round-robin results for three different corncob materials. *Energy & Fuels, 25*(7), 3251-3265. doi:10.1021/ef200450h

Wang, X. Y., Wan, X. J., Chen, M. Q., & Wang, J. (2012). Kinetic model of biomass pyrolysis based on three-component independent parallel first-order reactions. *Guocheng Gongcheng Xuebao/The Chinese Journal of Process Engineering, 12*(6), 1020-1024. Retrieved from http://www.scopus.com/inward/record.url?eid=2-s2.0-84872227037&partnerID=40&md5=db7f9f47b41717d346ac4ce828d9edbf

Wang, Z., Cao, J., & Wang, J. (2009). Pyrolytic characteristics of pine wood in a slowly heating and gas sweeping fixed-bed reactor. *Journal of Analytical and Applied Pyrolysis, 84*(2), 179-184. doi:10.1016/j.jaap.2009.02.001

White, J. E., Catallo, W. J., & Legendre, B. L. (2011). Biomass pyrolysis kinetics: A comparative critical review with relevant agricultural residue case studies. *Journal of Analytical and Applied Pyrolysis, 91*(1), 1-33. doi:10.1016/j.jaap.2011.01.004

Wigley, T., Pang, S., & Yip, A. (2014). *Development of the fast pyrolysis process to produce a high quality liquid fuel from woody biomass.* Paper presented at Pyro2014 20th International Symposium on Analytical and Applied Pyrolysis, Birmingham, United Kingdom.

Williams, P. T., & Besler, S. (1996). The influence of temperature and heating rate on the slow pyrolysis of biomass. *Renewable Energy, 7*(3), 233-250. doi:10.1016/0960-1481(96)00006-7

Wu, L., Guo, S., Wang, C., & Yang, Z. (2009). Production of alkanes (C7–C29) from different part of poplar tree via direct deoxy-liquefaction. *Bioresource Technology, 100*(6), 2069-2076. doi:10.1016/j.biortech.2008.10.024

Yu, J., Wang, C., Wang, Y., & Yang, Z. (2011). Deoxy-liquefaction products obtained from Crofton weed at different temperatures. *Journal of Analytical and Applied Pyrolysis, 92*(1), 68-75. doi:10.1016/j.jaap.2011.04.009

Zhu, G., Zhu, X., Xiao, Z., & Yi, F. (2012). Study of cellulose pyrolysis using an in situ visualization technique and thermogravimetric analyzer. *Journal of Analytical and Applied Pyrolysis, 94*(0), 126-130. doi:10.1016/j.jaap.2011.11.016

Chapter 4 Effect of Catalysts on Pyrolysis

4.1 Introduction

In chapter 2 it was discussed that the yield of char can not only be increased by prolonged vapour-phase residence times but also by catalysis. Catalysts that have been reported are alkali and alkaline earth metals (Khelfa, Bensakhria, & Weber, 2013; Wang, Wang, Cao, & Wang, 2010), as well as dehydrating acids (Fu, Argyropoulos, Tilotta, & Lucia, 2008; Mamleev, Bourbigot, Le Bras, & Yvon, 2009). The aim of this chapter is to investigate their impact on pyrolysis, in particular their effect on the char yield and how this compares to the yield increases caused by the prolonged vapour-phase residence times (secondary reactions) studied in chapter 3. A central question is whether or not they catalyse primary or secondary reactions or both. Potassium and magnesium were chosen to represent the class of alkali and alkaline earth metals respectively, and phosphoric acid was selected as an acid catalyst. They were chosen on the basis that they are plant macronutrients (Barker & Pilbeam, 2007; Schachtman, Reid, & Ayling, 1998), and have been shown to improve crop growth (Rajkovich et al., 2012).

4.2 Material and Methods

4.2.1 Feedstock

The feedstock used was radiata pine wood sawdust with a particle size < 1 mm, as described in 3.2.1.1.

4.2.2 Catalysts and Impregnation Procedure

The metals mentioned in 4.1 were added as chlorides (KCl and $MgCl_2 \cdot 6H_2O$), because chlorine is a plant micronutrient, and chlorides do not affect the gas composition during pyrolysis like carbonates or hydroxides do, which release gases upon their decomposition (Khelfa et al., 2013; Wang et al., 2010). Furthermore, chlorides are easily soluble, which is ideal for impregnating the biomass feedstock (Khelfa et al., 2013). Potassium chloride (grade: EMSURE®), KCl, and magnesium chloride hexahydrate (grade: UNIVAR® analytical reagents), $MgCl_2 \cdot 6H_2O$, were supplied by Merck KGaA (Darmstadt, Germany) and Thermo Fisher Scientific New Zealand Ltd (North Shore City, New Zealand) respectively.

The impregnation method was based on Khelfa et al. (2013). In the case of K impregnation 0.5747 g of KCl was dissolved in 180 g distilled Millipore water. After complete dissolution 15 g of sawdust was added to the solution in order to obtain sawdust impregnated with 2 % (wt/wt) potassium metallic cations. The mixture was subsequently stirred on a hot plate with a magnetic stirrer from Schott Instruments GmbH (Mainz, Germany) for approximately 7 h at 75 °C, then left stirring overnight without heating, and the next day heating was continued at a temperature of approximately 90 °C to speed up the evaporation process. Once the solid concentration was too high for stirring, the beaker was transferred into a Series 5 Contherm Digital Series Oven (Contherm Scientific, Upper Hutt, New Zealand) and heated at 105 °C for 24 h. Subsequently, the dried sawdust was stored over silica gel (grade: LABCHEM® general purpose reagents) supplied by Thermo Fisher Scientific New Zealand Ltd (North Shore City, New Zealand) to ensure the sawdust was completely dry.

The impregnation of sawdust with magnesium ions was done in a supervised 4th year engineering project with the title “Catalysis of char formation” (Alyami, 2014). It was aimed to impregnate the pine sawdust with 2 and 5 % (wt/wt) of magnesium ions

respectively. Similar to the procedure for K impregnation $MgCl_2 \cdot 6H_2O$ was first dissolved in approximately 120 g distilled Millipore water; that is, 3.346 and 8.365 g $MgCl_2 \cdot 6H_2O$ for the case of 2 and 5 % (wt/wt) Mg impregnation respectively. After complete dissolution 20 g of pine sawdust was added and the mixture stirred on a hot plate MS7-H550-Pro from Scilogex (Rocky Hill, Connecticut, USA) at 75 °C for approximately 7 to 9 h. Subsequently it was placed in the oven at 105 °C for 12 h analogue to K impregnation, and then stored over silica gel until used for pyrolysis.

The effect of phosphoric acid on pyrolysis was studied as part of the above mentioned 4th year engineering project (Alyami, 2014). Orthophosphoric acid (analytical reagent grade with a concentration of 85 % (wt/wt)) from Fisher Scientific (Loughborough, UK) was used for impregnation. The procedure was based on Fu et al. (2008). Two solutions were prepared by adding 1.3 and 3.161 g of Orthophosphoric acid in 100 g of analytical reagent grade methanol from Thermo Fisher Scientific New Zealand Ltd (North Shore City, New Zealand) respectively. Subsequently the mixtures were stirred and in each 20 g of pine sawdust introduced. The resulting solutions were stirred for about an hour. Next, the methanol was evaporated by the use of a rotary evaporator, and then stored over silica gel to prevent moisture absorption. In this way, theoretically, sawdust with a P content of 1.75 and 4.25 % (wt/wt) is obtained.

To verify that the impregnation was successful, the ash content of the impregnated samples was determined by ROI according to Bridges (2013), as discussed in 3.2.1.4. The ash content was calculated as the average of three samples. Table 4-1 summarises the results.

Table 4-1. Ash content of impregnated radiata pine sawdust.

Targeted impregnation	2 % (wt/wt) K	2 % (wt/wt) Mg	5 % (wt/wt) Mg	1.75 % (wt/wt) P	4.25 % (wt/wt) P
μ in % (wt/wt)	3.959	3.107	6.174	2.008	4.057
σ in pp	0.033	0.136	0.300	0.228	0.203
CV	0.008	0.044	0.049	0.113	0.050
Ash impregnated-Ash pine in % (wt/wt)	3.657	2.804	5.871	1.706	3.755
Element impregnated in % (wt/wt)	1.918	0.716	1.499	1.706	3.755
Δ in % (wt/wt)	0.091	1.285	3.502	0.041	0.491

Note. The ash content was determined by Residue on Ignition according to Bridges (2013). The measured ash content of untreated radiata pine wood is 0.303 % (wt/wt). The results represent averages of 3 samples. *CV* = coefficient of variation; pp = percent point; wt = weight; Δ = difference between targeted element impregnation and actually achieved impregnation; μ = average; σ = standard deviation.

Table 4-1 shows that impregnation was successful in the sense that the target concentrations of the desired element were quite closely attained (see Δ in Table 4-1, which represents the difference of the obtained concentration to the target concentration) except in the case of Mg. Reasons for the differences could be the volatilisation of some of the alkali and alkaline earth metals, as well as chlorine (Björkman & Strömberg, 1997; Keown, Favas, Hayashi, & Li, 2005; Okuno et al., 2005) or incomplete impregnation. Chapter 7 discusses how some of the inorganic compounds volatilise during pyrolysis although this could not be confirmed for Mg. Therefore, in the following section when reporting the impregnated amount, the % (wt/wt) of the targeted impregnation is stated as theoretically the observed difference could be due to volatilisation. For the calculations in Table 4-1 it has been assumed that in the case of K, Mg and P impregnation, the ash consisted of KCl, $MgCl_2$ and P respectively.

4.2.3 Pyrolysis

Pyrolysis of impregnated sawdust was investigated by laboratory scale TGA as described in 3.2.2. Non impregnated sawdust was also pyrolysed where KCl was added physically to the crucible, the purpose being to investigate the presence of a catalyst but

without the intimate contact acquired during impregnation. The applied temperature programme was similar to the one in Table 3-11 (3.2.2) with the *HTT* being set to 750 °C except for the experiments where the catalyst was added physically, it was set to 720 °C. Again experiments were performed with and without a lid to investigate the impact of catalyst on primary and secondary reactions respectively. In the case of K impregnation eight and seven samples were pyrolysed with and without a lid respectively, but with varying initial sample weights in the range 5 to 13 mg. In contrast, only two repetitions were performed on the pyrolysis experiments with and without a lid that employed Mg and P impregnated pine sawdust. The initial sample weight for these experiments was in the range 9 to 12 mg.

In order to be able to manipulate the TGA data, e.g. plot difference curves between various runs, the raw data had to be adjusted to a common temperature, which was done with the Matlab program described in 3.2.2. It is important to note that the TGA data was smoothed as discussed in 3.2.2.

4.2.4 Curve-fitting

The applied curve-fitting procedure is based on the method outlined in 3.3.8. In this catalysis study the curve-fitting was done on average curves, *viz.*, the recorded weight-loss curves and derivative weight-loss curves of repeat experiments were averaged. Interpolation was selected as it allows obtaining a higher number of experimental points for curve-fitting, which is essential to obtain a good fit. Interpolation was done by cubic spline interpolation in Matlab. For the sample component compositions, x_i, a different set of initial values was selected than in Table 3-22 in section 3.3.8, because the samples used here had a lower extractives content due to their longer storage time, the effect of which is discussed in 3.3.1. The compositions used are based on the extractives content of sample 1 in Table 3-1 (section 3.2.1.2) and are 0.0281, 0.2437, 0.3984, and 0.3298 for extractives, hemicellulose, cellulose and lignin respectively. The reference temperatures for scaling the pre-exponential factor were chosen on the basis of the respective experimental derivative weight loss curves.

4.2.5 Summary of Experimental Plan

In Table 4-2 is the experimental plan summarised to give an overview.

Table 4-2. Experimental plan.

Objective	Experimental plan	Measurements performed
Investigate if physical addition of catalyst is sufficient or impregnation is required to obtain increased char yields	• Pyrolyse physically added KCl in crucibles with sawdust and covered with lid in labscale TGA to allow long vapour-phase residence times, and compare to results in chapter 3	• Weight loss with temperature/time
Investigate role of catalyst on pyrolysis		
• Alkali and alkaline earth metals	• Pyrolyse different weights of sawdust impregnated with 2 % (wt/wt) K in crucibles with and without a lid in a labscale TGA • Pyrolyse sawdust impregnated with 2 and 5 % (wt/wt) Mg in crucibles with and without a lid in a labscale TGA	• Weight loss with temperature/time • Heat flow (discussed in chapter 5)
• Dehydrating acids	• Perform experiments analogue to Mg impregnated samples for samples impregnated with 1.75 and 4.25 % (wt/wt) P, as Orthophosphoric acid	• Weight loss with temperature/time • Heat flow (discussed in chapter 5)

4.3 Results and Discussion

4.3.1 Physical Addition versus Impregnation

Before impregnation, preliminary experiments were carried out in which KCl was added physically onto the sawdust in the TGA crucibles, and subsequently pyrolysed with a lid. This was based on the work of Wang et al. (2010), who observed a catalytic effect of potassium carbonate and calcium hydroxide in a fixed-bed reactor by having mixed the salt with the wood sample in an agate mortar for approximately 15 min without strong forcing. The aim was to investigate, whether or not the salt catalyses vapour-phase char formation. The purpose of using the lid was to encourage these vapour-phase secondary reactions. The sawdust used was the one described in 4.2.1 but was additionally oven-dried at 110 °C in a Series 5 Contherm Digital Series Oven (Contherm Scientific, Upper Hutt, New Zealand) and then stored over silica gel (grade: LABCHEM® general purpose reagents) supplied by Thermo Fisher Scientific New Zealand Ltd (North Shore City, New Zealand) to ensure the sawdust was completely dry. The results of the experiments are depicted in Figure 4-1 and Figure 4-2.

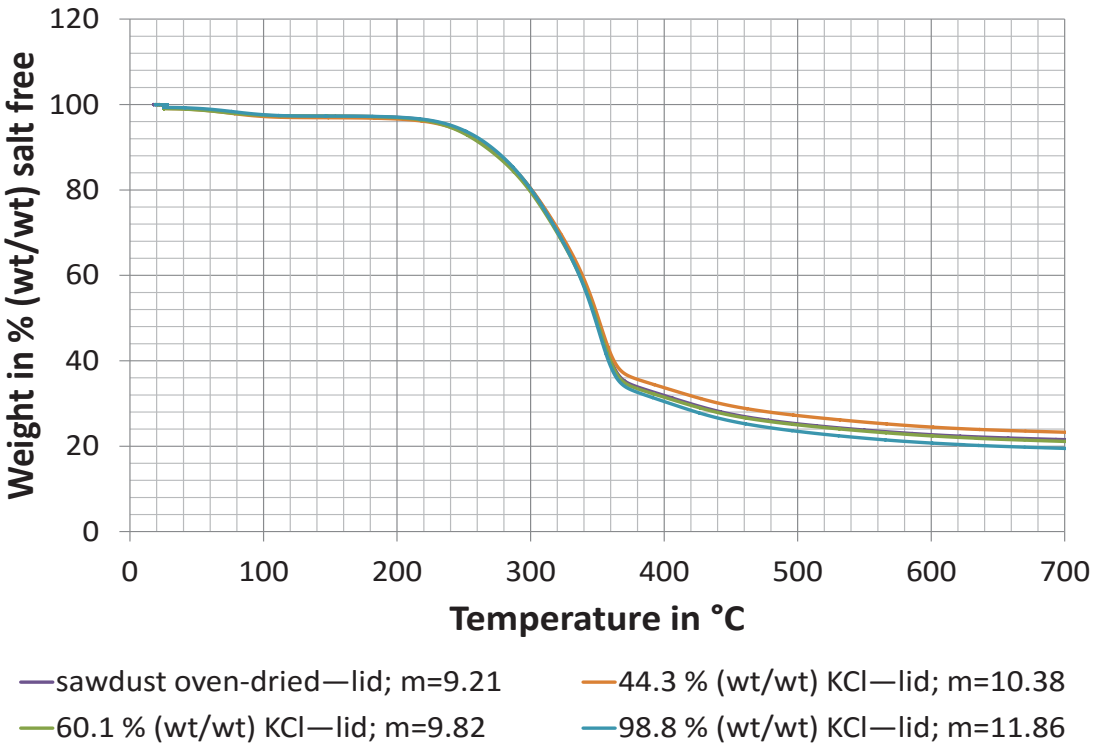

Figure 4-1. Comparison of weight-loss curves of pine sawdust with and without physically added KCl on a salt free basis. The % (wt/wt) refers to the amount of KCl added on the basis of the pine sawdust present in the crucible. Legend: sample description—lid or no lid; sawdust weight in mg on a salt free basis. m = initial sawdust weight in mg on a salt free basis.

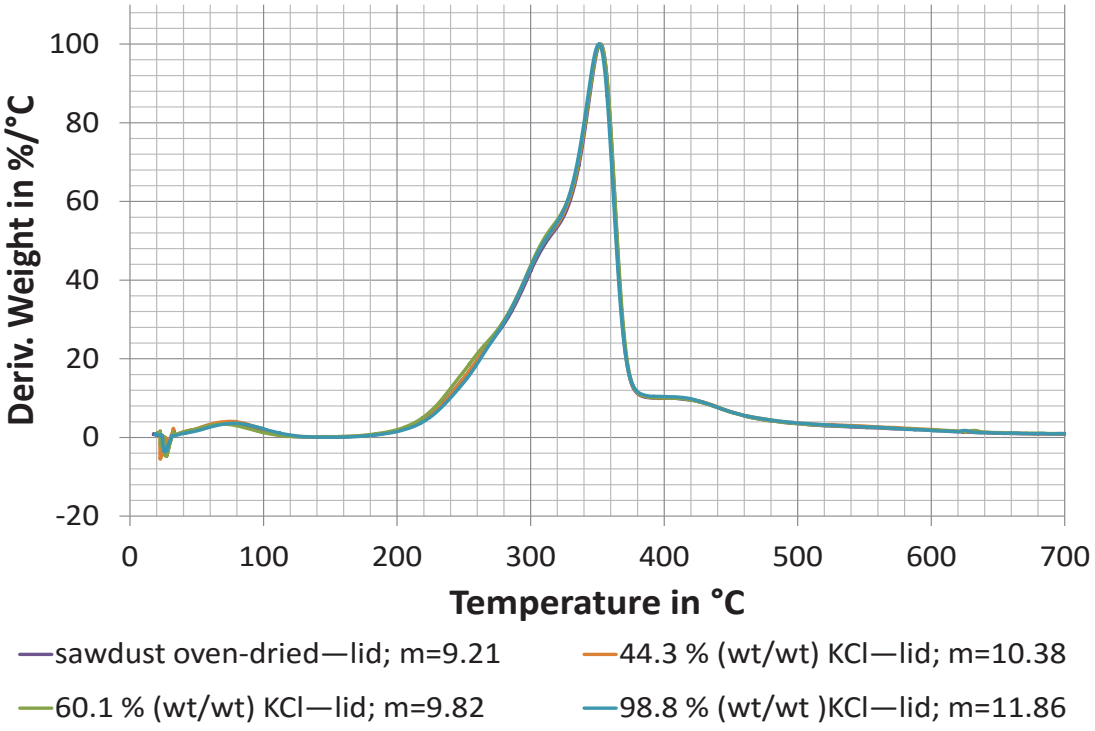

Figure 4-2. Comparison of derivative weight-loss curves of pine sawdust with and without physically added KCl on a salt free basis. The % (wt/wt) refers to the amount of KCl added on the basis of the pine sawdust present in the crucible. Legend: sample description—lid or no lid; sawdust weight in mg on a salt free basis. m = initial sawdust weight in mg on a salt free basis.

Figure 4-1 shows that there is not much difference between the runs with added KCl compared to a pure sawdust sample without the addition of salt. The present scatter in the final char yield, visible above approximately 360 °C in Figure 4-1, is believed to be caused by natural variation and sample inhomogeneity as observed in chapter 3. This is supported by the conforming results of the derivative weight-loss curves in Figure 4-2, and evidenced in Figure 4-3, where the char yield of the KCl added pyrolysis experiments is plotted together with the yields of untreated sawdust pyrolysis experiments with and without a lid from section 3.3.1 and 3.3.6.

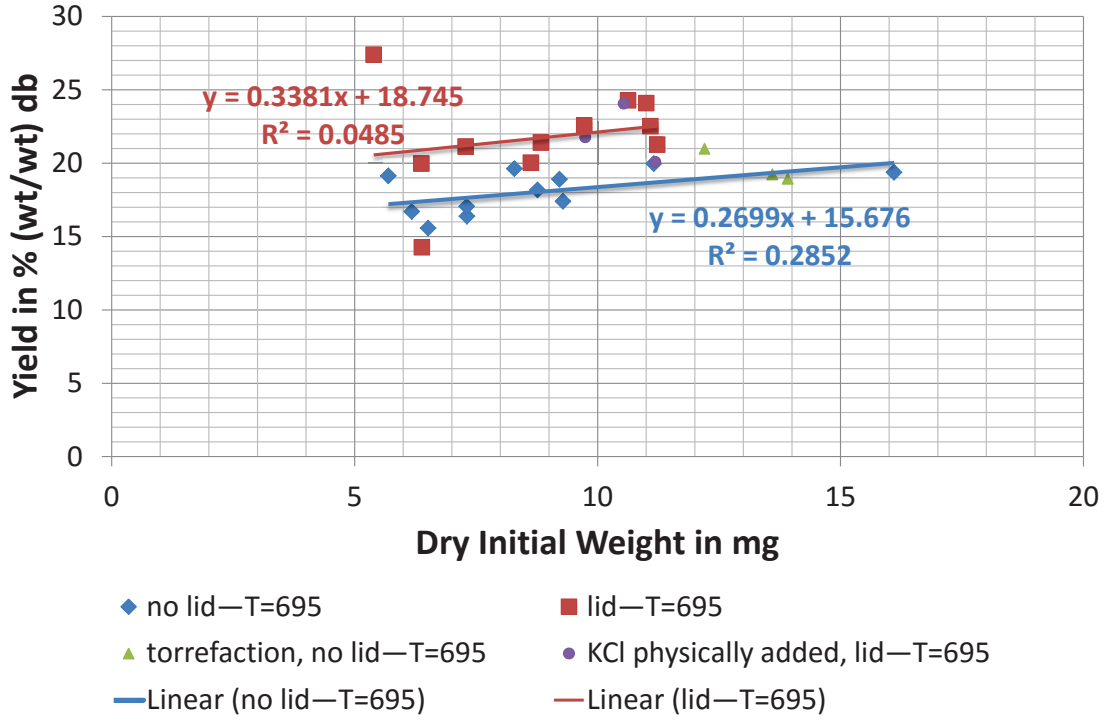

Figure 4-3. Comparison of char yields at 695 °C on a dry basis of various pyrolysis experiments with and without a lid as a function of the initial dry sample weight. The torrefaction experiments did not employ a lid, and the dry initial weight and the yield of the experimental runs with KCl addition is reported on a salt free basis. The dry weight was determined for lid and no lid experiments at 152 and 126 °C respectively. db = dry basis; R^2 = coefficient of determination; T = temperature in °C.

Considering the results in Figure 4-2 and Figure 4-3 it can be concluded that, for catalysis to occur, more intimate contact is required between the pyrolysing solid and the salt. Wang et al. (2010) appeared to achieve this by grinding the wood sample together with the salt for about 15 min. However, this is believed to result in the particle disintegration described by them. Therefore, it was decided to use impregnation as a means of studying catalytic effects during pyrolysis.

4.3.2 Catalytic Effect of Impregnated Samples

A simple correlation analysis was performed on the trials with K impregnation (2 % (wt/wt)) to see if a correlation exists between char yield and the presence or absence of a lid, and the initial sample weight. The results are shown in Table 4-3.

Table 4-3. Correlation analysis for 2 % (wt/wt) K impregnated sawdust.

	Char yield daf	**Lid/no lid**	**Dry sample weight[a]**
Char yield daf	1		
Lid/no lid	0.709466	1	
Dry sample weight[a]	-0.04419	-0.14036	1

Note. The raw data is given in Table C-1 in Appendix C.1.1. The analysis was performed with Microsoft Excel (Microsoft, Redmond, WA, USA). daf = dry ash free basis.

[a]Dry weight was determined for lid and no lid experiments at 152 and 126 °C respectively.

Table 4-3 shows that for the 2 % (wt/wt) K impregnated samples, the char yield correlates to the presence or absence of a lid but not to the initial sample weight. This is illustrated in Figure 4-4.

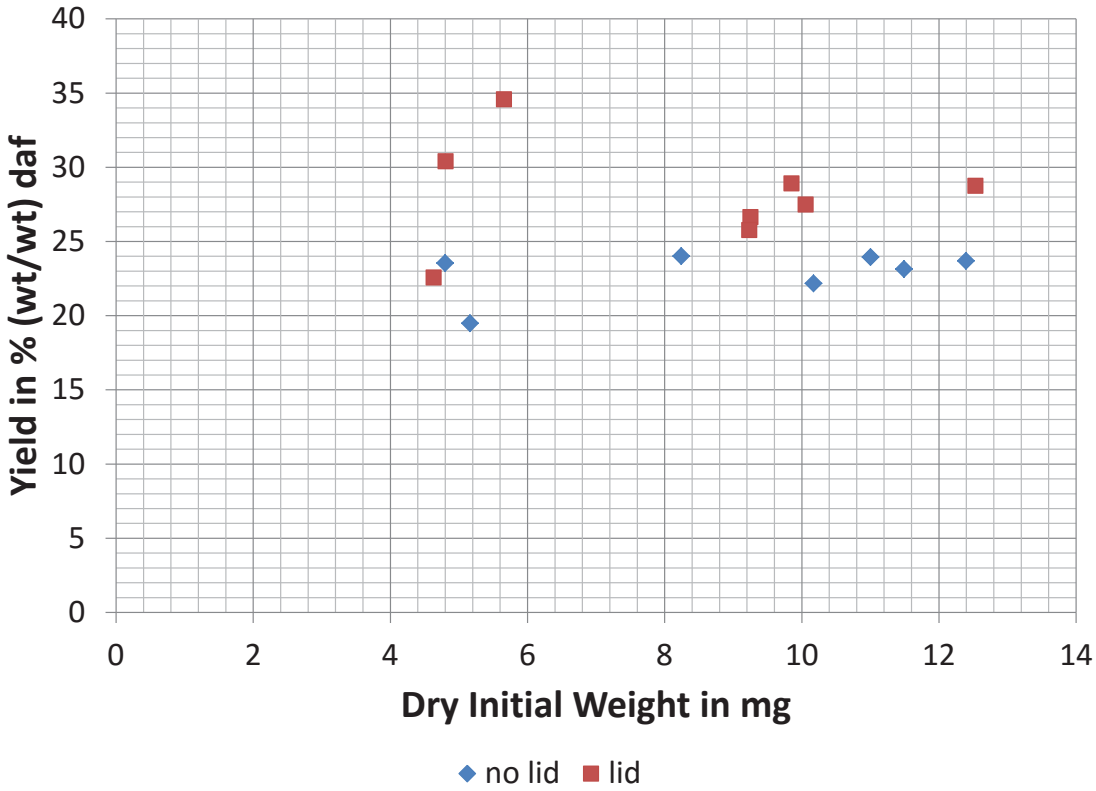

Figure 4-4. Comparison of char yields at 695 °C of 2 % (wt/wt) K impregnated sawdust pyrolysed with and without a lid. The dry sample weight was determined for lid and no lid experiments at 152 and 126 °C respectively. daf = dry ash free.

The difference in yield between runs with and without a lid in Figure 4-4 was tested for significance. A preliminary test for the equality of variances, one tail F-test, with a significance level of 0.05 was performed revealing unequal variance, as shown in Table 4-4.

Table 4-4. F-test for equality of variances on data in Figure 4-4.

	Lid	**No lid**
Mean	28.13	22.86
Variance	12.42	2.59
Observations	8	7
df	7	6
F	4.79	
P(F<=f) one-tail	0.037	
F Critical one-tail	4.21	

Note. The analysis was performed with Microsoft Excel (Microsoft, Redmond, WA, USA). The significance level was set to 0.05. df = degrees of freedom; F = F-test for null hypothesis; P(F<=f) one-tail = P-value for one tail F-test.

Therefore, a t-test assuming unequal variances was performed, Table 4-5.

Table 4-5. t-test for equality of means assuming unequal variances.

	Lid	**No lid**
Mean	28.13	22.86
Variance	12.42	2.59
Observations	8	7
Hypothesized Mean Difference	0	
df	10	
t Stat	3.80	
P(T<=t) one-tail	0.002	
t Critical one-tail	1.81	
P(T<=t) two-tail	0.003	
t Critical two-tail	2.23	

Note. The analysis was performed with Microsoft Excel (Microsoft, Redmond, WA, USA). The significance level was set to 0.05. df = degrees of freedom; P(T<=t) one-tail = P-value for one tail t-test; P(T<=t) two-tail = P-value for two tail t-test; t Stat = t-statistics.

Table 4-5 shows that the null hypothesis of equal means was rejected (two tail t-test) with 99.7 % confidence (P-value of 0.003) showing that the presence of a lid also increases the yield of K impregnated samples. The resulting yield increase is compared to non-impregnated sawdust in Figure 4-5.

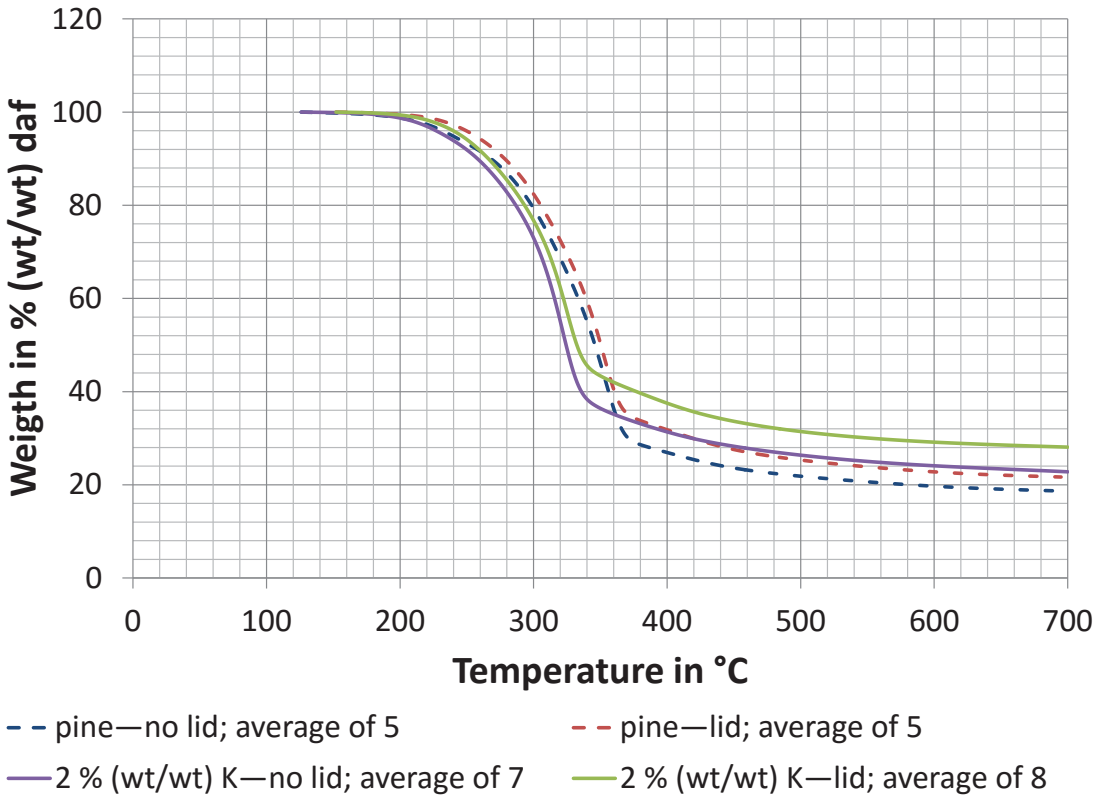

Figure 4-5. Comparison of average weight-loss curves of impregnated, 2 % (wt/wt) K, and non-impregnated pine sawdust pyrolysed in crucibles with and without a lid. The dry sample weight was determined for lid and no lid experiments at 152 and 126 °C respectively. Legend: sample description—lid or no lid; number of averaged experiments. daf = dry ash free.

Figure 4-5 shows that the char yield is higher and overall weight-loss occurs earlier in the impregnated samples compared to the untreated sawdust confirming a catalytic effect of potassium. The effect of a lid is enhanced in the impregnated samples. This is illustrated in Figure 4-6 for the char yield at 695 °C.

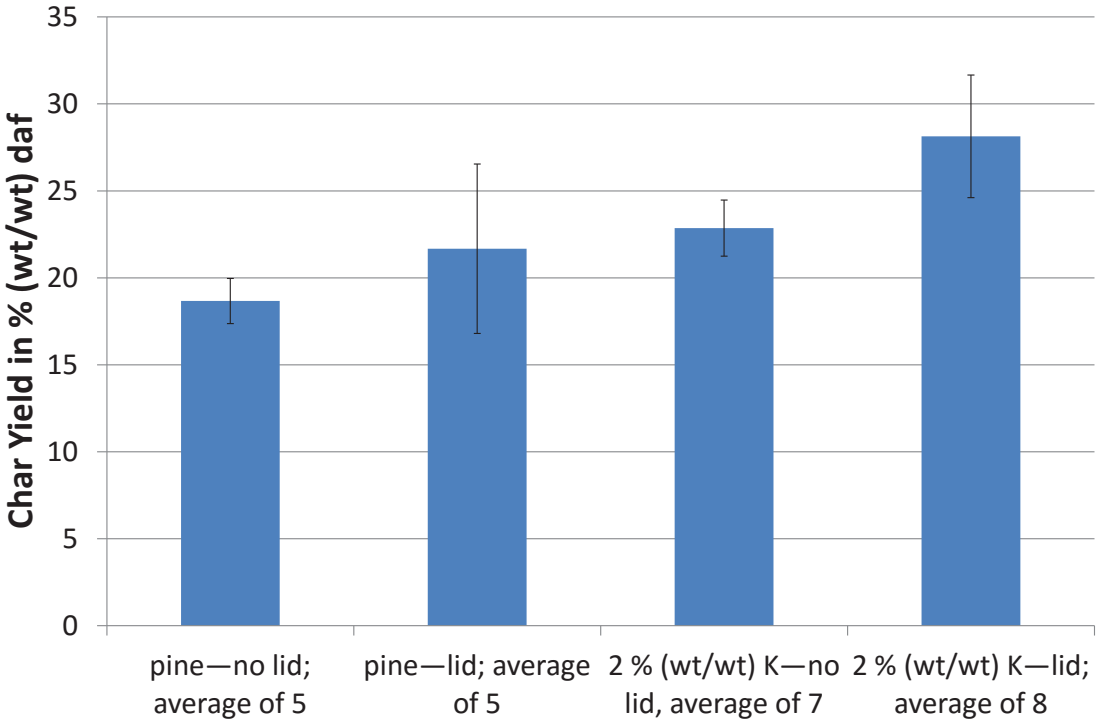

Figure 4-6. Comparison of the char yield obtained at 695 °C of 2 % (wt/wt) K impregnated pine sawdust pyrolysed with and without a lid with pine sawdust pyrolysed with and without a lid. The dry sample weight was determined for lid and no lid experiments at 152 and 126 °C respectively. The error bars denote the standard deviation in percent points. Legend: sample description—lid or no lid; number of averaged experiments. daf = dry ash free.

Figure 4-6 shows that the yield increases with lid and impregnation and that the variability is larger when a lid is applied, which agrees with Figure 4-3. The difference in the yield on a daf basis between experiments with and without a lid in Figure 4-6 is 3.0 and 5.3 % (wt/wt) for untreated pine and pine impregnated with 2 % (wt/wt) K respectively. This indicates that the effect of vapour-phase residence time and thus secondary reactions is enhanced by mineral matter. However, why no yield increase with initial sample weight is observed is unknown. Note, for reference purposes, the pine average curves depicted in Figure 4-5 are those shown in Figure B-9 in Appendix B.5.1. It was decided to use them instead of the ones in Figure 3-10 in section 3.3.1 as they were done within a close time frame and therefore had similar amounts of extractives present (variation of extractives content with storage time was discussed in 3.3.1). The catalytic effect is further investigated in the respective derivative weight-loss curves in Figure 4-7.

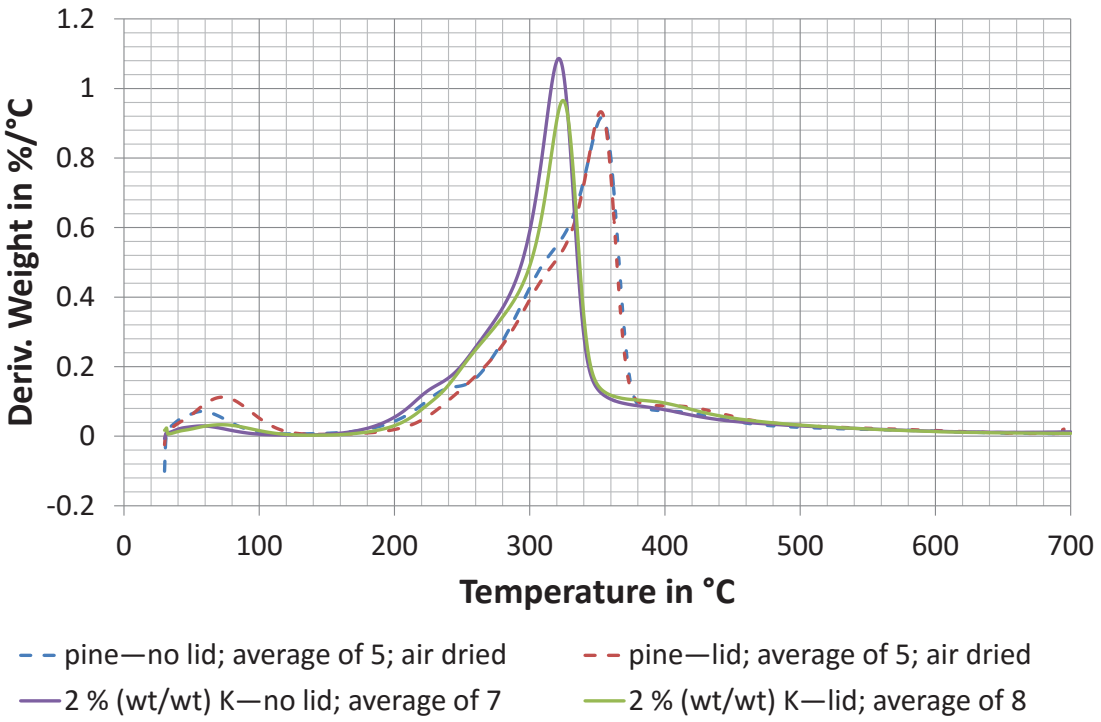

Figure 4-7. Comparison of average derivative weight-loss curves of impregnated, 2 % (wt/wt) K, and non-impregnated pine sawdust pyrolysed in crucibles with and without a lid. Legend: sample description—lid or no lid; number of averaged experiments; drying information (the K impregnated samples were oven-dried as discussed in 4.2.2).

Figure 4-7 shows that impregnation/catalysis causes pyrolysis to occur at lower temperatures. Overall, the curves appear similar in shape. The moisture peak, below 140 °C, is larger for the non-impregnated runs in Figure 4-7, because these samples were air-dried (3.2.1.1), whereas the impregnated samples were oven-dried (4.2.2). As an aside, it is interesting to note that a small amount of moisture is still present in the dried samples despite being oven-dried at 105 °C for 24 h and subsequent storage over silica gel. This shows that dried wood easily absorbs moisture but also a *MC* of 0 % cannot be practically attained (Rowell, 2013). Characteristic temperatures describing the main weight-loss region are given in Table 4-6.

Table 4-6. Characteristic temperatures of the derivative weight-loss curves in Figure 4-7.

Sample	**Lid/no lid**	**Tinitial**[a]	**Tpeak**	**Ttransition**[b]
		°C	**°C**	**°C**
pine	no lid	156.35	353.26	374.62
	lid	183.96	352.38	372.85
2 % (wt/wt) K	no lid	162.71	321.42	346.60
	lid	175.79	324.71	348.08

Note. The listed temperatures represent averages. In case of untreated pine the average temperatures were obtained by averaging of the curves in Figure B-11 and Figure B-12 in Appendix B.5.1. This was possible as a t-test showed there was no statistically significant difference between the characteristic temperatures despite the varying amount of extractives. The impregnated samples have been averaged over all the experiments.

[a]Temperature where the weight-loss equals 0.01%/°C. [b]This temperature was determined with TA Universal Analysis 2000 (TA Instruments, New Castle, Delaware) as the step transition temperature between the point where the second derivative of the derivative weight-loss curve has a minimum and 400 °C.

The differences in the temperatures displayed in Table 4-6 were verified to be statistically significant. The initial temperatures are within ~ 10 °C, whereas the peak temperatures and transition temperatures are ~ 30 °C apart. This shows that pyrolysis in K impregnated samples occurs over a narrower temperature range (time period) than for non-impregnated samples. The reason is believed to be the increased reaction exothermicity of the impregnated samples which causes the internal particle temperature to rise and so accelerates the rate of conversion (details are discussed in chapter 5). Further evidence that the K impregnated samples have indeed a reduced reaction heat (more exothermic) compared to the untreated pine sawdust is qualitatively confirmed by comparing Figure 5-9 in 5.3.2 with Figure D-14 and Figure D-15 in Appendix D.2. In particular Figure D-15 shows that, in the case of pyrolysing the 2 % (wt/wt) K impregnated samples with a lid, the overall heat of pyrolysis appears to become exothermic or close to exothermic. Comparing ‘lid’ and ‘no lid’ trials, in contrast to pine, the peak temperature of the derivative weight-loss curves for the impregnated samples increases, albeit slightly, by ~3 °C, as shown in Table 4-6. This trend is contrary to the one observed for the pine samples, which was discussed in 3.3.5, and is the reason that the difference curves “no lid-lid” for the untreated and impregnated pine in Figure 4-8 differ (last peak of the pine curve is caused by the fact that the peak occurs earlier for the lid samples).

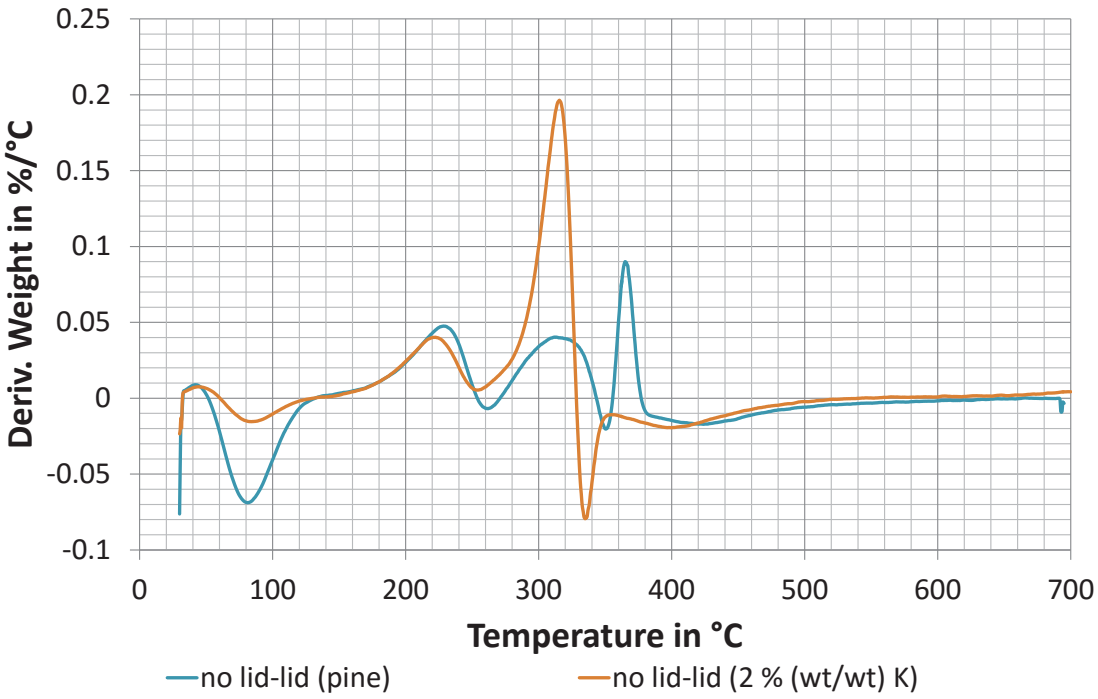

Figure 4-8. Comparison of difference curves "no lid-lid" of derivative weight-loss curves of impregnated, 2 % (wt/wt) K, and non-impregnated pine sawdust samples. The difference curves correspond to the derivative weight-loss curves in Figure 4-7.

The statistical test for significance of the above discussed increase in the peak temperatures for the 2 % (wt/wt) K impregnated samples is given in Appendix C.1.2. The null hypothesis that they are equal means was rejected (two tail t-test) with 99.7 % confidence (P-value of 0.003), as shown in Table C-4 in Appendix C.2.2. This means the ~3 °C difference is significant. The reason for the above result are not obvious. As an example, the work of Gomez, Velo, Barontini, and Cozzani (2009) yielded, in washed samples with reduced mineral content, a char yield increase, caused by the presence of a lid. This they argued is associated with a greater reduction in the heat of pyrolysis (increased exothermicity) compared to unwashed samples, which indicates possibly reduced secondary reaction heat effects with increasing mineral content. This points towards a different underlying reaction mechanism that results in higher char yield attained by secondary reactions in the presence of minerals. However, they also showed that overall the heat of pyrolysis can be fitted linearly to the char yield no matter whether or not the differences in the yield were caused by differing sample size, sample washing or the presence of a lid. This demonstrates the large effect secondary reactions have in general on the heat of pyrolysis and the char yield and that these effects are independent of the presence or absence of minerals. The fact that minerals

appear to lower the change in the heat of pyrolysis between the 'lid' and 'no lid' cases as indicated by Gomez et al. (2009) would explain a reduced difference in the peak temperature between the two cases of the K impregnated samples in Table 4-6 compared to the untreated pine samples but not a higher peak temperature for the runs with a lid. Therefore, increased mass transfer limitations are likely in combination with a smaller reaction heat effect, which would result in a right shift of the derivative weight loss peak. Chapter 5 attempts to examine the reaction heat, but unfortunately usable quantitative results were not obtained as a consequence of the inherent inaccuracy of the equipment (see chapter 5 for details). The hypothesis of increased mass transfer limitations in the case of K impregnated samples is supported by the observation in Figure 4-7 that the maximum derivative weight-loss is higher for the impregnated samples. However, there is quite a bit of variation between repeat runs, which is illustrated in Figure C-1 and Figure C-2 in Appendix C.1.3. Nevertheless, the maximum derivative weight-loss appears to be higher for the impregnated samples but this could also be related to the lower moisture content of the impregnated samples. To verify this it is necessary to determine the degree of conversion of the dried samples and plot it as a function of time. The result is depicted in Figure 4-9 and Figure 4-10 for the cases no lid and lid respectively.

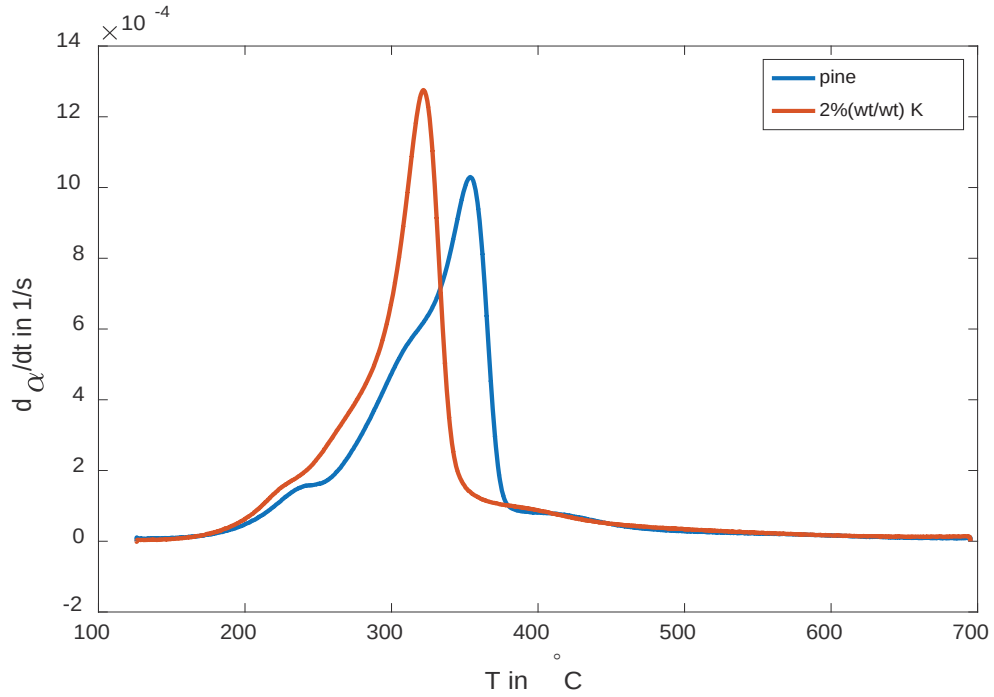

Figure 4-9. Comparison of the average derivative conversion curves of untreated pine sawdust and pine sawdust impregnated with 2 % (wt/wt) K pyrolysed in crucibles without a lid. The conversion was calculated for dried samples with a starting temperature of 126 °C. The pine sawdust represents the average of 5 experiments corresponding to Figure B-10 in Appendix B.5.1 and the impregnated curve the average of 7 experiments. T = temperature; dα/dt = time derivative of the degree of conversion.

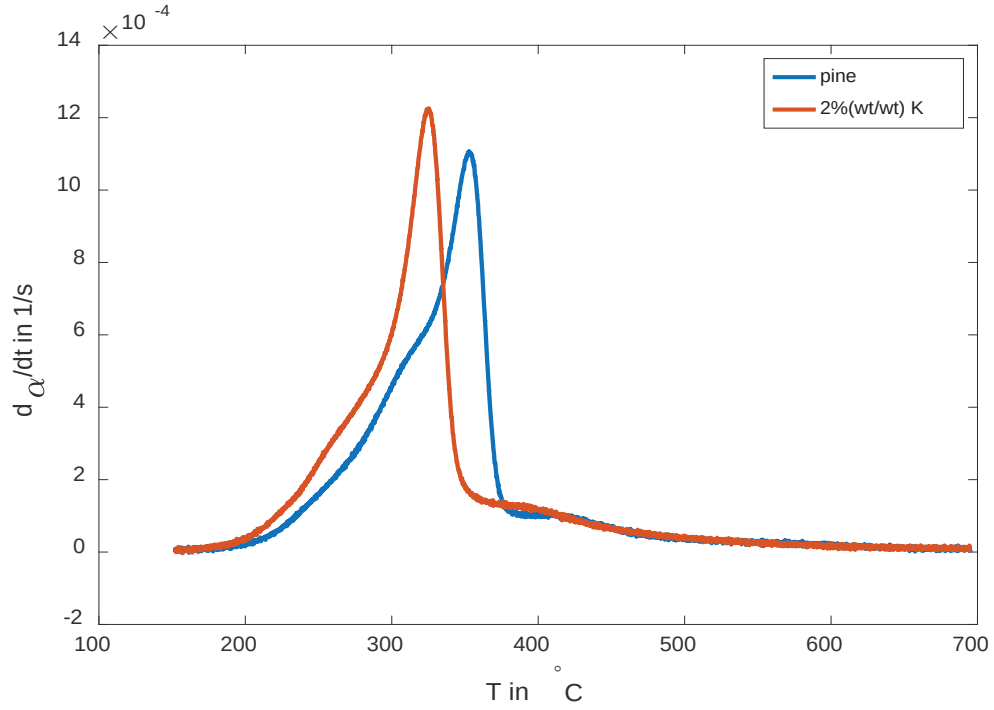

Figure 4-10. Comparison of the average derivative conversion curves of untreated pine sawdust and pine sawdust impregnated with 2 % (wt/wt) K pyrolysed in crucibles with a lid. The conversion was calculated for dried samples with a starting temperature of 152 °C. The pine sawdust represents the average of 5 experiments corresponding to Figure B-10 in Appendix B.5.1 and the impregnated curve the average of 8 experiments. T = temperature; dα/dt = time derivative of the degree of conversion.

Figure 4-9 and Figure 4-10 reveal that indeed the maximum conversion is higher in the impregnated samples, that is, more volatiles are released in a shorter time. Therefore, mass transfer limitations associated with the main pyrolysis peak are likely to occur earlier in the K impregnated samples explaining the delay in the maximum conversion and its reduced value in the case of the application of a lid in Figure 4-10. It further indicates that the higher char yield in the case of a lid might be associated with char formation from a liquid phase, noting that its formation is favoured under conditions of mass transfer limitations as was discussed in chapter 2. Figure 4-9 and Figure 4-10 also indicate that the majority of the difference between the impregnated and non-impregnated samples originates from the holocellulose fraction, though in the case of a lid more lignin appears to decompose.

The other catalysts have a similar effect on the derivative weight loss curves in that they cause a shift of the main pyrolysis peak to lower temperatures, which is illustrated in Figure 4-11 and Figure 4-12 for the Mg and P impregnated samples respectively.

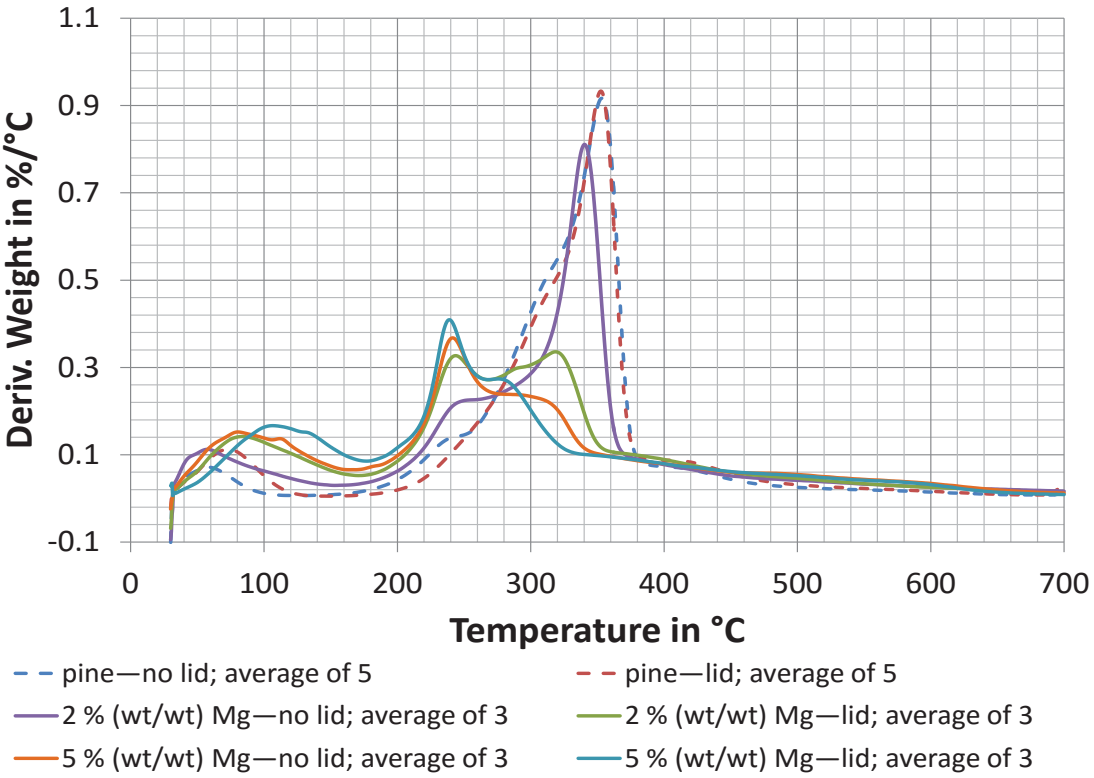

Figure 4-11. Comparison of average derivative weight-loss curves of pine sawdust impregnated with 2 and 5 % (wt/wt) Mg pyrolysed in crucibles with and without a lid. The derivative weight-loss curves of untreated pine sawdust (dashed lines) have been included for comparison. Legend: sample description—lid or no lid; number of averaged experiments.

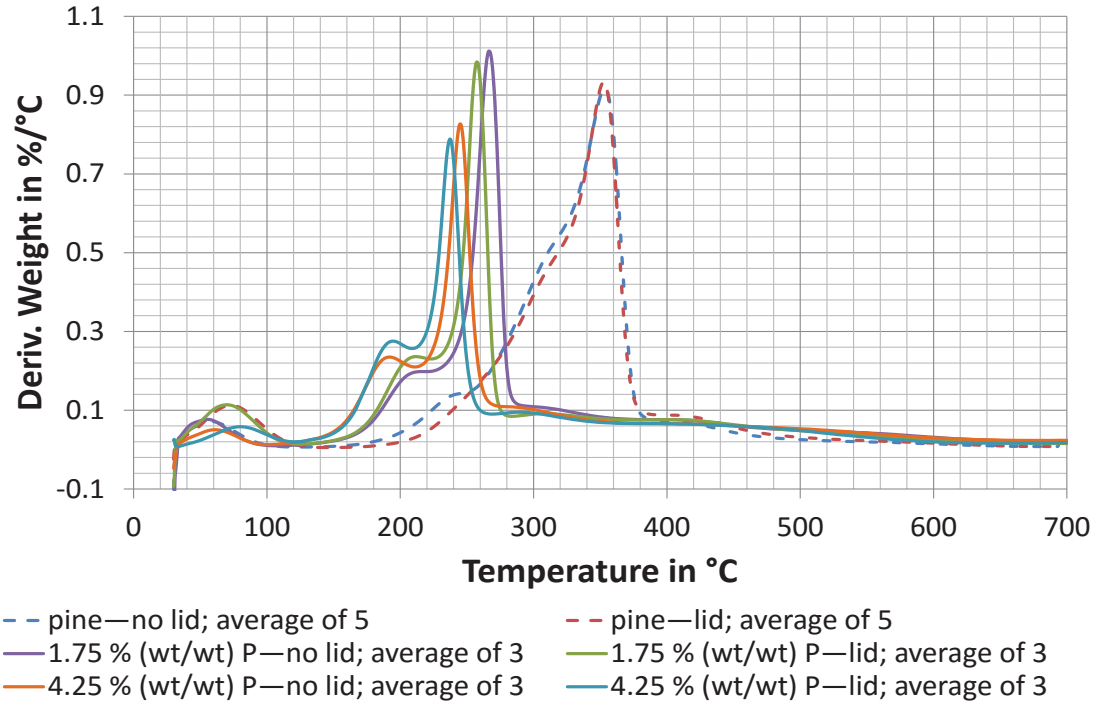

Figure 4-12. Comparison of average derivative weight-loss curves of pine sawdust impregnated with 1.75 and 4.25 % (wt/wt) P pyrolysed in crucibles with and without a lid. The derivative weight-loss curves of untreated pine sawdust (dashed lines) have been included for comparison. Legend: sample description—lid or no lid; number of averaged experiments.

The shift in the main weight loss peak, which is generally associated with the holocellulose fraction as discussed in 3.3.8, indicates that lignin might be unaffected by catalysis and secondary reactions. That Mg does not have a big impact on lignin was shown by Khelfa et al. (2013). In general, their results for Mg impregnation support the observed trend in Figure 4-11 except the large peak around 100 °C, which was not observed by them. The non-averaged curves of the impregnated experiments in Figure 4-11 are supplied in Appendix C.1.5 in Figure C-3 to Figure C-6 to demonstrate the repeatability of the experiments, which was generally good except for the last peak associated with cellulose decomposition. The observed variation in the decomposition profile was found to follow the trend in Figure 4-11, that is, with increasing char yield (Figure 4-13), caused by the presence of a lid or increased content of Mg, the main peak decreased and shifted towards lower temperatures. Thus, the variation in this peak (e.g. Figure C-3 in Appendix C.1.5) is believed to be genuine and could be related to inhomogeneous catalyst distribution. The initial sample mass was ruled out as a contributing factor as the experiments employed similar initial sample weights and run "003" in Figure C-3 in Appendix C.1.5 with the highest char yield employed the lowest initial sample weight out of the three experiments. These changes also explain the relatively large deviations observed in Figure 4-13, e.g. in the case of 2 % (wt/wt) Mg impregnated sawdust pyrolysed without a lid.

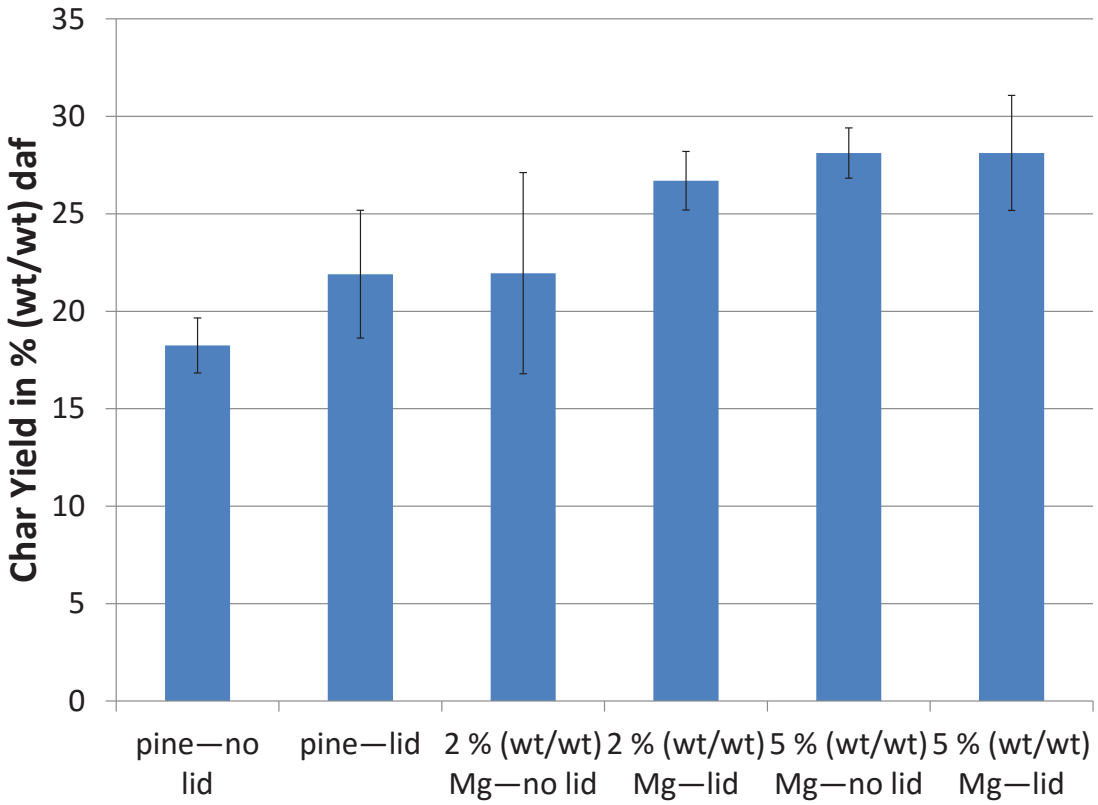

Figure 4-13. Comparison of the char yield obtained at 650 °C of Mg impregnated pine sawdust pyrolysed with and without a lid with pine sawdust pyrolysed with and without a lid. The dry temperature was selected as 30 °C for the Mg impregnated samples, as they were previously oven-dried at 105 °C and subsequently stored over silica gel. In the case of pine sawdust the dry sample weight was determined for lid and no lid experiments at 152 and 126 °C respectively. The yields of the Mg impregnated samples and pine sawdust represent averages of 3 and 11 respectively. The error bars denote the standard deviation in percent points. daf = dry ash free.

It is important to note that Figure 4-13 shows the effect of Mg impregnation and the presence of a lid on the char yield at 650 °C instead of the 695 °C used in Figure 4-6 as the aim was to calculate the average of at least three experiments but one experiment (run "003" in Figure C-4 in Appendix C.1.5) stopped recording after 650 °C. Due to the above discussed variation and the small number of replicates carried out, there was no statistical difference in yield between the experiments with and without a lid for the 2 % (wt/wt) Mg impregnated samples. However, when considering the derivative weight-loss profiles, it is believed that the difference is authentic between the experiments with and without a lid; that is, the yield increases with Mg impregnation and the presence of a lid, although maximum limit seems to be reached at 5% (wt/wt) Mg impregnation, at which the presence of a lid also does not cause any further yield increase. This is supported by Figure 4-11 where the differences between the derivative weight-loss curves become smaller with increasing Mg concentration. Figure 4-11 shows that with increasing impregnation and vapour-phase residence time (increased by

the presence of a lid) the pyrolysis range of the holocellulose fraction occurs at lower temperatures and the overall devolatilisation decreases (char yield increases). This is related to the catalytic action of Mg and the decreasing reaction heat (becoming increasingly exothermic, Figure 5-16 and Figure 5-17 in 5.3.2 and Figure D-12 and Figure D-13 in Appendix D.2) with increasing char yield (chapter 5). In this manner the Mg results in Figure 4-11 agree with the findings in 3.3.5, where the peak temperature of the main peak for untreated pine wood was found to decrease with the presence of a lid. Note that this is contrary to the observation for the K impregnated samples reported in Table 4-6 where the peak temperature increased in the presence of a lid. Figure 4-11 also indicates that the maximum weight-loss rate decreases with both increasing Mg impregnation and the presence of a lid. This suggests that mass transfer limitations are not a dominant factor for Mg impregnation, which is the opposite conclusion to that drawn for the K impregnation trials earlier.

Figure 4-11 also reveals that an increasingly large proportion is decomposed prior to 200 °C. In the case of untreated pine sawdust the first peak below 200 °C is associated with the evaporation of water (chapter 3). However, the Mg treated samples were oven-dried at 105 °C and subsequently stored over silica gel. Thus, this peak is too large to solely derive from absorbed moisture (this would be expected to be in the order of that reported for K impregnation in Figure 4-7). Remarkably, Mg promotes pyrolysis reactions even below 100 °C, which was evidenced by leaving the Mg impregnated samples for longer than 12 hours in the oven, which caused decolourisation similar to that observed during torrefaction. This initial peak increases and shifts right with increasing metal impregnation and the presence of a lid, revealing that it is not only affected by catalyst concentration but also by mass transfer limitations, which is a consequence of the low wood porosity compared to char. However, the existence of transfer limitations in this region could also be a manifestation of the presence of a liquid phase given that the majority of reactions occurring are dehydration reactions. That Mg impregnation favours dehydration of holocellulose was reported in the literature (Khelfa et al., 2013; Khelfa, Finqueneisel, Auber, & Weber, 2008).

Interestingly, the results presented here show that the impregnated metals affect the main peak that is associated with cellulose decomposition (in particular for Mg impregnation), which in the literature is reported to be limited (Khelfa et al., 2013). Mamleev, Bourbigot, and Yvon (2007) demonstrate that the solid matrix of cellulose is

impenetrable for chemical reagents with van der Waals radii larger than oxygen, which lead Khelfa et al. (2013) to conclude that mineral impregnation cannot be important for cellulose pyrolysis as it is merely a surface phenomenon that affects the thermal degradation of cellulose minimally. However, looking in more detail at the proposed two-phase model of Mamleev et al. (2007), which proposes that cellulose pyrolysis "is a migration of chain ends from the phase of polymer cellulose into the phase of products (char, gases and high-boiling tar)" (p. 151) that continuously changes the cellulose polymer into a microporous char with liquid tar inclusions, it can be concluded that the change observed here in the thermal decomposition profile of cellulose with increasing mineral concentration and vapour-phase residence time is indeed the result of secondary reactions that takes place in the product phase. This indicates that minerals catalyse secondary reactions of cellulose and supports the importance of secondary char forming reactions for cellulose as found by Antal and Varhegyi (1995) as discussed in 3.3.2.

The effect of phosphoric acid impregnation (1.75 and 4.25 % (wt/wt) P) is shown in Figure 4-12. That acids dehydrate sugar is a well-known fact, and the dehydration of sugar by concentrated sulphuric acid is a popular science experiment (Mamleev et al., 2009). The non-averaged curves of the impregnated experiments in Figure 4-12 are provided in Figure C-11 to Figure C-14 in Appendix C.2.1 showing a good reproducibility. In general Figure 4-12 depicts similar trends to Figure 4-11, that is, with increasing amount of impregnated P and prolonged vapour-phase residence time, the main weight-loss peak shifts to lower temperatures. In addition the key peak associated with cellulose pyrolysis becomes narrower, while the shoulder peak associated with hemicellulose becomes more differentiated. In contrast to Figure 4-11 the large initial peak, below 200 °C, is absent. Instead, the relatively small peak below 120 °C in Figure 4-12 is due to the evaporation of moisture, which matches that of the untreated pine sawdust in the case of the sawdust impregnated with 1.75 % (wt/wt) P. The moisture peak of the sawdust impregnated with 4.25 % (wt/wt) P is smaller as it was stored longer over silica gel. The absence of the "thought to be" dehydration peak below 200 °C in Figure 4-12 comes as a surprise as dehydration was anticipated. The maximum weight-loss rate of the impregnated sample with the lowest concentration, associated with cellulose decomposition, appears higher than the one for the untreated wood. This was verified to be authentic by plotting the time derivative of the conversion of the dried pine sawdust impregnated with 1.75 % (wt/wt) P pyrolysed in

crucibles without a lid, which showed the highest weight-loss in Figure 4-12 with respect to temperature, in Figure 4-14.

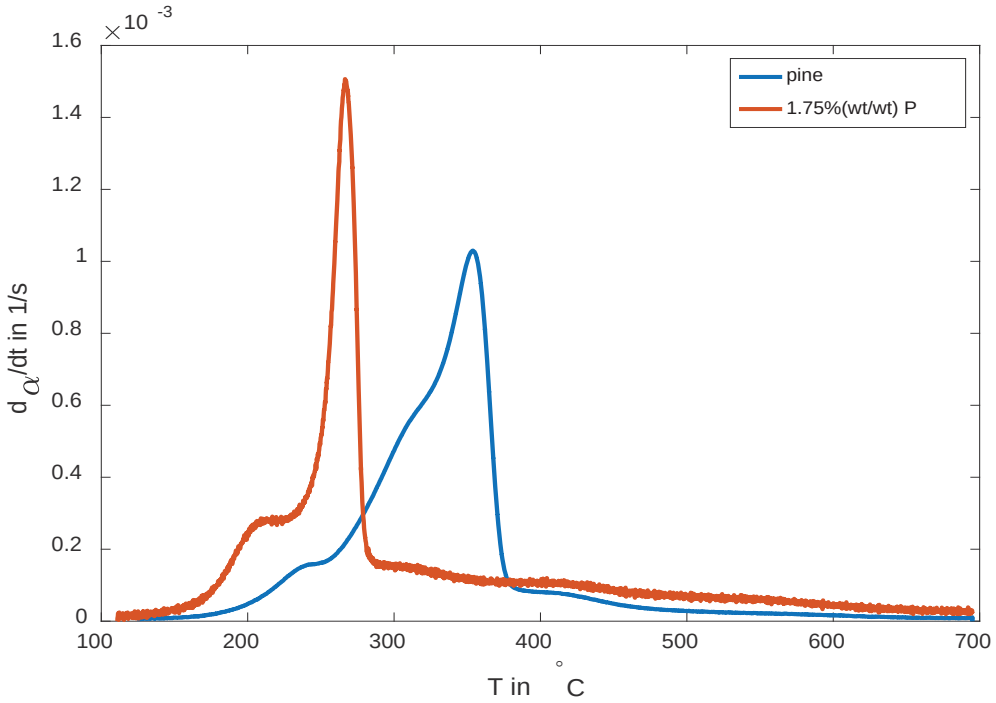

Figure 4-14. Comparison of the average derivative conversion curves of untreated pine sawdust and pine sawdust impregnated with 1.75 % (wt/wt) P pyrolysed in crucibles without a lid. The conversion was calculated for dried samples with a starting temperature of 126 and 111 °C for the untreated and treated pine sawdust respectively. The pine sawdust represents the average of 5 experiments corresponding to Figure B-10 in Appendix B.5.1 and the impregnated curve the average of 3 experiments. T = temperature; dα/dt = time derivative of the degree of conversion.

Figure 4-14 reveals that the conversion rate for the P impregnated sample is even faster than the one observed in Figure 4-9 for the 2 % (wt/wt) K impregnated sample. This could be due to the lower concentration of P that is naturally present in the wood compared to K, resulting in a greater change when it is present. Despite this fast conversion rate, there appears to occur no mass transfer limitations (the peak width decreases with increased impregnation and presence of lid, and the main pyrolysis peak shifts to lower temperatures) as was the case for the K impregnated samples. The reason could be a different reaction mechanism with a higher reaction rate associated with a larger decrease in the reaction heat compared to the K impregnated samples. This idea is supported by comparing the heat flow data in Figure D-16 to Figure D-19 in Appendix D.2 for the P impregnated samples with those in Figure D-14 and Figure D-15 in Appendix D.2 for the K impregnated samples. The initial increase and subsequent decrease of the cellulose peak, shown in Figure 4-12 and Figure 4-14

indicates that P also impacts cellulose depolymerisation, which is associated with the main weight-loss peak according to Collard and Blin (2014). In the same manner as Mg impregnation, P impregnation does not allow the cellulose matrix to be penetrated by the reagent (Mamleev et al., 2007). Therefore, the change in the decomposition profile observed in Figure 4-12 is believed once again to be a consequence of secondary reactions.

The char yields at 695 °C to the runs in Figure 4-12 are depicted in Figure 4-15.

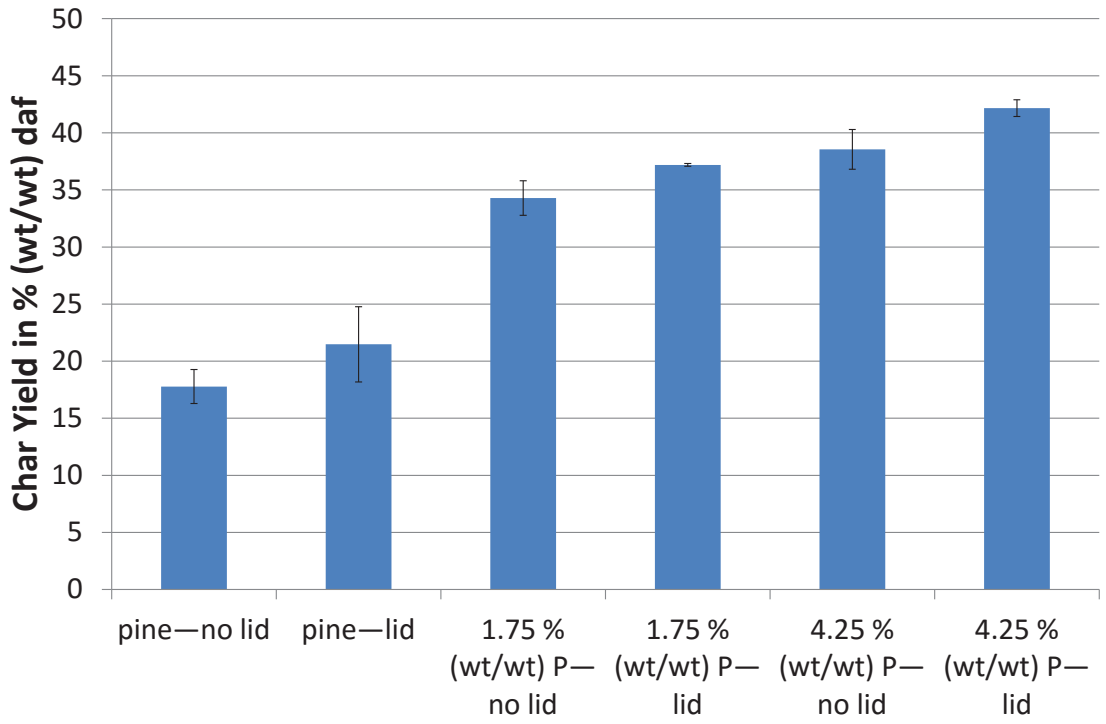

Figure 4-15. Comparison of the char yield obtained at 695 °C of P impregnated pine sawdust pyrolysed with and without a lid with pine sawdust pyrolysed with and without a lid. The dry temperature was taken at the minimum in the derivative weight-loss curve between 60 to 200 °C for the P impregnated samples. In the case of pine sawdust the dry sample weight was determined for lid and no lid experiments at 152 and 126 °C respectively. The yields of the P impregnated samples and pine sawdust represent averages of 3 and 11 respectively. The error bars denote the standard deviation in percent points. daf = dry ash free.

Figure 4-15 shows a similar trend to Figure 4-13, that is, the total char yield increases with impregnation and presence of a lid, which confirms that P catalyses char formation and that secondary vapour-phase reactions are active in the presence of P. Intriguing is that the char yield of P impregnated samples at 695 °C is higher than the Mg treated samples at 650 °C revealing the stronger catalytic effect of P.

It was attempted to model the decomposition curves of the impregnated samples by the first order model described in 3.3.8, which is illustrated for the 2 % (wt/wt) K

impregnated samples pyrolysed without and with a lid in Figure 4-16 and Figure 4-17 respectively.

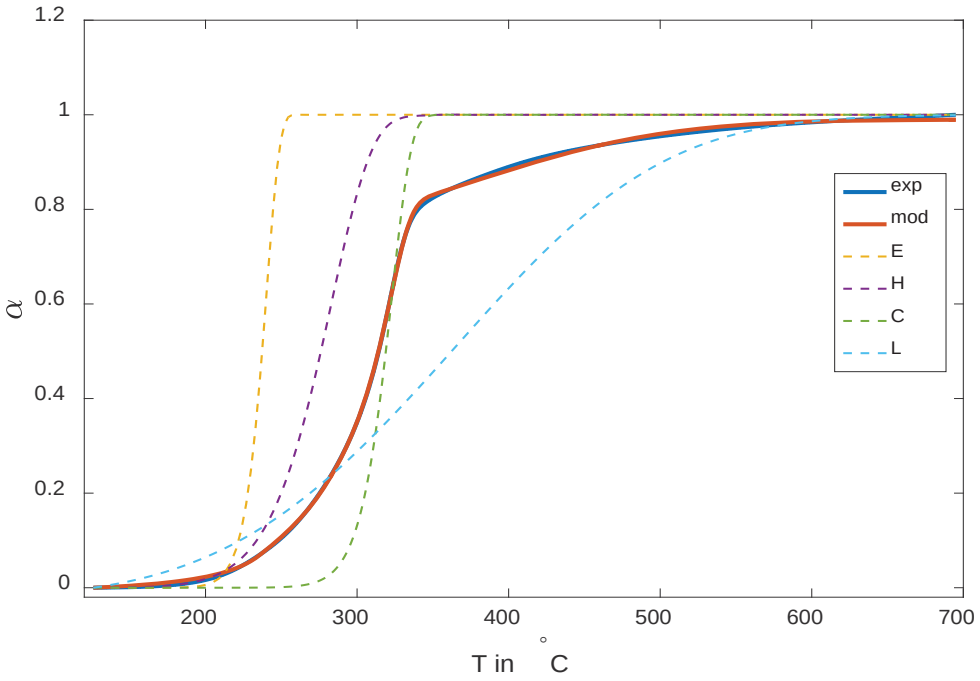

Figure 4-16. Conversion curves of the experimental and modelled data of 2 % (wt/wt) K impregnated sawdust pyrolysed without a lid. The thinner dashed lines represent the conversion curves of the four biomass constituents extractives, hemicellulose, cellulose and lignin. The fitted parameters are given in Table C-5 in Appendix C.2.4. exp = experimental data; E = extractives; C = cellulose; H = hemicellulose; L = lignin; mod = modelled data; T = temperature; α = degree of conversion.

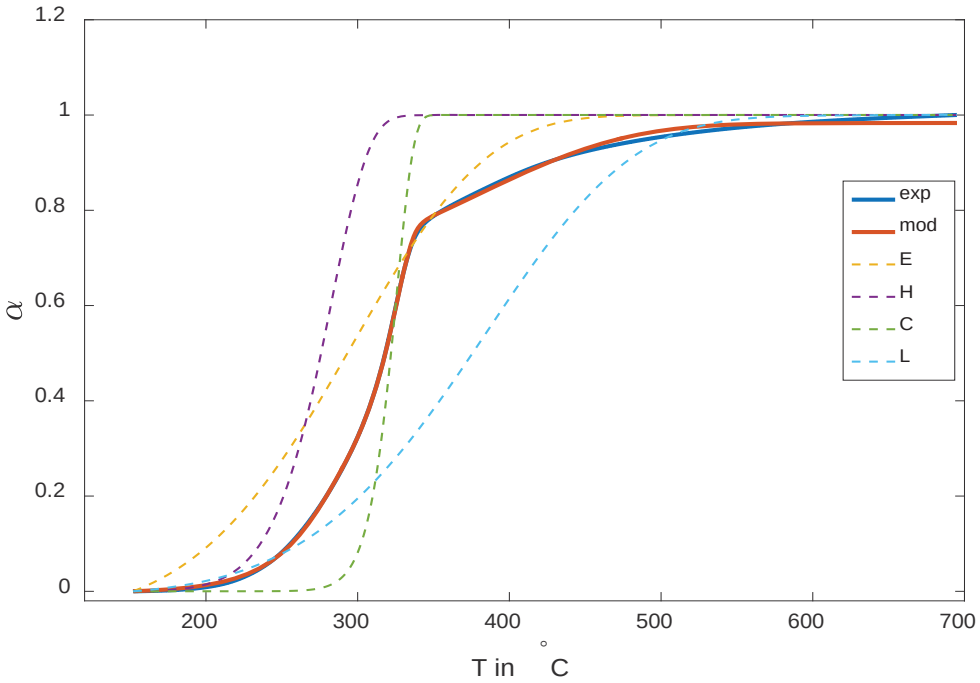

Figure 4-17. Conversion curves of the experimental and modelled data of 2 % (wt/wt) K impregnated sawdust pyrolysed with a lid. The thinner dashed lines represent the conversion curves of the four biomass constituents extractives, hemicellulose, cellulose and lignin. The fitted parameters are given in Table C-6 in Appendix C.2.4. exp = experimental data; E = extractives; C = cellulose; H = hemicellulose; L = lignin; mod = modelled data; T = temperature; α = degree of conversion.

Figure 4-16 and Figure 4-17 show that it is possible to fit a first order model to the decomposition curve but it was found that the fit gets worse with presence of lid and increasing concentration of catalyst (average difference in Figure 4-16 and Figure 4-17 is 0.31 % and 0.42 % respectively). For the Magnesium and Potassium impregnated samples the curve fitting results are given in Appendix C.1.6 and C.2.2 respectively, where it becomes clear that fitting is still possible due to the fact that four components, each with three adjustable parameters, are available for fitting. However, this does not represent reality as demonstrated by the unrealistic decomposition behaviour of the constituents and their respective char yields as shown in Table C-7 to Table C-10 and Table C-11 to Table C-14 for the Mg and P impregnated samples respectively. Thus, a first order reaction model is not valid to describe catalysed pyrolysis and pyrolysis with enhanced secondary reactions (see 3.3.8). This is also revealed by the changing shape of the thermal analysis curves compared to pine wood (see Figure 4-11, Figure 4-12, Appendix C.1.6 and Appendix C.2.2); it is the shape which determines the mechanistic model, as reviewed by Brown (1988). Therefore, alternative models have to be researched. It is also important to analyse the volatile product composition profile as a function of temperature to identify pseudo-component decomposition ranges if distinguishable, which has been done for untreated pine wood in chapter 6. Therefore, these findings support the conclusion made in chapter 3 that this commonly used devolatilisation model is an over-simplification for any process that involves the formation of significant amounts of char (due to either the action of secondary reactions or catalyst). It is important to note that in particular a large uncertainty is associated with the lignin peak. The tail region (zone V and VI) seems to have two peaks around 300 and 420 °C in Figure 4-12 indicating that the tailing region cannot be described by a single lignin peak; rather re-arrangement reactions with associated weight-loss are expected from all four biomass pseudo-components. Ambiguity is also associated with the extractives and hemicellulose decomposition as they overlap. It is questionable if extractives were present after the rotary evaporation step described in 4.2.2; although water was still present as discussed above.

4.3.3 Summary of Catalysts Performance

The effect of the above studied catalysts on the decomposition rate is compared in Figure 4-18.

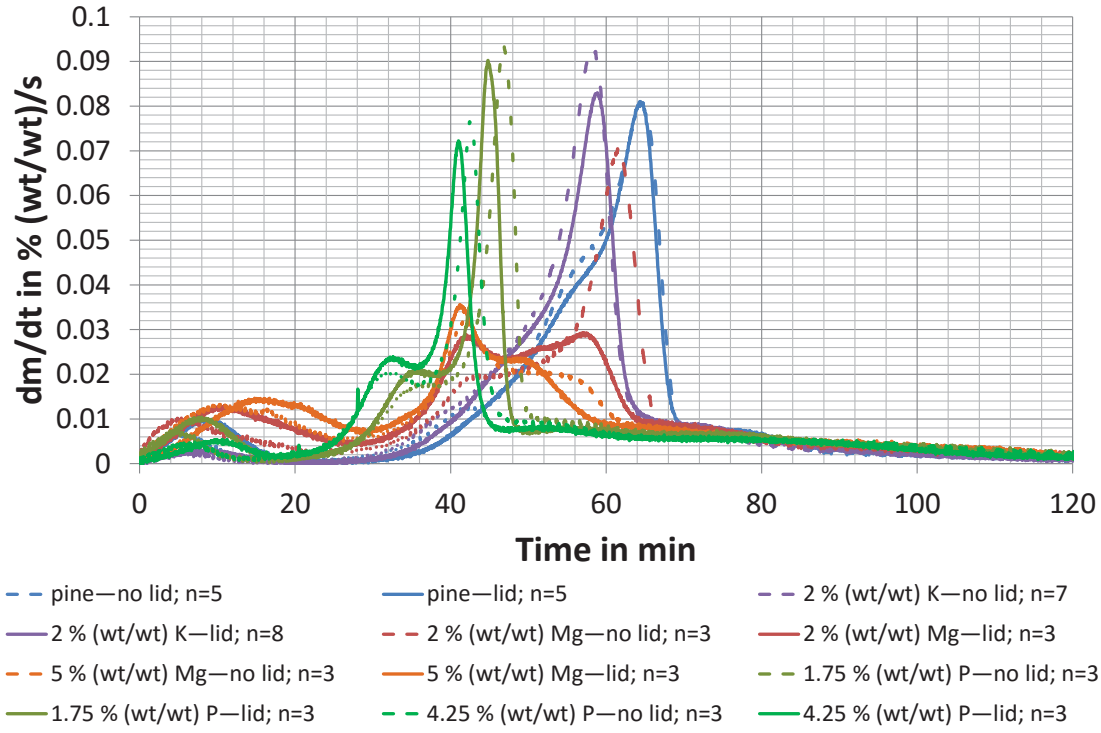

Figure 4-18. Comparison of the weight-loss rate of untreated pine sawdust and sawdust impregnated with K, Mg and P pyrolysed in crucibles with and without a lid. The depicted weight-loss rate is calculated on the basis of the sample weight at 30 °C. It is important to note that the samples treated with K and Mg were previously oven-dried while the others were not. Legend: experiment—lid or no lid; number of averaged experiments. m = weight in % (wt/wt); n = number of averaged experiments; t = time; wt = weight.

The graphs in Figure 4-18 are plotted as a function of time as the temperature recordings are skewed due to the reaction heat. It clearly shows that catalysis and the presence of a lid affects the reaction rate and decomposition profile in general. Overall, pyrolysis is completed in shorter time with increasing catalyst concentration and presence of a lid, which also correlates with an increase in char yield (Figure 4-19). This supports the findings in chapter 3 that it is not the time-temperature history that causes the char yield increase; although the differing decomposition profiles of the varying catalysts show that they affect pyrolysis by a different mechanism, but also that secondary reactions form an integral part of the mechanism. While the pseudo component model has been shown to be inadequate, catalysis appears to most affect the holocellulose region (i.e., the cellulose and hemicellulose).

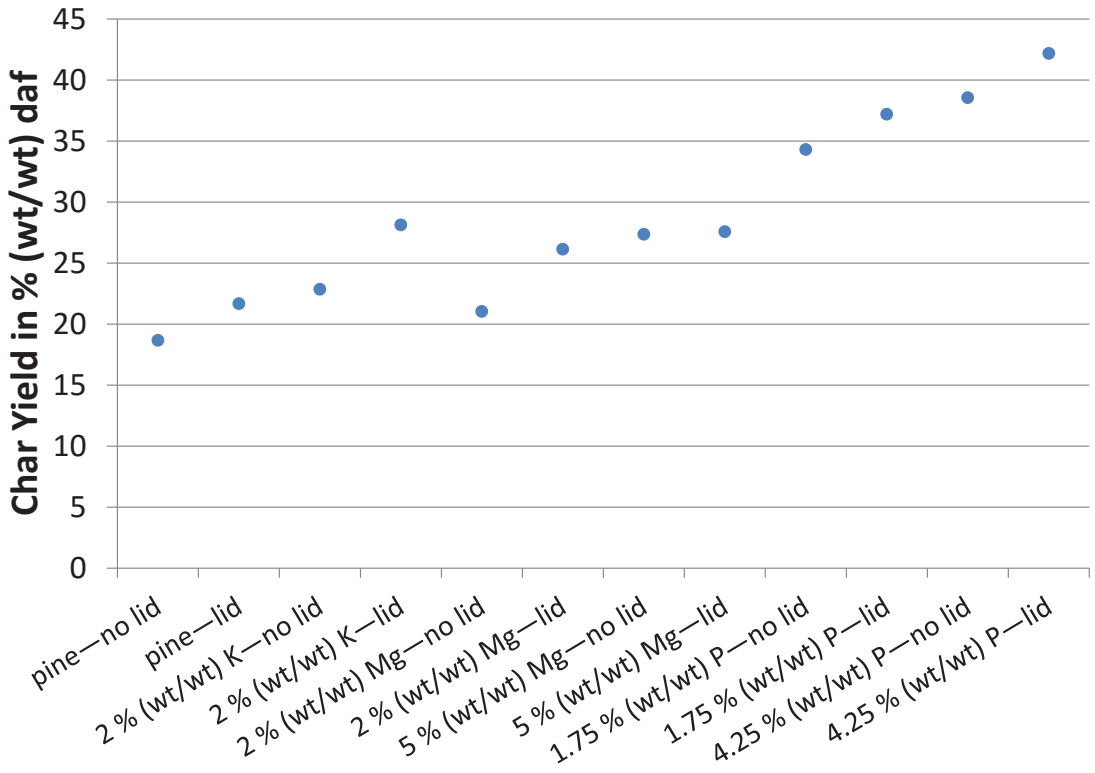

Figure 4-19. Comparison of the total char yield obtained at 695 °C on a dry ash free basis of pine sawdust and sawdust impregnated with K, Mg and P pyrolysed in crucibles with and without a lid. Axis name: experiment—lid or no lid. daf = dry ash free; wt = weight.

The reduction in volatile matter formation, that is, the increased production of char with impregnation of salts or phosphoric acid is one of the reasons why these materials are used as flame retardants (Fu et al., 2008; Shafizadeh, 1968). The most efficient catalyst with respect to char yield increase and possibly reduced required reaction heat (see chapter 5) is phosphoric acid treatment. Phosphorous is one of the main plant nutrients and is added to agricultural soils on a large scale. Thus, if available to plants, it can have additional benefits to soil. Moreover phosphoric acid is also been used for chemical activation offering additional advantages for the application of biochar (Downie, Crosky, & Munroe, 2009). In general, all the catalysts used in this study are plant nutrients (4.1) and therefore naturally present in the ash of the feedstock. This means that all the observations made here take place to a smaller or larger extent (depending on the ash content of the feedstock) during pyrolysis of any untreated biomass feedstock, highlighting the important role of catalysis and secondary reactions during char formation.

4.4 Conclusion

All the investigated catalysts in this chapter, K, Mg and P, were found to be catalytic during pyrolysis. In this work, intimate contact between the samples and catalyst was achieved by impregnation. In general catalysis leads to an earlier onset and completion of pyrolysis. It primarily affects the holocellulose fraction, which leads to progressively higher char yields with catalyst concentration. Similar to the results of untreated pine sawdust in chapter 3, increased vapour-phase residence time, by the application of a lid, leads to higher char yields in the presence of catalyst indicating that there is a relationship between catalyst and secondary reactions. This was confirmed by the observation that enhancing secondary reactions by using of a lid changed the decomposition profile, although the effect varied with catalyst and its concentration. This shows that the catalysts are active towards secondary reactions. However, merely increasing the sample weight to improve/ prolong the vapour-solid contact/ vapour-phase residence time did not result in a char yield increase. Conclusions about the catalytic action towards primary reactions are not possible from the results presented here.

Impregnation and the presence of a lid force the pyrolysis reactions to be more exothermic. Therefore, decisive conclusions about the temperature range of catalysed reactions (either by impregnation or presence of lid) are not possible without measuring the internal sample temperature as this also shows that caution has to be exerted when comparing char yields of different feedstocks or samples with different catalyst impregnation at pre-defined temperatures as this could relate to different stages in the actual pyrolysis process. This is pursued in more detail in chapter 5.

Mass transfer limitations during the holocellulose decomposition range appear to be less of an issue with impregnation except in the case of K impregnation where mass transfer limitations were apparent in the case when a lid was used.

The first order pseudo component reaction model is not able to describe pyrolysis accurately enough with increasing catalyst concentration and vapour-phase residence time in the presence of catalyst. Therefore, it can be concluded that the model presented in 3.3.8 is only applicable for pyrolysis in the absence of catalyst and secondary reactions. However, the catalysts used in this study are naturally present in biomass and, as discussed in chapter 3, secondary reactions cannot be completely

prevented in most lab scale TGA's. Thus, this commonly used devolatilisation model is an over-simplification for any process that involves the formation of significant amounts of char, and alternative models have to be researched.

4.5 References

Alyami, S. (2014). *Catalysis of char formation* (Unpublished final year project report). Massey University, Palmerston North, New Zealand. The report can be accessed by contacting J.R.Jones@massey.ac.nz

Antal, M. J., & Varhegyi, G. (1995). Cellulose pyrolysis kinetics: The current state of knowledge. *Industrial & Engineering Chemistry Research, 34*(3), 703-717. doi:10.1021/ie00042a001

Barker, A. V., & Pilbeam, D. J. (Eds.). (2007). *Handbook of plant nutrition*. Boca Raton, FL: CRC Press.

Björkman, E., & Strömberg, B. (1997). Release of chlorine from biomass at pyrolysis and gasification conditions. *Energy & Fuels, 11*(5), 1026-1032. doi:10.1021/ef970031o

Bridges, R. (2013). *Design and characterisation of an 'open source' pyrolyser for biochar production* (Master's thesis, Massey University, Palmerston North, New Zealand). Retrieved from http://mro.massey.ac.nz/handle/10179/5864

Brown, M. E. (1988). *Introduction to thermal analysis: Techniques and applications*. London, United Kingdom: Chapman and Hall.

Collard, F.-X., & Blin, J. (2014). A review on pyrolysis of biomass constituents: Mechanisms and composition of the products obtained from the conversion of cellulose, hemicelluloses and lignin. *Renewable and Sustainable Energy Reviews, 38*, 594-608. doi:10.1016/j.rser.2014.06.013

Downie, A., Crosky, A., & Munroe, P. (2009). Physical properties of biochar. In J. Lehmann & S. Joseph (Eds.), *Biochar for environmental management: Science and technology* (pp. 13-32). London, England, United Kingdom: Earthscan.

Fu, Q., Argyropoulos, D. S., Tilotta, D. C., & Lucia, L. A. (2008). Understanding the pyrolysis of CCA-treated wood: Part II. Effect of phosphoric acid. *Journal of Analytical and Applied Pyrolysis, 82*(1), 140-144. doi:10.1016/j.jaap.2008.02.007

Gomez, C., Velo, E., Barontini, F., & Cozzani, V. (2009). Influence of secondary reactions on the heat of pyrolysis of biomass. *Industrial & Engineering Chemistry Research, 48*(23), 10222-10233. doi:10.1021/ie9007985

Keown, D. M., Favas, G., Hayashi, J.-i., & Li, C.-Z. (2005). Volatilisation of alkali and alkaline earth metallic species during the pyrolysis of biomass: Differences between sugar cane bagasse and cane trash. *Bioresource Technology, 96*(14), 1570-1577. doi:10.1016/j.biortech.2004.12.014

Khelfa, A., Bensakhria, A., & Weber, J. V. (2013). Investigations into the pyrolytic behaviour of birch wood and its main components: Primary degradation mechanisms, additivity and metallic salt effects. *Journal of Analytical and Applied Pyrolysis, 101*, 111-121. doi:10.1016/j.jaap.2013.02.004

Khelfa, A., Finqueneisel, G., Auber, M., & Weber, J. (2008). Influence of some minerals on the cellulose thermal degradation mechanisms: Thermogravimetic and pyrolysis-mass spectrometry studies. *Journal of Thermal Analysis and Calorimetry, 92*(3), 795-799. doi:10.1007/s10973-007-8649-8

Mamleev, V., Bourbigot, S., Le Bras, M., & Yvon, J. (2009). The facts and hypotheses relating to the phenomenological model of cellulose pyrolysis: Interdependence of the steps. *Journal of Analytical and Applied Pyrolysis, 84*(1), 1-17. doi:10.1016/j.jaap.2008.10.014

Mamleev, V., Bourbigot, S., & Yvon, J. (2007). Kinetic analysis of the thermal decomposition of cellulose: The main step of mass loss. *Journal of Analytical and Applied Pyrolysis, 80*(1), 151-165. doi:10.1016/j.jaap.2007.01.013

Okuno, T., Sonoyama, N., Hayashi, J.-i., Li, C.-Z., Sathe, C., & Chiba, T. (2005). Primary release of alkali and alkaline earth metallic species during the pyrolysis of pulverized biomass. *Energy & Fuels, 19*(5), 2164-2171. doi:10.1021/ef050002a

Rajkovich, S., Enders, A., Hanley, K., Hyland, C., Zimmerman, A., & Lehmann, J. (2012). Corn growth and nitrogen nutrition after additions of biochars with varying properties to a temperate soil. *Biology and Fertility of Soils, 48*(3), 271-284. doi:10.1007/s00374-011-0624-7

Rowell, R. M. (2013). Moisture properties. In R. M. Rowell (Ed.), *Handbook of wood chemistry and wood composites* (2nd ed., pp. 75-98). Boca Raton, FL: CRC Press.

Schachtman, D. P., Reid, R. J., & Ayling, S. M. (1998). Phosphorus uptake by plants: From soil to cell. *Plant physiology, 116*(2), 447-453. doi:10.1104/pp.116.2.447

Shafizadeh, F. (1968). Pyrolysis and combustion of cellulosic materials. In L. W. Melville & R. S. Tipson (Eds.), *Advances in carbohydrate chemistry* (Vol. 23, pp. 419-474). New York, NY: Academic Press.

Wang, Z., Wang, F., Cao, J., & Wang, J. (2010). Pyrolysis of pine wood in a slowly heating fixed-bed reactor: Potassium carbonate versus calcium hydroxide as a catalyst. *Fuel Processing Technology, 91*(8), 942-950. doi:10.1016/j.fuproc.2009.09.015

Chapter 5 Heat of Pyrolysis

5.1 Introduction

Knowledge of the heat of pyrolysis during pyrolysis is important for studying and modelling pyrolysis, as well as controlling the *HTT* in a pyrolysis process. In chapter 3 and 4 it was discovered that the heat of pyrolysis is affected by secondary reactions and the presence of minerals. This chapter contains two investigations. First, the heat of pyrolysis is analysed by means of the time derivative of the temperature difference between the centre temperature of pine cylinders and the chamber heater temperature. Cylinders range in size from 20 to 75 mm diameter, which mass loss was studied in chapter 3. The results are interpreted with respect to the overall heat of pyrolysis and related to the decomposition of the biomass pseudo-components discussed in chapter 3. Second, the heat flows are analysed for TGA experiments of untreated pine sawdust, sawdust impregnated with metals and sawdust treated with phosphoric acid (chapter 4) that have been pyrolysed with and without a lid. The results are compared to literature to gain a better understanding of secondary reactions and the role of catalysts on the heat of pyrolysis.

5.2 Material and Methods

5.2.1 Feedstock

The feedstock used is radiata pine wood as described in 3.2.1.1.

5.2.2 Temperature Recording in Wood Cylinders

In this chapter the temperature recordings in cylindrical wood samples undergoing pyrolysis described in 3.2.3 in chapter 3 have been further analysed, and the reader is referred to this section for detailed information about the experimental procedure. Additionally to these experiments the temperature has been recorded for large cylindrical wood samples with a diameter of 120 mm and a height of 60 mm, which have been pyrolysed in the same equipment as described in 3.2.3. The positioning of the thermocouples and the respective labelling is illustrated in Figure 5-1.

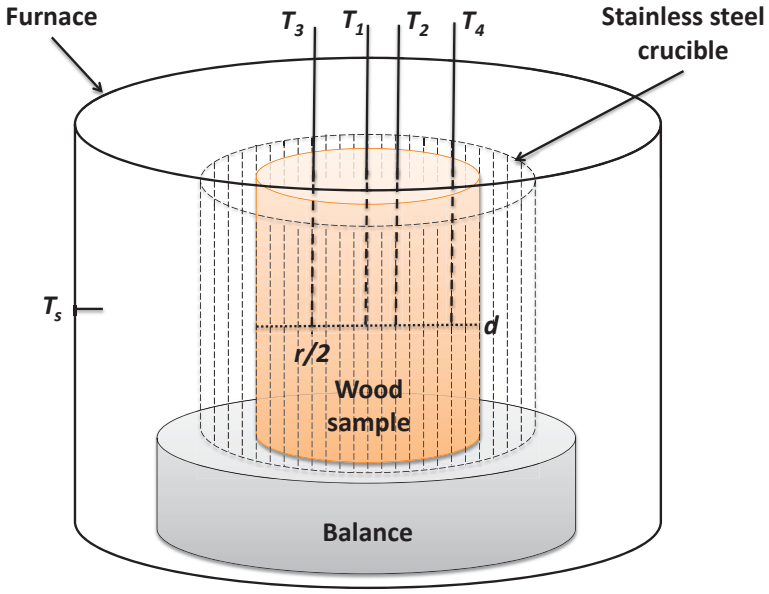

Figure 5-1. Stainless steel perforated crucible with loaded sample in the case of the pyrolysis of large wood cylinders with a diameter of 120 mm and a height of 60 mm. d = diameter; r = radius; T_n = thermocouple position (thermocouples have been evenly distributed at 0, 0.25, 0.5 and 0.75 of the radius); TGA = Thermogravimetric analyser.

The large cylinders were previously oven-dried at 110 °C and then directly transferred into the Macro-TGA for analysis. The pyrolysis conditions were the same as described in 3.2.3, except for the temperature programme. The aim was to study the thermal runaway in large cylindrical wood samples for which reason the wood was heated from room temperature to 120 °C at 2 °C/min, where it was held for 180 min before pyrolysis

continued at a heating rate of ≈ 1 °C/min to a *HTT* of 500 °C. One experiment involved two runs, one to record the sample weight loss with time, the other to collect the sample temperature-time history, because they could not be collected concurrently as discussed in 3.2.3. Each pair of experiments was only repeated once due to time constraints. A temperature experiment was also done where the initial hold temperature and time was 140 °C and 120 min, respectively. However, this experiment had to be stopped at 280 °C due to time limitations, and thus could only be used for comparing temperature profiles during the initial holding period.

5.2.3 Heat Flow Analysis of TGA Experiments

Heat flow analysis was carried out on a range of selected TGA experiments in chapter 3 and 4. The lab-scale TGA used in this research was calibrated with a sapphire standard as mentioned in 3.2.1.4 to obtain meaningful heat flow data. The applied method is based on the work of Rath et al. (2003). The wood samples and treated wood samples were pyrolysed as described in 3.2.2 and 4.2.3 respectively. After pyrolysis was completed and the sample cooled back to room temperature the char was re-pyrolysed, according to the method of the respective feedstock, over the temperature range of interest, 30 to 700 °C, to allow for baseline correction. Re-pyrolysing the char instead of pyrolysing an empty crucible for baseline correction has the added benefit that it accounts for changes in the radiative heat exchange due to varying emissivity between the solid and the reference crucible in the experiments when no lid is employed (Wolfinger, Rath, Krammer, Barontini, & Cozzani, 2001). To calculate the actual reaction heat it is necessary to remove radiation effects, the equipment specific baseline and the various sensible heats. Starting with the pyrolysis run of the feedstock, the measured heat flow, Q_{wood}, in W consists of:

$$Q_{wood} = Q_{blank} + Q_{wood,se} + Q_{\,char,feed,se} + Q_{ash} + Q_{impreg} + Q_{rad/conv} + Q_P \ , \tag{5.1}$$

where $Q_{wood,se}$, $Q_{char,feed,se}$, Q_{ash}, and Q_{impreg} are the sensible heats in W required to heat the wood, the produced char, the ash in the wood, and the impregnated compounds in the wood in the case of experiments with treated feedstock. Q_{blank} in W represents the equipment specific baseline, which is a function of the operating conditions, and the sensible heat required to heat the lid in case a lid is applied as the reference crucible of

the TGA had no lid. $Q_{rad/conv}$ is the heat flow in W that has to be supplied due to losses by radiation (Wolfinger et al., 2001) as mentioned above, which is of particular importance in the case where no lid is applied, and in the case of the applied TGA convection due to the horizontal balance and furnace design and the applied nitrogen purge gas flow of 20 ml/min. Q_P in equation (5.1) is the desired pyrolysis heat in W. It does not solely encompass reaction energetics but also the latent heat of evaporation of volatile pyrolysis products, or the enthalpy of condensation if for example temperature gradients exist within the sample or polymerisation reactions have taken place resulting in the formation of less volatile compounds.

Re-pyrolysing the obtained char, after the sample was cooled back down to room temperature, under the same conditions as previously results in the following measured heat flow, Q_{char}, in W:

$$Q_{char} = Q_{blank} + Q_{char,se} + Q_{ash} + Q_{impreg} + Q_{rad/conv} \ . \qquad (5.2)$$

It is assumed that Q_{ash}, Q_{impreg}, and $Q_{rad/conv}$ are the same as in equation (5.1), that is, the volatilisation of ash and impregnated compound during pyrolysis are negligible and the convective and radiative heat losses of wood and char are the same. The latter assumption is believed to be valid despite char and pine wood having a different emissivity, 0.80 and 0.95 respectively (Engineering ToolBox, n.d.; Green & Perry, 2008), because at high temperatures when radiation becomes significant (according to the Stefan-Boltzmann law radiation is directly proportional to the fourth power of the temperature) most of the wood has turned into char. The sensible heat of char, $Q_{char,se}$, in equation (5.2) differs from $Q_{char,feed,se}$ in equation (5.1). $Q_{char,se}$ is a fixed value but $Q_{char,feed,se}$ varies with temperature as the char is formed during the pyrolysis run of the feedstock. Q_{blank} in equation (5.1) and (5.2) are identical as the equipment set up and pyrolysis conditions remain unchanged. Thus, substituting

$$Q_{se} = Q_{wood,se} + Q_{char,feed,se} \qquad (5.3)$$

in equation (5.1), solving equation (5.2) for Q_{blank} and inserting into equation (5.1) results in:

$$Q_{wood} = Q_{char} - Q_{char,se} + Q_{se} + Q_P \ , \qquad (5.4)$$

Equation (5.4) is used for calculating Q_P:

$$Q_P = Q_{wood} - Q_{char} + Q_{char,se} - Q_{se} \ . \tag{5.5}$$

The only unknowns in equation (5.5) are $Q_{char,se}$ and Q_{se} as Q_{wood} and Q_{char} are determined experimentally. It is important to note that equation (5.5) is the same as the one used in the work of Rath et al. (2003) to calculate the heat flow of the reaction thermal effects except that in their case the term $-\left(Q_{char} - Q_{char,se}\right)$ represents the above discussed radiation term (Wolfinger et al., 2001) whereas here it accounts for Q_{blank}. Q_{se} in equation (5.5) can be calculated according to Rath et al. (2003) by:

$$Q_{se} = \left[\left(1 - \alpha(T)\right)m_{wood,in}c_{p,wood} + \alpha(T)m_{char}c_{p,char}\right]\frac{dT}{dt} \ , \tag{5.6}$$

and $Q_{char,se}$ by:

$$Q_{char,se} = m_{char}c_{p,char}\frac{dT}{dt} \ . \tag{5.7}$$

In equation (5.6) is $\alpha(T)$ the dimensionless sample conversion that is a function of the temperature and is calculated analogous to equation (3.10) in 3.3.8, $m_{wood,in}$ and m_{char} are the feedstock weight before pyrolysis and the char weight after pyrolysis in kg, $c_{p,wood}$ and $c_{p,char}$ are the specific heat capacity of wood and char in J/(kg·K) and dT/dt is the heating rate in K/s. The heating rate is given by the experimental conditions, and $c_{p,wood}$ and $c_{p,char}$ are approximated by equation (5.8) and (5.9) respectively:

$$c_{p,wood} = 1113.68 + 4.8567(T - 273.15) \ , \tag{5.8}$$

and

$$c_{p,char} = \frac{8314}{5.75}\left[e^{\frac{380}{T}}\left(\frac{e^{\frac{380}{T}} - 1}{\frac{380}{T}}\right)^{-2} + 2e^{\frac{1800}{T}}\left(\frac{e^{\frac{1800}{T}} - 1}{\frac{1800}{T}}\right)^{-2}\right] , \tag{5.9}$$

where T is the temperature in K. Equation (5.8) and (5.9) are from Kollmann (1982, as cited in Rath et al., 2003) and Merrick (1988, as cited in Rath et al., 2003). Finally, the heat of pyrolysis, H_P, in J/g is calculated as follows (Rath et al., 2003):

$$H_P = \frac{1}{m_{wood,in}} \int_{T_{in}}^{T_f} Q_p \frac{dT}{\beta} \,, \tag{5.10}$$

where T_{in} is the initial temperature and T_f the final temperature in K over which the heat of pyrolysis is determined. The temperature interval $[T_{in},\ T_f]$ over which it is integrated is dependent on the sample and the pyrolysis conditions, and is determined from the respective derivative weight-loss curve.

To process the TGA data the Matlab program described in 3.2.2 was used to select the TGA data closest to a common temperature in the range 30 to 700 °C at 0.5 °C increments. Alternatively interpolation is a viable option, which was used in chapter 4.

5.3 Results and Discussion

5.3.1 Derivation of Reaction Heat Effects from Internal Temperature Recordings

One of the main findings of chapter 3 is that secondary reactions take place over the entire pyrolysis range concurrently to primary reactions, and that the internal temperature profile recorded at the centre of a cylindrical wood sample, in which internal temperature gradients do not affect the derivative weight loss curve, tracks the difference curve between TGA pine sawdust runs with and without a lid, shown previously in Figure 3-46 in section 3.3.7. This indicates that the reaction heat effects are a function of secondary reactions. But before investigating this further, it was decided to examine if the events observed in the time derivative of the difference between the centre temperature and the heater temperature can also be related to the decomposition of the biomass constituents, as discussed in 3.3.8 similarly to the work of Di Blasi, Branca, Masotta, and De Biase (2013). The breakdown is presented in Figure 5-2.

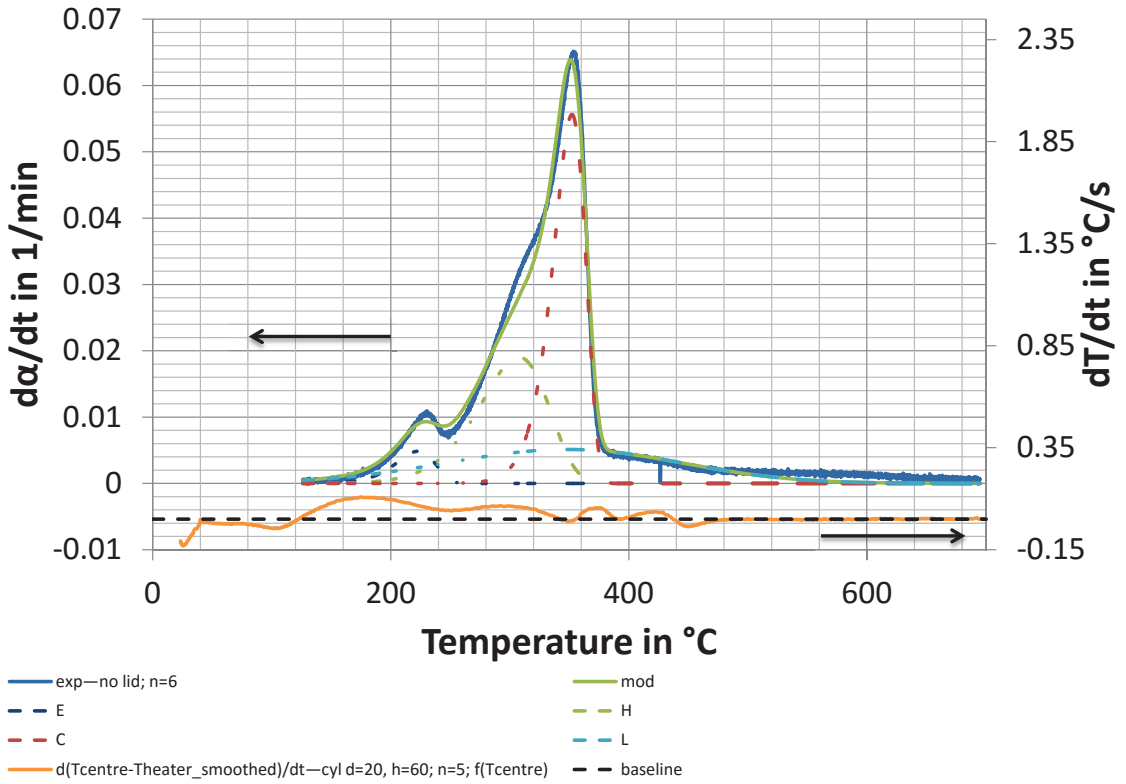

Figure 5-2. Comparison of the time derivative conversion curves of pine sawdust and its pseudo-components pyrolysed in crucibles without a lid with the average time derivative of the temperature difference between the centre and heater temperature observed during the pyrolysis of cylinders with a diameter of 20 mm and a height of 60 mm in a Macro-TGA. Curve-fitting of the pseudo-components was done on the average pine sawdust curve in Figure 3-46 in 3.3.7 that was pyrolysed without a lid according to the method in section 3.3.8. The time derivative conversion curves start at 126 °C as this is the temperature where drying is completed and pyrolysis begins (chapter 3). The baseline refers to the secondary axis showing the time derivative of the temperature difference, and denotes zero difference between the centre heating rate of the sample and the heater heating rate. C = cellulose; cyl = cylinder; d = diameter in mm; E = extractives; exp = experimental data; f(Tcentre) = plotted as a function of the measured centre temperature of the sample; H = hemicellulose; h = height in mm; L = lignin; mod = modelled data; n = number of runs over which was averaged; t = time in s; TGA = Thermogravimetric analysis.

The centre temperature of cylinders in Figure 5-2 is ideal for representing the reaction heat effects due to the symmetry condition, *viz.* there is no more inwards heat transfer (Di Blasi, Branca, Galgano, & Gallo, 2015; Di Blasi, Branca, Sarnataro, & Gallo, 2014). A differential temperature rise characterises an underlying exothermic process and/or heat gain, and a differential temperature decrease an endothermic process and/or heat loss respectively. It is important to note that there was conduction along the thermocouple in the sample, which means that the actual endothermic processes are more endothermic and the exothermic processes are more exothermic. Figure 5-2 reveals that as soon as the evaporation of moisture, below 126 °C, is completed (see for comparison Figure 3-46 in chapter 3) the sample temperature increases faster than the

heater temperature, which is initially caused by the large thermal lag (large temperature gradient) caused by the removal of moisture but overall remains globally exothermic till the end of the majority of the weight-loss. That the initial temperature rise in Figure 5-2 is not just a consequence of the initially high temperature gradient caused by the thermal lag resulting from the evaporation of moisture (section 3.3.5 in chapter 3) is demonstrated in Figure 5-3.

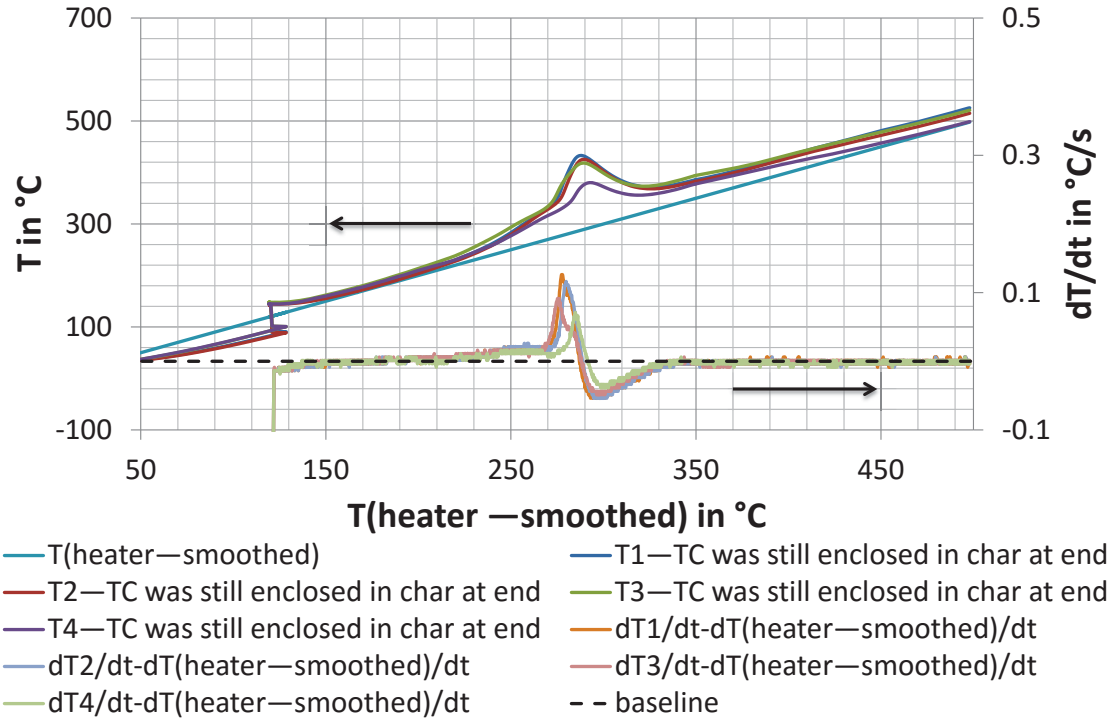

Figure 5-3. Temperature profile including differential temperature change recorded in a large pine cylinder (d = 120 mm, h = 60 mm) undergoing pyrolysis. The cylinder was pyrolysed from room temperature to 120 °C at 2 °C/min, where the temperature was held for 180 min before pyrolysis continued at 0.83 °C/min to 500 °C. T1 to T4 refer to the thermocouple positions in Figure 5-1. The sample shrunk onto the thermocouples and did not crack or fracture during pyrolysis in proximity of the thermocouples providing exact temperature readings. The baseline refers to the secondary axis showing the difference of the time derivative of the recorded temperature to the time derivative of the heater temperature, and denotes zero difference. d = diameter in mm; h = height in mm; T = Temperature in °C; TC = thermocouple; t=time in s.

Figure 5-3 reveals that in slowly heated samples a thermal runaway occurs from the onset of pyrolysis (≈ 120 °C). It also shows that no major temperature gradients exist over the radius of the sample despite its large diameter, which is a consequence of the slow heating rate and the reaction exothermicity. The exception is thermocouple 4 (T4 in Figure 5-3), which exhibits a large temperature difference in the region of the heater temperature from ≈ 270 to 330 °C. The reason is believed to be its position in close proximity to the sample surface (Figure 5-1), which is affected by external heat transfer

that intensifies as a result of the increasing temperature overshoot leading to a cooling of the sample surface and its adjacent layers. A repeat run can be found in Figure D-1 in Appendix D.1. This run is similar to the one in Figure 5-3 but shows a reduced temperature gradient between thermocouple 3 and 4. That the thermal runaway occurs indeed from ≈ 120 °C is confirmed by Figure 5-3 and Figure D-1 in Appendix D.1 by the fact that before the hold temperature of 120 °C the sample temperature was lagging behind the heater temperature due to moisture evaporation and heat transfer limitations (section 3.3.5), and during the hold time increased above the heater temperature. This becomes more evident when plotting the temperature as a function of time, Figure D-2 and D-3 in Appendix D.1. The temperature increase slows down with time during the hold time, probably due to heat losses. The slowing down of the temperature increase with time decreases when the hold temperature is increased as illustrated in Figure D-4 in Appendix D.1. This shows that for large samples it is difficult to keep a sample at the desired torrefaction temperature as outlined in section 3.3.6 in chapter 3. The thermal runaway further explains why the charcoal yield approaches an asymptote as the heating rate is decreased when pyrolysis conditions are otherwise constant (Antal, Mok, Varhegyi, & Szekely, 1990); that is, a further decrease in the external heating rate does not result in a char yield increase because a thermal runaway causes the sample heating rate to be higher than the set heater heating rate at least for large samples. Intriguingly, the magnitude of the maximum temperature overshoot for the centre temperature is 145.7 and 130.7 °C respectively for Figure 5-3 and Figure D-1 in Appendix D.1. This is higher than the 53 °C reported by Di Blasi et al. (2014) for softwood pellets with a diameter and length of 5-6 mm; and the here presented temperature overshoot is even an under prediction as the thermocouples conducted heat. The reason is believed to be the larger sample size (cylinders with diameter of 120 mm and a height of 60 mm) used in this study, which promotes secondary reactions and char formation leading to an increased heat release and consequently greater temperature overshoot, Figure 5-4.

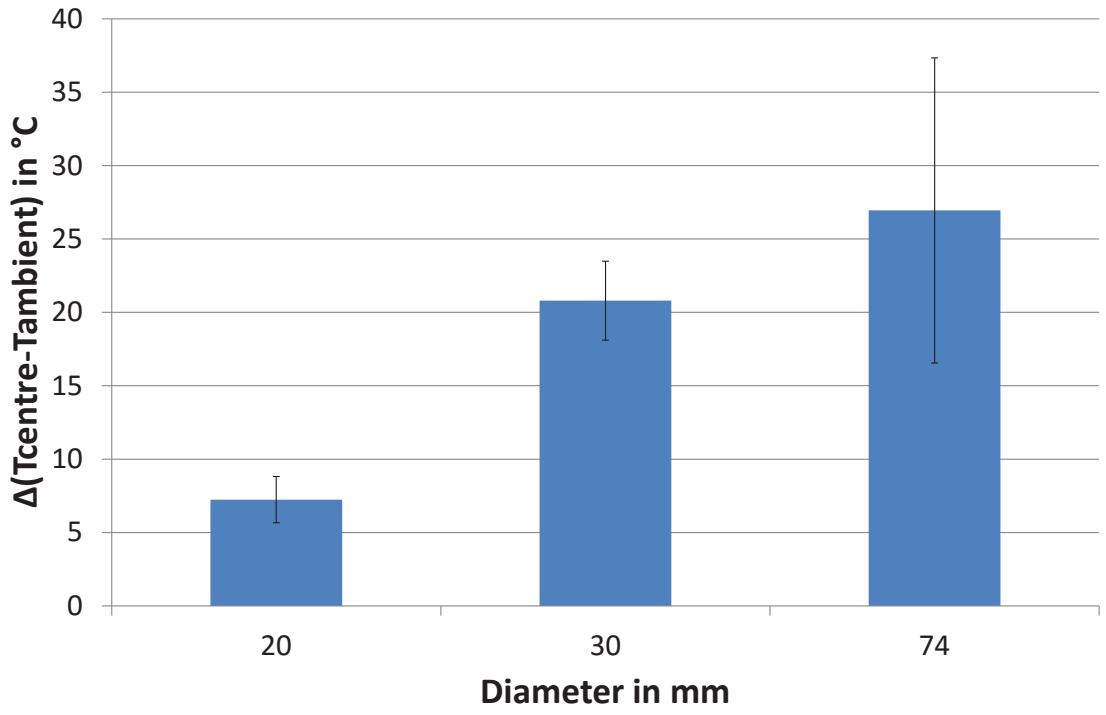

Figure 5-4. Maximum temperature overshoot observed in the pyrolysis of pine cylinders with a height of 60 mm and varying diameter. The samples were heated at approximately 5.5 °C/min from room temperature to 700 °C. The temperature overshoot was measured between the centre temperature and the recorded heater temperature. The error bars represent the standard deviation. For the samples with a diameter of 20, 30, and 74 mm the number of experiments over which was averaged is 5, 2 and 2 respectively. The respective temperature profiles are depicted in 3.3.5 in chapter 3. T = Temperature in °C.

Figure 5-4 shows that with increasing sample size the temperature overshoot increases. The large standard deviation for the samples with a diameter of 74 mm can be explained by the occurrence of cracks and fractures, which partly exposed the thermocouples and limit the extent of secondary reactions. The formation of cracks and fractures with increasing sample size and their impact on secondary reactions are discussed in detail in 3.3.4. It is important to note that the third experiment was omitted for averaging in Figure 5-4 for the samples with a diameter of 30 and 74 mm respectively, as the experiments performed in this particular week deviated for some unknown reason, which was eliminated by subsequent maintenance of the equipment. Overall, Figure 5-4 confirms the hypothesis that enhanced secondary reactions caused by increasing sample size lead to larger temperature overshoots. This agrees with the findings of Di Blasi et al. (2015). In Figure 5-5 it appears that the main temperature overshoot occurs once the majority of the weight-loss has taken place. It also shows that there is a relatively large variation between repeat runs, which is observed in both the temperature and weight measurements. It is believed to be related to the sample heterogeneity.

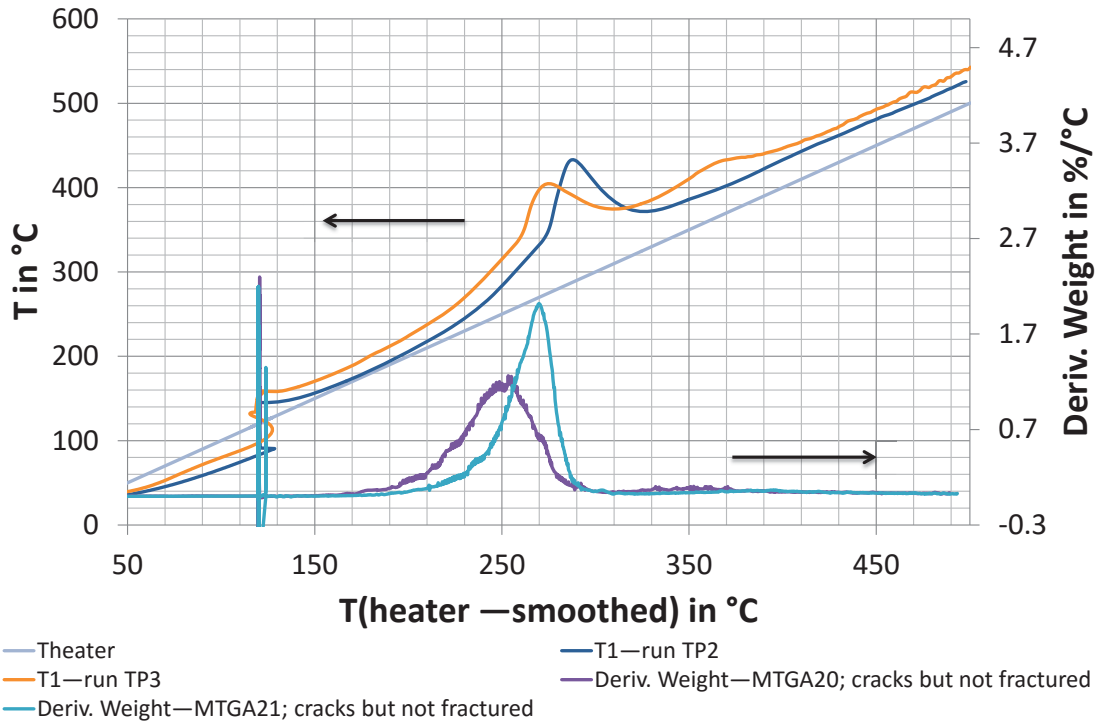

Figure 5-5. Comparison of the centre temperature profiles with the derivative weight-loss curves of large pine cylinders (d = 120 mm, h = 60 mm) undergoing pyrolysis. Run TP2 is the one depicted in Figure 5-3 and run TP3 the one in Figure D-1 in Appendix D.1 respectively. The derivative weight-loss measurements were carried out separately under the same conditions as the temperature measurements interfered with the weight-loss measurements. Legend: Investigated parameter—sample name; description. d = diameter in mm; h = height in mm; T = Temperature in °C.

However, when plotting the results in Figure 5-5 as a function of time shown in Figure 5-6 it is revealed that the apparent difference between the maximum temperature overshoot and the main weight-loss peak is merely a consequence of the temperature difference between sample and heater; reiterating the significance of thermal lag in TGA analysis. This endorses the statement above with respect to Figure 5-2 that pyrolysis appears to be overall exothermic over the main weight-loss region.

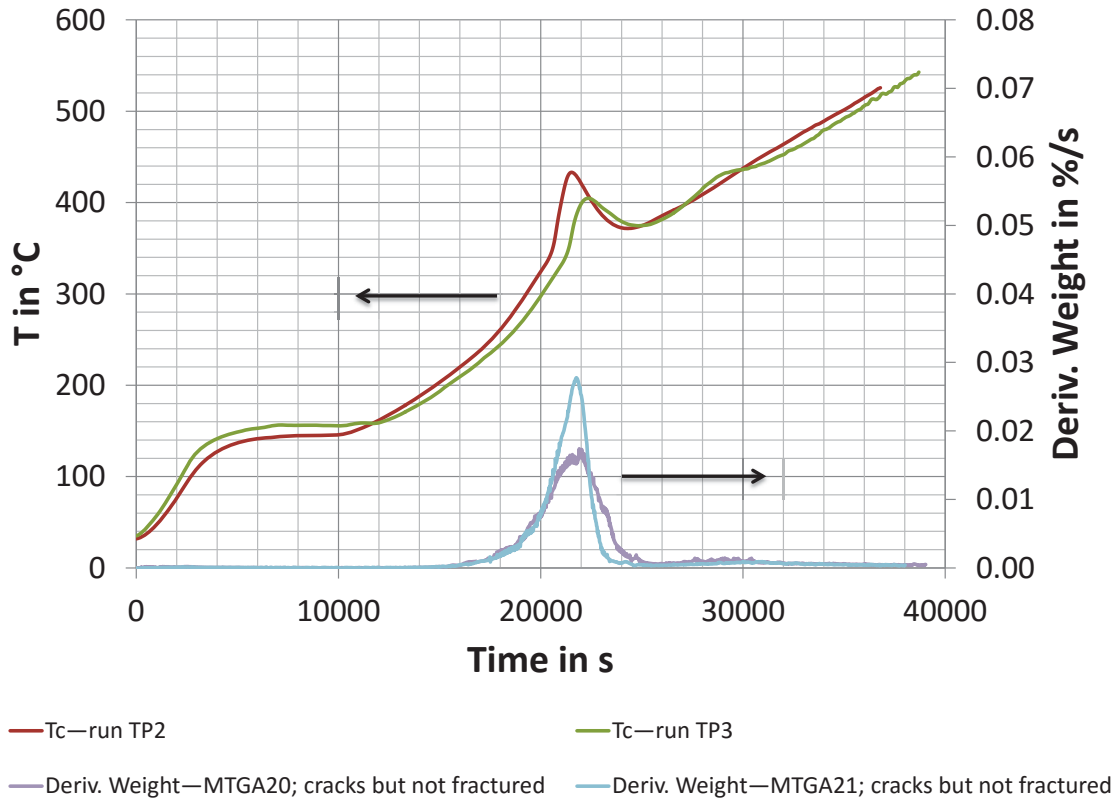

Figure 5-6. Comparison of the centre temperature profiles with the derivative weight-loss curves of large pine cylinders (d = 120 mm, h = 60 mm) undergoing pyrolysis as a function of time. Run TP2 is the one depicted in Figure 5-3 and run TP3 the one in Figure D-1 in Appendix D.1 respectively. The derivative weight-loss measurements were carried out separately under the same conditions as the temperature measurements interfered with the weight-loss measurements. The starting time was selected as the time when the heater temperature was at 30 °C. Legend: Investigated parameter—sample name; description. d = diameter in mm; h = height in mm; T = Temperature in °C; Tc = Temperature at the centre of the cylinder in °C.

One might argue that the curves in Figure 5-2 are flawed in a similar manner as in Figure 5-5. However, they are not flawed when plotted against time as shown in Figure 5-7. It shows that there is no difference between the temperature profile in relation to the weight-loss profile for a sample with the dimensions of $d = 20$ mm and $h = 60$ mm when plotted as a function of time compared to the TGA heater temperature in Figure 3-38 in 3.3.5, which also agrees with the labscale TGA curve as demonstrated in chapter 3.

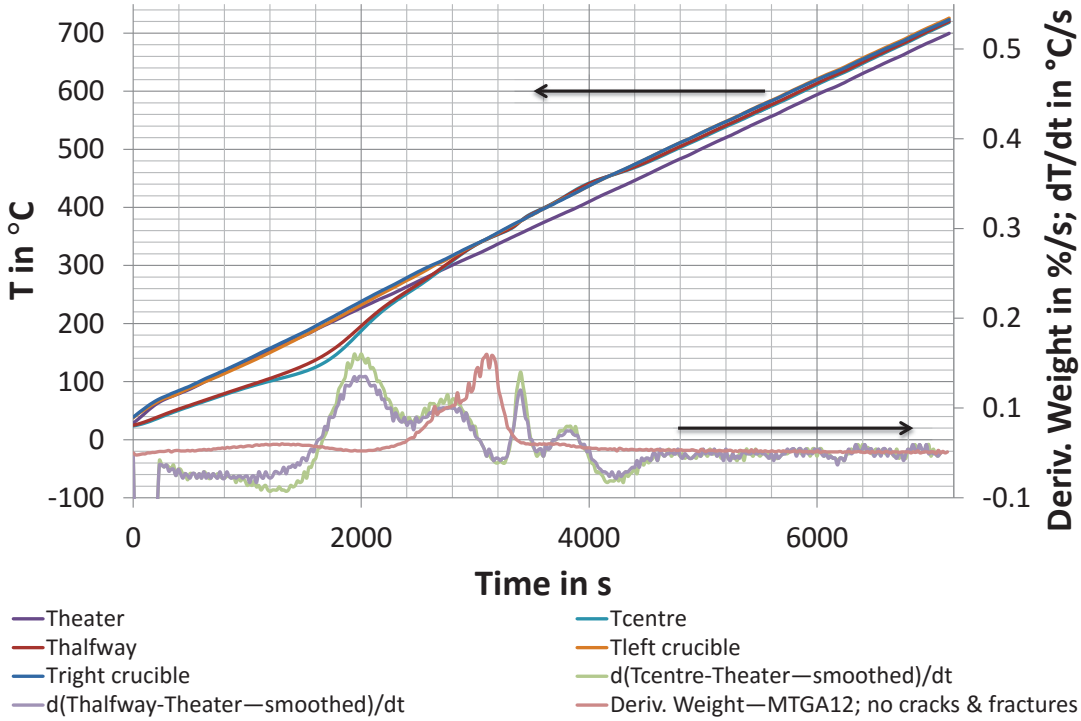

Figure 5-7. Results of thermocouple run 10 (see Figure 3-38 in 3.3.5) employing a cylinder with a diameter of 20 mm and a height of 60 mm depicted as a function of time. The sample showed no cracks and fractures at the end of the run. Cracking means the samples are still in one piece at the end of the run and fracturing means the sample broke into separate pieces. The derivative weight curve of experiment MTGA12 is included to illustrate the relationship between temperature and weight-loss events. "Tleft crucible" and "Tright crucible" are thermocouples T_1 and T_2 in Figure 3-5 in 3.2.3 respectively.

Four peaks can be distinguished when investigating the differential temperature curve in Figure 5-2 (see also Figure 5-7) in more detail. The first one extending from ≈ 126 to ≈ 250 °C falls into the region of the pyrolysis of the extractives before the onset of the main pyrolysis. The second peak from ≈ 250 to ≈ 350 °C coincides with the degradation of hemicellulose, and the exothermicity diminishes with increasing progress of the cellulose decomposition. Note that the minimum in the time derivative of the temperature difference at ≈ 350 °C almost matches the peak of the cellulose pseudo-component curve. There are two further peaks observed in the range ≈ 350 °C to ≈ 390 °C and ≈ 390 °C to ≈ 440 °C. The former one occurs in the region where lignin degradation is slightly past its maximum and the weight-loss from the cellulose component sharply decreases. The fourth peak is entirely in a range where only lignin pyrolysis arises according to the curve fitting in Figure 5-2. However, as discussed in chapter 4, it is unlikely that the weight-loss is exclusively from lignin, which would explain why this last peak is encompassed by two endothermic processes in a region dominated by lignin pyrolysis that is believed to be exothermic (Di Blasi et al., 2015; Di Blasi et al., 2013; Di Blasi et al., 2014). From 480 °C onwards the internal heating rate

was following the external heating rate confirming that the main pyrolysis is completed. Rearrangement reactions that proceed in the solid after 480 °C (Collard & Blin, 2014) seem to be overall neutral or not detectable. In general the presented results agree with the findings of Di Blasi et al. (2015; 2013; 2014), who state that pyrolysis is characterised by a sequence of (a) exothermic, (b) endothermic or neutral, and (c) exothermic processes linked to the primary and secondary pyrolysis of extractives and hemicellulose, cellulose and lignin, and lignin respectively. However, the reaction heat profile observed in Figure 5-2 is more detailed than in their work, which is believed to be due to the presence of transfer limitations in the latter hiding smaller reaction heat effects. This is depicted in Figure 5-8.

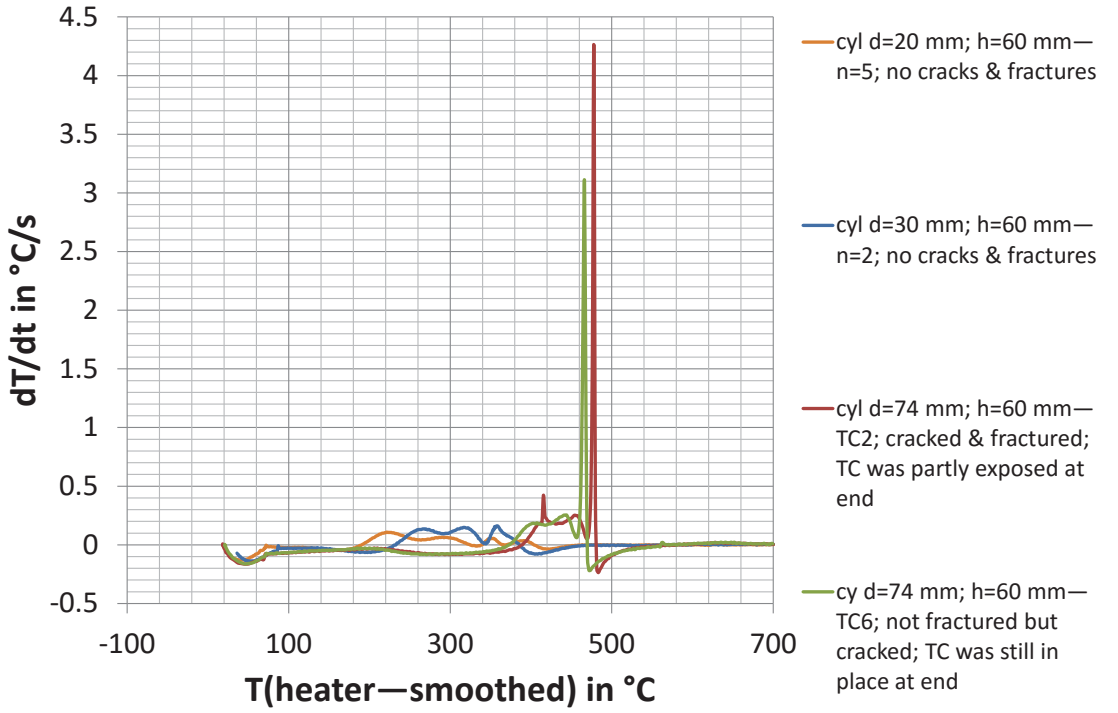

Figure 5-8. Time derivative of the difference between the centre temperature and the smoothed heater temperature of pine cylinders of various size being pyrolysed at ≈ 5.5 °C/min in a Macro-TGA. Legend: sample size—number of averaged experiments or name of single experiment; description of sample and thermocouple position. Cyl = cylinder; d = diameter in mm; h = height in mm; n = number of experiments over which was averaged; T = temperature in °C; t = time in s; TC = thermocouple; TGA = thermogravimetric analyser.

Figure 5-8 demonstrates that larger samples have thermal insulation (see also 3.3.5), which causes (a) the characteristic temperature profile of the centre temperature to shift to higher temperatures, (b) an increase in internal heating rate, and (c) a reduction in the number of observed peaks. The large samples, having a diameter of 74 mm, show a similar time derivative centre temperature profile to the one observed by Di Blasi et al. (2013; 2014), and the one in Figure 5-3. The reduction in peaks derives from the progressive merging of the last two peaks with increasing diameter (for details the reader is also referred to Figure 3-38 to Figure 3-40 in 3.3.5). Thus, it is believed that the presence of transfer limitations in the work of Di Blasi et al. (2013; 2014), caused by the pyrolysis in a relatively large cylindrical fixed bed that was radiatively heated, is responsible for the simplified observed reaction heat profile. Transfer limitations were present in the work of Di Blasi et al. because their recorded bed temperatures exhibited a gradient over the radius of the bed. Therefore, it is believed that the depicted temperature profile in Figure 5-2 is a more accurate representation of the reaction heat effects during pyrolysis. It shows that pyrolysis does in fact consist of a sequence of exothermic and endothermic processes that can be related to the pyrolysis of the

biomass constituents except towards the end of pyrolysis, above 380 °C, where supposedly only lignin decomposition takes place according to Figure 5-2. Reasons for the occurrence of exothermic and endothermic reactions above 380 °C could be the ongoing decomposition or rearrangement reactions of the other bio-components, or alternatively the occurrence of secondary tar decomposition (Pattanotai, Watanabe, & Okazaki, 2013). The first explanation appears more reasonable as chapter 3 revealed that secondary reactions occur over the entire pyrolysis range concurrently to primary reactions. Thus, a reaction heat effect due to secondary reactions is not expected towards the end of the weight-loss region, especially in light of the fact that there are no more volatiles present that can undergo secondary reactions. Rather, the decrease in reaction heat with enhanced secondary reactions and associated char yield increase (Basile, Tugnoli, Stramigioli, & Cozzani, 2014; Gomez, Velo, Barontini, & Cozzani, 2009; Mok & Antal, 1983; Rath et al., 2003) is believed to be a consequence of reaction heat changes over the entire pyrolysis range, as evidenced by changes in the volatile release over the whole pyrolysis range as discussed in chapter 3. For example, the observed decrease in endothermic cellulose volatilisation with increased secondary reactions or the presence of a catalyst (chapter 4) will cause a decrease in reaction heat demand. Overall, the reaction heat is likely to be not a consequence of the pseudo-component composition rather a function of the reaction mechanism that changes with product and catalyst interaction. Thus the effect of secondary reactions and catalysis on the pyrolysis heat demand is discussed further in 5.3.2 by investigating the heat flow obtained from the TGA.

5.3.2 Heat Flow Analysis of TGA Experiments

The raw heat flow data, as obtained from the TGA, for pine sawdust pyrolysed in crucibles with and without a lid is depicted in Figure 5-9. Four samples were pyrolysed for the cases with and without a lid. The initial sample mass was varied in order to achieve a range of yields (see section 3.3.1 for the effect of sample size on yield).

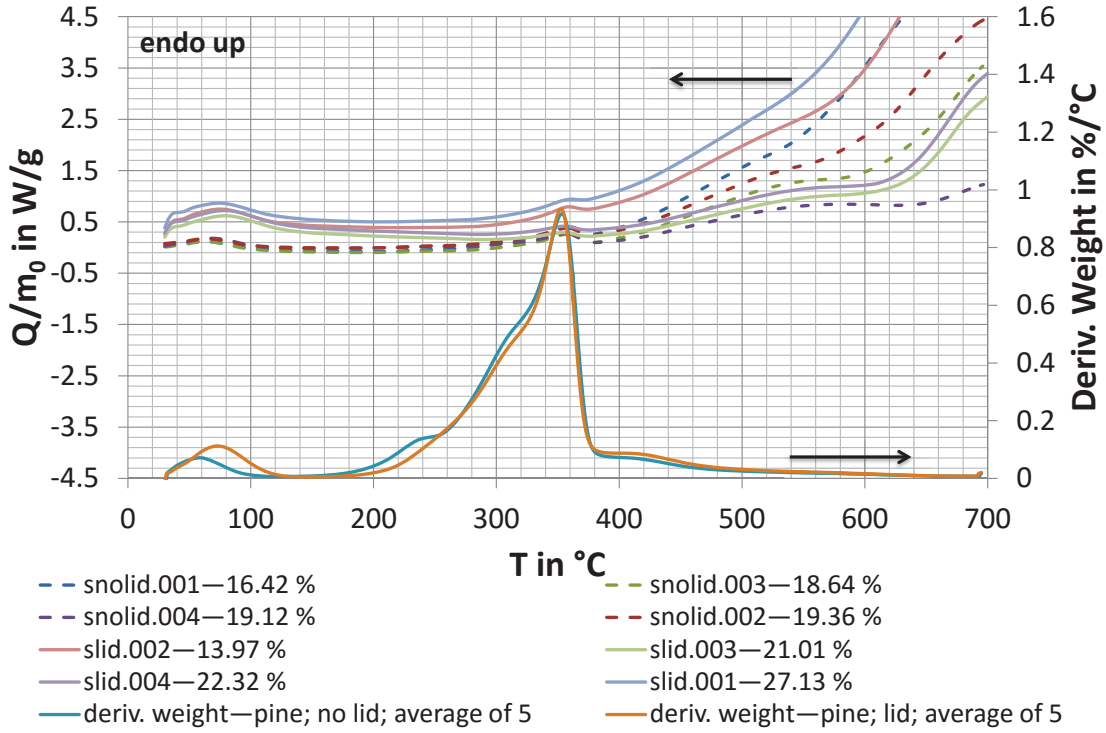

Figure 5-9. Raw heat flow data as obtained from the TGA analysis of pine sawdust pyrolysed in crucibles with and without a lid divided by the initial dry ash free feedstock weight. The secondary y-axis shows the corresponding average derivative weight-loss. Legend: sample name—char yield at 695 °C in % (wt/wt) daf. daf = dry ash free; deriv. = derivative; m_0 = dry ash free initial feedstock weight in mg; Q = heat flow in W; T = temperature in °C; TGA = thermogravimetric analyser.

In the first instance Figure 5-9 shows that the heat flow curves have corresponding peaks to the moisture peak, 30 to 140 °C, and the main pyrolysis peak, 200 to 380 °C, in the respective derivative weight-loss curve, which agrees with the literature (Basile et al., 2014; Gomez et al., 2009; Rath et al., 2003). However, an unexpected result was that there is no difference in the apparent baseline between the experiments with and without a lid as found by Wolfinger et al. (2001) and Rath et al. (2003), which they attributed to radiative heat exchange as discussed in 5.2.3. The reason is believed to be the fundamentally different design of the SDT Q600 used compared to the DSC (Mettler DSC 25) used in their studies. In their equipment the sample and reference crucible are laterally heated, whereas here they are surrounded by a pipe furnace. Thus, in the SDT Q600 less radiative heat exchange is expected between the sample/ reference

crucible and the surrounding furnace. Instead the main heat transfer will be associated with the purge gas (flow rate of 20 ml/min) through convection and radiation. Therefore, the term $Q_{rad/conv}$ was introduced into equation (5.1) and (5.2), and baseline correction was performed in both cases by re-pyrolysing the char as described in 5.2.3. Figure 5-9 also shows that the weight-loss seems to be associated with an endothermic peak, contrary to the findings in 5.3.1, but that appears to be affected by the presence of a lid, which causes a smaller peak.

Also surprising is the change in the heat flow above 500 °C. These phenomena are analysed further by determining Q_P, the heat of pyrolysis, according to the method outlined in 5.2.3. While calculating Q_P it was discovered that the measured heat flows varied between subsequent runs, which is illustrated in Figure D-5 in Appendix D.2 showing that in blank runs (empty crucibles) with and without a lid, performed before subsequent pyrolysis experiments, the onset points and shapes of the heat flow curves differed. This reveals the inherent equipment variability/ sensitivity to slight experimental changes. For example, modifications in the crucible positioning can have an effect, which was minimised by having a small groove in the crucible that allowed aligning the crucible in the same way after, for example, taring. Reasons for the different shapes of the baseline could be the "aging" of the sample crucible, which became evident by its progressive discolouration despite thorough cleaning (ethanol and flame cleaning). Also the SDT Q600 is not actually a "true" DSC (crucible and reference crucible are not thermally coupled) but rather a calibrated thermogravimetric differential thermal analyser, TG-DTA, in DSC mode, providing only semi-quantitative data, which leads to relatively low enthalpy accuracy and repeatability (A. Gillen, personal communication, February 9, 2015). The vertical variation of the heat flow curve has an effect on the pyrolysis heat flow in that it influences the endothermicity/ exothermicity of the pyrolysis process. For instance, in Figure 5-10, the Q_P curve appears too much in the endothermic region; evidence for this assertion is that, after the evaporation of moisture, the first peak in the Q_P curve, the heat flow should be zero or very close to zero as pyrolysis reactions have not started or are minimal. This was confirmed by determining the enthalpy change in the region of moisture evaporation in the Q_P curve and comparing this to the latent heat of water evaporation. In the unadjusted Q_P curve in Figure 5-10 this would mean a latent heat of moisture volatilisation of approximately 11,000 kJ/kg, which is far higher than the ~1,500 kJ/kg

found directly from integration of the heat flow curves of the TGA data. This shows that significant errors are introduced by the inherent variability between runs as discussed above.

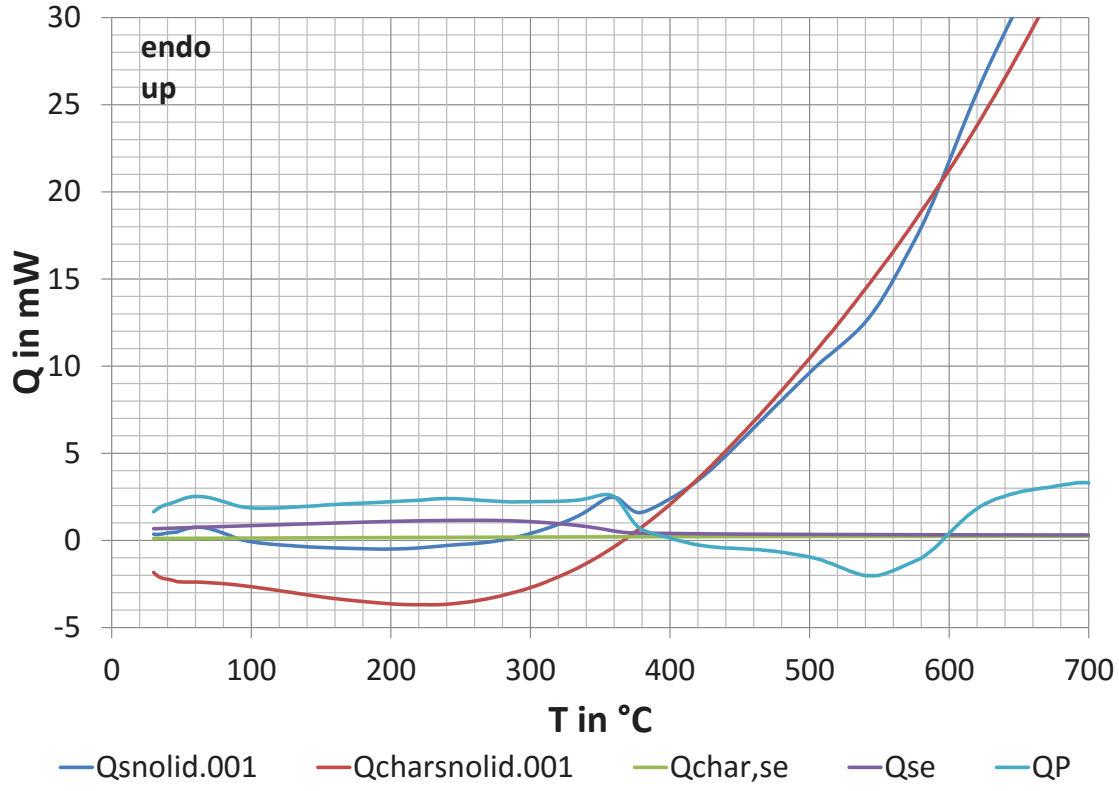

Figure 5-10. Pyrolysis heat flow and its component heat flows in the case of pine sawdust pyrolysed in crucibles without a lid. "Qsnolid.001" and "Qcharsnolid.001" are the heat flow measured during pyrolysis of the pine sawdust and the resulting char respectively. "Qse" and "Qchar,se" are the calculated sensible heat flows required to heat the solid in "Qsnolid.001" and "Qcharsnolid.001" correspondingly. Q = heat flow in mW; T = temperature in °C.

Therefore, in order to use the data, the pyrolysis heat flow had to be adjusted by assuming that after the evaporation of moisture the heat flow is merely due to the sensible heating of the feedstock:

$$Q_{wood} - Q_{char} = Q_{se} - Q_{char,se} \ . \tag{5.11}$$

Thus, the required offset, OFF, in W was calculated by determining the minimum in the heat flow between 60 and 200 °C of the curve "$Q_{wood} - Q_{char}$" and solving:

$$OFF = (Q_{wood} - Q_{char}) - \left(Q_{se} - Q_{char,se}\right) \tag{5.12}$$

at this point. This is depicted in Figure D-6 in Appendix D.2. Subsequently, the offset corrected pyrolysis heat flow, $Q_{P,cor}$, was calculated according to:

$$Q_{P,cor} = \sum_{n} Q_P - OFF \ , \tag{5.13}$$

where n is the number of experimental data points. The corrected heat flows divided by the dry ash free initial feedstock weight (determined at the point where OFF was derived) are shown in Figure 5-11 and Figure 5-12 for the cases no lid and lid respectively. For the experiment "snolid.001" in Figure 5-10, the latent heat of moisture evaporation was now calculated to be 1,700 kJ/kg, which is much less than the figure of 11,000 kJ/kg mentioned above. The average of the determined latent heat of moisture volatilisation of the experiments in Figure 5-11 and Figure 5-12 is given in Table 5-1 illustrating the error associated with this technique.

Table 5-1. Latent heat of moisture evaporation.

μ kJ/kg	σ kJ/kg	*CV*
1975	321	0.16

Note. Averaged was over the 8 latent heats determined from the first peak in the $Q_{P,cor}$ curves in Figure 5-11 and Figure 5-12. μ = average; σ = standard deviation; *CV* = coefficient of variation.

An example of the weight-loss of the feedstock and subsequent char when pyrolysed is depicted in Figure D-7 and Figure D-8 in Appendix D.2 for the cases no lid and lid respectively. It is important to note though that the example in Figure D-7 represents an extreme case, that is, it has the highest char weight-loss as shown in Table D-1 in Appendix D.2. Partly this is believed to result from absorption revealed by the initially similar shape of the weight-loss of the char compared to the feedstock. It also appears that the weight-loss for char pyrolysed without a lid is slightly higher than for char pyrolysed with a lid, seen when comparing Table D-1 and Table D-2 in Appendix D.2. This is discussed further in chapter 7.

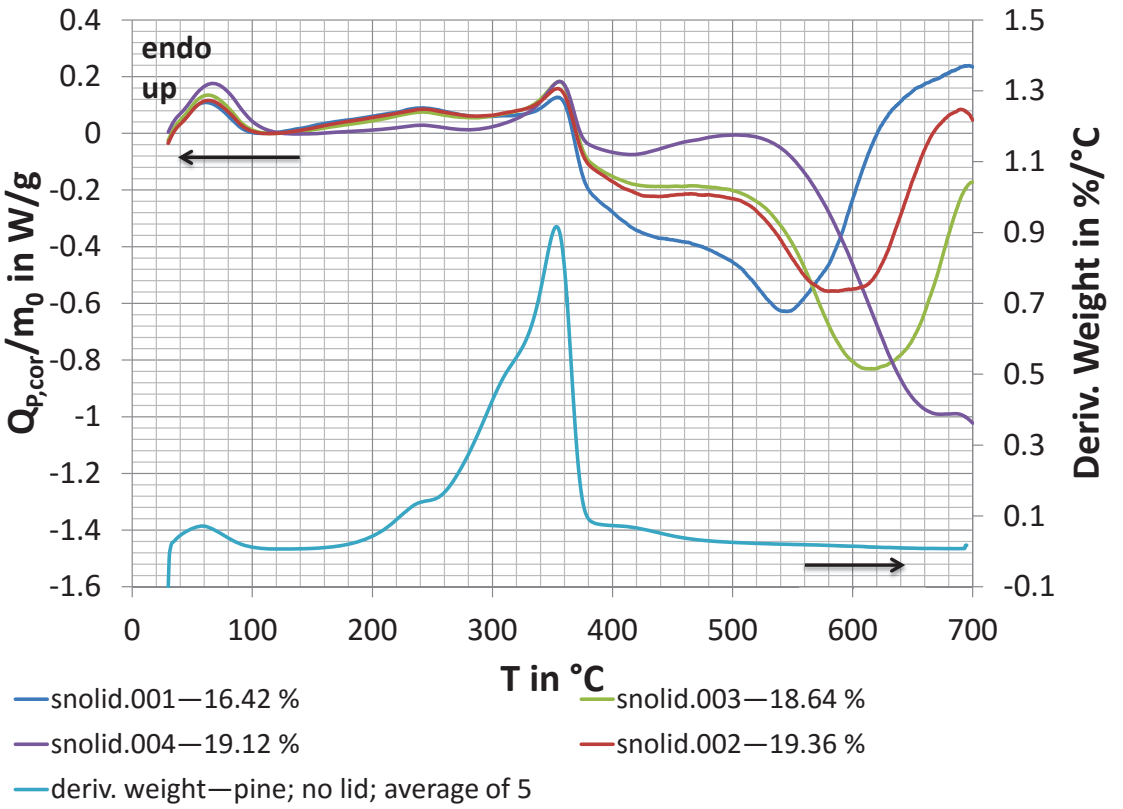

Figure 5-11. Offset corrected pyrolysis heat flows of pine sawdust pyrolysed in crucibles without a lid. The secondary y-axis shows the corresponding average derivative weight-loss. Legend: sample name—char yield at 695 °C in % (wt/wt) daf. daf = dry ash free; deriv. = derivative; m_0 = initial daf weight in mg; $Q_{P,cor}$ = offset corrected pyrolysis heat flow in mW; T = temperature in °C; TGA = thermogravimetric analyser.

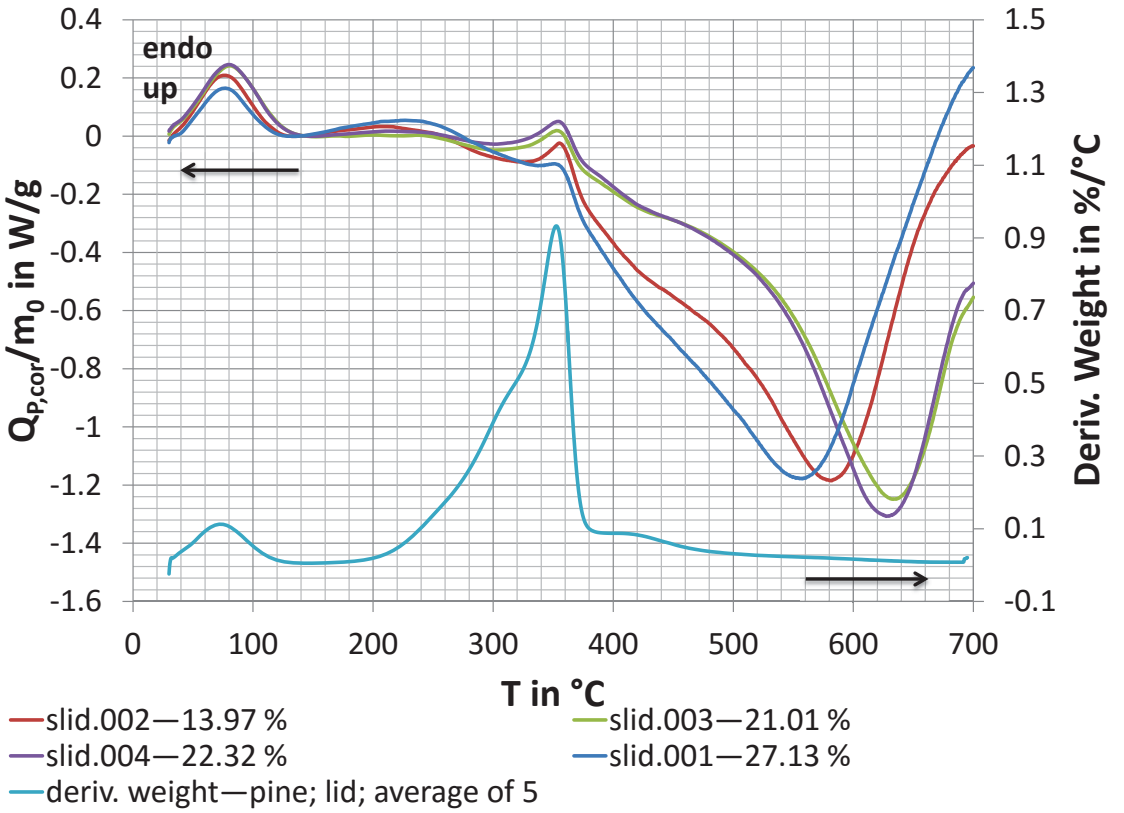

Figure 5-12. Offset corrected pyrolysis heat flows of pine sawdust pyrolysed in crucibles with a lid. The secondary y-axis shows the corresponding average derivative weight-loss. Legend: sample name—char yield at 695 °C in % (wt/wt) daf. daf = dry ash free; deriv. = derivative; m_0 = initial daf weight in mg; $Q_{P,cor}$ = corrected pyrolysis heat flow in mW; T = temperature in °C; TGA = thermogravimetric analyser.

Looking at Figure 5-11 and Figure 5-12 in more detail, they are similar to the literature below *c.* 380 °C, but quite different above (Basile et al., 2014; Gomez et al., 2009; Rath et al., 2003). Specifically, the exothermic region after the main peak in the derivative weight-loss curve has not been observed in the aforementioned studies to this extent; although it is important to note that they do not report the heat flow beyond about 500 °C. Discontinuing analysis at about 500 °C is supported by the fact that no more reaction heat effects were observed after ≈ 480 °C in the temperature difference plot of Figure 5-2. The presence of this larger than usual exothermic region is accompanied by large variation between repeat runs indicating inherent problems with the equipment precision. Even though these experiments were done after major equipment maintenance/ repair work and re-calibration, repeated blank TGA runs, without opening the furnace in between to eliminate effects caused by interfering with the sample crucible, resulted in significant variation. The results are depicted in Figure D-9 in Appendix D.2 showing that the baseline started to deviate between repeat runs above 200 °C. Note, the blanks were adjusted to have the same starting point, and the curves are different to the ones in Figure D-5 in Appendix D.2 due to the repair work and re-

calibration. The larger difference between "blank 1" and the other runs is believed to be due to the fact that it was the first run and the crucible may have adsorbed substances. Nevertheless, it shows that the TGA heat flow data obtained cannot be used to quantitatively determine the heat of pyrolysis.

Despite this, a rough comparison with the literature was possible by calculating the heat of pyrolysis in Figure 5-11 and Figure 5-12 in the range after moisture evaporation was completed (104.5-144.5 °C) till the transition temperature at the end of the main peak in the derivative weight-loss curve (372-376 °C), which was determined with TA Universal Analysis 2000 (TA Instruments, New Castle, Delaware) as the step transition temperature between the point where the second derivative of the derivative weight-loss curve has a minimum and 400 °C. This was possible as in this range the impact of the baseline variation was small enough for purposes of comparison. The resulting heat of pyrolysis is plotted in Figure 5-13 together with literature data as a function of the char yield.

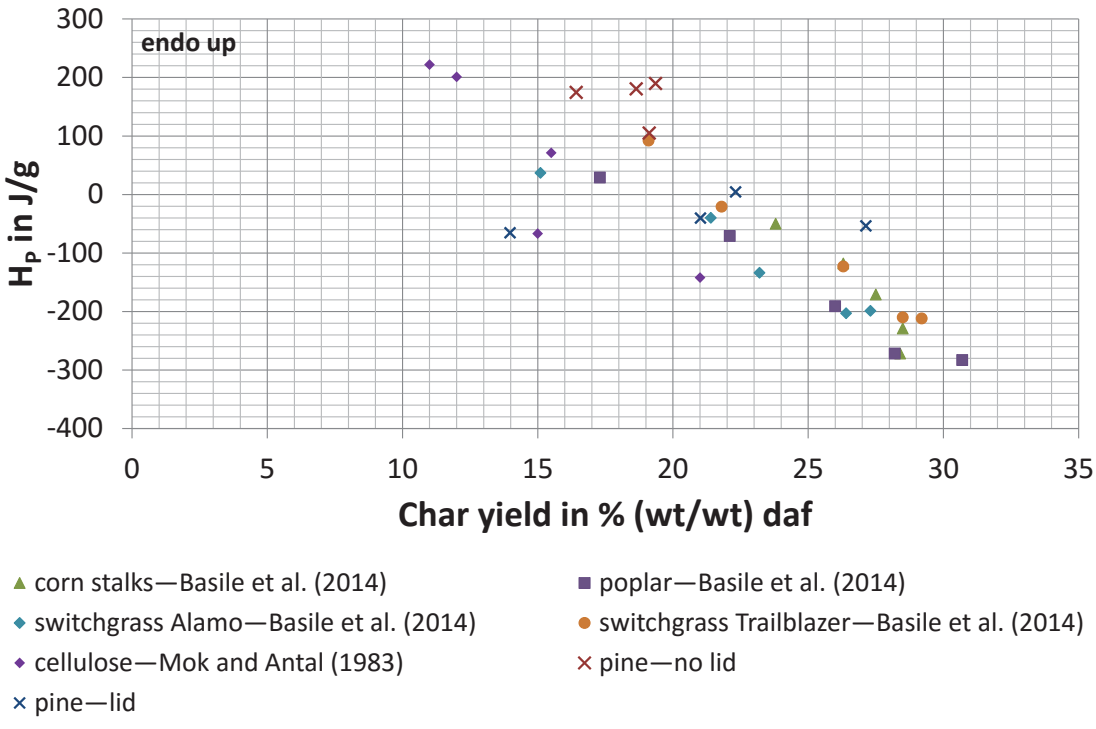

Figure 5-13. Heat of pyrolysis as a function of the char yield. Literature data (Basile et al., 2014; Mok & Antal, 1983) is included for comparison. daf = dry ash free; H_P = heat of pyrolysis in J/g.

Figure 5-13 shows that the data is within the range of previously reported data, and that the action of secondary char forming reactions (enhanced by the application of a lid) causes a decrease in the heat of pyrolysis from endothermicity to exothermicity as

indicated in 3.3.5 and reported by Mok, Antal, Szabo, Varhegyi, and Zelei (1992). The effect of sample size is not visible in the experimental results of this study due to the large inaccuracies of the equipment as discussed above. Due to these inaccuracies a sensitivity analysis of the correction process for the calculation of the heat of pyrolysis was not performed but needs to be done on data obtained with for example a DSC. Nevertheless, the results confirm the findings in the literature that the exothermicity increases with the char yield.

That the heat flow curves in Figure 5-11 and Figure 5-12 are reasonably accurate till about 380 °C was confirmed by sending a pine sawdust sample to NETZSCH Scientific Instruments Trading (Shanghai) Ltd (Waigaoqiao Free Trade Zone Shanghai, P.R. China) for analysis on a NETZSCH (Selb, Germany) STA449 F3 Jupiter TG/DSC employing the same heating conditions as used in Figure 5-11. The resulting DSC heat flow measurement and weight-loss is depicted in Figure D-10 in Appendix D.2. It shows a similar heat flow profile as observed in Figure 5-11, but without the large fluctuation above 500 °C. It is important to note here that the STA449 F3 Jupiter TG/DSC employed a true heat flux-DSC sensor (thermally coupled) providing a more precise, accurate and repeatable result (A. Gillen, Netzsch, personal communication, February 9, 2015). Thus, the differences between heat flow curves in Figure 5-11 and Figure 5-12 are indeed authentic. Furthermore, they agree with the differences observed by Rath et al. (2003) for spruce wood pyrolysed in crucibles with and without a lid. The differences reveal that the decreasing endothermicity is associated with changes in the extractives and holocellulose fraction. Therefore, enhanced secondary reactions are believed to be the cause for the exothermic peaks in Figure 5-2 (large particle size) while these regions were dominantly endothermic in Figure 5-11 (sawdust with particle size < 1 mm).

Overall Figure 5-11 and Figure 5-12 reveal that (a) pyrolysis consists of a sequence of endothermic and exothermic reactions agreeing with the findings in 5.3.1, (b) the order of the sequence is affected by secondary reactions, and (c) volatile product formation from the decomposition of cellulose appears to be the main endothermic process, which becomes progressively less endothermic with increasing extent of secondary reactions. An exothermic peak after 400 °C as observed in Figure 5-2 was also detected by Rath et al. (2003) and is indicated by both Figure 5-11 and Figure 5-12. Rath et al. treated this peak separately from the main pyrolysis peak, and discovered that

its reaction heat is less correlated with the char yield than the heat of the primary pyrolysis from the onset of pyrolysis till 400 °C. This is believed to be due to the fact that after this temperature pyrolysis is almost completed and mainly light pyrolysis gases are released, which are not subject to secondary char forming reactions. Thus the observed exothermicity might be a result of solid re-arrangement reactions. Unfortunately, due to the inaccuracy of the TGA used here, it was not possible to completely verify the heat of reaction profile observed in Figure 5-2, but in general the outlined findings validate its accuracy. The endothermic peak detected in Figure D-10 in Appendix D.2 between 420 and 500 °C highlights that reactions are still occurring after the main weight loss and supports the observed changes in the time derivative of the temperature difference in Figure 5-2.

The aim was to further investigate the reaction heat effects of heartwood samples with increased extractives content and of the impregnated samples in chapter 4 but, because of the above described equipment imprecisions, this could only be done qualitatively by analysing the raw heat flow data of the TGA results. First, the heat flow data of heartwood slices pyrolysed in crucibles without a lid, Figure 5-14, are compared to heartwood slices pyrolysed in crucibles with a lid, Figure 5-15, in an attempt to get a better understanding of the role of extractives on the heat of pyrolysis.

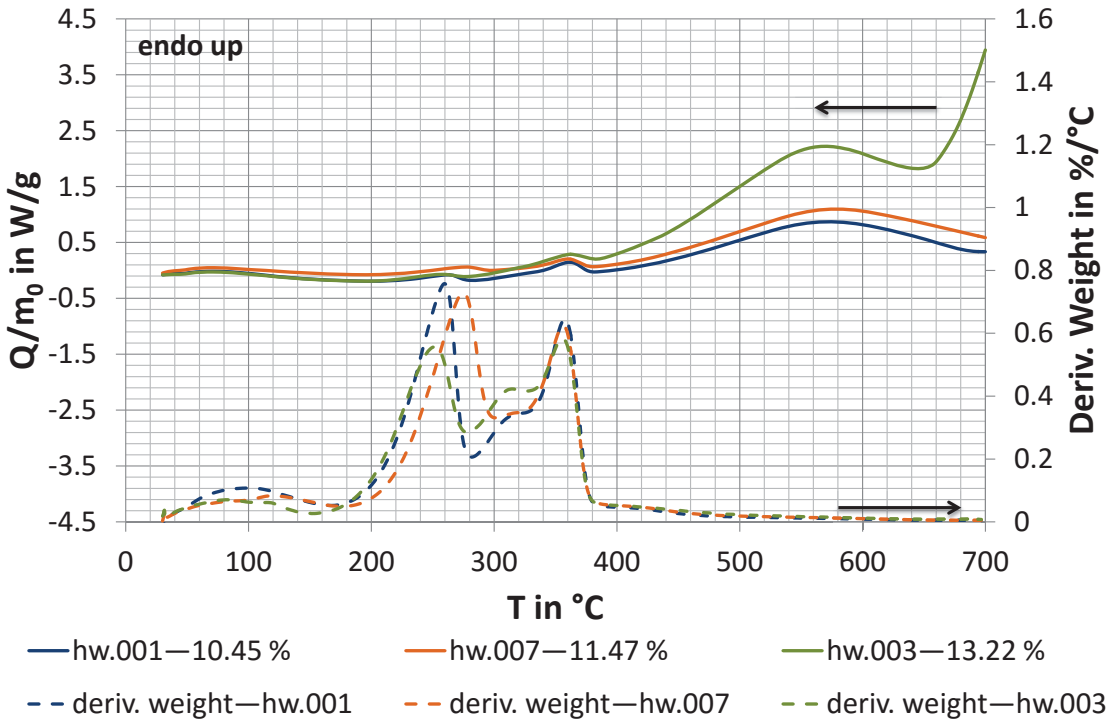

Figure 5-14. Raw heat flow data of heartwood slices pyrolysed in crucibles without a lid. The secondary y-axis shows the corresponding derivative weight-loss curves. Legend: sample name—char yield at 695 °C in % (wt/wt) daf. daf = dry ash free; deriv. = derivative; m_0 = initial dry ash free weight in mg; Q = heat flow in mW; T = temperature in °C.

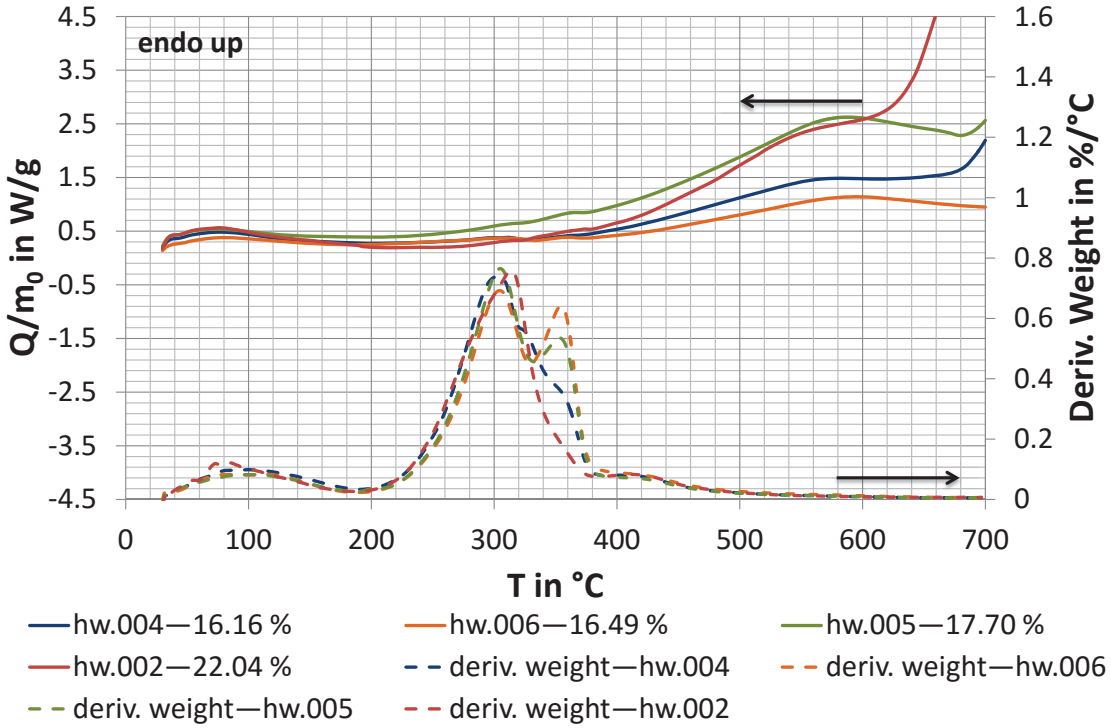

Figure 5-15. Raw heat flow data of heartwood slices pyrolysed in crucibles with a lid. The secondary y-axis shows the corresponding derivative weight-loss curves. Legend: sample name—char yield at 695 °C in % (wt/wt) daf. daf = dry ash free; deriv. = derivative; m_0 = initial dry ash free weight in mg; Q = heat flow in mW; T = temperature in °C.

Figure 5-14 exhibits similar trends to those observed for pine sawdust in Figure 5-11. That is, the derivative weight-loss peaks associated with the pyrolysis of extractives (≈ 180-300 °C) and holocellulose (≈ 300-380 °C) correspond to an endothermic peak, as does the evaporation of water at lower temperatures. Both endothermic peaks decrease with the presence of a lid, which confirm the findings above that extractives and holocellulose can undergo exothermic secondary reactions. The decrease in the endothermicity of cellulose appears to be a consequence of the reduction in weight-loss from cellulose as expressed by the diminishing peak in the derivative weight-loss curve in the range 320 to 380 °C when a lid is applied, compare Figure 5-14 and Figure 5-15. This shows that the formation of volatile pyrolysis products from cellulose is an endothermic process.

A decrease in volatile pyrolysis products is also expected for the extractives fraction (see chapter 3 for detail) although this is not directly apparent from the derivative weight-loss curves in Figure 5-14 and Figure 5-15. The reason is that the derivative weight-loss peak, constituting the pyrolysis products of the extractives, shifts to higher temperatures with the presence of a lid and consequently overlaps with hemicellulose decomposition. However, the endothermic peak in the decomposition range of the extractives is not entirely due to the extractives. Evidence for this is shown by the endothermic peak for sapwood which contains a minimum of extractives in the range 240 to 300 °C in Figure D-11 in Appendix D.2. This peak aligns with a minimum in the time derivative of the centre temperature in Figure 5-2 in this region, and might be partly related to the hemicellulose fraction. In conclusion, the formation of volatile pyrolysis products from the components of extractives and holocellulose is an overall endothermic process that becomes less endothermic with increasing secondary char formation.

Heat flows for the impregnated samples were also significantly different with and without a lid. This is illustrated for the case of 2 % (wt/wt) Mg impregnated sawdust in Figure 5-16 and Figure 5-17 for the case no lid and lid respectively. Again, the presence of a lid decreases the endothermicity, which is mainly associated with the volatilisation of the cellulose component. Figure 5-17 also shows that more compounds are released at temperatures below 200 °C. This causes an increase in endothermicity at lower temperatures but cannot be attributed to a specific pseudo-component, as discussed in chapter 4.

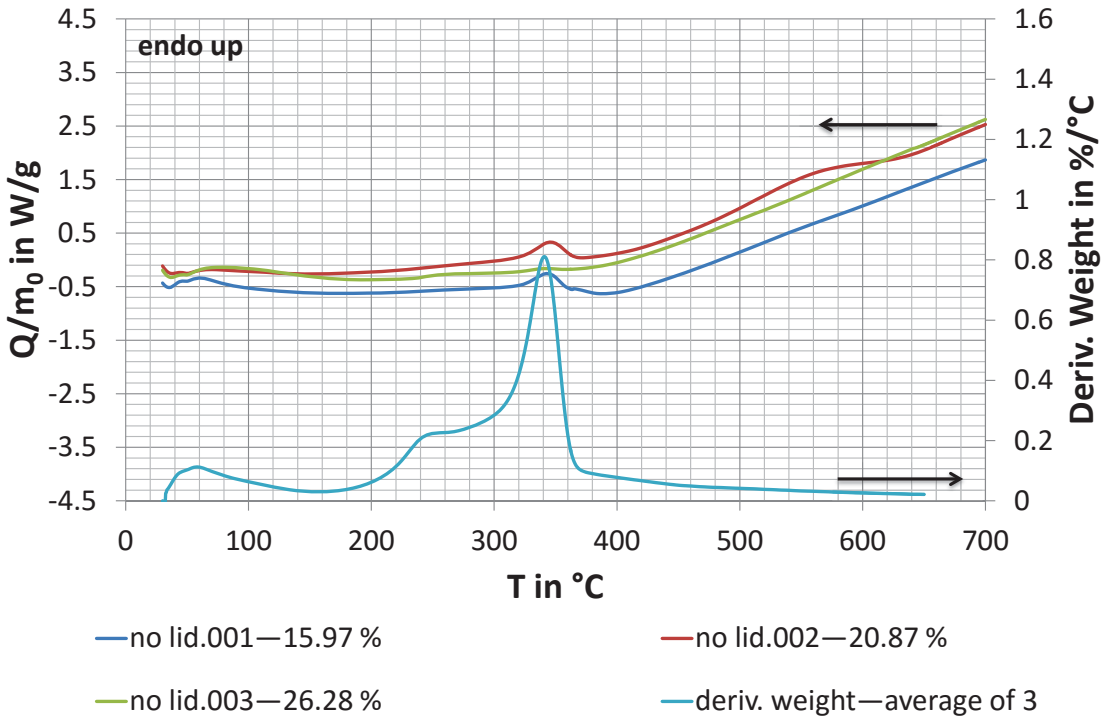

Figure 5-16. Raw heat flow data of pine sawdust impregnated with 2 % (wt/wt) Mg pyrolysed in crucibles without a lid. The secondary y-axis shows the corresponding average derivative weight-loss curve. Legend: sample name—char yield at 695 °C in % (wt/wt) daf. daf = dry ash free; deriv. = derivative; m_0 = initial dry ash free weight in mg; Q = heat flow in mW; T = temperature in °C.

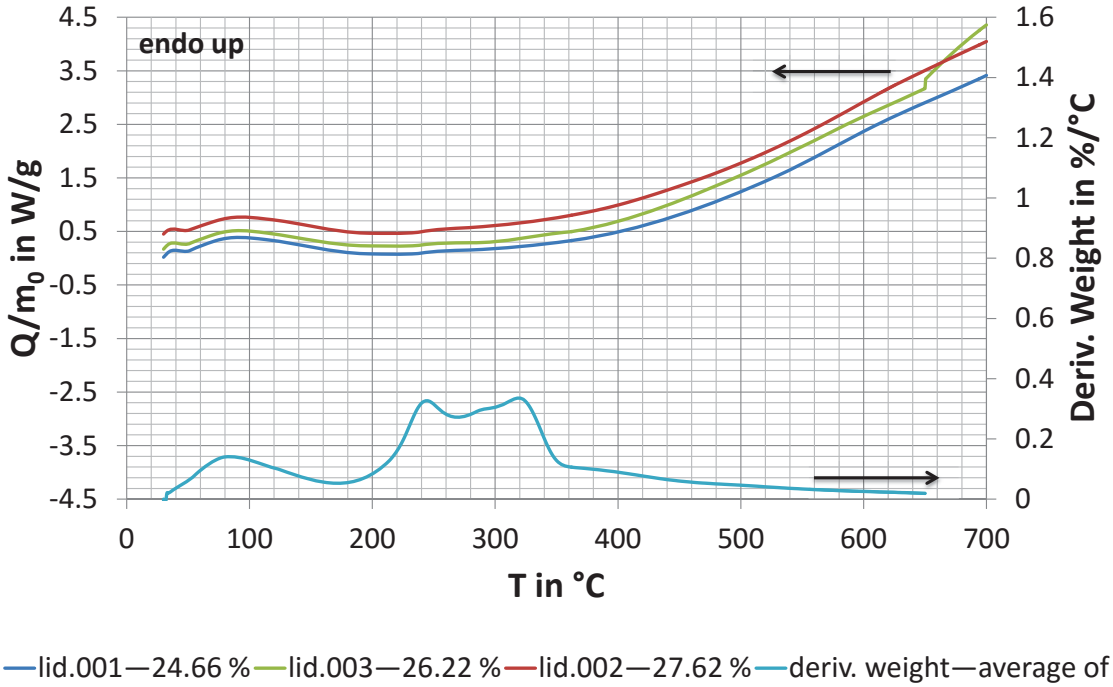

Figure 5-17. Raw heat flow data of pine sawdust impregnated with 2 % (wt/wt) Mg pyrolysed in crucibles with a lid. The secondary y-axis shows the corresponding average derivative weight-loss curve. Legend: sample name—char yield at 695 °C in % (wt/wt) daf except for run "lid.003" where the char yield was determined at 650 °C as the experiment halted at this temperature. daf = dry ash free; deriv. = derivative; m_0 = initial dry ash free weight in mg; Q = heat flow in mW; T = temperature in °C.

The differences are less visible when pine sawdust is impregnated with 5 % (wt/wt) Mg, Figure D-12 and Figure D-13 in Appendix D.2, but at this concentration there was no significant difference in the char yield between runs with and without a lid, as shown earlier in Figure 4-13 in 4.3.2, indicating that the maximum potential of secondary char forming reactions under the present conditions was achieved. However, it is impossible to conclude whether or not the pyrolysis process becomes globally exothermic with the increasing extent of secondary reactions, as suggested by the large cylinder experiments in 5.3.1. Indications for this are given by the K impregnated samples, Figure D-14 and Figure D-15 in Appendix D.2, and by the samples treated with phosphoric acid, Figure D-16 to Figure D-19 in Appendix D.2; in both a clear exothermic peak can be identified from the heat flow curves in the case when a lid is present compared to the case where no lid is present. The exothermicity increases with P concentration, as shown by comparing Figure D-18 and Figure D-19 in Appendix D.2 to Figure D-16 and Figure D-17 in Appendix D.2. This again confirms that the exothermicity observed in the large cylinder trials, in 5.3.1, is a consequence of secondary reactions, but also shows that catalytic char formation contributes to reaction exothermicity, in particular over the range of cellulose which, due to its limited accessibility to impregnation (see chapter 4), must be related to secondary reactions as well. Here, the observed effects of catalysts on the heat of pyrolysis agree with the findings of Gomez et al. (2009), who demonstrated that removing extractives and minerals increases reaction endothermicity in particular in the region where extractives and holocellulose decompose. The findings are also further supported by the work of Di Blasi et al. (2015). Furthermore, the heat of reaction always seems to have a linear correlation with the char yield, no matter whether the yield increase is caused catalytically or by enhanced vapour-phase residence times (Basile et al., 2014; Gomez et al., 2009; Mok & Antal, 1983; Mok et al., 1992; Rath et al., 2003). Considered together, these results support the hypothesis that both methods lead to increased char formation by favouring secondary char forming reactions (see chapter 4), which are exothermic.

5.4 Conclusions

It was found that the pyrolysis reaction heat effects can be successfully represented by the time derivative of the temperature difference between the recorded sample centre temperature and the heater temperature of pine cylinders with a diameter of 20 mm and a height of 60 mm. These relatively large cylindrical samples exhibit a temperature profile consisting of four peaks in the range ≈ 126 to ≈ 250 °C, ≈ 250 to ≈ 350 °C, ≈ 350 °C to ≈ 390 °C and ≈ 390 °C to ≈ 440 °C, which are separated by endothermic or less exothermic zones but showing an overall exothermic heat of pyrolysis. The separation of these zones becomes less distinguished with increasing heat transfer limitations explaining the reduced number of peaks reported previously in the literature. In general with increasing thermal insulation the characteristic temperature profile of the centre temperature shifts to higher temperatures, the internal heating rate increases and the number of observed peaks diminishes due to a progressive overlapping of the last two peaks, which increase in intensity caused by a feedback loop between exothermic reactions and heat transfer limitations.

The findings in this chapter show that the sequence of exothermic and endothermic or neutral processes cannot be entirely related to the pyrolysis of the biomass constituents as the heat of pyrolysis appears to be more a function of the char yield and the presence of catalyst. That is, the heat of pyrolysis depends on the underlying mechanism not the feedstock constituents. Exothermic reactions are linked to char formation which increases due to secondary reactions leading to the aforementioned higher internal heating rates in larger samples causing increasingly higher temperature overshoots towards the end of pyrolysis. In the absence of these secondary char forming reactions, the volatilisation and degradation of the extractives and holocellulose components into volatile pyrolysis products is an endothermic process. This explains why the small samples pyrolysed in the labscale TGA appear to have an endothermic heat of pyrolysis and the large cylindrical samples pyrolysed in the Macro-TGA display an overall exothermic heat of pyrolysis. The exothermic nature of pyrolysis was demonstrated by pyrolysing large cylindrical samples with a diameter of 120 mm and height of 60 mm at slow heating rates, ≈ 1 °C/min, displaying a thermal runaway leading to a temperature overshoot of 145.7 °C at a heater temperature of ≈ 290 °C. This explains why an asymptote in the char yield is reached when the external heating rate is decreased, at least for large samples. Further, it reveals the

difficulty in controlling the *HTT* at the lower end of the biochar production range or in the torrefaction regime. This is especially true for batch processes, or for large capacity continuous processes, as it does not allow the control of heat loss.

Another main finding was that calibrated TG-DTA in DSC mode is not accurate enough to determine the heat of pyrolysis quantitatively. Despite this, a semi-quantitative and qualitative analysis of untreated and treated sawdust samples was conducted. The findings support the literature in that the heat of pyrolysis decreases (becomes exothermic) with increasing char yield no matter whether it is due to secondary reactions induced by mass and heat transfer limitations or by catalysis. For the latter, catalysis clearly affects the heat flow peak in the region associated with cellulose decomposition, which supports the hypothesis of chapter 4 that catalysis increases char formation by secondary reactions.

To sum up, reaction heat effects correlate partly with the decomposition zones of the organic biomass constituents because of the varying char formation mechanism of the biomass components but these mechanisms are affected by secondary reactions caused by prolonged vapour-phase residence times and/ or catalysis, explaining the commonly observed linear correlation between char yield and heat of pyrolysis (heat of pyrolysis decreases with char yield) reported in the literature. However, there are also interactions between the biomass constituents and their volatile pyrolysis products as discussed in chapter 6 that require further research.

5.5 References

Antal, M. J., Mok, W. S.-L., Varhegyi, G., & Szekely, T. (1990). Review of methods for improving the yield of charcoal from biomass. *Energy & Fuels, 4*(3), 221-225. Retrieved from http://www.scopus.com/inward/record.url?eid=2-s2.0-0025434090&partnerID=40&md5=e397506586bcbfac82518a387556e697

Basile, L., Tugnoli, A., Stramigioli, C., & Cozzani, V. (2014). Influence of pressure on the heat of biomass pyrolysis. *Fuel, 137*, 277-284. doi:10.1016/j.fuel.2014.07.071

Collard, F.-X., & Blin, J. (2014). A review on pyrolysis of biomass constituents: Mechanisms and composition of the products obtained from the conversion of cellulose, hemicelluloses and lignin. *Renewable and Sustainable Energy Reviews, 38*, 594-608. doi:10.1016/j.rser.2014.06.013

Di Blasi, C., Branca, C., Galgano, A., & Gallo, B. (2015). Role of pretreatments in the thermal runaway of hazelnut shell pyrolysis. *Energy & Fuels, 29*(4), 2514-2526. doi:10.1021/acs.energyfuels.5b00171

Di Blasi, C., Branca, C., Masotta, F., & De Biase, E. (2013). Experimental analysis of reaction heat effects during beech wood pyrolysis. *Energy & Fuels, 27*(5), 2665-2674. doi:10.1021/ef4001709

Di Blasi, C., Branca, C., Sarnataro, F. E., & Gallo, A. (2014). Thermal runaway in the pyrolysis of some lignocellulosic biomasses. *Energy & Fuels, 28*(4), 2684-2696. doi:10.1021/ef500296g

Engineering ToolBox. (n.d.). *Emissivity coefficients of some common materials.* Retrieved June 4, 2015, from http://www.engineeringtoolbox.com/emissivity-coefficients-d_447.html

Gomez, C., Velo, E., Barontini, F., & Cozzani, V. (2009). Influence of secondary reactions on the heat of pyrolysis of biomass. *Industrial & Engineering Chemistry Research, 48*(23), 10222-10233. doi:10.1021/ie9007985

Green, D. W., & Perry, R. H. (Eds.). (2008). *Perry's chemical engineers' handbook* (8th ed.). New York, NY: McGraw-Hill.

Mok, W. S.-L., & Antal, M. J. (1983). Effects of pressure on biomass pyrolysis. II. Heats of reaction of cellulose pyrolysis. *Thermochimica Acta, 68*(2-3), 165-186. doi:10.1016/0040-6031(83)80222-6

Mok, W. S.-L., Antal, M. J., Szabo, P., Varhegyi, G., & Zelei, B. (1992). Formation of charcoal from biomass in a sealed reactor. *Industrial & Engineering Chemistry Research, 31*(4), 1162-1166. doi:10.1021/ie00004a027

Pattanotai, T., Watanabe, H., & Okazaki, K. (2013). Experimental investigation of intraparticle secondary reactions of tar during wood pyrolysis. *Fuel, 104*(0), 468-475. doi:10.1016/j.fuel.2012.08.047

Rath, J., Wolfinger, M. G., Steiner, G., Krammer, G., Barontini, F., & Cozzani, V. (2003). Heat of wood pyrolysis. *Fuel, 82*(1), 81-91. doi:10.1016/S0016-2361(02)00138-2

Wolfinger, M. G., Rath, J., Krammer, G., Barontini, F., & Cozzani, V. (2001). Influence of the emissivity of the sample on differential scanning calorimetry measurements. *Thermochimica Acta, 372*(1–2), 11-18. doi:10.1016/S0040-6031(01)00438-5

Chapter 6 Effect of Autogenous Pressure on Volatile Pyrolysis Products

6.1 Introduction

Long vapour-phase residence times have been shown to increase the char yield in chapter 3 by the action of secondary reactions, which were found to be responsible for the majority of the char formation over the whole pyrolysis range (≈ 140 to 500 °C). Understanding the underlying reaction mechanism is of paramount importance to make the manufacture of charcoal more efficient and environmentally friendly. To achieve this goal, it is necessary to know how secondary reactions affect the composition of the volatile pyrolysis products. This is the subject of this chapter, which is aimed at detecting the changes, caused by the presence of secondary reactions, in the gas chromatograph-mass spectrometer (GC/MS) detectable pyrolysis products. Therefore, samples of *pinus radiata* were pyrolysed in a pyrolysis-gas chromatograph-mass spectrometer, Py-GC/MS. The samples were sealed in glass capsules during the course of pyrolysis which were then subsequently broken for analysis. The glass capsules prevent the escape of volatile pyrolysis products, leading to autogenous pressure with associated long vapour-phase residence times and intimate contact between the volatile pyrolysis products and the pyrolysing solid. The assumption is that this allows secondary reactions to take place. The resulting pyrograms are compared to open crucible runs, where secondary reactions are minimal. Subsequently, the chapter discusses the results with respect to possible pyrolysis mechanisms.

6.2 Materials and Methods

This chapter is based on the combined work of two supervised 4th year engineering projects titled "GC/MS analysis of volatile species formed during the pyrolysis of wood" (Evanson, 2012), and "Analysis of secondary char formation during the pyrolysis of pinus radiata" (Kirwan, 2013), who are gratefully acknowledged for their input.

6.2.1 Py-GC/MS

Pyrolysis-gas chromatograph-mass spectrometry, Py-GC/MS, was carried out with a Frontier Laboratories Ltd (Fukushima, Japan) Multi-Shot Pyrolyser model EGA/PY-3030D connected to the inlet of a Shimadzu (Kyoto, Japan) gas chromatograph mass spectrometer GCMS-QP2010 Ultra. The resulting pyrograms were evaluated with GCMSsolution software version 2.71 from Shimadzu (Kyoto, Japan) for Windows (Microsoft, Redmond, WA, USA). For compound identification the NIST/EPA/NIH Mass Spectral Library NIST 11 (National Institute of Standards and Technology, Gaithersburg, MD, USA) was used in combination with literature. No standards have been used, as complete compound identification was not the subject of this research. Therefore, the pyrograms are to be viewed as prospective (Nowakowski & Jones, 2008). Consequently, the compounds have been analysed qualitatively, because overlapping peaks along with the presence of a large amount of unidentified substances, makes a semi quantitative analysis based on peak area or characteristic ion intensity somewhat arbitrary. Additionally, pyrograms were obtained at varying temperatures, meaning that the substance pool for semi quantitative analysis varied and the actual fraction detectable by Py-GC/MS is not known.

Three different types of experiments were carried out: (a) Evolved Gas Analysis (EGA), (b) pyrolysis in open crucibles, and (c) pyrolysis in sealed glass capsules. The respective Py-GC/MS parameters were developed on the basis of available literature similar to the experiments carried out in this study (Alén, Kuoppala, & Oesch, 1996; Arias et al., 2006; Evanson, 2012; Gao, Li, Quan, Du, & Duan, 2013) and preliminary experiments. A relatively large sample mass of 6.0 ± 0.1 mg was chosen to ameliorate sample inhomogeneity. This value was based on the work of Khelfa, Bensakhria, and Weber (2013).

6.2.1.1 Evolved Gas Analysis

EGA has already been described in 3.2.6 to which the reader is referred for more detail. Though, at this point it is helpful to include a picture of the employed crucibles, shown in Figure 6-1, as the crucible geometry affects the extent of secondary reactions, which was elucidated in chapter 3 and is further discussed in 6.3.1.

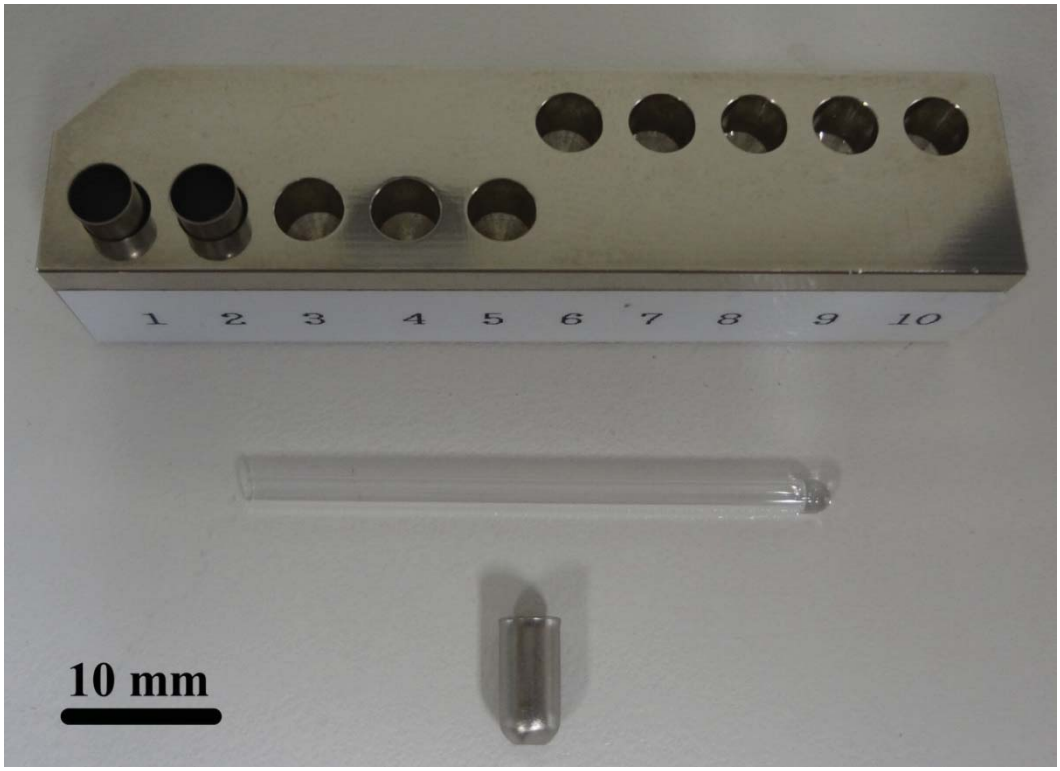

Figure 6-1. Py-GC/MS crucibles and glass capsule. At the top is the Eco-cup stand with an Eco-cup LF in position 1 and 2 shown. A side view of the Eco-cup LF is seen at the bottom. In the middle is the glass capsule, used for autogenous pyrolysis runs in the On-line Micro Reaction Sampler, depicted. GC = Gas Chromatograph; MS = Mass Spectrometer; Py = Pyrolysis.

6.2.1.2 Open Crucible Experiments

Open crucible pyrolysis runs were done with the same pyrolyser setup as EGA, utilising red heated Eco-cup LF crucibles with 6.0 ± 0.1 mg air-dried pine sawdust. However, different pyrolyser heating profiles were applied. Double-Shot experiments were carried out following the experimental procedure illustrated in Figure 6-2.

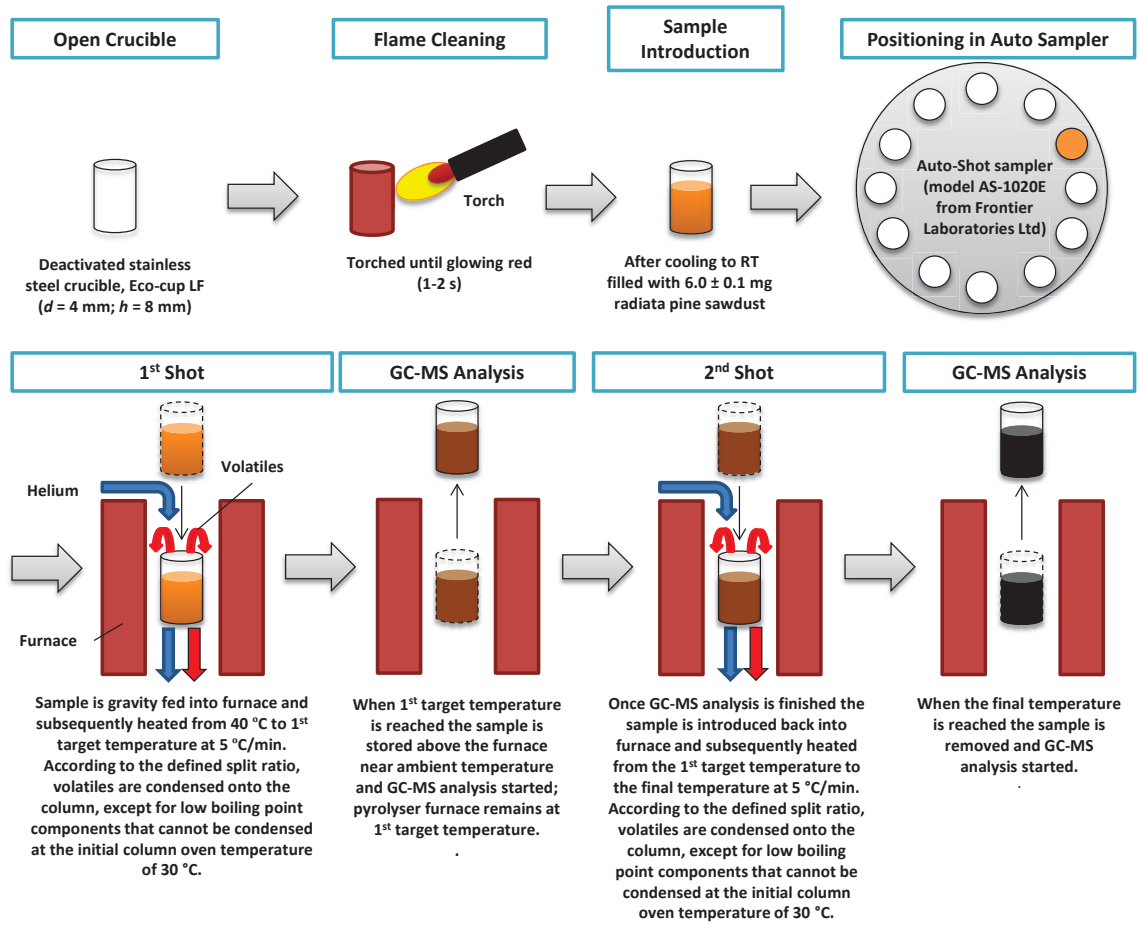

Figure 6-2. Experimental procedure for pyrolysis runs in open crucibles minimising the effect of secondary reactions. *d* = diameter; GC = Gas Chromatograph; *h* = height; MS = Mass Spectrometer; Py = pyrolysis; RT = room temperature.

In the first Shot, a thermal desorption step, the sample is heated from 40 °C to the first target temperature at 5 °C/min. During thermal desorption the volatiles are condensed onto the column according to the split ratio, except for low boiling point components that cannot be condensed at the initial column oven temperature of 30 °C. When the target temperature is reached the sample is stored above the furnace near ambient temperature and GC/MS analysis started; that is, the column oven temperature program commences, shown in Table 6-1, and the MS detector is turned on. Separation of the condensed pyrolysis products occurs in the column according to their boiling point and interaction with the stationary phase. A Frontier Lab Ultra ALLOY^{+}-5-30M-0.25F (l = 30 m; ID = 0.25 mm; film thickness = 0.25 µm) general purpose column was employed. The stationary phase is 5 % diphenyl 95 % dimethylpolysiloxane, which has an extreme low polarity (Frontier Laboratories Ltd, 2011, n.d.). The Py-GC/MS parameters are given in Table 6-1. Meanwhile the pyrolyser furnace remained at the first target temperature and once the GC/MS analysis is finished the second thermal

desorption step begins by introducing the sample back into the furnace and heating it from the first target temperature to the final temperature at 5 °C/min. When the final temperature is reached the sample is removed from the furnace and the second GC/MS analysis is started using the same program. In some cases only one thermal desorption step was carried out. The Double-Shot target temperatures are given in Table 6-1, and are based on the pyrolysis zones in section 3.3.7. Each set was repeated three times.

Table 6-1. Py-GC/MS parameters for open crucible pyrolysis runs.

Py parameters	**GC parameters**	**MS parameters**
Double-Shot Target Temperatures (Initial *T*=>1st Target *T*=>2nd Target *T*): 40 °C=>240 °C=>280 °C 40 °C=>280 °C=>350 °C 40 °C=>350 °C=>380 °C 40 °C=>380 °C=>500 °C 40 °C=>500 °C=>700 °C 40 °C=>700 °C	Column Oven *T* program: Initial *T*: 30 °C Initial Hold Time: 4 min Heating Rate: 5 °C/min Final *T*: 300 °C Final Hold Time: 15 min	Ionisation Mode: EI at 70 eV
Heating Rate: 5 °C/min	Injection *T*: 325 °C	Ion Source *T*: 230 °C
Hold Time at Target *T*: 0 min	Injection Mode: Split	Interface *T*: 250 °C
Interface *T*: 325 °C (Auto[a])	Flow Control Mode: Linear velocity	Solvent Cut Time: 0 min
	Pressure: 46.6 kPa	Micro Scan Width: 0 u
	Total Flow: 185.8 ml/min	Start Time: 0 min
	Column flow: 1.01 ml/min	End Time: 70 min[b]
	Linear Velocity: 36.1 cm/s	Acq. Mode: Scan
	Purge Flow: 3.0 ml/min	Event Time: 0.3 s
	Split Ratio: 180	Scan Speed: 2000
		Start *m/z*: 40
		End *m/z*: 550

Note. EGA = Evolved Gas Analysis; EI = Electron Ionisation; GC = Gas Chromatograph; MS = Mass Spectrometer; *m/z* = mass-to-charge ratio; Py = pyrolysis; *T* = temperature.

[a]Auto means that the interface temperature is set automatically 100 °C above the furnace temperature but 325 °C is the maximum temperature. [b]based on column oven temperature program.

6.2.1.3 Sealed Glass Capsule Experiments

The Auto-Shot Sampler was replaced with a Frontier Laboratories Ltd (Fukushima, Japan) On-line Micro Reaction Sampler model PY1-1050 for studying pyrolysis under autogenous pressure in sealed glass capsules (*OD* = 2.5 mm, *ID* = 2 mm, length 30-35 mm), Figure 6-1. The quartz pyrolysis tube inside the pyrolyser furnace was exchanged for a stainless steel tube to avoid damaging of the former caused by breaking the sealed glass capsule at the end of the pyrolysis run. The experimental procedure is depicted in Figure 6-3.

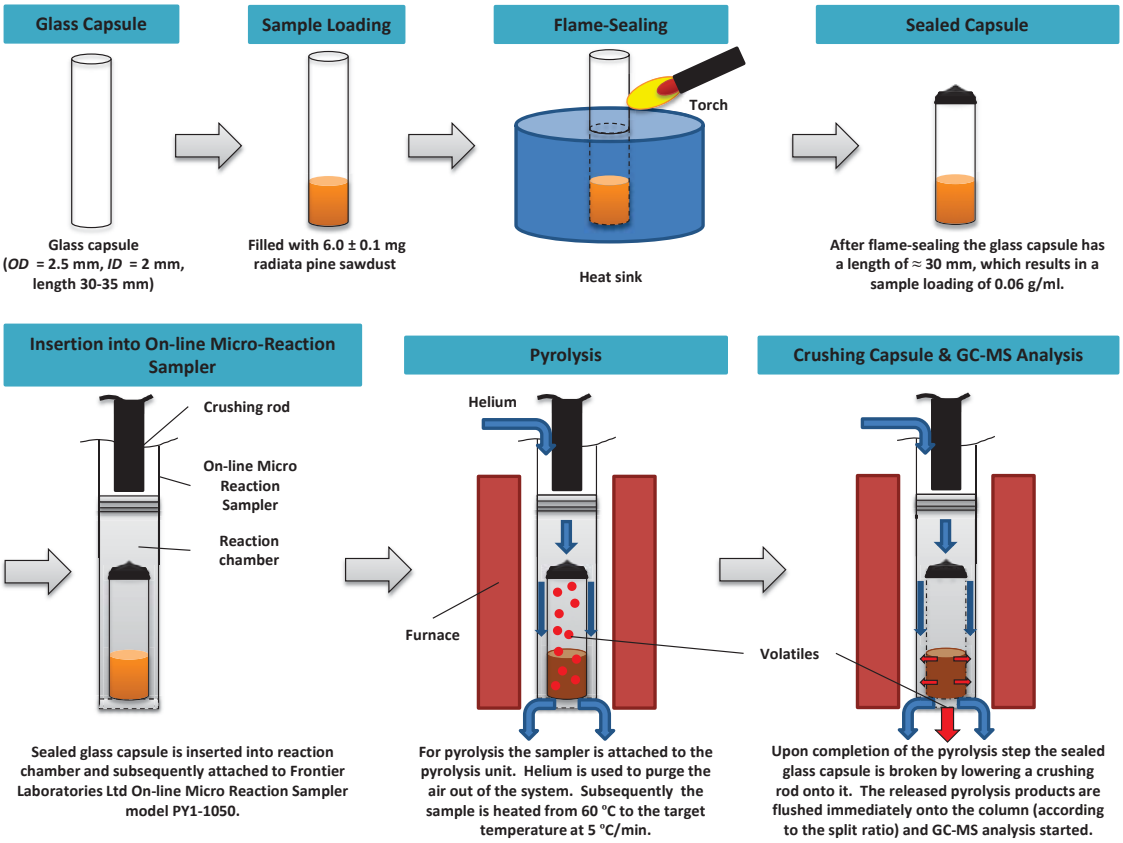

Figure 6-3. Experimental procedure for pyrolysis runs in sealed glass capsules. The sealed capsule prevents the escape of volatile pyrolysis products causing a pressure increase in the glass capsule resulting in long vapour-phase residence times and intimate contact between the volatile pyrolysis products and the pyrolysing solid enabling secondary reactions. GC = Gas Chromatograph; *ID* = inside diameter; MS = Mass Spectrometer; *OD* = outside diameter; Py = Pyrolysis.

In accordance with the open crucible experiments 6.0 ± 0.1 mg of air-dried pine sawdust was inserted into a capsule. The capsule had to be tapped on a flat surface for filling to allow the sample to move to the bottom. Subsequently, it was inserted into a heat sink that had been chilled beforehand in a freezer to protect the pine sawdust from pyrolysing while flame-sealing the glass capsule with a torch. It is important to note that the glass capsules were sealed under ambient conditions in air. Thus oxygen was

present. Taking a conservative approach and assuming that the sealed glass capsules have all a length of 35 mm, an internal diameter of 2 mm, and the volume of the wood is negligible shows that the oxygen of the trapped air inside the sealed glass capsules is only 1.24 %(wt/wt) of the oxygen of the wood sample, using the oxygen content from Table 3-3. Therefore, it was deemed unnecessary to prepare the samples in an inert atmosphere. After flame-sealing the glass capsule had a length of approximately 30 mm, which results in a sample loading of 0.06 g/ml. Ethanol was used to remove contaminants from the sealed tube that was then inserted into the reaction chamber attached to the Online Micro Reaction sampler. To start the experiment the reaction chamber was slid into the stainless steel pyrolysis tube inside the pyrolysis furnace and the heating profile for pyrolysis started. The initial temperature of the pyrolysis furnace was 60 °C. Originally, it was aimed to start the runs at 40 °C in accordance with the open crucible runs. However, with the installation of the Online Micro-Reaction sampler it was not possible to cool the furnace to 40 °C, and 60 °C was chosen instead. This difference has no impact on the results as pyrolysis reactions do not occur below ≈ 140 °C, Figure 3-45. Again a so-called Double-Shot analysis was carried out. Though, this time only one thermal desorption could be applied. The following runs were done (Initial *T*=>Final *T*): 60 °C=>240 °C, 60 °C=>280 °C, 60 °C=>350 °C, 60 °C=>380 °C, and 60 °C=>500 °C utilising the heating rate, hold time and interface temperature stated under “Py parameters” in Table 6-1. Replicates were done except for the experiment 60 °C=>280 °C. During pyrolysis the sealed glass capsule prevents the escape of volatile pyrolysis products causing a pressure increase in the glass capsule resulting in a long vapour-phase residence time and intimate contact between the vapour-phase and the pyrolysing solid. Upon completion of this step the glass capsule was broken by lowering a crushing rod onto it. The released pyrolysis products were flushed immediately onto the column and GC/MS analysis started according to the GC and MS parameters in Table 6-1. The same column was used as for the open crucible runs.

6.3 Results and Discussion

6.3.1 Open Crucible Experiments

Pyrolysis in open crucibles was done to obtain an overview of primary volatile pyrolysis products. Of course secondary reactions cannot be completely ruled out. In fact they were most likely present as the results in chapter 3 show, which agree with the study of L. Wang et al. (2011) who found that slight changes in the crucible geometry have large effects on the char and fixed carbon yield. Figure 6-1 shows that the crucibles used in this study were relatively deep; the height to diameter ratio is two, inhibiting the egress of volatile pyrolysis products and so enabling secondary reactions. The significant impact that sample size and geometry of the pyrolysis equipment have on the final products is also discussed in a recent review by Morgan and Kandiyoti (2013). They particularly mention that commercially available pyrolyser for GC/MS are not optimized for geometry independence. However, this might be impossible, as the results in chapter 3 indicate (at least for slow pyrolysis); and the fact that open crucible runs will have a minimum of secondary reactions compared to the sealed glass capsule experiments makes the application of the crucibles in Figure 6-1 valid for this research.

The pyrograms corresponding to pyrolysis zone I in Figure 3-45 (RT to 240 °C) in 3.3.7 are depicted in Figure 6-4.

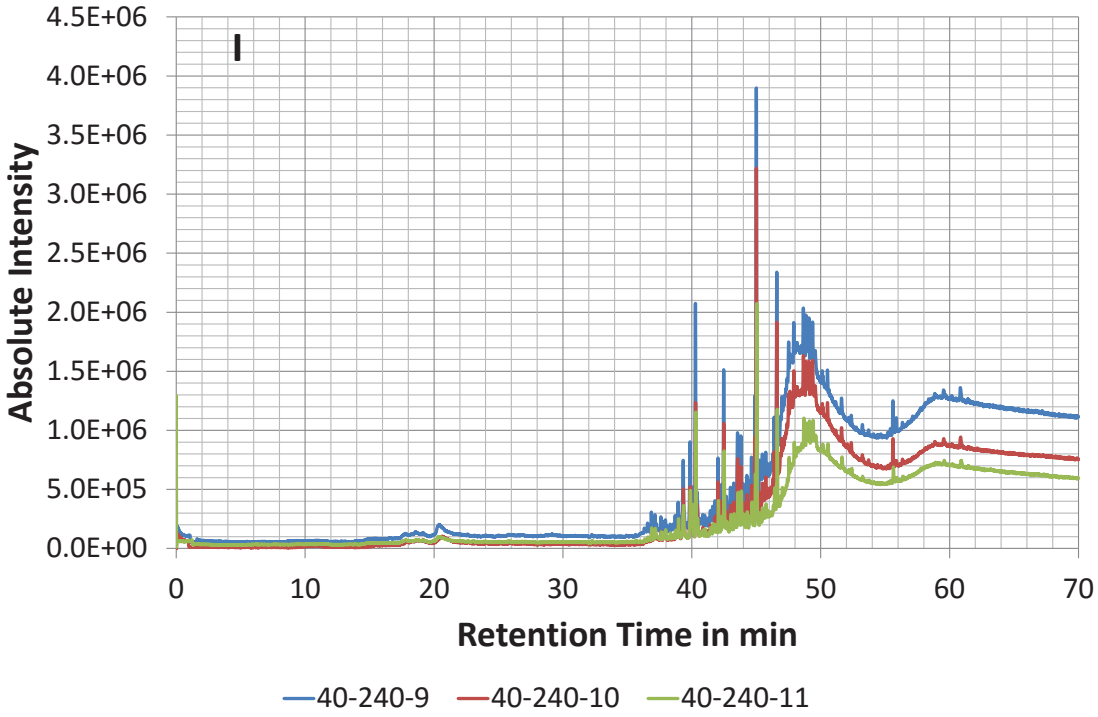

Figure 6-4. Pyrograms of pine sawdust heated in open crucibles from 40 to 240 °C. A compound list is given in the provided Excel file in Appendix E.3 in the sheet "pine240-9". The Roman numeral in the top left corner refers to the pyrolysis zone defined in Figure 3-45 in 3.3.7. Legend: start temperature in °C-highest treatment temperature in °C-run number.

Figure 6-4 shows the good reproducibility of the runs, which was encountered consistently throughout all open crucible experiments (see Figure E-1 to E-10 in Appendix E.1). The increasing slope in Figure 6-4 after a retention time of 30 min is expected, and caused by column bleed, which increases exponentially with temperature, and levels off when attaining a constant temperature (Antonio, n.d.). In this study a constant temperature is reached at a retention time of 58 min. This effect is more visible when looking at the pyrograms in Figure E-9 in Appendix E.1. The analysed peaks of Figure 6-4, including compound identification, are listed in the provided Excel file in Appendix E.3 in the sheet "pine240-9". It was found that the volatiles released prior to 240° C primarily originate from the extractives content of radiata pine wood. This confirms the findings of chapter 3, where the local peak at about 230 °C of the "no lid" derivative weight curve and the EGA curve in Figure 3-46 was identified to originate from the extractives present in heartwood. In chapter 3 it was also discussed that these extractives are lost with time due to their partial pressure, which explains why this peak is often not encountered in the literature (Kang, Lee, Park, Park, & Kim, 2006; Khelfa et al., 2013; Park, Park, & Kim, 2008; Skreiberg, Skreiberg, Sandquist, & Sørum, 2011; X. Y. Wang, Wan, Chen, & Wang, 2012). Thus, in the majority of cases

biomass decomposition is described by three pseudo-components, that is, hemicellulose, cellulose, and lignin (Biagini & Tognotti, 2014; Di Blasi, 2008), which was already discussed in 3.3.8. Abietic acid is by far the main substance identified in the pyrogram in Figure 6-4. It is the peak extending from a retention time, *Rt*, of 36 min to 57 min with its peak at 48.3 min. The majority of the other substances are fronting and tailing on this peak. Fiebach and Grimm (2000) state that the primary compound in rosin acid is levopimaric acid, 30 to 50 %, but that this isomerises to abietic acid in the temperature range 100 to 200 °C. This explains the large proportion of abietic acid detected in the pyrograms of this study. The vast amount of unidentified compounds in sheet "pine240-9" in Appendix E.3 can be explained by the presence of a multitude of tricyclic resin acid isomers (Fiebach & Grimm, 2000), which generally show a poor chromatographic behaviour along with the formation of decarboxylation products (Anderson & Winans, 1991).

Analysis can be improved by methylation, Anderson and Winans (1991), and silylation (Egenberg, Aasen, Holtekjølen, & Lundanes, 2002; Egenberg, Holtekjølen, & Lundanes, 2003; Nolte, Schauer, Cass, & Simoneit, 2001). Further, oxime-trimethylsilylation has been suggested as a quantification method for pyrolysis products from wood polysaccharides (Hosoya, Kawamoto, & Saka, 2006). However, those methods were disregarded as this study is focused on identifying differences in volatile pyrolysis products rather than identifying and quantifying the exact composition. Hence, the substances from an *Rt* of 36 min onwards are generalised as extractives. Apart from the extractives a lignin compound, coniferaldehyde (*Rt* 36.316 min in sheet "pine240-9" in Appendix E.3) was also identified. This is expected as lignin degradation occurs over the entire pyrolysis range. In section 3.3.8 it was shown to decompose in the temperature range 140 to 646 °C. Other possible benzene derivatives like 2-t-Butylxanthen-9-one (*Rt* 40.022 or 40.670 min in sheet "pine240-9" in Appendix E.3) were found, which could also derive from lignin (Hosoya, Kawamoto, & Saka, 2009a). The peaks at the beginning of the pyrogram in Figure 6-4 (*Rt* 0 to 2 min in sheet "pine240-9" in Appendix E.3) are attributed to light pyrolysis gases which can be derived from any of the four biomass constituents but due to the pyrolysis temperature are believed to mainly result from the fragmentation of the extractives.

The pyrograms and compound tables of zone II and III in Figure 3-45 are given in Appendix E in Figure E-1 and sheet "pine240-280-10" in the Excel file in Appendix

E.3, and Figure E-3 and sheet "pine280-350-5" in the Excel file in Appendix E.3 respectively. Over both zones is a shoulder visible in the derivative weight curve in Figure 3-45, which corresponds to the degradation of hemicellulose (Babu, 2008; Grønli, Várhegyi, & Di Blasi, 2002; X. Y. Wang et al., 2012). This is demonstrated in section 3.3.8 were the hemicellulose decomposition range was found to be between 226 to 339 °C. A typical hemicellulose degradation product that was identified is cyclohexanone (*Rt* 13.649 and 11.099 min in sheet "pine240-280-10" and "pine280-350-5" in Appendix E.3 respectively) (Nowakowski & Jones, 2008) along with a range of non-specific carbohydrates (e.g. furfuryl alcohol *Rt* 12.370 and 6.143 min in sheet "pine240-280-10" and "pine280-350-5" in Appendix E.3 respectively), which can originate from either cellulose or hemicellulose degradation (Lourenço, Gominho, Marques, & Pereira, 2013). Hydroxypropanone (*Rt* 2.910 and 1.866 min in sheet "pine240-280-10" and "pine280-350-5" in Appendix E.3 respectively), deriving from hexose (Faix et al., 1992; Lourenço et al., 2013), was identified in zone II indicating the onset of cellulose (hexose) pyrolysis. As expected, more hexose markers, 1,4:3,6-Dianhydro-.alpha.-d-glucopyranose (*Rt* 20.930 min in sheet "pine280-350-5" in Appendix E.3) (Faix et al., 1992; Lourenço et al., 2013), 5-Hydroxymethylfurfural (*Rt* 23.178 min in sheet "pine280-350-5" in Appendix E.3) (Faix et al., 1992; Lourenço et al., 2013), D-Allose (*Rt* 28.820 min in sheet "pine280-350-5" in Appendix E.3) and levoglucosan (*Rt* 30.811 min in sheet "pine280-350-5" in Appendix E.3) (Dobele, Rossinskaja, Telysheva, Meier, & Faix, 1999; Lourenço et al., 2013; Nowakowski & Jones, 2008; Shen, Gu, & Bridgwater, 2010b) were identified in zone III. This agrees with the temperature range for cellulose decomposition, which was identified in section 3.3.8 to occur in the temperature range 297 to 392 °C, and has its maximum at the peak of the derivative weight curve. Present again are light pyrolysis gases at the beginning of the pyrograms, which, in this temperature range, derive less from the extractives and more from the other biomass constituents. They are followed by other low molecular weight pyrolysis products like acetic acid (*Rt* 1.942 and 1.432 min in sheet "pine240-280-10" and "pine280-350-5" in Appendix E.3 respectively), which can originate from either carbohydrate or lignin pyrolysis. The number of methoxyl substituted aromatics (e.g. 4-Vinylguaiacol *Rt* 24.517 and 23.433 min in sheet "pine240-280-10" and "pine280-350-5" in Appendix E.3 respectively) increases significantly in zone II and III, revealing the increasing decomposition of lignin. Typical compounds of the extractive fraction like terpenes, terpenoids, and steroids are still released.

In zone IV of Figure 3-45 the weight-loss rapidly decreases and the main compounds identified are (a) non-specific carbohydrates (e.g. furfuryl alcohol *Rt* 10.886 min in sheet "pine350-380-6" in Appendix E.3), (b) 2,5-Dimethyl-4-hydroxy-3(2H)-furanone (*Rt* 16.722 min in sheet "pine350-380-6" in Appendix E.3) (Nowakowski & Jones, 2008), levoglucosenone (*Rt* 17.490 min in sheet "pine350-380-6" in Appendix E.3) (Dobele et al., 2005; Y. M. Wu, Zhao, Li, & He, 2009), 1,4:3,6-Dianhydro-.alpha.-d-glucopyranose (*Rt* 20.943 min in sheet "pine350-380-6" in Appendix E.3) (Faix et al., 1992; Lourenço et al., 2013), and possibly levoglucosan (*Rt* 29.796 min in sheet "pine350-380-6" in Appendix E.3) as hexose/ cellulose marker, and (c) lignin derivatives (e.g. guaiacol *Rt* 16.877 min in sheet "pine350-380-6" in Appendix E.3). The amount of detected extractives is greatly reduced, and a few light pyrolysis gases and low molecular weight pyrolysis products are again observed at the beginning of the pyrogram. The pyrograms and compound table is given in Figure E-5 and sheet "pine350-380-6" in Appendix E.1 and E.3 respectively. The findings agree well with the constituent decomposition profile outlined in section 3.3.8.

The pyrograms and compound table of zone V are given in Figure E-7 and sheet "pine380-500-5" in Appendix E.1 and E.3 respectively. Interesting is that, apart from a few expected lignin derivatives, long chain alkanes and alkenes are also present, which have not been observed in the other zones to this extent. Separation into long chain and short chain has been done according to C. Wang, Du, Pan, Li, and Yang (2007), who defined a chain length shorter than 17 carbon atoms as short chain. The presence of alkanes in the six pyrolysis zones in Figure 3-45 is demonstrated in Figure 6-5, where the characteristic Mass Ion Chromatograms, MIC, for alkanes with the mass-to-charge ratio *m/z* 57+71 (P. Buurman, personal communication, March 4, 2013) have been plotted.

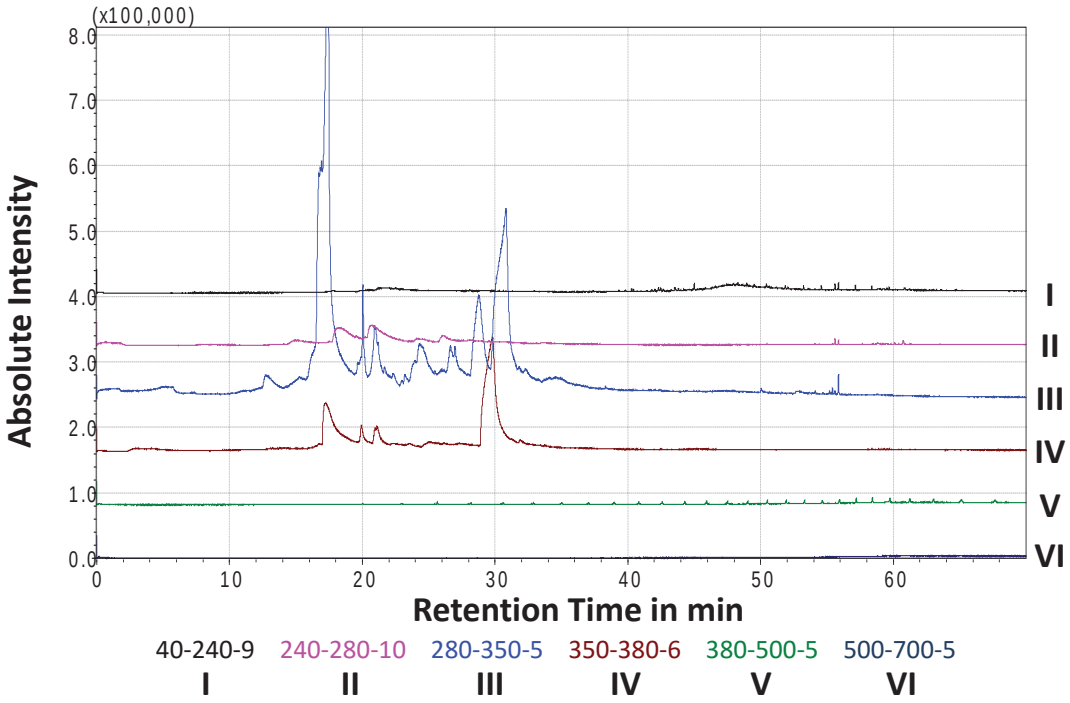

Figure 6-5. Mass Ion Chromatograms consisting of *m/z* 57+71 of the six pyrolysis zones in Figure 3-45. The mass-to-charge ratio *m/z* 57+71 is characteristic for alkanes (P. Buurman, personal communication, March 4, 2013). Legend: start temperature in °C-highest treatment temperature in °C-run number. Samples that have a start temperature above 40 °C have previously been heated to their start temperature, thus containing only the volatiles released in their respective pyrolysis range. The roman numerals refer to the pyrolysis zones in Figure 3-45. *m/z* = mass-to-charge ratio.

Figure 6-5 shows in the first instance that *m/z* 57+71 is not only present in alkanes but also carbohydrate derivatives, e.g. cyclopropyl carbinol *Rt* 17.4 min and levoglucosan *Rt* 30.8 min in curve "280-350-5" (see sheet "pine280-350-5" in Appendix E.3). The peaks in the curve "380-500-5" represent alkanes and alkenes (include *m/z* 57+71) as carbohydrate decomposition is already completed at this stage, as discussed above and shown in sheet "pine380-500-5" in Appendix E.3 by the absence of typical holocellulose markers. It can be seen that the intensities are very low, which could be a reason that they are not detected in the curves "280-350-5" and "350-380-6". However, Figure 6-5 clearly shows that the alkanes and alkenes, released in the volatile fraction between 380 to 500 °C, are primarily long chain alkanes and alkenes with an $Rt \geq 35$ min, where no carbohydrate products are present in the lower temperature pyrograms. This suggests that alkanes and alkenes are primarily formed at temperatures between 380 and 500 °C. It is important to note that they were also detected in the curve "40-240-9" (sheet "pine240-9" in Appendix E.3) but that their intensities appear smaller than in the curve "380-500-5" in Figure 6-5. Another interesting observation in temperature zone V is the presence of phenol (*Rt* 16.063 min in sheet "pine380-500-5"

in Appendix E.3) and alkyl substituted phenols (e.g. o-cresol *Rt* 17.362 min in sheet "pine380-500-5" in Appendix E.3) next to the typical methoxyl substituted phenols (e.g. guaiacol *Rt* 17.975 min in sheet "pine380-500-5" in Appendix E.3), which are lignin markers. Commonly, phenol and the alkyl substituted phenols are attributed to lignin pyrolysis as well (Faix et al., 1992; Lourenço, Gominho, marques, & Pereira, 2012; Lourenço et al., 2013). This makes sense as, in this temperature zone, carbohydrate decomposition is completed (explained above). However, in their review Collard and Blin (2014) outline that even though the main weight-loss of carbohydrates is completed, charring still takes place in this temperature zone (till ≈ 800 °C), which is characterised by the formation of benzene rings in the solid residue that possibly could lead to the release of some into the vapour-phase due to cracking reactions. The ongoing rearrangement reactions are also associated with the release of light pyrolysis gases like CO, H_2, and CH_4 resulting essentially in a char structure similar to lignin (Collard & Blin, 2014). Thus, the detected pyrolysis gases at the beginning of the pyrograms in Figure E-7 originate from the three biomass constituents hemicellulose, cellulose and lignin. Extractives reactions are believed to be already completed at the temperatures in zone V although a single extractives compound (18-Norabieta-8,11,13-triene *Rt* 39.416 min in sheet "pine380-500-5" in Appendix E.3) was identified. Benzene derivatives appear in this zone without oxygen such as the polycyclic aromatic hydrocarbon, PAH, Phenanthrene, 2,3,5-trimethyl- (*Rt* 42.083 min in sheet "pine380-500-5" in Appendix E.3).

In zone VI no more pyrolysis products were detected with Py-GC/MS, except a few unidentified low molecular weight gaseous compounds as can be seen by the pyrograms of Figure E-9 and the compound list in sheet "pine500-700-5" in Appendix E.1 and E.3 respectively. They are likely to originate from holocellulose and lignin combined as mentioned in the paragraph above. That no typical methoxyphenol lignin markers are present, even though lignin pyrolysis occurs till a temperature of 646 °C as mentioned above, and illustrated by the still ongoing weight-loss in Figure 3-45 in 3.3.7 and Figure 3-10 in 3.3.1, could be due to the fact that only high molecular weight lignin markers are formed that are non-detectable by Py-GC/MS or lignin mainly decomposes to form char and light molecular weight gases that are non-condensable in the column and hence are not detectable by GC/MS as discussed in the experimental section. The EGA results reveal that indeed the majority are light pyrolysis gases. It was found that

at the beginning of zone VI 88 % of the absolute peak intensity are caused by $m/z \leq 44$, which increases to 97 % at the end of zone VI. Dominant *m/z* ratios at 500 °C with decreasing absolute intensity are 28, 18, 2, 16, and 44, which indicate the presence of molecular ions of CO, H_2O, H_2, CH_4, and CO_2 respectively. It is important to note that the ions of H_2O and H_2 were swapped around in one out of the three recorded mass spectra. These findings agree with literature where CO, CO_2, H_2 and CH_4 are reported to be the main compounds detected in the pyrolysis gas (Grieco & Baldi, 2011; Neves, Thunman, Matos, Tarelho, & Gómez-Barea, 2011; Ratte, Marias, Vaxelaire, & Bernada, 2009; Z. Wang, Cao, & Wang, 2009; Williams & Besler, 1996). Water is present in the EGA runs because no condensation step was included in this set up. Pyrolysis gas, as discussed in the introduction, is defined as the non-condensable fraction of the volatile pyrolysis products at room temperature, and thus water has to be disregarded for comparison with literature values. That CO has the highest gas release rate at this temperature followed by CH_4, CO_2 and H_2 has been shown by Z. Wang et al. (2009). This agrees with the EGA results except for H_2. The reason for the difference in the position of H_2 can be explained by its almost exponential increase with temperature above 400 °C as shown by Z. Wang et al. (2009). This onset temperature or the increased rate could have been different in our experiments due to the heterogeneity or species of the pine used, or the experimental set up, which, for example, could have impacted on the presence of secondary reactions. Overall these findings support that the main pyrolysis is finished at 500 °C, and that after 500 °C mainly light pyrolysis gases are released as a consequence of the charring processes (Collard & Blin, 2014; Neves et al., 2011).

Looking at the compound tables, sheet “pine240-9” to “pine500-700-5” in Appendix E.3, it can be concluded that these results agree with literature, that is, the majority of lignin markers are from the guaiacyl-type, which is the building block of softwood lignin (Brown, 2009; Rowell, Pettersen, & Tshabalala, 2013), and that holocellulose primary decomposition products are anhydrosugars, low molecular weight carbonyls, carboxylic acids and furans (Hosoya, Kawamoto, & Saka, 2007c, 2008b).

To illustrate the discussed differences in volatile products released in the different pyrolysis zones in Figure 3-45, the respective pyrograms are compared in Figure 6-6.

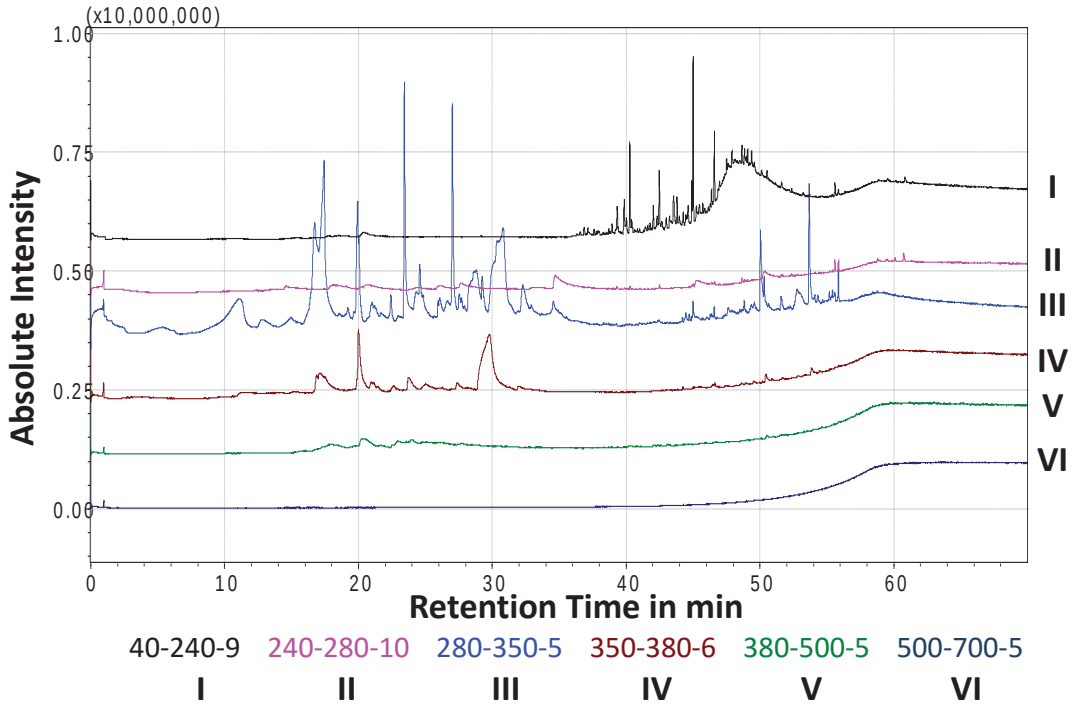

Figure 6-6. Pyrograms of the six pyrolysis zones in Figure 3-45. Samples that have a start temperature above 40 °C have previously been heated to their start temperature thus containing only the volatiles released in their respective pyrolysis range. The roman numerals refer to the pyrolysis zones in Figure 3-45. Legend: start temperature in °C-highest treatment temperature °C-run number.

Figure 6-6 clearly shows the formation of different pyrolysis products at different temperatures; explaining the changes in the smell of wood smoke observed with temperature, which is of particular interest for food smoking (Haris, 2012).

The two thermal desorption steps in a Double-Shot experiment were found to be additive till 350 °C apart from a few minor differences. This is illustrated in Figure 6-7 and Figure 6-8, where the pyrogram of sawdust heated from 40 to 280 °C contains the sum of the peaks observed in the chromatogram of the volatile fractions released between 40 to 240 °C and 240 to 280 °C, and the pyrogram of sawdust heated from 40 to 350 °C contains the sum of the peaks observed in the chromatogram of the volatile fractions released between 40 to 280 °C and 280 to 350 °C respectively.

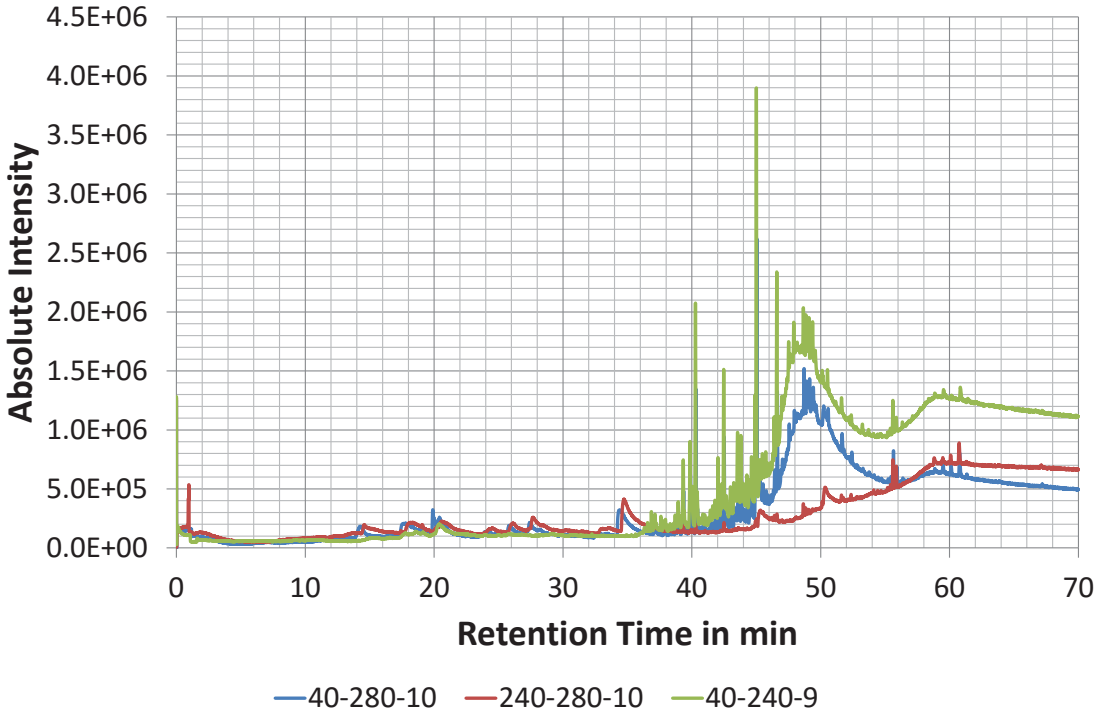

Figure 6-7. Open crucible pyrograms of pine sawdust pyrolysed from 40 to 280 °C, 240 to 280 °C, and 40 to 240 °C. The sample that has been pyrolysed from 240 to 280 °C was previously pyrolysed to 240 °C, therefore containing only the volatile fraction released between 240 to 280 °C. Legend: start temperature in °C-highest treatment temperature in °C-run number.

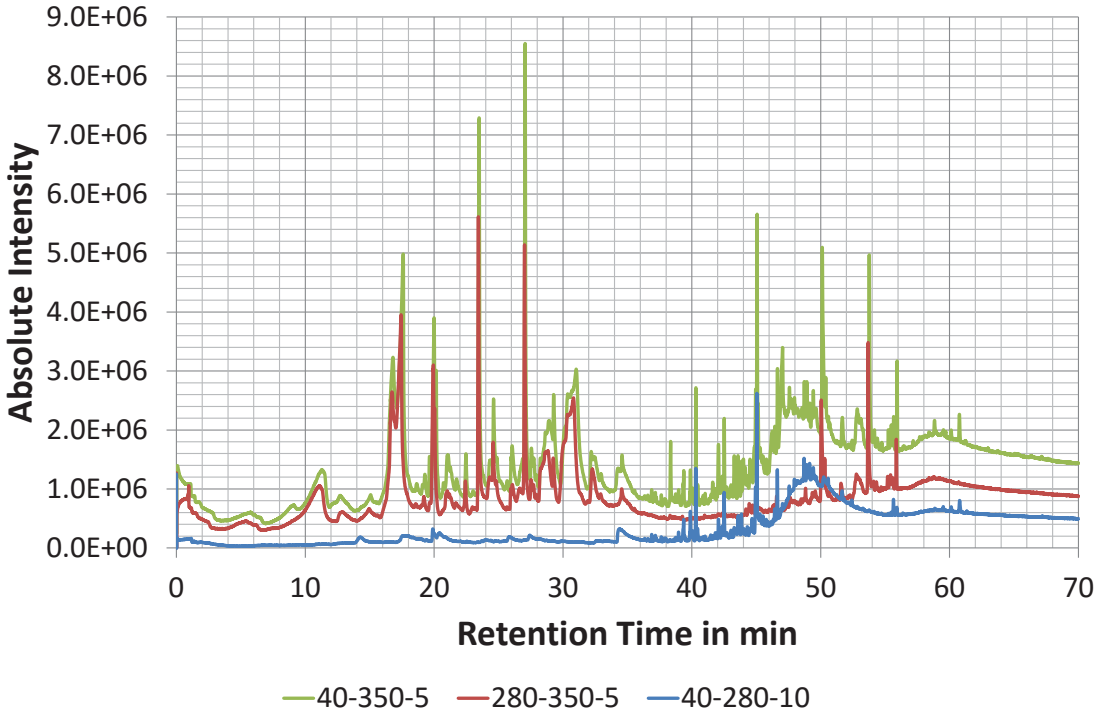

Figure 6-8. Open crucible pyrograms of pine sawdust pyrolysed from 40 to 350 °C, 280 to 350 °C, and 40 to 280 °C. The sample that has been pyrolysed from 280 to 350 °C was previously pyrolysed to 280 °C, therefore containing only the volatile fraction released between 280 to 350 °C. Legend: start temperature in °C-highest treatment temperature in °C-run number.

Above 350 °C the additivity is difficult to determine as the pyrograms of the volatile fraction released between 350 to 380 °C (Figure E-5 in Appendix E.1) and 380 to 500 °C (Figure E-7 in Appendix E.1) have a greatly reduced intensity compared to their sum pyrograms in Figure E-6 and Figure E-8 in Appendix E.1. This is illustrated in Figure 6-9 and Figure 6-10.

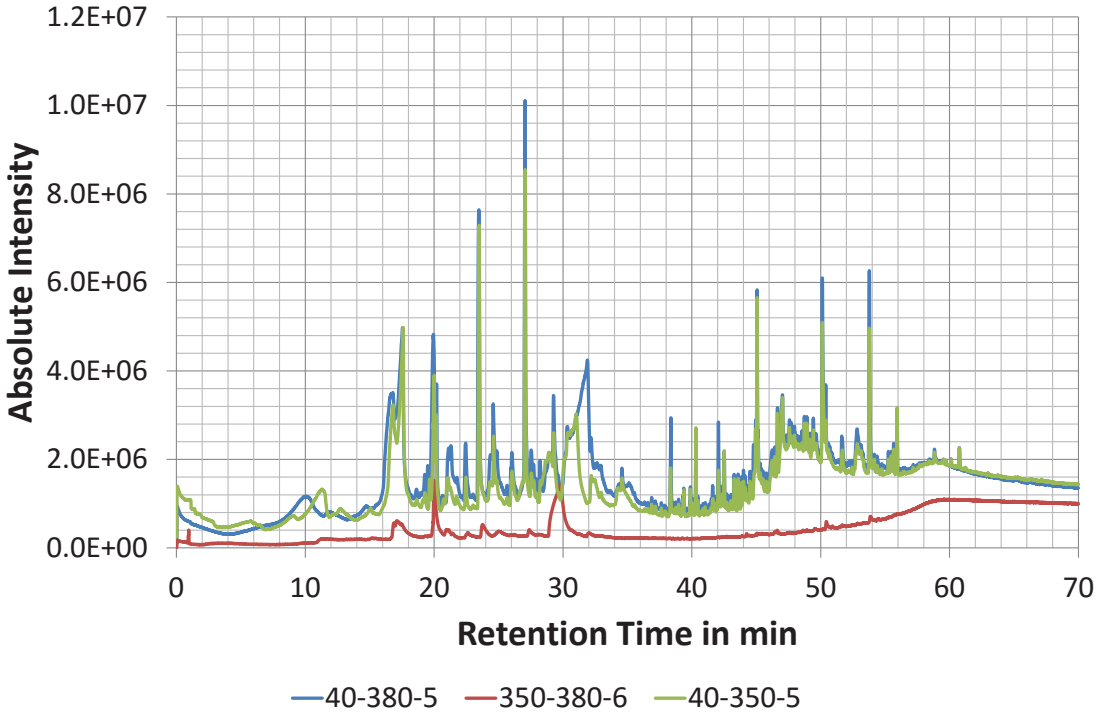

Figure 6-9. Open crucible pyrograms of pine sawdust pyrolysed from 40 to 380 °C, 350 to 380 °C, and 40 to 350 °C. The sample that has been pyrolysed from 350 to 380 °C was previously pyrolysed to 350 °C, therefore containing only the volatile fraction released between 350 to 380 °C. Legend: start temperature in °C-highest treatment temperature in °C-run number.

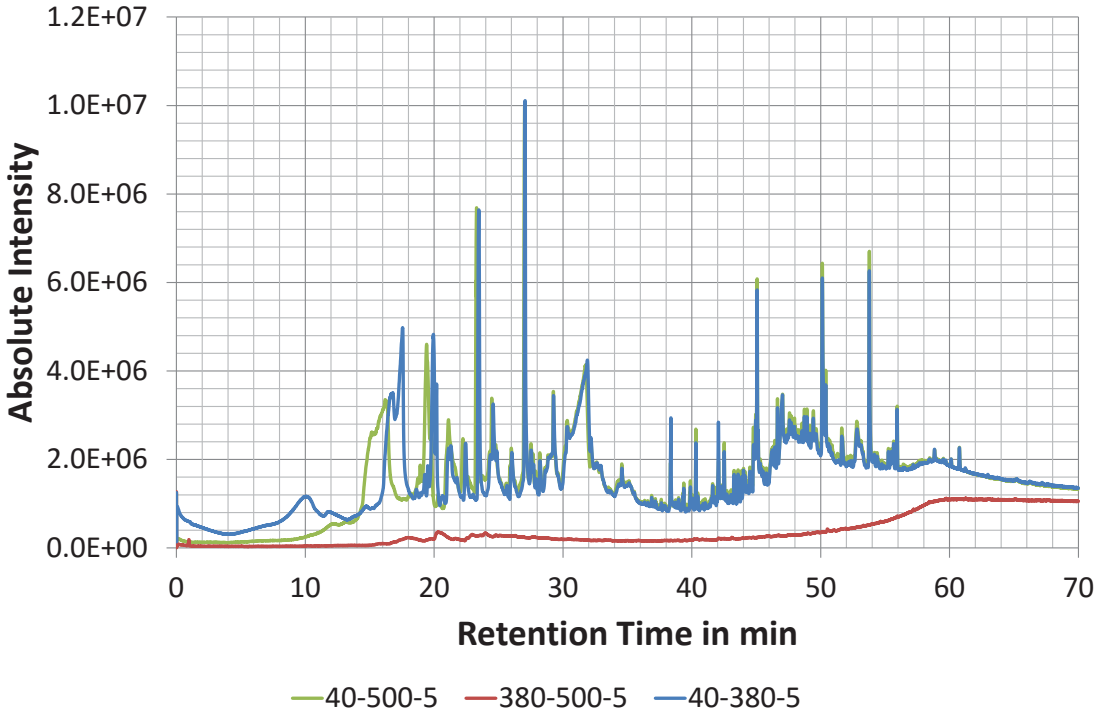

Figure 6-10. Open crucible pyrograms of pine sawdust pyrolysed from 40 to 500 °C, 380 to 500 °C, and 40 to 380 °C. The sample that has been pyrolysed from 380 to 500 °C was previously pyrolysed to 380 °C, therefore containing only the volatile fraction released between 380 to 500 °C. Legend: start temperature in °C-highest treatment temperature in °C-run number.

Furthermore, at the higher temperatures above 350 °C, the pyrograms change below an *Rt* of 27 min depending on the final pyrolysis temperature as shown in Figure 6-11.

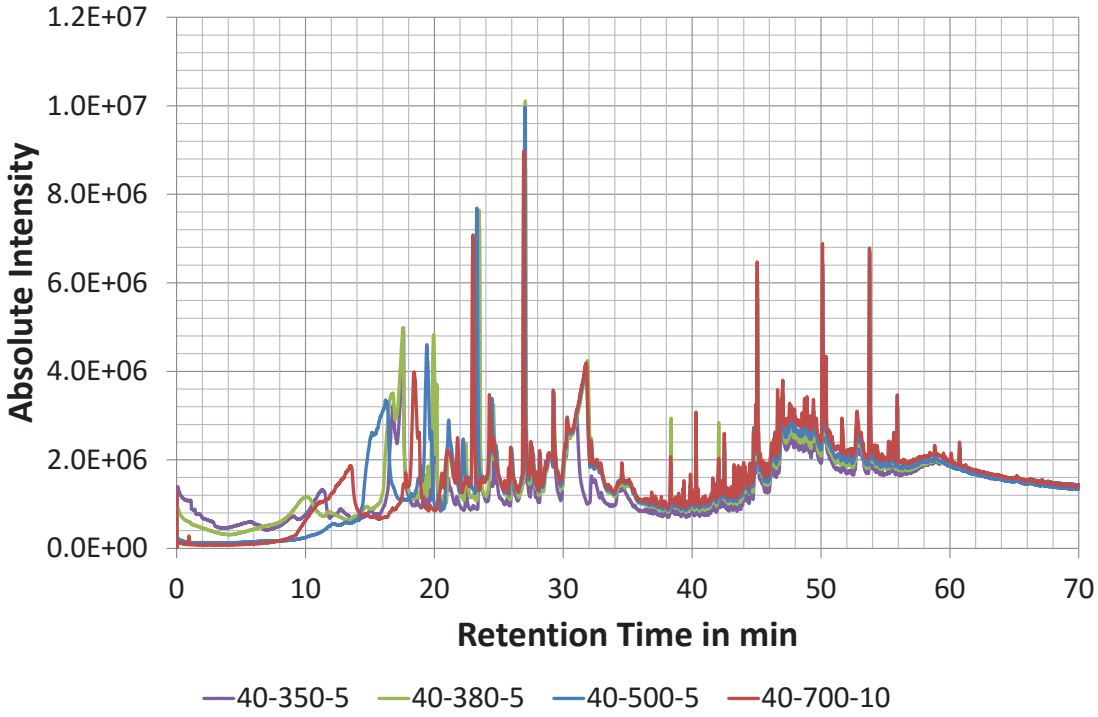

Figure 6-11. Comparison of pyrograms obtained by heating samples of pine wood from 40 °C to a highest treatment temperature of 350, 380, 500, and 700 °C respectively. Legend: start temperature in °C-highest treatment temperature in °C-run number.

The corresponding compound tables to Figure 6-11 are given in sheet “pine350-5”, “pine380-5”, “pine500-5” and “pine700-10” in Appendix E.3. The results show that with increasing pyrolysis temperature low molecular weight pyrolysis products are lost and the peaks at a low retention time shift to the left and widen. This indicates that if product identification is the aim of experiments lower pyrolysis temperatures are desired.

6.3.2 Sealed Glass Capsule Experiments

The aim of the sealed capsule (autogenous pressure) runs was to investigate the effect of secondary reactions on the volatile pyrolysis products. Contrary to the open crucible runs, these experiments provide intimate contact between the pyrolysing solid and the primary pyrolysis products, in particular the primary char and tar, enabling secondary reactions like cracking, re-polymerisation and re-condensation (Di Blasi, 2008; Z. Wang et al., 2009).

Before runs were carried out in the Online Micro Reaction Sampler, the glass capsules were pressure tested by varying the sample amount and pyrolysis temperature, Figure 6-12.

Figure 6-12. Glass capsule pressure test. The weights in the figure refer to the feedstock weight initially sealed in the respective capsule, and the subsequently stated temperature is the set point temperature to which the electric furnace was heated in the respective experiment. The picture on the right depicts the remnants of a broken capsule and the conditions which led to its destruction.

Figure 6-12 illustrates that 6 mg pine sawdust samples could be heated to 500 °C without breaking the glass capsules, and that heating to 700 °C caused the glass capsule to burst. Heating above 500 °C is not necessary as the open crucible runs showed that at this temperature mainly light pyrolysis gases are formed and bulk pyrolysis is over.

However, doing the actual sample run to 500 °C with 6 mg sawdust caused the ampoule to break before the heating profile was finished. The reason is that for pressure testing the ampoules were slightly longer than the maximum possible length inside the Online Micro Reaction Sampler. Therefore, the pyrolysis runs to 500 °C were repeated with 4.5 mg and 4.2 mg, which represent a sample loading of 0.05 g/ml and 0.04 g/ml respectively.

In contrast to the open crucible runs, two to three blank runs had to be carried out after each experiment to obtain a peak free chromatogram, which was necessary so that subsequent experiments were not affected by those before it. This was required as some of the volatile pyrolysis products condensed on cooler parts inside the furnace, like the crushing rod, once the capsule is crushed. This indicates the difficulty in detecting high molecular weight substances. Morgan and Kandiyoti (2013) discuss this in their review. They reported that only a small fraction of the volatile pyrolysis products is accessible for GC/MS analysis as a large portion consists of high boiling compounds that cannot travel through the column, because mass limits are 300 u and 500 u for aromatic and aliphatic compounds respectively. The former limit applies also for highly oxygenated, that is highly polar, substances (Pindoria et al., 1997). Z. Wang et al. (2009; 2010) also reported a large heavy tarry fraction that cannot be analysed by GC/MS. Heat sensitivity of molecules as well as coelution are further limitations (Morgan & Kandiyoti, 2013; Omais, Charon, Courtiade, Ponthus, & Thiébaut, 2013; Omais, Courtiade, Charon, Thiébaut, & Quignard, 2010). However, this study reported here was not aimed at completely resolving all the pyrolysis products, but rather at getting a glimpse of the secondary reactions taking place.

The pyrograms of sealed capsule runs heated from 60 to 240 °C are depicted in Figure 6-13.

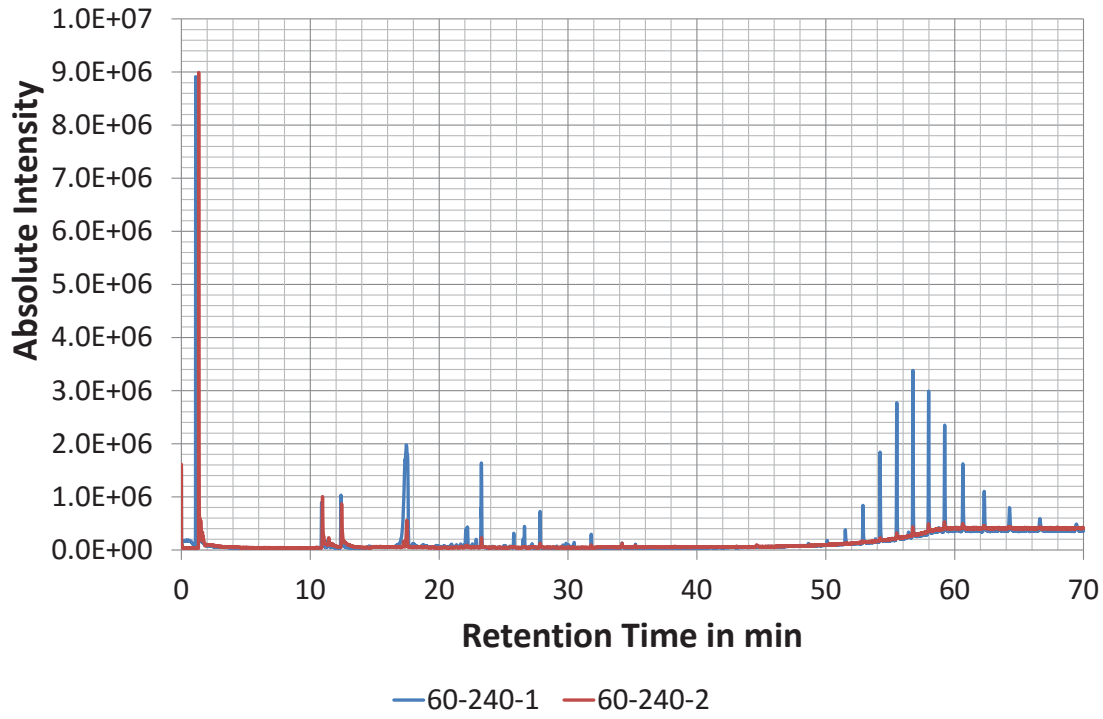

Figure 6-13. Pyrograms of pine sawdust heated in a sealed glass capsule from 60 to 240 °C. A compound list is given in the provided Excel file in Appendix E.3 in the sheet "A (60-240-1)" and "A (60-240-2)" for run "60-240-1" and "60-240-2" respectively. Legend: start temperature in °C-highest treatment temperature in °C-run number.

Figure 6-13 shows that the pyrograms are significantly different to the respective open crucible runs in Figure 6-4. The differences were consistent for the higher pyrolysis temperatures as can be seen by comparing Figure E-11 to Figure E-14 with Figure E-2, Figure E-4, Figure E-6 and Figure E-8 in Appendix E.2 and E.1 respectively. The corresponding compound tables are given in Appendix E.3.

In general the sealed capsule runs show more variability between runs than the open crucible experiments. The variation in peak intensity and compound presence between replicate runs is believed to be caused by varying sample loadings. That is, the weight varied by ± 0.1 mg for the 6 mg samples and by 0.3 mg for the capsule runs heated to 500 °C. This in combination with a varying capsule length due to manual flame sealing, which easily could vary by ± 2 mm, results in a sample loading difference of 0.01 g/ml. Mok, Antal, Szabo, Varhegyi, and Zelei (1992) discovered that this has an impact on pyrolysis, and needs to be investigated further. Another possibility is the inhomogeneity of the sample. However, this was also the case for the open crucible experiments and did not affect the results. Thus, it is believed to have a negligible role compared to the effect of sample loading. Despite those variations the pyrograms show overall similar patterns as illustrated in Figure 6-14.

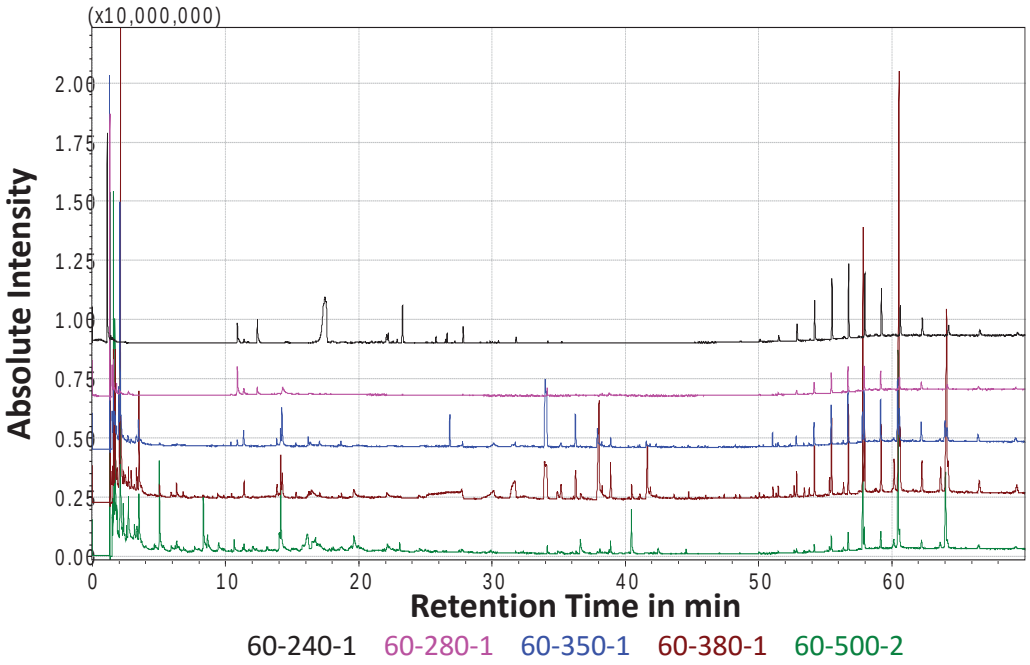

Figure 6-14. Comparison of pyrograms of pine sawdust heated in a sealed glass capsule from 60 to 240 °C, 60 to 280 °C, 60 to 350 °C, 60 to 380 °C, and 60 to 500 °C. Compound identification is given in sheet "A (60-240-1)", "A (60-280-1)", "A (60-350-1)", "A (60-380-1)", and "A (60-500-2)" in Appendix E.3 for run "60-240-1", "60-280-1", "60-350-1", "60-380-1", and "60-500-2" respectively. For all the experiments were 6 mg sawdust used except run "60-500-2" which used 4.2 mg due to the pressure limitation of the glass capsules. Legend: start temperature in °C-highest treatment temperature in °C-run number.

Run 2 was chosen for the pyrolysis run to 500 °C ("60-500-2") in Figure 6-14 as for some unknown reason the low molecular weight substances were absent in run 1 ("60-500-1") and compounds with a *Rt* below 20 min were shifted to lower *Rt's* (Figure E-14, and sheet "A (60-500-1)" and "A (60-500-2)" in Appendix E.2 and E.3 respectively).

The pyrograms in Figure 6-14 and the compound tables in Appendix E.3 show that the numbers of identified compounds increases with pyrolysis temperature due to the increasing severity of the pyrolysis reactions at higher temperatures. Again, as in the open crucible runs, the pyrograms with the highest *HTT* comprise more or less the compounds of the pyrograms at lower *HTT's*. When considered together Figure 6-13 and Figure 6-14 indicate that secondary reactions might be more dependent on pressure than temperature.

Figure 6-14 shows the formation of a distinctive set of compounds with a *Rt* smaller than ten minutes and a *Rt* above fifty minutes. The former compounds are characterised by low molecular weight substances. At 240 °C (sheet "A (60-240-1)"

and "A (60-240-2)" in Appendix E.3) these are pyrolysis gas, a branched alkene, and acetone (a ketone). They are joined by other ketones, cyclopentene (a cycloalkene), and furan, 2-methyl- (a furan derivative) at 280 °C (sheet "A (60-280-1)" in Appendix E.3). The proportion of these compound groups increases with increasing temperature (Figure 6-14), and at 350 °C (sheet "A (60-350-1)" and "A (60-350-2)" in Appendix E.3) are additionally present aldehydes, short chain alkene, ester, carboxylic acid, benzene derivative without oxygen, and terpenes. Again their amounts are increased at 380 °C, and newly detected are cycloalkane, and cycloketones (sheet "A (60-380-1)" and "A (60-380-2)" in Appendix E.3). At the final *HTT* of 500 °C (sheet "A (60-500-1)" and "A (60-500-2)" in Appendix E.3) short chain alkanes are also present.

The characteristic compound profile above a *Rt* of 50 min represents primarily long chain alkanes, alkenes, methylketones and alcohols (sheet "A (60-240-1)" to "A (60-500-2)" in Appendix E.3). Methylketones only start to appear at a temperature of 350 °C.

In the mid-range, *Rt* 10 min to 50 min, at a temperature of 240 °C (sheet "A (60-240-1)" and "A (60-240-2)" in Appendix E.3) are mainly terpenes, terpenoids, long chain alkanes, and silicon containing peaks from the column material present. This is also true for the pyrogram at 280 °C (sheet "A (60-280-1)" in Appendix E.3). At a temperature of 350 °C (sheet "A (60-350-1)" and "A (60-350-2)" in Appendix E.3) additionally appear alkyl substituted aromatics without oxygen (Cymene and Cymenene), methoxyl substituted aromatics (e.g. Creosol and 4-Ethylguaiacol), carboxylic acid (e.g. Diethyl Phthalate), and long chain methylketone. When the temperature is increased to 380 °C (sheet "A (60-380-1)" and "A (60-380-2)" in Appendix E.3) furan derivatives (e.g. 2-Acetyl-5-methylfuran) are detected, as well as a cycloketone (3,4,5-Trimethyl-2-cyclopenten-1-one). At the final *HTT* of 500 °C (sheet "A (60-500-1)" and "A (60-500-2)" in Appendix E.3) short chain alkanes and alkenes, and phenol derivatives with alkyl side chains (Methylphenol, Dimethylphenol and Trimethylphenol) are also present. Throughout all pyrograms a range of unidentified substances were present, as was the case in the open crucible experiments. The beginning of the pyrograms were characterised by pyrolysis gases and low molecular weight pyrolysis products, which can be derived from all of the biomass constituents.

Looking at all the compounds released at the different temperatures (sheet "A (60-240-1)" to "A (60-500-2)" in Appendix E.3), it is evident that the characteristic extractive, hemicellulose, cellulose and lignin decomposition profile with its typical markers, as discussed for the open crucible experiments, is absent. The extractives fraction that is primarily released before 240 °C, as seen in Figure 3-45 in 3.3.7, comprises in the sealed capsule experiments mainly of low molecular weight volatile organic compounds (e.g. .alpha.-Pinene *Rt* 10.877 min in sheet "A (60-240-1)" in Appendix E.3), compared to the large number of fused ring high molecular weight extractives like abietic acid (*Rt* 48.265 min in sheet "pine240-9" in Appendix E.3) found in the open crucible runs. The disappearance of these fused ring substances in the sealed capsule experiments reveals that they are reactants in secondary reactions or their formation is inhibited in the first place. No specific hemicellulose or cellulose markers are present. Although, diethyl phthalate (*Rt* 30.104 min in sheet "A (60-350-1)" in Appendix E.3), which has been reported in the literature in cellulose pyrolysis (S. Wang, Liao, Liu, Luo, & Cen, 2007), that has been identified in pyrograms from 350 °C onwards. It was not detected in the open crucible experiments indicating that it might be a secondary reaction product. Furan derivatives (e.g. Furan, 2-methyl- *Rt* 2.094 min in sheet "A (60-280-1)" in Appendix E.3) and ketones (e.g. 2,3-butanedione *Rt* 2.013 min in sheet "A (60-280-1)" in Appendix E.3) are the main non-specific carbohydrate markers, and start to appear at a temperature of 280 °C, indicating that holocellulose decomposition was taking place. As expected their number increases with pyrolysis temperature (sheet "A (60-350-1)" to "A (60-500-2)" in Appendix E.3). The first specific lignin markers (e.g. creosol *Rt* 19.980 min in sheet "A (60-350-1)" in Appendix E.3) appear at a *HTT* of 350 °C. Also present are alkyl substituted benzene derivatives (e.g. toluene *Rt* 5.033 min in sheet "A (60-350-1)" in Appendix E.3), which contain no oxygen. Y. Lu et al. (2012) generally attributed the benzene ring containing substances to lignin pyrolysis. However, benzene and phenol derivatives can also be derived from the carbohydrate decomposition as reviewed by Collard and Blin (2014) and mentioned with respect to the open crucible experiments in 6.3.1. For this reason the alkyl substituted aromatics have not been specifically assigned to any biomass constituent in this study. Phenol derivatives with alkyl side chains were not observed until a temperature of 500 °C (sheet "A (60-500-1)" and "A (60-500-2)" in Appendix E.3). In general, the amount of alkyl substituted aromatics and methoxyl substituted aromatics increases with pyrolysis temperature. PAHs (e.g. 2-Isopropyl-10-

methylphenanthrene *Rt* 42.551 min in sheet "A (60-380-2)" in Appendix E.3) start to appear, as in the open crucible runs, at 380 °C, and increase with temperature.

An interesting observation is that of the non methoxyl substituted aromatics the proportion of the phenols with alkyl groups is smaller than the alkyl substituted benzene derivatives without oxygen, which is contrary to the literature (W. Lu, Guo, Zhang, & Wang, 2013; W. Lu, Wang, & Yang, 2009; C. Wang et al., 2007; C. Wang, Pan, Li, & Yang, 2008) but goes along with the presence of alkyl substituted aromatics without oxygen at 350 °C and 380 °C, while the phenol derivatives without methoxyl groups were not detected till above 500 °C.

From a liquid fuel perspective, the long chain alkanes, alkenes and methylketones are the most interesting fraction. To illustrate their presence, the mass-to-charge ratio *m/z* 57+71, which is characteristic for alkanes but also for alkenes, alcohols and methylketones (P. Buurman, personal communication, March 4, 2013) is depicted in Figure 6-15 for the pyrograms with a *HTT* of 240 to 350 °C, and in Figure 6-16 for the pyrograms with a *HTT* of 380 to 500 °C.

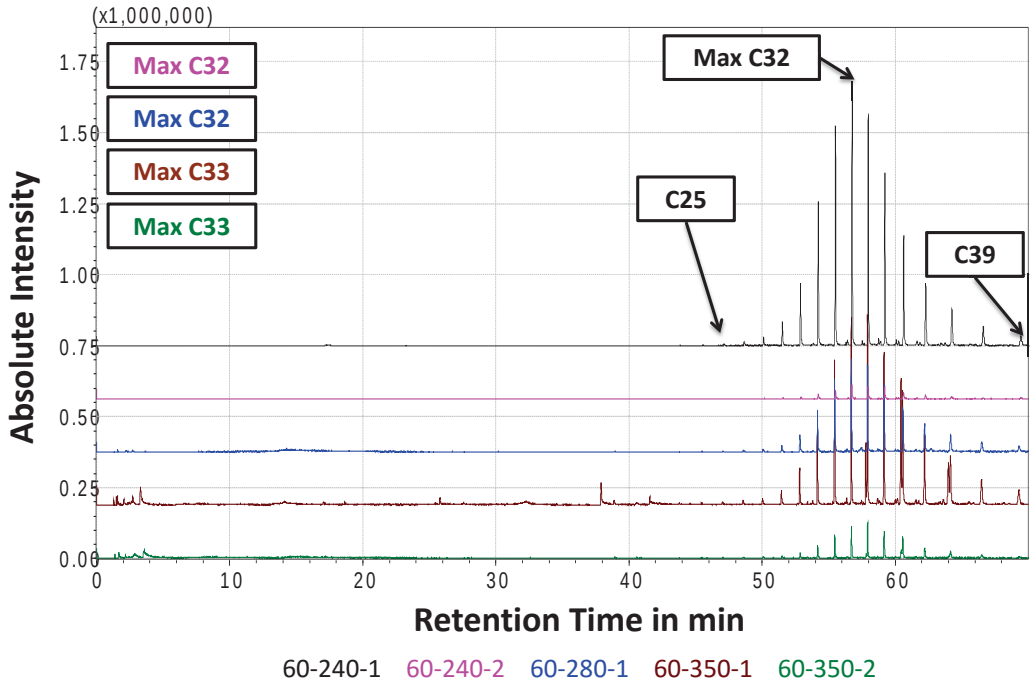

Figure 6-15. Mass Ion Chromatograms consisting of *m/z* 57+71 of sealed capsule experiments "60-240-1", "60-240-2", "60-280-1", "60-350-1", and "60-350-2". The mass-to-charge ratio *m/z* 57+71 is characteristic for alkanes but is also typical for alkenes, alcohols and methylketones (P. Buurman, personal communication, March 4, 2013). Legend: start temperature in °C-highest treatment temperature in °C-run number. C = Carbon chain length; Max = maximum; *m/z* = mass-to-charge ratio.

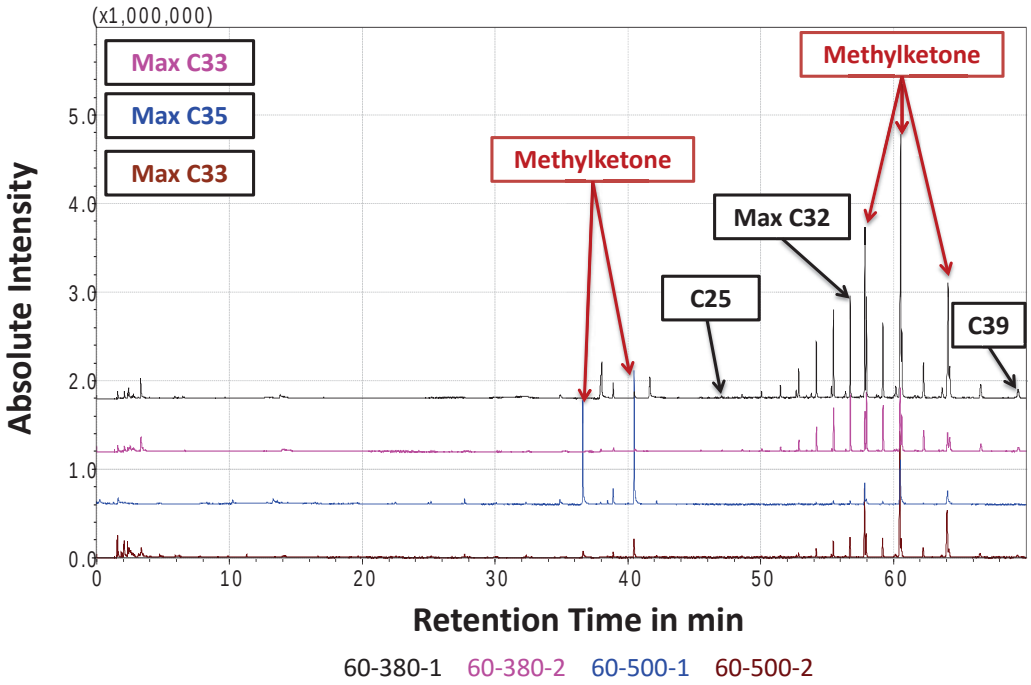

Figure 6-16. Mass Ion Chromatograms consisting of *m/z* 57+71 of sealed capsule experiments "60-380-1", "60-380-2", "60-500-1", and "60-500-2". The mass-to-charge ratio *m/z* 57+71 is characteristic for alkanes but is also typical for alkenes, alcohols and methylketones (P. Buurman, personal communication, March 4, 2013). It is important to note that the runs with *HTT* 380 °C employed a feedstock weight of 6 mg while runs "60-500-1" and "60-500-2" used 4.5 and 4.2 mg respectively due to the pressure limitation of the glass capsules. Legend: start temperature in °C-highest treatment temperature in °C-run number. C = Carbon chain length; *HTT* = highest treatment temperature; Max = maximum; *m/z* = mass-to-charge ratio.

Figure 6-15 and Figure 6-16 show that the majority of alkanes and alkenes appear in the *Rt* range 50 to 70 min, which corresponds to a carbon chain length of C_{27} to C_{39} (sheet "A (60-240-1)" to "A (60-500-2)" in Appendix E.3). The maximum alkane peak is observed at C_{32} (*Rt* 56.7-56.8 min) for run "60-240-1", "60-240-2" and run "60-280-1" in Figure 6-15, and run "60-380-1" in Figure 6-16. In run "60-350-1" and "60-350-2" in Figure 6-15, and run "60-380-2" and "60-500-2" in Figure 6-16 it was observed at C_{33} (*Rt* 57.9-58.0 min). The maximum was also observed at C_{35} (*Rt* 60.6 min) in experiment "60-500-1" in Figure 6-16. That the intensity of the *HTT* 500 °C runs in Figure 6-16 is slightly reduced compared to the other runs in Figure 6-15 and Figure 6-16 is due to the reduced weight that had to be applied because of the strength limitations of the glass capsules used. However, the above mentioned variation between the repeat runs, shown for example in Figure 6-13, is at least of the same magnitude.

The observed maximum alkane peak, C_{33} to C_{35} in Figure 6-15 and Figure 6-16, is much higher compared to literature, where C. Wang et al. (2007) observed it between

C_8 and C_{20}. Similar results have been reported by C. Wang et al. (2008). However, in these studies the carbon chain length did not continuously increase with *Rt* but fluctuated strongly. It is believed to be caused by the difficulty in detecting the molecular weight ion of long chain alkanes, alkenes and methylketones in the mass spectrum; but generally the chain length should increase with *Rt* (P. Buurman, personal communication, March 4, 2013). Thus, the result from this study is thought to be more accurate. Other reasons that could play a role are the different sample loading: both studies C. Wang et al. (2007; 2008) employed a sample loading of 0.64 g/ml mixed with an additional 15 % water, as well as the differing feedstocks, which were rice straw in C. Wang et al. (2007), and legume and wheat straw, and cotton and corn stalk in C. Wang et al. (2008). Nevertheless, as stated by C. Wang et al. (2007), the formation mechanism of these long-chain alkanes is not yet understood and requires further investigation.

Figure 6-15 and Figure 6-16 along with sheet "A (60-240-1)" to "A (60-500-2)" in Appendix E.3 show also that more short chain alkanes and alkenes were formed at higher temperatures above 350 °C but that their amount was negligible compared to the long-chain alkanes and alkenes.

The peaks in Figure 6-16 at a *Rt* of 36.6-36.8, 40.5-40.6, 57.8, 60.4-60.5, and 64.0-64.1 min are identified as C_{17}, C_{19}, C_{31}, C_{33}, and C_{35} methylketones (sheet "A (60-350-1)" to "A (60-500-2)" in Appendix E.3). To better illustrate the methylketones the mass-to-charge ratio *m/z* 58+59, which is characteristic for methylketones (P. Buurman, personal communication, March 4, 2013), is depicted in Figure 6-17 for the pyrograms with a *HTT* of 350 °C onwards, because this is the temperature where methylketones start to appear as discussed above.

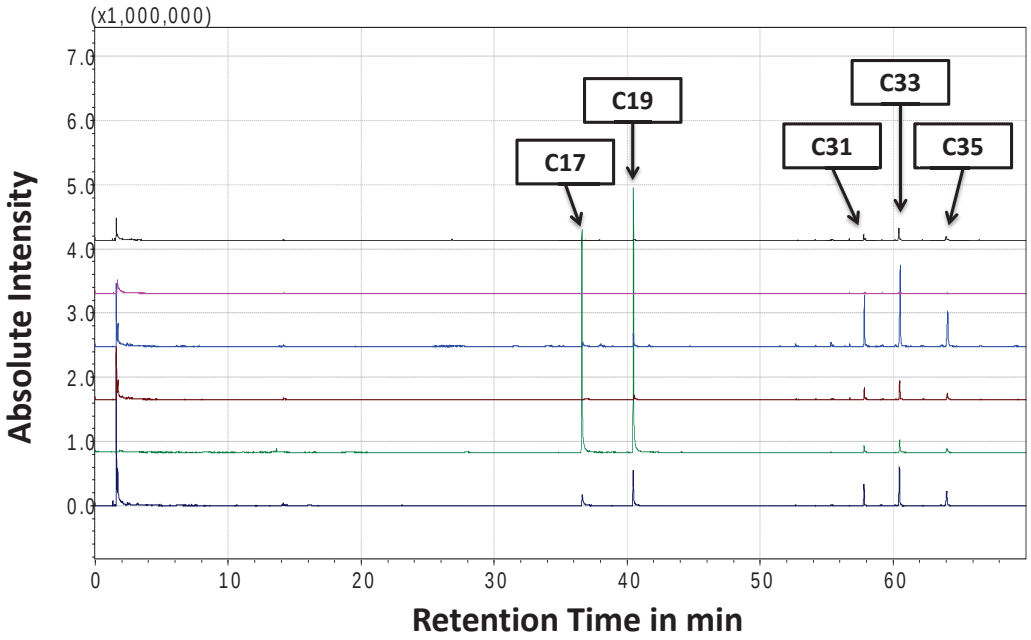

Figure 6-17. Mass Ion Chromatograms consisting of *m/z* 58+59 of sealed capsule experiments "60-350-1", "60-350-2", "60-380-1", "60-380-2", "60-500-1", and "60-500-2". The mass-to-charge ratio *m/z* 58+59 is characteristic for methylketones (P. Buurman, personal communication, March 4, 2013). It is important to note that the runs employed a feedstock weight of 6 mg except runs "60-500-1" and "60-500-2" used 4.5 and 4.2 mg respectively due to the pressure limitation of the glass capsules. Legend: start temperature in °C-highest treatment temperature in °C-run number. C = Carbon chain length; *m/z* = mass-to-charge ratio.

Figure 6-17 in combination with sheet "A (60-350-1)" to "A (60-500-2)" in Appendix E.3 reveals that methylketones with an uneven C number are dominant.

6.3.3 Comparison between Open Crucible and Sealed Capsule Experiments

As indicated above, exposing the pine samples to autogenous pressure during the course of pyrolysis changes the composition of the volatile pyrolysis products significantly. The findings of the open crucible and sealed capsule runs are summarised in Figure 6-18 for a *HTT* of 500 °C, as these pyrograms contain the substances detected in pyrograms at lower pyrolysis temperatures.

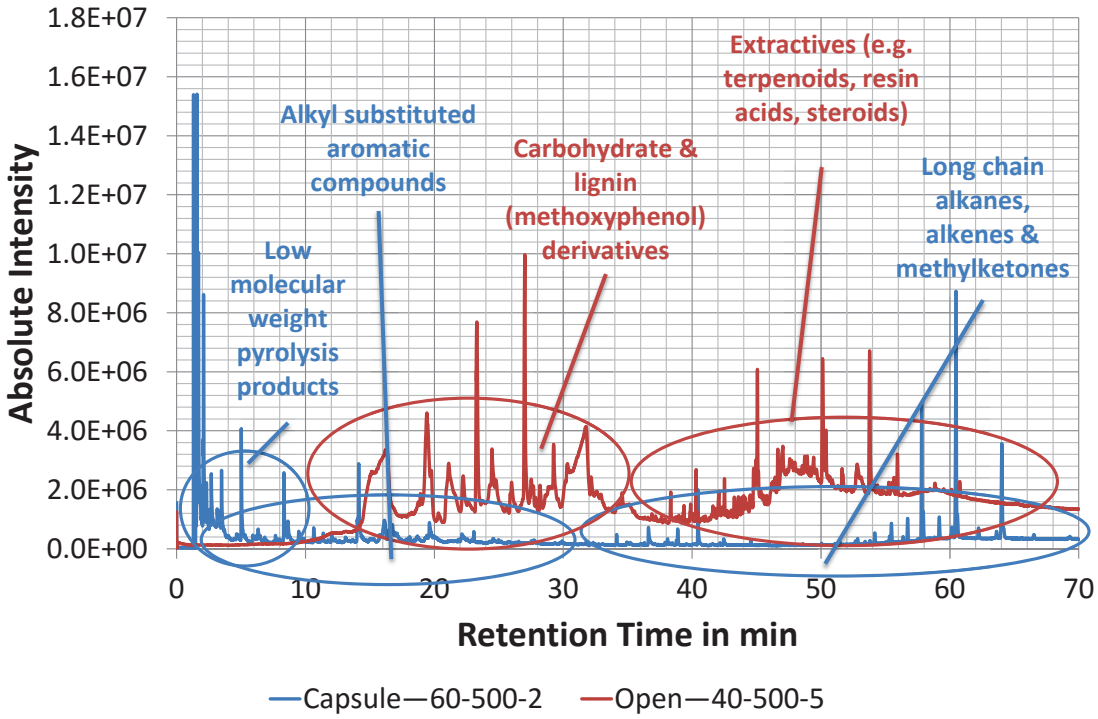

Figure 6-18. Comparison of pyrograms obtained by pyrolysing pine sawdust in sealed capsules and open crucibles in the temperature range 60 to 500 °C and 40 to 500 °C respectively. Compound lists are given in the provided Excel file in Appendix E.3 in the sheet "A (60-500-2)" and "pine500-5" for run "60-500-2" and "40-500-5" respectively. The open crucible run employed 6 mg sawdust while the sealed capsule experiment used 4.2 mg due to the pressure limitation of the glass capsules. Legend: start temperature in °C-highest treatment temperature in °C-run number.

Figure 6-18 shows that secondary reactions lead to the formation of low molecular weight pyrolysis products, alkyl substituted aromatics and long chain alkanes, alkenes and methylketones at the expense of extractives, carbohydrate, and lignin derivatives. As shown in Figure 6-14 these differences were similar for the different *HTT's*. The extractives in the open crucible experiments, *Rt* 36 to 61 min in Figure 6-18 were mainly released up to a *HTT* of 240 °C (Figure 6-4). Their constituents were identified to be largely high molecular weight fused ring compounds like resin acids and steroids. These classes of substances were almost entirely absent in the sealed crucible

pyrograms (Figure 6-13 and Figure 6-18). Instead, low molecular weight pyrolysis products (e.g. pyrolysis gases) were detected below an *Rt* of 10 min along with long chain alkanes, alkenes and alcohols above a *Rt* of 40 min. This implies that secondary reactions cause the side chains of those high molecular weight extractives to cleave resulting in the formation of low molecular weight pyrolysis products as well as the formation of long chain alkanes, alkenes and alcohols. The majority of the alkanes have a chain length ranging from C_{28} to C_{39} with the maximum being around C_{33}, Figure 6-15 and Figure 6-16. The reaction mechanism is not yet resolved (C. Wang et al., 2007), but it is possible that under these autogenous pressure conditions Fischer Tropsch type polymerisation reactions take place. The considerable difference in the presence of alkanes, alkenes, and at higher temperatures methylketones between open crucible and sealed capsule experiments is illustrated in Figure 6-19. It compares the MIC of *m/z* 57+71 of the primary volatiles released in pyrolysis zone V in Figure 3-45, which contains the majority of the alkanes and alkenes of the open crucible experiments, with the MIC's of the pyrograms of Figure 6-18 and the pyrogram of a sealed capsule experiment that has been heated to 240 C, as it appeared that at this temperature the majority of alkanes was formed.

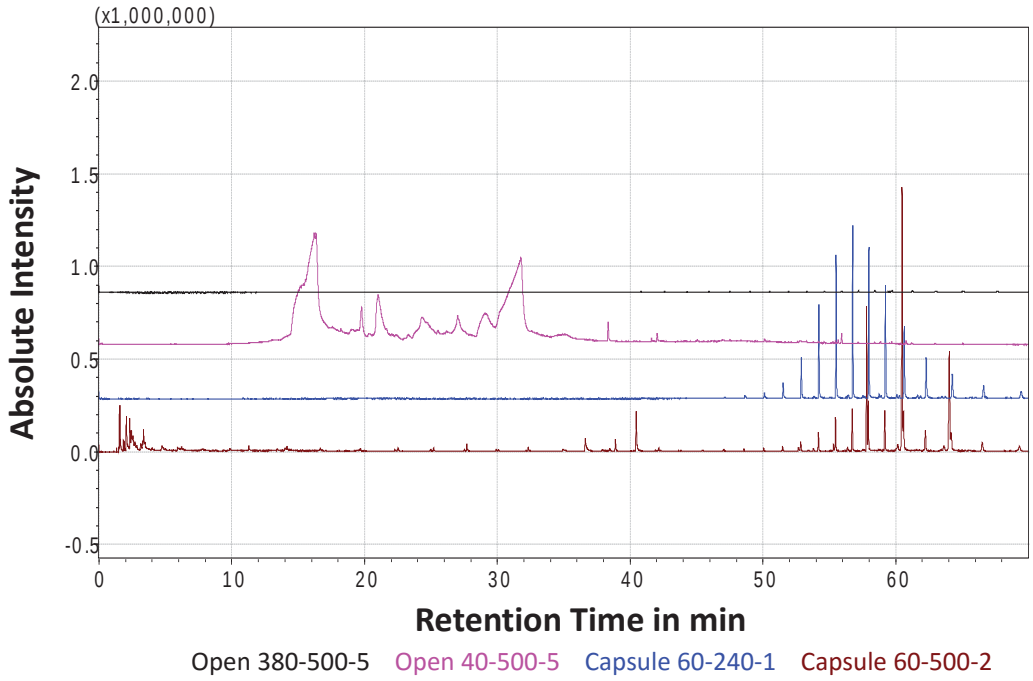

Figure 6-19. Comparison of Mass Ion Chromatograms consisting of *m/z* 57+71 of open crucible experiments "380-500-5" and "40-500-5" with the sealed capsule runs "60-240-1" and "60-500-2". The mass-to-charge ratio *m/z* 57+71 is characteristic for alkanes but is also typical for alkenes and methylketones (P. Buurman, personal communication, March 4, 2013). The sample in experiment "Open 380-500-5" has previously been heated to 380 °C thus containing only the volatiles released in the temperature range 380 to 500 °C. The open crucible runs and the sealed capsule experiment to 240 °C employed 6 mg sawdust while the sealed capsule experiment heated to 500 °C used 4.2 mg due to the pressure limitation of the glass capsules. Legend: start temperature in °C-highest treatment temperature in °C-run number. *m/z* = mass-to-charge ratio.

It is clearly visible in Figure 6-19 that the intensities of the peaks of alkanes, alkenes, and methylketones for the sealed capsule runs are substantially increased, even at a lower sample weight in the case of run "Capsule 60-500-2". This confirms that they are mainly secondary reactions products. It is important to note that the large peaks below a *Rt* of 40 min in the run "Open 40-500-5" in Figure 6-19 are not alkanes, alkenes, and methylketones as discussed in 6.3.1.

The findings of chapter 3 showed that already from the extractive fraction secondary char is formed. A higher char yield in parts of the feedstock with higher extractives contents has also been observed by Yu, Wang, Wang, and Yang (2011) despite having a lower lignin content, but their feedstock also had a high ash content, which could have had an impact (see chapter 4). Looking at the substances present in the extractives fraction, it is believed that secondary char is formed from the fused ring terpenoids. In the sealed capsule experiments low molecular weight volatile organic compounds like pinene were detected, which were absent in the open crucible runs but

are typical for pine wood (McDonald, Dare, Gifford, Steward, & Riley, 2002). The reason is believed to be that those compounds could not be retained in the column before GC/MS analysis started in the open crucible experiments, which commenced after the pyrolysis run was completed. However, in the sealed capsule experiment the GC/MS analysis took place immediately upon crushing the capsule in the sealed capsule experiments, which allowed the detection of substances that could not be retained in the column.

The large carbohydrate and lignin compound section in the open crucible runs, *Rt* 10 to 35 min in Figure 6-18, is formed between 240 °C and 500 °C. The vast majority of this portion is missing in the sealed capsule runs. Only non-specific carbohydrate markers remain, of which furan derivatives represent the majority. Also, the number of the typical lignin markers present is greatly reduced. Methoxyphenols that are still present in the sealed run in Figure 6-18 are guaiacol (*Rt* 16.490 min), creosol (*Rt* 19.617 min), 4-ethylguaiacol (*Rt* 22.142 min), and 4-propylguaiacol (*Rt* 24.546 min). Quantitatively they cannot be directly compared to the open crucible run in Figure 6-18, as the sample mass had to be reduced in the sealed capsule experiment due to the pressure limitation of the employed glass capsules. However, comparing their peaks in the open (guaiacol *Rt* 16.791 min, creosol *Rt* 19.943 min, 4-ethylguaicol *Rt* 22.437 min, and 4 propylguaiacol *Rt* 24.868 min) and sealed (guaiacol *Rt* 16.690 min, creosol *Rt* 19.799 min, 4-ethylguaicol *Rt* 22.433 min, and 4 propylguaiacol *Rt* 25.075 min) pyrograms that have been obtained by pyrolysis to 380 °C, shown in Figure 6-20, gives a good indication that their amount is greatly reduced in the sealed runs.

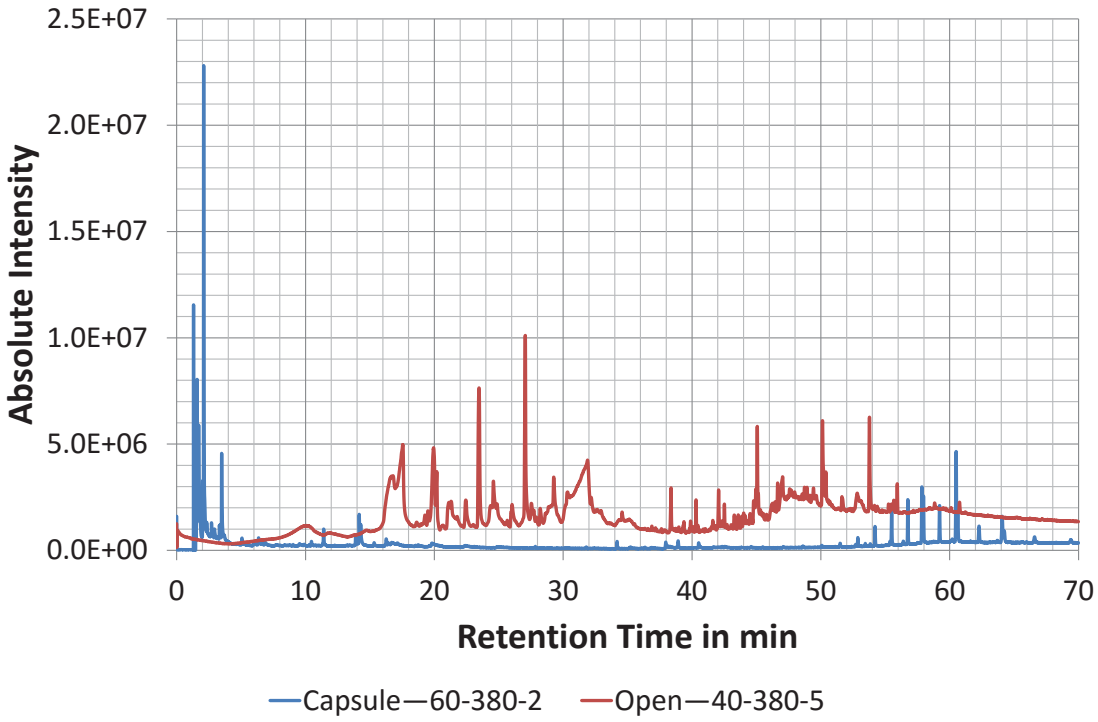

Figure 6-20. Comparison of pyrograms obtained by pyrolysing pine sawdust in sealed capsules and open crucibles in the temperature range 60 to 380 °C and 40 to 380 °C respectively. Compound lists are given in the provided Excel file in Appendix E.3 in the sheet "A (60-380-2)" and "pine380-5" for run "60-380-2" and "40-380-5" respectively. Both runs had a feedstock weight of 6 mg. Legend: start temperature in °C-highest treatment temperature in °C-run number.

The methoxyphenols that are still present (in greatly reduced quantity) in the sealed capsule experiments are only those with saturated side chains. The reason is the higher polymerisation reactivity of the methoxyphenols with unsaturated side chains like 4 vinylguaiacol and vanillin (Hosoya, Kawamoto, & Saka, 2008c; Hosoya et al., 2009a; Nakamura, Kawamoto, & Saka, 2007). This shows that carbohydrates and methoxyphenols are reactants in secondary reactions. Similar to the observations made for the extractives, their disappearance goes along with an increase in low molecular weight pyrolysis products, which continue to increase with *HTT*, Figure 6-14. Also the large portion of long chain alkanes, alkenes and alcohols remains present with additionally long chain methylketones appearing at a *HTT* of 350 °C. However, looking at Figure 6-15 and Figure 6-16, it appears that the long chain alkanes and alkenes start to decrease with increasing temperature indicating that they might originate merely from the decomposition of extractives, which has also been suggested in the literature (W. Lu et al., 2013; L. Wu, Guo, Wang, & Yang, 2009; Yu et al., 2011). However, Yu et al. (2011) found that alkane production exhibits a maximum for crofton weed at 425 to 450 °C after which it decreases. The high temperature of 425 to 450 °C indicates that

the alkanes do not solely originate from the extractives. This is supported by W. Lu et al. (2013), who state that the long chain hydrocarbons may also be formed from lignin (propyl group), hemicellulose (5-carbon-chain), and cellulose (6-carbon-chain). There is a larger presence of long chain alkanes and alkenes in the open crucible experiments in pyrolysis zone V (380 to 500 °C) compared to pyrolysis zone I (RT to 240 °C) giving further support to the hypothesis that they are not only derived from the extractives content. A decrease of alkanes with temperature could be due to aromatisation of alkanes (Yu et al., 2011), or fragmentation, which is supported by the appearance of short chain alkanes at a *HTT* of 500 °C, but which could also be due to fragmentation of other substances.

In the sealed capsule experiments alkyl substituted aromatics appear that contain no oxygen from a *HTT* of 350 °C, which increase in number with increasing *HTT*. Their *Rt* ranges from 5 to 30 min in Figure 6-18. To name a few, toluene (*Rt* 5.015 min), ethylbenzene (*Rt* 8.324 min), dimethylbenzene (*Rt* 8.640 and 9.476 min), cumene (*Rt* 10.640 min), ethyltoluene (*Rt* 12.049, 12.252, and 12.630 min), trimethylbenzene (*Rt* 13.101 and 14.015 min), and cymene (*Rt* 14.061 and 14.129 min), sheet "A (60-500-2)" in Appendix E.3. Again the large majority of the benzene derivatives contain saturated side chains, indicating their higher stability compared to unsaturated side chains. Alkyl substituted aromatics without oxygen were also present in the open crucible runs, sheet "pine240-9", "pine380-500-5" and "pine700-10" in Appendix E.3. However, they are mainly PAHs, and their number and amount is negligible compared to the sealed capsule runs.

At 500 °C phenol derivatives with alkyl side chains were detected in the sealed capsule runs. In Figure 6-18 these are methylphenols (*Rt* 15.761 and 16.662 min), dimethylphenols (*Rt* 18.400 and 18.686 min), and trimethylphenol (*Rt* 19.970 min), sheet "A (60-500-2)" in Appendix E.3 (same substances are present in sheet "A (60-500-1)" in Appendix E.3). Phenol derivatives with alkyl side chains were also identified in the open crucible pyrograms. There they start to appear in the volatile fraction released between 380 to 500 °C, sheet "pine380-500-5" in Appendix E.3. Again they are methylphenol (*Rt* 17.362 min) and dimethylphenol (*Rt* 19.647 min), as well as methylcatechol (*Rt* 23.851 min). Methylcatechols were also detected in the open crucible pyrograms of pyrolysis runs that have been carried out to a *HTT* of 500 and 700 °C, sheet "pine500-5" and "pine700-10" in Appendix E.3. It is difficult to

quantitatively judge whether or not they were present in a larger proportion in the sealed or open crucible experiments, particularly as the weight was smaller in the sealed capsule runs to 500 °C. However, looking at the respective peaks in the pyrogram in Figure E-14 and Figure E-7 in Appendix E.2 and E.1 respectively, and taking into account the slightly larger number of compounds of this class detected in the sealed runs in sheet "A (60-500-1)" and "A (60-500-2)" in Appendix E.3 (each 5) compared to the open runs in sheet "pine380-500-5" (3), "pine500-5" (2) and "pine700-10" (3) in Appendix E.3 it can be assumed that their presence is slightly more prevalent in the autogenous pressure runs. This suggests they could be secondary reaction products, which cannot be ruled out in the open crucible experiments as discussed 6.3.1. In the open crucible runs phenol (*Rt* 16.063 min) and catechol (*Rt* 23.352 min) were identified in the temperature range 380 to 500 °C (sheet "pine380-500-5" in Appendix E.3). Further, catechol has been detected in the sum pyrograms of the open crucible experiments heated to 350, 380, 500, and 700 °C (sheet "pine350-5" to "pine700-10" in Appendix E.3). Alkyl substituted phenols, phenols, and catechols are secondary reaction products as reported by Hosoya et al. (2008b, 2008c).

The phenol derivatives with alkyl groups and without methoxyl groups appear to be less common than the alkyl substituted aromatics that contain no oxygen. This is contrary to the observations in the deoxy-liquefaction studies in the literature (W. Lu et al., 2013; W. Lu et al., 2009; C. Wang et al., 2007; C. Wang et al., 2008), and other pyrolysis studies (Kantarelis, Yang, & Blasiak, 2013). These authors found a higher content of phenolic compounds than benzene compounds, which has been attributed to the high bond energy, 414 kJ/mol, of the hydroxyl group in phenol (W. Lu et al., 2013; C. Wang et al., 2007). The reasons why this study observed less alkyl substituted phenol derivatives are not obvious, but there were several differences. Here the heating rate was slower, 5 K/min compared to 10 K/min in C. Wang et al. (2007; 2008), or 80 K/min in W. Lu et al. (2013). However, C. Wang et al. (2007; 2008) employed a long holding time of 2 to 3 h at the *HTT*, which resulted in a longer vapour-phase residence time than in this study. Also, this study used a lower sample loading (0.04 to 0.06 g/ml) compared to 0.64 g/ml in C. Wang et al. (2007; 2008) and 0.51 g/ml in W. Lu et al. (2013). But one would expect that the higher sample loading with its higher resulting pressure has a higher potential to break bond c in Figure 6-21. Another marked difference between this study and others was the addition of water as a medium,

which was 15 % in C. Wang et al. (2007; 2008) and 20 % in W. Lu et al. (2013), but in this study were air dried samples with a moisture content of 9.3 % (wt/wt), Table 3-7 in 3.2.1.4, used. Of course, the difference in feedstock is also a probable cause. However, the deoxy-liquefaction studies employed a range of feedstock materials (W. Lu et al., 2013; C. Wang et al., 2007; C. Wang et al., 2008; L. Wu, Guo, Wang, & Yang, 2008; Yu et al., 2011), which lead to similar results indicating that this was probably not the determining factor. To establish the cause a more detailed analysis of all the pyrolysis products is required, especially the high molecular weight fraction that are not detectable by Py/GC-MS. Morgan and Kandiyoti (2013) report that GC-MS analysis of pyrolysis tars from sugar cane bagasse and eucalyptus imply that only a fraction ≤ 10 % of this tar is able to be analysed. This means that the results of this study reflect only a small portion of the volatile pyrolysis products. Thus, the findings regarding a possible oxygen loss have to be treated with caution as no knowledge is available about the heavier fraction like pyrolytic lignins. To get a definitive answer about the oxygen content elemental analysis of the liquid product is needed. This was done by the deoxy-liquefaction studies indicating that the oxygen loss in the GC-MS detectable fraction in this study might be able to be extrapolated to the non-detectable fraction. In order to carry out elemental analysis on the liquid products a larger experimental kit is required that supplies sufficient sample for analysis (addressed in chapter 8). Other methods for compound identification in the heavy, non GC-MS detectable, range have been discussed by Morgan and Kandiyoti (2013) but generally compound identification in this range is difficult.

6.3.4 Possible Reaction Mechanisms from the Literature Explaining the Observed Results

One of the main observations in 6.3.3 was the disappearance of the methoxyl substituted aromatics, and the formation of alkyl substituted phenols and benzenes. W. Lu et al. (2013) proposed a radical mechanism that starts with the demethylation, bond b in Figure 6-21, due to its low bond energy. Cleavage of O-CH_3 has also been reported by Hosoya et al. (2008b).

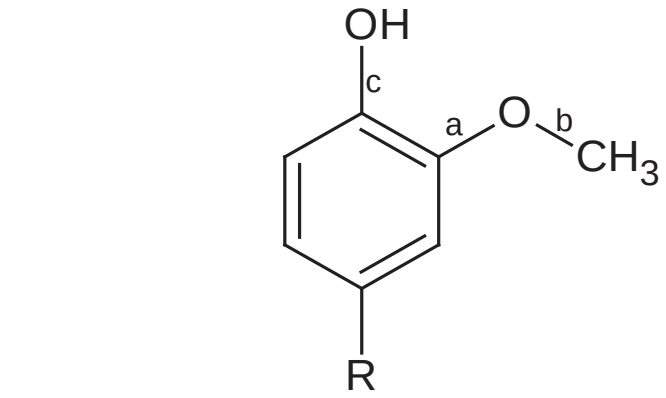

Figure 6-21. Bond energy in methoxyphenol. a, b, and c = bonds; R = rest. Adapted from W. Lu et al. (2013).

In a subsequent step W. Lu et al. (2013) suggest that the resulting phenoxy radical, PhO•, is intercepted by CO, a product of cellulose pyrolysis which is enhanced with residence time/ secondary reactions (Shen & Gu, 2009), resulting in the formation of a phenol radical, Ph•, and CO_2. This mechanism is supported by the findings of Gomez, Velo, Barontini, and Cozzani (2009), who reported the enhanced production of CO and CO_2 with increased secondary reactions. They state that CO is formed by two different mechanisms (a) it derives from the hydroxyl groups and oxygen atoms in the natural cell wall polymers and (b) it is formed as a cracking product during char formation, explaining its increased formation with secondary reactions. This demethoxylation reaction is not just limited to phenol as the disappearance of 6-methoxy-3-methylbenzofuran (sheet “pine280-350-5” and “pine350-380-6” in Appendix E.3) in the open crucible experiments suggests, while methylbenzofuran (sheet “A (60-380-1)”, “A (60-500-1)”, and “A (60-500-2)” in Appendix E.3) appears in the sealed capsule experiments.

The Ph• can then combine with hydrogen, methyl, ethyl, or propyl radicals to form alkyl substituted phenols (W. Lu et al., 2013). W. Lu et al. (2013) further state that the presence of benzene derivatives suggests that under the high temperature/ high pressure conditions enough energy is present to break bond c in Figure 6-21 that leads to the formation of alkyl substituted benzenes upon reaction with hydrogen, methyl or propyl radicals. In this study, the small amount of alkyl substituted phenols and benzenes present indicate that the former were changed into benzene radicals, which have reacted further to produce secondary char.

A slightly different mechanism has been proposed by Hosoya et al. (2009a), who developed it based on the observation that char formation is accompanied by the disappearance of the O-CH_3 group in the aromatic rings resulting from lignin decomposition (Hosoya et al., 2008b). Hosoya et al. (2009a) propose, for char formation, a radical induced reaction rather than homolysis, which leads to the formation of catechols and methane by abstracting hydrogen (Asmadi, Kawamoto, & Saka, 2011b). The formation of catechols is prevented in the scheme of W. Lu et al. (2013) due to the interception by CO, which resulted in the formation of the Ph•. In the mechanism of Hosoya et al. (2009a) the radical induced reaction leads to the formation of o-quinone methide as an intermediate, which can then polymerise through Diels-Alder type reactions to form char. Asmadi et al. (2011c, 2011d) refer to this char as first stage coke. A definition for the differentiation between char and coke is given by Asmadi, Kawamoto, and Saka (2011a), who state that char is defined as the methanol insoluble substance at the end of pyrolysis, which is found at the bottom of the capsule where the feedstock was originally placed, and coke is the methanol insoluble substance that stuck on the reactor wall. This was based on the fact that coke is usually referred to as the carbonaceous substance that is formed from low molecular weight volatile pyrolysis products (primary pyrolysis products) (Asmadi et al., 2011a). Therefore, Asmadi et al. (2011c, 2011d) referred to the char formed by the mechanism of Hosoya et al. (2009a) as coke as it is a secondary char forming mechanism that proceeds in the vapour-phase. However, this might not be entirely exact if one bases it on the definition of coke according to McNaught and Wilkinson (1997), who classify it as a high carbon containing solid in the nongraphitic state but of the graphitisable variety that has formed from, or at least in part, a liquid phase. In chapter 7 it is outlined that both chars, formed from the solid or volatiles, are believed to be of the non-graphtisable variety.

This outlines the importance of being cautious when it comes to comparing various studies, as different authors apply different definitions depending on the focus of their research, which has been already discussed in chapter 2. Here a simplistic definition of coke is used, that is, char formed from volatiles or a liquid (see chapter 2).

The o-quinone methide, as outlined by Hosoya et al. (2009a) and Asmadi et al. (2011d), can also form cresols and xylenols depending on the type of lignin. Asmadi et al. (2011d) show that these, in turn, can decompose to form CH_4, H_2, phenol, cresol, and second stage coke by a similar path via o-quinone methide. Second stage coke formation along with CH_4, and H_2 also occurs from catechols/ pyrogallols but via a different mechanism (Asmadi et al., 2011d), which they argue possibly involves a cyclopentadienyl radical (Khachatryan, Adounkpe, Maskos, & Dellinger, 2006; Marinov, Pitz, Westbrook, Castaldi, & Senkan, 1996; Marinov et al., 1998; Melius, Colvin, Marinov, Pit, & Senkan, 1996) as a reactive intermediate. They also report that this second stage coke formation is associated with the formation of PAHs (catechols/ pyrogallols form mainly biphenyl, naphthalenes, and phenanthrene; cresols/ xylenols form mainly xanthene and anthracene). Phenanthrenes and naphthalenes are the main PAHs detected in this study. Asmadi et al. also observed an increasing reactivity with additional substituent groups on phenol, and noted that the effect is larger for hydroxyl groups compared to methyl groups, meaning that the homolysis path of the mechanism of Hosoya et al. (2009a) yields more reactive substances than the rearrangement path with methyl substituted aromatics as products. This would explain why no catechols were present in the sealed capsule results while they were present in the open crucible results.

Hosoya et al. (2009a) further report that o-quinone methide is expected to be a key intermediate in the formation of primary char in the solid-phase as well, which was corroborated by Asmadi et al. (2011a) for the solid/ liquid phase. Asmadi et al. (2011a) give a good overview (as a schematic) of the vapour-phase and solid/ liquid-phase pathway of lignin pyrolysis. None of the xanthene derivatives, which are intermediates in the char formation mechanism of Hosoya et al. (2009a) have been detected in the sealed crucible experiments or the deoxy-liquefaction studies. Reasons could be the lower sample loading (0.002 g/ml) and the shorter residence time (80 s) applied by Hosoya et al., which means that these reactions were already completed under the conditions in this study and in the aforementioned deoxy-liquefaction studies. This is

supported by the presence in the open crucible pyrograms of a possible xanthene derivative 2-t-Butylxanthen-9-one (*Rt* 40.022 or 40.670 min in sheet "pine240-9", *Rt* 40.035 min in sheet "pine240-280-10", and *Rt* 40.032 min in sheet "pine700-10" in Appendix E.3 respectively). Furthermore, dibenzopyran-type structures (e.g. 6H-Dibenzo[b,d]pyran-6-one, 7,9-dihydroxy-3-methoxy-1-methyl-) were detected in the open crucible pyrograms (sheet "pine240-280-10", "pine280-350-5", and "pine700-10" in Appendix E.3) indicating the occurrence of Diels-Alder type reactions, and thus supporting the proposed mechanism of Hosoya et al. (2009a).

Hosoya et al. (2007c, 2008b, 2009a) report that the secondary char/ coke formation from lignin occurs in the vapour-phase which, they state, is contrary to secondary char/ coke formation from polysaccharides which occurs through condensation on cooler reactor parts. However, Hosoya et al. mention that this behaviour is different in wood samples compared to the isolated wood constituents due to both the ash content and the interaction between the constituent polymers in the wood (Hosoya, Kawamoto, & Saka, 2007a, 2007b, 2009b). Hosoya et al. (2009b) show that the interaction between cellulose and lignin occurs in the solid/liquid and vapour-phase. This agrees with the findings in this research, where ash was found to impact char formation during extended vapour-solid contact (see chapter 4) and in the liquid-phase (section 7.3.2).

Figure 6-12 shows similar phenomena as observed by Hosoya et al. (2007c), which lead to the conclusion that secondary char formation for lignin occurs in the vapour-phase and for polysaccharides, it occurs after condensation. It is important to note that the sample in Figure 6-12 was positioned at the bottom of the capsules but moved due to handling (when taking the photograph); and also that the entire capsule was positioned in the furnace during each run so that no temperature gradient was present. At low sample loading, slight deposition of secondary char/ coke was observed at the bottom of the capsule, where the sample was placed, which appeared more towards the top of the capsule (away from the sample) with increasing sample loading. This indicates secondary char formation from a liquid-phase after condensation at the top of the glass capsule at high sample loadings. The temperature gradient necessary for condensation to occur is believed to come from the exothermic nature of pyrolysis as shown in chapter 3 and 5, and by Mok et al. (1992), who report that the exothermic heat of reaction increased with sample loading in a sealed reactor. This explains the

increased char formation from a liquid-phase resulting from an increased temperature gradient due to an increased exothermic heat of reaction with higher sample loading. These findings support that secondary char/ coke formation is complex and involves vapour-phase and liquid-phase reactions. It would be interesting to know whether or not the secondary char/ coke formation from a liquid-phase in Figure 6-12 is merely a result of an existing temperature gradient and would otherwise form from the vapour-phase if the temperature gradient was absent under autogenous pressure conditions as this would provide information about the underlying reaction mechanism (e.g. necessity of a liquid phase for catalytic reactions). It seems that the sample loading does not have a large impact on the volatile pyrolysis products above a certain threshold as indicated by the similar results of this study (sample loading 0.04 to 0.06 g/ml) compared to the work of W. Lu et al. (2013) and C. Wang et al. (2007; 2008), who employed a sample loading of 0.51 and 0.64 g/ml respectively, indicating that the same secondary reactions occur. However, no data is available about the char/ coke and its characteristics. For this reason a pyrolysis experiment needs to be designed that allows the analysis of the char/ coke product as well. This is addressed in chapter 8.

Having a more detailed look at the polysaccharide reaction products, it becomes evident in Figure 6-18 that levoglucosan (*Rt* 31.766 min in sheet "pine500-5" in Appendix E.3), which is the major product of cellulose pyrolysis (Kawamoto, Murayama, & Saka, 2003; Patwardhan, Dalluge, Shanks, & Brown, 2011), is not present in the sealed capsule experiments. Kawamoto et al. (2003) proposed a reaction pathway for cellulose that explains the disappearance of levoglucosan by two concurrently occurring secondary reactions. These are (a) transformation into low molecular weight pyrolysis products and (b) ring-opening polymerisation into polysaccharides (the reaction is reversible), which is a key reaction for secondary char/ coke formation (Kawamoto et al., 2003). Kawamato et al. state that both reactions can proceed by similar mechanisms, e.g. dehydration and fragmentation, but that reaction (a) essentially forms volatile products by increasing the volatility, and reaction (b) leads to carbonisation as the non-volatile carbohydrates remain in the heated zone. That reaction (b) indeed occurs in the liquid/ solid-phase is corroborated by the work of Hosoya, Kawamoto, and Saka (2008a), who studied levoglucosan pyrolysis in a dual-space closed ampoule reactor. They found that, upon melting, liquid levoglucosan is subject to volatilisation and polymerisation, which are competing. Hosoya et al. further

explain that, if the volatile levoglucosan does not condense, it is decomposed/ gasified to CO and CO_2 by a radical chain reaction. The low molecular weight pyrolysis products like furfural, hydroxyacetone, and 5-hydroxymethylfurfural, which are formed during the liquid/ solid-phase polymerisation of levoglucosan, prevent its decomposition in the vapour-phase by H-donation, quenching the radical chain reaction (Hosoya et al., 2008a). This in turn allows the levoglucosan in the gas phase to condense and form secondary char/ coke. Those H-donating aldehydes also derive from the pyrolysis of hemicellulose, which commences earlier than the formation and volatilisation (estimated boiling point 300 °C (Milosavljevic, Oja, & Suuberg, 1996)) of levoglucosan. Furthermore, under autogenous pressure, volatilisation of the pyrolysis products is inhibited due to a higher pressure, which promotes polymerisation and thus char/ coke formation. The above description illustrates the complicated interplay between physical processes, chemical reactions, and the different pyrolysis products.

Similar interactions are anticipated for the products of the other biomass constituents. Small amounts of levoglucosan also derive from the pyrolysis of glucomannan (Alén et al., 1996; Branca, Di Blasi, Mango, & Hrablay, 2013; Hosoya et al., 2007c). Glucomannans, that is, hemicelluloses, are reported to form higher char yields than cellulose due to their higher mineral contents and their amorphous nature, which allows rearrangement reactions to take place forming a more reticulated solid matrix leading to a higher char yield as reviewed by Collard and Blin (2014) and discussed in 3.3.8. Cellulose, which consists of both crystalline and amorphous zones (Shen & Gu, 2009), produces less char as the crystalline fraction mainly undergoes depolymerisation reactions that occur due to the cleavage of the glycosidic linkages resulting in the production of levoglucosan (Collard & Blin, 2014). After condensation the depolymerisation products can then undergo rearrangement reactions forming a reticulated solid matrix and thus secondary char/ coke as observed by Hosoya et al. (2007c). The fact that secondary char/ coke formation of polysaccharides requires a condensation step also renders the possibility of an ionic mechanism (Evans & Milne, 1987; Mamleev, Bourbigot, Le Bras, & Yvon, 2009; Shafizadeh, 1982).

In general the findings with respect to carbohydrate derived pyrolysis products agree with the literature in that secondary reactions lead to the disappearance of:

- anhydromonosaccharides (Kawamoto et al., 2003; Patwardhan et al., 2011), e.g. 1,4:3,6-Dianhydro-.alpha.-d-glucopyranose *Rt* 20.915 min, 3,4-Anhydro-d-galactosan *Rt* 21.030 min, 2,3-Anhydro-d-mannosan *R*t 21.646 min, 3,4-Anhydrohexopyranose *Rt* 27.010 min, levoglucosan *Rt* 31.766 min, and 1,6-Anhydro-.alpha.-d-galactofuranose *Rt* 32.611 min in Figure 6-18 and sheet "pine500-5" in Appendix E.3 respectively;
- other pyran derivatives, e.g. Maltol *Rt* 16.910 min, and 3,5-Dihydroxy-2-methyl-4H-pyran-4-one *Rt* 20.314 min in Figure 6-18 and sheet "pine500-5" in Appendix E.3 respectively; and
- furan derivatives with aldehyde, hydroxyl, and carbonyl groups (W. Lu et al., 2013; Patwardhan et al., 2011; S. Wang, Guo, Liang, Zhou, & Luo, 2012), e.g. 5-Hydroxymethyl furfural *Rt* 22.481 min, and 2(3H)-Furanone, dihydro-4-hydroxy- *Rt* 21.025 min in Figure 6-18 and sheet "pine500-5" in Appendix E.3 respectively, 2-Furaldehyde (furfural) *Rt* 11.378 min, and 2-Furan methanol (furfuryl alcohol) *Rt* 12.370 min in Figure E-1 and sheet "pine240-280-10" in Appendix E.3 respectively.

The loss of these substances goes along with an increase in low molecular weight pyrolysis products as discussed above, which indicates the decomposition of primary pyrolysis products of carbohydrates into low molecular weight compounds and gases (Patwardhan et al., 2011; S. Wang et al., 2012). Another major path, responsible for the loss of anhydrosugars, is the oligomerisation of the anhydrosugars (Patwardhan et al., 2011), which was discussed above for levoglucosan using the mechanism of Kawamoto et al. (2003). The decrease in pyran derivatives (non-aromatic ring) can be explained by their lower stability compared to furan rings (aromatic ring) (S. Wang et al., 2012). S. Wang et al. (2012) state that the first linear intermediates are formed from the pyran ring by cleavage of the C-O bond, which subsequently form furans by cyclisation along with low molecular weight products like acetic acid, which has been detected in the sealed capsule experiment in Figure 6-18 (*Rt* 2.815 min in sheet "A (60-500-2)" in Appendix E.3). While acetic acid was not detected in the open crucible run in Figure 6-18 it was identified in the open crucible experiments in the temperature range 240 to 280 °C (sheet "pine240-280-10" in Appendix E.3), and 280 to 350 °C (sheet "pine280-350-5" in Appendix E.3) showing that these reactions also occurred in the open crucible runs, along with the formation of furans, e.g. furfural and 5-hydroxymethylfurfural.

However, acetic acid is also a fragmentation product of the acetyl groups from hemicellulose (Collard & Blin, 2014; Peng & Wu, 2010; Prins, Ptasinski, & Janssen, 2006; Shen, Gu, & Bridgwater, 2010a) explaining its presence below 350 °C, which is the main hemicellulose decomposition range. The secondary decomposition of acetic acid at higher temperatures into gases has been reported by Peng and Wu (2010). The formation of furan rings from pyran rings in the solid phase along with the release of furans in the vapour-phase has also been discussed in a review by Collard and Blin (2014). They report that char is formed from the solid cellulose matrix by dehydration reactions and cyclisation, and that this cyclisation can be accompanied by oxygen loss resulting in the formation of furan rings in the solid-phase. During this process some of the glycosidic linkages can be ruptured causing the formation of the typical furan derivatives, like 5-hydroxymethylfurfural, in the vapour-phase (Collard & Blin, 2014). Thus, the higher stability of furans, and their formation from the solid-phase/ liquid-phase explains their presence in the sealed capsule runs while the pyran derivatives disappear.

The vanishing of the furan derivatives with aldehyde, hydroxyl, and carbonyl groups like 5-Hydroxymethyl furfural has been attributed to the secondary decomposition into low molecular weight pyrolysis products and non-condensable gases by Patwardhan et al. (2011). They based this on the work of Girisuta, Janssen, and Heeres (2006), who showed that acid catalysed decomposition of 5-hydroxymethylfurfural leads to the formation of formic acid and levulinic acid. However, none of these substances have been identified in the pyrograms of this study which could indicate that they were further decomposed to CO and other gaseous species (Patwardhan et al., 2011). The relatively large proportion of furan derivatives detected in the sealed capsule experiments with alkyl side chains without hydroxyl, aldehyde or carbonyl groups (e.g. Furan, 2-methyl-*Rt* 2.090 min in sheet "A (60-500-2)" in Appendix E.3) suggests the cleavage of these functional groups due to secondary reactions leading to the presence of small chain compounds like acetone (*Rt* 1.575 min in sheet "A (60-500-2)" in Appendix E.3). This pathway is supported by the findings that furfural is a decomposition product of 5-hydroxymethylfurfural (S. Wang et al., 2012). Shen and Gu (2009) state that this is due to the dehydroxymethylation reaction of the side chain of 5-hydroxymethylfurfural leading to the formation of furfural and formaldehyde. Another possible reaction of 5-hydroxymethylfurfural is

decarbonylation leading to the formation of furfuryl alcohol and CO (Shen & Gu, 2009). If both reactions take place in sequence furan is obtained, which has been detected in Figure 6-18 at *Rt* 1.580 min (sheet "A (60-500-2)" in Appendix E.3) in the sealed capsule experiment but was missing in all the open crucible experiments (sheet "pine240-9" to "pine500-5" in Appendix E.3). The formation of furan along with CO, vinyl acetylene, vinyl ketene and benzene from 5-hydroxymethylfurfural has been reported by Shin, Nimlos, and Evans (2001) showing that both gaseous species and furan can be decomposition products of 5-hydroxymethylfurfural. The formation of benzene suggests a possible char formation pathway. This shows that furan and furan derivatives with alkyl side chains are secondary reaction products, which might be subject to further decomposition (Grela, Amorebieta, & Colussi, 1985) under more severe conditions (temperature and pressure), but this requires more research.

The formation of the long chain methylketones with uneven carbon number at a temperature above 350 °C require further investigation, as their formation mechanism is currently unknown. The formation of the long chain alkanes and alkenes, which are already formed from the extractives section at 240 °C is also unknown. In general, not much is known about the reactions of the extractives under autogenous pressure.

It is import to add that aromatic compounds (phenol and benzene derivatives) not only derive from the thermal degradation of lignin but can also originate from holocellulose decomposition as reviewed by Collard and Blin (2014). C. Wang et al. (2008) state that under the extreme conditions in deoxy-liquefaction (350 °C and 12 to 13 MPa) aromatic compounds are possibly formed by dehydration, deoxygenation, condensation or cyclisation reactions from cellulose. Other sources of aromatic compounds could be dehydrogenation reactions of extractive compounds. The formation of p- and o-cymene along with 1,2,4- and 1,2,3-trimethylbenzene from catalytic dehydrogenation of pinane has been reported by Pines, Olberg, and Ipatieff (1948). If similar reactions occur under autogenous pressure pyrolysis has to be investigated. If so, it supports the conclusion that all four biomass constituents (extractives, hemicellulose, cellulose, and lignin) form char/ coke.

Overall, the results of this study support the mechanisms given in the literature, as discussed above. These indicate that oxygen is removed from the condensable volatiles under autogenous pressure, for which a good overview of possible reactions is

given by W. Lu et al. (2013). However, the exact reaction mechanisms remain unknown due to the complexity of the processes and reactions involved. In particular research is required looking at the formation of long chain alkanes, alkenes, and methylketones. It appears that it is likely that there exists a mix of radical reaction mechanisms (e.g. char/ coke formation from lignin pyrolysis products, which can proceed in the vapour-phase (Hosoya et al., 2009a)) and (liquid-phase) ionic mechanisms (Dufour, Ouartassi, Bounaceur, & Zoulalian, 2011; Mamleev et al., 2009; Shafizadeh, 1982), which are both catalysed by either acid (chapter 4) or base catalysis (Antal, Leesomboon, Mok, & Richards, 1991; Evans & Milne, 1987; Mamleev et al., 2009; Ponder & Richards, 1993; Zhang, Li, Yang, & Blasiak, 2011). Furthermore, secondary char/ coke is formed from all biomass constituents.

The presence of inorganics is expected to affect the volatile product composition, where the results in chapter 4 revealed that they increase the char yield by catalysing secondary reactions. This has been shown to be true by Nowakowski and Jones (2008), who demonstrated that K impregnation in the case of cellulose and levoglucosan (cellulose model compound and intermediate product) leads to the decomposition of levoglucosan and other anhydrosugars, and the formation of cyclopenten derivatives and phenol derivatives, which agrees with the here analysed effect of increased vapour-phase residence time. (Compare the open and sealed crucible pyrograms in Appendix E.3.) Nowakowski and Jones attribute this to a base catalysed heterolytic mechanism supporting the conclusion that the overall pyrolysis mechanism consists of homolytic and heterolytic reactions. Similarly, analogies exist in the case of lignin pyrolysis with K impregnation (*ibid*) and the here observed effect of vapour-phase residence time, which lead to the decrease or disappearance of some methoxyl compounds. Nowakowski and Jones also used chlorogenic acid, a model compound for lignin, and discovered that the presence of K promoted secondary reactions. Their findings support the hypothesis in chapter 4 that inorganics catalyse secondary reactions, and that the majority of char is formed from secondary reactions (see chapter 3). Unfortunately, due to the time constraints of this research it was not possible to repeat the in this chapter outlined experiments with the impregnated samples in chapter 4, which is advised for future research as it would give more insight into the catalysis mechanism and secondary reactions.

6.4 Conclusions

The open crucible pyrograms in this study were found to agree with the literature. The analysis of the six pyrolysis zones established in chapter 3 revealed that the volatiles released up till a temperature of 240° C (zone I) originate primarily from the extractives content of radiata pine wood, which confirms the findings of chapter 3. The major extractive compound was identified as abietic acid, which is the isomerisation product of levopimaric acid. The compounds determined in zone II and III (240 to 350 °C) agree with the well-established fact that the shoulder of the derivative weight curve between 240 and 350 °C is associated with hemicellulose decomposition. The cellulose markers increased over this temperature range and subsequently decreased in zone IV (350 to 380 °C) highlighting that the peak of the derivative weight curve at ≈ 353 °C is related to the decomposition of cellulose. Typical lignin markers (mainly from the guaiacyl-type, which is the building block of softwood lignin) were detected in zone I to V (240 to 500 °C) showing that lignin decomposes over the whole pyrolysis range. These findings confirm the decomposition regions stated in the literature for the biomass constituents (hemicellulose, cellulose and lignin). Additionally, a small fraction of long chain alkanes and alkenes appeared to be formed at temperatures between 380 and 500 °C (zone V), although smaller intensities were detected in the extractives fraction. Above 500 °C (zone VI) only light pyrolysis gases (CO, CO_2, H_2 and CH_4) were detected revealing that the main pyrolysis is finished at this temperature, and that the released gases are a consequence of ongoing charring processes (rearrangement and fragmentation reactions in the solid). Overall, the pyrograms of the six different pyrolysis zones illustrate very clearly the formation of different pyrolysis products at different temperatures explaining, for example, the changes in the smell of wood smoke observed with temperature.

The two thermal desorption steps in a Double-Shot experiment were found to be additive except that above 350 °C the pyrograms change below a *Rt* of 27 min depending on the final pyrolysis temperature. This means that, with increasing pyrolysis temperature, low molecular weight pyrolysis products are lost and the peaks at a low retention time shift to the left and widen. This indicates that if product identification is the aim of experiments, lower pyrolysis temperatures are desired.

The pyrograms of the sealed capsule experiments revealed that autogenous pressure changes the composition of volatile pyrolysis products significantly to form the low molecular weight products, alkyl substituted aromatic compounds, long chain alkanes, alkenes and methylketones, at the expense of extractives, carbohydrate and lignin derivatives. The characteristic extractive, hemicellulose, cellulose and lignin decomposition profile with its typical markers, as discussed for the open crucible experiments, is not present anymore. The methoxyl substituted aromatics, typical for lignin decomposition, disappear while alkyl substituted aromatics appear, indicating oxygen loss in the condensable fraction. This was also evidenced in the fraction of the non methoxyl substituted aromatics, where the proportion of the phenols with alkyl groups is smaller than the alkyl substituted benzene derivatives without oxygen. It was found that the side chains in the autogenous pressure experiments are saturated showing that the less stable unsaturated side chains are more reactive during secondary reactions (i.e., they have higher polymerisation reactivities). The majority of the detected alkanes and alkenes were found to have a carbon chain length of C_{27} to C_{39} with the maximum alkane peak being between C_{33} to C_{35}. The methylketones, which started to appear at 350 °C, consisted primarily of uneven C numbers (C_{17}, C_{19}, C_{31}, C_{33}, and C_{35}). These changes are due to the action of secondary reactions which, this research shows, take place over the entire pyrolysis range, ≈ 140 to 500 °C, concurrently to primary reactions. This confirms the results in chapter 3. Furthermore, it appears that secondary reactions are more a function of vapour-phase concentration than temperature (in contrast to the open crucible experiments in the sealed capsule experiments the pyrograms obtained at varying *HTT's* are similar), and involve all major wood components, i.e. extractives, hemicellulose, cellulose, and lignin. The discussed findings support the conclusion that secondary reactions are a set of cracking, depolymerisation, and re-polymerisation reactions. Similar to the open crucible experiments the numbers of identified compounds were observed to increase with pyrolysis temperature in the sealed capsule experiments due to the increasing severity of these pyrolysis reactions at higher temperatures.

In both experiments, open crucibles and sealed capsules, PAHs started to appear at 380 °C and then increased with temperature, which could be related to the ongoing charring process.

The results of this study along with the proposed mechanisms in the literature indicate that oxygen is removed from the condensable volatiles under autogenous pressure but the exact reaction mechanisms remain unknown due to the complexity of the processes and reactions involved. In particular, research is required to look at the formation of long chain alkanes, alkenes, and methylketones, and the secondary reactions of the extractives fraction. It seems likely that there exists a mix of homolytic and heterolytic reaction mechanisms during biomass pyrolysis, and that secondary char/ coke is formed from all biomass constituents (extractives, hemicellulose, cellulose, and lignin). When comparing the autogenous pressure results with the literature, it appears that there is a threshold above which the sample loading does not affect the composition of the volatile pyrolysis products, but more research is required which also considers the gas and solid products.

Overall, this chapter shows that autogenous pressure experiments are invaluable for studying pyrolysis and the development of a pyrolysis mechanism.

6.5 References

Alén, R., Kuoppala, E., & Oesch, P. (1996). Formation of the main degradation compound groups from wood and its components during pyrolysis. *Journal of Analytical and Applied Pyrolysis, 36*(2), 137-148. doi:10.1016/0165-2370(96)00932-1

Anderson, K. B., & Winans, R. E. (1991). Nature and fate of natural resins in the geosphere. I. Evaluation of pyrolysis-gas chromatography mass spectrometry for the analysis of natural resins and resinites. *Analytical Chemistry, 63*(24), 2901-2908. doi:10.1021/ac00024a019

Antal, M. J., Leesomboon, T., Mok, W. S., & Richards, G. N. (1991). Mechanism of formation of 2-furaldehyde from d-xylose. *Carbohydrate Research, 217*, 71-85. doi:10.1016/0008-6215(91)84118-X

Antonio, J. (n.d.). *Column Bleed - what is it and what does it really mean?* Retrieved December 15, 2013, from http://www.truepr.co.uk/news/sgeuk/0506/003.asp

Arias, M. E., Polvillo, O., Rodríguez, J., Hernández, M., González-Pérez, J. A., & González-Vila, F. J. (2006). Thermal transformations of pine wood components under pyrolysis/gas chromatography/mass spectrometry conditions. *Journal of Analytical and Applied Pyrolysis, 77*(1), 63-67. doi:10.1016/j.jaap.2005.12.013

Asmadi, M., Kawamoto, H., & Saka, S. (2011a). Gas- and solid/liquid-phase reactions during pyrolysis of softwood and hardwood lignins. *Journal of Analytical and Applied Pyrolysis, 92*(2), 417-425. doi:10.1016/j.jaap.2011.08.003

Asmadi, M., Kawamoto, H., & Saka, S. (2011b). Pyrolysis and secondary reaction mechanisms of softwood and hardwood lignins at the molecular level. *Green Energy and Technology, 66*, 129-135. doi:10.1007/978-4-431-53910-0_16

Asmadi, M., Kawamoto, H., & Saka, S. (2011c). Thermal reactions of guaiacol and syringol as lignin model aromatic nuclei. *Journal of Analytical and Applied Pyrolysis, 92*(1), 88-98. doi:10.1016/j.jaap.2011.04.011

Asmadi, M., Kawamoto, H., & Saka, S. (2011d). Thermal reactivities of catechols/pyrogallols and cresols/xylenols as lignin pyrolysis intermediates. *Journal of Analytical and Applied Pyrolysis, 92*(1), 76-87. doi:10.1016/j.jaap.2011.04.012

Babu, B. V. (2008). Biomass pyrolysis: A state-of-the-art review. *Biofuels, Bioproducts and Biorefining, 2*(5), 393-414. doi:10.1002/bbb.92

Biagini, E., & Tognotti, L. (2014). A generalized procedure for the devolatilization of biomass fuels based on the chemical components. *Energy & Fuels, 28*(1), 614-623. doi:10.1021/ef402139v

Branca, C., Di Blasi, C., Mango, C., & Hrablay, I. (2013). Products and kinetics of glucomannan pyrolysis. *Industrial & Engineering Chemistry Research, 52*(14), 5030-5039. doi:10.1021/ie400155x

Brown, R. C. (2009). Biochar production technology. In J. Lehmann & S. Joseph (Eds.), *Biochar for environmental management: Science and technology* (pp. 127-146). London, England, United Kingdom: Earthscan.

Collard, F.-X., & Blin, J. (2014). A review on pyrolysis of biomass constituents: Mechanisms and composition of the products obtained from the conversion of cellulose, hemicelluloses and lignin. *Renewable and Sustainable Energy Reviews, 38*, 594-608. doi:10.1016/j.rser.2014.06.013

Di Blasi, C. (2008). Modeling chemical and physical processes of wood and biomass pyrolysis. *Progress in Energy and Combustion Science, 34*(1), 47-90. doi:10.1016/j.pecs.2006.12.001

Dobele, G., Rossinskaja, G., Dizhbite, T., Telysheva, G., Meier, D., & Faix, O. (2005). Application of catalysts for obtaining 1,6-anhydrosaccharides from cellulose and wood by fast pyrolysis. *Journal of Analytical and Applied Pyrolysis, 74*(1–2), 401-405. doi:10.1016/j.jaap.2004.11.031

Dobele, G., Rossinskaja, G., Telysheva, G., Meier, D., & Faix, O. (1999). Cellulose dehydration and depolymerization reactions during pyrolysis in the presence of phosphoric acid. *Journal of Analytical and Applied Pyrolysis, 49*(1–2), 307-317. doi:10.1016/S0165-2370(98)00126-0

Dufour, A., Ouartassi, B., Bounaceur, R., & Zoulalian, A. (2011). Modelling intra-particle phenomena of biomass pyrolysis. *Chemical Engineering Research and Design, 89*(10), 2136-2146. doi:10.1016/j.cherd.2011.01.005

Egenberg, I. M., Aasen, J. A. B., Holtekjølen, A. K., & Lundanes, E. (2002). Characterisation of traditionally kiln produced pine tar by gas chromatography-mass spectrometry. *Journal of Analytical and Applied Pyrolysis, 62*(1), 143-155. doi:10.1016/S0165-2370(01)00112-7

Egenberg, I. M., Holtekjølen, A. K., & Lundanes, E. (2003). Characterisation of naturally and artificially weathered pine tar coatings by visual assessment and gas chromatography-mass spectrometry. *Journal of Cultural Heritage, 4*(3), 221-241. doi:10.1016/S1296-2074(03)00048-7

Evans, R. J., & Milne, T. A. (1987). Molecular characterization of the pyrolysis of biomass. 1. Fundamentals. *Energy & Fuels, 1*(2), 123-137. doi:10.1021/ef00002a001

Evanson, U. (2012). *GC/MS analysis of volatile species formed during the pyrolysis of wood* (Unpublished final year project report). Massey University, Palmerston North, New Zealand. The report can be accessed by contacting J.R.Jones@massey.ac.nz

Faix, O., Bremer, J., Meier, D., Fortmann, I., Scheijen, M. A., & Boon, J. J. (1992). Characterization of tobacco lignin by analytical pyrolysis and Fourier transform-infrared spectroscopy. *Journal of Analytical and Applied Pyrolysis, 22*(3), 239-259. doi:10.1016/0165-2370(92)85017-F

Fiebach, K., & Grimm, D. (2000). Resins, Natural. In *Ullmann's encyclopedia of industrial chemistry* (Vol. 31, pp. 478-494). Weinheim, Germany: Wiley-VCH Verlag.

Frontier Laboratories Ltd. (2011). *Stainless steel capillary column. Ultra Alloy* [Brochure]. Fukushima, Japan: Author.

Frontier Laboratories Ltd. (n.d.). *Multi-Shot Pyrolyser model EGA/PY-3030D operation manual* (Version 1.10) [Operation manual]. Retrieved from Fukushima, Japan: http://www.frontier-lab.com/manual/en/EGA_PY-3030D_E.pdf

Gao, N., Li, A., Quan, C., Du, L., & Duan, Y. (2013). TG–FTIR and Py–GC/MS analysis on pyrolysis and combustion of pine sawdust. *Journal of Analytical and Applied Pyrolysis, 100*(0), 26-32. doi:10.1016/j.jaap.2012.11.009

Girisuta, B., Janssen, L. P. B. M., & Heeres, H. J. (2006). A kinetic study on the decomposition of 5-hydroxymethylfurfural into levulinic acid. *Green chemistry, 8*(8), 701-709. doi:10.1039/b518176c

Gomez, C., Velo, E., Barontini, F., & Cozzani, V. (2009). Influence of secondary reactions on the heat of pyrolysis of biomass. *Industrial & Engineering Chemistry Research, 48*(23), 10222-10233. doi:10.1021/ie9007985

Grela, M. A., Amorebieta, V. T., & Colussi, A. J. (1985). Very low pressure pyrolysis of furan, 2-methylfuran and 2,5-dimethylfuran. The stability of the furan ring. *The Journal of Physical Chemistry, 89*(1), 38-41. doi:10.1021/j100247a011

Grieco, E., & Baldi, G. (2011). Analysis and modelling of wood pyrolysis. *Chemical Engineering Science, 66*(4), 650-660. doi:10.1016/j.ces.2010.11.018

Grønli, M. G., Várhegyi, G., & Di Blasi, C. (2002). Thermogravimetric analysis and devolatilization kinetics of wood. *Industrial & Engineering Chemistry Research, 41*(17), 4201-4208. doi:10.1021/ie0201157

Haris, N. A. (2012). *Smoke generator for food smoking* (Unpublished final year project report). Massey University, Palmerston North, New Zealand. The report can be accessed by contacting J.R.Jones@massey.ac.nz

Hosoya, T., Kawamoto, H., & Saka, S. (2006). Oxime-trimethylsilylation method for analysis of wood pyrolysate. *Journal of Analytical and Applied Pyrolysis, 77*(2), 121-126. doi:10.1016/j.jaap.2006.02.009

Hosoya, T., Kawamoto, H., & Saka, S. (2007a). Cellulose-hemicellulose and cellulose-lignin interactions in wood pyrolysis at gasification temperature. *Journal of Analytical and Applied Pyrolysis, 80*(1), 118-125. doi:10.1016/j.jaap.2007.01.006

Hosoya, T., Kawamoto, H., & Saka, S. (2007b). Influence of inorganic matter on wood pyrolysis at gasification temperature. *Journal of Wood Science, 53*(4), 351-357. doi:10.1007/s10086-006-0854-8

Hosoya, T., Kawamoto, H., & Saka, S. (2007c). Pyrolysis behaviors of wood and its constituent polymers at gasification temperature. *Journal of Analytical and Applied Pyrolysis, 78*(2), 328-336. doi:10.1016/j.jaap.2006.08.008

Hosoya, T., Kawamoto, H., & Saka, S. (2008a). Different pyrolytic pathways of levoglucosan in vapor- and liquid/solid-phases. *Journal of Analytical and Applied Pyrolysis, 83*(1), 64-70. doi:10.1016/j.jaap.2008.06.008

Hosoya, T., Kawamoto, H., & Saka, S. (2008b). Pyrolysis gasification reactivities of primary tar and char fractions from cellulose and lignin as studied with a closed ampoule reactor. *Journal of Analytical and Applied Pyrolysis, 83*(1), 71-77. doi:10.1016/j.jaap.2008.06.002

Hosoya, T., Kawamoto, H., & Saka, S. (2008c). Secondary reactions of lignin-derived primary tar components. *Journal of Analytical and Applied Pyrolysis, 83*(1), 78-87. doi:10.1016/j.jaap.2008.06.003

Hosoya, T., Kawamoto, H., & Saka, S. (2009a). Role of methoxyl group in char formation from lignin-related compounds. *Journal of Analytical and Applied Pyrolysis, 84*(1), 79-83. doi:10.1016/j.jaap.2008.10.024

Hosoya, T., Kawamoto, H., & Saka, S. (2009b). Solid/liquid- and vapor-phase interactions between cellulose- and lignin-derived pyrolysis products. *Journal of Analytical and Applied Pyrolysis, 85*(1-2), 237-246. doi:10.1016/j.jaap.2008.11.028

Kang, B.-S., Lee, K. H., Park, H. J., Park, Y.-K., & Kim, J.-S. (2006). Fast pyrolysis of radiata pine in a bench scale plant with a fluidized bed: Influence of a char separation system and reaction conditions on the production of bio-oil. *Journal of Analytical and Applied Pyrolysis, 76*(1–2), 32-37. doi:10.1016/j.jaap.2005.06.012

Kantarelis, E., Yang, W., & Blasiak, W. (2013). Production of liquid feedstock from biomass via steam pyrolysis in a fluidized bed reactor. *Energy & Fuels, 27*(8), 4748-4759. doi:10.1021/ef400580x

Kawamoto, H., Murayama, M., & Saka, S. (2003). Pyrolysis behavior of levoglucosan as an intermediate in cellulose pyrolysis: Polymerization into polysaccharide as a key reaction to carbonized product formation. *Journal of Wood Science, 49*(5), 469-473. doi:10.1007/s10086-002-0487-5

Khachatryan, L., Adounkpe, J., Maskos, Z., & Dellinger, B. (2006). Formation of cyclopentadienyl radical from the gas-phase pyrolysis of hydroquinone, catechol, and phenol. *Environmental Science & Technology, 40*(16), 5071-5076. doi:10.1021/es051878z

Khelfa, A., Bensakhria, A., & Weber, J. V. (2013). Investigations into the pyrolytic behaviour of birch wood and its main components: Primary degradation mechanisms, additivity and metallic salt effects. *Journal of Analytical and Applied Pyrolysis, 101*, 111-121. doi:10.1016/j.jaap.2013.02.004

Kirwan, C. (2013). *Analysis of secondary char formation during the pyrolysis of pinus radiata* (Unpublished final year project report). Massey University, Palmerston North, New Zealand. The report can be accessed by contacting J.R.Jones@massey.ac.nz

Lourenço, A., Gominho, J., marques, A. V., & Pereira, H. (2012). Variation of lignin monomeric composition during Kraft pulping of eucalyptus globulus heartwood and sapwood. *Journal of Wood Chemistry and Technology, 33*(1), 1-18. doi:10.1080/02773813.2012.703284

Lourenço, A., Gominho, J., Marques, A. V., & Pereira, H. (2013). Py-GC/MS(FID) assessed behavior of polysaccharides during kraft delignification of Eucalyptus globulus heartwood and sapwood. *Journal of Analytical and Applied Pyrolysis, 101*(0), 142-149. doi:10.1016/j.jaap.2013.01.018

Lu, W., Guo, Y., Zhang, B., & Wang, C. (2013). Comprehensive analysis on elements, energy recovery, and oil compositions of biomass deoxy-liquefaction. *Energy and Fuels, 27*(4), 2157-2166. doi:10.1021/ef400157e

Lu, W., Wang, C., & Yang, Z. (2009). The preparation of high caloric fuel (HCF) from water hyacinth by deoxy-liquefaction. *Bioresource Technology, 100*(24), 6451-6456. doi:10.1016/j.biortech.2009.07.032

Lu, Y., Wei, X.-Y., Cao, J.-P., Li, P., Liu, F.-J., Zhao, Y.-P., . . . Zong, Z.-M. (2012). Characterization of a bio-oil from pyrolysis of rice husk by detailed compositional analysis and structural investigation of lignin. *Bioresource Technology, 116*(0), 114-119. doi:10.1016/j.biortech.2012.04.006

Mamleev, V., Bourbigot, S., Le Bras, M., & Yvon, J. (2009). The facts and hypotheses relating to the phenomenological model of cellulose pyrolysis: Interdependence of the steps. *Journal of Analytical and Applied Pyrolysis, 84*(1), 1-17. doi:10.1016/j.jaap.2008.10.014

Marinov, N. M., Pitz, W. J., Westbrook, C. K., Castaldi, M. J., & Senkan, S. M. (1996). Modeling of aromatic and polycyclic aromatic hydrocarbon formation in premixed methane and ethane flames. *Combustion Science and Technology, 116-117*(1-6), 211-287. doi:10.1080/00102209608935550

Marinov, N. M., Pitz, W. J., Westbrook, C. K., Vincitore, A. M., Castaldi, M. J., Senkan, S. M., & Melius, C. F. (1998). Aromatic and polycyclic aromatic hydrocarbon formation in a laminar premixed n-butane flame. *Combustion and Flame, 114*(1–2), 192-213. doi:10.1016/S0010-2180(97)00275-7

McDonald, A. G., Dare, P. H., Gifford, J. S., Steward, D., & Riley, S. (2002). Assessment of air emissions from industrial kiln drying of Pinus radiata wood. *Holz als Roh- und Werkstoff, 60*(3), 181-190. doi:10.1007/s00107-002-0293-1

McNaught, A. D., & Wilkinson, A. (1997). *IUPAC. Compendium of chemical terminology Gold Book*. doi:10.1351/goldbook.

Melius, C. F., Colvin, M. E., Marinov, N. M., Pit, W. J., & Senkan, S. M. (1996). Reaction mechanisms in aromatic hydrocarbon formation involving the C_5H_5 cyclopentadienyl moiety. *Symposium (International) on Combustion, 26*(1), 685-692. doi:10.1016/S0082-0784(96)80276-1

Milosavljevic, I., Oja, V., & Suuberg, E. M. (1996). Thermal effects in cellulose pyrolysis: Relationship to char formation processes. *Industrial & Engineering Chemistry Research, 35*(3), 653-662. doi:10.1021/ie9504381

Mok, W. S.-L., Antal, M. J., Szabo, P., Varhegyi, G., & Zelei, B. (1992). Formation of charcoal from biomass in a sealed reactor. *Industrial & Engineering Chemistry Research, 31*(4), 1162-1166. doi:10.1021/ie00004a027

Morgan, T. J., & Kandiyoti, R. (2013). Pyrolysis of coals and biomass: Analysis of thermal breakdown and its products. *Chemical Reviews*. doi:10.1021/cr400194p

Nakamura, T., Kawamoto, H., & Saka, S. (2007). Condensation reactions of some lignin related compounds at relatively low pyrolysis temperature. *Journal of Wood Chemistry and Technology, 27*(2), 121-133. doi:10.1080/02773810701515143

Neves, D., Thunman, H., Matos, A., Tarelho, L., & Gómez-Barea, A. (2011). Characterization and prediction of biomass pyrolysis products. *Progress in Energy and Combustion Science, 37*(5), 611-630. doi:10.1016/j.pecs.2011.01.001

Nolte, C. G., Schauer, J. J., Cass, G. R., & Simoneit, B. R. T. (2001). Highly polar organic compounds present in wood smoke and in the ambient atmosphere. *Environmental Science & Technology, 35*(10), 1912-1919. doi:10.1021/es001420r

Nowakowski, D. J., & Jones, J. M. (2008). Uncatalysed and potassium-catalysed pyrolysis of the cell-wall constituents of biomass and their model compounds. *Journal of Analytical and Applied Pyrolysis, 83*(1), 12-25. doi:10.1016/j.jaap.2008.05.007

Omais, B., Charon, N., Courtiade, M., Ponthus, J., & Thiébaut, D. (2013). A novel analytical approach for oxygen speciation in coal-derived liquids. *Fuel, 104*, 805-812. doi:10.1016/j.fuel.2012.04.049

Omais, B., Courtiade, M., Charon, N., Thiébaut, D., & Quignard, A. (2010). Characterization of oxygenated species in coal liquefaction products: An overview. *Energy & Fuels, 24*(11), 5807-5816. doi:10.1021/ef100894n

Park, H. J., Park, Y.-K., & Kim, J. S. (2008). Influence of reaction conditions and the char separation system on the production of bio-oil from radiata pine sawdust by fast pyrolysis. *Fuel Processing Technology, 89*(8), 797-802. doi:10.1016/j.fuproc.2008.01.003

Patwardhan, P. R., Dalluge, D. L., Shanks, B. H., & Brown, R. C. (2011). Distinguishing primary and secondary reactions of cellulose pyrolysis. *Bioresource Technology, 102*(8), 5265-5269. doi:10.1016/j.biortech.2011.02.018

Peng, Y., & Wu, S. (2010). The structural and thermal characteristics of wheat straw hemicellulose. *Journal of Analytical and Applied Pyrolysis, 88*(2), 134-139. doi:10.1016/j.jaap.2010.03.006

Pindoria, R. V., Lim, J.-Y., Hawkes, J. E., Lazaro, M.-J., Herod, A. A., & Kandiyoti, R. (1997). Structural characterization of biomass pyrolysis tars/oils from eucalyptus

wood waste: Effect of H_2 pressure and sample configuration. *Fuel, 76*(11), 1013-1023. doi:10.1016/S0016-2361(97)00092-6

Pines, H., Olberg, R. C., & Ipatieff, V. N. (1948). Studies in the terpene series. VIII. Effect of catalyst, solvent and temperature on the dehydrogenation of pinane and p-menthane. *Journal of the American Chemical Society, 70*(2), 533-537. doi:10.1021/ja01182a031

Ponder, G. R., & Richards, G. N. (1993). Pyrolysis of some ^{13}C-labeled glucans: A mechanistic study. *Carbohydrate Research, 244*(1), 27-47. doi:10.1016/0008-6215(93)80003-W

Prins, M. J., Ptasinski, K. J., & Janssen, F. J. J. G. (2006). Torrefaction of wood: Part 2. Analysis of products. *Journal of Analytical and Applied Pyrolysis, 77*(1), 35-40. doi:10.1016/j.jaap.2006.01.001

Ratte, J., Marias, F., Vaxelaire, J., & Bernada, P. (2009). Mathematical modelling of slow pyrolysis of a particle of treated wood waste. *Journal of Hazardous Materials, 170*(2-3), 1023-1040. doi:10.1016/j.jhazmat.2009.05.077

Rowell, R. M., Pettersen, R., & Tshabalala, M. A. (2013). Cell wall chemistry. In R. M. Rowell (Ed.), *Handbook of wood chemistry and wood composites*. Boca Raton, FL: CRC Press.

Shafizadeh, F. (1982). Introduction to pyrolysis of biomass. *Journal of Analytical and Applied Pyrolysis, 3*(4), 283-305. doi:10.1016/0165-2370(82)80017-X

Shen, D. K., & Gu, S. (2009). The mechanism for thermal decomposition of cellulose and its main products. *Bioresource Technology, 100*(24), 6496-6504. doi:10.1016/j.biortech.2009.06.095

Shen, D. K., Gu, S., & Bridgwater, A. V. (2010a). Study on the pyrolytic behaviour of xylan-based hemicellulose using TG–FTIR and Py–GC–FTIR. *Journal of Analytical and Applied Pyrolysis, 87*(2), 199-206. doi:10.1016/j.jaap.2009.12.001

Shen, D. K., Gu, S., & Bridgwater, A. V. (2010b). The thermal performance of the polysaccharides extracted from hardwood: Cellulose and hemicellulose. *Carbohydrate Polymers, 82*(1), 39-45. doi:10.1016/j.carbpol.2010.04.018

Shin, E.-J., Nimlos, M. R., & Evans, R. J. (2001). Kinetic analysis of the gas-phase pyrolysis of carbohydrates. *Fuel, 80*(12), 1697-1709. doi:10.1016/S0016-2361(01)00056-4

Skreiberg, A., Skreiberg, O., Sandquist, J., & Sørum, L. (2011). TGA and macro-TGA characterisation of biomass fuels and fuel mixtures. *Fuel, 90*(6), 2182-2197. doi:10.1016/j.fuel.2011.02.012

Wang, C., Du, Z., Pan, J., Li, J., & Yang, Z. (2007). Direct conversion of biomass to bio-petroleum at low temperature. *Journal of Analytical and Applied Pyrolysis, 78*(2), 438-444. doi:10.1016/j.jaap.2006.10.016

Wang, C., Pan, J., Li, J., & Yang, Z. (2008). Comparative studies of products produced from four different biomass samples via deoxy-liquefaction. *Bioresource Technology, 99*(8), 2778-2786. doi:10.1016/j.biortech.2007.06.023

Wang, L., Trninic, M., Skreiberg, Ø., Grønli, M. G., Considine, R., & Antal, M. J. (2011). Is elevated pressure required to achieve a high fixed-carbon yield of charcoal from biomass? Part 1: Round-robin results for three different corncob materials. *Energy & Fuels, 25*(7), 3251-3265. doi:10.1021/ef200450h

Wang, S., Guo, X., Liang, T., Zhou, Y., & Luo, Z. (2012). Mechanism research on cellulose pyrolysis by Py-GC/MS and subsequent density functional theory studies. *Bioresource Technology, 104*, 722-728. doi:10.1016/j.biortech.2011.10.078

Wang, S., Liao, Y., Liu, Q., Luo, Z., & Cen, K. (2007). Experimental study of the influence of acid wash on cellulose pyrolysis. *Frontiers of Chemical Engineering in China, 1*(1), 35-39. doi:10.1007/s11705-007-0007-7

Wang, X. Y., Wan, X. J., Chen, M. Q., & Wang, J. (2012). Kinetic model of biomass pyrolysis based on three-component independent parallel first-order reactions. *Guocheng Gongcheng Xuebao/The Chinese Journal of Process Engineering, 12*(6), 1020-1024. Retrieved from http://www.scopus.com/inward/record.url?eid=2-s2.0-84872227037&partnerID=40&md5=db7f9f47b41717d346ac4ce828d9edbf

Wang, Z., Cao, J., & Wang, J. (2009). Pyrolytic characteristics of pine wood in a slowly heating and gas sweeping fixed-bed reactor. *Journal of Analytical and Applied Pyrolysis, 84*(2), 179-184. doi:10.1016/j.jaap.2009.02.001

Wang, Z., Wang, F., Cao, J., & Wang, J. (2010). Pyrolysis of pine wood in a slowly heating fixed-bed reactor: Potassium carbonate versus calcium hydroxide as a catalyst. *Fuel Processing Technology, 91*(8), 942-950. doi:10.1016/j.fuproc.2009.09.015

Williams, P. T., & Besler, S. (1996). The influence of temperature and heating rate on the slow pyrolysis of biomass. *Renewable Energy, 7*(3), 233-250. doi:10.1016/0960-1481(96)00006-7

Wu, L., Guo, S., Wang, C., & Yang, Z. (2008). Direct deoxy-liquefaction of poplar leaves to biopetroleum with two kinds of catalysts. *Industrial & Engineering Chemistry Research, 47*(23), 9248-9255. doi:10.1021/ie801129b

Wu, L., Guo, S., Wang, C., & Yang, Z. (2009). Production of alkanes (C7–C29) from different part of poplar tree via direct deoxy-liquefaction. *Bioresource Technology, 100*(6), 2069-2076. doi:10.1016/j.biortech.2008.10.024

Wu, Y. M., Zhao, Z. L., Li, H. B., & He, F. (2009). Low temperature pyrolysis characteristics of major components of biomass. *Ranliao Huaxue Xuebao/Journal of Fuel Chemistry and Technology, 37*(4), 427-432. Retrieved from http://www.scopus.com/inward/record.url?eid=2-s2.0-70349243489&partnerID=40&md5=b426bad743e2c5ce56612863e0d81b02

Yu, J., Wang, C., Wang, Y., & Yang, Z. (2011). Deoxy-liquefaction products obtained from Crofton weed at different temperatures. *Journal of Analytical and Applied Pyrolysis, 92*(1), 68-75. doi:10.1016/j.jaap.2011.04.009

Zhang, X., Li, J., Yang, W., & Blasiak, W. (2011). Formation mechanism of levoglucosan and formaldehyde during cellulose pyrolysis. *Energy & Fuels, 25*(8), 3739-3746. doi:10.1021/ef2005139

Chapter 7 Tar-char/ Coke *versus* Wood-char/ Charcoal

7.1 Introduction

Throughout the previous chapters it was discussed that char can form from the solid or liquid pyrolysis products. The solid is called charcoal and, as discussed earlier (3.3.4), forms during pyrolysis from a highly viscous but immobile phase resembling the parent feedstock. The liquid is the condensable phase which, when pyrolysed a second time, produces a solid char (see chapter 6) called coke. The aim of this chapter is to investigate if the different char types, charcoal and coke, have an effect on the biochar properties.

The properties of the charcoal, which are of main concern to the manufacture of biochar, have already been widely established (Lehmann & Joseph, 2009). However, the properties of coke and its contribution to the overall char properties is less researched. Coke is formed by the condensation of volatile pyrolysis products onto the pyrolysing feedstock with resulting co-carbonisation and self-charring. The fraction of coke in the char is believed to increase with enhanced secondary char formation, leading to a significant char yield increase. Thus, it contributes to a large portion of the overall biochar yield, as demonstrated by Huang, Kudo, Masek, Norinaga, and Hayashi (2012).

In this chapter coke (here also called tar-char) is produced by self-charring of pine tar, and charcoal (here also called wood-char or pine-char) is obtained by traditional/ conventional pyrolysis of wood. Both types of char are compared to establish similarities and differences between them. Parameters analysed are macro- and microscopic structure by microscopy (light and scanning electron microscopy) and Raman spectroscopy, yield, ultimate analysis, proximate analysis, electrical conductivity, pH, true density, surface area and calorific value.

7.2 Material and Methods

7.2.1 Feedstock

Radiata pine rods with a diameter of 20 mm and varying height were used as feedstock for the production of wood-char. The wood is the same as described in 3.2.1.1.

The pine wood was also used as the starting material for the production of tar that was subsequently self-charred for the manufacture of tar-char/ coke, see 7.2.2 for details.

7.2.2 Tar and Coke Production

Tar was produced from the feedstock in 7.2.1 by pyrolysis employing two different processes. The first process involved condensing the volatile pyrolysis products generated in a gas-fired drum pyrolyser during pyrolysis of radiata pine beams with differing cross-sections to varying *HTT's*, as described in 3.2.4. Condensation was achieved by utilising two pot condensers in sequence, both with a water cooled double wall, made in the Engineering Workshop at the School of Engineering and Advanced Technology (Massey University, New Zealand). A range of the obtained tar samples, produced at different *HTT's,* were subsequently selected and re-pyrolysed in a furnace from W D Mcgregor Ltd (Manukau, New Zealand) with Eurotherm (now Schneider Electric, Rueil-Malmaison, France) temperature control. Before pyrolysis, the water-phase of the condensables was decanted and the heavy fraction, here referred to as tar, stirred and filled into 10 ml Kimble® beakers (Kimble® Life Science and Research Products LLC, Rockwood, USA). Subsequently they were placed into a specially designed reactor (built in the previously mentioned Engineering workshop), Figure 7-1, to prevent air from getting in contact with the hot sample (prevent oxidising damage) during pyrolysis. The tar was pyrolysed from room temperature to a set temperature of either 300 or 600 °C. This resulted in a heating rate of approximately 10 to 15 °C/min, meaning that pyrolysis was done in the slow pyrolysis regime.

Figure 7-1. Tar pyrolysis vessel with 10 ml beaker from Kimble®.

Additionally tar and tar-char/ coke were produced in a supervised 4th year engineering project looking at the differences between wood-char and tar-char titled "Understanding the differences between wood-char and tar-char" (Caco, 2014). As part of this project, a tar production reaction vessel was designed and built that fits inside the Wild Barfield Ltd (Northampton, United Kingdom) furnace that was used during this project for manufacturing tar, tar-char and wood-char respectively. For detailed information the reader is referred to Caco (2014). Here follows only a brief summary. For tar production approximately 300 g of pine wood, in the form of cylindrical samples with a diameter of 20 mm and a height of 50 mm, were placed inside the tar production vessel that was subsequently sealed with clay, positioned in the above mentioned furnace and heated by setting the furnace temperature to 500 °C. Upon attainment of the final *HTT* the furnace temperature was held at this temperature for 30 to 60 min or until no further gas production occurred. The tar was collected in the same condensers described above which were fitted onto the tar production reactor. The obtained tar consisted of ≈ 70 % (vol/vol) water, which was removed before tar-pyrolysis for coke production by decanting the water and subsequently drying it at 105 °C overnight. The tar-char/ coke production was done in a larger version of the reactor depicted in Figure 7-1, which accommodated a 30 ml Kimble® beaker. The beaker was filled with tar, enclosed in the reactor and subsequently heated in the Wild Barfield furnace at approximately 10 °C/min to a final *HTT* of 300, 450 and 600 °C. At the *HTT* the sample was held for about 10 min before the furnace was switched off and left for cooling.

7.2.3 Wood-char Production

Wood-char was produced for comparison from the pine rods described in 7.2.1 in the same reaction vessels and under the same conditions as the respective tars discussed in 7.2.2.

7.2.4 Microscopy

Photographs of pine-char and tar-char samples were taken with a stereomicroscope Leica MZ12 (Leica Microsystems GmbH, Wetzlar, Germany) at the Manawatu Microscopy and Imaging Centre (Palmerston North, New Zealand).

Scanning electron microscopy, SEM, was done with a FEI (Hillsboro, OR, USA) Quanta 200 Environmental Scanning Electron Microscope. Analysis was performed by Doug Hopcraft at the Manawatu Microscopy and Imaging Centre (Palmerston North, New Zealand). In the work of Caco (2014) analysis was performed by Nicki Murray at the Manawatu Microscopy and Imaging Centre. Before analysis, samples were dried at 105 °C and subsequently stored over silica gel.

Additional SEM analysis was performed by John McDonald-Wharry from the University of Waikato (Hamilton, New Zealand).

7.2.5 Ultimate Analysis

Ultimate analysis was done with the equipment and procedure outlined in 3.2.1.3. It was aimed at making two replicates for each sample analysis. This however was not always possible due to the limited amount of sample available. Details are given in 7.3.3. The sulphur content is neglected in this study, because of its marginal presence in the feedstock, as shown in Table 3-3 in 3.2.1.3.

7.2.6 Raman Analysis

Raman analysis was carried out by John McDonald-Wharry from the University of Waikato (Hamilton, New Zealand). The analysis and interpretation is based on McDonald-Wharry, Manley-Harris, and Pickering (2013).

7.2.7 Proximate Analysis

The proximate analysis was performed according to the procedure outlined in Table 3-5 in 3.2.1.4 using the same equipment. In the experiments of Caco (2014) no lid was used, whereas all other analysis runs employed a lid (more details are provided in 7.3.3). The crucibles were filled with 6 to 47 mg ground char samples. Grinding was carried out using a ring mill from Rocklabs (Auckland, New Zealand) and a stainless steel mortar and pestle were used.

7.2.8 Electrical Conductivity and pH

Electrical conductivity, EC, and pH measurement are based on the recommendations of the International Biochar Initiative (2014) following the method of Rajkovich et al. (2012). The samples analysed were ground (with mortar and pestle) pine-char and tar-char. They were dried prior to analysis at 105 °C for 24 hours and stored over silica gel. Subsequently 0.5 g of the char or coke were measured and added into 10 ml Milli-Q® water (EMD Millipore, Billerica, MA, USA). The mixture was then thoroughly shaken by hand and placed on an electric shaker for 1.5 h at 250 rpm, and shaken by hand every 30 min to ensure good mixing. Next, the electrical conductivity and pH were determined with a HANNA Instruments (Woonsocket, RI, USA) HI 8633 conductivity meter and a Radiometer (Brønshøj, Denmark) Copenhagen PHM 83 AUTOCAL pH meter respectively. The analyses were performed in triplicate.

7.2.9 True Density

True or solid density measurement was done with an AccuPyc II 1340 pycnometer (Micromeritics Instrument Corporation, Norcross, GA, USA) by Micromeritics Analytical Services (Norcross, GA, USA) for radiata pine wood (1 sample), wood-char (3 samples with a *HTT* of 383, 552 and 713 °C respectively) and tar-char (2 samples each produced at 300 and 600 °C respectively). The analysis was carried out with Helium as measuring gas, and ten measuring cycles per sample were performed.

In the study of Caco (2014) an AccuPyc II 1340 Pycnometer (Micromeritics Instrument Corporation, Norcross, GA, USA) was used as well with Helium as a displacement medium. The exact operating procedure is given by Caco (2014).

All samples were ground with a mortar and pestle, and dried at 105 °C prior to analysis.

7.2.10 Surface Area

Surface area was analysed by Nitrogen physisorption at 77.35 K and carried out by the team of Dr. Geoff Waterhouse at the University of Auckland (Auckland, New Zealand). Only single samples of wood-char and tar-char produced at both 300 and 600 °C were analysed.

7.2.11 Calorific Value

The calorific values were determined by the Nutrition Laboratory of the Institute of Food, Nutrition and Human Health (Massey University, Palmerston North, New Zealand). Details of the method and sample preparation are given by Caco (2014).

7.3 Results and Discussion

7.3.1 Appearance

First, the two types of char are compared visually and the resulting structural implications discussed. Conventional charcoal typically retains the parent structure with its rudimentary morphology (Downie, Crosky, & Munroe, 2009; Joseph et al., 2010; Keiluweit, Nico, Johnson, & Kleber, 2010; Wildman & Derbyshire, 1991), Figure 7-2, but tar-char/ coke, which as a result of its formation from a liquid-phase, has a glassy appearance very different from the feedstock, Figure 7-3.

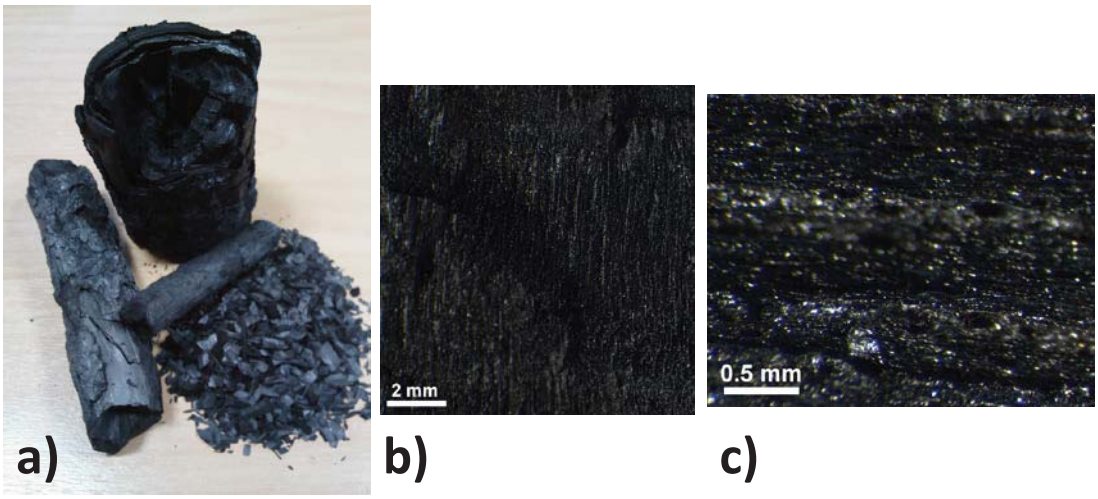

Figure 7-2. Conventional char from radiata pine pyrolysis. a) Char obtained from pyrolysing branches and twigs including a pile of crushed char. b) and c) Radiata pine char as viewed under a stereomicroscope. The chars depicted had highest treatment temperatures in the range 400 to 700 °C.

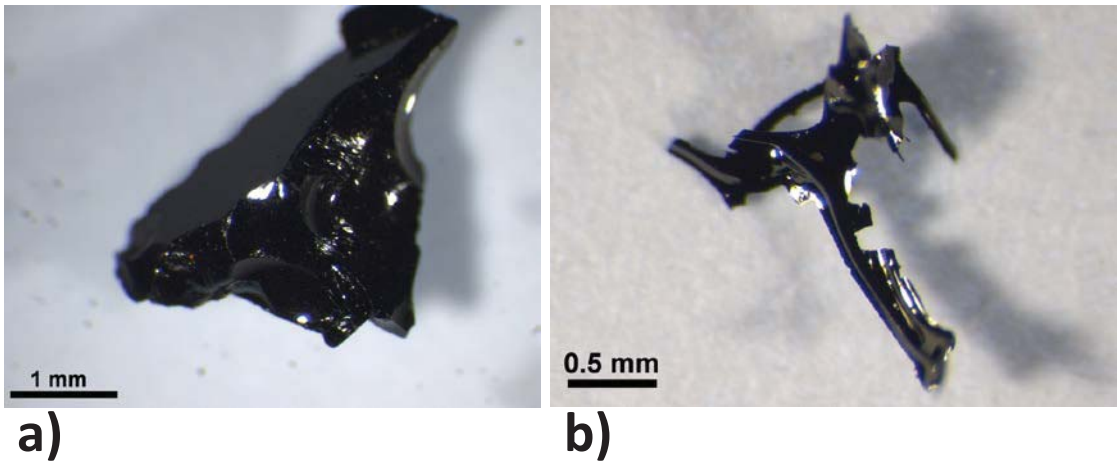

Figure 7-3. Photographs of tar-char produced from radiata pine tar as viewed under a stereomicroscope. a) Tar-char pyrolysed at 300 °C from radiata pine tar collected at a *HTT* of ≈ 700 °C. b) Tar-char pyrolysed at 600 °C from radiata pine tar collected at a *HTT* of ≈ 400 °C. *HTT* = highest treatment temperature.

Figure 7-2 clearly shows that the wood-char retains the structure of the feedstock. For instance in Figure 7-2 a) one can still distinguish the bark form the wood and in Figure 7-2 c) the parent softwood structure, discussed in 2.5.1, is recognisable. In contrast, Figure 7-3 shows a glassy material with smooth surfaces that display spherical surfaces in Figure 7-3 a) resulting from internal air pockets that have formed due to tar boiling. In Figure 7-3 b) the remnants of these internal air pockets are no longer visible, as at this temperature the boiling was so violent that a porous "carbon tower" was formed; similar to the well-known tower that forms from the experiment of dehydrating sugar with sulphuric acid. The tower was subsequently crushed to obtain the particle shown in Figure 7-3 b).

In terms of biochar, charcoal with its macroscopic structure is the desired product, as it is the physical properties of the char that affect directly (e.g. hydrology) and indirectly (e.g. soil microbe habitat (Brady and Weil, 2008, as cited in Downie et al., 2009)) the soil system (Downie et al., 2009).

That both charcoal and coke, depicted in Figure 7-2 and Figure 7-3, can occur concurrently during pyrolysis without intentional tar condensation, as is the case in the work of Huang et al. (2012), is illustrated in Figure 7-4, which displays the presence of coke nodules in Manuka bisquettes pyrolysed at 340 °C in a modified Bradley food smoker (Auckland, New Zealand) (Haris, 2012). Haris (2012) observed the formation of these so-called coke nodules from 260 °C when heating Oak and Manuka bisquettes.

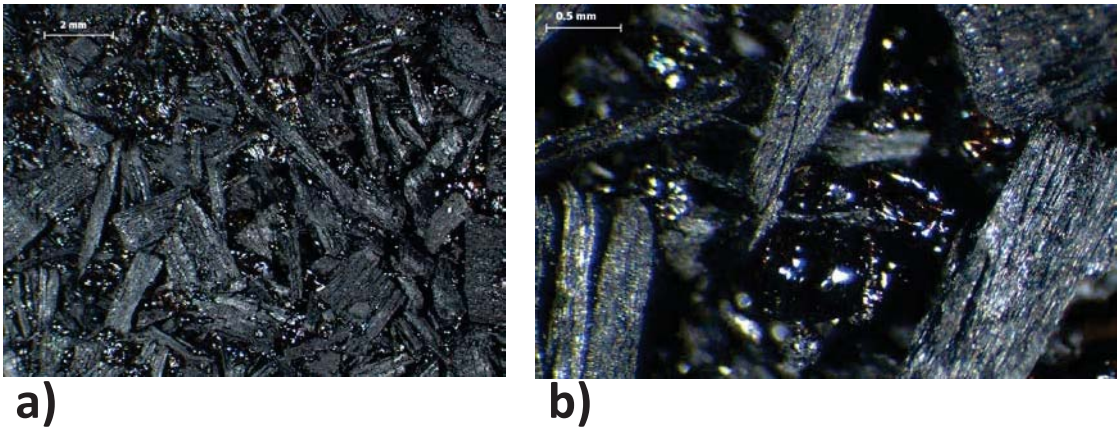

Figure 7-4. Photographs of Manuka bisquettes pyrolysed on a modified Bradley Smoker (Auckland, New Zealand) at 340 °C. The samples were obtained from Haris (2012), and the pictures were taken with a stereomicroscope. a) Tar-char/ coke formation between sawdust particles of Manuka bisquettes. b) Magnified coke bubble.

The presence of solid nodules/ bubbles in Figure 7-4 highlights the presence of a liquid phase during pyrolysis, which is either subject to boiling or through which internally generated volatiles escape. The liquid tar then solidifies more rapidly than the bubble can collapse leading to the presence of coke nodules in Figure 7-4. SEM micrographs confirmed that the formed nodules are indeed thin walled bubbles, Figure F-1 and F-2 in Appendix F.1. The fact that the bubbles appear to be formed separately on top of the "conventional" char indicates that liquid tar has blocked some of the pores of the pyrolysing solid and subsequent internal volatile formation lead to the occurrence of the bubbles. The reason for the presence of the nodules in the bisquettes, while they are absent in Figure 7-2, is unknown but could be due to the different pyrolysis conditions that for instance enabled condensation of volatile pyrolysis products in the bisquettes.

However, they appeared in the charred layer adjacent to the heating element, which has the highest temperature in the sample, indicating a more intricate mechanism. Other reasons could be the presence of binder in the bisquettes, which was corn starch in the case of Manuka and/ or differences in the amount of extractives present compared to radiata pine wood. The latter one is believed to be unlikely as for instance oak, a hardwood, has a similar extractives fraction to pine (Ruiz-Aquino, González-Peña, Valdez-Hernández, Revilla, & Romero-Manzanares, 2015). The same is thought to be true for Manuka; although it is known for its oil, but this is mainly obtained from its foliage (Porter et al., 1998; Stephens, Molan, & Clarkson, 2005).

The possibility of the wood cell wall components itself going through a liquid phase was discussed in 2.5.4 and 3.3.4. In particular the loss of structural complexity in the cell wall, as observed by Haas, Nimlos, and Donohoe (2009), was stated as evidence for the presence of a liquid phase during conventional atmospheric pressure pyrolysis. This, however, is not believed to be the reason for the tar nodules in Figure 7-4, as they appear in random locations in the bisquettes on top of the macroscopically intact charcoal pieces. Nevertheless, loss of structural complexity was observed microscopically in the SEM micrographs taken as part of this research, Figure F-3 and F-4 in Appendix F.1 respectively. Figure F-3 displays the fibrous heterogeneous nature of the cell wall of radiata pine tracheids (see white arrows), which disappears with increasing *HTT*, Figure F-4. In the latter, the cell wall appears very homogenous, in particular at 450 and 600 °C. This observation is the basis for the discussed hypothesis of Mamleev, Bourbigot, Le Bras, and Yvon (2009) in 3.3.4 that the cell wall is like a porous viscous suspension.

The presence of a liquid-phase in the cell wall itself would imply that the formed charcoal, according to the definition in 2.6.1, is actually coke, and the structure of the parent material is merely maintained due to a minimal short lived fluidity caused by the interaction of cell wall components (hemicellulose, cellulose, lignin and mineral matter) (Dufour, Castro-Diaz, Brosse, Bouroukba, & Snape, 2012). Dufour et al. (2012) report the greatest fluidity for isolated lignin, and observed its glass transition below 200 °C, which illustrates that liquid phases could be involved right from the beginning of pyrolysis, and not just associated with the depolymerisation of carbohydrates as suggested by Mamleev et al. (2009). The fluidity in the study of Dufour et al. (2012) was determined by ^{1}H NMR spectroscopy as elucidated in 3.3.4. Their results are

corroborated by the findings of Sharma et al. (2004) discussed in 2.5.4, who observed a liquid phase during lignin fast pyrolysis at 250 °C, and state that the temperature of its occurrence is dependent on the interaction between the biomass constituents in the wood. Morgan and Kandiyoti (2013) argue that the observation of a transient liquid-phase during rapid biomass pyrolysis can also be related to coal plasticity phenomena. That is, during rapid heating, internally released hydrogen may quench the free radicals involved in retrogressive recombination reactions, which lead to the formation of char, and thus enables melting and swelling behaviour (Morgan & Kandiyoti, 2013). This proposed mechanism is able to explain why, at slow heating of biomass, the macroscopic structure of the parent material is visible, while the microscopic cell wall structure (middle lamella, primary and secondary cell wall), as discussed above, disappears. This mechanism purports that, during slow pyrolysis, the "softening" (internal liquefaction) process is short lived (but long enough to destroy the microscopic cell wall structure), due to the absence of hydrogen and the presence of hydrogen scavenging oxygen, meaning that char forming recombination reactions take place before the macroscopic structure is destroyed. This mechanism is most likely to relate to lignin, as this involves a radical char forming mechanism (see 6.3.4). It also highlights the important role of hydrogen, its mobility and transfer during pyrolysis, which have been identified to play a major part in biomass pyrolysis (Balonek, Colby, Persson, & Schmidt, 2010; Dufour et al., 2012; Morgan & Kandiyoti, 2013). It is supported by the mechanisms discussed in 6.3.4 and by the pyrolysis processes elucidated in 2.8. In 2.5.4 it was elaborated that, in the case of cellulose, the viscosity of the intermediate liquid compound, which is dependent on the heating rate, affects the char structure. This highlights the complexity of processes involved in the formation of liquid phases or melts during pyrolysis, and outlines the interdependence of pyrolysis mechanism and structural properties. The main implication however is that processes traditionally associated with primary char formation could in fact be secondary mechanisms, which agrees with the observation in chapter 3 that the majority of the char yield is formed by secondary reactions.

Another instance where a molten phase has been observed is under pressure (L. Wang, Skreiberg, Grønli, Specht, & Antal, 2013). L. Wang et al. (2013) argue that this is due to the increased saturation pressure and temperature of the liquid products preventing volatilisation and thus enabling char formation from the liquid phase,

impairing the macroscopic structure of the feedstock. This was also discussed for secondary char formation from levoglucosan in 6.3.4. If the processes occur under autogenous pressure, the above discussed quenching of retrogressive recombination reactions by hydrogen may play an important role due to the prolonged presence of hydrogen. L. Wang et al. (2013) further mention that "hints of melting" (p. 2154) were observed in large particles. This implies that the macroscopic structure of the char is to a large extent dependent on physical processes and not just chemical.

Comparing the pine charcoal and coke at very high SEM magnifications, Figure 7-5, it becomes evident that their microstructure looks very similar indicating that the glassy appearance of the tar-char in Figure 7-3 is a consequence of the absence of the biomass textural structure, and is not actually caused by a higher amorphicity in the nanostructure (J. McDonald-Wharry, personal communication, November 5, 2012), although tar-char might be slightly more amorphous than wood-char at low *HTT's*, see section 7.3.4 and 7.3.7. This supports the discussion above and shows that charcoal and coke are nanostructurally very similar.

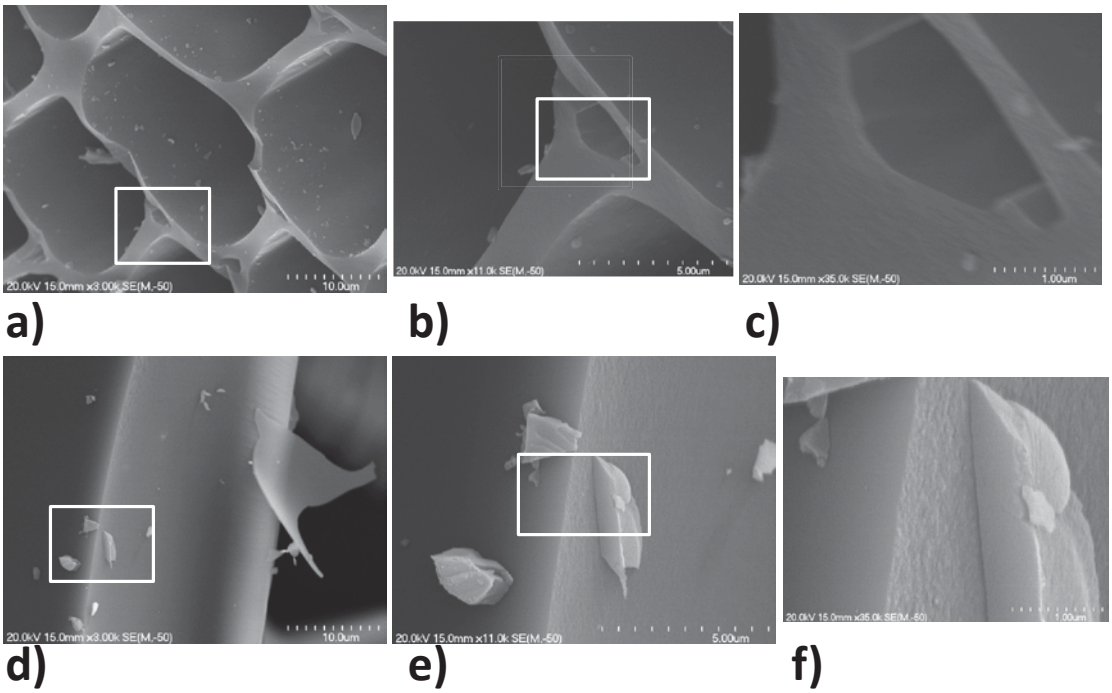

Figure 7-5. Comparison of SEM micrographs of pine-char and tar-char/ coke produced at a *HTT* of 600 °C. a) to c) Wood-char. d) to f) Tar-char/ coke. Magnification increases from left to right and the white rectangle represents the respective area of magnification. SEM analysis was performed by John McDonald-Wharry from the University of Waikato (Hamilton, New Zealand). *HTT* = highest treatment temperature; SEM = Scanning electron microscope.

In summary, the discussion in this section reveals that both chars, charcoal and coke, can be present in biochar and their distinction is primarily a consequence of the differing macroscopic structure. The macroscopic structure of the feedstock is desired for the application as biochar but can be impaired if there is a pronounced liquid phase present in the solid matrix during char formation, or volatile pyrolysis products condense and subsequently self-char within the matrix.

7.3.2 Yield

The yield of pine-char and tar-char as a function of the *HTT* determined by Caco (2014) is depicted in Figure 7-6.

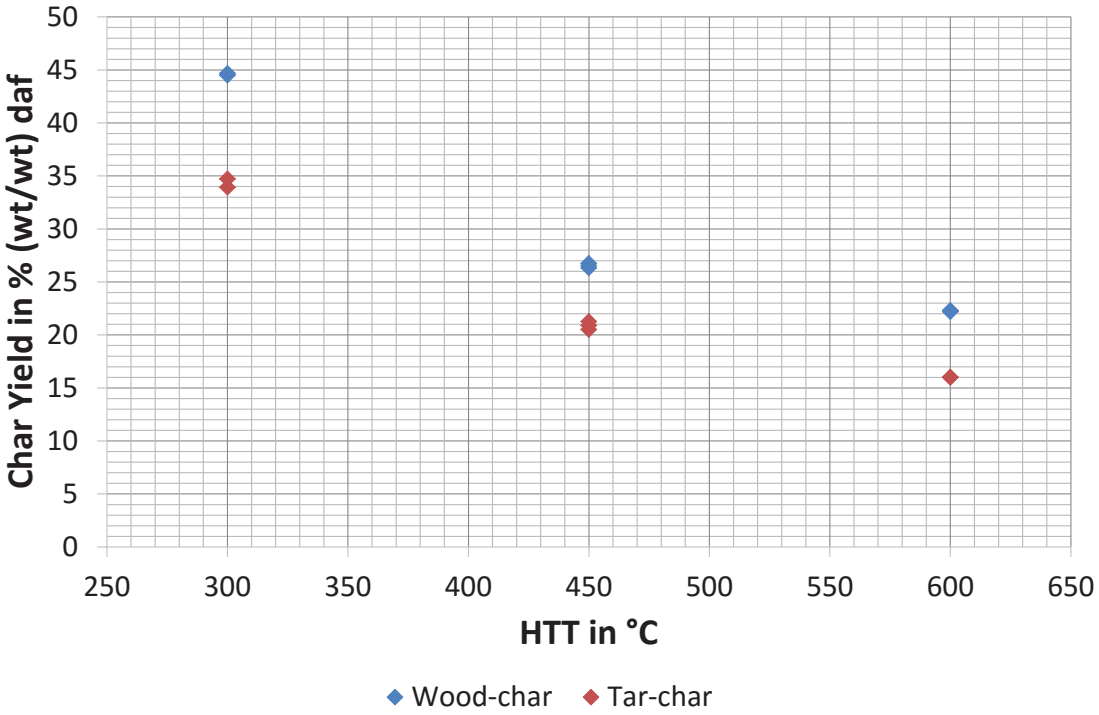

Figure 7-6. Comparison of wood-char and tar-char yield on a dry ash free basis. The tar used for producing coke was collected from pine pyrolysis with a HTT of 500 °C. It is important to note that the yield of wood-char and tar-char is calculated based on the initial weight of the wood and tar respectively, and that for calculating the ash content of the feed the assumption was made that no inorganics are lost during pyrolysis as the ash content was only measured for the char/ coke. For each experiment one repetition was done except for the run at 450 °C where two repetitions were performed. Adapted from Caco (2014). daf = dry ash free basis; HTT = highest treatment temperature; wt = weight.

Figure 7-6 shows that the yield of wood-char and tar-char decreases with increasing *HTT*, and that pyrolysis of tar led to a lower yield than pyrolysis of wood. It is important to note that the yield of wood-char and tar-char is calculated based on the initial weight of the wood and tar respectively. Lower yields with increasing *HTT's* were anticipated as decomposition and volatilisation of the pyrolysing compounds progresses with increasing temperature as discussed in chapter 3. These results confirm that a significant amount of char/ coke can be formed by self-charring of tar. Similar trends are observed for the fixed carbon yield, Figure F-5 in Appendix F.2.

In chapter 6 it is shown that the tar composition is a function of the *HTT* for which reason the yield of coke, produced at 300 and 600 °C, from tars collected at varying *HTT's* is compared in Figure 7-7.

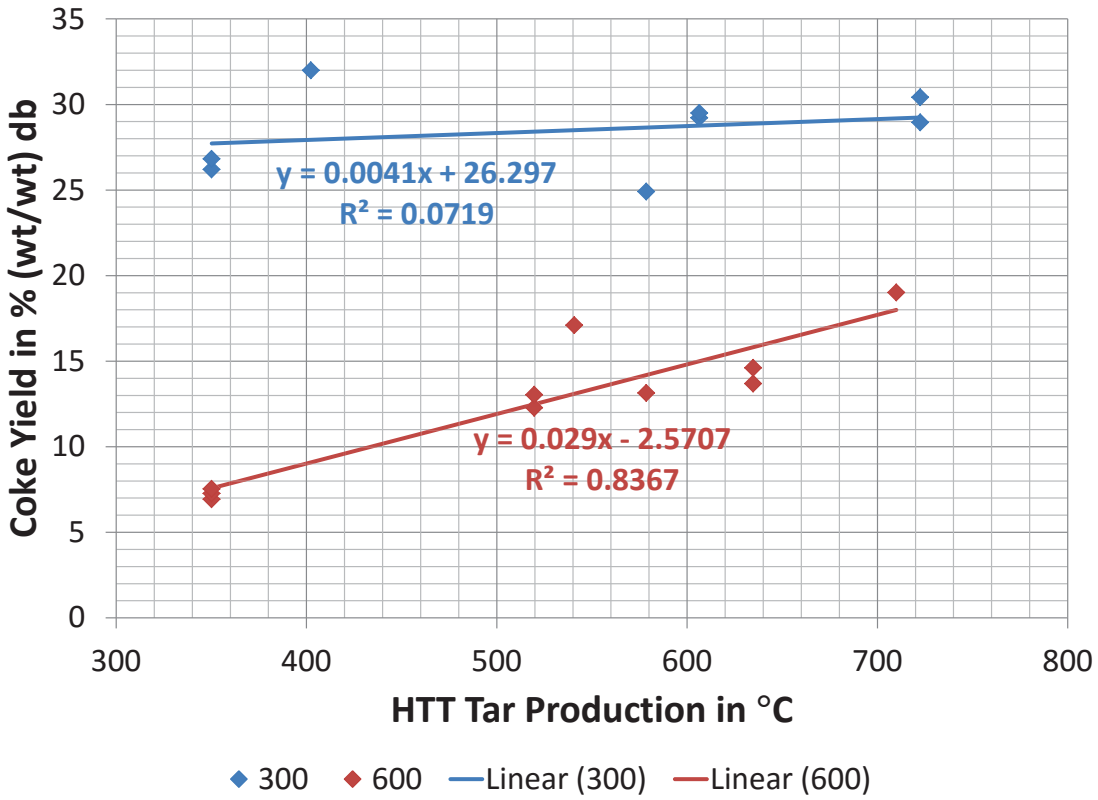

Figure 7-7. Coke yield of various tars pyrolysed at 300 and 600 °C as a function of their production temperature (HTT of tar production). It is important to note that the yield of tar-char is calculated based on the initial weight of the tar. Legend: Temperature of coke production in °C. db = dry basis; HTT = highest treatment temperature in °C of the pyrolysis process in which the tar was collected; R^2 = coefficient of determination; wt = weight.

Figure 7-7 shows that the coke yield from tar produced at 300 °C is higher than that produced at 600 °C over the entire *HTT* range analysed, which confirms the decreasing trend in coke yield with increasing *HTT* observed in Figure 7-6. It also shows that the yield of coke appears to be independent of the *HTT* of tar production for pyrolysis at 300 °C but for pyrolysis at 600 °C a correlation with the *HTT* of tar production is present. The reason is believed to be varying ash contents of tars collected at different *HTT's*. This is evidenced by the fact that wood-char and tar-char appear to have a maximum in the ash content, Figure 7-8.

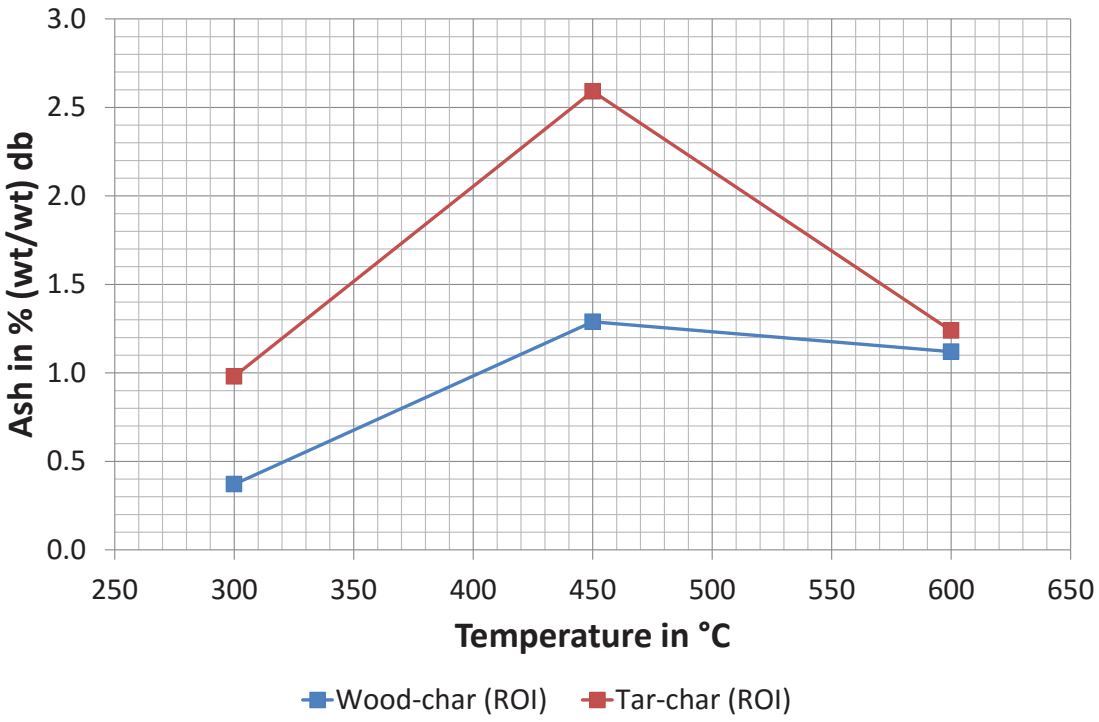

Figure 7-8. Ash content of wood-char and tar-char produced at 300, 450 and 600 °C. The ash content was determined by Residue on Ignition (ROI) according to Bridges (2013). Only one analysis per sample was performed due to the limited amount of sample available. The tar for coke production was collected at a HTT of 500 °C. Adapted from Caco (2014). db = dry basis; wt = weight.

Thus, Figure 7-8 illustrates that ash compounds are lost above 450 °C from wood-char and tar-char. It is important to note that only one analysis per run was performed due to the limited amount of sample available. However, the results are believed to be reproducible as the method was found to be accurate as demonstrated by the determination of the wood ash content, Table 3-7 in 3.2.1.4. That ash compounds indeed volatilise during pyrolysis is supported by the fact that ash can be detected in the tar-char, which can only be explained by a volatilisation of the feedstock inorganics or carryover of char particles into the volatile phase. A picture of the resulting ash of the experiments in Figure 7-8 is depicted in Figure 7-9.

Figure 7-9. Ash of wood-char and tar-char produced at 300, 450 and 600 °C. The top row shows the ash of pine-char and the bottom row of tar-char from left to right produced at 300, 450 and 600 °C respectively. Picture taken from Caco (2014).

The colour difference between the ash of wood-char and tar-char in Figure 7-9 indicates that the inorganics are present in a different form.

Ash loss above 450 °C can also be inferred from the TGA results of char when comparing the no-lid and lid runs shown in Figures D-7 and D-8 in Appendix D-2. The no-lid case has significantly more char mass loss above 450 °C. While the inference that this mass loss also includes ash is not able to be made from the TGA results alone, it does allow the supposition to be made that ash is carried off with the volatiles or, indeed, is volatile itself, which supports the findings above where less ash is obtained at temperatures above 450°C. This supposition is further supported when examining the K impregnated samples (K is one of the major ash fractions in biomass (Cetin, Gupta, & Moghtaderi, 2005; Mohan, Pittman, & Steele, 2006)) which, in the no-lid trial, shows a peak in the respective derivative weight-loss curve of char at approximately 420 °C in Figure F-6 in Appendix F.2. Applying a lid still resulted in a weight-loss of the char but seemingly less pronounced, as shown in Figure F-7 in Appendix F.2, indicating that the presence of a lid also impacts the volatilisation of compounds from char which, it can now be supposited, also includes ash. In the samples impregnated with Mg (Figure F-8 to Figure F-11 in Appendix F.2) or P (Figure F-12 to Figure F-15 in Appendix F.2) such a distinguishable peak in the derivative weight-loss curve of char around 400 °C is not present; instead the derivative weight-loss is increasing with rising temperature from 400 °C onwards. The effect is larger with lower impregnation concentration, and for Mg compared to P impregnation. Again with the presence of a lid the weight-loss is

less distinct. Thus, the type of impregnated compound and the presence of a lid affect the release of volatile compounds from char; however, whether or not the discussed effects are due to inorganics volatilisation has yet to be clarified. In the literature volatilisation of, for instance, potassium has been reported but beginning at temperatures between 800 to 900 °C (Misra, Ragland, & Baker, 1993). Though, in a more recent study Okuno et al. (2005) showed that volatilisation of alkali and alkaline earth metals can occur at much lower temperatures during slow pyrolysis for instance in the case of K and Mg at 400 °C and 600 °C respectively, when secondary reactions/ interactions are minimised. This agrees with the above discussed weight-loss profiles of K and Mg. Further they explain that under conditions enhancing secondary reactions (here in the case of a lid) the volatile alkali and alkali earth metallic species go through a sequence of desorption and adsorption steps onto the char surface leading to their transformation into less volatile char-bonded compounds and/ or the formation of non-volatile compounds like silicates. This could explain the reduced weight-loss for the above described samples with a lid, and shows that secondary reactions, requiring an intimate contact between the volatile species and char, also affect the inorganics release. That these effects are observed by pyrolysing the char is due to the fact that char undergoes cracking even after tar volatilisation is completed leading to the release of char bonded alkali or alkaline earth metals (Okuno et al., 2005).

Thus, it can be concluded that the increased ash content at higher temperatures in the tar minimises tar volatilisation and therefore increases coke formation as observed in Figure 7-7 for the coke produced at 600 °C. This confirms that catalysis also enhances the char yield of pyrolysis products present in a liquid-phase, which supports the finding in chapter 4 that catalysis by inorganics is with respect to secondary reactions. That the effect appears to be absent for coke produced at 300 °C indicates that tar decomposition is still in its initial phase at this temperature. However, these trends need to be confirmed by carrying out more experiments to obtain statistically meaningful results.

The findings with respect to the ash content imply that some ash is volatilised during its process of determination by ROI, which means that the assumption used to plot Figure 7-6, i.e., that no inorganics are lost during pyrolysis, is an oversimplification. However, the overall trend remains the same as illustrated in,

Figure 7-10, where the results are plotted on a dry basis and combined with previous analysis results of pine-char and tar-char.

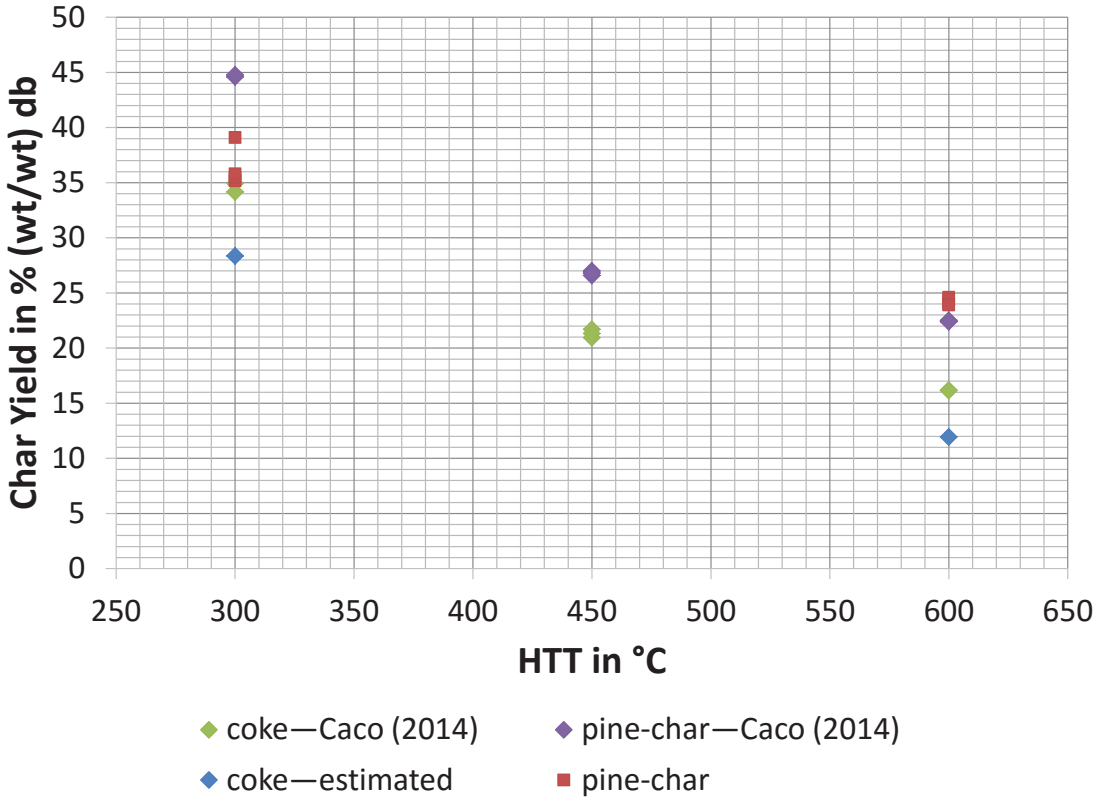

Figure 7-10. Yield of pine-char and tar-char pyrolysed at 300, 450 and 600 °C on a dry basis. It is important to note that the yield of wood-char and tar-char is calculated based on the initial weight of the wood and tar respectively. The estimated coke yields are derived from the equation in Figure 7-7 for a HTT of tar production of 500 °C. The pine-char yields represent values obtained by pyrolysing cylinders of pine wood in the same equipment as the tar in Figure 7-7 (different from the furnace used by Caco (2014)). db = dry basis; HTT = highest treatment temperature in °C; wt = weight.

Figure 7-10 shows again the decreasing trend in the yield with increasing *HTT*, as well as that there is variation between the results of Caco (2014) and the additional ones, which were done in a separate furnace. The application of different furnaces with varying accuracy of temperature control is believed to be the reason for the observed discrepancies. That is, smaller temperature overshoots (± 26 °C) were observed in the work of Caco (2014), Figure F-16 in Appendix F.3, compared to temperature overshoots of approximately 80 °C in the McGregor furnace used for the production of the additional samples. Despite this, the set point temperatures were plotted in Figure 7-10 as no continuous temperature recordings were obtained for all the samples. Nevertheless, it supports the findings of Figure 7-6, i.e., decreasing trend in the yield with increasing *HTT*. Another possible reason for the lower estimated coke yields compared to the measured values determined by Caco (2014) could be the fact that the

tar in the experiments by Caco was oven-dried before the coke production, which was not the case for the tar used in Figure 7-7 (see 7.2.2). However, this is believed to be of minor influence.

7.3.3 Ultimate Analysis

Ultimate analysis was done, as biochar production can be assessed by its changes in the elemental composition with increasing *HTT* (Krull, Baldock, Skjemstad, & Smernik, 2009), which was discussed in chapter 2.

First, it was investigated whether or not the elemental composition of tar-char is dependent on the *HTT* of the tar collection process, Figure 7-11.

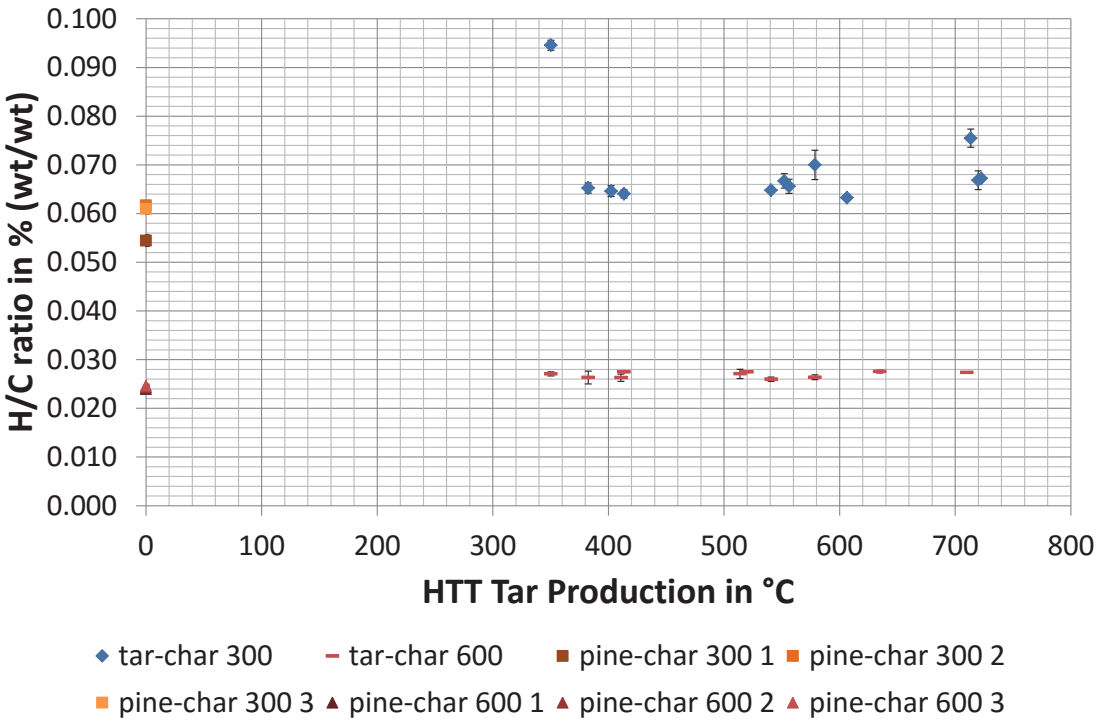

Figure 7-11. H/C ratio of tar-char produced at 300 and 600 °C as a function of the HTT of the tar collection process. Pine-char samples at a tar HTT of 0 °C were included for comparison. The error bars represent the standard deviation. Two repetitions per analysis were done except in a few cases of tar-char samples where only enough sample was present for one repeat analysis. Legend: sample name_HTT of pyrolysis process_sample number (in case of pine-char samples). C = carbon; H = hydrogen; HTT = highest treatment temperature; wt = weight.

Figure 7-11 illustrates that the H/C ratio of tar-char is unaffected by the *HTT* of tar collection, as shown in Figure F-17 to Figure F-20 in Appendix F.4. Further, it appears that tar-char has a slightly higher H/C weight ratio than the respective pine-char. The N

content of tar-char, produced at 300 and 600 °C (Figure F-21 and Figure F-22 in Appendix F.4 respectively), is also independent of the *HTT* of the tar collection process.

The second investigation was whether or not there is a difference between the elemental composition of pine-char and tar-char at the different *HTT's* as suggested by Figure 7-11. Of main interest is the carbon content, which may be able to serve as an alternative means to the weight for determining the char formation rate as was hypothesised in 2.6.2, Figure 7-12.

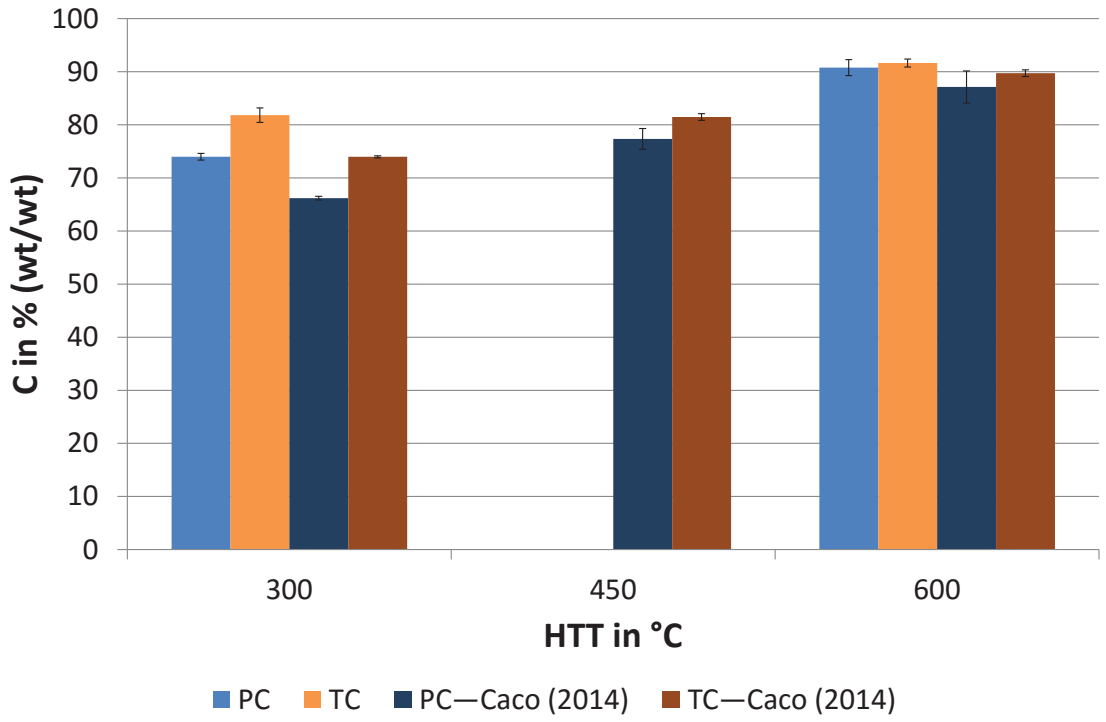

Figure 7-12. Comparison of carbon content of pine-char and tar-char as a function of the HTT of the pyrolysis process. The error bars represent the standard deviation. In the case of pine-char three samples at 300 and 600 °C were analysed with two repetitions per sample. For the tar-char twelve and ten samples were analysed at 300 and 600 °C respectively with at least one repeat ultimate analysis per sample. The results of Caco (2014) represent the average of two samples for pine-char and tar-char at 300 and 600 °C respectively with two repetitions for each analysis. In the case of 450 °C three samples were analysed with at least one repetition per sample. C = carbon; HTT = highest treatment temperature; PC = pine-char; TC = tar-char; wt = weight.

Figure 7-12 reveals a difference between the two experimental sets, with the samples analysed by Caco (2014) showing a lower carbon content. This is related to the different final oven temperatures of the experiments as discussed earlier in 7.3.2. Overall, they display the same trend, that is, there is initially a difference between the pine-char and tar-char, with tar-char having a higher carbon content. The difference decreases with increasing temperature, which indicates that from the carbon content only a conversion rate can be inferred but not a carbon formation rate of the two

different chars. In the case of the hydrogen content no clear trend is visible, Figure F-23 in Appendix F.4. This leads to an inconclusive trend in the atomic H/C ratio, Figure 7-13, that is, it appears there is no significant difference between pine-char and tar-char.

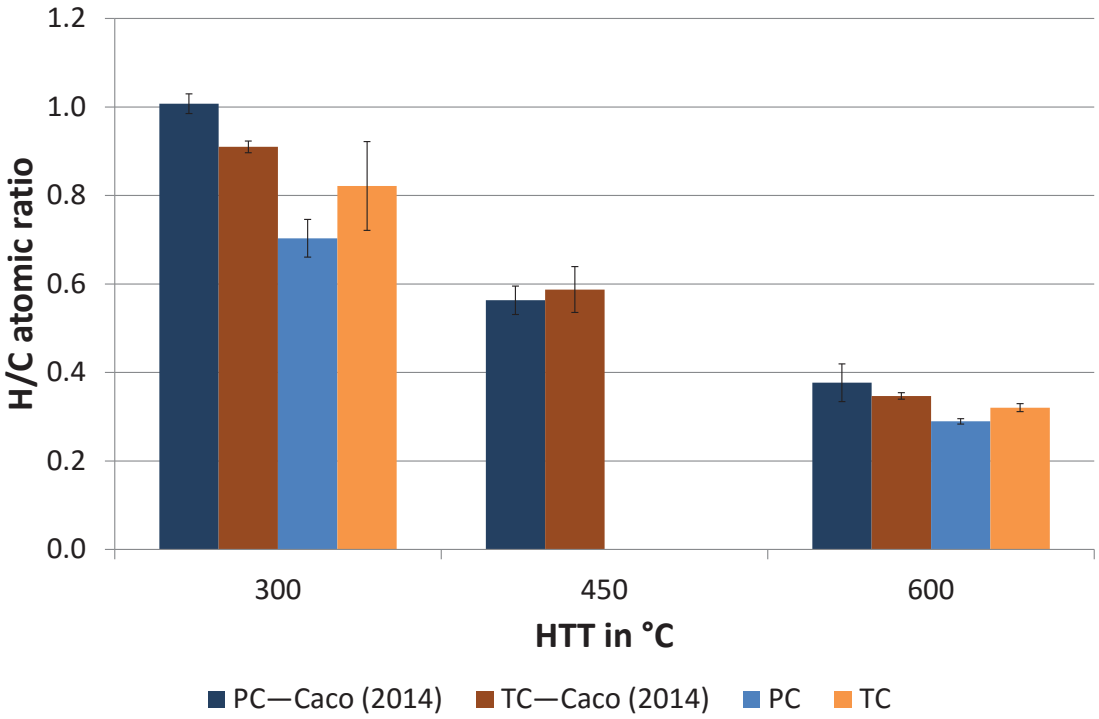

Figure 7-13. Comparison of atomic H/C ratio of pine-char and tar-char as a function of the HTT of the pyrolysis process. The error bars represent the standard deviation. In the case of pine-char three samples at 300 and 600 °C were analysed with two repetitions per sample. For the tar-char twelve and ten samples were analysed at 300 and 600 °C respectively with at least one repeat ultimate analysis per sample. The results of Caco (2014) represent the average of two samples for pine-char and tar-char at 300 and 600 °C respectively with two repetitions for each analysis. In the case of 450 °C three samples were analysed with at least one repetition per sample. C = carbon; H = hydrogen; HTT = highest treatment temperature; PC = pine-char; TC = tar-char; wt = weight.

Figure 7-13 displays an overall decreasing trend in the atomic H/C ratio with increasing *HTT*, which has been proposed as a method for biochar classification by the International Biochar Initiative (2014). That is, char with an H/C_{org} (C_{org} is the organic carbon content) ratio below 0.7 is considered to have a large enough proportion of fused aromatic rings and thus stability to be called biochar (*ibid*). The inorganic carbon content for the here studied samples can be neglected because of the low ash content of radiata pine (Table 3-6 in 3.2.1.4) and thus the manufactured char, Figure 7-8. Accordingly the chars produced at 300 °C in Figure 7-13 do not classify as biochar and the tar-char and pine-char are expected to have a similar stability although char produced in a confined reactor with enhanced secondary reactions has been reported to be less stable by Gangil (2014). However, their char included the condensed volatiles

and not just the additionally produced coke as was the case in this study, indicating that poorly carbonised coke is less stable.

The changes in the nitrogen content between pine-char and tar-char as a function of the *HTT* are illustrated in Figure F-24 in Appendix F.4. The nitrogen content exhibits the highest standard deviation due to their low presence in the feedstock, as shown in Table 3-3 in 3.2.1.3. Overall, the nitrogen content appeared to increase with pyrolysis temperature, which is believed to be due to their relative inertness leading to their accumulation in the solid (Caco, 2014) and agrees with the literature (Keiluweit et al., 2010).

The maturation of thermally altered biomass is often depicted in a van Krevelen diagram, Figure 7-14 (Baldock & Smernik, 2002; Krull et al., 2009).

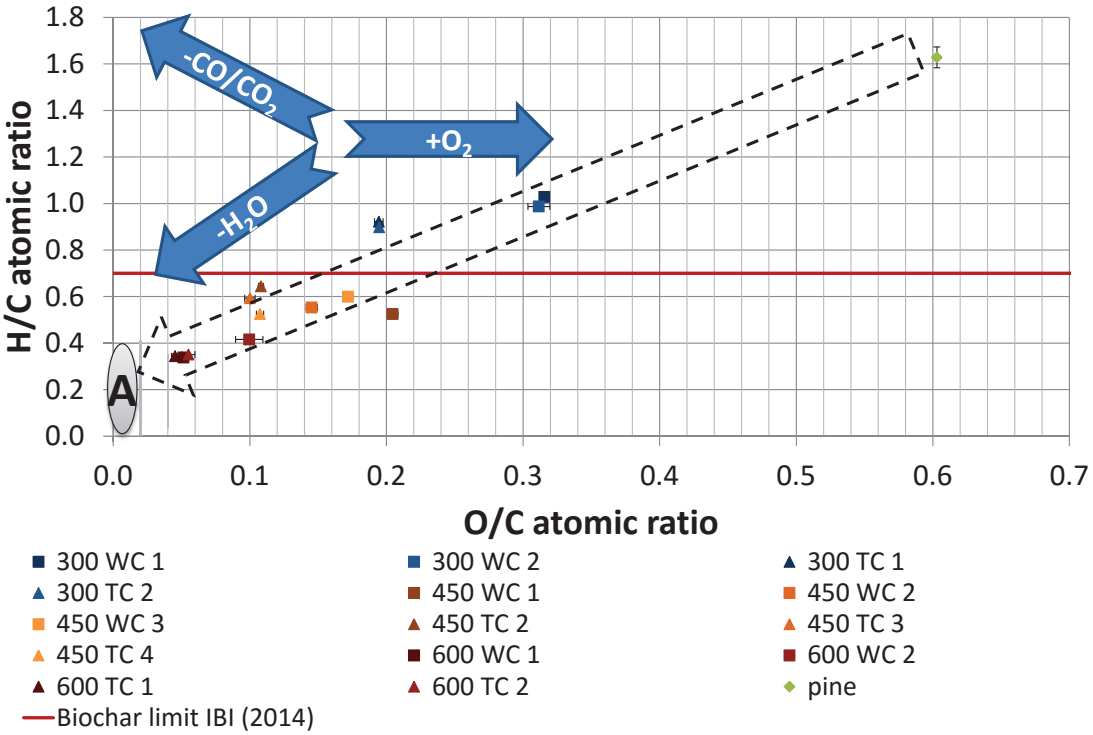

Figure 7-14. Van Krevelen diagram of pine-char and tar-char produced at 300, 450 and 600 °C. The error bars represent the standard deviation. Two repetitions per sample were done except for the sample "450 WC 1" where only one repeat analysis was done. The large dashed black arrow depicts the change in the elemental composition from the feedstock with thermal conversion, *viz.* increasing HTT (Krull et al., 2009). The elemental ratio of Anthracite, A, is included for comparison (McKendry, 2002). The blue arrows are adapted from Baldock and Smernik (2002) representing the van Krevelen trajectory. The red line denotes the upper limit for biochars as proposed by the International Biochar Initiative (2014). Legend: HTT of pyrolysis process_sample type_sample number. C = carbon; H = hydrogen; HTT = highest treatment temperature; PC = pine-char; TC = tar-char. Tar-char and wood-char values adapted from Caco (2014).

Figure 7-14 reveals that a large portion of the thermal alteration is caused by dehydration reactions combined with the formation of carbon monoxide and/ or carbon dioxide (Baldock & Smernik, 2002), which was discussed in more detail in chapter 6. It also shows that biomass becomes more graphitic with increasing *HTT* (Baldock & Smernik, 2002; Downie et al., 2009), and it appears that pine-char has a higher O/C ratio compared to tar-char but that this difference diminishes with increasing *HTT*. The latter trend was confirmed by Energy-dispersive X-ray spectroscopy done in combination with SEM by John McDonald-Wharry from the University of Waikato (Hamilton, New Zealand).

The oxygen content in the tar-char in combination with the surface area development of the coke with increasing temperature, section 7.3.8, indicates that it is non-graphitisable carbon (J. McDonald-Wharry, personal communication, March 3, 2015). Thus, terming it coke is debatable as, according to McNaught and Wilkinson

(1997), coke refers to graphitisable carbon before the onset of graphitisation. However, more detailed analysis like Transmission electron microscopy and heat treatment above 2000 °C is required to exactly know how graphitisable or non-graphitisable it is (J. McDonald-Wharry, personal communication, March 3, 2015). Nevertheless, it supports the observation in 7.3.1 that both char, tar-char and pine-char, are nanostructurally very similar, in particular at higher *HTT's*.

7.3.4 Raman Analysis

Raman analysis was performed to gain information of the nanostructural development of both types of char with increasing *HTT*. The Raman G band position, which was found to correlate well with the *HTT* of chars and thus the extent of carbonisation (McDonald-Wharry, Manley-Harris, et al., 2013; McDonald-Wharry, Ripberger, Manley-Harris, & Pickering, 2013), revealed that both types of chars exhibit a similar G band position and therefore nanostructural development, Figure 7-15.

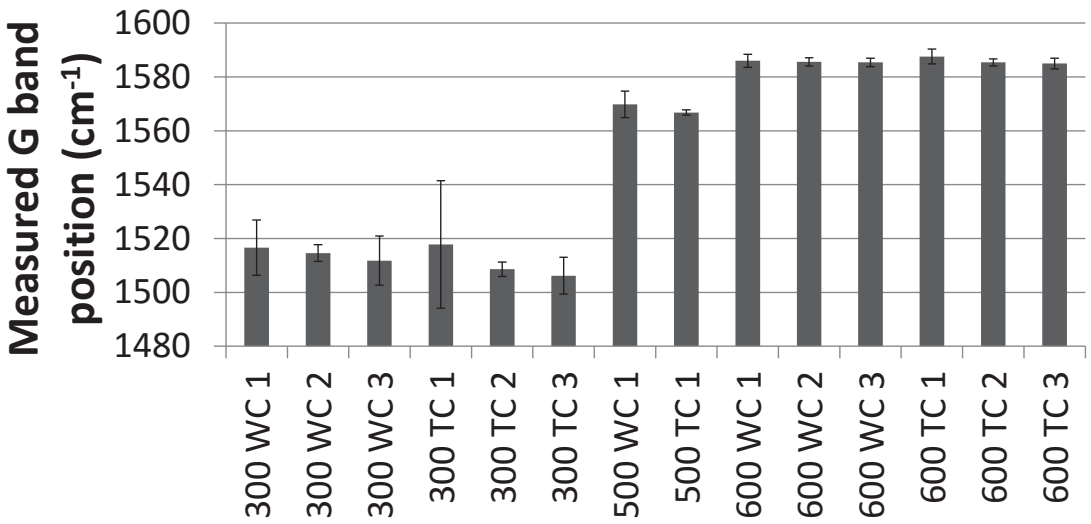

Figure 7-15. Measured G band positions of wood-chars and tar-chars with increasing *HTT*. The error bars represent the 99 % confidence intervals generated from five separately obtained Raman spectra. Legend: *HTT* in °C_char type_sample number. *HTT* = highest treatment temperature; TC = tar-char; WC = wood-char. Adapted from John McDonald-Wharry from the University of Waikato (Hamilton, New Zealand).

Figure 7-15 shows a close agreement of the G band positions of chars produced at the same *HTT*, in particular of chars produced at 600 °C. This indicates that at higher temperatures initial differences in the nanostructure of the chars disappear. Similarities in the nanostructure were also confirmed by the I_D/I_G and I_A/I_G ratios in Figure 7-16.

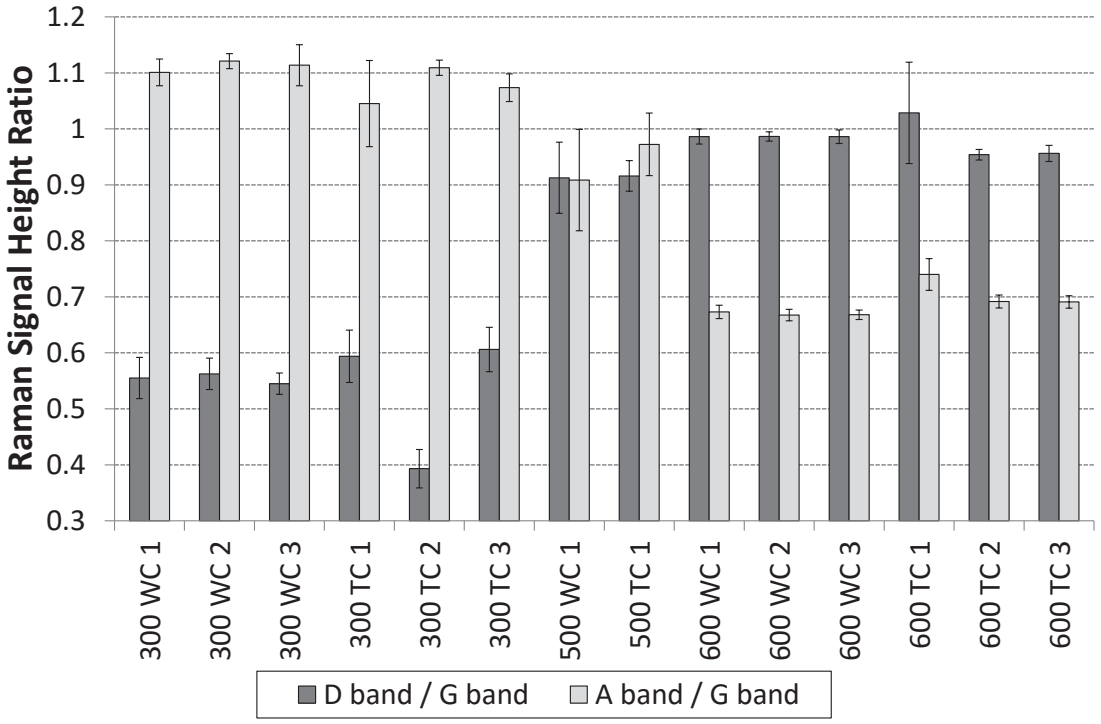

Figure 7-16. Comparison of I_D/I_G and I_A/I_G ratios of wood-chars and tar-chars with increasing *HTT*. The error bars represent the 99 % confidence intervals generated from five separately obtained Raman spectra. Legend: *HTT* in °C_char type_sample number. *HTT* = highest treatment temperature; I_A = Intensity/ height of A band; I_D = Intensity/ height of D band; I_G = Intensity/ height of G band; TC = tar-char; WC = wood-char. Adapted from John McDonald-Wharry from the University of Waikato (Hamilton, New Zealand).

The increasing I_D/I_G ratio with rising *HTT* in Figure 7-16 describes the growth of graphene-like structures in the char with increasing *HTT* (McDonald-Wharry, Manley-Harris, et al., 2013). In Figure 7-16 tar- and wood-chars produced at the same *HTT* exhibit similar I_D/I_G ratios, except tar-char "300 TC 2", which had a significantly lower value. The reason is unknown but could be related to differences in the tar production process, namely the *HTT* (compare Figure 7-7). Contrary to the I_D/I_G ratio the I_A/I_G ratio is a measure of the amorphicity, which decreases with increasing *HTT*. Thus, the opposite trend to the I_D/I_G ratio was expected. Comparing both values in Figure 7-16 indicates that there might be a slight difference between both types of char, which was investigated further by dividing the valley height by the G band height, I_V/I_G, as it is a measure of the conversion of amorphous carbon into larger aromatic or graphene like clusters (McDonald-Wharry, Manley-Harris, et al., 2013), Figure 7-17.

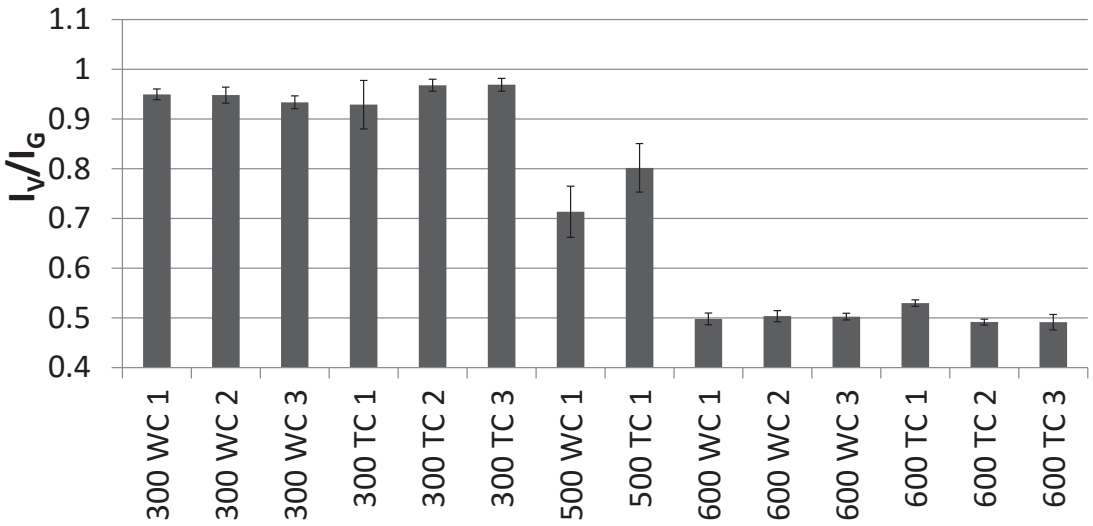

Figure 7-17. Comparison of I_V/I_G signals of wood-char and tar-char with increasing *HTT*. The error bars represent the 99 % confidence intervals generated from five separately obtained Raman spectra. Legend: *HTT* in °C_char type_sample number. *HTT* = highest treatment temperature; I_G = Intensity/ height of G band; I_V = Intensity/ height of Valley; TC = tar-char; WC = wood-char. Adapted from John McDonald-Wharry from the University of Waikato (Hamilton, New Zealand).

As anticipated, Figure 7-17 shows a decrease in the I_V/I_G height ratio with increasing temperature revealing that the disordered carbon structure is converted into a structure containing turbostratic crystallites at the expense of amorphous carbon, which agrees with the structural models reported in the literature (Downie et al., 2009; Keiluweit et al., 2010). It appears that at lower *HTT's* tar-chars have marginally higher amorphous carbon contents than wood-chars. This is, however, opposite to the findings in Figure 7-16. The difference between wood-chars and tar-chars is not anymore apparent at 600 °C, which agrees with the observation in Figure 7-15, indicating that at high temperatures no differences are present between the two types of chars. This is supported by the findings of McDonald-Wharry, Manley-Harris, et al. (2013), who demonstrated that between various pre-cursors, deriving from carbohydrate based feedstocks or feedstocks rich in oxygen, differences in the nanostructure disappear above 700 °C. This is further in agreement with the observation that the chars from the biomass constituents become increasingly similar with higher *HTT's* as well, as reviewed by Collard and Blin (2014).

Generally, the char formation from lignin is more intuitive as its structure is already made up of aromatic rings (Collard & Blin, 2014). The occurring rearrangement reactions are likely to involve the O-CH_3 group as discussed in 6.3.4. Other reactions taking place are the conversion of the side chains of the phenylpropane units, and the breakage of ether bonds between them (*ibid*). These reactions are

associated with the formation of oxygenated compounds like H_2O, CO_2, CO, and formaldehyde (Cao, Xiao, Xu, Shen, & Jin, 2013; Collard & Blin, 2014; Jakab, Faix, Till, & Székely, 1995; S. Wang et al., 2009). This leads to an oxygen loss in the solid-phase with increasing temperature, leading to a lignin char with almost no organic oxygen at 600 °C (Sharma et al., 2004). Oxygen loss also occurs during char formation from cellulose, which below 300 °C mainly takes place by dehydration reactions (Collard & Blin, 2014). With increasing temperature the char structure changes from pyran rings to furan rings (see 6.3.4), and subsequently to benzene rings linked with aliphatic and oxygenated groups giving it a structure similar to lignin char at 400 °C as reviewed by Collard and Blin (2014). The char will then undergo similar reactions to lignin char at higher temperatures, and similar rearrangement reactions are expected for polysaccharides of hemicellulose. This explains the observed oxygen loss in the solid-phase as revised by Neves, Thunman, Matos, Tarelho, and Gómez-Barea (2011) and depicted in Figure 7-14, and indicates that these different chars become increasingly similar chemically and nanostructurally with severity of the heat treatment.

Furthermore, the photoluminescence slope divided by I_G, which is believed to be related to the hydrogen content in the amorphous phase (McDonald-Wharry, Manley-Harris, et al., 2013), was determined and is depicted in Figure 7-18.

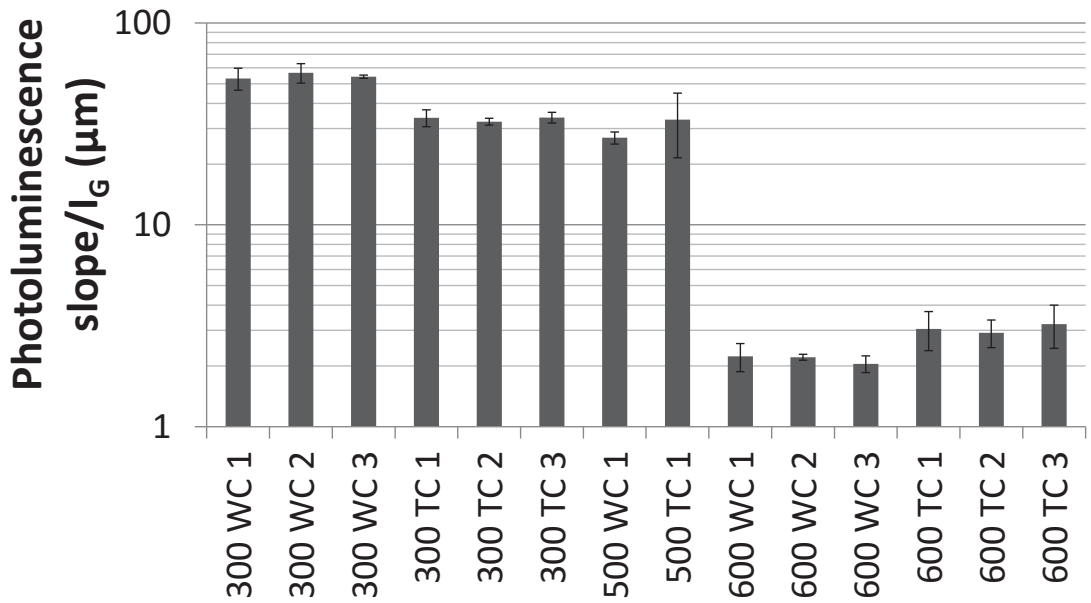

Figure 7-18. Comparison of photoluminescence slope/I_G signals of wood-char and tar-char with increasing *HTT*. The error bars represent the 99 % confidence intervals generated from five separately obtained Raman spectra. Legend: *HTT* in °C_char type_sample number. *HTT* = highest treatment temperature; I_G = Intensity/ height of G band; TC = tar-char; WC = wood-char. Adapted from John McDonald-Wharry from the University of Waikato (Hamilton, New Zealand).

Figure 7-18 shows that tar-chars appear to have a lower photoluminescence slope than wood-chars at 300 °C but that this trend reverses with increasing *HTT*. The lower slope value at 300 °C was identified to be related to a negative fluorescence slope contribution from the presence of a liquid tar phase (McDonald-Wharry, Ripberger, et al., 2013). The higher photoluminescence slope values of tar-chars produced at higher *HTT's* compared to wood-chars indicate the presence of slightly more hydrogen-rich amorphous carbon in tar-chars. The overall decrease in the photoluminescence slope/I_G value with rising *HTT* is the consequence of hydrogen loss and decreasing H/C atomic ratio, Figure 7-13, (McDonald-Wharry, Ripberger, et al., 2013).

The above discussion shows that the nanostructural development of chars is more a function of the *HTT* than the feedstock origin.

7.3.5 Proximate Analysis

In 7.3.2 it was shown that the presence or absence of a lid during char pyrolysis can impact the proximate analysis results. Therefore, the effect of the presence of a lid together with the sample preparation method was investigated on the proximate analysis results of pine-char and tar-char. Sample preparation in form of size reduction was required as the resulting char and coke pieces were too large for the TGA crucibles and

the coke had internal gas pockets (see 7.3.1). Due to the latter it was decided to use a tar-char sample for studying the effect of size reduction method on proximate analysis. A tar-char sample produced at 300 °C, Figure 7-19, was selected as it has a higher volatile matter content and thus, if differences exist, they are expected to be larger in this sample compared to one produced at 600 °C.

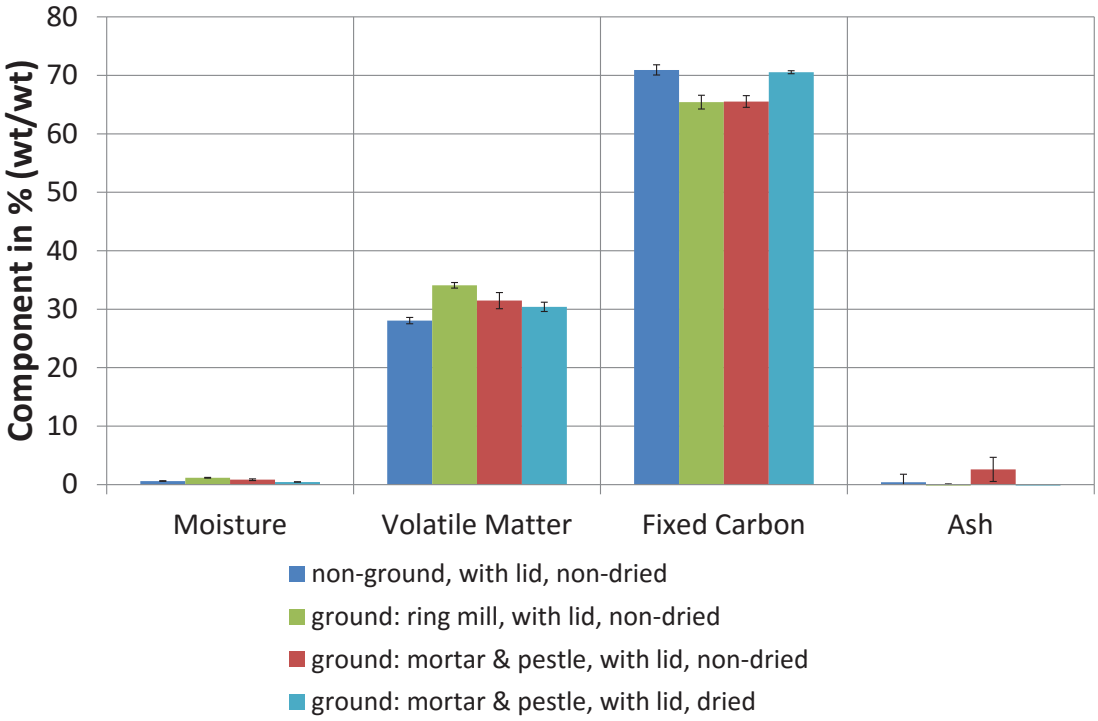

Figure 7-19. Proximate analysis results of coke produced form tar pyrolysis with a *HTT* of 300 °C. The tar for coke production was collected from pine pyrolysis with a *HTT* of 606 °C. Non-ground means the coke was crushed with tweezers to fit the TGA crucible. Dried means the sample was previously oven-dried at 105 °C for 24 h. The grinding time of the ring mill was ≈ 10 s. The error bars represent the standard deviation. Two repetitions for each analysis were carried out except for the dried sample was only one repeat analysis done. *HTT* = highest treatment temperature; wt = weight.

Figure 7-19 shows that the standard deviation between analysis runs is relatively small and that there is a larger difference between the runs applying different methods. Despite this, the effect of the sample treatment in Figure 7-19 is inconclusive because, for instance, a lower volatile matter and higher fixed carbon content were expected for the samples ground electrically in the ring mill as they are subject to more heating. Samples of the coke were also oven-dried at 105 °C to see whether or not that impacts the so-called moisture content as tar-char does not appear to have a large surface area for the adsorption of water. Differences were found to be minimal for the moisture and volatile matter content but relatively large for the fixed carbon and ash content. The respective weight-loss compared to the non-dried case is depicted in Figure F-25 in

Appendix F.5. The difference in the fixed carbon and ash content seem to be more related to sample inhomogeneity and equipment error than to the analysis method. It is argued that the equipment error is more important as the standard deviation between repeat analyses is generally fairly small (excluding the ash content). Thus, the variation between the methods in Figure 7-19 could be merely due to equipment error, which is supported by comparing the proximate analysis results of non-ground and ground coke produced at 600 °C in Figure F-26 in Appendix F.5. An F-test with subsequent t-test revealed that the differences between the fixed carbon content and volatile matter content are not statistically significant (p-value of 0.054 and 0.167 for the fixed carbon and volatile matter content respectively; the significance level was selected as 0.05).

Due to the inconclusiveness of the findings and the recommendations of the International Biochar Initiative (2014) it was decided to grind the samples in a metal mortar and pestle to minimise the risk of sample heating. When grinding the different samples the following observations were made:

1. wood-char is more difficult to grind than tar-char,
2. lower temperature char/ coke is harder to grind than higher *HTT* char/ coke,
3. tar-char produced at 300 °C is sticky, has a brownish colour, a tarry odour and differences seem to exist between cokes produced from tars collected at varying *HTT's*; and
4. coke produced at a *HTT* of 600 °C does not stick and has a silvery shine.

The observations of number 3 confirm the findings in Figure 7-18 that a lower photoluminescence slope in the tar-char samples produced at 300 °C is caused by the presence of a liquid phase. One sample even became liquid when oven-drying at 105 °C, then solid again upon cooling. This illustrates that there are differences between the cokes and that during the course of pyrolysis they may solidify, liquefy and re-solidify several times. Also some volatilisation and re-condensation is likely. These findings further support the discussion associated with Figure 7-7 that at 300 °C the tar decomposition is in its initial stages explaining the negligible effect of the tar *HTT* on the coke yield compared to pyrolysis at 600 °C. These observations also reveal that the mechanical strength of the chars/ cokes is affected by the *HTT*, and that the tar-char has the ability to alter the physical properties, like porosity, which is important for soil functions (e.g. hydrology). It has been reported that condensed liquids or adsorbed

volatile pyrolysis products in char can exert a phytotoxic effect on plants (Buss & Mašek, 2014; Buss, Mašek, Graham, & Wüst, 2015). Thus, the longer vapour-phase residence times, desired for secondary char formation, can have negative effects for biochar-soil-plant interaction, if pyrolysis is carried out at low *HTT's*.

It was observed that tar-char is very electrostatic and that this increases with *HTT*. Therefore, it might be advantageous to apply a lid for analysis in the case of large electrostatic forces to avoid loss of sample. The effect a lid exerts on the proximate analysis of char/ coke was investigated and is illustrated in Figure 7-20.

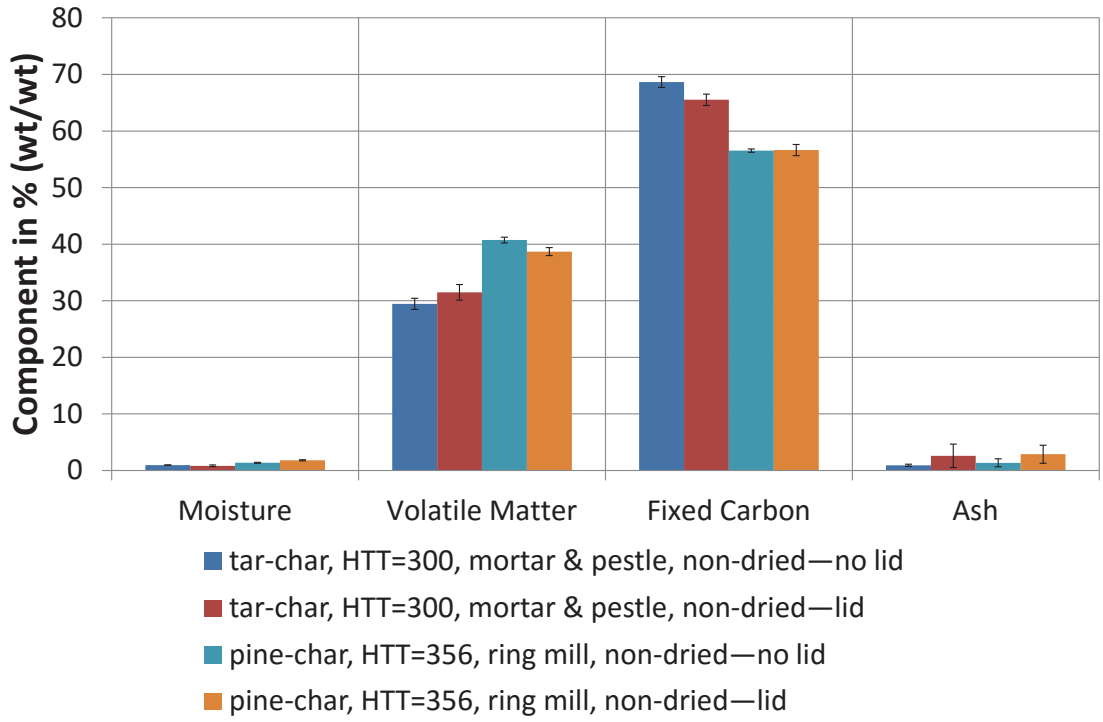

Figure 7-20. Effect of a lid on the proximate analysis of tar-char and pine-char. The tar for coke production was collected from pine pyrolysis with a HTT of 606 °C. The error bars represent the standard deviation. Two repetitions for each analysis run were done except for the pine-char where only one was done. Legend: char type, HTT of char production in °C, grinding information, drying information—lid or no lid. The pine-char proximate analysis was taken from Bridges (2013), who analysed the samples of Bashir (2012). HTT = highest treatment temperature; wt = weight.

For comparison of the lid and no lid case in Figure 7-20 was char/ coke selected with a low HTT (similar to Figure 7-19) as it has a higher volatile matter content and is thus expected to be more sensitive to the presence or absence of a lid. Pine-char samples ground with the ring mill were included as wood-char is generally harder to grind and the grinding method has no effect on the comparison of the cases lid and no lid as the unlikely heating during grinding (see above) affects only the feedstock composition minimally but not directly the actual proximate analysis test. The differences in the

volatile matter and fixed carbon content of the pine-char were found to be not statistically significant by doing a t-test assuming equal variance (p-value 0.08 and 0.90 for volatile matter and fixed carbon content respectively; the significance level was selected as 0.05). The t-test assuming equal variance was also performed on the tar-char for the volatile matter and fixed carbon content respectively. The difference was found to be not statistically significant for the volatile matter content (p-value 0.09; significance level was selected as 0.05) but significant for the fixed carbon content (p-value 0.02; significance level was selected as 0.05). However, the difference observed in the fixed carbon content in the tar-char could be associated with the uncertainty in the measurement as expressed above and revealed by the large variation in the ash content. The weight-loss and derivative weight-loss data of the proximate analysis runs in Figure 7-20 are depicted in Figure F-27 and Figure F-28 in Appendix F.5 for the pine-char and tar-char respectively. The large difference above 200 min between the cases lid and no lid in these figures is due to mass transfer limitations as the lid hinders the access of air to the sample, which is introduced for combustion to determine the fixed carbon and oxygen content.

The more interesting region is the region to 700 °C in the above carried out proximate analysis, because this is the here investigated pyrolysis range relevant for the manufacture of biochar, which is depicted in Figure 7-21 for the pine-char and tar-char compared to radiata pine.

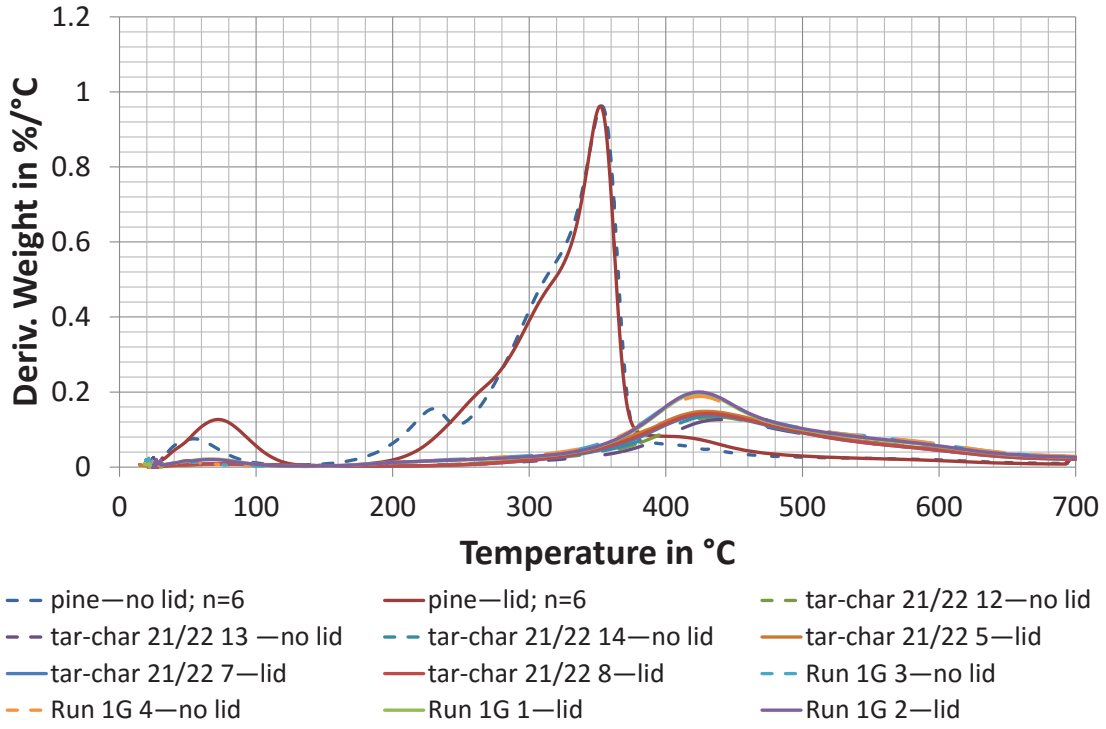

Figure 7-21. Comparison of derivative weight-loss curves obtained by pyrolysis with and without a lid of pine, tar-char and pine-char. The samples labelled "pine", "Run", and "tar-char" refer to the feedstock radiate pine, the pine-char and tar-char respectively. Legend: sample name—lid or no lid; number over which was averaged in the case of pine samples.

Figure 7-21 confirms that there is no difference between pine-char proximate analysis with and without a lid but that there might be a small difference in the tar-char analysis. Mass transfer limitations can be disregarded due to the fact that in the case of a lid the derivative weight-loss appears to be higher and earlier compared to the case without a lid (see 3.3.5 for details). This means that the volatiles released from tar-char may interact although less volatiles are released compared to pine-char. In the case of pine-char some moisture is initially absorbed by the char and its release is again transfer limited as exhibited by the right shift of the moisture peak in Figure 7-21. This characteristic right shift for the case with lid in the initial peak is absent for the tar-char samples.

Overall, for the purpose of proximate analysis of the tar-char and pine-char samples, it can be concluded that no significant effect on the results is exerted by the presence or absence of a lid, which was anticipated as few volatiles are released from the chars that have the ability to interact. These findings are opposite to the ones for the ash content.

A comparison between pine-char and tar-char volatile matter and fixed carbon content measured by Caco (2014) is displayed in Figure 7-22 and Figure 7-23 respectively.

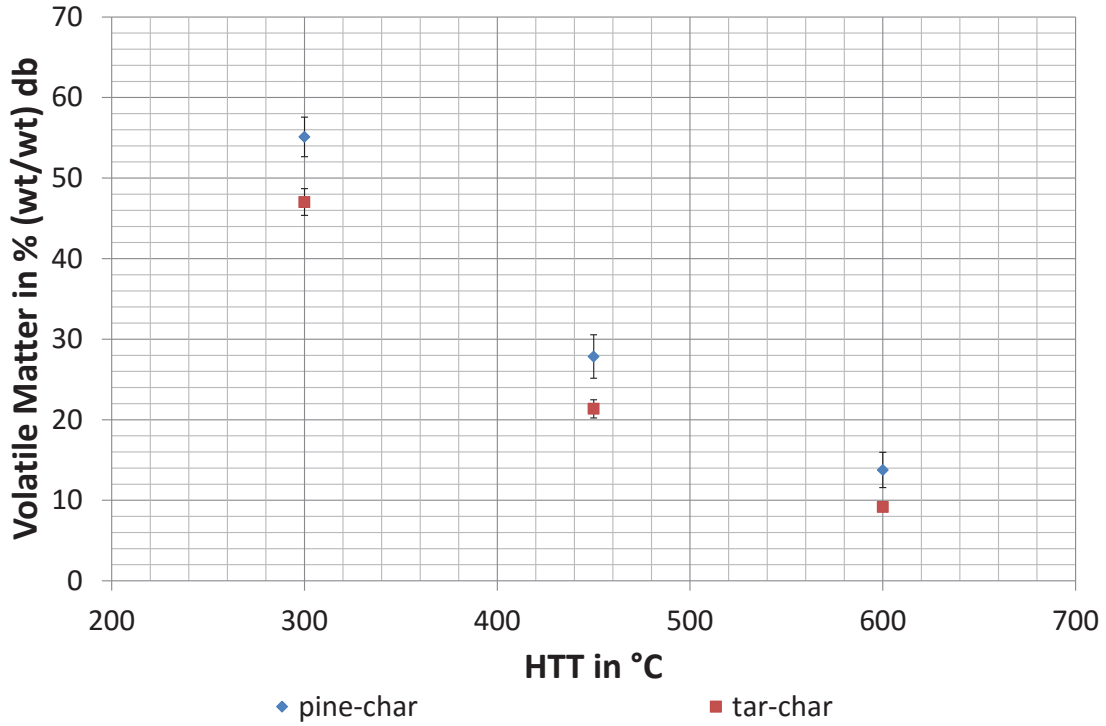

Figure 7-22. Comparison between averaged pine-char and tar-char volatile matter content. The error bars represent the standard deviation. One repetition was done for each char/ coke sample produced at 300 and 600 °C, and two and three for the char and coke produced at 450 °C respectively. The original data is depicted in Figure F-29 in Appendix F.5. db = dry basis; HTT = highest treatment temperature; wt = weight. Adapted from Caco (2014).

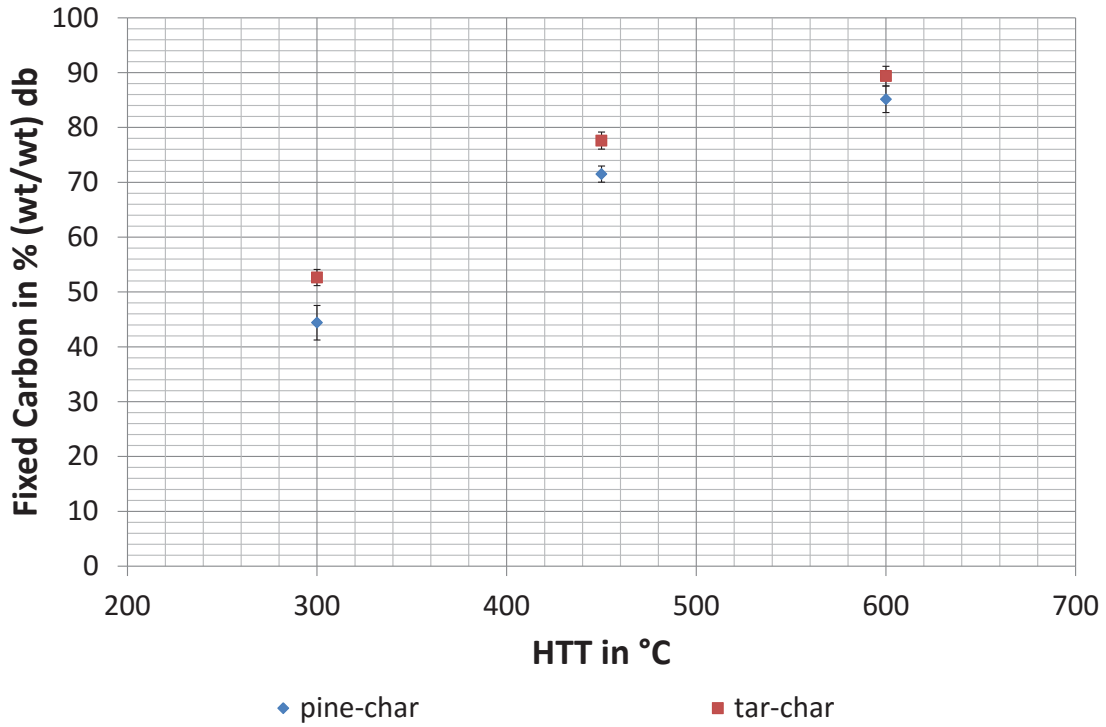

Figure 7-23. Comparison between pine-char and tar-char fixed carbon content. The error bars represent the standard deviation. One repetition was done for each char/ coke sample produced at 300 and 600 °C, and two and three for the char and coke produced at 450 °C respectively. The original data is depicted in Figure F-30 in Appendix F.5. db = dry basis; HTT = highest treatment temperature; wt = weight. Adapted from Caco (2014).

Figure 7-22 and Figure 7-23 show that with decreasing *HTT* the volatile matter increases and the fixed carbon content decreases, and that pine-char has a higher volatile matter and lower fixed carbon content than tar-char. The original data combined with additional tar-char analysis results are depicted in Figure F-29 and Figure F-30 in Appendix F.5 for the volatile matter and fixed carbon content respectively. The added values do not fit as well, which is believed to be caused by the different oven used for pyrolysis that was subject to a higher temperature overshoot as discussed in 7.3.2, *viz.* the actual *HTT* is thought to be higher. Nevertheless, these supplementary data points confirm that tar-char has lower volatile matter and higher fixed carbon contents, indicating that it is more stable than wood-char (Zimmerman, 2010). However, this is not supported by the atomic H/C ratio in Figure 7-13, and the findings of the Raman analysis, which suggest that the tar-char is slightly more amorphous and hence less stable. It is important to note that for averaging in Figure 7-22 and Figure 7-23 the analysis of sample "TC 450 1" was excluded as it displayed a significantly different pyrolysis behaviour, Figure F-31 in Appendix F.5. Further the original data displayed in Figure F-29 and Figure F-30 in Appendix F.5 indicates that the difference between the two types of char decrease with increasing *HTT*, supporting the findings in 7.3.4.

7.3.6 Electrical Conductivity and pH

The cation exchange capacity, CEC, a measure of cations present in plant-available form, of soil organic matter in general and biochar in particular increases with pH (Lehmann, 2007). Lehmann (2007) showed that biochar pH is dependent on the *HTT* and can range from 4 to 12; generally increasing with *HTT*. Therefore, the aim here was to investigate whether or not there are any differences between pine-char and tar-char pH as a function of *HTT*, Figure 7-24.

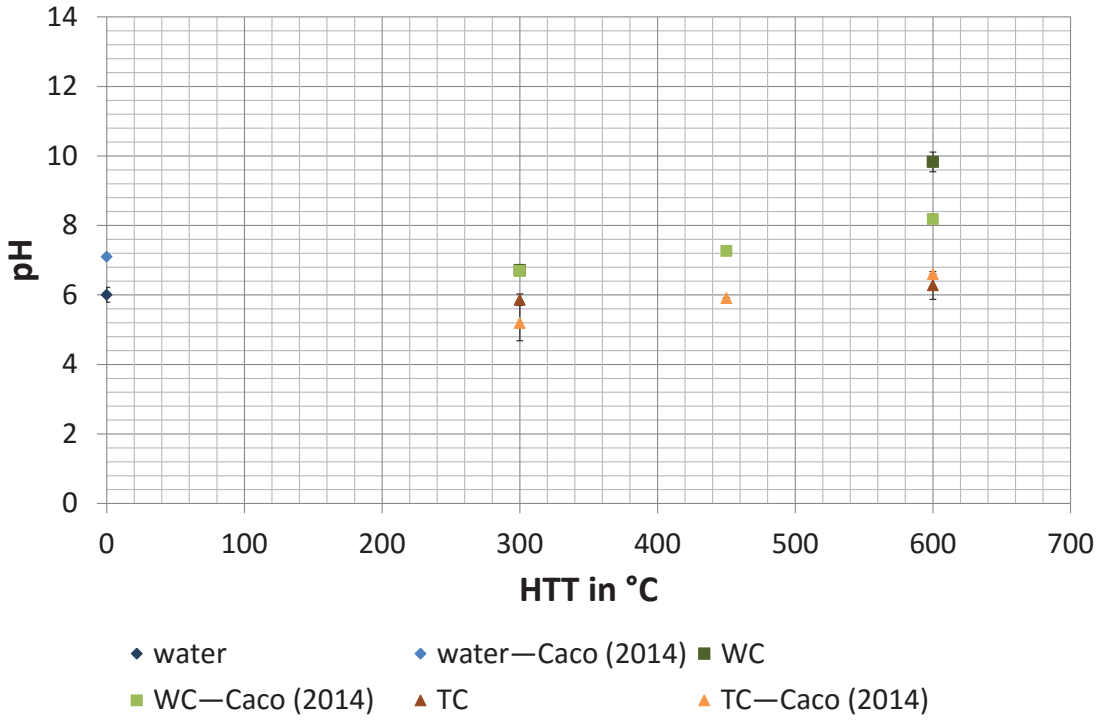

Figure 7-24. pH of pine-char and tar-char in water solution as a function of HTT. The error bars represent the standard deviation. Two repetitions were done per sample. HTT = highest treatment temperature; TC = tar-char; WC = wood-char; water = Milli-Q® water.

Figure 7-24 confirms the increasing trend in biochar pH with *HTT* as reported by Lehmann (2007), despite there being a relatively large variation between the two experimental sets. At 300 °C the pH of pine-char appears to be slightly lower than that of neutral water although the pH of the neutral water was initially measured at 6.01 ± 0.21 indicating some calibration error. However, the analyses of Caco (2014) revealed a pH of 7.1 ± 0.01 for the Milli-Q® water and verified the values for pine-char. The measured pH values of pine-char agree with the work of Rajkovich et al. (2012) at 300 °C but differ at higher temperatures, where they remained below 6 for pine char obtained at 400, 500 and 600 °C in the work of Rajkovich and his team. The reasons are unknown but could be related to the pine species and pyrolysis conditions. Comparing the pH of pine-char and tar-char exposes a clear difference between both types of char, with tar-char having a lower pH and possibly a lower temperature dependence. That the presence of liquids or adsorbed volatiles in char can cause an acidic pH was shown by Buss and Mašek (2014), and as discussed above (7.3.4 and 7.3.5) liquids were found to be present in the low *HTT* coke, and thus could have contributed to the low pH.

The electrical conductivities of the samples in Figure 7-24 were determined before the pH measurement and are depicted in Figure 7-25.

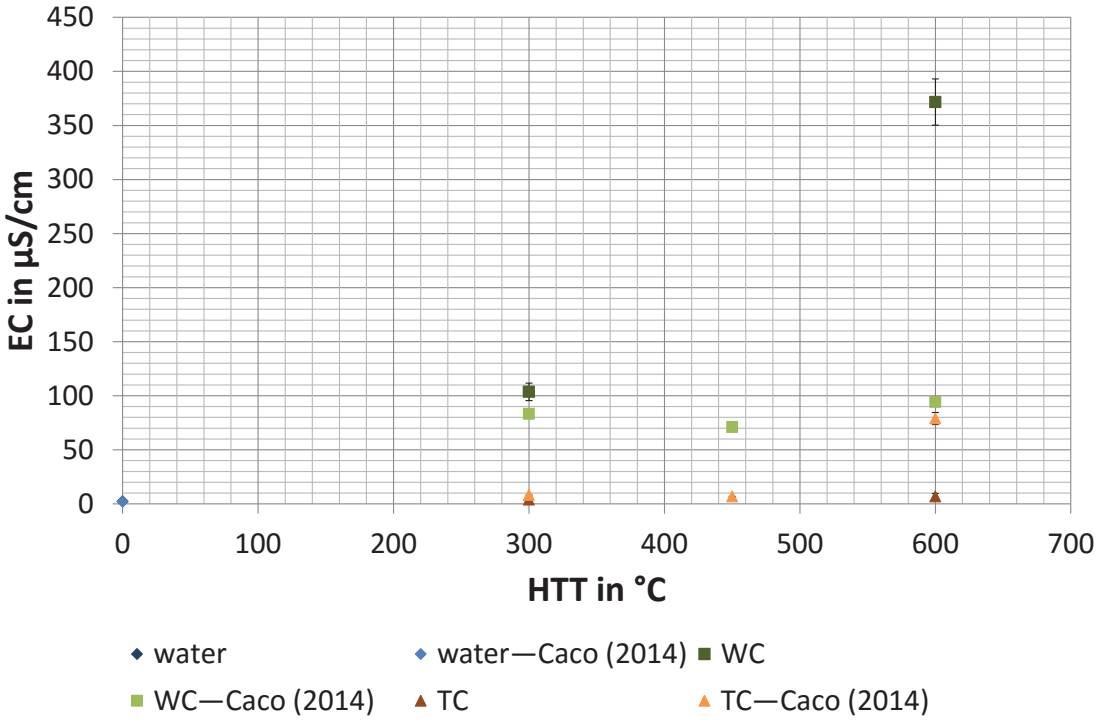

Figure 7-25. Electrical conductivity of pine-char and tar-char in water solution as a function of HTT. The error bars represent the standard deviation. Two repetitions were done per sample. EC = electrical conductivity; HTT = highest treatment temperature; TC = tar-char; WC = wood-char; water = Milli-Q® water.

Figure 7-25 shows an even larger variation in electrical conductivity between the different experimental sets compared to pH in Figure 7-24. The reasons for the uncertainties are not known. An increase in EC with the addition of pine-char was anticipated due to the introduction of ions associated with the char. However, the apparent increase with *HTT* was not expected, as the ash content was found to decrease with increasing *HTT*, Figure 7-8. A decreasing trend with *HTT* is reported by Rajkovich et al. (2012) for pine pyrolysed at 300, 400, 500 and 600 °C; although some fluctuations for other feedstock's with *HTT* were present. Tar-char on the other side seems to have no effect on the EC, which is believed to be due to its glassy nature that prevents the ions from entering the water.

These two results reveal that enhancement of secondary reactions in biochar manufacture can impact plant-soil interactions.

7.3.7 True Density

The change in true or solid density of tar-char and pine-char with *HTT* is illustrated in Figure 7-26, and compared to the solid density of radiata pine.

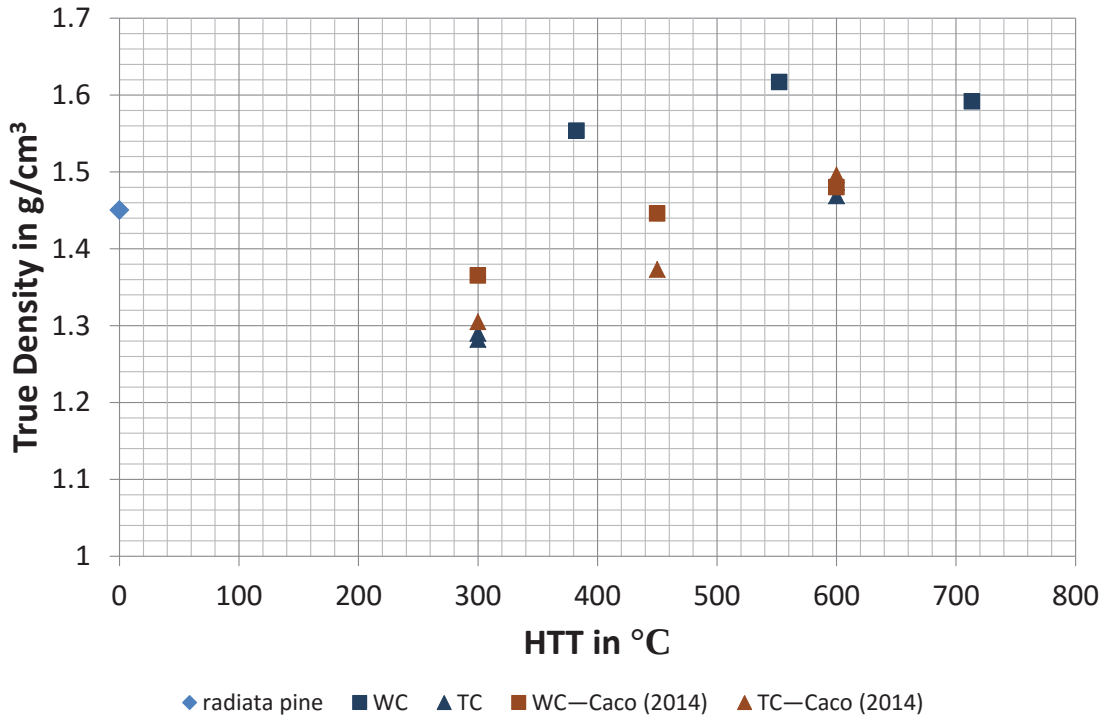

Figure 7-26. True density of pine-char and tar-char as a function of HTT. The true density of radiata pine has been included for comparison. HTT = highest treatment temperature; TC = tar-char; WC = wood-char.

Figure 7-26 shows that there is a good agreement between the tar-char samples of the different experimental sets but also that there is a relatively large variation between the wood-char samples. The differences in the wood-char samples are believed to be caused by the different pyrolysis methods, that is the wood-char samples were not produced in an electric furnace like the tar-char samples or the samples of Caco (2014) but were taken from the gas fired drum pyrolyser described in 3.2.4. Despite this the results reveal that the true density increases with *HTT*, which agrees with the literature and is caused by the conversion of highly disordered carbon in an amorphous mass into a turbostratic carbon structure with a higher density as reviewed by Downie et al. (2009) (see also 7.3.4). Another major observation is that the tar-char appears to have a lower density than pine-char at temperatures below 600 °C indicating that it is more amorphous than wood char, which agrees with some of the findings in 7.3.4. The initial decrease in the solid density of char compared to wood is caused by the destruction of

the ordered cell wall structure. Bulk density was not analysed as tar-char does not have macroscopic porosity like wood-char (see 7.3.1).

7.3.8 Surface Area

The results of surface area analysis are presented in Table 7-1.

Table 7-1. BET N_2 surface area of wood-char and tar-char.

T in °C	Wood-char in m^2/g	Tar-char in m^2/g
300	0.7239	0.1962
600	400.3918	205.0244

Note. Surface area was analysed by Nitrogen physisorption at 77.35 K and carried out by the team of Dr. Geoff Waterhouse at the University of Auckland (Auckland, New Zealand). The original analysis data is provided in Appendix F.6.

The results in Table 7-1 show that wood-char has about three times and two times the surface area of tar-char at 300 and 600 °C respectively, and that the surface area increases significantly with *HTT*. The higher surface area of wood-char was anticipated due to the presence of the textural structure of the feedstock (section 7.3.1). Similar values for the surface area of wood-char at 300 and 600 °C are reported by Keiluweit et al. (2010). The large increase in the surface area with increasing *HTT* in both types of chars is due to micro pore formation associated with the nanostructural development of chars as demonstrated in the dynamic molecular structure model of Keiluweit et al. (2010). This confirms that both tar-char and wood-char undergo the same structural development with increasing *HTT* as suggested in 7.3.4. The isotherms are provided in Appendix F.6. It is important to note that the data for the samples other than the wood-char produced at a *HTT* of 600 °C, which displays a typical adsorption isotherm for a microporous material, is poor due to their low specific surface areas that are characteristic for biochars produced at temperatures below 500 °C (G. Waterhouse, personal communication, January 7, 2015). Nevertheless, the results can be used for comparison as the analysis conditions were the same and the aim was a comparative analysis of the nanostructural development.

7.3.9 Calorific Values

The *HHV* was determined for the pine-char and tar-char manufactured at the different *HTT's* and compared to radiata pine (see also 3.2.1.5) to evaluate their use as a fuel, Figure 7-27.

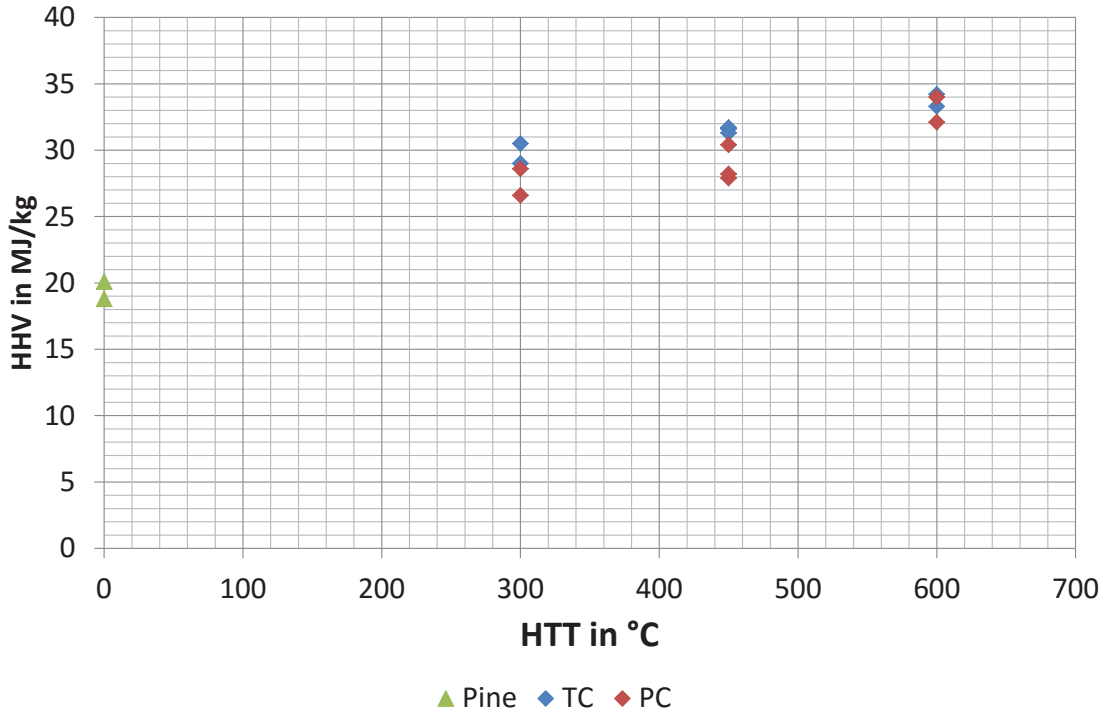

Figure 7-27. Higher heating values of pine, pine-char and tar-char as a function of the *HTT*. HHV = higher heating value; HTT = highest treatment temperature; PC = pine-char; TC = tar-char.

Figure 7-27 shows that the *HHV* increases with *HTT* but that there appears to be not much difference between pine-char and tar-char. The increase in *HHV* with *HTT* is a consequence of the increased carbon and fixed carbon content, Figure 7-12 and Figure 7-23 respectively, while at the same time the oxygen content decreases, Figure 7-14. This relationship is evidenced by the multitude of correlation equations available in the literature, which are based on these values. For details see 3.2.1.5 or Sheng and Azevedo (2005). Considering this, it is evident that tar-char has a higher *HHV* as it has a higher carbon content, fixed carbon content and reduced oxygen content compared to pine-char (see 7.3.3 and 7.3.5). As the differences between tar-char and pine-char generally decreases with *HTT* the difference in the *HHV* value diminishes correspondingly, Figure 7-27. The variation is larger in Figure 7-27 for pine-char because it is more heterogeneous than tar-char. This is likely to be due to the experimental process of pine-char formation which will probably include some

deposition of coke as secondary char within the relatively large cylindrical samples (see 3.3.2). Thus, it can be concluded that coke is generally a better fuel than pine-char especially if produced at lower *HTT*'s.

7.4 Conclusions

It was discovered that self-charring of tar can significantly contribute to the char yield, and that ash compounds catalyse this coke formation at temperatures above 300 °C. This supports the findings of chapter 4 that the catalytic action of inorganics is with respect to secondary reactions as coke formation from tar is a secondary mechanism. However, it also reveals that below 300 °C other mechanisms than self-charring of tar are catalysed.

Characterising the structure of pine-char and tar-char revealed that their nanostructures are very similar, where initial differences, that tar-char is slightly more amorphous and contains less oxygen, diminish with increasing *HTT* as the amorphous carbon mass turns into an increasingly structured turbostratic char. Both chars are believed to belong to the non-graphitisable carbon, which explains their increasing micro porosity with increasing *HTT*. However, the surface area of tar-char is two to three times smaller than wood-char in the temperature range 300 to 700 °C, because it lacks the textural structure of the biomass. This lack of macro porosity reduces the biochar value of self-charred tar-char where soil functions like hydrology are important. In addition tar-char produced at low temperatures was found to contain liquid pyrolysis products, which can have a phytotoxic effect on plants, and might be part of the reason that tar-char was found to have a lower pH value than wood-char. Differences were also detected in the electrical conductivity with tar-char but the effect will be minimal due to its reduced porosity, making inorganics less accessible to water, as well as reduced presence of inorganics due to their previous volatilisation. Therefore, the structural properties important for biochar are related to the effect that pyrolysis has on the macroscopic structure rather than the microscopic structure. This shows that the different chars may cause various soil responses.

To sum it up, pine-char and tar-char are nanostructurally similar, especially at higher *HTT*'s, but their different macroscopic structure along with differences in the ash content and possibly the presence of functional groups are likely to impact biochar-soil-plant interactions, which has to be regarded when maximising the char yield by enhancing secondary char formation. Overall, it appears that separation of primary and secondary char is not straightforward.

7.5 References

Baldock, J. A., & Smernik, R. J. (2002). Chemical composition and bioavailability of thermally altered Pinus resinosa (Red pine) wood. *Organic Geochemistry, 33*(9), 1093-1109. doi:10.1016/S0146-6380(02)00062-1

Balonek, C. M., Colby, J. L., Persson, N. E., & Schmidt, L. D. (2010). Rapid ablative pyrolysis of cellulose in an autothermal fixed-bed catalytic reactor. *ChemSusChem, 3*(12), 1355-1358. doi:10.1002/cssc.201000257

Bashir, F. (2012). *Fracturing of wood during pyrolysis* (Unpublished final year project report). Massey University, Palmerston North, New Zealand. The report can be accessed by contacting J.R.Jones@massey.ac.nz

Bridges, R. (2013). *Design and characterisation of an 'open source' pyrolyser for biochar production* (Master's thesis, Massey University, Palmerston North, New Zealand). Retrieved from http://mro.massey.ac.nz/handle/10179/5864

Buss, W., & Mašek, O. (2014). Mobile organic compounds in biochar – A potential source of contamination – Phytotoxic effects on cress seed (Lepidium sativum) germination. *Journal of Environmental Management, 137*, 111-119. doi:10.1016/j.jenvman.2014.01.045

Buss, W., Mašek, O., Graham, M., & Wüst, D. (2015). Inherent organic compounds in biochar–Their content, composition and potential toxic effects. *Journal of Environmental Management, 156*, 150-157. doi:10.1016/j.jenvman.2015.03.035

Caco, N. (2014). *Understanding the differences between char and tar-char* (Unpublished final year project report). Massey University, Palmerston North, New Zealand. The report can be accessed by contacting J.R.Jones@massey.ac.nz

Cao, J., Xiao, G., Xu, X., Shen, D., & Jin, B. (2013). Study on carbonization of lignin by TG-FTIR and high-temperature carbonization reactor. *Fuel Processing Technology, 106*, 41-47. doi:10.1016/j.fuproc.2012.06.016

Cetin, E., Gupta, R., & Moghtaderi, B. (2005). Effect of pyrolysis pressure and heating rate on radiata pine char structure and apparent gasification reactivity. *Fuel, 84*(10), 1328-1334. doi:10.1016/j.fuel.2004.07.016

Collard, F.-X., & Blin, J. (2014). A review on pyrolysis of biomass constituents: Mechanisms and composition of the products obtained from the conversion of cellulose, hemicelluloses and lignin. *Renewable and Sustainable Energy Reviews, 38*, 594-608. doi:10.1016/j.rser.2014.06.013

Downie, A., Crosky, A., & Munroe, P. (2009). Physical properties of biochar. In J. Lehmann & S. Joseph (Eds.), *Biochar for environmental management: Science and technology* (pp. 13-32). London, England, United Kingdom: Earthscan.

Dufour, A., Castro-Diaz, M., Brosse, N., Bouroukba, M., & Snape, C. (2012). The origin of molecular mobility during biomass pyrolysis as revealed by in situ ^{1}H NMR spectroscopy. *ChemSusChem, 5*(7), 1258-1265. doi:10.1002/cssc.201100442

Gangil, S. (2014). Thermogravimetric evidence for better thermal stability in char produced under unconfined conditions. *Environmental Engineering Science, 31*(4), 183-192. doi:10.1089/ees.2013.0415

Haas, T. J., Nimlos, M. R., & Donohoe, B. S. (2009). Real-Time and post-reaction microscopic structural analysis of biomass undergoing pyrolysis. *Energy & Fuels, 23*(7), 3810-3817. doi:10.1021/ef900201b

Haris, N. A. (2012). *Smoke generator for food smoking* (Unpublished final year project report). Massey University, Palmerston North, New Zealand. The report can be accessed by contacting J.R.Jones@massey.ac.nz

Huang, Y., Kudo, S., Masek, O., Norinaga, K., & Hayashi, J.-i. (2012). Simultaneous maximization of the char yield and volatility of oil from biomass pyrolysis. *Energy & Fuels, 27*(1), 247-254. doi:10.1021/ef301366x

International Biochar Initiative. (2014). *Standardized product definition and product testing guidelines for biochar that is used in soil* (Document Reference Code: IBI-STD-2.0) [Product Definition and Specification Standards]. Retrieved from International Biochar Initiative website: http://www.biochar-international.org/sites/default/files/IBI_Biochar_Standards_V2%200_final_2014.pdf

Jakab, E., Faix, O., Till, F., & Székely, T. (1995). Thermogravimetry/mass spectrometry study of six lignins within the scope of an international round robin test. *Journal of Analytical and Applied Pyrolysis, 35*(2), 167-179. doi:10.1016/0165-2370(95)00907-7

Joseph, S., Camps-Arbestain, M., Lin, Y., Munroe, P., Chia, C. H., Hook, J., . . . Amonette, J. E. (2010). An investigation into the reactions of biochar in soil. *Soil Research, 48*(7), 501-515. doi:10.1071/SR10009

Keiluweit, M., Nico, P. S., Johnson, M. G., & Kleber, M. (2010). Dynamic molecular structure of plant biomass-derived black carbon (biochar). *Environmental Science & Technology, 44*(4), 1247-1253. doi:10.1021/es9031419

Krull, E. S., Baldock, J. A., Skjemstad, J. O., & Smernik, R. J. (2009). Characteristics of biochar: Organo-chemical properties. In J. Lehmann & S. Joseph (Eds.), *Biochar for environmental management: Science and technology* (pp. 53-66). London, England, United Kingdom: Earthscan.

Lehmann, J. (2007). Bio-energy in the black. *Frontiers in Ecology and the Environment, 5*(7), 381-387. Retrieved from http://www.jstor.org/stable/20440704

Lehmann, J., & Joseph, S. (Eds.). (2009). *Biochar for environmental management: Science and technology*. London, England, United Kingdom: Earthscan.

Mamleev, V., Bourbigot, S., Le Bras, M., & Yvon, J. (2009). The facts and hypotheses relating to the phenomenological model of cellulose pyrolysis: Interdependence of the steps. *Journal of Analytical and Applied Pyrolysis, 84*(1), 1-17. doi:10.1016/j.jaap.2008.10.014

McDonald-Wharry, J., Manley-Harris, M., & Pickering, K. (2013). Carbonisation of biomass-derived chars and the thermal reduction of a graphene oxide sample studied using Raman spectroscopy. *Carbon, 59*, 383-405. doi:10.1016/j.carbon.2013.03.033

McDonald-Wharry, J., Ripberger, G. D., Manley-Harris, M., & Pickering, K. (2013, July). *Studying carbonisation with raman spectroscopy.* Paper presented at New Zealand 2013 Biochar Workshop - The final answer?, Palmerston North, New Zealand.

McKendry, P. (2002). Energy production from biomass (part 1): Overview of biomass. *Bioresource Technology, 83*(1), 37-46. doi:10.1016/S0960-8524(01)00118-3

McNaught, A. D., & Wilkinson, A. (1997). *IUPAC. Compendium of chemical terminology Gold Book*. doi:10.1351/goldbook.

Misra, M. K., Ragland, K. W., & Baker, A. J. (1993). Wood ash composition as a function of furnace temperature. *Biomass and Bioenergy, 4*(2), 103-116. doi:10.1016/0961-9534(93)90032-Y

Mohan, D., Pittman, C. U., & Steele, P. H. (2006). Pyrolysis of wood/biomass for bio-oil: A critical review. *Energy & Fuels, 20*(3), 848-889. doi:10.1021/ef0502397

Morgan, T. J., & Kandiyoti, R. (2013). Pyrolysis of coals and biomass: Analysis of thermal breakdown and its products. *Chemical Reviews*. doi:10.1021/cr400194p

Neves, D., Thunman, H., Matos, A., Tarelho, L., & Gómez-Barea, A. (2011). Characterization and prediction of biomass pyrolysis products. *Progress in Energy and Combustion Science, 37*(5), 611-630. doi:10.1016/j.pecs.2011.01.001

Okuno, T., Sonoyama, N., Hayashi, J.-i., Li, C.-Z., Sathe, C., & Chiba, T. (2005). Primary release of alkali and alkaline earth metallic species during the pyrolysis of pulverized biomass. *Energy & Fuels, 19*(5), 2164-2171. doi:10.1021/ef050002a

Porter, N. G., Smale, P. E., Nelson, M. A., Hay, A. J., Van Klink, J. W., & Dean, C. M. (1998). Variability in essential oil chemistry and plant morphology within a Leptospermum scoparium population. *New Zealand Journal of Botany, 36*(1), 125-133. doi:10.1080/0028825x.1998.9512551

Rajkovich, S., Enders, A., Hanley, K., Hyland, C., Zimmerman, A., & Lehmann, J. (2012). Corn growth and nitrogen nutrition after additions of biochars with varying properties to a temperate soil. *Biology and Fertility of Soils, 48*(3), 271-284. doi:10.1007/s00374-011-0624-7

Ruiz-Aquino, F., González-Peña, M. M., Valdez-Hernández, J. I., Revilla, U. S., & Romero-Manzanares, A. (2015). Chemical characterization and fuel properties of wood and bark of two oaks from Oaxaca, Mexico. *Industrial Crops and Products, 65*, 90-95. doi:10.1016/j.indcrop.2014.11.024

Sharma, R. K., Wooten, J. B., Baliga, V. L., Lin, X., Chan, W. G., & Hajaligol, M. R. (2004). Characterization of chars from pyrolysis of lignin. *Fuel, 83*(11–12), 1469-1482. doi:10.1016/j.fuel.2003.11.015

Sheng, C., & Azevedo, J. L. T. (2005). Estimating the higher heating value of biomass fuels from basic analysis data. *Biomass and Bioenergy, 28*(5), 499-507. doi:10.1016/j.biombioe.2004.11.008

Stephens, J. M. C., Molan, P. C., & Clarkson, B. D. (2005). A review of Leptospermum scoparium (Myrtaceae) in New Zealand. *New Zealand Journal of Botany, 43*(2), 431-449. doi:10.1080/0028825x.2005.9512966

Wang, L., Skreiberg, Ø., Grønli, M. G., Specht, G. P., & Antal, M. J. (2013). Is elevated pressure required to achieve a high fixed-carbon yield of charcoal from biomass? Part 2: The importance of particle size. *Energy & Fuels, 27*(4), 2146-2156. doi:10.1021/ef400041h

Wang, S., Wang, K., Liu, Q., Gu, Y., Luo, Z., Cen, K., & Fransson, T. (2009). Comparison of the pyrolysis behavior of lignins from different tree species. *Biotechnology Advances, 27*(5), 562-567. doi:10.1016/j.biotechadv.2009.04.010

Wildman, J., & Derbyshire, F. (1991). Origins and functions of macroporosity in activated carbons from coal and wood precursors. *Fuel, 70*(5), 655-661. doi:10.1016/0016-2361(91)90181-9

Zimmerman, A. R. (2010). Abiotic and microbial oxidation of laboratory-produced black carbon (biochar). *Environmental Science & Technology, 44*(4), 1295-1301. doi:10.1021/es903140c

Chapter 8 High Temperature High Pressure Reactor

8.1 Introduction

The literature review in chapter 2 along with the results in chapter 3 and 6 revealed that secondary reactions are best studied under autogenous pressure. This type of experiment has been carried out as early as 1853 by Violette, who sealed wood samples in glass tubes (as cited in Antal & Grønli, 2003). Antal and Grønli state that Violette's "observations are intriguing, and his experiments remain novel even today" (Antal & Grønli, 2003, p. 1628). This statement represents the scarcity of literature that can be found on the topic, even twelve years later, despite its great potential demonstrated in chapter 6. Limited knowledge is available in particular when it comes to the characteristics of the solid (char) product. This was also evidenced in a recent review on the comparison between wet and dry pyrolysis by Libra et al. (2011), who stated that "better quantification, reporting and standardization of char characteristics and production conditions are required in order to understand the wide variability found in experimental investigations" (p.116), which especially is true for biochar. The reason for the scarcity of data on char characteristics, in particular under autogenous pressure, is the limited capacity of existing laboratory equipment like Py-GC/MS (chapter 6), TGA, and DSC. The aim of this chapter is to design a research reactor that overcomes this limitation by enabling the pyrolysis of large enough samples to obtain sufficient char for analysis under a wide range of operating conditions relevant for the manufacture of biochar, and to investigate char formation in general. The purpose of the reactor is to create new research capabilities to quantify the relationship between pyrolysis conditions and product properties, and to understand the underlying primary and secondary reaction mechanisms, and transfer processes.

8.2 Design Objectives

8.2.1 Principal Design Features

The main objective, as indicated in 8.1, is the investigation of primary and secondary pyrolysis reactions; that is, their effect on the produced char and (ideally) the kinetics of char formation. In the latter case it was proposed to investigate if kinetic data can be derived from the rising carbon content with temperature, see chapter 2. However, the findings in 7.3.3 indicate that this is not possible, and thus cumulative experiments with subsequent weight measurements are proposed instead.

Chapters 2, 3 and 6 revealed that secondary reactions are best studied under autogenous pressure. Therefore, to study primary pyrolysis and control the extent of secondary reactions it is necessary to be able to manipulate the vapour-phase concentration and residence time. This can be achieved by controlling the autogenous pressure, pyrolysis atmosphere, and pyrolysis time. Thus, a reactor is required that can be operated under vacuum and pressure (inert and autogenous, or a combination of both) that can be set and controlled. The details of the desired pressure envelope are given in 8.2.2.

Intrinsically related to the study of primary and secondary reactions is the avoidance/ minimisation of internal transfer processes, at least in the case of primary reactions, as discussed in chapter 3, while at the same time maintaining a big enough sample size for product characterisation. Associated with this is the requirement of uniform heating. This is discussed further in 8.2.4. The relevant temperature and heating rate regime is outlined in 8.2.3.

Chapter 3 and 5 revealed that the heat of pyrolysis is a function of secondary reactions and can range from endothermic to exothermic. Therefore, it is desired to record the sample temperature as accurately as possible in order to obtain information about process energetics (see 5.3.1).

Essential to this research is the obtainment of complete mass and energy balances, which requires measuring the temperature and flow of all the inlet and outlet streams, as well as collecting the produced char, volatiles (requires condensing) and gases. These mass and energy balances are essential to determine the process thermokinetics.

8.2.2 Pressure Envelope

In section 2.8 in chapter 2 pyrolysis processes involving or closely related to autogenous pressure pyrolysis were reviewed, and it was found that water can play an important role during this process for which reason they were depicted in Figure 2-24 (see 2.8.7) superimposed on the phase diagram of water. Based on the pyrolysis methods in Figure 2-24 it was decided to choose as an upper limit for autogenous pressure pyrolysis 200 bar, as this is generally the maximum pressure applied in hydrothermal liquefaction (Babu, 2008). Higher pressures are disregarded as this will get into the regime of hydrothermal gasification, which is not the subject of this research and will push the material characteristics even further. The lower end of the pressure has been fixed to the vacuum available at the laboratories at Massey University, which is -60 kPa(g).

To attain such high pressures autogenously the dead volume inside the reactor is required to be at a minimum.

8.2.3 Temperature Range and Heating Rate

The temperature range and heating rate is specified by the typical regime used for the manufacture of biochar, that is, slow conventional pyrolysis to *HTT's* of up to 700 °C (chapter 2). However, the results in chapter 3 and 6 showed that the actual pyrolysis process, associated with the release of volatile pyrolysis products involved in secondary reactions, is completed at 500 °C allowing a reduction of the *HTT* to this temperature, if required by material constraints due to the high pressures involved (see 8.2.2). Changes in the char characteristics at higher temperatures could then be studied by re-pyrolysing the char in a separate furnace to the desired temperatures. In this case no high pressures are required as the majority of the volatile formation is completed.

The maximum heating rate for conventional pyrolysis has been stated in the literature (Babu, 2008) as 1 K/s (60 °C/min), which has been adopted as the upper limit for the reactor design. However, the target heating rate in this research is 5 °C/min, as this is the heating rate applied throughout this study adding flexibility to the upper limit, which can thus be reduced if required by constraints of available heaters.

8.2.4 Sample Size and Shape

In 8.2.1 it was indicated that it is essential to avoid heat and mass transfer limitations for studying reaction kinetics, which was also discussed in the literature where the minimisation of thermal lag is stated (Grønli, Antal, & Várhegyi, 1999; Lin, Cho, Tompsett, Westmoreland, & Huber, 2009; White, Catallo, & Legendre, 2011). That thermal lag, which increases with sample size, can be considerable was shown in chapter 3 in section 3.3.5. Therefore, for studying primary reaction kinetics, sample size, vapour-phase residence time and volatile concentration need to be minimised.

Independently from the results in chapter 3, it was believed that this can be best achieved with thin slices of radiata pine wood. Thus, in a first estimate the heat transfer was analysed since thermal properties are readily available and, in the case of no heat transfer limitations, mass transfer limitations were assumed to be negligible (Di Blasi & Branca, 2001; Lin et al., 2009). In chapter 2 the maximum characteristic length for no heat transfer limitations was calculated as 480 μm for a heat transfer coefficient of 25 $W/(m^2 \cdot K)$. This is larger than the range of sizes suggested in the literature; for example Di Blasi and Branca (2001) experimentally determined the layer thickness of beech wood powder required for uniform sample temperature to be below 200 μm for a heating rate of 1000 K/min and a *HTT* of 708 K. For cellulose pyrolysis Di Blasi (1996) state that for a particle half thickness of 10 μm the pure kinetic regime is obtained. They considered a planar one-dimensional radiative heated cellulose particle. Contrary, Lin et al. (2009) found no heat and mass transfer limitations in the particle size range from 110 to 50 μm by TGA analysis. The thermal conductivity of cellulose, 0.13 W/(m·K) (Pyle and Zaror, 1984, as cited in Narayan & Antal, 1996), is similar to that of softwood. The reason for the larger characteristic length calculated in chapter 2 is the relatively low heat transfer coefficient.

The aim of the experiments in section 3.3.2 in chapter 3 was to experimentally determine the thickness at which transfer limitations are negligible. It was found that the derivative weight loss curves were not affected by apparent heat transfer limitations in the particle size range of 1 mm but also that the yield seemed to continually decrease with reduction in sample size without attaining a minimum value indicating that mass transfer processes are still relevant at this scale, which is supported by the fact that a strong interaction was observed if samples were placed in close proximity to each other. This gave support to the hypothesis that a primary char, at least for cellulose as

suggested by Antal and his team (Antal, 2014; Antal & Varhegyi, 1995; Grønli et al., 1999), does not exist or is negligible, which lead to a rethink of the initially proposed design, Figure G-1 in Appendix G.1. The initially proposed design was based on the fact that there is a minimum yield that can be obtained when the sample size is reduced below a characteristic value, as found by Di Blasi and Branca (2001). The pipe design was chosen as it allows the pyrolysis of a single slice layer (minimising the interaction between the released volatiles and the pyrolysing solid) while providing enough sample for simple analysis. It makes use of the natural curling effect of the pine shavings, which could be kept in place with the help of a wire mesh. Additionally, vacuum could be applied to assure that the vapour-phase residence time and concentration remain at a minimum. However, this set up would have only catered for determining reaction kinetics by either gravimetry, or as proposed earlier by elemental analysis for the char (see 8.2.1) and not for thorough product characterisation due to the limited amount of feedstock that can be pyrolysed in this manner. It is important to note that this design does not allow continuous weight measurement, and thus cumulative experiments are required, that is, by carrying out pyrolysis repeatedly to increasing *HTT's*. But this is necessary for analysis techniques like ultimate analysis anyway. It is believed that cumulative experiments are feasible, because primary pyrolysis is endothermic as demonstrated in chapter 5, and even if it becomes exothermic with the presence of a large amount of catalyst the small sample mass (thin monolayer of pine shavings with thickness of ≈ 90 μm) compared to the large thermal mass of the reactor, and the ability to flush with "cold" nitrogen is believed to quench the reaction fairly quickly.

In order to carry out a more detailed char characterisation, in particular in the case of enhanced secondary reactions where the minimisation of mass transfer is not relevant anymore, more feedstock volume is required, which was accounted for in the proposed design in Figure G-2 and Figure G-3 in Appendix G.1 by making the inner pipe removable leading to a larger reactor volume.

But since the results of chapter 3 along with the discussion in chapter 6 revealed that the majority of char is formed by so-called "secondary reactions", and the fact that pyrolysis of such small single particles will never be subject of any process that aims at the manufacture of char, it was decided to dismiss the reactor designs in Appendix G.1; and focus on a more realistic scenario in which primary and secondary reactions are studied in a frame that is relevant for the industrial manufacture of char. Thus, the focus

shifted from avoiding secondary reactions completely to minimising them to a scale that can occur in industrial processes. Nevertheless, the importance of minimising heat transfer limitations and thermal lag remains.

Considering the findings of chapter 3 it was decided to use cylindrical samples with a diameter of 20 mm, as it was discovered that sample sizes up to 20 mm have a negligible effect on the derivative weight loss curve at a heating rate of 5 °C/min. The larger thermal lag can be accounted for by recording the centre temperature, which is also desired for gaining information of reaction energetics (8.2.1). The ability to accurately observe reaction energetics from the recorded centre temperature was demonstrated in chapter 5. Further, cylindrical samples are advantageous from the point of view that they allow uniform sample heating and are ideal for modelling. It was decided to use cylinders with a length of 30 cm to minimise end effects and have sufficient sample mass for analysis. For the pyrolysis of radiata pine wood this means a feedstock weight of ≈ 42 g taking the density of 450 kg/m^3 determined in 3.2.1.6 in chapter 3. For atmospheric pressure conditions this will result in a char yield of ≈ 10.5 g at 695 °C (see 3.3.2 in chapter 3), which is enough to carry out product characterisation, similar to the one done in chapter 7. The application of vacuum will decrease this yield but even in the case of a yield of 10 % (wt/wt) this will be sufficient for the majority of the product characterisation; in the worst case an experiment can be repeated to collect enough char for analysis.

8.2.5 Pyrolysis Environment/ Atmospheres

In 8.2.1 it was discussed that the reactor needs to accommodate autogenous pressure operation, that is, the reactor is sealed and the produced volatiles forced to remain in close contact with the pyrolysing solid, which is the main mode for studying secondary reactions. To minimise secondary reactions a vacuum mode is required. Additionally, to make the reactor more flexible for research purposes the application of an inert purge gas, primarily nitrogen, is desired and to be able to adjust the inert gas pressure from atmospheric pressure to the maximum pressure (200 bar), as the literature shows that absolute pressure alone will increase the char yield and decrease the reaction heat (Basile, Tugnoli, Stramigioli, & Cozzani, 2014) due to an increase of the volatile residence time inside the pyrolysing particle and affect the char properties (Antal & Grønli, 2003; Recari, Berrueco, Abelló, Montané, & Farriol, 2014); further, as

discussed in chapter 6, the increased pressure will inhibit the vaporisation of the liquid pyrolysis products possibly favouring char formation.

An inert purge gas is also important for flushing the reactor before commencement of an experiment to prevent oxidative damage (pyrolysis is the thermal decomposition that occurs during heating in the absence of oxygen). The capability of connecting other gases than inert nitrogen or argon is a feature worth having as well, as studies under atmospheres like CO, CO_2, CH_4, H_2, and H_2O (steam) are less studied (Kantarelis, 2014). Thus, the connection of various gas cylinders is desired. Of particular importance is the addition of steam as it can improve the physical properties of the char (Minkova et al., 2001; Zanzi, Bai, Capdevila, & Bjornbom, 2001), which are anticipated to be deteriorated by secondary reactions and high pressures, that is, autogenous and inert (Violette, 1853, as cited in Antal, 2014; Recari et al., 2014). Nevertheless, there will be a trade-off for example reduced char yield (Minkova et al., 2001; A. Pütün, Özbay, & Pütün, 2006; E. Pütün, Ateş, & Pütün, 2008). The properties of bio-oil will also be affected (Kantarelis, 2014; Önal, Uzun, & Pütün, 2011; A. Pütün et al., 2006; E. Pütün et al., 2008). In fact, Önal et al. (2011) report that steam pyrolysis oil has a higher yield, is more paraffinic, has a decreased elemental oxygen content and higher calorific value than oil obtained under static and nitrogen atmosphere. Therefore, having the ability of steam injection is vital for researching the relationship between pyrolysis conditions and product yield/ properties. It becomes even more important when considering the autocatalytic effect water can have on char formation under autogenous pressure, which was discussed in chapter 2, 3 and 6, and is illustrated in Figure 2-24.

8.3 Final Design

8.3.1 Preliminary Considerations

Before coming up with the final design, outlined in this section, different options were carefully considered, which are only briefly summarised here. First the option of high pressure simultaneous thermal analysis, STA, was investigated. Equipment considered were a high pressure STA HP/1 from Linseis Messgeräte GmbH (Selb, Germany) and the DynTHERM thermogravimetry analyser range from Rubotherm (Bochum, Germany) using magnetic suspension balances. However, none of these devices allowed a high vapour-phase concentration or a sample size which yields enough char for characterisation. Because of the inherent difficulty of combining high pressures (8.2.2), a large sample size (8.2.4) and internal temperature recording with simultaneous gravimetric measurement it was decided to abandon gravimetric measurement during an experimental run; weight-loss data can be obtained cumulatively by quenching pyrolysis at various *HTT's*. A literature review revealed that not many research reactors with similar capabilities as outlined in 8.2 are available. Noteworthy reactors are the ones used in the deoxy-liquefaction studies e.g. Li, Wu, and Yang (2008), and the set-up of Capunitan and Capareda (2012). However, they do not meet the requirements detailed in 8.2. During the course of this research and the findings of chapter 3 the design changed gradually from the one in Figure G-1 in Appendix G.1 to a design that allowed the pyrolysis of either shavings or cylindrical rods, Figure G-2 and G-3 in Appendix G.1, to the here described reactor, which is based on the pyrolysis of a single rod described in 8.2.4.

After having contacted various national and international companies, it was decided to seek professional consultancy services from Worley Parsons New Zealand (formerly Transfield Worley Ltd, Christchurch, New Zealand) to assist with the procurement and installation of the high pressure and high temperature reactor to ensure the manufacture and operation of the desired kit is within New Zealand law and safety standards. Such a step was necessary due to the high demand on the materials (high temperature and pressure), and to minimise the risk involved with building a highly specialised pilot plant with its associated relatively large investment costs. The procurement of the reactor was set up as a stage gate project with the following three phases:

1. Development of tender documents and equipment specifications with subsequent selection of the most suitable tenderer;
2. Detailed engineering by tenderer (e.g. calculation sheets, general assembly drawings, layout drawings, final piping and instrumentation diagram (P&ID), equipment lists, valve lists, safety review, compliance codes, and control strategy); and
3. Fabrication, assembly, and commissioning.

The tender documents (phase 1) are given in Appendix G.2, and the tenderer of choice was Fitzroy Engineering Group Limited (Auckland, New Zealand). Following the outcome of stage gate 2 is elucidated with the help of the final P&ID (8.3.2) and by explaining the operational modes of the designed experimental kit (8.3.3). The supplied documents of the detailed engineering from Fitzroy Engineering are given in Appendix G.3.

8.3.2 P&ID

Succeeding the final P&ID is depicted. The P&ID is also available through the provided CD in the location chapter 8/data/final reactor design/Pyrolysis report drawings-20150204.pdf, where it is given on page 1.

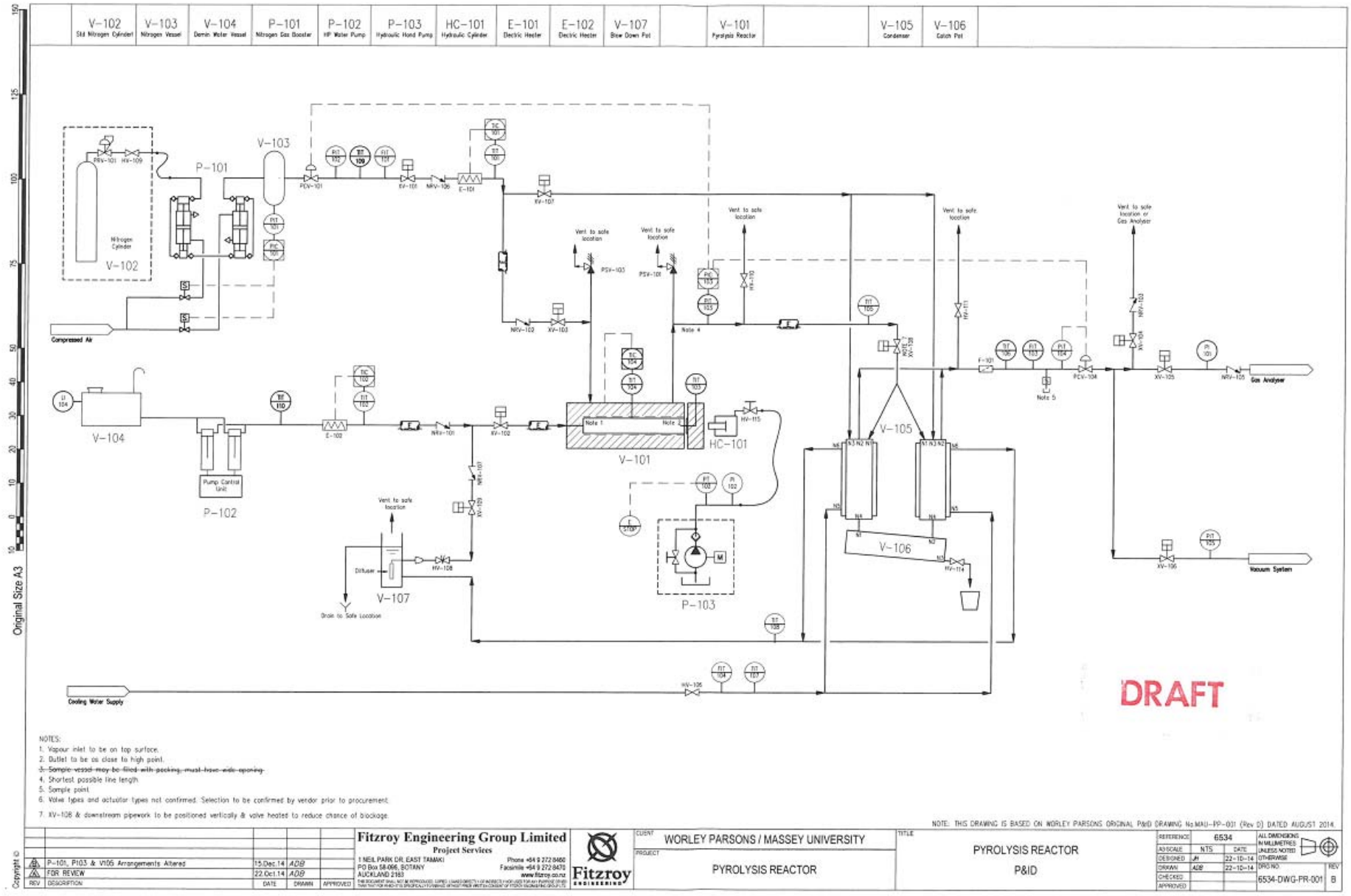
V-102 Std Nitrogen Cylinder
V-103 Nitrogen Vessel
V-104 Demin Water Vessel
P-101 Nitrogen Gas Booster
P-102 HP Water Pump
P-103 Hydraulic Hand Pump
HC-101 Hydraulic Cylinder
E-101 Electric Heater
E-102 Electric Heater
V-107 Blow Down Pot
V-101 Pyrolysis Reactor
V-105 Condenser
V-106 Catch Pot
Nitrogen Cylinder
Compressed Air
Pump Control Unit
Diffuser
Drain to Safe Location
Vent to safe location
Vent to safe location or Gas Analyser
Gas Analyser
Vacuum System
Cooling Water Supply
Note 1
Note 2
Note 4
Note 5
DRAFT
NOTES:
1. Vapour inlet to be on top surface.
2. Outlet to be as close to high point.
3. Sample vessel may be filled with packing, must have side opening.
4. Shortest possible line length.
5. Sample point.
6. Valve types and actuator types not confirmed. Selection to be confirmed by vendor prior to procurement.
7. XV-108 & downstream pipework to be positioned vertically & valve heated to reduce chance of blockage.
NOTE: THIS DRAWING IS BASED ON WORLEY PARSONS ORIGINAL P&ID DRAWING No.MAU-PP-031 (Rev 0) DATED AUGUST 2014.
Original Size A3
Copyright ©
REV P-101, P103 & V105 Arrangements Altered 15.Dec.14 ADB
REV FOR REVIEW 22.Oct.14 ADB
REV DESCRIPTION DATE DRAWN APPROVED
Fitzroy Engineering Group Limited
Project Services
1 NEIL PARK DR, EAST TAMAKI
PO Box 58-066, BOTANY
AUCKLAND 2163
Phone +64 9 272 8460
Facsimile +64 9 272 8470
www.fitzroy.co.nz
Fitzroy ENGINEERING
CLIENT WORLEY PARSONS / MASSEY UNIVERSITY
PROJECT PYROLYSIS REACTOR
TITLE PYROLYSIS REACTOR
P&ID
REFERENCE 6534
ALL DIMENSIONS IN MILLIMETRES UNLESS NOTED OTHERWISE
AS SCALE NTS DATE
DESIGNED JH 22-10-14
DRAWN ADB 22-10-14
CHECKED
APPROVED
DRG NO. 6534-DWG-PR-001
REV B

8.3.3 Process Description

The final design and experimental set up (8.3.2) of the experimental kit was based on the four main operating modes:

1. autogenous operation;
2. augmented operation;
3. vacuum operation; and
4. steam/ water vapour injection.

The detailed operational steps of each mode are given in Appendix G.4. Here they are only briefly summarised.

Mode 1, as mentioned in 8.2, is the main mode for studying secondary reactions, as it allows intimate vapour-solid/ liquid contact and long vapour-phase residence times. Essentially in this mode the sample, which just fits the reactor, is sealed in the reactor and subsequently heated according to its heating profile. The vapour-phase concentration can be controlled by setting the maximum autogenous pressure. Once that pressure is attained or the pyrolysis process completed the volatiles are partly or completely released, and collected as gas or tar, which then can be analysed.

In mode 2, augmented operation, the volatile pyrolysis products are continuously removed from the pyrolysis zone by the application of an inert purge gas or a reactive gas that can be applied at atmospheric pressure up to 200 bar allowing the control of the pyrolysis atmosphere and vapour-phase residence time. The condensable pyrolysis products are collected and the gaseous products can be sampled if required.

The third mode is the operation under vacuum (-60 kPa(g)), which is primarily used for studying pyrolysis under conditions minimising secondary reactions. The liquid pyrolysis products are removed by the condenser and the non-condensable products are collected in the vacuum system in this mode.

In the last mode, mode 4 (steam/ water vapour injection), water can be injected into the main reactor if the temperature is above the saturation temperature at the respective set point pressure enabling gasification reactions and char activation to take place. Again the liquid (condensable) products will be collected in this mode.

8.3.4 Final Process Parameters

The pyrolysis reactor, V-101 in 8.3.2, which forms the core of the experimental kit was designed for a pressure of 250 bar(g), which corresponds to an operating pressure of 220 bar(g). The design temperature was 700 °C as given in 8.2.3 but the operational temperature is limited to 600 °C due to the available process valves, which are not warranted for temperatures > 600 °C (for details see Appendix G.3).

8.4 Proposed Experiments/ Research Capabilities

Unfortunately the project was halted at stage gate 2 due to the limited funds and time available in this PhD research. The costs spend on stage gate 1 and 2 were 10 % of the final cost for stage gate 3, which is in the range that is typically expected for chemical engineering design projects (Towler & Sinnott, 2013). Since the experimental kit could not be built, an overview of the main proposed experiments is given in Table 8-1 demonstrating the research capabilities of the designed reactor.

Table 8-1. Proposed experiments.

No.	Research Question/ Task	Proposed Method	Outcome
1	Can char formation kinetics be inferred from recording a change in elemental composition of the solid with pyrolysis temperature/ time? (confirm or disprove preliminary findings in chapter 7)	• Pyrolysis of cylindrical rods ($d \leq 20$ mm; $l = 300$ mm) at various heating rates (1 to 20 K/min[a]) to stepwise increasing *HTT's* in the range from ambient to 600 °C; first it is proposed to do these experiments under vacuum (minimising "secondary" char formation) followed by augmented and autogenous pressure pyrolysis; Risk: reactions cannot be quenched in the range of interest due to increasing exothermicity as a consequence of secondary char formation • Analyse the elemental composition at each *HTT* & obtain complete mass balance • Plot elemental composition and weight of products as a function of *T* and *t*	• If possible derive char formation or feed conversion kinetics from change in elemental composition, particular C, with time • Comparison of kinetics from elemental analysis (if possible) with kinetics determined from weight-loss measurements and kinetic data available in the literature • Insight into the relationship between char formation and vapour-phase residence time and vapour-phase concentration

(continued)

No.	Research Question/ Task	Proposed Method	Outcome
2	How are char formation kinetics affected by moisture content and mineral matter?	• See no. 1 • Add moisture or mineral matter (by impregnation) in various amounts respectively	• Conclusions regarding the autocatalytic effect of moisture, and the effect of mineral matter can be drawn
3	At what autogenous pressure is the maximum char yield obtained?/ Is it possible to attain the theoretical char yield in this manner?	• Pyrolyse pine rods (d = 20 mm; l = 300 mm) at a defined heating rate to a designated *HTT* at various autogenous pressures • Determine the yield/ fixed carbon yield	• Char yield/ fixed carbon yield as a function of autogenous pressure for different *HTT's* and heating rates
4	How does the yield achievable by autogenous pressure pyrolysis compare to the yield attainable by mineral impregnation and acid catalysis (dehydrating acid)?	• Pyrolyse impregnated pine rods (d = 20 mm; l = 300 mm) in the augmented mode at atmospheric pressure to the same *HTT* as in no. 3 applying the identical heating rate; possibly extent to include autogenous pressure • Determine the yield/ fixed carbon yield	• Comparison to yield determined in no. 3 • Information about best method for obtaining the highest char yields • Conclusions about the underlying char formation mechanisms
5	What is the effect of moisture on the char yield?	• Pyrolyse pine rods (d = 20 mm; l = 300 mm) with various amounts of initial water present (either soak samples in water or add various amounts of liquid water) at a defined heating rate to a designated *HTT* (corresponding to the experiments in no. 3 and 4) • Determine the yield/ fixed carbon yield	• If autocatalytic effect of moisture is confirmed, data can be used to establish optimum water content

(continued)

No.	Research Question/ Task	Proposed Method	Outcome
6	What is the effect of total inert pressure on the char yield and characteristics?	• Pyrolyse pine rods (d = 20 mm; l = 300 mm) at a defined heating rate to a designated *HTT* at various pressures in the augmented mode • Determine the yield/ fixed carbon yield and product characteristics as outlined in no. 9	• Insight into transfer processes at play/ conclusions regarding the presence of a liquid phase, i.e. at what absolute pressures does char appear to be molten (due to inhibiting the evaporation of the liquid pyrolysis products) • Comparison of char yield under inert pressure to autogenous pressure (see no. 3) • Conclusion in how far external mass transfer limitations contribute to the char yield by increasing the internal vapour-phase residence time as well as enabling carbonisation reactions in the liquid phase
7	How does maximum yield increase under autogenous pressure (no. 3) compare to the yield that can be attained if the produced tars under conditions minimising secondary reactions are collected and re-pyrolysed?	• Re-pyrolyse tar, previously collected in condenser from experiments minimising secondary reactions, under same heating profile as in no. 3, 4 and 6 • Determine the yield/ fixed carbon yield	• The role of tar self-charring • Comparison to no. 3, 4 and 6 • Information about best method for obtaining the highest char yields
8	What is the role of co-carbonisation of tar and feedstock or char?	• Re-pyrolyse tar according to no. 7 in the presence of feedstock or char • Determine the yield/ fixed carbon yield	• The role of co-carbonisation • Comparison to no. 3, 4, 6 and 7 • Conclusion about underlying pyrolysis mechanism

(continued)

No.	Research Question/ Task	Proposed Method	Outcome
9	Characterise pyrolysis products (quality and quantity), especially char, under a wide range of operating conditions including different atmospheres	• Pyrolyse pine rods (d = 20 mm; l = 300 mm) at a defined heating rate to a designated *HTT* under various conditions utilising the four operation modes stated in 8.3.3 • Determine product yields • Determine product characteristics: (a) gaseous (e.g. composition by gas chromatography), (b) liquid (composition by various chromatographic methods e.g. GC/MS, elemental analysis to determine total oxygen content), and (c) solid/ char (see chapter 7 and IBI guidelines (International Biochar Initiative, 2014))	• Knowledge of how pyrolysis conditions affect a range of char properties (development of a property database as a function of operating conditions); e.g. characterisation of similarities and differences between hydrochar and dry pyrolysis char • Obtained data can be used to fine tune the pyrolysis conditions to produce a char that matches the desired product application • Knowledge about whether or not a high quality liquid and solid product can be co-produced • Insight into geological formation of coal
10	How do the different pyrolysis conditions/ modes affect the process energetics?	• See no. 9 combined with a heat balance of the overall system (inclusive temperature data analysis; determination of heating values of pyrolysis products, …)	• Information about process economics and thus process feasibility

Note. C = carbon; d = diameter; *HTT* = highest treatment temperature; l = length; no. = number; *T* = temperature; *t* = time.

[a]Heating rate range is fixed by reactor capability.

It is important to note that the list in Table 8-1 is not exhaustive and some of the research questions can be investigated concurrently.

Being able to study number 3 in Table 8-1 allows the determination of the minimum pressure required for obtaining the theoretical char yield, which according to Antal (2014) is above 200 psi(g) (≈ 14 bar(g)) for ash-free cellulose. This combined with the "large" sample that can be pyrolysed enables not just the determination of the fixed carbon yield but also thorough product characterisation that, to the best of our

knowledge, is currently not available in the literature under these conditions. Knowledge and data is existing regarding the yield of char but literature becomes scarce in predicting the properties of the solid product as a function of its manufacturing conditions. Noteworthy work has been done by Antal and his co-workers (Antal, 2014; Antal et al., 2000; Antal et al., 1996; Antal & Grønli, 2003; Mok, Antal, Szabo, Varhegyi, & Zelei, 1992; Wang, Skreiberg, Grønli, Specht, & Antal, 2013; Wang et al., 2011), who are continuously advancing the understanding of good quality high-yield charcoals. However, their studies have been mainly carried out with the aim to use charcoal as a reductant in the iron and steel industry or for the manufacture of silicon. Thus, their final product requirements, mainly low volatile matter content (Antal et al., 1996), differ from the ones destined for soil application.

There is not "one" exact, very specific and well-defined biochar product (Brown, 2009; Lehmann & Joseph, 2009); rather, research indicates that depending on the soil type, different biochars with specific properties are necessary (Joseph et al., 2012; Lehmann et al., 2011; Noguera et al., 2010; Verheijen, Jeffery, Bastos, van der Velde, & Diafas, 2009). Joseph et al. (2012) goes even further and suggests that a blend of different biochars is required for soil application. This shows that, when talking about manufacturing biochar efficiently, it is not enough to look at high yields alone; the properties have to be considered as well! Research suggests that there are differences between traditionally produced "primary" and secondary char (Violette 1853, as cited in Antal, 2014; Antal & Grønli, 2003; Boroson, Howard, Longwell, & Peters, 1989; Mok & Antal, 1983), and that secondary reactions are responsible for the formation of PAH's (Dieguez-Alonso, Anca-Couce, Zobel, & Behrendt, 2015; Hilber, Blum, Leifeld, Schmidt, & Bucheli, 2012). Macroscopic structural differences that exist between traditional charcoal and coke were outlined in chapter 7. Thus, producing a high yield biochar, which is desired from an economic and carbon sequestration point of view, might be in conflict with other biochar quality parameters, which requires further research.

The designed reactor in 8.3 enables one to conduct this research. It also permits the establishment of hydrochar characteristics as a function of operating conditions and thus allows defining clear differences between hydrochar and dry pyrolysis char. Knowledge in this field is currently lacking (Libra et al., 2011).

Because of its wide operating range the reactor can also be used to study the natural process of coal formation, and aid in clarifying the role of water and autogenous pressure in this process (hydrous pyrolysis *versus* confined pyrolysis in section 2.8 in chapter 2). Related to this, it can be used to investigate if it is possible to co-produce a high value liquid and solid product from biomass, as suggested in chapter 6.

In chapter 6 it was also discussed that the increase in autogenous pressure above a certain threshold can provide the high activation energy to break the hydroxyl group in the phenol and thus reduce the oxygen content in the liquid product considerably (deoxy-liquefaction), which makes the operation under autogenous pressure distinctively different from re-cycling the volatile pyrolysis products under atmospheric pressure. Thus, autogenous pressure is an important pyrolysis parameter that can be researched with the designed reactor over a large pressure range.

Analysing the occurrence of a molten phase (number 6 in Table 8-1) will aid in understanding transfer processes during pyrolysis, and thus will assist in the modelling of pyrolysis processes. In general with respect to modelling Antal (2014) state that modelling autogenous pressure phenomena will reveal much about the underlying pyrolysis mechanism. The use of cylindrical rods with internal sample temperature measurement is ideal for this purpose. An energetic analysis (no. 10 Table 8-1) combined with a thorough product characterisation, as discussed above and extending to the volatile pyrolysis products (no. 9 Table 8-1), will aid in making economic feasibility estimates. The economics will certainly depend on the maximum pressure required. The use of pressure equipment is generally very costly and challenging in industrial manufacturing processes. However, utilising it for studying pyrolysis will help in understanding the mechanisms involved. The knowledge gained can then be applied to develop alternative processes and/ or improve existing ones.

The recently published work of Williams, Higashi, Phothisantikul, Van Wesenbeeck, and Antal (2015) confirms the here proposed venture into studying pyrolysis under very high temperature and pressure (inert and autogenous) conditions. They report that the solid carbon residue produced at high autogenous pressures (above 1.68 MPa) has a “true, fascinating appearance” (p.228) similar to the earlier findings of Violette (1853, as cited in Williams et al., 2015). That is, the char passed through a liquid phase, had a bubbly inner surface, was brittle, appeared to be deep black, and was

glittery (Williams et al., 2015), which sounds similar to the description of the coke reported in chapter 7. However, they give no detailed analysis. They further report that under these conditions the theoretical fixed carbon yield is attained and even exceeds the theoretical limit determined by thermodynamic calculations. Surprisingly, this was also the case when the reactor was initially pressurised to 2.28 MPa with oxygen before commencement of the autogenous pressure pyrolysis to 300 °C. Their results show that not only the vapour-phase concentration affects the pyrolysis products (solid and volatile) but also the absolute pressure and pyrolysis atmosphere. Additionally, they report a high volatile matter content of the char at the applied *HTT* of 300 °C, which decreases at 400 °C, while still maintaining the high fixed carbon yields. However, their experiments were limited to these temperatures because of safety concerns at these high temperatures and pressures (Williams et al., 2015). This outlines the importance of the here proposed reactor design and its extended operating conditions (20 MPa at 600 °C) which can advance the knowledge and understanding of pyrolysis. Furthermore, it allows studying pyrolysis in one reactor over a large range of operating conditions and parameters, which eliminate differences caused by differing reactor designs and geometries, making the results directly comparable. Further the experiments will deliver the data required for modelling pyrolysis and will allow either confirming or disproving of the proposed pyrolysis mechanism in chapter 9.

8.5 Conclusion

An experimental kit has been designed to meet the requirements, outlined in the previous chapters, needed to advance knowledge in the field of pyrolysis with particular emphasis on char characterisation. It also enables one to study the natural formation of fossil fuels from biomass, hydrothermal carbonisation and liquefaction, and deoxy-liquefaction. The reactors key specifications are:

- Temperature range: RT to 600 °C;
- Pressure range: -60 to 20,000 kPa(g);
- Heating rate: 1 to 20 °C/min;
- Sample size: cylindrical wood rods with a diameter of 2 cm and a length of 30 cm, which fill the reactor with minimal dead volume (high autogenous pressures up to 200 bar are possible);
- Operating modes: autogenous (self-generated pressure), augmented (different pyrolysis atmospheres at various pressures), vacuum, and steam/ water vapour injection; and
- Special features: recording of sample centre temperature, ability to obtain complete mass and energy balances.

The designed experimental kit creates unique research capabilities, which to the best of our knowledge, currently is not available in the literature.

8.6 References

Antal, M. J. (2014). *The fundamentals of biocarbon formation at elevated pressure: from 1850 to the 21st century.* Paper presented at Pyro2014 20th International Symposium on Analytical and Applied Pyrolysis, Birmingham, United Kingdom.

Antal, M. J., Allen, S. G., Dai, X., Shimizu, B., Tam, M. S., & Grønli, M. G. (2000). Attainment of the theoretical yield of carbon from biomass. *Industrial & Engineering Chemistry Research, 39*(11), 4024-4031. doi:10.1021/ie000511u

Antal, M. J., Croiset, E., Dai, X., DeAlmeida, C., Mok, W. S.-L., Norberg, N., . . . Al Majthoub, M. (1996). High-yield biomass charcoal. *Energy & Fuels, 10*(3), 652-658. doi:10.1021/ef9501859

Antal, M. J., & Grønli, M. G. (2003). The art, science, and technology of charcoal production. *Industrial & Engineering Chemistry Research, 42*(8), 1619-1640. doi:10.1021/ie0207919

Antal, M. J., & Varhegyi, G. (1995). Cellulose pyrolysis kinetics: The current state of knowledge. *Industrial & Engineering Chemistry Research, 34*(3), 703-717. doi:10.1021/ie00042a001

Babu, B. V. (2008). Biomass pyrolysis: A state-of-the-art review. *Biofuels, Bioproducts and Biorefining, 2*(5), 393-414. doi:10.1002/bbb.92

Basile, L., Tugnoli, A., Stramigioli, C., & Cozzani, V. (2014). Influence of pressure on the heat of biomass pyrolysis. *Fuel, 137*, 277-284. doi:10.1016/j.fuel.2014.07.071

Boroson, M. L., Howard, J. B., Longwell, J. P., & Peters, W. A. (1989). Heterogeneous cracking of wood pyrolysis tars over fresh wood char surfaces. *Energy & Fuels, 3*(6), 735-740. doi:10.1021/ef00018a014

Brown, R. C. (2009). Biochar production technology. In J. Lehmann & S. Joseph (Eds.), *Biochar for environmental management: Science and technology* (pp. 127-146). London, England, United Kingdom: Earthscan.

Capunitan, J. A., & Capareda, S. C. (2012). Assessing the potential for biofuel production of corn stover pyrolysis using a pressurized batch reactor. *Fuel, 95*(0), 563-572. doi:10.1016/j.fuel.2011.12.029

Di Blasi, C. (1996). Kinetic and heat transfer control in the slow and flash pyrolysis of solids. *Industrial & Engineering Chemistry Research, 35*(1), 37-46. doi:10.1021/ie950243d

Di Blasi, C., & Branca, C. (2001). Kinetics of primary product formation from wood pyrolysis. *Industrial & Engineering Chemistry Research, 40*(23), 5547-5556. doi:10.1021/ie000997e

Dieguez-Alonso, A., Anca-Couce, A., Zobel, N., & Behrendt, F. (2015). Understanding the primary and secondary slow pyrolysis mechanisms of holocellulose, lignin and wood with laser-induced fluorescence. *Fuel, 153*, 102-109. doi:10.1016/j.fuel.2015.02.097

Grønli, M. G., Antal, M. J., & Várhegyi, G. (1999). A round-robin study of cellulose pyrolysis kinetics by thermogravimetry. *Industrial & Engineering Chemistry Research, 38*(6), 2238-2244. doi:10.1021/ie980601n

Hilber, I., Blum, F., Leifeld, J., Schmidt, H.-P., & Bucheli, T. D. (2012). Quantitative determination of PAHs in biochar: A prerequisite to ensure its quality and safe

application. *Journal of Agricultural and Food Chemistry*. doi:10.1021/jf205278v

International Biochar Initiative. (2014). *Standardized product definition and product testing guidelines for biochar that is used in soil* (Document Reference Code: IBI-STD-2.0) [Product Definition and Specification Standards]. Retrieved from International Biochar Initiative website: http://www.biochar-international.org/sites/default/files/IBI_Biochar_Standards_V2%200_final_2014.pdf

Joseph, S., Camps-Arbestain, M., Lin, Y., Munroe, P., Hook, J., Chia, C., . . . Thomas, P. (2012, February). *Labile organic molecules in biochar; Their role in plant health and nutrition; More questions than answers.* Paper presented at New Zealand Biochar Workshop 2012, Palmerston North, New Zealand.

Kantarelis, E. (2014). *Catalytic steam pyrolysis of biomass for production of liquid feedstock* (Doctoral dissertation, Royal Institute of Technology, Stockholm, Sweden). Retrieved from http://www.diva-portal.org/smash/get/diva2:703293/FULLTEXT01.pdf

Lehmann, J., & Joseph, S. (2009). Biochar for environmental management: An introduction. In J. Lehmann & S. Joseph (Eds.), *Biochar for environmental management: Science and technology* (pp. 1-12). London, England, United Kingdom: Earthscan.

Lehmann, J., Rillig, M. C., Thies, J., Masiello, C. A., Hockaday, W. C., & Crowley, D. (2011). Biochar effects on soil biota – A review. *Soil Biology and Biochemistry, 43*(9), 1812-1836. doi:10.1016/j.soilbio.2011.04.022

Li, J., Wu, L., & Yang, Z. (2008). Analysis and upgrading of bio-petroleum from biomass by direct deoxy-liquefaction. *Journal of Analytical and Applied Pyrolysis, 81*(2), 199-204. doi:10.1016/j.jaap.2007.11.004

Libra, J. A., Ro, K. S., Kammann, C., Funke, A., Berge, N. D., Neubauer, Y., . . . Kern, J. (2011). Hydrothermal carbonization of biomass residuals: A comparative review of the chemistry, processes and applications of wet and dry pyrolysis. *Biofuels, 2*(1), 71-106. doi:10.4155/bfs.10.81

Lin, Y.-C., Cho, J., Tompsett, G. A., Westmoreland, P. R., & Huber, G. W. (2009). Kinetics and mechanism of cellulose pyrolysis. *The Journal of Physical Chemistry C, 113*(46), 20097-20107. doi:10.1021/jp906702p

Minkova, V., Razvigorova, M., Bjornbom, E., Zanzi, R., Budinova, T., & Petrov, N. (2001). Effect of water vapour and biomass nature on the yield and quality of the pyrolysis products from biomass. *Fuel Processing Technology, 70*(1), 53-61. doi:10.1016/s0378-3820(00)00153-3

Mok, W. S.-L., & Antal, M. J. (1983). Effects of pressure on biomass pyrolysis. II. Heats of reaction of cellulose pyrolysis. *Thermochimica Acta, 68*(2-3), 165-186. doi:10.1016/0040-6031(83)80222-6

Mok, W. S.-L., Antal, M. J., Szabo, P., Varhegyi, G., & Zelei, B. (1992). Formation of charcoal from biomass in a sealed reactor. *Industrial & Engineering Chemistry Research, 31*(4), 1162-1166. doi:10.1021/ie00004a027

Narayan, R., & Antal, M. J. (1996). Thermal lag, fusion, and the compensation effect during biomass pyrolysis. *Industrial & Engineering Chemistry Research, 35*(5), 1711-1721. doi:10.1021/ie950368i

Noguera, D., Rondón, M., Laossi, K.-R., Hoyos, V., Lavelle, P., Cruz de Carvalho, M. H., & Barot, S. (2010). Contrasted effect of biochar and earthworms on rice growth and resource allocation in different soils. *Soil Biology and Biochemistry, 42*(7), 1017-1027. doi:10.1016/j.soilbio.2010.03.001

Önal, E. P., Uzun, B. B., & Pütün, A. E. (2011). Steam pyrolysis of an industrial waste for bio-oil production. *Fuel Processing Technology, 92*(5), 879-885. doi:10.1016/j.fuproc.2010.12.006

Pütün, A., Özbay, N., & Pütün, E. (2006). Effect of steam on the pyrolysis of biomass. *Energy Sources, Part A: Recovery, Utilization, and Environmental Effects, 28*(3), 253-262. doi:10.1080/009083190890012

Pütün, E., Ateş, F., & Pütün, A. E. (2008). Catalytic pyrolysis of biomass in inert and steam atmospheres. *Fuel, 87*(6), 815-824. doi:10.1016/j.fuel.2007.05.042

Recari, J., Berrueco, C., Abelló, S., Montané, D., & Farriol, X. (2014). Effect of temperature and pressure on characteristics and reactivity of biomass-derived chars. *Bioresource Technology, 170*, 204-210. doi:10.1016/j.biortech.2014.07.080

Towler, G., & Sinnott, R. K. (2013). *Chemical engineering design - Principles, practice and economics of plant and process design* (2nd ed.). Amsterdam, Netherlands: Elsevier.

Verheijen, F., Jeffery, S. L., Bastos, A. C., van der Velde, M., & Diafas, I. (2009). *Biochar application to soils - A critical scientific review of effects on soil properties, processes and functions* (EUR 24099 EN) [JRC Scientific and Technical Reports (EUR collection)]. Retrieved from http://publications.jrc.ec.europa.eu/repository/handle/111111111/13558

Wang, L., Skreiberg, Ø., Grønli, M. G., Specht, G. P., & Antal, M. J. (2013). Is elevated pressure required to achieve a high fixed-carbon yield of charcoal from biomass? Part 2: The importance of particle size. *Energy & Fuels, 27*(4), 2146-2156. doi:10.1021/ef400041h

Wang, L., Trninic, M., Skreiberg, Ø., Grønli, M. G., Considine, R., & Antal, M. J. (2011). Is elevated pressure required to achieve a high fixed-carbon yield of charcoal from biomass? Part 1: Round-robin results for three different corncob materials. *Energy & Fuels, 25*(7), 3251-3265. doi:10.1021/ef200450h

White, J. E., Catallo, W. J., & Legendre, B. L. (2011). Biomass pyrolysis kinetics: A comparative critical review with relevant agricultural residue case studies. *Journal of Analytical and Applied Pyrolysis, 91*(1), 1-33. doi:10.1016/j.jaap.2011.01.004

Williams, S., Higashi, C., Phothisantikul, P., Van Wesenbeeck, S., & Antal, M. J. (2015). The fundamentals of biocarbon formation at elevated pressure: From 1851 to the 21st century. *Journal of Analytical and Applied Pyrolysis, 113*, 225-230. doi:10.1016/j.jaap.2014.12.021

Zanzi, R., Bai, X., Capdevila, P., & Bjornbom, E. (2001). *Pyrolysis of biomass in presence of steam for preparation of activated carbon, liquid and gaseous products*. Paper presented at the 6th World Congress of Chemical Engineering, Melbourne, Australia. Paper retrieved from http://hem.fyristorg.com/zanzi/paper/paper6.pdf

Chapter 9 Project Conclusion

9.1 Introduction

The main conclusions from this research presented in chapters 3-7, in conjunction with what is known in the literature, are drawn together to propose a simplified pyrolysis mechanism. The reactor in chapter 8 was designed to address the further investigation of the intricacies of the proposed mechanism. Finally, suggestions for future work are given to assist with the progression of prospective research tasks.

9.2 Pyrolysis Mechanism

As this work has shown, pyrolysis mechanisms are highly complex and remained unresolved, but are also significantly affected by secondary reactions.

From an engineering perspective, where the desired outcome is to predict the product yield and establish the energy requirements of the process, a mechanistic model does not need to delve deeply into the underlying chemistry. Rather, it needs appropriate kinetic terms that accurately account for the presence of secondary reactions, which are a sequence of subsequent reactions involving the multitude of primary volatile pyrolysis products and consequently lead to a continuous change in product composition. This is proposed in Figure 9-1, as a model adapted from the work of others.

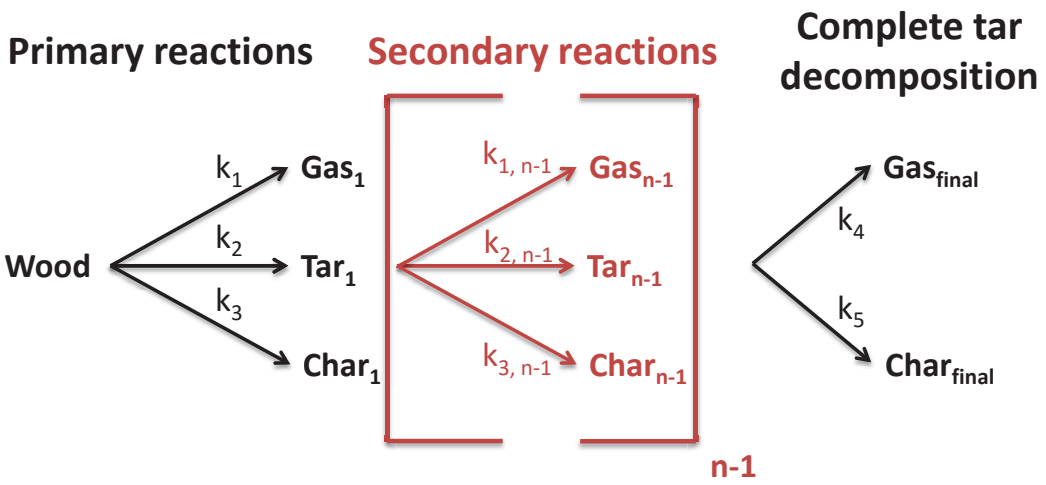

Figure 9-1. Modified pyrolysis mechanism based on Shafizadeh and Chin (1977), and the modifications of Thurner and Mann (1981) and Di Blasi (1996). Char is an unspecific term referring to charcoal, coke or soot. The subscript on the pyrolysis products refers to the pyrolysis stage e.g. primary reactions are denoted by 1. final = final reaction product; k_1 to k_5 are reaction rates; n = number of reaction steps.

Intimate contact between the volatile pyrolysis products and the pyrolysing solid is critical for some of the reactions in Figure 9-1, in particular for secondary char formation reactions. This is demonstrated in chapter 3 and 4, and by research indicating that the secondary reactions are catalysed by the char itself (Boroson, Howard, Longwell, & Peters, 1989; Brandt, Larsen, & Henriksen, 2000; Zaror, Hutchings, Pyle, Stiles, & Kandiyoti, 1985). However, homogenous reactions will be present too (Boroson, Howard, Longwell, & Peters, 1987) and a mechanism that allows for intimate contact, while it does not rule them out, also accounts for self-charring reactions of the tar which can have a significant impact on the char yield as demonstrated in chapter 7. For a simplistic model it does not matter whether the actual interaction is caused by vapour-phase solid-phase interactions (Antal & Varhegyi, 1995) or vapour-phase liquid-phase interactions (Mamleev, Bourbigot, Le Bras, & Yvon, 2009) or a combination of both, as the principle mechanism of intimate contact remains the same. Intimate contact between interacting molecular species is also promoted by pressure, either applied to the system, or generated internally by mass transfer resistance and by time of contact, as an imposed residence time or by an extended tortuous path length of volatile transport. To express this interaction in the scheme in Figure 9-1 it is proposed to introduce a "recycle factor", *RF*, depicted in Figure 9-2.

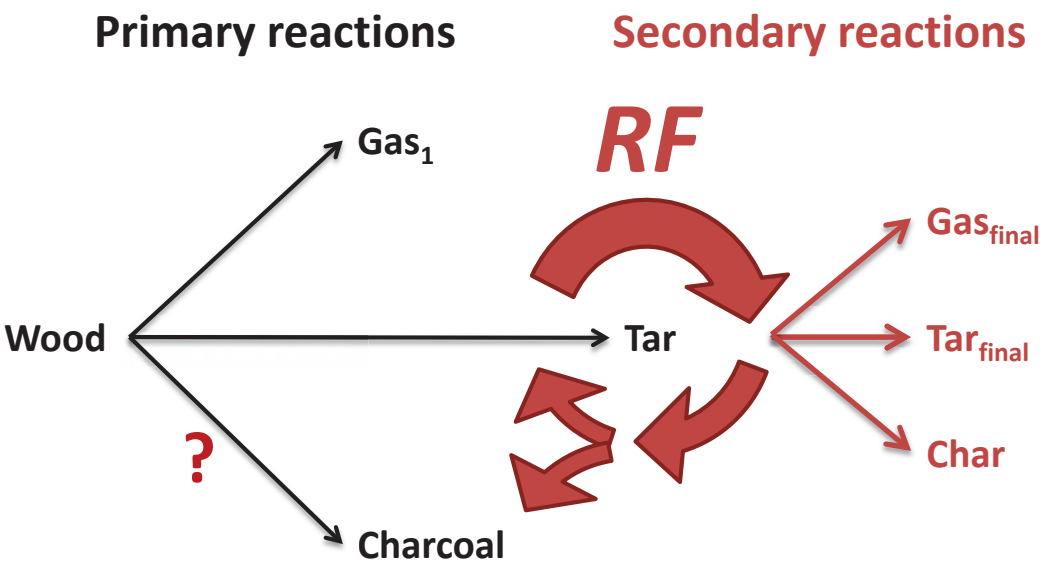

Figure 9-2. Proposed pyrolysis mechanism. Charcoal is char that retains the morphology of the feedstock, and char is an unspecific term, which refers in this case to coke and/ or soot. The question mark is introduced to denote that the extent of primary charcoal formation is currently unknown. The subscript on the pyrolysis products refers to the pyrolysis stage e.g. primary reactions are denoted by 1. *RF* = recycle factor. final = final reaction stage.

The *RF* term in Figure 9-2 quantifies how the extent/ progress of secondary reactions affect the product quantity and quality. Intuitively property predictions seem feasible for the liquid and gaseous products as their properties are determined by their composition where, as shown in 6.3.4, a fairly good knowledge pool already exists about how reaction conditions, and in particular secondary reactions, affect volatile composition. For the solid product this is more complex as physical properties like porosity and surface area play a major role for product application like biochar and activated carbon, and these properties are affected by the char formation pathway (e.g. whether out of a liquid phase or a rigid phase). In Figure 9-2 this is illustrated by the separation into charcoal and char. The question mark is introduced to highlight that the extent of primary charcoal formation remains unknown as demonstrated in chapter 3, and nanostructurally there appears to be not much difference between charcoal and coke in particular at high temperatures (see chapter 7). The introduction of *RF* is also beneficial because factors accounting for particle size, sample size, and the ability of volatiles to escape from the pyrolysis zone could be included in its determination. Doing this would make the simulation of pyrolysis more accurate, as discussed by Wang, Skreiberg, Grønli, Specht, and Antal (2013). Furthermore, the introduction of *RF* in Figure 9-2 highlights the inherent importance of transfer processes during pyrolysis and their role during product formation (see chapter 3 and 6).

The mechanism in Figure 9-2, while simple, applies equally to intraparticle and extraparticle secondary reactions (in chapter 3 it was demonstrated that they are essentially the same) over the entire pyrolysis range, that is, the thermal decomposition range associated with volatile product formation. At a more intricate level, illustrated in Figure 9-3, the recycle factor, *RF*, straddles the pre- and primary-pyrolysis and intra- and extra-particle processes regions. This figure is an adaptation of Figure 2-1 in section 2.2.2 and highlights the parameters that have the biggest impact on the reaction mechanism and the product quantity and quality as found in this research and the literature.

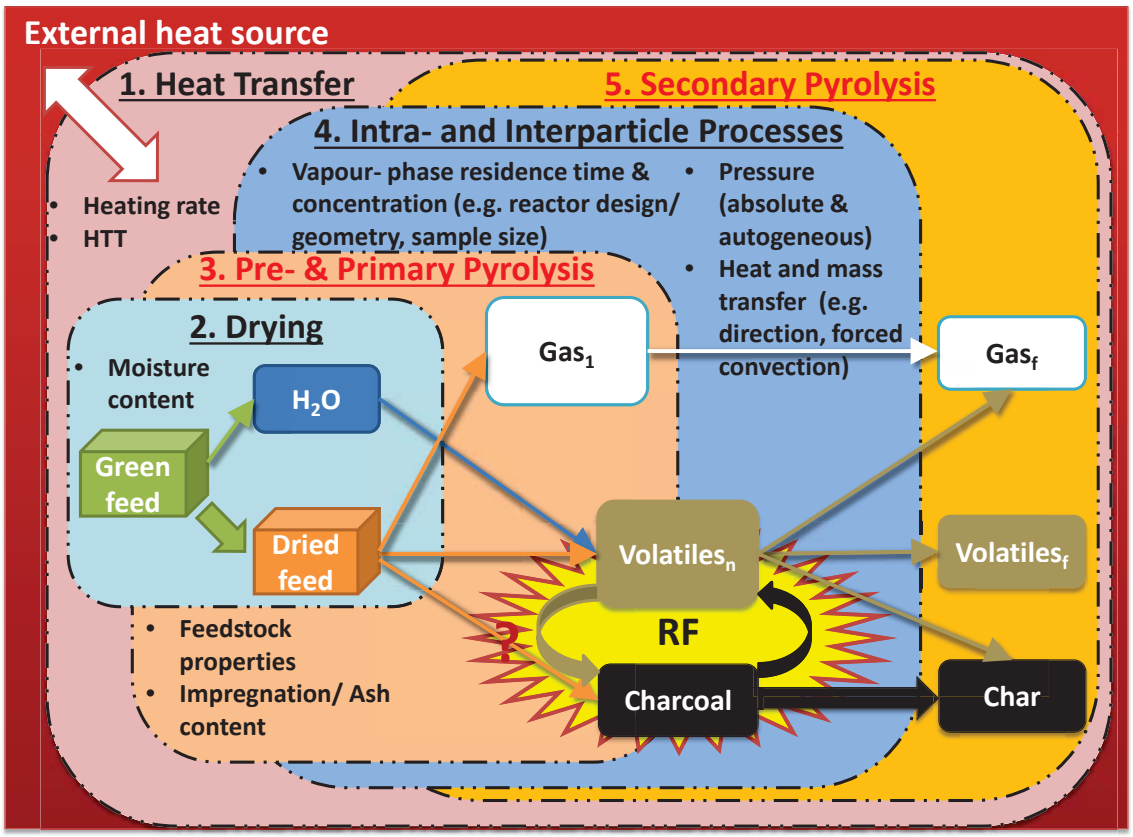

Figure 9-3. Proposed pyrolysis mechanism including the relevant physical processes, and the main parameters of influence. The coloured boxes with the dashed boundaries represent the physical, black headings, and chemical, red headings, processes. Overlapping boxes illustrate their interactions. The toothed ellipse around RF signifies the exothermic nature of this reaction step. The scheme with the arrows in the lower centre of the figure, apart from the drying step, illustrates the proposed mechanism in Figure 9-2. Charcoal is char that retains the morphology of the feedstock, and char is an unspecific term, which refers in this case to coke and/ or soot. The question mark is introduced to denote that the extent of primary charcoal formation is currently unknown. The subscript on the pyrolysis products refers to the pyrolysis stage e.g. primary reactions are denoted by 1. f = final reaction stage; HTT = highest treatment temperature; n = number of reaction steps; RF = Recycle factor. The presented illustration is a modification of Figure 2-1 in chapter 2, and is an adaption from Neves, Thunman, Matos, Tarelho, and Gómez-Barea (2011).

Figure 9-3 shows that pyrolysis always begins with the addition of heat to increase the sample temperature to facilitate the subsequent drying step and the onset of thermal decomposition. The parameters of main importance to thermal decomposition are the heating rate and the *HTT*. The heating rate was not investigated in this research but its effect was discussed in chapter 2. It can for example affect product distribution by promoting re-arrangement reactions (slow pyrolysis) or depolymerisation reactions (fast pyrolysis) leading to increased char or liquid formation respectively, as reviewed by Collard and Blin (2014). The heating rate can further affect the timing of the hydrogen transfer processes, which in turn impacts on the ability of donor hydrogen molecules to quench free radicals involved in retrogressive char forming reactions (Morgan & Kandiyoti, 2013), which was discussed in section 7.3.1. The influence of *HTT* was

observed first hand in this study. In section 3.3.8 it was shown that it determines the decomposition of the biomass constituents, and thus the release of volatile pyrolysis products (see chapter 6). It also directly impacts on the nanostructural development of the char, as was demonstrated in chapter 7.

The drying step is important for almost all feedstocks where the moisture initial content is the primary adjustable variable. The influence of moisture content on pyrolysis was not investigated in this study but according to the literature can have an autocatalytic effect (Mok, Antal, Szabo, Varhegyi, & Zelei, 1992). This was discussed in detail in chapter 2, where also the role of water in hydrous pyrolysis and hydrothermal liquefaction was discussed. However, the exact role of water during pyrolysis remains unknown for which reason steam/ water vapour injection was a main design criterion for the reactor design in chapter 8.

In the subsequent step, pre-and primary pyrolysis occur which, as stated above, can be affected by the presence of water from the previous drying step if water vapour remains in the system. Other important parameters are the feedstock properties of porosity and composition. Porosity affects directly the intimacy of contact between the vapour-phase of the released primary volatile pyrolysis products and the solid/liquid-phase, and so affects the extent of subsequent secondary reactions (see chapter 3). With respect to the feedstock composition, the ash content and its mineralogy are of major importance as they induce catalysis and affect the char yield and the heat of pyrolysis as demonstrated in chapter 4 and 5 respectively. However, the findings in chapter 4 indicate that the catalytic action impacts secondary reactions rather than primary. As a result, this meant no conclusions could be made about the role of ash content on primary reactions.

The occurrence of secondary reactions and their extent are primarily determined by mass transfer processes because of the way these affect the intimacy of contact between mobile volatiles and stationary liquid and solid phases. In chapter 3, 4 and 6 it was shown that long vapour-phase residence times and high volatile concentrations increase the char yield and change the volatile composition significantly. Both this research and the review of the literature in chapter 2 revealed that these conditions are best attained under autogenous pressure because, without pressure, there is a maximum

particle size limit (see 3.3.4) which affects the maximum intra-particle vapour-phase residence time and concentration that can be attained.

The absolute pressure is also believed to be a parameter of major importance. For instance in 6.3.4 it was discussed that a combination of high temperature and high pressure could supply enough energy to break the hydroxyl group in methoxyphenols (Lu, Guo, Zhang, & Wang, 2013), and thus alter the reaction pathway and product quality. High pressures also favour char formation out of a liquid phase by altering the saturation pressure and temperature as discussed in 6.3.4 and 7.3.1, affecting the physical char properties as discussed in chapter 7.

The saw tooth ellipse, shown in Fig 9-3 with the red outline and yellow filling encompassing the secondary reaction step and containing *RF*, represents the exothermic nature of this interaction that leads to increased char yields and makes controlling the *HTT* difficult at the lower end of the biochar production range or in the torrefaction regime. This has been discussed in chapter 5. The here proposed mechanism is supported by the recent work of Dieguez-Alonso, Anca-Couce, Zobel, and Behrendt (2015), and Zobel and Anca-Couce (2015), who showed that the reaction exothermicity is correlated with the production of char and PAH by heterogeneous secondary reactions of the primary volatile pyrolysis products. However, the extent of primary char formation and its effect on the global heat of reaction remains unknown, for which reason the question mark in Figure 9-2 and Figure 9-3 is included. The arrow in Figure 9-3 illustrates that charcoal can be turned into char under high pressures (autogenous and absolute) by inhibiting the evaporation of pyrolysis products and thus causing char formation to proceed through a liquid phase resulting in the destruction of the macroscopic structure of the parent material as mentioned in the paragraph above.

It is important to highlight that the recently published work of Williams, Higashi, Phothisantikul, Van Wesenbeeck, and Antal (2015) confirms the research approach taken here, of focussing on autogenous pressure pyrolysis, as they demonstrate for the first time that the achievement or even over-achievement of the theoretically calculated fixed carbon yield of cellulose is possible under autogenous pressure; even when the sample is initially pressurised with oxygen. They report that the produced char is characterised by a high volatile matter content which is of concern for metallurgical applications but attributed this to the relative low *HTT* that was

restricted to 300 °C due to equipment limitations (associated to obtaining high pressures, i.e., equipment rating 13.9 MPa at 400 °C) but they mention that recent findings at 400 °C corroborate that lower volatile matter contents (≈25 % (wt/wt)) are possible at fixed carbon yields of cellulose that exceed the theoretical value of 28 % (wt/wt). This justifies the design of the high temperature high pressure reactor in chapter 8, which aimed to increase the research capabilities by allowing pyrolysis to 600 °C at 20 MPa. It also enables one to control the maximum autogenous pressure.

Chapter 7 showed that ash compounds are vaporised during pyrolysis. In their recent study Williams et al. (2015) confirmed the findings of Violette that autogenous pressure pyrolysis leads to anomalously high ash yields which appears to be related to the aforementioned observation in chapter 7 (7.3.2). However, Van Wesenbeeck, Higashi, Legarra, Wang, and Antal (2015) demonstrated that the increased ash yield in their studies is caused by contamination from glass and kao wool illustrating that there are still many unknowns in the field of autogenous pressure pyrolysis and that it is subject to on-going research and hence change. Williams et al. (2015) also state that the presence of a liquid phase (discussed in chapter 2, 3 and 7) "links high pressure pyrolysis chemistry to high heating rate pyrolysis chemistry" (Williams et al., 2015, p. 230). They explain this relationship by giving a short review of the literature. Most notably the work of Bai, Brown, and co-workers (Bai & Brown, 2014; Bai, Johnston, & Brown, 2013; Bai, Johnston, Sadula, & Brown, 2013) showed that levoglucosan is the primary product of cellulose and the so-called intermediate liquid compound, ILC, discussed in 2.5.4, which is subject to two competing reactions evaporation and polymerisation. Polymerisation in the liquid phase, which leads to the formation of char and low molecular weight volatiles (Bai, Johnston, Sadula, et al., 2013), is favoured under conditions minimising the evaporation of levoglucosan. With respect to the heating rate Lédé (2012) state in their review that the formation of ILC is rate limited at low temperatures whereas at high temperatures during fast pyrolysis the subsequent processes are rate limited, which explains why liquid phases are observed during fast pyrolysis and not slow pyrolysis. Condensation reactions, which lead to the polymerisation of levoglucosan, are favoured in the liquid phase (discussed in 6.3.4). Thus, the limited evaporation at high heating rates in combination with the presence of a liquid phase promotes the polymerisation pathway as stated above. However, under very high heating rates (flash pyrolysis: $\beta > 10{,}000$ °C/s) no char is observed as the

dehydration of polymers to low molecular weight volatiles is enhanced rather than char formation (Bai & Brown, 2014; Bai, Johnston, & Brown, 2013) explaining why Lédé, Blanchard, and Boutin (2002) observed no char formation under high heat flux densities whereas some was observed under lower heat flux densities. This reveals that there is an optimum for levoglucosan formation, the platform chemical for biofuels and biobased products (Bai & Brown, 2014), because depolymerisation to levoglucosan is enhanced at high heating rates, as stated above and reviewed by Collard and Blin (2014), while at very high heating rates its evaporation is minimised and its polymerisation and decomposition to gas is enhanced (Bai & Brown, 2014).

The above discussion reveals the important role transport phenomena play when it comes to the effect of heating rate on product distribution, because heating rate affects pressure which drives the mass transfer of levoglucosan to the vapour phase, in particular if the external pressure exceeds the vapour pressure which leads to the presence of liquid levoglucosan and its subsequent polymerisation (Bai & Brown, 2014; Bai, Johnston, & Brown, 2013; Bai, Johnston, Sadula, et al., 2013; Williams et al., 2015). Therefore, any condition that minimises the evaporation of levoglucosan, like increased sample size, reduced sweep gas flow rate and prolonged vapour-phase residence time (Bai, Johnston, & Brown, 2013), increases the char yield if the heating rate is not very high. It is important to note that Williams et al. (2015) employed fast heating rates by inserting the sealed bomb reactor in a pre-heated fluidised sand bath at 300 °C showing that slow pyrolysis is not a necessary requirement to obtain high char yields.

Overall these findings reveal that char formation from cellulose occurs only by secondary reactions and that the structure of the char is primarily affected by transport phenomena. This means that specific to cellulose, the arrow from the feedstock to the charcoal in Figure 9-2 and Figure 9-3 does not exist. It needs to be noted here that these findings agree with the two-phase model for cellulose pyrolysis proposed by Mamleev et al. (2009), which underlines the important role of catalysis and supports the introduction of the recycle factor, *RF*, proposed in this work. However, the char formation mechanism for wood or for the other biomass constituents remains uncertain although Dufour, Castro-Diaz, Brosse, Bouroukba, and Snape (2012) show that proton mobility and transfer play an important role and that there is an interaction between the

biomass polymers, and their mineral matter content. Without doubt, wood and other biomass constituents require further research.

Further, Williams et al. (2015) found that autogenous pressure pyrolysis leads to increased CO_2 yields, which links to the deoxy-liquefaction studies (e.g. Lu et al. (2013)) discussed in 2.8.2 and 6.3.4. This reiterates that autogenous pressure pyrolysis is invaluable for understanding pyrolysis mechanism and makes the designed reactor in chapter 8 a valuable asset.

It is important to note here that the introduction of *RF* is merely a concept at this stage. It is envisioned that it would be imbedded within a kinetic model by an array of RF_i representing the various reaction pathways like polymerisation, dehydration, volatilisation, *etc*., which are weighted according to the reaction conditions. Clearly more research is needed to determine the values for such a model.

9.3 Suggestions for Future Work

As with any research project this work had to deal with a large range of challenges and un-resolved issues, which are highlighted briefly and warrant future research.

1. Measure accurately weight loss of single particles in the range of single tracheid cells to draw conclusion about primary char formation. This is suggested as Figure 3-19 in 3.3.2 indicates a char yield of 0 % (wt/wt) for small samples. However this was at the limit of the applied TGA, and a TGA with a better resolution could provide more insight.
2. Perform weight loss measurements at different heating rates to get a better understanding of the time-temperature history and to account for the compensation effect when determining the Arrhenius parameters. In the former case perform additional experiments including isothermal temperature steps.
3. Account for and minimise the conduction of heat by the thermocouples (use thinner thermocouples), and position thermocouples closer to the sample surface to get a better understanding of the internal temperature profile. The benefit of doing this is to validate the relationship between thermal lag effects and reaction heat effects.
4. Model pyrolysis to verify the role of time-temperature history and secondary reactions.
5. Development of a new kinetic model to describe char formation in the presence of catalyst and enhanced secondary reactions. This includes optimising the reference temperature for re-parameterisation of the Arrhenius equation (Schwaab, Lemos, & Pinto, 2008; Schwaab & Pinto, 2007), optimisation of the reaction order, and more fundamentally a review of the applicability of the Arrhenius kinetics for heterogeneous reactions as outlined in the review by White, Catallo, and Legendre (2011).
6. Since the TGA heat flow data used in this study was unsuitable for determining the heat of reaction it is proposed to repeat the experiments in chapter 5 with a true DSC.
7. With respect to the Py/ GC-MS study in chapter 6 it is beneficial to select some key pyrolysis products or constituents (e.g. a guaiacol standard) and carry out a quantitative analysis in open crucibles and sealed glass capsules to gain more information about detailed reaction mechanism. The standard will be compared

against the pyrograms to establish/ verify the compounds existence and quantitatively evaluate its change due to secondary reactions.

8. Build the reactor in chapter 8 and perform the experiments outlined and explained in 8.4 to study the intricacies of the proposed mechanism in Figure 9-3.
9. Carry out a thorough product characterisation of all the pyrolysis products (solid, liquid and gaseous). When analysing the char it is recommended to perform a detailed char characterisation according to IBI (International Biochar Initiative, 2014) and European Biochar Certificate (European Biochar Foundation, 2012) guidelines. It is advisable to include a chemical analysis (e.g. functional groups and presence of phytotoxic compounds—especially when tar is condensed on the char), as well as structural analysis by transmission electron microscopy and possibly pore analysis by mercury porosimetry. For characterising the liquid product it is suggested to apply elemental analysis for oxygen determination (directly related to product quality), as well as a range of analysis techniques for determination of the pyrolytic lignin, as discussed in the literature (Scholze, Hanser, & Meier, 2001; Scholze & Meier, 2001). Simulating these results will aid in resolving the pyrolysis mechanisms as suggested by Williams et al. (2015).
10. When studying the catalytic effect of ash compounds and dehydrating acids it is proposed to record the internal sample temperatures, which can be done by utilising the designed reactor in chapter 8, and analysing the volatile pyrolysis products to gain a better understanding of the decomposition temperature ranges and the underlying reaction mechanism. Unique information about catalytic reactions can already be obtained by repeating the experiments in chapter 6 with the impregnated samples in chapter 4. This will provide much needed information about their influence on primary and secondary reaction mechanism, and help identify what bio-components or pyrolysis products are affected by catalysis.
11. Perform analysis on the fate of the ash compounds during pyrolysis to confirm whether or not the observed trend in chapter 7 (maximum in ash profile of char) is genuine. Also the colour changes observed in the tar ash compared to the char ash can be examined by analysing the elemental and chemical compositions by Inductively Coupled Plasma Emission Spectroscopy (ICPES) and X-Ray

Diffraction (XRD) (Misra, Ragland, & Baker, 1993) to gain more information of ash behaviour during pyrolysis.

9.4 Conclusion

To sum it up, the objective stated in chapter 1 of maximising the yield of biochar in the slow pyrolysis regime by understanding how secondary reactions affect the char yield and pyrolysis process was achieved. That is, secondary reactions were identified to be responsible for the majority of the char formed by the principle mechanism of intimate contact between the pyrolysis products and the pyrolysing solid. This conclusion was derived by the careful analysis of TGA data, which has not been performed in literature to this extent to analyse and verify the effect of secondary reactions on pyrolysis. This method also revealed a strong relationship between the presence of catalyst and secondary reactions as it showed that they affect pyrolysis in the same manner. Overall this research clearly highlights the central role of secondary reactions in pyrolysis, and the best method for studying them was identified to be autogenous pressure pyrolysis, where applying the new method of slowly pyrolysing wood in sealed crucibles in a Pyrolysis gas-chromatograph mass spectrometer revealed their effect on the volatile product composition right from the onset of pyrolysis. The final key contribution of this PhD to the field of research is the open accessible design of a high pressure high temperature reactor that creates new research capabilities to study the underlying reaction mechanism in detail.

For the manufacture of biochar specifically, this research shows that reactors are desired that use large samples and limit the escape of the volatile pyrolysis products to enhance the char yield. With respect to biochar properties, the formation of coke and char out of a liquid phase due to increased pressure can destroy the important macroscopic structure required for soil application highlighting a conflict between yield and properties, and sequestration and economics.

9.5 References

Antal, M. J., & Varhegyi, G. (1995). Cellulose pyrolysis kinetics: The current state of knowledge. *Industrial & Engineering Chemistry Research, 34*(3), 703-717. doi:10.1021/ie00042a001

Bai, X., & Brown, R. C. (2014). Modeling the physiochemistry of levoglucosan during cellulose pyrolysis. *Journal of Analytical and Applied Pyrolysis, 105*, 363-368. doi:10.1016/j.jaap.2013.11.026

Bai, X., Johnston, P., & Brown, R. C. (2013). An experimental study of the competing processes of evaporation and polymerization of levoglucosan in cellulose pyrolysis. *Journal of Analytical and Applied Pyrolysis, 99*, 130-136. doi:10.1016/j.jaap.2012.10.012

Bai, X., Johnston, P., Sadula, S., & Brown, R. C. (2013). Role of levoglucosan physiochemistry in cellulose pyrolysis. *Journal of Analytical and Applied Pyrolysis, 99*, 58-65. doi:10.1016/j.jaap.2012.10.028

Boroson, M. L., Howard, J. B., Longwell, J. P., & Peters, W. A. (1987). *Effects of extra-particle secondary reactions of fresh tars on liquids yields in hardwood pyrolysis*. Paper presented at the 193rd National meeting of the American Chemical Society, Denver, CO. Paper retrieved from https://web.anl.gov/PCS/acsfuel/preprint%20archive/Files/32_2_DENVER_04-87_0051.pdf

Boroson, M. L., Howard, J. B., Longwell, J. P., & Peters, W. A. (1989). Heterogeneous cracking of wood pyrolysis tars over fresh wood char surfaces. *Energy & Fuels, 3*(6), 735-740. doi:10.1021/ef00018a014

Brandt, P., Larsen, E., & Henriksen, U. (2000). High tar reduction in a two-stage gasifier. *Energy & Fuels, 14*(4), 816-819. doi:10.1021/ef990182m

Collard, F.-X., & Blin, J. (2014). A review on pyrolysis of biomass constituents: Mechanisms and composition of the products obtained from the conversion of cellulose, hemicelluloses and lignin. *Renewable and Sustainable Energy Reviews, 38*, 594-608. doi:10.1016/j.rser.2014.06.013

Di Blasi, C. (1996). Heat, momentum and mass transport through a shrinking biomass particle exposed to thermal radiation. *Chemical Engineering Science, 51*(7), 1121-1132. doi:10.1016/S0009-2509(96)80011-X

Dieguez-Alonso, A., Anca-Couce, A., Zobel, N., & Behrendt, F. (2015). Understanding the primary and secondary slow pyrolysis mechanisms of holocellulose, lignin and wood with laser-induced fluorescence. *Fuel, 153*, 102-109. doi:10.1016/j.fuel.2015.02.097

Dufour, A., Castro-Diaz, M., Brosse, N., Bouroukba, M., & Snape, C. (2012). The origin of molecular mobility during biomass pyrolysis as revealed by in situ ^{1}H NMR spectroscopy. *ChemSusChem, 5*(7), 1258-1265. doi:10.1002/cssc.201100442

European Biochar Foundation. (2012). *European biochar certificate - Guidelines for a sustainable production of biochar*. Retrieved from European Biochar Foundation website: http://www.european-biochar.org/biochar/media/doc/ebc-guidelines.pdf

International Biochar Initiative. (2014). *Standardized product definition and product testing guidelines for biochar that is used in soil* (Document Reference Code: IBI-STD-2.0) [Product Definition and Specification Standards]. Retrieved from International Biochar Initiative website: http://www.biochar-

international.org/sites/default/files/IBI_Biochar_Standards_V2%200_final_2014.pdf

Lédé, J. (2012). Cellulose pyrolysis kinetics: An historical review on the existence and role of intermediate active cellulose. *Journal of Analytical and Applied Pyrolysis, 94*, 17-32. doi:10.1016/j.jaap.2011.12.019

Lédé, J., Blanchard, F., & Boutin, O. (2002). Radiant flash pyrolysis of cellulose pellets: Products and mechanisms involved in transient and steady state conditions. *Fuel, 81*(10), 1269-1279. doi:10.1016/S0016-2361(02)00039-X

Lu, W., Guo, Y., Zhang, B., & Wang, C. (2013). Comprehensive analysis on elements, energy recovery, and oil compositions of biomass deoxy-liquefaction. *Energy and Fuels, 27*(4), 2157-2166. doi:10.1021/ef400157e

Mamleev, V., Bourbigot, S., Le Bras, M., & Yvon, J. (2009). The facts and hypotheses relating to the phenomenological model of cellulose pyrolysis: Interdependence of the steps. *Journal of Analytical and Applied Pyrolysis, 84*(1), 1-17. doi:10.1016/j.jaap.2008.10.014

Misra, M. K., Ragland, K. W., & Baker, A. J. (1993). Wood ash composition as a function of furnace temperature. *Biomass and Bioenergy, 4*(2), 103-116. doi:10.1016/0961-9534(93)90032-Y

Mok, W. S.-L., Antal, M. J., Szabo, P., Varhegyi, G., & Zelei, B. (1992). Formation of charcoal from biomass in a sealed reactor. *Industrial & Engineering Chemistry Research, 31*(4), 1162-1166. doi:10.1021/ie00004a027

Morgan, T. J., & Kandiyoti, R. (2013). Pyrolysis of coals and biomass: Analysis of thermal breakdown and its products. *Chemical Reviews*. doi:10.1021/cr400194p

Neves, D., Thunman, H., Matos, A., Tarelho, L., & Gómez-Barea, A. (2011). Characterization and prediction of biomass pyrolysis products. *Progress in Energy and Combustion Science, 37*(5), 611-630. doi:10.1016/j.pecs.2011.01.001

Scholze, B., Hanser, C., & Meier, D. (2001). Characterization of the water-insoluble fraction from fast pyrolysis liquids (pyrolytic lignin): Part II. GPC, carbonyl goups, and 13C-NMR. *Journal of Analytical and Applied Pyrolysis, 58–59*, 387-400. doi:10.1016/S0165-2370(00)00173-X

Scholze, B., & Meier, D. (2001). Characterization of the water-insoluble fraction from pyrolysis oil (pyrolytic lignin). Part I. PY–GC/MS, FTIR, and functional groups. *Journal of Analytical and Applied Pyrolysis, 60*(1), 41-54. doi:10.1016/S0165-2370(00)00110-8

Schwaab, M., Lemos, L. P., & Pinto, J. C. (2008). Optimum reference temperature for reparameterization of the Arrhenius equation. Part 2: Problems involving multiple reparameterizations. *Chemical Engineering Science, 63*(11), 2895-2906. doi:http://dx.doi.org/10.1016/j.ces.2008.03.010

Schwaab, M., & Pinto, J. C. (2007). Optimum reference temperature for reparameterization of the Arrhenius equation. Part 1: Problems involving one kinetic constant. *Chemical Engineering Science, 62*(10), 2750-2764. doi:http://dx.doi.org/10.1016/j.ces.2007.02.020

Shafizadeh, F., & Chin, P. P. S. (1977). Thermal deterioration of wood. In I. S. Goldstein (Ed.), *Wood Technology: Chemical Aspects* (Vol. 43, pp. 57-81).

Thurner, F., & Mann, U. (1981). Kinetic investigation of wood pyrolysis. *Industrial & Engineering Chemistry Process Design and Development, 20*(3), 482-488. doi:10.1021/i200014a015

Van Wesenbeeck, S., Higashi, C., Legarra, M., Wang, L., & Antal, M. J. (2015). Biomass pyrolysis in sealed vessels. Fixed-carbon yields from Avicel cellulose

that realize the theoretical limit. *Energy & Fuels*. doi:10.1021/acs.energyfuels.5b02628

Wang, L., Skreiberg, Ø., Grønli, M. G., Specht, G. P., & Antal, M. J. (2013). Is elevated pressure required to achieve a high fixed-carbon yield of charcoal from biomass? Part 2: The importance of particle size. *Energy & Fuels, 27*(4), 2146-2156. doi:10.1021/ef400041h

White, J. E., Catallo, W. J., & Legendre, B. L. (2011). Biomass pyrolysis kinetics: A comparative critical review with relevant agricultural residue case studies. *Journal of Analytical and Applied Pyrolysis, 91*(1), 1-33. doi:10.1016/j.jaap.2011.01.004

Williams, S., Higashi, C., Phothisantikul, P., Van Wesenbeeck, S., & Antal, M. J. (2015). The fundamentals of biocarbon formation at elevated pressure: From 1851 to the 21st century. *Journal of Analytical and Applied Pyrolysis, 113*, 225-230. doi:10.1016/j.jaap.2014.12.021

Zaror, C. A., Hutchings, I. S., Pyle, D. L., Stiles, H. N., & Kandiyoti, R. (1985). Secondary char formation in the catalytic pyrolysis of biomass. *Fuel, 64*(7), 990-994. doi:10.1016/0016-2361(85)90156-5

Zobel, N., & Anca-Couce, A. (2015). Influence of intraparticle secondary heterogeneous reactions on the reaction enthalpy of wood pyrolysis. *Journal of Analytical and Applied Pyrolysis, 116*, 281–286. doi:10.1016/j.jaap.2015.08.019

10. Nomenclature

Symbols	Definition	Units
A	Area	m^2
A	Pre-exponential factor in Arrhenius equation	s^{-1}, min^{-1}
Ash	Ash content	% (wt/wt)
Bi	Biot number	
BP	Before Present	
BTEX	Benzene, toluene, ethylbenzene, and xylenes	
C	Carbon content	% (wt/wt)
c_p	Specific heat capacity	J/(kg·K)
CCD	Charge-coupled device	
CEC	Cation exchange capacity	
CV	Coefficient of variation	
d	Diameter	m, mm
D	Diffusion coefficient	m^2/s
D_{AB}	Binary mass diffusivity	m^2/s
D_B	Bound water diffusion coefficient	m^2/s
D_V	Water vapour diffusion coefficient in air in lumens	m^2/s
Da	Average difference	
daf	Dry ash free	
db	Dry basis	
dim	Dimension	mm
DP	Degree of polymerisation	
DSC	Differential scanning calorimetry	
DTA	Differential thermal analysis	

E	Exponential factor in Arrhenius equation	kJ/mol
EBC	European Biochar Certificate	
EBF	European Biochar Foundation	
EC	Electrical conductivity	
EGA	Evolved gas analysis	
F	View factor	
FC	Fixed carbon	% (wt/wt)
FSP	Fibre saturation point	
FTIR	Fourier transform infrared spectroscopy	
G	Specific gravity	
GC	Gas chromatograph	
H	Hydrogen content	% (wt/wt)
h	Convection heat transfer coefficient	W/(m^{2}K)
h_m	Convection mass transfer coefficient	m/s
h	Height	m; mm
H_P	Heat of pyrolysis	J/g
HHV	Higher heating value	MJ/kg
HTC	Hydrothermal carbonisation	
HTT	Highest treatment temperature	°C, K
I	Intensity/height of Raman signal	
IBI	International Biochar Initiative	
ICPES	Inductively Coupled Plasma Emission Spectroscopy	
ID	Inside diameter	m, mm
ILC	Intermediate liquid compound	
IPCC	Intergovernmental Panel on Climate Change	
K	Permeability	m^3/(m·Pa·s)

k	Reaction rate constant	s^{-1}
l	Length, thickness	m, mm
LHV	Lower heating value	MJ/kg
LPG	Liquefied petroleum gas	
M	Moisture	% (wt/wt)
m	Mass	kg
$\dot{m}$	Mass flow	kg/s
MC	Moisture content	% (wt/wt)
MIC	Mass Ion Chromatogram	
MS	Mass spectrometry/spectrometer	
m/z	mass-to-charge ratio	
N	Nitrogen content	% (wt/wt)
n	Number of experimental data points	
O	Oxygen content	% (wt/wt)
OD	Outside diameter	m, mm
OF	Objective function	
OFF	Offset	W
p	Pressure	Pa, bar
$p(u)$	Arrhenius temperature integral	
PAH	Polycyclic aromatic hydrocarbons	
Ph•	Phenol radical	
PhO•	Phenoxy radical	
Py	Pyrolysis	
P&ID	Piping and instrumentation diagram	
Q	Heat flow	W
R	Correlation coefficient	
R^2	Coefficient of determination	
R_g	Universal gas constant	J/(mol·K)
R_m	Mass transfer resistance	s/m^3

R_t	Thermal resistance	K/W
r	Radial position/radius	m
RF	Recycle factor	
ROI	Residue on Ignition	
RT	Room temperature	
Rt	Retention time	min
S	Sulphur content	% (wt/wt)
SEM	Scanning electron microscope	
STA	Simultaneous thermal analysis	
T	Temperature	°C, K
t	Time	s, min, h
TGA	Thermogravimetric analysis/analyser	
TG-DTA	Thermogravimetric differential thermal analysis	
TIC	Total Ion Chromatogram	
V	Volume	m^3
$\dot{V}$	Volume flow	m^3/s
VM	Volatile Matter	% (wt/wt)
VTC	Vapothermal carbonisation	
x	Fraction of biomass component	
XRD	X-ray diffraction	
y	Yield	kg/kg
$\%\,FC$	Percentage of fixed carbon in the charcoal	%
$\%\,feed\ ash$	Percentage of ash in the feedstock	%

Greek Symbols

α	Degree of decomposition/conversion	% (wt/wt)

α_T	Thermal diffusivity	m^2/s
β	Heating rate	K/min, K/s
Δ	Difference	
ε	Porosity/void fraction	
λ	Thermal conductivity	W/(m·K)
ρ	Mass concentration/density	kg/m^3
τ	Tortuosity	
ω	Emissivity	

Subscripts

A	A band signal of Raman spectra
ash	Mineral matter/ash
B	Bound
b	Biomass
blank	Empty crucible
c	Centre
ch	Characteristic
calc	Calculated
char	Char
cond	Conduction
conv	Convection
cor	Offset corrected
D	D band signal of Raman spectra
d	Dry
eff	Effective
exp	Experimental
f	Final
FC	Fixed carbon

feed	Feedstock
G	G band signal of Raman spectra
h	Halfway
i	Component or phase *i*
impreg	Impregnated components
in	Initial
m	Mass
max	Maximum
mod	Model
moist	Moist
OD	Oven-dry
org	Organic
P	Pyrolysis
R	Reaction
r	Residue
rad	Radiation
ref	Reference
s	Surface
se	Sensible
T	Transverse
trans	Transition
V	Valley signal of Raman spectra
w	Wall
water	Water
wood	Wood

Appendix A Project Overview

A.1 Biochar: Potential and Concerns

Table A-1. Potential/ benefits of biochar production and application.

Potential/ Benefits	By
Agronomic	
Improve soil productivity/ Enabling plant growth on infertile soils	• Nutrient and moisture retention • Reducing soil acidity/ increasing pH • Increasing cation exchange capacity • Increasing microbial biomass • Supporting soil beneficial microorganism, e.g. earthworms • Enhancing arbuscular mycorrhizal fungi in soil
Reduce irrigation demand/ allow farming in dry regions	• Moisture retention
Make farming more secure	• Stabilizing soil conditions
Reduce amount or need for fertilizer and thus dependency on suppliers	• Nutrient retention • Reduced required application rate (research indicates that biochar does not need to be applied very often)
Environmental	
Reduce emissions from soil	• Storing carbon in soil for a sufficient long time (biochar could even sequester more carbon when buried) • Reducing emissions of other greenhouse gases, e.g. CH_4 and N_2O • Supporting nitrogen fixation
Prevent pollution of water streams and ground water	• Preventing leaching of nutrients • Binding agrochemicals
Compensate for greenhouse gas emissions	• Being carbon negative • Reducing emissions of greenhouse gases from soil • Increasing biomass and thus carbon uptake in biomass • Offsetting emissions associated with reduced fertilizer demand • Offsetting emission associated with reduced waste treatment • Reducing emissions associated with ponding of organic materials

(continued)

Potential/ Benefits	**By**
Biodiversity conservation	• Preventing forest clearances by supporting intensive sustainable agriculture
Waste management	
Reduce fire risk in forests	• Removing unused residues for biochar production
Reduce costs associated with sewage and animal waste treatment	• Converting sewage to biochar • Decreasing waste volume • Pyrolysis acts sterilising & destroys some veterinary pharmaceuticals
Soil remediation	
Reduce uptake of pesticides[a]	• High surface area, nanoporosity & capability to sequester organic compounds[a]
Reduce bioavailability and phytotoxicity of heavy metals[b]	• Partitioning metals to less bioavailable organic bound fraction[b]
Energy sector	
Support biofuel production	• Using volatile pyrolysis products for energy generation or as syngas supply • Utilising process heat
Social	
Opportunities for rural communities, e.g. Maori communities in New Zealand (Vision Mātauranga[c])	• Technology is relative easy & can be adopted widely, i.e. possible at village scale • Farmers used to slash and burn can easily switch to slash and char • Selling carbon offset on market

Note. The information in this table has been adapted from Barrow (2012).

[a]Yu, Ying, and Kookana (2009). [b]Bolan, Park, Choppala, Shenbagavalli, and Mahimairaja (2012). [c]Ministry of Research Science and Technology - Te Manatū Pūtaiao (2007).

Table A-2. Concerns and criticism of biochar.

Subject to Criticism	Annotation
Definition of biochar	• Biochar is not a chemically or physically well-defined product, i.e. its name is derived from its purpose
Soil carbon	• The stability of biochar in soil is highly variable and the reasons remain unknown • Field trials do not support that biochar consistently increases soil carbon
Soil fertility	• Different biochars affect various soils in an unpredictable manner • Terra Preta soils are complex and their "recipe" is unknown • Field trials have not been carried out over a sufficiently long time period and there is not enough evidence suggesting that biochar increases crop yields consistently
Mitigating climate change	• It is not proven that biochar can sequester carbon sufficiently long—see also soil carbon • There is no substantial evidence suggesting reduced nitrous oxide emissions from biochar application to soil • Biochar particles could become airborne and reduce albedo • Harvesting, transporting and pyrolysing of biomass and transporting and application of biochar to soil causes emissions, which could turn biochar from being carbon negative to being carbon positive
Manufacture	• Modern pyrolysis processes are still inefficient and uneconomic • The inefficiency of pyrolysis processes can lead to land-use changes, increase in monocultures and deforestation • The operation of pyrolyser is complex and difficult • Control of pyrolyser is problematic
Economics	• Biochar is not economic unless subsidised • Future of carbon markets is unclear and the European emission trading scheme, to which most trading worldwide is connected, does not presently include soils as sinks

Note. The information in this table presents a summary of the critical points raised in the report "Biochar: A critical review of science and policy," by Biofuelwatch. Retrieved from Biofuelwatch website: http://www.biofuelwatch.org.uk/wp-content/uploads/Biochar-Report3.pdf

A.2 References

Barrow, C. J. (2012). Biochar: Potential for countering land degradation and for improving agriculture. *Applied Geography, 34*(0), 21-28. doi:10.1016/j.apgeog.2011.09.008

Bolan, N. S., Park, J., Choppala, G., Shenbagavalli, S., & Mahimairaja, S. (2012, February). *Biochars enhance the remediation of metal contaminated soils.* presented at New Zealand Biochar Workshop 2012, Palmerston North, New Zealand.

Ministry of Research Science and Technology - Te Manatū Pūtaiao. (2007). *Vision Mātauranga* [Ministry of Business, Innovation and Employment website:]. Retrieved from http://www.msi.govt.nz/assets/MSI/Get-connected-documents/VM-Booklet.pdf

Yu, X.-Y., Ying, G.-G., & Kookana, R. S. (2009). Reduced plant uptake of pesticides with biochar additions to soil. *Chemosphere, 76*(5), 665-671. doi:10.1016/j.chemosphere.2009.04.001

Appendix B Role of Secondary Char Formation in the Manufacture of Biochar

B.1 TGA Proximate Analysis Results without Adjustment of Ash Content

Table B-1. Proximate analysis with lid of air-dried radiata pine in % (wt/wt) on an air-dry basis.

	Moisture	**Volatile matter**	**Fixed carbon**	**Ash**
μ in % (wt/wt)	9.409	72.064	17.784	0.746
σ in pp	0.384	1.844	0.431	2.028
CV	0.041	0.026	0.024	2.720

Note. The results represent averages of 5 samples. *CV* = coefficient of variation; μ = average; σ = standard deviation.

Table B-2. Proximate analysis without lid of air-dried radiata pine in % (wt/wt) on an air-dry basis.

	Moisture	**Volatile matter**	**Fixed carbon**	**Ash**
μ in % (wt/wt)	9.307	76.768	13.108	0.820
σ in pp	0.206	1.566	0.463	1.620
CV	0.022	0.020	0.035	1.974

Note. The results represent averages of 5 samples. *CV* = coefficient of variation; μ = average; σ = standard deviation.

B.2 Matlab Code for Selecting Data Corresponding to Temperatures in the Range 30 to 700 °C

```
function newdata = Tselect(data)

  indices = [];
  columnT = data(:,1);
  columnTnew = columnT;

  for T = 30:0.5:700

    index = [];

    for i = 1:length(columnT)
        columnTnew(i) = abs(columnT(i)-T);
    end

    minimum = min(columnTnew);

    for i = 1:length(columnT)
        if columnTnew(i) == minimum
            index = [index i];
        end
    end
    if length(index)>1
        index=index(1);
    end

    indices = [indices index];
  end
  Temperature = (30:0.5:700);
  dependent = data(indices,2:6);
  newdata = [Temperature' dependent];
```

B.3 Binder Burner/Macro-TGA

B.3.1 Equipment Pictures

Figure B-1. Binder Burner (Macro-TGA) with peripheral equipment.

Figure B-2. Binder Burner furnace with stainless steel crucible and pyrolysed wood sample MTGA16. The diameter and height of the crucible is 130 and 75 mm respectively.

Figure B-3. Condenser for Binder Burner. Designed as a counter current double hull condenser. The height, inner diameter, and hull thickness is 30 cm, 10 cm, and 3 mm respectively.

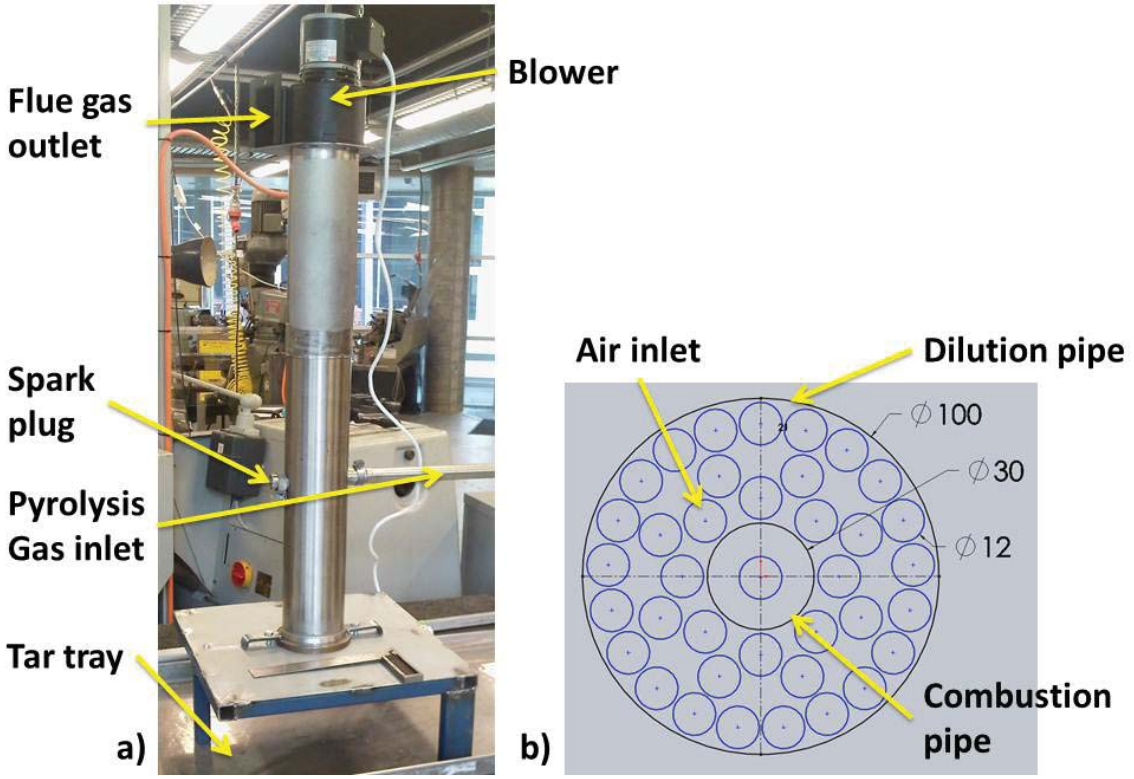

Figure B-4. Exhaust burner with air-inlet plate. a) Exhaust burner. The height of the whole assembly inclusive high-temperature blower is 1.05 m. b) Air-inlet plate. The dimensions are in mm.

B.3.2 Extended Operating Procedure for Pyrolysis Experiments in the Binder Burnout Furnace

This operating guide is intended as an extension only, and the trained operator is required to be familiar with the main operating instructions first. They outline the general steps of the operating procedure and thus are a necessity.

Before the Run

1. Ensure that the condenser with the downstream exhaust burner is connected to the gas outlet of the Binder Burnout Furnace instead of the vacuum pump, and that they are placed inside the provided tray to minimise the effect of an accidental spillage.
2. Check the water is on (one turn is usually enough) and flowing through the condenser (inlet: bottom; outlet: top), as well as through the heat exchanger in the furnace to protect the balance from overheating (if water flow is too low an error message will appear in the Binder Burnout software window; check the “Interlock status”—this is only visible when the software is running).

3. Insert thermocouples in exhaust burner (one near the pilot flame and a second one at the end of the stack just before the exhaust fan), and connect to handheld digital thermometer.
4. Make sure the exhaust pipe from the exhaust burner fan is placed inside the fume cupboard in the next door room, and the extraction fan of the fume cupboard is turned on—wait until pre-purging is finished before going to the next step.
5. Ascertain the controller power switch is on at the wall (Step 1 Main Operating Procedure).
6. Check that the balance is turned on and its display lit (Step 3 Main Operating Procedure).
7. Check for "Normal Operation under Nitrogen Gas"—Step 27 to 28—that enough nitrogen for a run is available in the respective cylinder outside. A pyrolysis run at a heating rate of 5 °C/min to 700 °C requires generally 2000 kPa (includes evacuating and backfilling of the bell jar twice; as well as additional nitrogen—with the backfill valve open—for increasing the cooling down rate).

Start-up Exhaust Burner

8. Turn on exhaust burner fan, spark plug and LPG-solenoid valve by plugging the respective power plug into the provided extension cord. Make sure the extension cord is placed away from the floor to prevent it from getting wet.
9. Slide the exhaust burner fan up so that there is a "hand width" gap between the fan and the end of the exhaust stack. The resulting reduced airflow in the stack allows one to light the pilot flame.
10. Turn on the LPG to light the pilot flame (pilot flame is lit automatically by the continuous sparking of the spark plug).
11. Make sure the pilot flame is going. This can be done acoustically or visually by reading the value of the pilot flame thermocouple. The temperature displayed should be several hundred degrees Celsius.
12. Reposition the exhaust fan so that it is flush with the stack. Ensure the pilot flame is still going; if not start again from step 8 and adjust the LPG flow with the needle valve.

13. Check that exhaust fan temperature, that is temperature at the top of the stack, does not exceed 232 °C (450 °F). In normal operation this temperature is expected to be below 100 °C.

Sample Loading

14. First the operator is referred to the "Loading" section of the Main Operating Procedure (Step 5 to 12).
15. Regarding Step 5 in the Main Operating Procedure before opening the bell-jar make sure that the furnace power switch at the controller fascia is turned off.
16. For the pyrolysis experiments a special steel sample basket is utilised. Before placing the sample basket into the furnace assure that the sample support tube connecting the silica glass plate inside the furnace to the balance is not touching the side wall, which would otherwise affect weighing.
17. Place the empty sample basket on the silica glass plate. Ensure that the basket is not touching the heating wires and the furnace thermocouple.
18. Tare the balance so that the sample net mass loss can be followed.
19. Position the sample inside the basket. It is important to note that the drilled holes for the thermocouples in the sample have to be slightly deeper than the thermocouple length that is penetrating the sample to avoid thermal expansion to interfere with weighing.
20. Position metal lid on furnace with the number of required thermocouples (maximum of four) evenly distributed. Note the number of the thermocouples and their position, which is important for data logging. Store thermocouples that are not required out of the way on the cooled balance plate (bottom plate).
21. Align the thermocouples with the silica glass gas exhaust tube so that the two-layer fibreboard lid can be placed on top of the furnace (Note the alignment notches). Before locating the fibreboard lid check that the support tube mentioned in point 16 is still in place.
22. Make sure the thermocouples or their wires do not interfere with the steel bell-jar and do not touch the hot plate (Tape them to the water cooled balance plate).
23. Carefully lower the steel cover and affirm that no wire or thermocouple is hanging out.

24. Re-engage the clips to seal the bell-jar.
25. Evacuate and backfill the bell-jar with nitrogen twice. For evacuation the reader is referred to Steps 13 to 15 of the Main Operating Procedure. To backfill the bell jar with nitrogen turn on the quarter turn valve by the wall and turn the handle of the centre large gas valve down. Subsequently turn the backfill valve on. Undo the last steps to evacuate again.
26. Turn on the furnace power switch at the controller fascia (Step 12 Main Operating Procedure).

Normal Operation under Nitrogen Atmosphere

27. The reader is referred to the "Normal operation under gas" section of the Main Operating Procedure (Step 16 to 19—Step 20 does not apply in this set up).
28. Regarding to step 19 adjust the flow so that the black ball of the glass rotameter is positioned at 150, which equals a nitrogen flow of 55 ml/min.

Control and Logging

29. The reader is referred to the "Control and Logging" section of the Main Operating Procedure (Step 21 to 29).
30. Output time of measurements has to be at least 20 s.
31. Stability filter has to be set to "very unstable" if high mass loss rates are expected and the balance settings have to be adjusted so that the data recording printout is set to "Manual Without stability" or the communication to the PC will fail (see Menu Structure Overview in the Balance Manual for detail).

At the End of Pyrolysis Experiments

32. Once the furnace temperature has reached 100 °C it is advised to evacuate the bell-jar to half scale and backfill it with nitrogen three times to get rid of pyrolysis gases that may have accumulated in the bell-jar, as the volume of the bell-jar is relative large compared to the sample.

33. The reader is referred to the "At the end of the run" section of the Main Operating Procedure (Step 30 to 35). Important to note is step 30 in the Main Operating Procedure, that is to switch off the primary power off the heater on the front fascia before raising the bell-jar.
34. If all experiments are finished the exhaust burner needs to be turned off. First close the LPG bottle and wait till the pilot flame extinguishes. This can be checked acoustically and visually as discussed in point 11. After it has been ensured that the pilot flame is off, turn off the power to the solenoid valve, spark plug and exhaust fan. As backup safety, in the event that the LPG is not turned off and the power is left on, the sparking plug ensures the LPG is ignited. When the power is turned off the solenoid valve closes, stopping the LPG flow.
35. Switch of the fume cupboard extraction.
36. Turn off the water.
37. Unplug thermocouples from the digital handheld thermometer and store it away safely.
38. Disconnect the water pipes from the condenser.
39. Open the condenser by unscrewing the bottom part of the condenser. Dispose the tar in the appropriate manner according to the local regulations and reassemble the condenser.
40. Clean the spillage tray and remove all the water if required.
41. Report any faults and issues to the Key Operator.

B.4 Drum Pyrolyser

B.4.1 Equipment Pictures

Figure B-5. Drum pyrolyser. Insert depicts installed venturi.

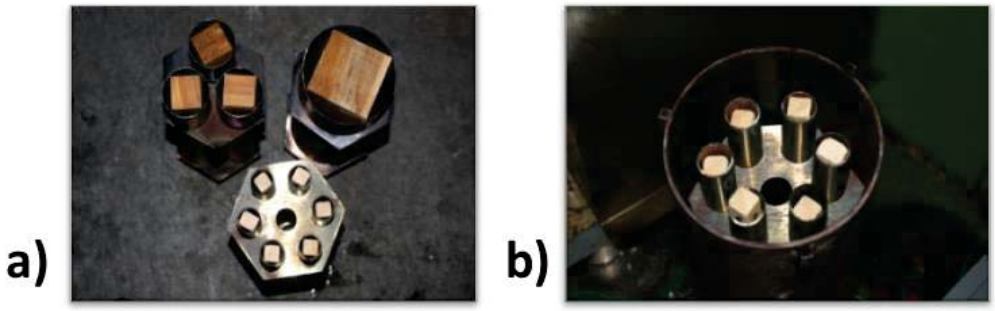

Figure B-6. Sample holder with samples for drum pyrolyser. a) Top view and b) sample holder for small samples with samples inside rotating drum. Pictures taken from Bashir (2012). The sample beams had a length of approximately 175 mm and a cross section of 15 x 15 mm, 32 x 32 mm, and 67 x 67 mm for the small, medium and large size respectively.

B.4.2 Modifications

The lab-scale pyrolyser was modified for this research:

- to cope with the required sample loads, 400 to 500 g, the motor for driving the drum was upgraded as well as the installed pressure relief valve;

- the gas burner was adjusted to achieve *HTT's* of 700 °C;
- installed were (a) a venturi to create a slightly negative pressure in the system to prevent pyrolysis gases from leaking into the workspace (insert Figure B-5), (b) a hood around the pressure relief valve to carry gases, released in the case of over-pressure, straight to the exhaust burner, and (c) a valve to regulate the LPG flow of the exhaust burner;
- the thermocouple for measuring the centre temperature was replaced;
- a faulty LPG mass flow controller repaired; and
- three sample holders built to accommodate the wood samples and prevent them from being damaged by the rotating movement of the drum, Figure B-6.

B.5 Extraparticle Secondary Char Formation

B.5.1 Differences between Experiments with and without a Lid

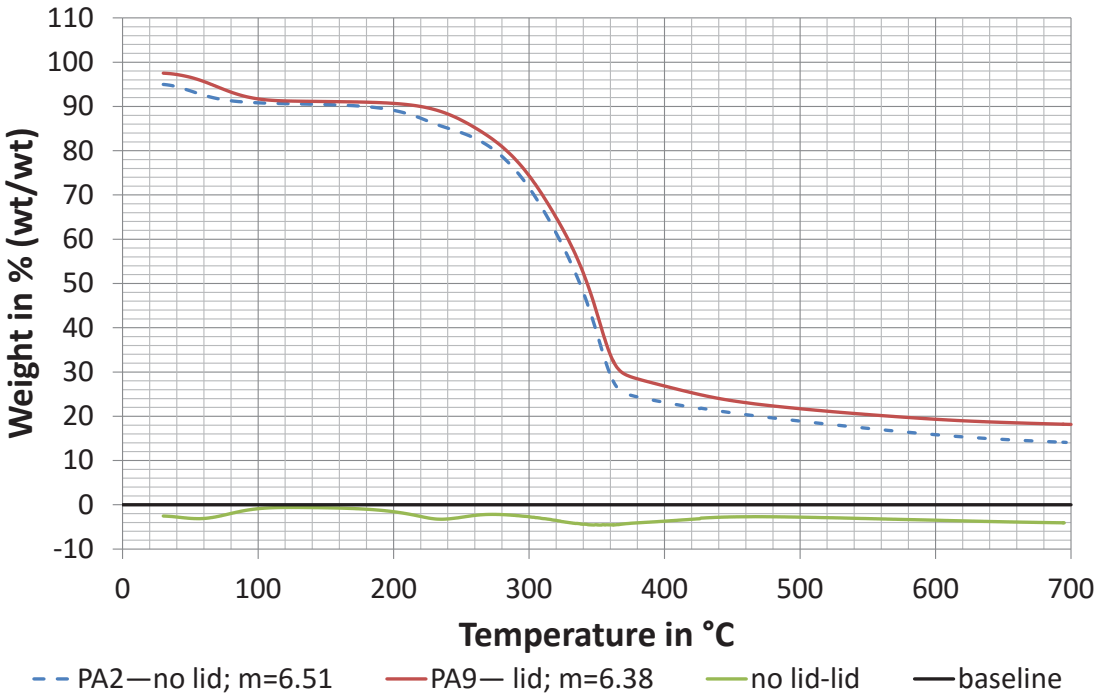

Figure B-7. Weight-loss curve of proximate analysis PA2 and PA9. The "no lid-lid curve" illustrates the difference between the two cases lid and no lid. Legend: Run number—lid or no lid; dry weight in mg. m = dry weight in mg determined for lid and no lid at 152 and 126 °C respectively.

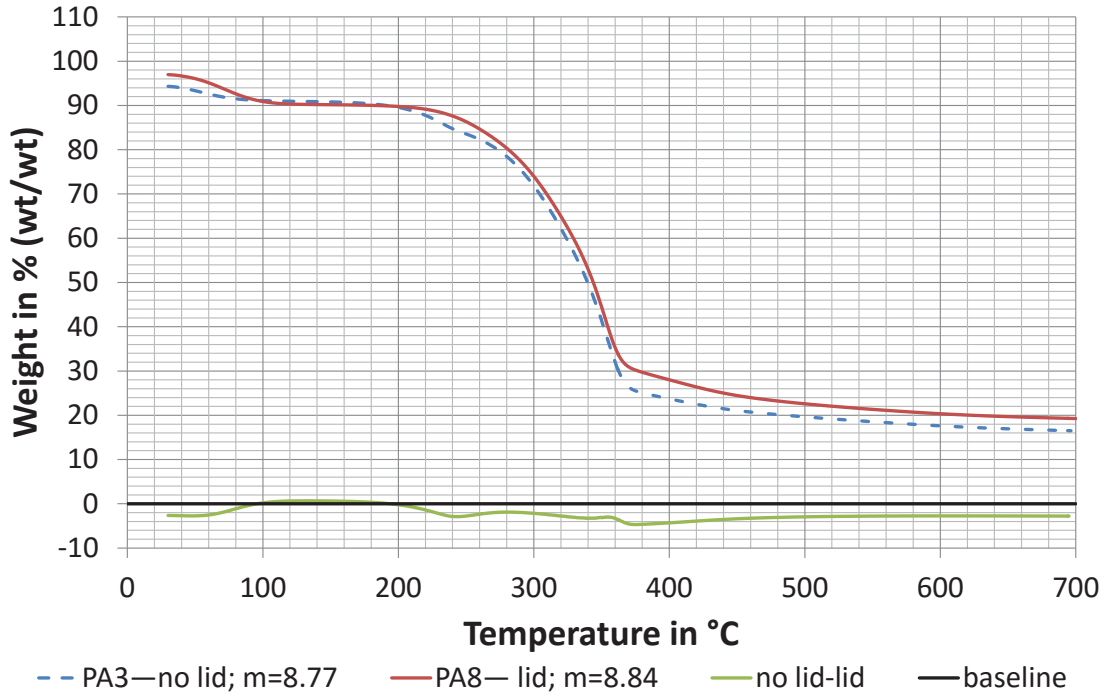

Figure B-8. Weight-loss curve of proximate analysis PA3 and PA8. The "no lid-lid curve" illustrates the difference between the two cases lid and no lid. Legend: Run number—lid or no lid; dry weight in mg. m = dry weight in mg determined for lid and no lid at 152 and 126 °C respectively.

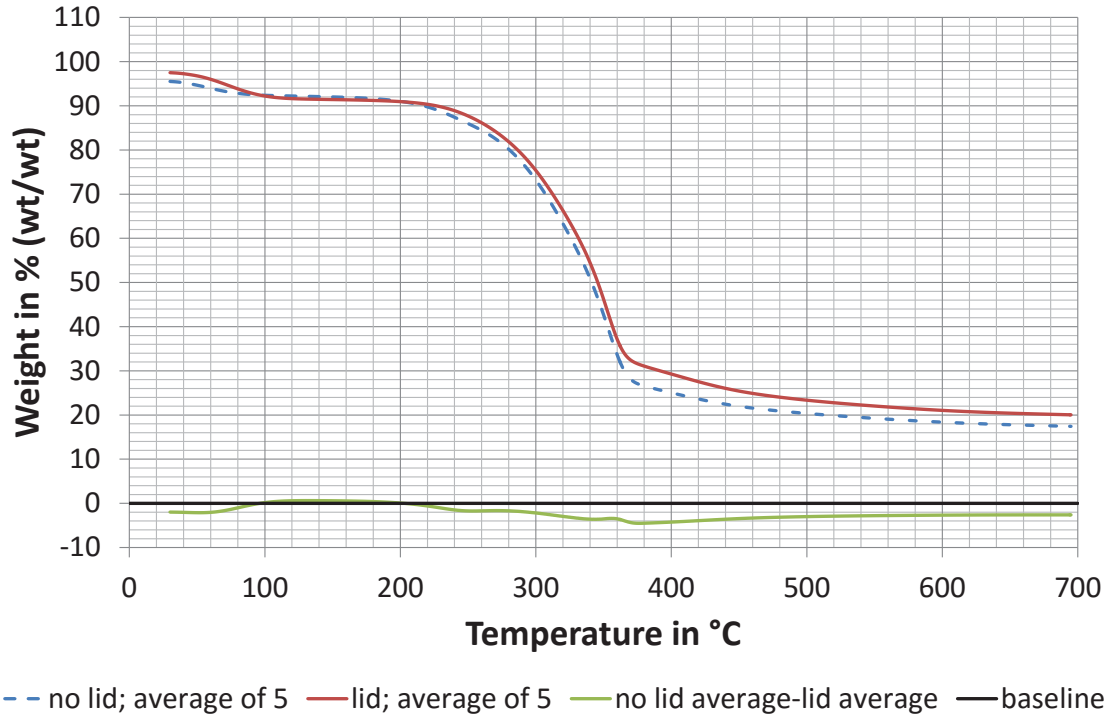

Figure B-9. Average weight-loss curve of additional pyrolysis experiments with and without a lid. The "no lid average-lid average" curve illustrates the difference between the two cases lid and no lid.

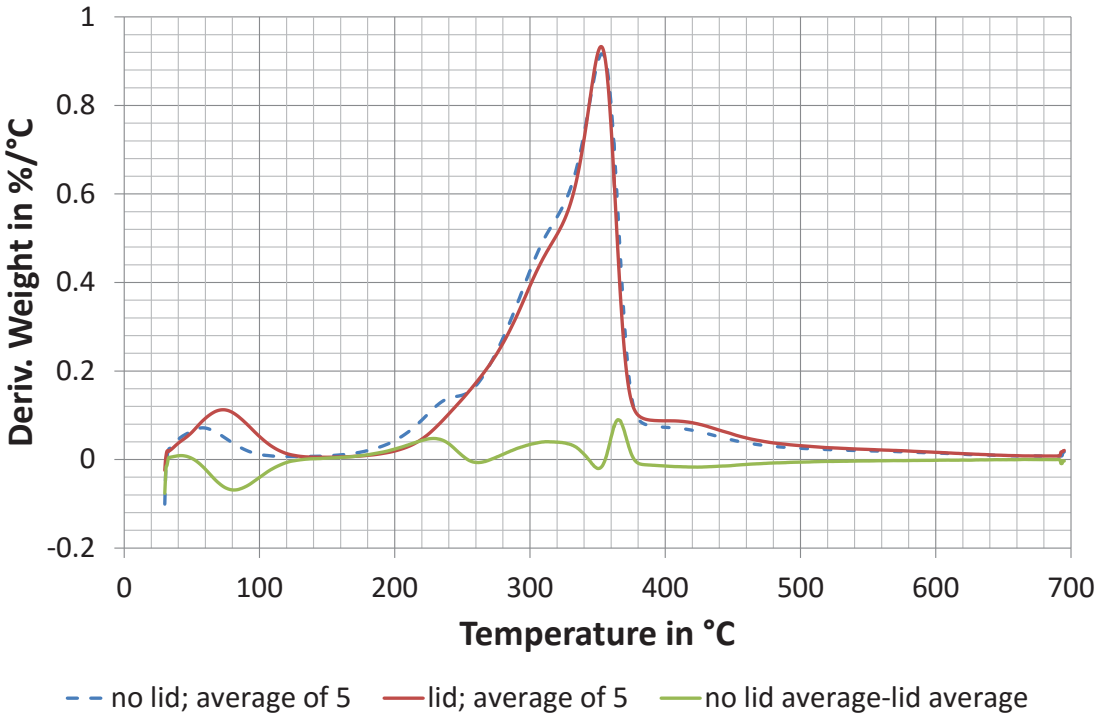

Figure B-10. Average derivative weight curve of additional pyrolysis experiments with and without a lid. The "no lid average-lid average" curve illustrates the difference between the two cases lid and no lid.

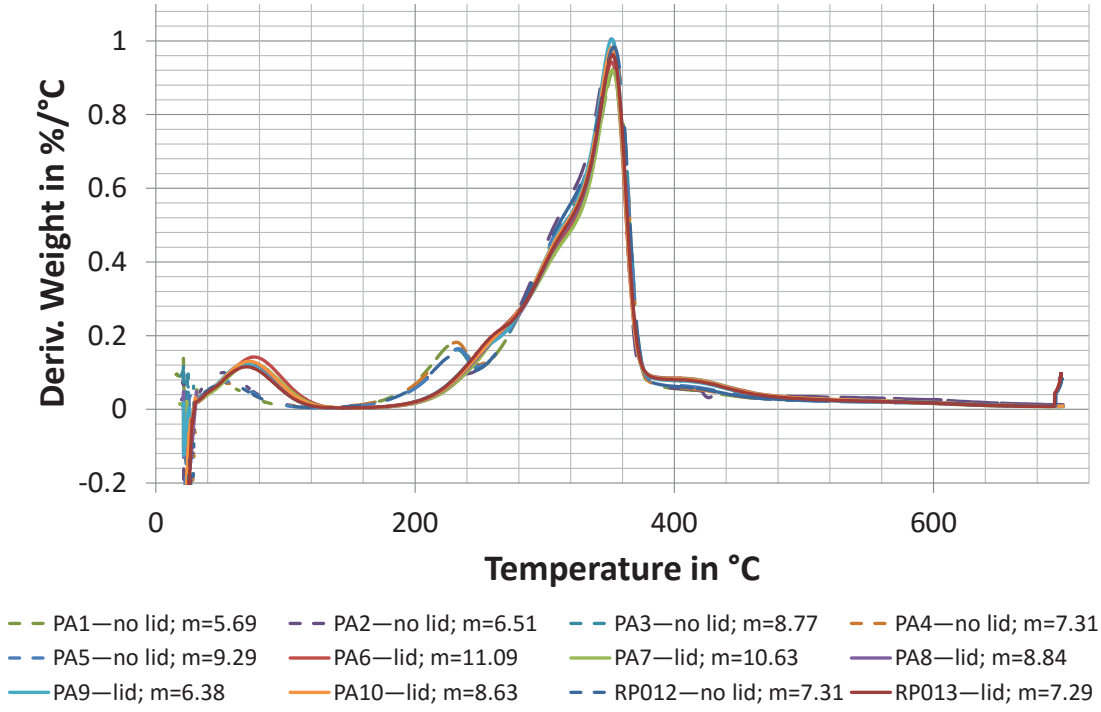

Figure B-11. Derivative weight curves of proximate analysis experiments with and without a lid inclusive an additional pyrolysis experiment to 700 °C for the cases lid and no lid. Un-averaged data of Figure 3-1. Legend: Run number—lid or no lid; dry weight in mg. m = dry weight in mg determined for lid and no lid at 152 and 126 °C respectively; PA = proximate analysis.

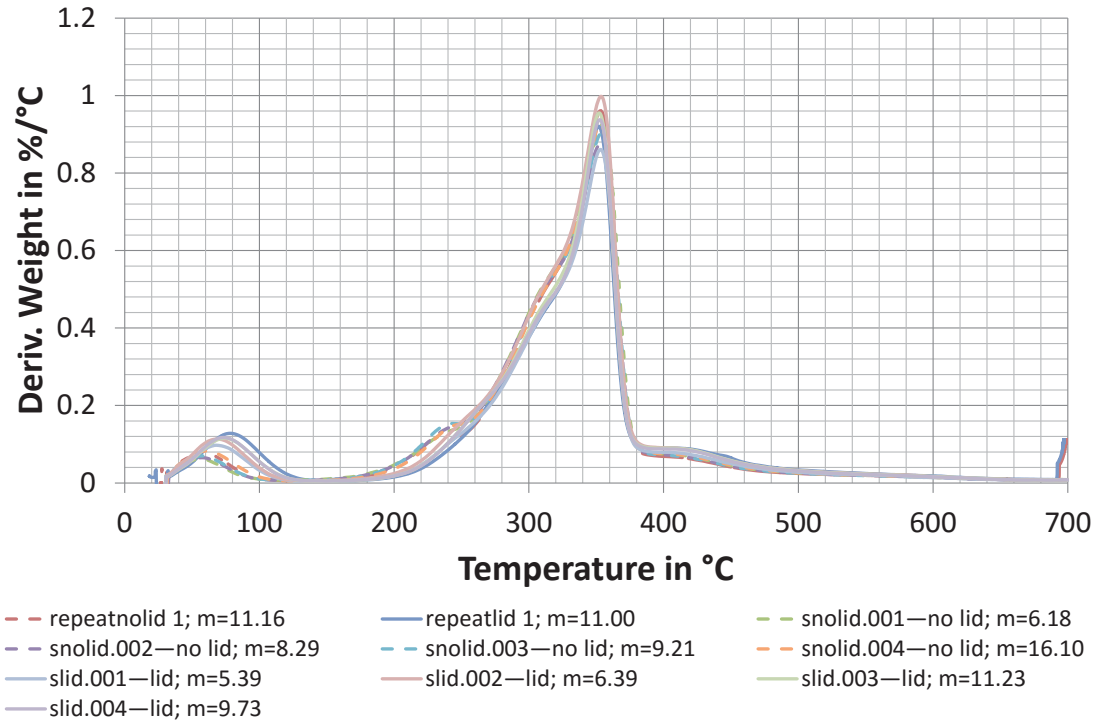

Figure B-12. Derivative weight curves of additional pyrolysis experiments with and without a lid. Un-averaged data of Figure B-10. Legend: Run number—lid or no lid; dry weight in mg. m = dry weight in mg determined for lid and no lid at 152 and 126 °C respectively.

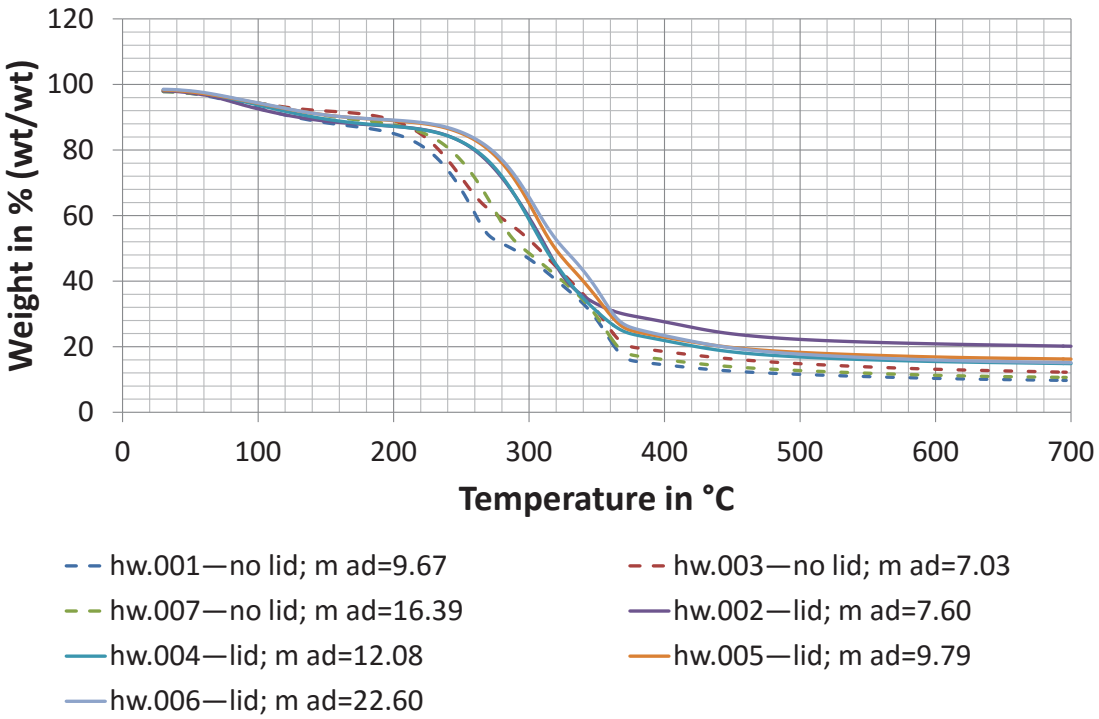

Figure B-13. Comparison of weight-loss curves of pyrolysis experiments with or without lid of heartwood strips containing resin. Legend: Run number—lid or no lid; air-dry weight in mg. m ad = air-dry weight in mg determined at 30 °C.

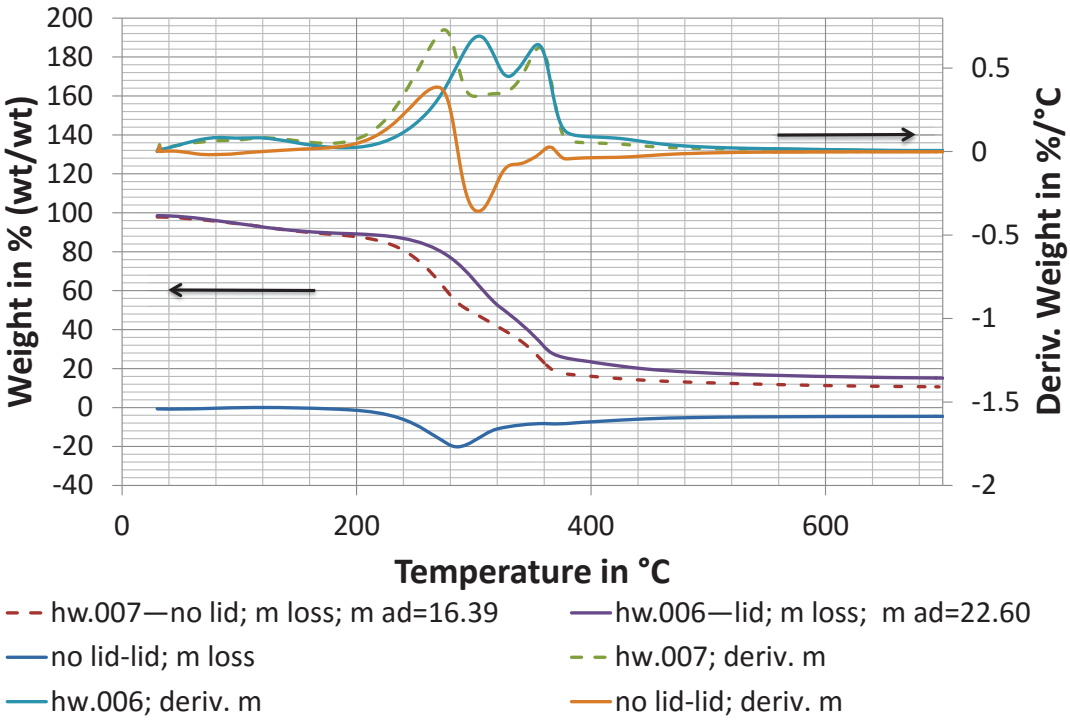

Figure B-14. Differences between weight-loss and derivative weight curves of heartwood strips containing resin during pyrolysis with and without a lid. The "no lid-lid curve" illustrates the difference between the two cases lid and no lid. Legend: Run number—lid or no lid; weight-loss or derivative weight curve; air-dry weight in mg. m ad = air-dry weight in mg determined at 30 °C; deriv. m = deriv. weight; m loss = weight-loss.

B.5.2 Relationship between Yield, Lid/No Lid and Initial Dry Sample Mass

Table B-3. Char yields at 695 °C and dry feedstock weight of pyrolysis experiments with and without a lid.

Sample	Char yield % (wt/wt)	Lid/no lid[a]	Dry sample weight mg
PA1	19.1273	0	5.6942
PA2	15.5805	0	6.5133
PA3	18.1679	0	8.7665
PA4	16.3878	0	7.3119
PA5	17.3977	0	9.2904
RP012	17.0618	0	7.3099
sawdustnolid.001	19.9660	0	11.158
snolid.001	16.7046	0	6.1772
snolid.002	19.6270	0	8.2877
snolid.003	18.9067	0	9.2146
snolid.004	19.3674	0	16.1014
PA6	22.5182	1	11.0875
PA7	24.2727	1	10.6290
PA8	21.4016	1	8.8357
PA9	19.9713	1	6.3775
PA10	20.0156	1	8.6329
RP013	21.1256	1	7.2890
sawdustlid.001	24.0868	1	11.0034
slid.001	27.3861	1	5.3926
slid.002	14.2526	1	6.3882
slid.003	21.2625	1	11.2313
slid.004	22.5625	1	9.7278

Note. The char yield is given on a dry basis. The dry sample weight was determined for lid and no lid experiments at 152 and 126 °C respectively.

[a]lid is 1 and no lid is 0.

B.5.3 Differences between Experiments with High and Low Initial Dry Sample Mass

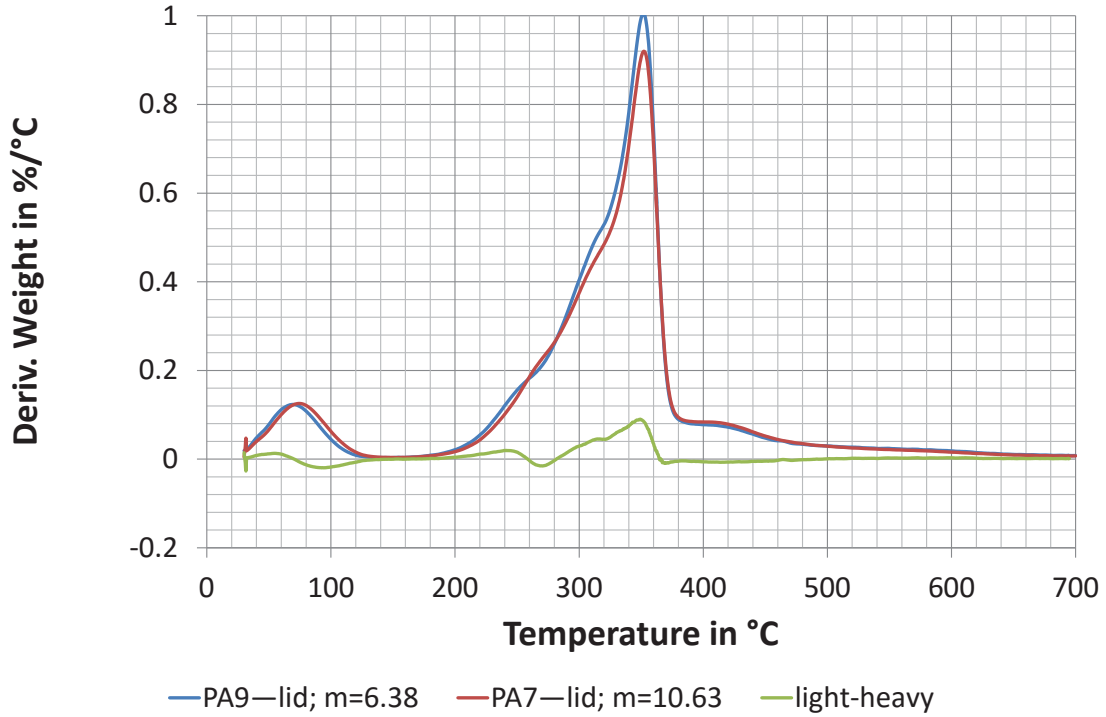

Figure B-15. Difference between derivative weight curves of pyrolysis experiments with a lid that have differing initial sample weights correlating to yield differences caused by the varying feedstock weight 1). The "light-heavy" curve illustrates the difference between the two pyrolysis runs with differing initial weights corresponding to the difference curve "no lid-lid" in Figure 3-1. Legend: Run number—lid or no lid; dry weight in mg. m = dry weight in mg determined at 152 °C.

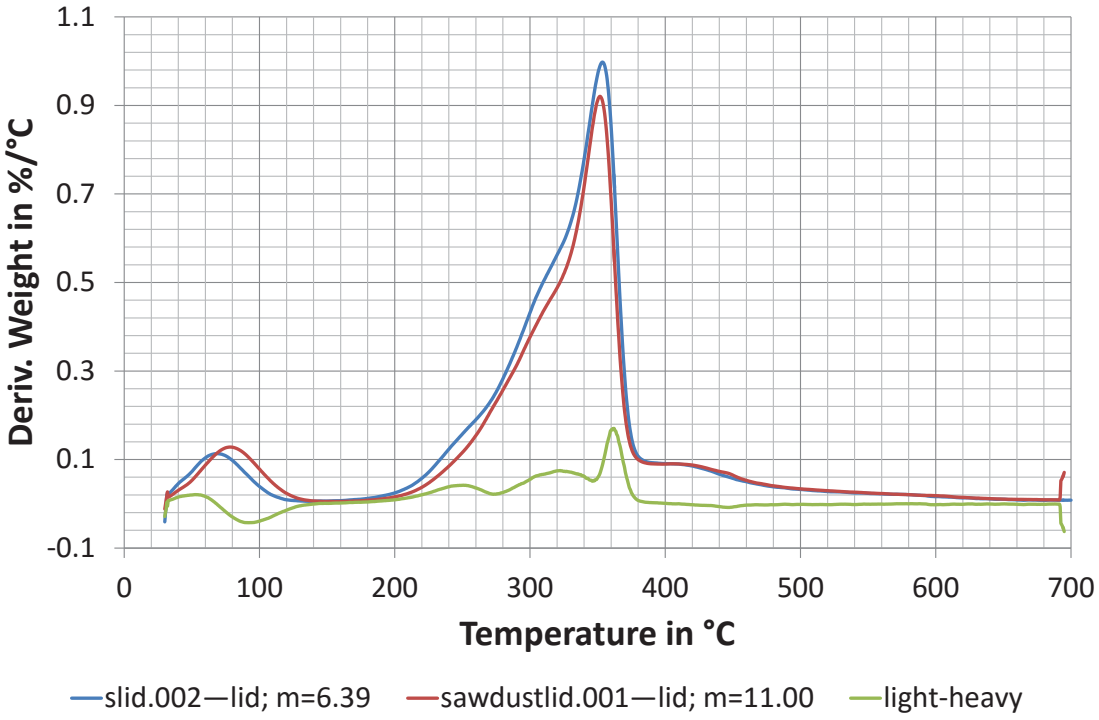

Figure B-16. Difference between derivative weight curves of pyrolysis experiments with a lid that have differing initial sample weights correlating to yield differences caused by the varying feedstock weight 2). The light-heavy curve illustrates the difference between the two pyrolysis runs with differing initial weights corresponding to the difference curve "no lid-lid" in Figure 3-1. Legend: Run number—lid or no lid; dry weight in mg. m = dry weight in mg determined at 152 °C.

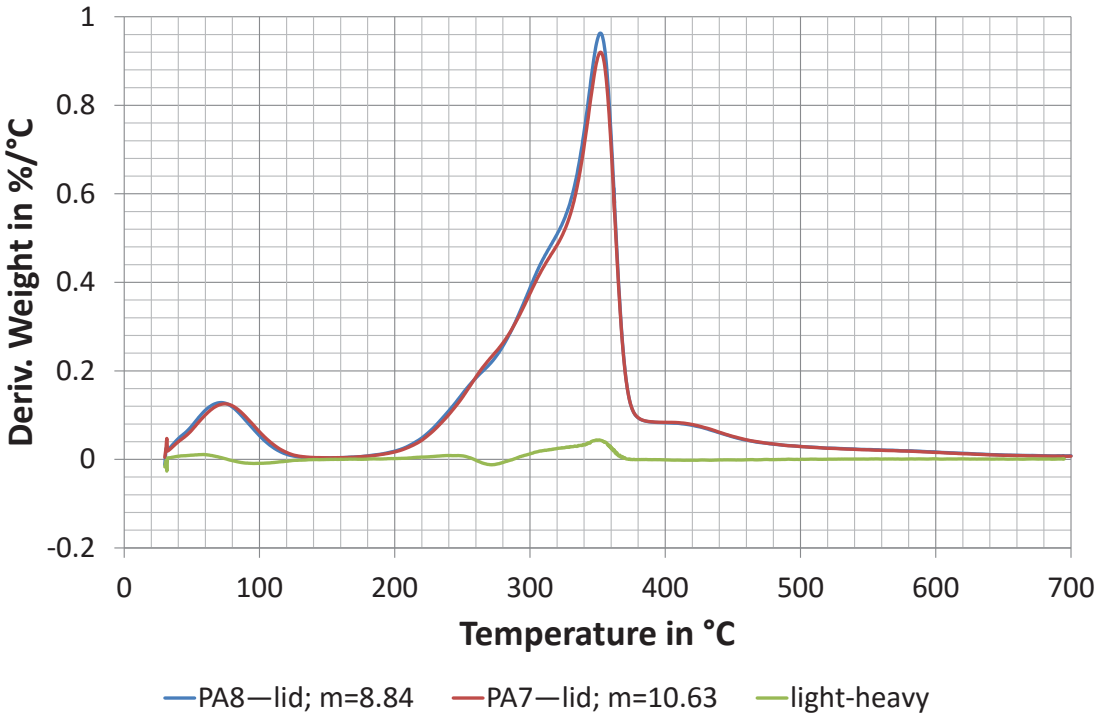

Figure B-17. Difference between derivative weight curves of pyrolysis experiments with a lid that have differing initial sample weights correlating to yield differences caused by the varying feedstock weight 3). The "light-heavy" curve illustrates the difference between the two pyrolysis runs with differing initial weights corresponding to the difference curve "no lid-lid" in Figure 3-1. Legend: Run number—lid or no lid; dry weight in mg. m = dry weight in mg determined at 152 °C.

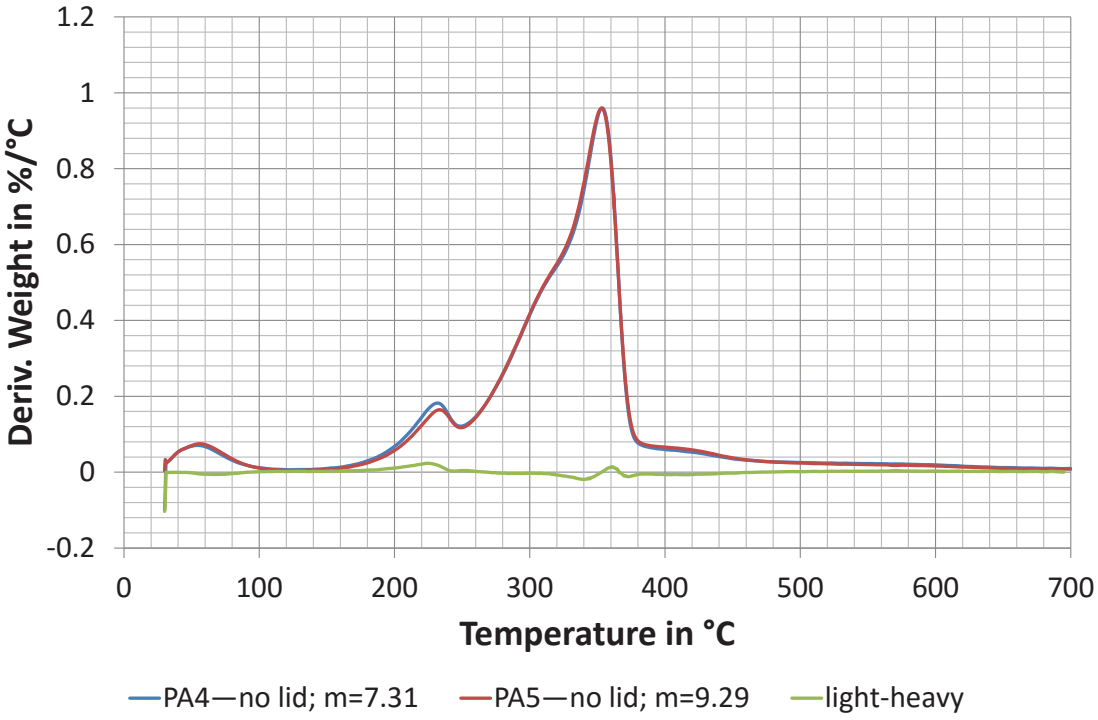

Figure B-18. Difference between derivative weight curves of pyrolysis experiments without a lid that have differing initial sample weights correlating to yield differences caused by the varying feedstock weight 1). The "light-heavy" curve illustrates the difference between the two pyrolysis runs with differing initial weights corresponding to the difference curve "no lid-lid" in Figure 3-1. Legend: Run number—lid or no lid; dry weight in mg. m = dry weight in mg determined at 126 °C.

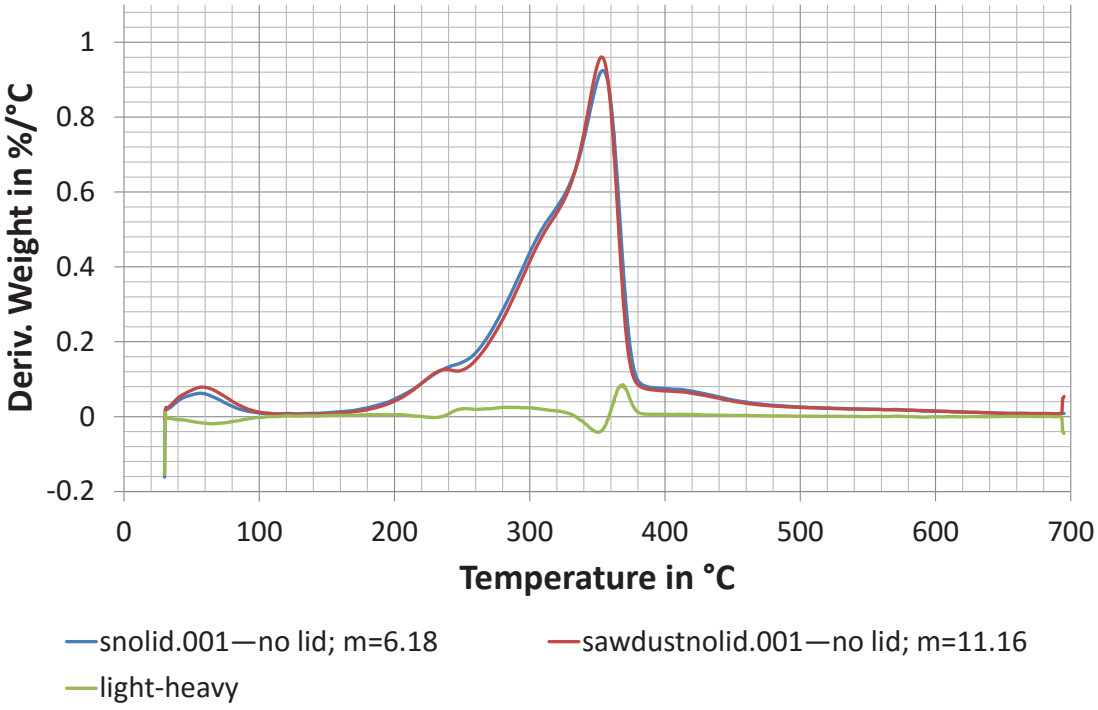

Figure B-19. Difference between derivative weight curves of pyrolysis experiments without a lid that have differing initial sample weights correlating to yield differences caused by the varying feedstock weight 2). The "light-heavy" curve illustrates the difference between the two pyrolysis runs with differing initial weights corresponding to the difference curve "no lid-lid" in Figure 3-1. Legend: Run number—lid or no lid; dry weight in mg. m = dry weight in mg determined at 126 °C.

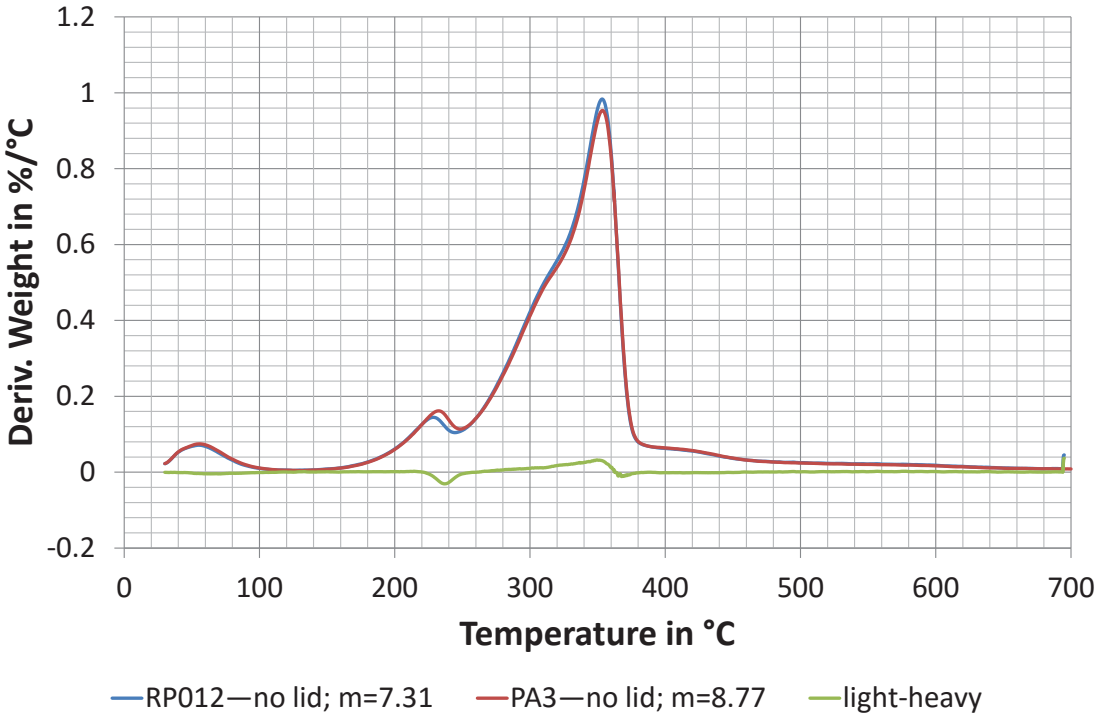

Figure B-20. Difference between derivative weight curves of pyrolysis experiments without a lid that have differing initial sample weights correlating to yield differences caused by the varying feedstock weight 3). The "light-heavy" curve illustrates the difference between the two pyrolysis runs with differing initial weights corresponding to the difference curve "no lid-lid" in Figure 3-1. Legend: Run number—lid or no lid; dry weight in mg. m = dry weight in mg determined at 126 °C.

B.6 Intraparticle Secondary Char Formation

B.6.1 Effect of Sample Size

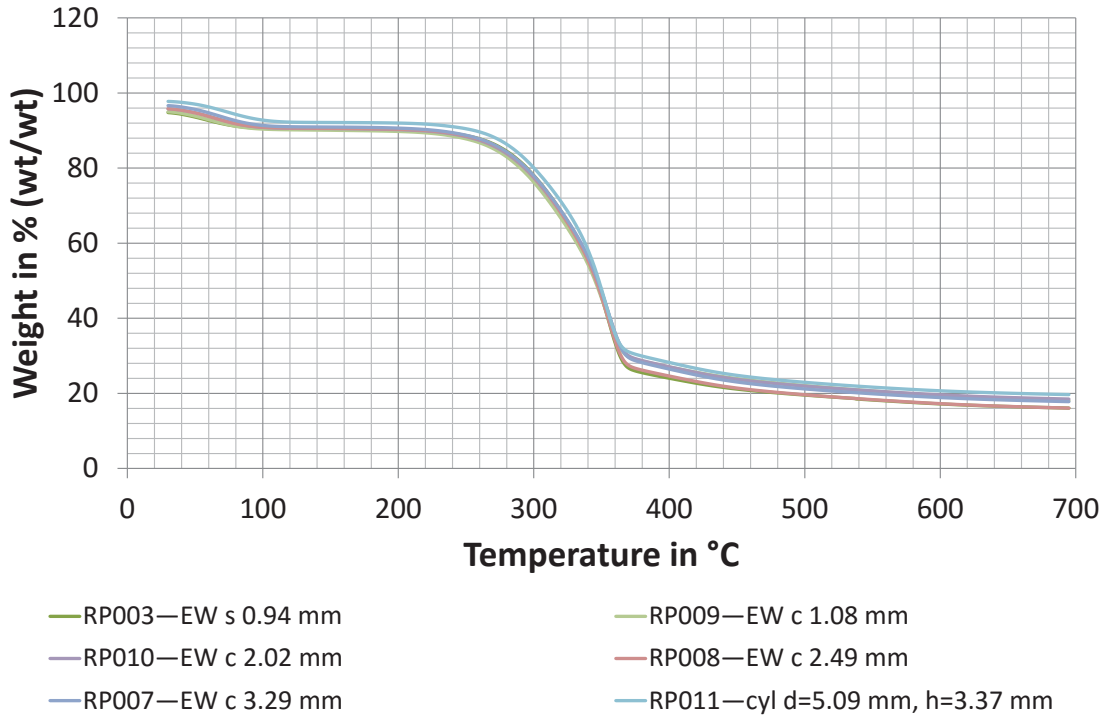

Figure B-21. Weight-loss curves of cuboid samples in Figure 3-19 compared to the weight-loss curve of a thick slice and a small cylindrical sample. Legend: Run number—wood type_shape_sample geometry. c = cuboid; cyl = cylinder; d = diameter in mm; EW = earlywood; h = height in mm; s = slice.

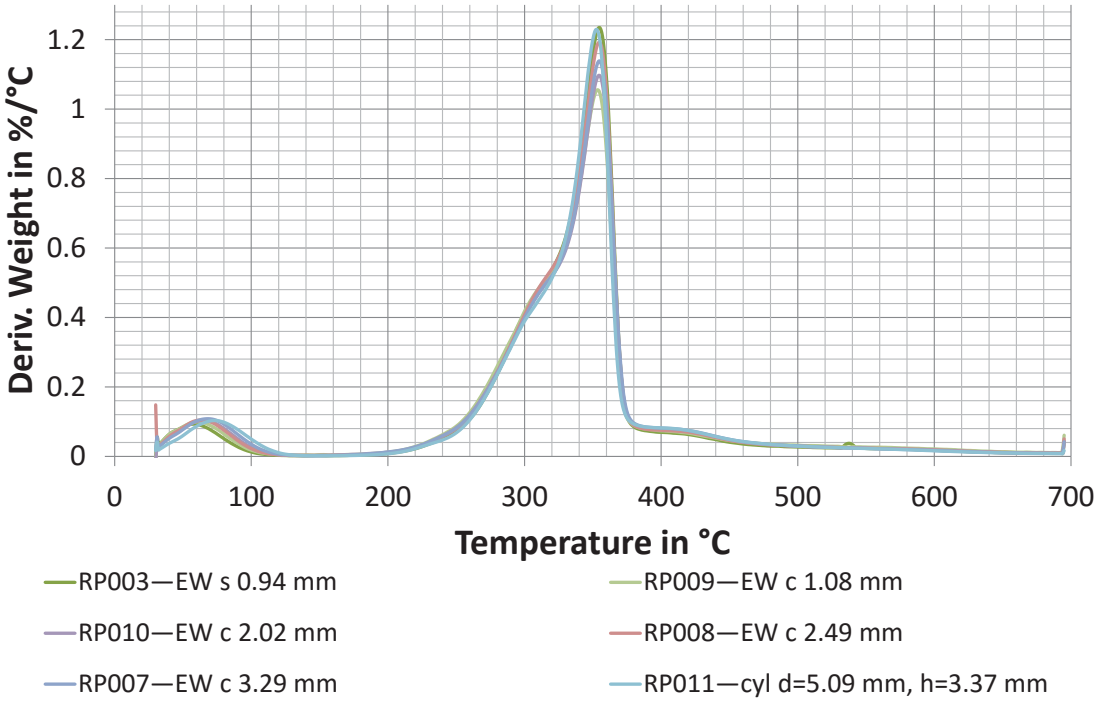

Figure B-22. Derivative weight curves of cuboid samples in Figure 3-19 compared to the derivative weight curve of a thick slice and a small cylindrical sample. Legend: Run number—wood type_shape_sample geometry. c = cuboid; cyl = cylinder; d = diameter in mm; EW = earlywood; h = height in mm; s = slice.

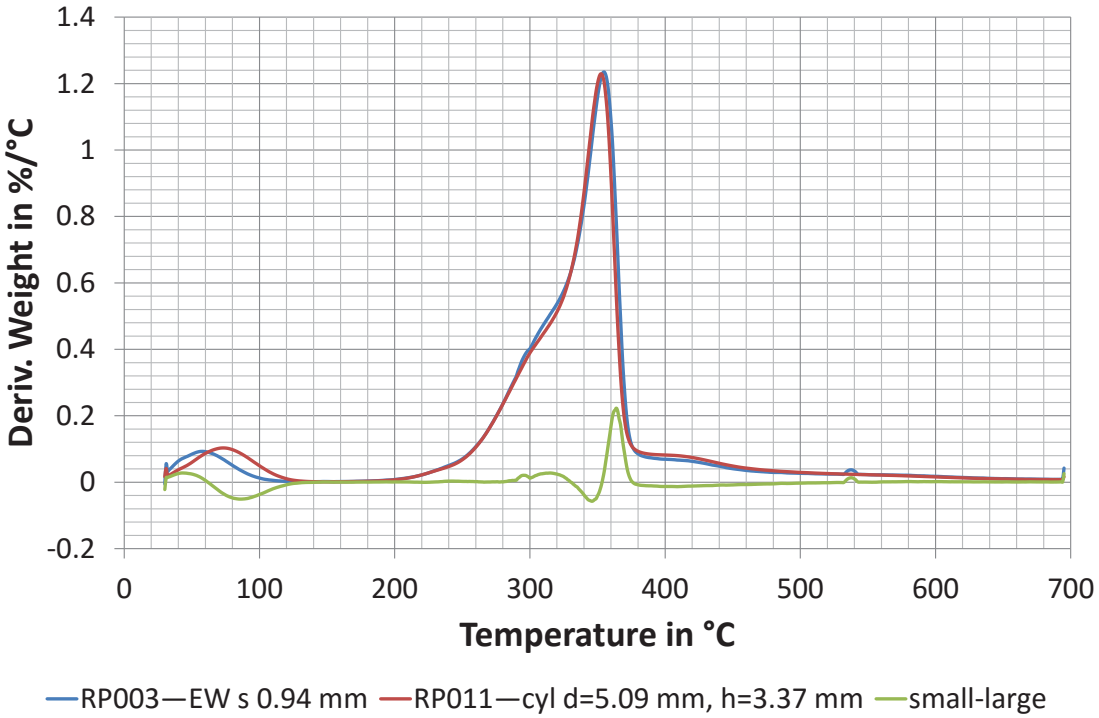

Figure B-23. Difference between derivative weight curves of a sample with small sample size compared to a sample with larger size showing a corresponding yield increase with size 1). The "small-large" curve illustrates the difference between the two pyrolysis runs with differing initial sample size corresponding to the difference curve "no lid-lid" in Figure 3-1. Legend: Run number—sample description. cyl = cylinder; d = diameter in mm; h = height in mm; EW = earlywood; s = slice.

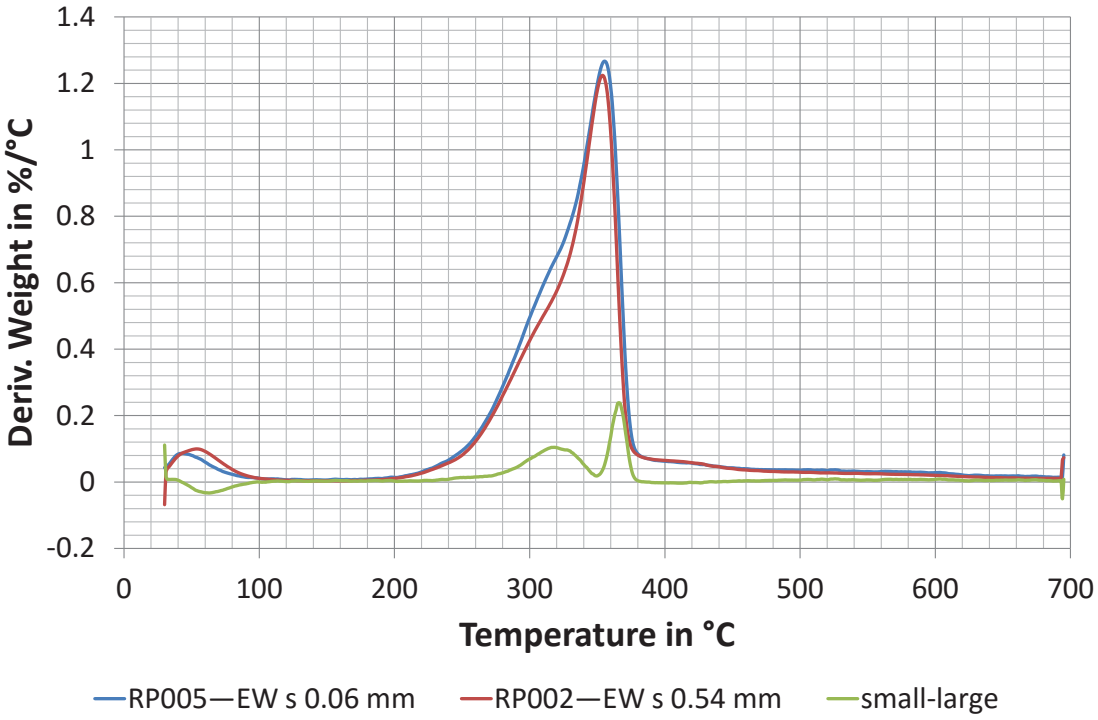

Figure B-24. Difference between derivative weight curves of a sample with small sample size compared to a sample with larger size showing a corresponding yield increase with size 2). The "small-large" curve illustrates the difference between the two pyrolysis runs with differing initial sample size corresponding to the difference curve "no lid-lid" in Figure 3-1. Legend: Run number—wood type_shape_thickness in mm. EW = earlywood; s = slice.

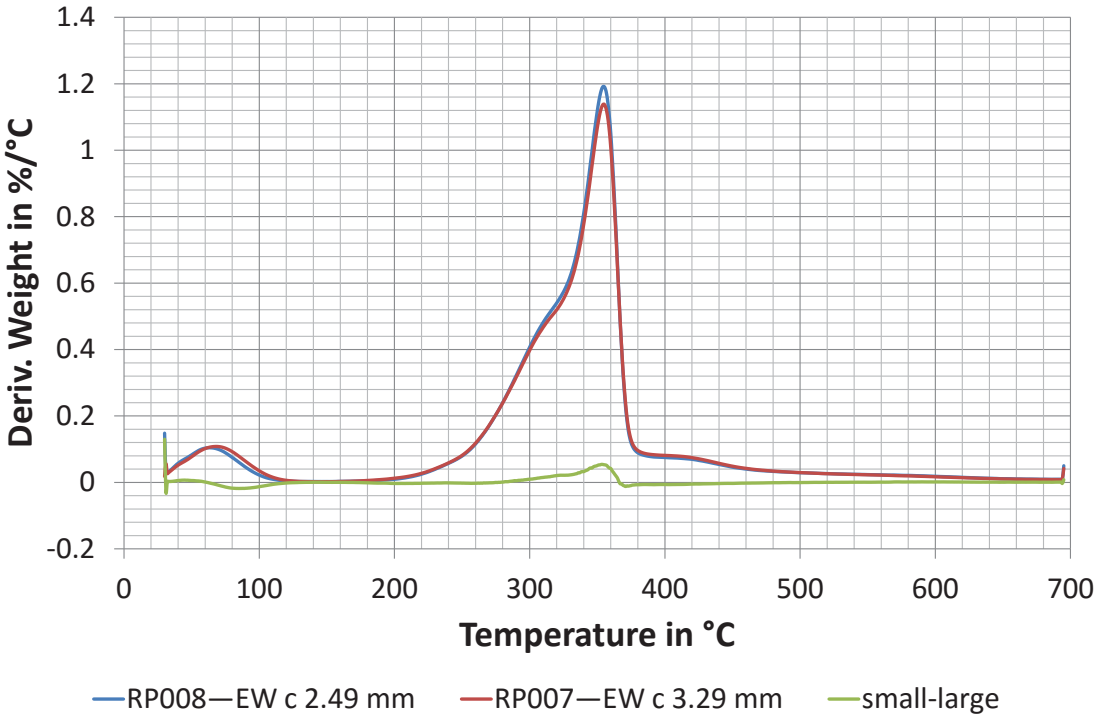

Figure B-25. Difference between derivative weight curves of a sample with small sample size compared to a sample with larger size showing a corresponding yield increase with size 3). The "small-large" curve illustrates the difference between the two pyrolysis runs with differing initial sample size corresponding to the difference curve "no lid-lid" in Figure 3-1. Legend: Run number—wood type_shape_thickness in mm. c = cuboid; EW = earlywood.

B.6.2 Thermocouple Experiments

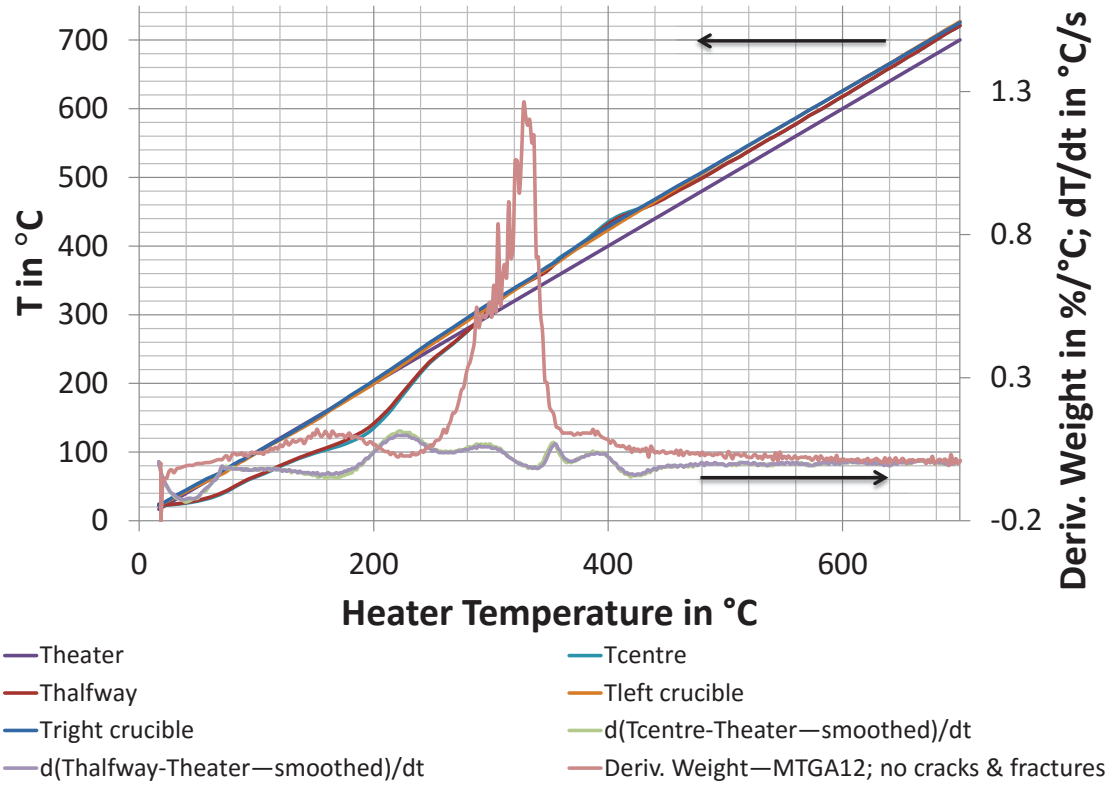

Figure B-26. Results of thermocouple run 11 employing a cylinder with a diameter of 20 mm and a height of 60 mm. The sample showed no cracks and fractures at the end of the run. Cracking means the samples are still in one piece at the end of the run and fracturing means the sample broke into separate pieces. The derivative weight curve of experiment MTGA12 is included to illustrate the relationship between temperature and weight-loss events. "Tleft crucible" and "Tright crucible" are thermocouples T_1 and T_2 in Figure 3-5 respectively.

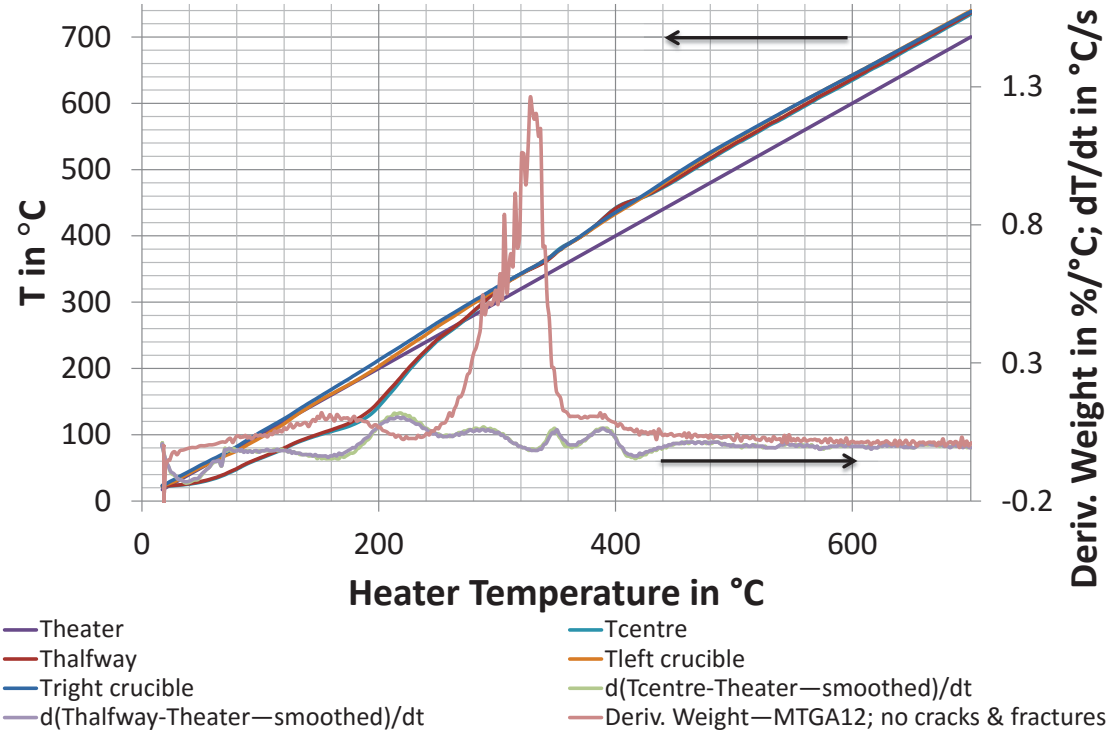

Figure B-27. Results of thermocouple run 12 employing a cylinder with a diameter of 20 mm and a height of 60 mm. The sample showed no cracks and fractures at the end of the run. Cracking means the samples are still in one piece at the end of the run and fracturing means the sample broke into separate pieces. The derivative weight curve of experiment MTGA12 is included to illustrate the relationship between temperature and weight-loss events. "Tleft crucible" and "Tright crucible" are thermocouples T_1 and T_2 in Figure 3-5 respectively.

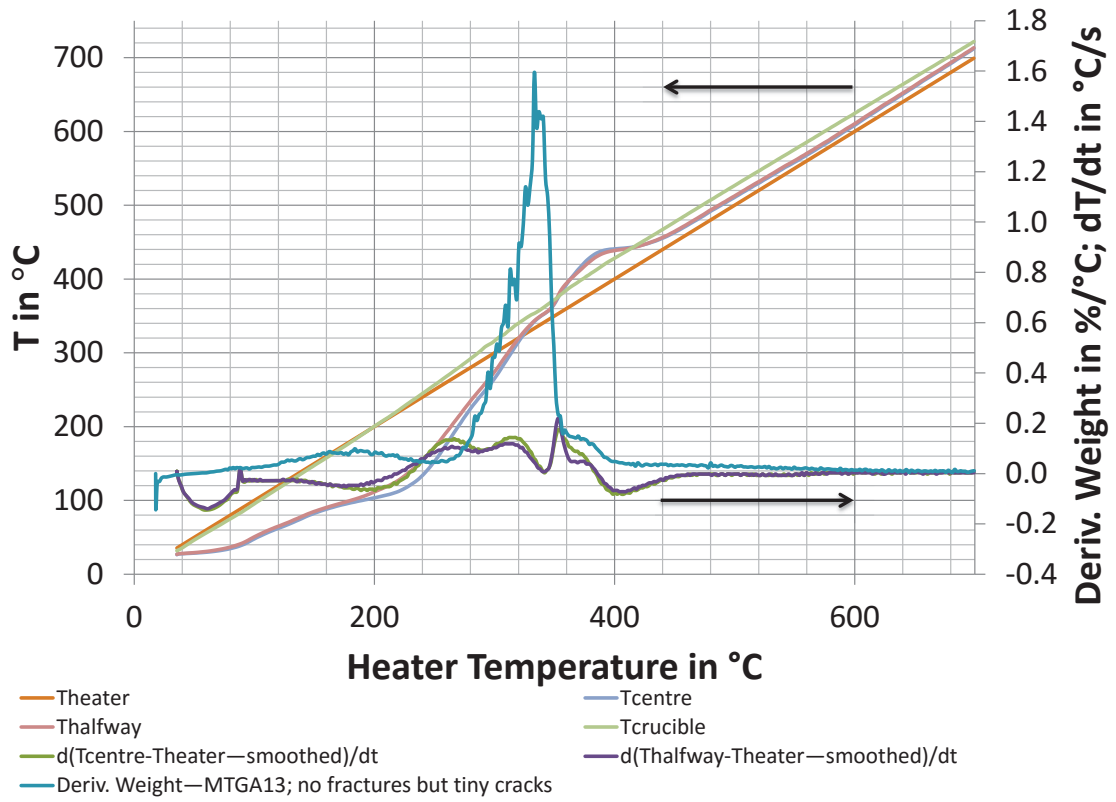

Figure B-28. Results of thermocouple run 5 employing a cylinder with a diameter of 30 mm and a height of 60 mm. The sample showed no cracks and fractures at the end of the run. Cracking means the sample is still in one piece at the end of the run and fracturing means the sample broke into separate pieces. The derivative weight curve of experiment MTGA13 is included to illustrate the relationship between temperature and weight-loss events.

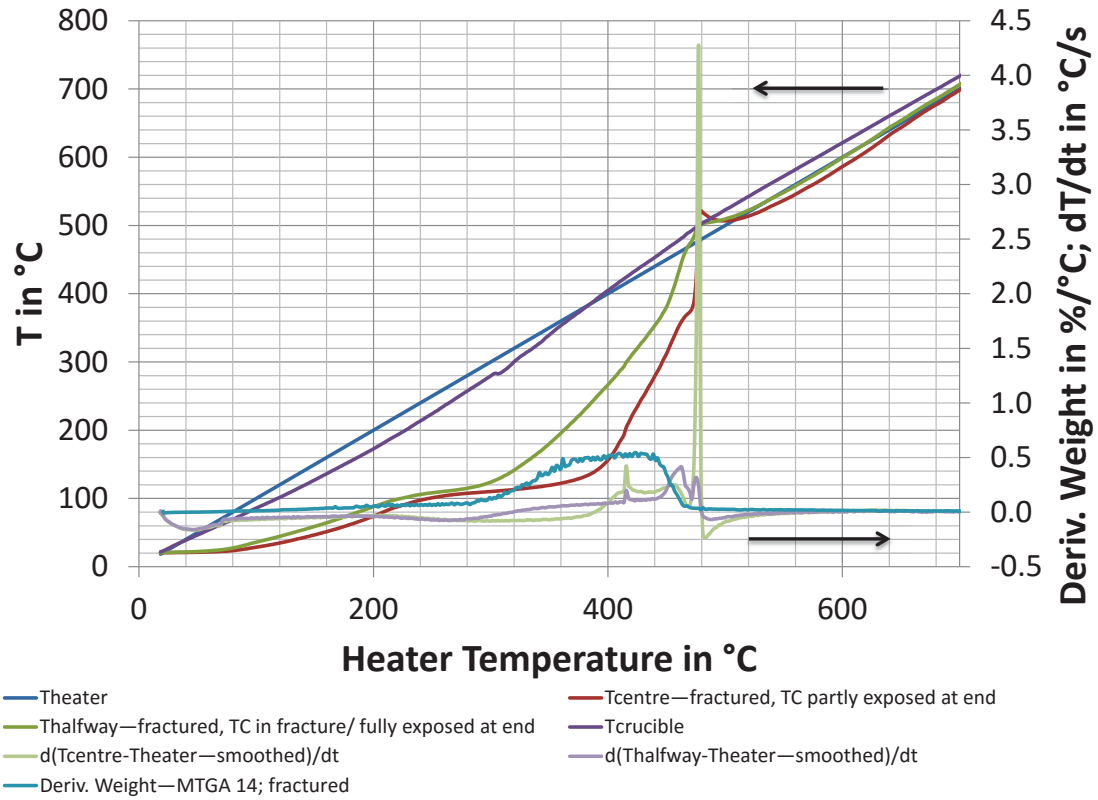

Figure B-29. Results of thermocouple run 2 employing a cylinder with a diameter of 74 mm and a height of 60 mm. The sample had cracks and fractured. Cracking means the sample is still in one piece at the end of the run and fracturing means the sample broke into separate pieces. The derivative weight curve of experiment MTGA14 is included to illustrate the relationship between temperature and weight-loss events.

B.6.3 Macro-TGA Graphs

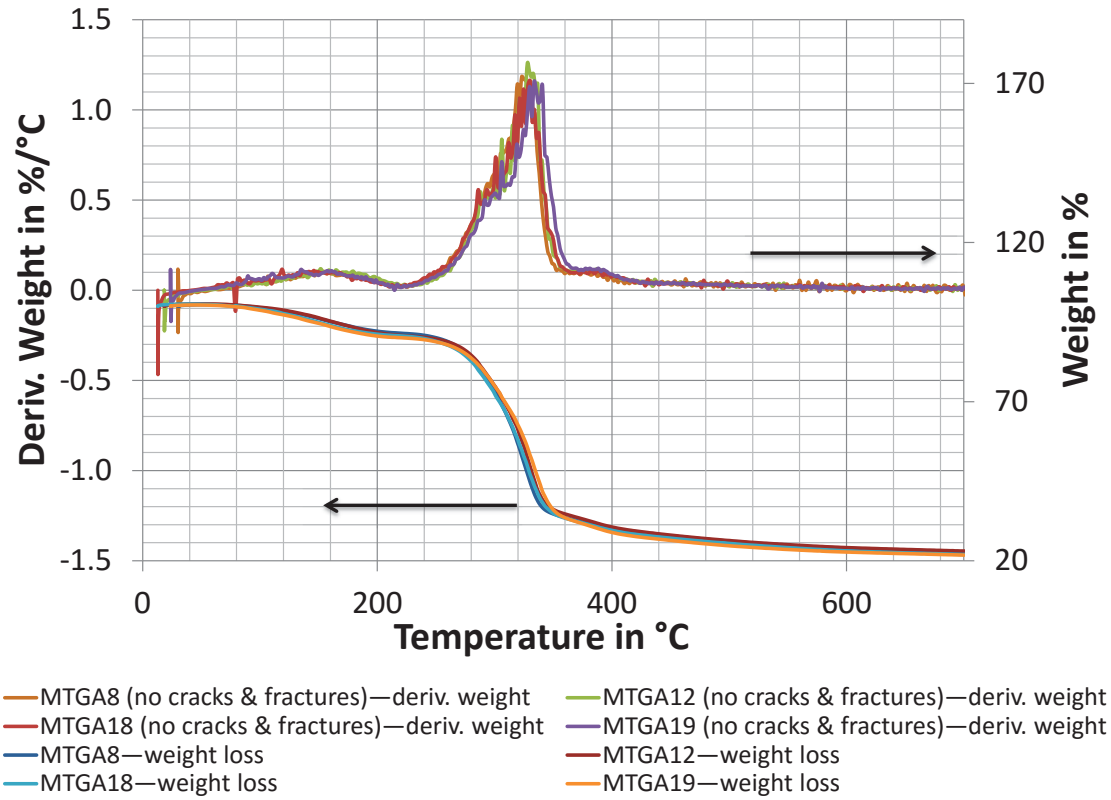

Figure B-30. Results of Macro-TGA of cylinders with a diameter of 20 mm and a height of 60 mm. Cracking means the sample is still in one piece at the end of the run and fracturing means the sample broke into separate pieces. deriv. = derivative.

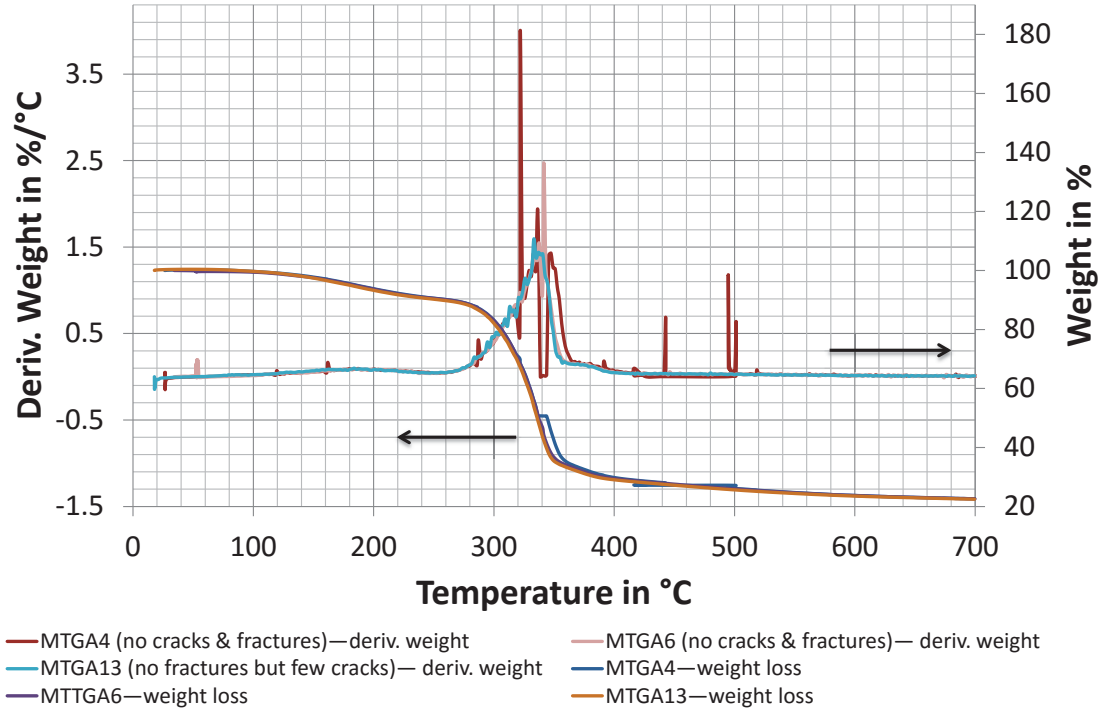

Figure B-31. Results of Macro-TGA of cylinders with a diameter of 30 mm and a height of 60 mm. Cracking means the sample is still in one piece at the end of the run and fracturing means the sample broke into separate pieces. The large noise in MTGA4 is due to a balance settings error in this run but is included here as it still fits the trend. deriv. = derivative.

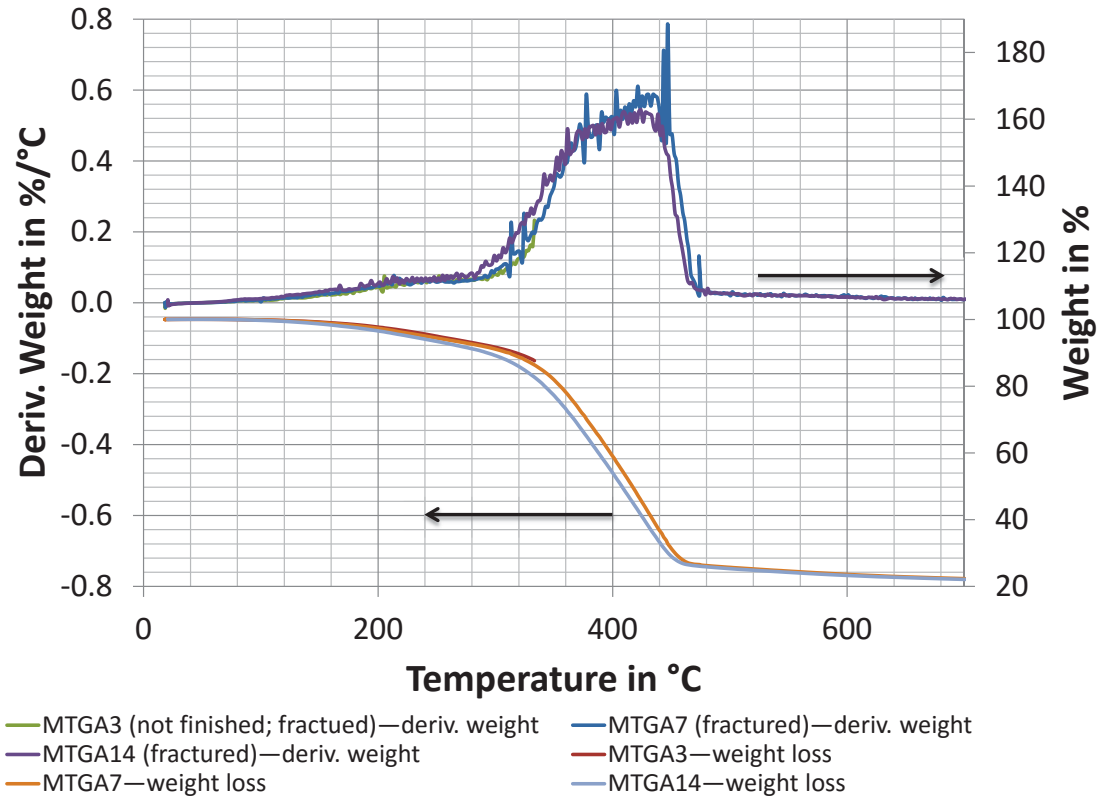

Figure B-32. Results of Macro-TGA of cylinders with a diameter of 74 mm and a height of 60 mm. Fractured means the sample broke into separate pieces. deriv. = derivative.

B.6.4 Comparison between Pyrolysis of Slices and Sawdust

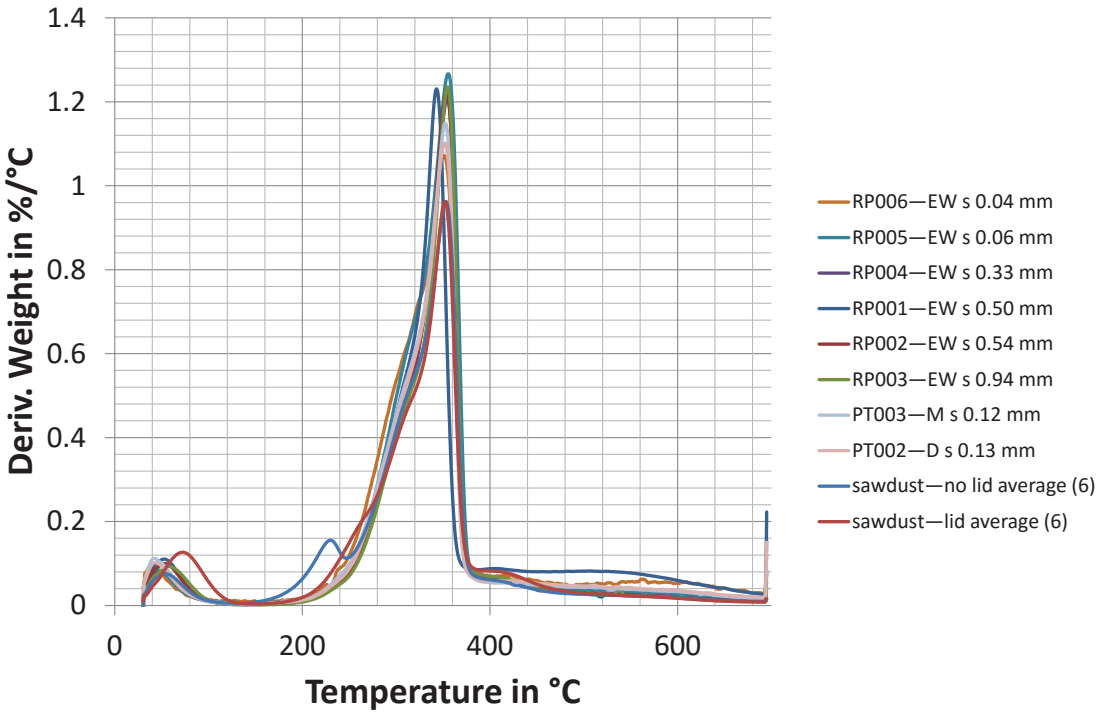

Figure B-33. Comparison of derivative weight curves of thin slices and sawdust that have been pyrolysed in the laboratory TGA. Legend: Run number—wood type_shape_sample geometry. EW = earlywood; s = slice.

B.7 Biomass Components and their Behaviour during Primary and Secondary Pyrolysis Reactions

B.7.1 Matlab Code

The Matlab code can be found on the provided CD in the location chapter 3/data/curve fitting. The file " kineticsnumintegr2" contains the Matlab code for the fitting procedure, the files "importDataFile1nolid_2.m" and "importDataFile1lid_2.m" are the files for importing the raw data, and the files "alpha_num2.m" and "arrhenius.m" contain the functions for calculating α and $\frac{d\alpha}{dt}$ respectively. The original data is provided in the excel file: "kinetic analysis.xlsx" in the same folder.

B.7.2 Curve-fitting

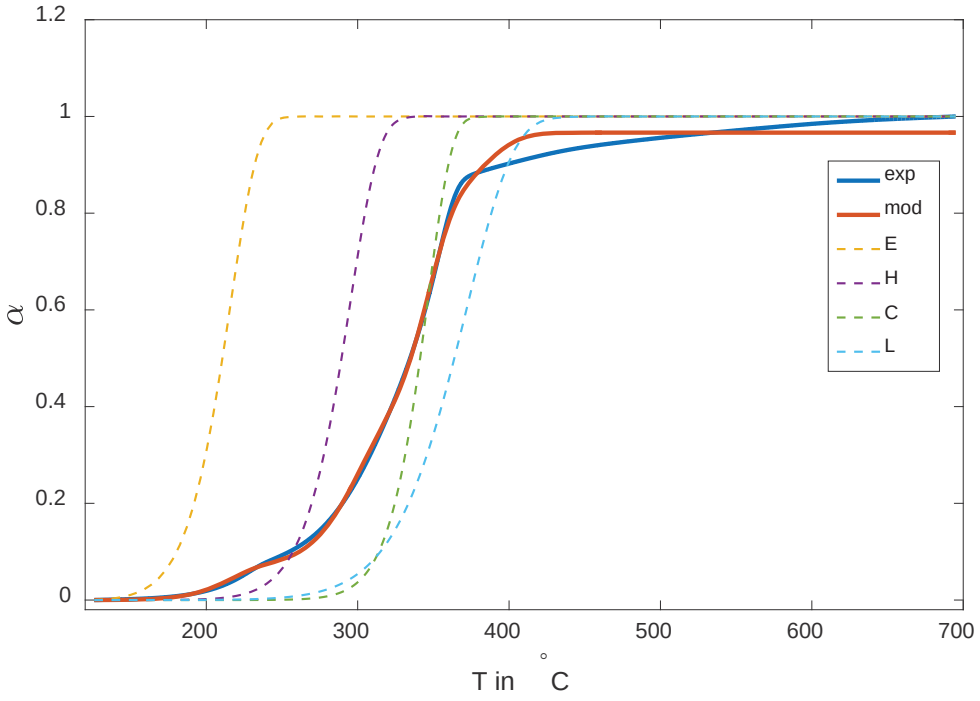

Figure B-34. Conversion curves of the experimental and modelled data of run RP012 representing pyrolysis experiments without a lid. The data has been fitted applying the starting values of Branca, Albano, and Di Blasi (2005) for the components hemicellulose, cellulose and lignin, and the values of Grønli et al. (2002) for the extractives fraction. The thinner dashed lines represent the conversion curves of the four biomass constituents extractives, hemicellulose, cellulose and lignin. exp = experimental data; E = extractives; C = cellulose; H = hemicellulose; L = lignin; mod = modelled data; T = temperature; α = degree of conversion.

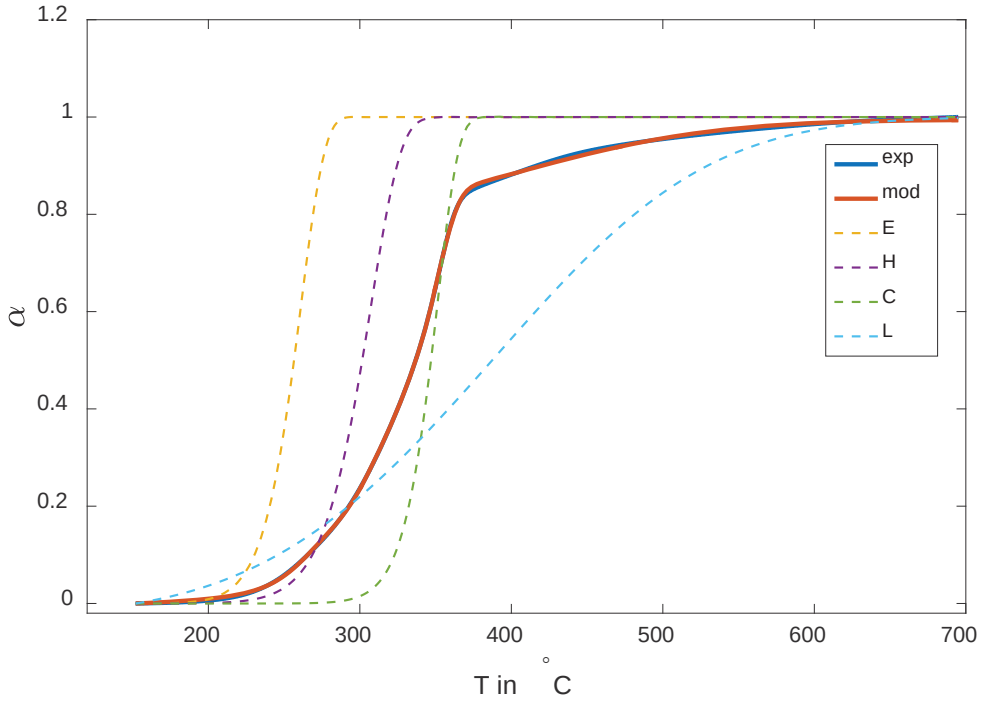

Figure B-35. Conversion curves of the experimental and modelled data of run RP013 representing pyrolysis experiments with a lid. The data has been fitted applying the starting values of Branca, Albano, and Di Blasi (2005) for the components hemicellulose, cellulose and lignin, and the values of Grønli et al. (2002) for the extractives fraction. The thinner dashed lines represent the conversion curves of the four biomass constituents extractives, hemicellulose, cellulose and lignin. exp = experimental data; E = extractives; C = cellulose; H = hemicellulose; L = lignin; mod = modelled data; T = temperature; α = degree of conversion.

Table B-4. Fitted parameters, char yield of the biomass constituents and char composition of run RP012 representing pyrolysis without a lid in Figure B-34.

Components	**A_i**	**E_i**	**x_i**	**Char yield**	**Char composition**	**Tstart**	**Tend**
	1/min	**kJ/mol**		**% (wt/wt)**	**%**	**°C**	**°C**
Extractives	5.43E+10	105.77	0.07	0.11	0.03	149.33	225.14
Hemicellulose	1.04E+12	137.00	0.23	19.77	23.58	221.94	322.22
Cellulose	1.45E+16	197.47	0.40	13.84	26.99	283.13	336.53
Lignin	1.39E+8	110.31	0.27	30.60	49.40	263.35	415.21

Note. The parameters were fitted in the temperature range 126 to 695 °C to capture the actual pyrolysis step without the removal of moisture. Tstart and Tend are the start and end temperature of the decomposition range of component *i*, which have been determined at $\alpha_i = 0.01$ and $\alpha_i = 0.98$ respectively. A_i = pre-exponential factor in Arrhenius equation for component *i*; E_i = exponential factor in Arrhenius equation for component *i*; x_i = fraction of component *i* that constitutes the overall weight-loss.

Table B-5. Fitted parameters, char yield of the biomass constituents and char composition of run RP013 representing pyrolysis with a lid in Figure B-35.

Components	**A_i**	**E_i**	**x_i**	**Char yield**	**Char composition**	**Tstart**	**Tend**
	1/min	**kJ/mol**		**% (wt/wt)**	**%**	**°C**	**°C**
Extractives	2.76E+14	152.60	0.06	9.58	2.49	201.44	282.51
Hemicellulose	8.62E+11	139.21	0.23	21.79	23.90	232.37	335.28
Cellulose	7.85E+18	231.07	0.45	8.14	14.60	295.45	385.06
Lignin	3.94	25.89	0.24	39.74	59.00	168.845	613.06

Note. The parameters were fitted in the temperature range 152 to 695 °C to capture the actual pyrolysis step without the removal of moisture. Tstart and Tend are the start and end temperature of the decomposition range of component *i*, which have been determined at $\alpha_i = 0.01$ and $\alpha_i = 0.98$ respectively. A_i = pre-exponential factor in Arrhenius equation for component *i*; E_i = exponential factor in Arrhenius equation for component *i*; x_i = fraction of component *i* that constitutes the overall weight-loss.

B.8 Torrefaction and Its Impact on Primary Char Formation

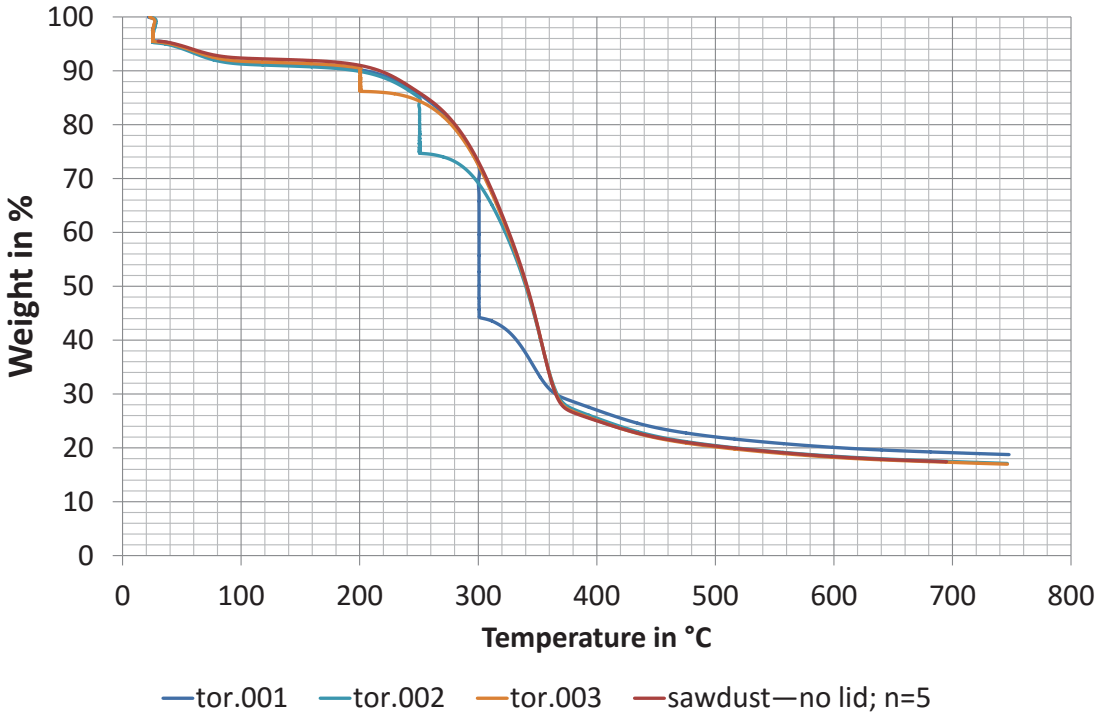

Figure B-36. Weight-loss of torrefaction experiments compared to pyrolysis without a torrefaction step. The graph "sawdust—no lid; n=5" represents the average curve without lid in Figure B-9.

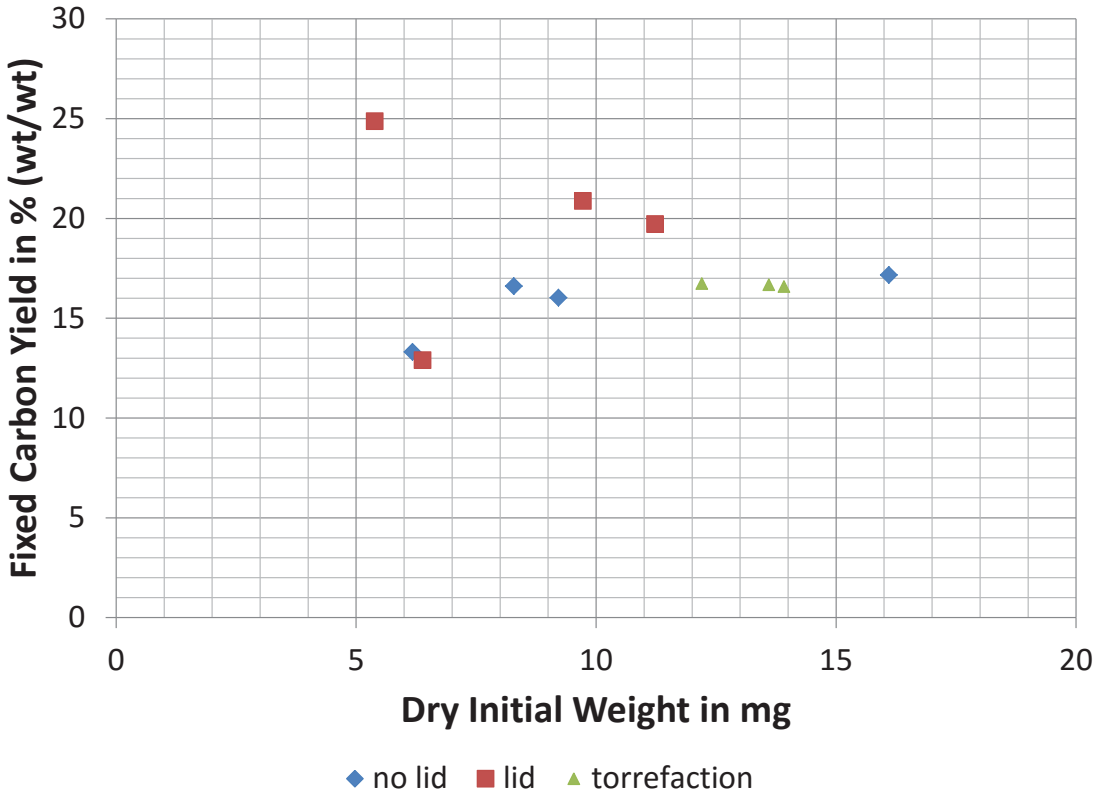

Figure B-37. Fixed carbon yield at a HTT of ≈ 745 °C of pyrolysis experiments including a torrefaction step compared to pyrolysis experiments without a torrefaction step with and without a lid as a function of the initial dry sample weight. The torrefaction experiments did not employ a lid. The dry weight was determined for lid and no lid experiments at 152 and 126 °C respectively.

References

Bashir, F. (2012). *Fracturing of wood during pyrolysis* (Unpublished final year project report). Massey University, Palmerston North, New Zealand. The report can be accessed by contacting J.R.Jones@massey.ac.nz

Branca, C., Albano, A., & Di Blasi, C. (2005). Critical evaluation of global mechanisms of wood devolatilization. *Thermochimica Acta, 429*(2), 133-141. doi:10.1016/j.tca.2005.02.030

Grønli, M. G., Várhegyi, G., & Di Blasi, C. (2002). Thermogravimetric analysis and devolatilization kinetics of wood. *Industrial & Engineering Chemistry Research, 41*(17), 4201-4208. doi:10.1021/ie0201157

Appendix C Effect of Catalysts on Pyrolysis

C.1 Catalysis by Metallic Salts

C.1.1 Relationship between Yield, Lid/No Lid and Initial Dry Sample Mass of K Impregnated Samples

Table C-1. Char yields at 695 °C and dry feedstock weight of pyrolysis experiments of 2 % (wt/wt) K impregnated sawdust pyrolysed with and without a lid.

Sample	Char yield daf % (wt/wt)	Lid/no lid[a]	Dry sample weight mg
impreg.001	23.94	0	11.001
impreg.002	22.18	0	10.172
impreg.004	24.01	0	8.242
impreg.012	19.49	0	5.163
impreg.013	23.14	0	11.491
impreg.014	23.69	0	12.395
impreg.015	23.55	0	4.798
impreg.003	28.91	1	9.851
impreg.005	27.48	1	10.059
impreg.006	26.64	1	9.254
impreg.007	30.39	1	4.808
impreg.008	34.58	1	5.660
impreg.009	22.56	1	4.635
impreg.010	28.74	1	12.535
impreg.011	25.76	1	9.236

Note. The char yield is given on a dry ash free basis. The dry sample weight was determined for lid and no lid experiments at 152 and 126 °C respectively. daf = dry ash free basis.

[a]lid is 1 and no lid is 0.

C.1.2 t-test Peak Temperatures of Derivative Weight-loss Curves of K Impregnated Sawdust Experiments With and Without a Lid

Table C-2. Peak temperatures of derivative weight-loss curves of K impregnated sawdust experiments with and without a lid.

Sample	Peak Temperature °C
impreg.001	322.40
impreg.002	322.08
impreg.004	322.14
impreg.012	322.08
impreg.013	321.78
impreg.014	322.00
impreg.015	317.43
impreg.003	326.64
impreg.005	326.61
impreg.006	326.01
impreg.007	324.82
impreg.008	325.06
impreg.009	323.04
impreg.010	323.04
impreg.011	322.47

Note. The peak temperature refers to the main peak of the derivative weight-loss curves.

Table C-3. F-test for equality of variances on data in Table C-2.

	No lid	Lid
Mean	321.4157	324.7113
Variance	3.1227	2.8221
Observations	7	8
df	6	7
F	1.1065	
P(F<=f) one-tail	0.4426	
F Critical one-tail	3.8660	

Note. The analysis was performed with Microsoft Excel (Microsoft, Redmond, WA, USA). The significance level was set to 0.05. df = degrees of freedom; F = F-test for null hypothesis; P(F<=f) one-tail = P-value for one tail F-test.

The preliminary test for the equality of variances, one tail F-test, in Table C-3 with a significance level of 0.05 resulted in the acceptance of the null hypothesis, that is, equal variance. Therefore, a t-test assuming equal variances was done, Table C-4.

Table C-4. t-test for equality of means assuming equal variances.

	No lid	**Lid**
Mean	321.4157	324.7113
Variance	3.1227	2.8221
Observations	7	8
Pooled Variance	2.9608	
Hypothesized Mean Difference	0	
df	13	
t Stat	-3.7006	
P(T<=t) one-tail	0.0013	
t Critical one-tail	1.7709	
P(T<=t) two-tail	0.0027	
t Critical two-tail	2.1604	

Note. The analysis was performed with Microsoft Excel (Microsoft, Redmond, WA, USA). The significance level was set to 0.05. df = degrees of freedom; P(T<=t) one-tail = P-value for one tail t-test; P(T<=t) two-tail = P-value for two tail t-test; t Stat = t-statistics.

C.1.3 Derivative Weight-loss Curves of K Impregnated Samples

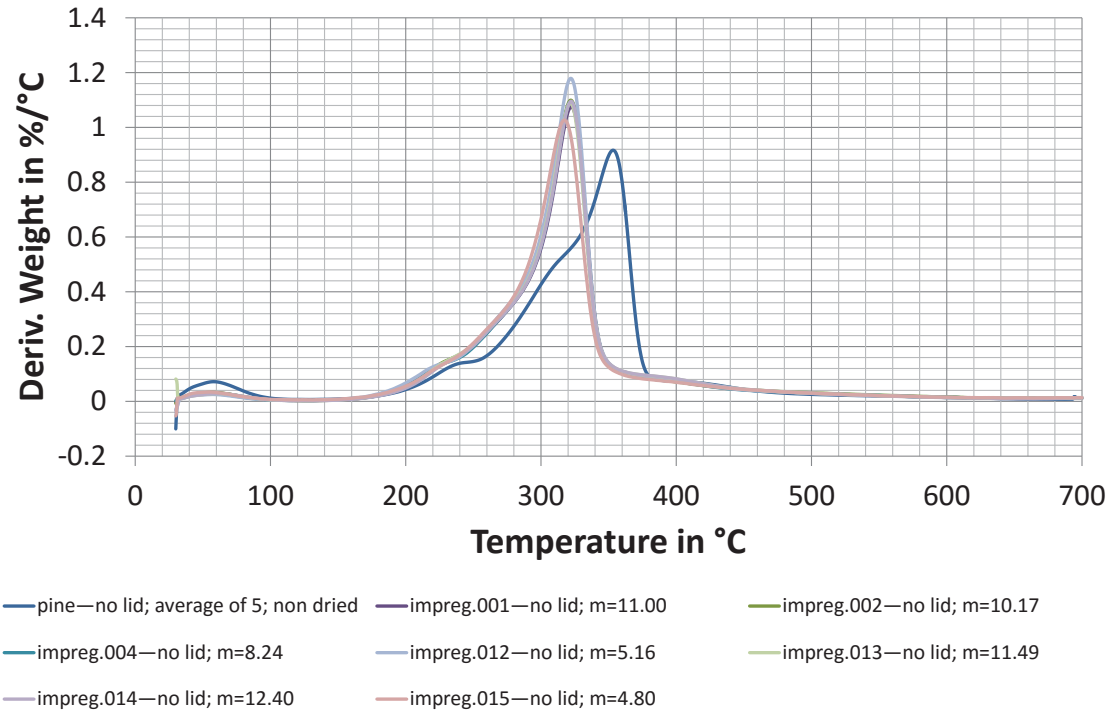

Figure C-1. Derivative weight-loss curves of 2 % (wt/wt) K impregnated pine sawdust pyrolysed without a lid. The average derivative weight-loss curve of untreated pine wood pyrolysed without a lid has been included for ease of comparison. Legend: Run number—lid or no lid; dry weight in mg. m = dry weight in mg determined at 126 °C; non dried = sample was air-dried not oven-dried.

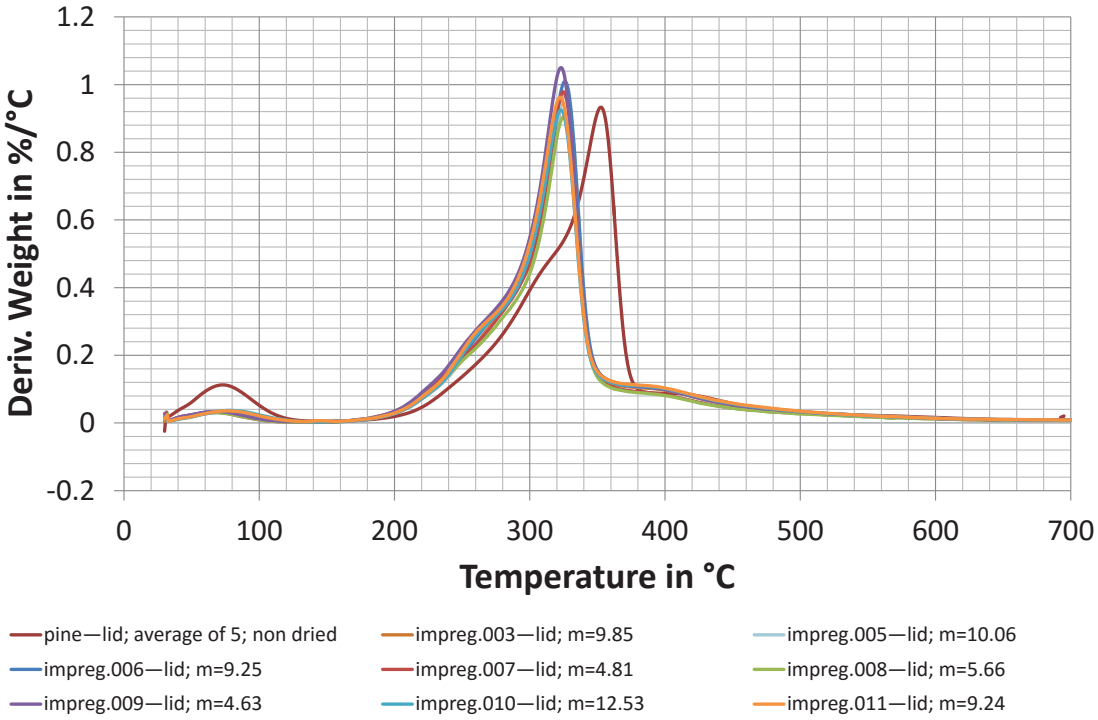

Figure C-2. Derivative weight-loss curves of 2 % (wt/wt) K impregnated pine sawdust pyrolysed with a lid. The average derivative weight-loss curve of untreated pine wood pyrolysed with a lid has been included for ease of comparison. Legend: Run number—lid or no lid; dry weight in mg. m = dry weight in mg determined at 152 °C; non dried = sample was air-dried not oven-dried.

C.1.4 Curve-fitting of K Impregnated Samples

Table C-5. Fitted parameters, resulting char yield of the biomass components and char composition of pine sawdust impregnated with 2 % (wt/wt) K in Figure 4-16.

Components	A_i	E_i	x_i	**Char yield**	**Char composition**
	1/min	**kJ/mol**		**% (wt/wt)**	**%**
Extractives	1.05E+25	248.29	0.017	52.44	6.23
Hemicellulose	1.39E+08	94.50	0.228	27.76	28.59
Cellulose	3.01E+19	227.07	0.453	12.35	20.79
Lignin	3.58	24.35	0.291	31.83	44.38

Note. The parameters were fitted in the temperature range 126 to 695 °C to capture the actual pyrolysis step without the removal of moisture. A_i = pre-exponential factor in Arrhenius equation for component i; daf = dry ash free; E_i = exponential factor in Arrhenius equation for component i; x_i = fraction of component i that constitutes the overall weight-loss.

Table C-6. Fitted parameters, resulting char yield of the biomass components and char composition of pine sawdust impregnated with 2 % (wt/wt) K in Figure 4-17.

Components	A_i	E_i	x_i	Char yield	Char composition
	1/min	kJ/mol		% (wt/wt)	%
Extractives	44.5	31.45	0.030	24.18	2.32
Hemicellulose	6.56E+08	101.19	0.254	25.11	20.85
Cellulose	3.50E+22	262.38	0.395	28.69	38.95
Lignin	45.7	37.10	0.304	33.71	37.88

Note. The parameters were fitted in the temperature range 152 to 695 °C to capture the actual pyrolysis step without the removal of moisture. A_i = pre-exponential factor in Arrhenius equation for component i; daf = dry ash free; E_i = exponential factor in Arrhenius equation for component i; x_i = fraction of component i that constitutes the overall weight-loss.

C.1.5 Magnesium Impregnation

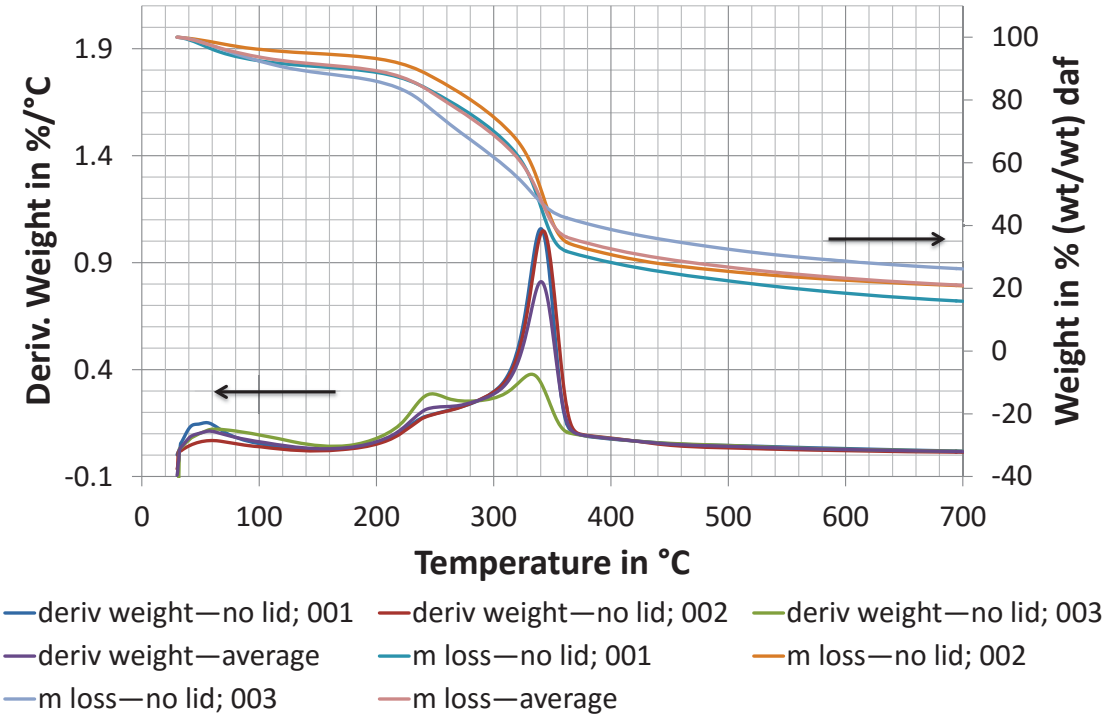

Figure C-3. Derivative weight-loss and weight-loss curves of pine sawdust impregnated with 2 % (wt/wt) Mg pyrolysed in crucibles without a lid. The dry weight was taken as the weight at 30 °C as the samples were previously oven-dried and stored over silica gel. Legend: Parameter displayed—lid or no lid; run number. daf = dry ash free; deriv weight = derivative weight-loss; m loss = weight-loss.

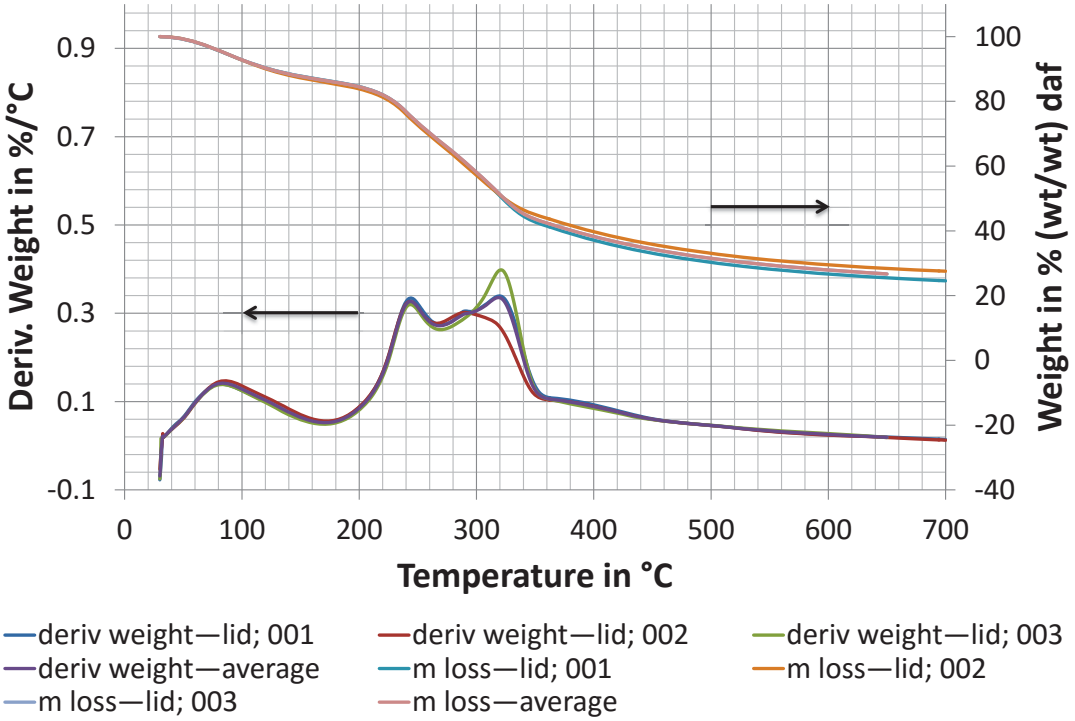

Figure C-4. Derivative weight-loss and weight-loss curves of pine sawdust impregnated with 2 % (wt/wt) Mg pyrolysed in crucibles with a lid. The dry weight was taken as the weight at 30 °C as the samples were previously oven-dried and stored over silica gel. Legend: Parameter displayed—lid or no lid; run number. daf = dry ash free; deriv weight = derivative weight-loss; m loss = weight-loss.

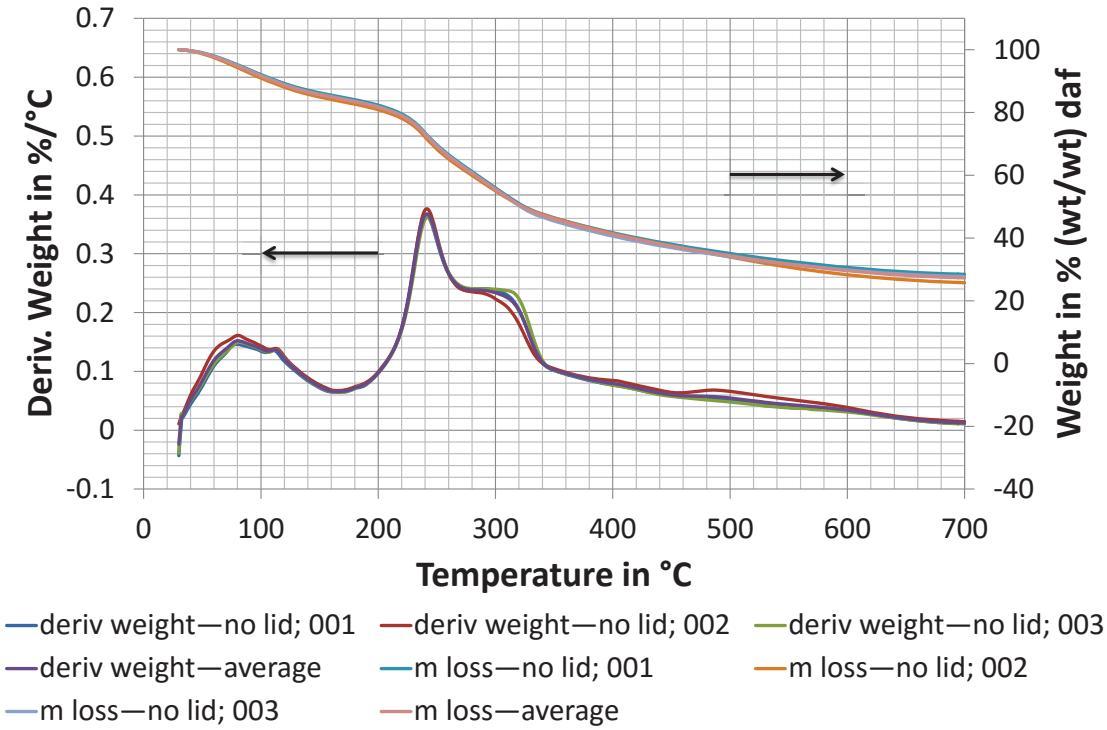

Figure C-5. Derivative weight-loss and weight-loss curves of pine sawdust impregnated with 5 % (wt/wt) Mg pyrolysed in crucibles without a lid. The dry weight was taken as the weight at 30 °C as the samples were previously oven-dried and stored over silica gel. Legend: Parameter displayed—lid or no lid; run number. daf = dry ash free; deriv weight = derivative weight-loss; m loss = weight-loss.

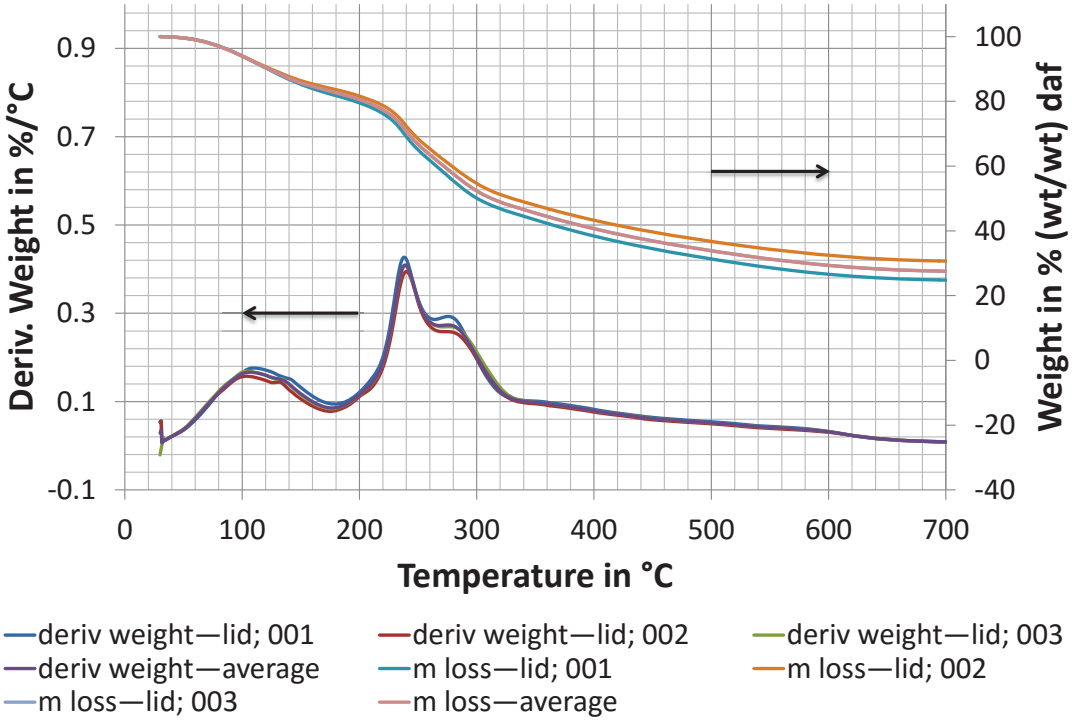

Figure C-6. Derivative weight-loss and weight-loss curves of pine sawdust impregnated with 5 % (wt/wt) Mg pyrolysed in crucibles with a lid. The dry weight was taken as the weight at 30 °C as the samples were previously oven-dried and stored over silica gel. Legend: Parameter displayed—lid or no lid; run number. daf = dry ash free; deriv weight = derivative weight-loss; m loss = weight-loss.

C.1.6 Curve-fitting of Mg Impregnated Samples

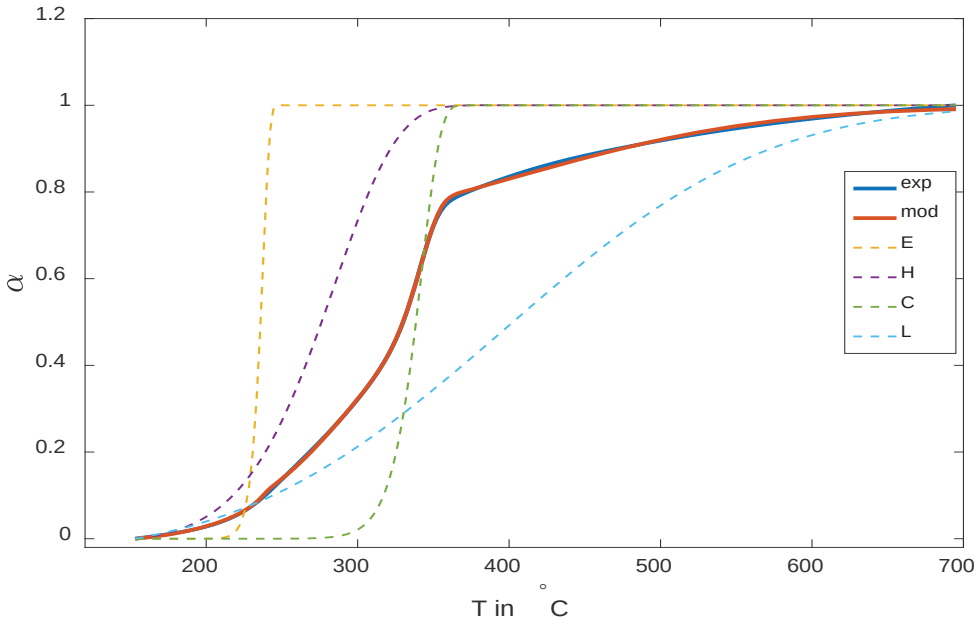

Figure C-7. Conversion curves of the experimental and modelled data of 2 % (wt/wt) Mg impregnated sawdust pyrolysed without a lid. The thinner dashed lines represent the conversion curves of the four biomass constituents extractives, hemicellulose, cellulose and lignin. The fitted parameters are given in Table C-7. exp = experimental data; E = extractives; C = cellulose; H = hemicellulose; L = lignin; mod = modelled data; T = temperature; α = degree of conversion.

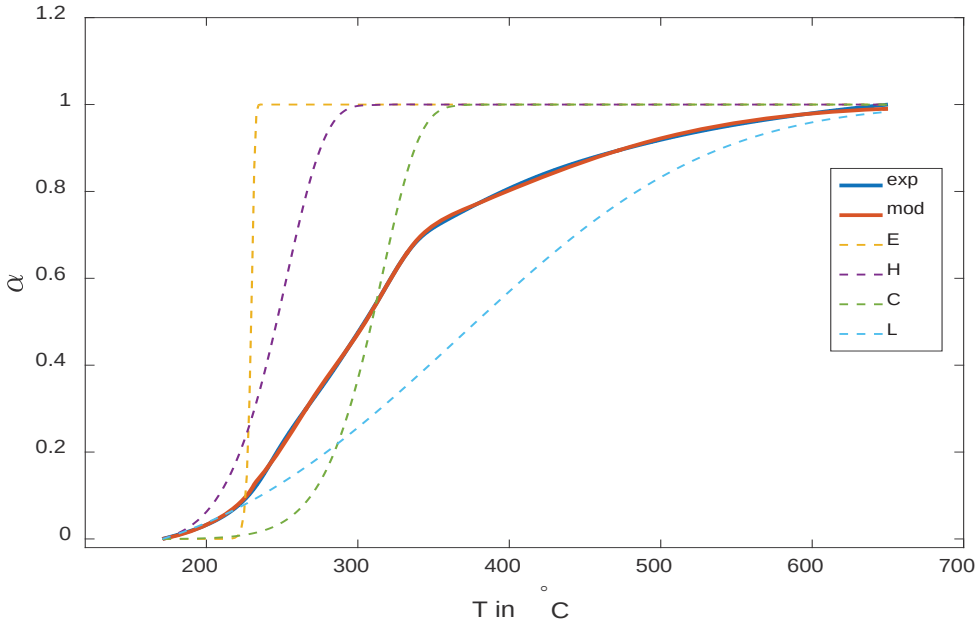

Figure C-8. Conversion curves of the experimental and modelled data of 2 % (wt/wt) Mg impregnated sawdust pyrolysed with a lid. The thinner dashed lines represent the conversion curves of the four biomass constituents extractives, hemicellulose, cellulose and lignin. The fitted parameters are given in Table C-8. exp = experimental data; E = extractives; C = cellulose; H = hemicellulose; L = lignin; mod = modelled data; T = temperature; α = degree of conversion.

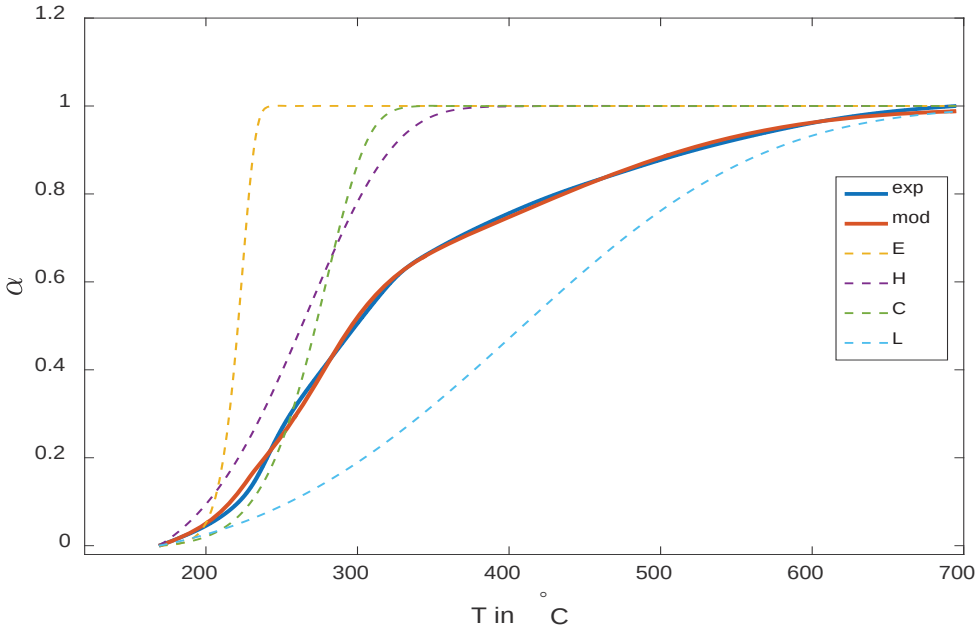

Figure C-9. Conversion curves of the experimental and modelled data of 5 % (wt/wt) Mg impregnated sawdust pyrolysed without a lid. The thinner dashed lines represent the conversion curves of the four biomass constituents extractives, hemicellulose, cellulose and lignin. The fitted parameters are given in Table C-9. exp = experimental data; E = extractives; C = cellulose; H = hemicellulose; L = lignin; mod = modelled data; T = temperature; α = degree of conversion.

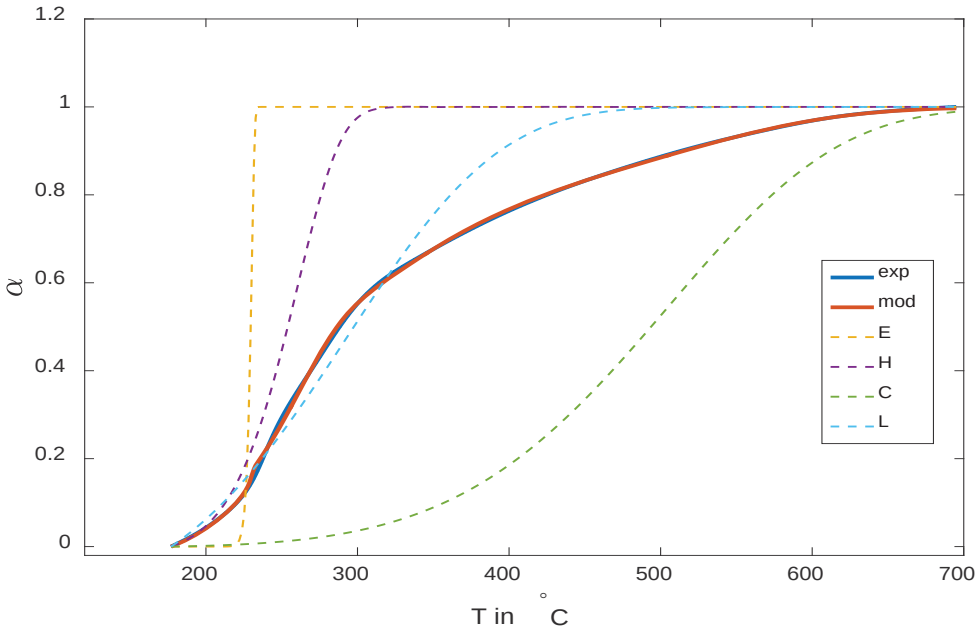

Figure C-10. Conversion curves of the experimental and modelled data of 5 % (wt/wt) Mg impregnated sawdust pyrolysed with a lid. The thinner dashed lines represent the conversion curves of the four biomass constituents extractives, hemicellulose, cellulose and lignin. The fitted parameters are given in Table C-10. exp = experimental data; E = extractives; C = cellulose; H = hemicellulose; L = lignin; mod = modelled data; T = temperature; α = degree of conversion.

Table C-7. Fitted parameters, resulting char yield of the biomass components and char composition of pine sawdust impregnated with 2 % (wt/wt) Mg in Figure C-7.

Components	A_i	E_i	x_i	**Char yield**	**Char composition**
	1/min	**kJ/mol**		**% (wt/wt)**	**%**
Extractives	8.12E+47	467.5	0.018	51.57	6.12
Hemicellulose	7.05E0+4	61.5	0.311	2.08	2.14
Cellulose	1.64E+21	254.3	0.341	34.36	57.79
Lignin	1.48	21.8	0.325	24.38	33.95

Note. The parameters were fitted in the temperature range 153 to 695 °C to avoid fitting the peak below 200 °C, which origin is unknown. A_i = pre-exponential factor in Arrhenius equation for component *i*; daf = dry ash free; E_i = exponential factor in Arrhenius equation for component *i*; x_i = fraction of component *i* that constitutes the overall weight-loss.

Table C-8. Fitted parameters, resulting char yield of the biomass components and char composition of pine sawdust impregnated with 2 % (wt/wt) Mg in Figure C-8.

Components	A_i	E_i	x_i	**Char yield**	**Char composition**
	1/min	**kJ/mol**		**% (wt/wt)**	**%**
Extractives	2.56E+111	1068.7	0.011	73.29	6.57
Hemicellulose	1.10E+08	88.0	0.237	33.03	25.67
Cellulose	2.94E+09	114.5	0.295	48.99	62.24
Lignin	1.42	20.5	0.454	5.25	5.53

Note. The parameters were fitted in the temperature range 171 to 650 °C to avoid fitting the peak below 200 °C, which origin is unknown. The maximum temperature was 650 °C as one run stopped recording after that temperature. A_i = pre-exponential factor in Arrhenius equation for component *i*; daf = dry ash free; E_i = exponential factor in Arrhenius equation for component *i*; x_i = fraction of component *i* that constitutes the overall weight-loss.

Table C-9. Fitted parameters, resulting char yield of the biomass components and char composition of pine sawdust impregnated with 5 % (wt/wt) Mg in Figure C-9.

Components	A_i	E_i	x_i	**Char yield**	**Char composition**
	1/min	**kJ/mol**		**% (wt/wt)**	**%**
Extractives	9.06E+23	230.1	0.033	21.74	1.82
Hemicellulose	1.24E+03	42.9	0.364	0.24	0.17
Cellulose	7.59E+07	91.1	0.131	78.00	92.40
Lignin	1.89	23.2	0.466	5.72	5.61

Note. The parameters were fitted in the temperature range 169 to 695 °C to avoid fitting the peak below 200 °C, which origin is unknown. A_i = pre-exponential factor in Arrhenius equation for component *i*; daf = dry ash free; E_i = exponential factor in Arrhenius equation for component *i*; x_i = fraction of component *i* that constitutes the overall weight-loss.

Table C-10. Fitted parameters, resulting char yield of the biomass components and char composition of pine sawdust impregnated with 5 % (wt/wt) Mg in Figure C-10.

Components	A_i	E_i	x_i	**Char yield**	**Char composition**
	1/min	**kJ/mol**		**% (wt/wt)**	**%**
Extractives	1.24E+111	1065.5	0.03	23.33	1.92
Hemicellulose	1.74E+07	81.6	0.302	18.38	13.13
Cellulose	42.51	44.4	0.240	60.27	70.41
Lignin	14.54	26.6	0.425	15.03	14.53

Note. The parameters were fitted in the temperature range 177 to 695 °C to avoid fitting the peak below 200 °C, which origin is unknown. A_i = pre-exponential factor in Arrhenius equation for component *i*; daf = dry ash free; E_i = exponential factor in Arrhenius equation for component *i*; x_i = fraction of component *i* that constitutes the overall weight-loss.

C.2 Catalysis by Acid Treatment

C.2.1 TGA Data

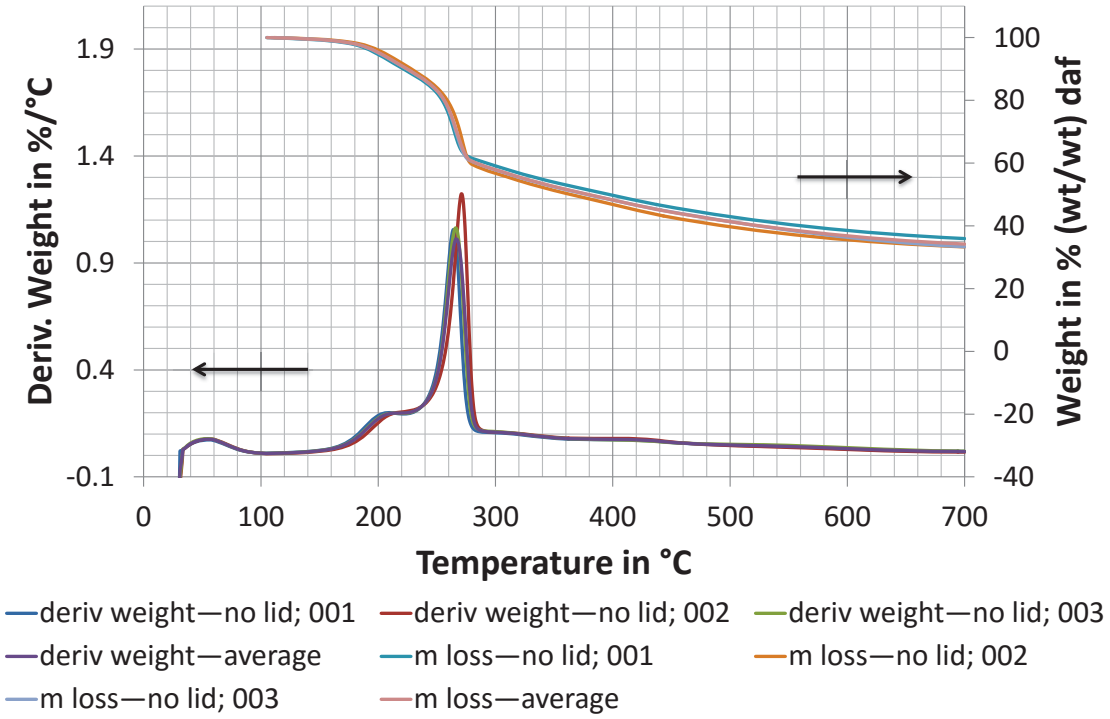

Figure C-11. Derivative weight-loss and weight-loss curves of pine sawdust impregnated with 1.75 % (wt/wt) P pyrolysed in crucibles without a lid. The dry weight was determined at the minimum in the derivative weight-loss curve between 60 and 200 °C. Legend: Parameter displayed—lid or no lid; run number. daf = dry ash free; deriv weight = derivative weight-loss; m loss = weight-loss.

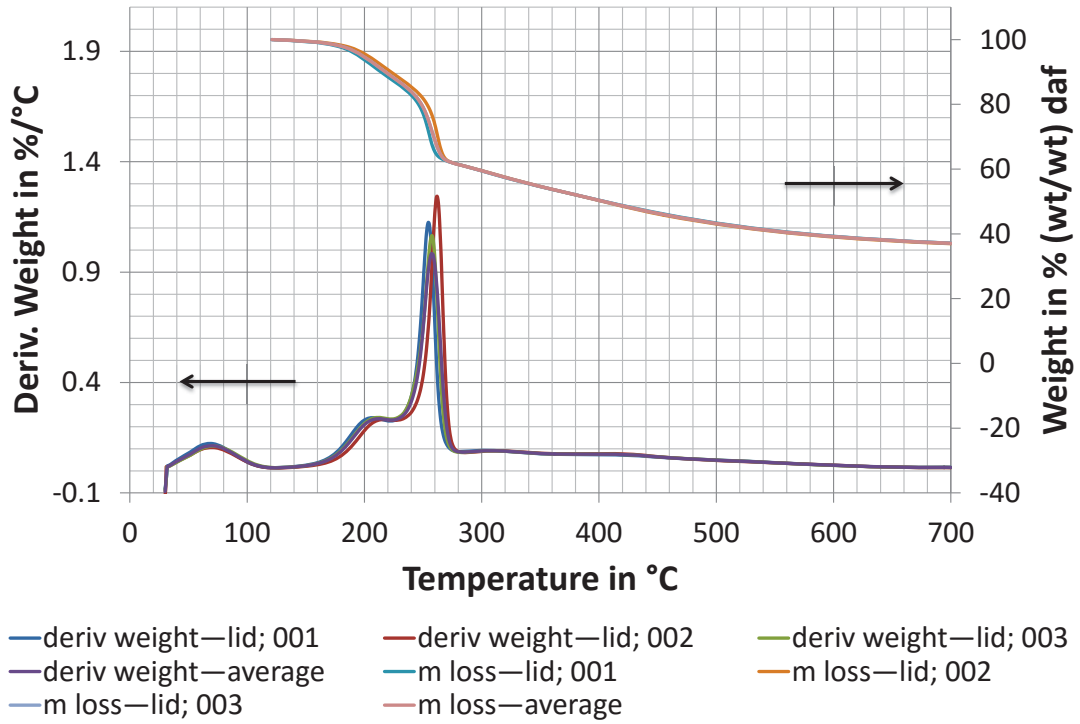

Figure C-12. Derivative weight-loss and weight-loss curves of pine sawdust impregnated with 1.75 % (wt/wt) P pyrolysed in crucibles with a lid. The dry weight was determined at the minimum in the derivative weight-loss curve between 60 and 200 °C. Legend: Parameter displayed—lid or no lid; run number. daf = dry ash free; deriv weight = derivative weight-loss; m loss = weight-loss.

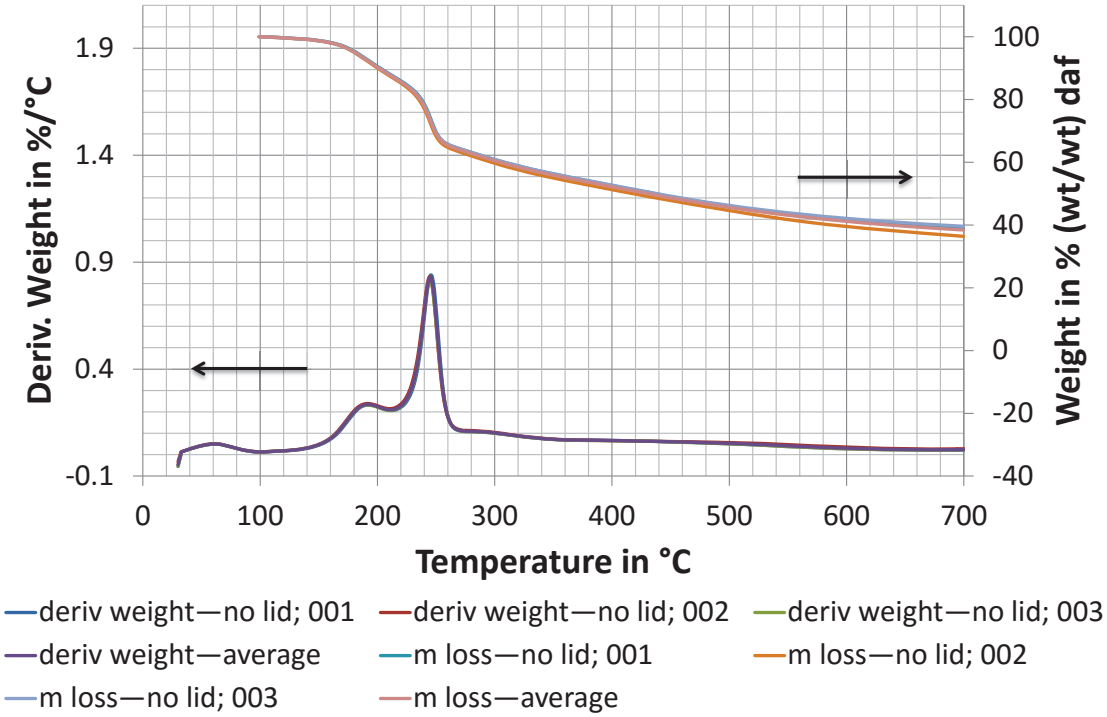

Figure C-13. Derivative weight-loss and weight-loss curves of pine sawdust impregnated with 4.25 % (wt/wt) P pyrolysed in crucibles without a lid. The dry weight was determined at the minimum in the derivative weight-loss curve between 60 and 200 °C. Legend: Parameter displayed—lid or no lid; run number. daf = dry ash free; deriv weight = derivative weight-loss; m loss = weight-loss.

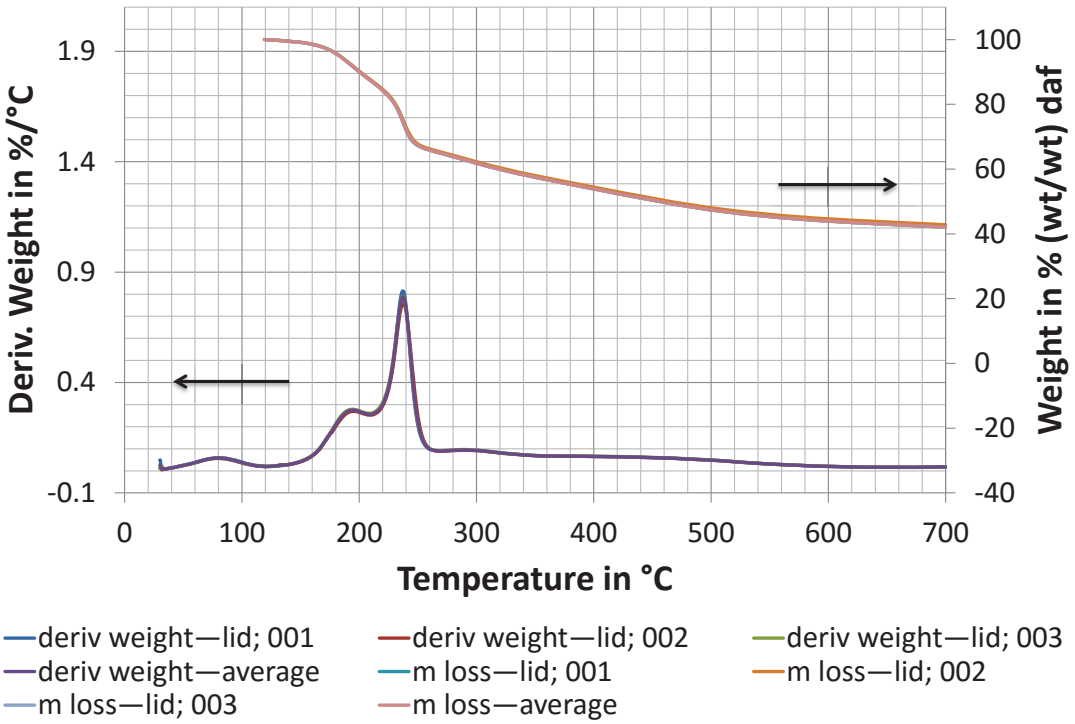

Figure C-14. Derivative weight-loss and weight-loss curves of pine sawdust impregnated with 4.25 % (wt/wt) P pyrolysed in crucibles with a lid. The dry weight was determined at the minimum in the derivative weight-loss curve between 60 and 200 °C. Legend: Parameter displayed—lid or no lid; run number. daf = dry ash free; deriv weight = derivative weight-loss; m loss = weight-loss.

C.2.2 Curve-fitting of P Impregnated Samples

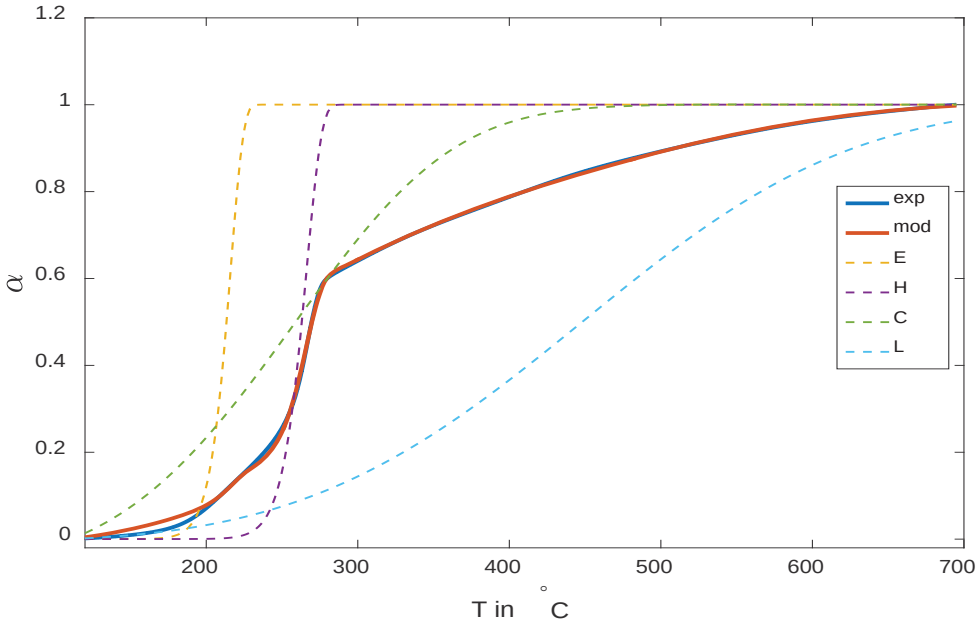

Figure C-15. Conversion curves of the experimental and modelled data of 1.75 % (wt/wt) P impregnated sawdust pyrolysed without a lid. The thinner dashed lines represent the conversion curves of the four biomass constituents extractives, hemicellulose, cellulose and lignin. The fitted parameters are given in Table C-11. exp = experimental data; E = extractives; C = cellulose; H = hemicellulose; L = lignin; mod = modelled data; T = temperature; α = degree of conversion.

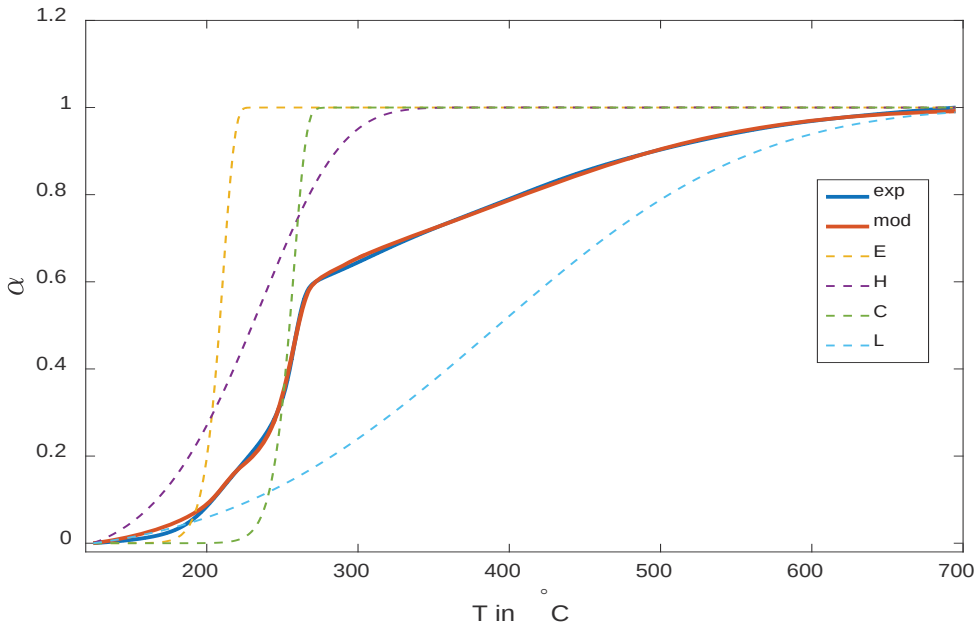

Figure C-16. Conversion curves of the experimental and modelled data of 1.75 % (wt/wt) P impregnated sawdust pyrolysed with a lid. The thinner dashed lines represent the conversion curves of the four biomass constituents extractives, hemicellulose, cellulose and lignin. The fitted parameters are given in Table C-12. exp = experimental data; E = extractives; C = cellulose; H = hemicellulose; L = lignin; mod = modelled data; T = temperature; α = degree of conversion.

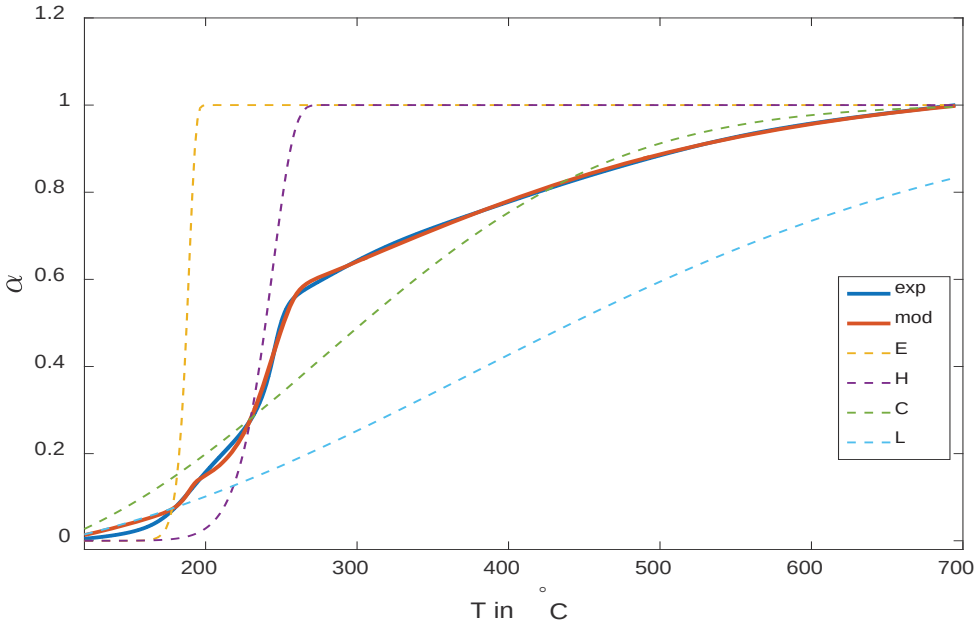

Figure C-17. Conversion curves of the experimental and modelled data of 4.25 % (wt/wt) P impregnated sawdust pyrolysed without a lid. The thinner dashed lines represent the conversion curves of the four biomass constituents extractives, hemicellulose, cellulose and lignin. The fitted parameters are given in Table C-13. exp = experimental data; E = extractives; C = cellulose; H = hemicellulose; L = lignin; mod = modelled data; T = temperature; α = degree of conversion.

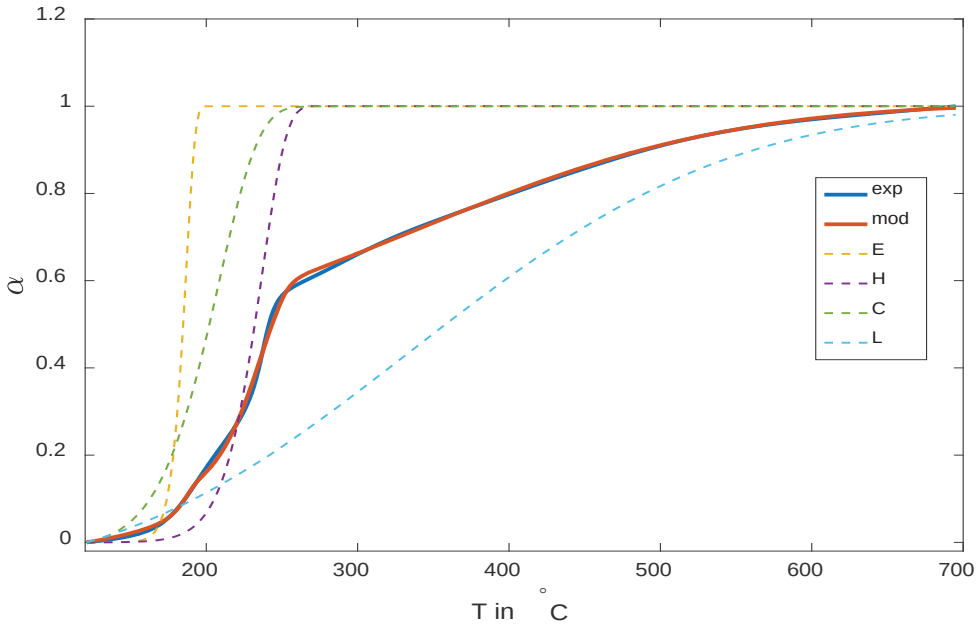

Figure C-18. Conversion curves of the experimental and modelled data of 4.25 % (wt/wt) P impregnated sawdust pyrolysed with a lid. The thinner dashed lines represent the conversion curves of the four biomass constituents extractives, hemicellulose, cellulose and lignin. The fitted parameters are given in Table C-14. exp = experimental data; E = extractives; C = cellulose; H = hemicellulose; L = lignin; mod = modelled data; T = temperature; α = degree of conversion.

Table C-11. Fitted parameters, resulting char yield of the biomass components and char composition of pine sawdust impregnated with 1.75 % (wt/wt) P in Figure C-15.

Components	A_i	E_i	x_i	**Char yield**	**Char composition**
	1/min	**kJ/mol**		**% (wt/wt)**	**%**
Extractives	9.23E+24	235.6	0.04	0.24	0.02
Hemicellulose	2.13E+23	243.5	0.37	0.47	0.34
Cellulose	7.54E+00	22.3	0.27	56.15	66.50
Lignin	1.69	24.5	0.33	33.80	33.14

Note. The parameters were fitted in the temperature range 111 to 695 °C to describe pyrolysis without the evaporation of moisture. A_i = pre-exponential factor in Arrhenius equation for component *i*; daf = dry ash free; E_i = exponential factor in Arrhenius equation for component *i*; x_i = fraction of component *i* that constitutes the overall weight-loss.

Table C-12. Fitted parameters, resulting char yield of the biomass components and char composition of pine sawdust impregnated with 1.75 % (wt/wt) P in Figure C-16.

Components	A_i	E_i	x_i	**Char yield**	**Char composition**
	1/min	**kJ/mol**		**% (wt/wt)**	**%**
Extractives	1.95E+27	254.2	0.04	0.001	0.00
Hemicellulose	1.48E+03	40.8	0.20	47.696	31.05
Cellulose	2.24E+27	279.5	0.31	50.803	54.07
Lignin	1.37	21.1	0.44	16.881	14.87

Note. The parameters were fitted in the temperature range 125 to 695 °C to describe pyrolysis without the evaporation of moisture. A_i = pre-exponential factor in Arrhenius equation for component *i*; daf = dry ash free; E_i = exponential factor in Arrhenius equation for component *i*; x_i = fraction of component *i* that constitutes the overall weight-loss.

Table C-13. Fitted parameters, resulting char yield of the biomass components and char composition of pine sawdust impregnated with 4.25 % (wt/wt) P in Figure C-17.

Components	A_i	E_i	x_i	**Char yield**	**Char composition**
	1/min	**kJ/mol**		**% (wt/wt)**	**%**
Extractives	2.92E+44	392.6	0.05	0.006	0.00
Hemicellulose	1.85E+15	155. 3	0.36	8.376	5.86
Cellulose	4.46E-01	13.0	0.29	56.035	64.07
Lignin	0.09	9.8	0.37	31.773	30.07

Note The parameters were fitted in the temperature range 102 to 695 °C to describe pyrolysis without the evaporation of moisture. A_i = pre-exponential factor in Arrhenius equation for component *i*; daf = dry ash free; E_i = exponential factor in Arrhenius equation for component *i*; x_i = fraction of component *i* that constitutes the overall weight-loss.

Table C-14. Fitted parameters, resulting char yield of the biomass components and char composition of pine sawdust impregnated with 4.25 % (wt/wt) P in Figure C-18.

Components	A_i	E_i	x_i	**Char yield**	**Char composition**
	1/min	**kJ/mol**		**% (wt/wt)**	**%**
Extractives	2.06E+33	293.6	0.049	0.00	0.00
Hemicellulose	2.89E+13	135.9	0.37	11.11	6.48
Cellulose	1.37E+07	72.3	0.058	91.54	87.22
Lignin	0.42	14.4	0.525	7.98	6.30

Note. The parameters were fitted in the temperature range 121 to 695 °C to describe pyrolysis without the evaporation of moisture. A_i = pre-exponential factor in Arrhenius equation for component *i*; daf = dry ash free; E_i = exponential factor in Arrhenius equation for component *i*; x_i = fraction of component *i* that constitutes the overall weight-loss.

Appendix D Heat of Pyrolysis

D.1 Derivation of Reaction Heat Effects from Internal Temperature Recordings

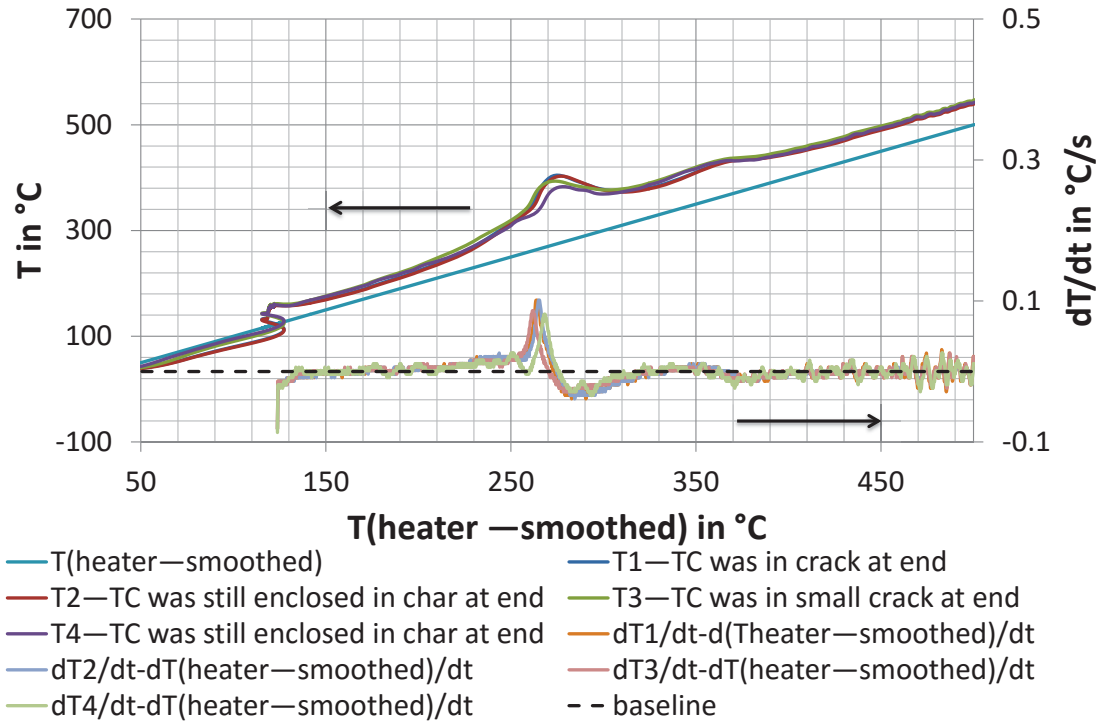

Figure D-1. Temperature profile including differential temperature change recorded in a large pine cylinder (d = 120 mm, h = 60 mm) undergoing pyrolysis. The cylinder was pyrolysed from room temperature to 120 °C at 2 °C/min, where the temperature was held for 180 min before pyrolysis continued at 0.85 °C/min to 500 °C. T1 to T4 refer to the thermocouple positions in Figure 5-1. The sample shrunk onto the thermocouples providing exact temperature readings except in the case of TC1 and TC3 where a crack was present at the end of the run. The baseline refers to the secondary axis showing the difference of the time derivative of the recorded temperature to the time derivative of the heater temperature, and denotes zero difference. d = diameter in mm; h = height in mm; T = Temperature in °C; TC = thermocouple; t = time in s.

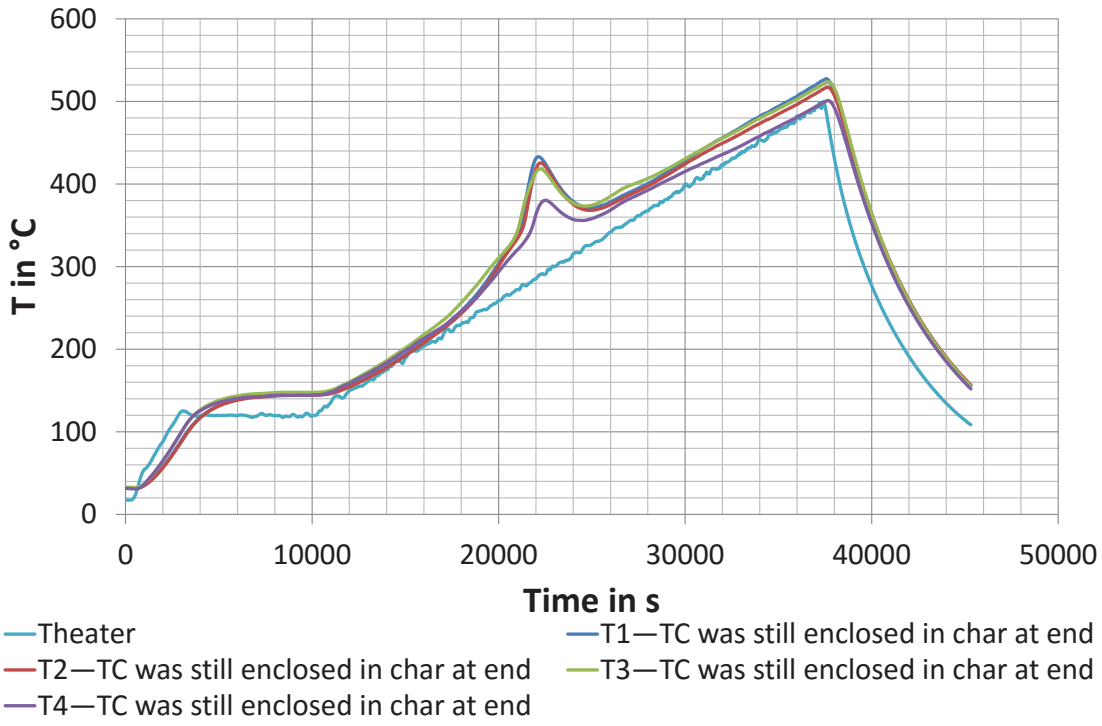

Figure D-2. Corresponding temperature profile to Figure 5-3 as a function of time. T1 to T4 refer to the thermocouple positions in Figure 5-1. The sample shrunk onto the thermocouples and did not crack or fracture during pyrolysis in proximity of the thermocouples providing exact temperature readings. T = Temperature in °C; TC = thermocouple; t = time in s.

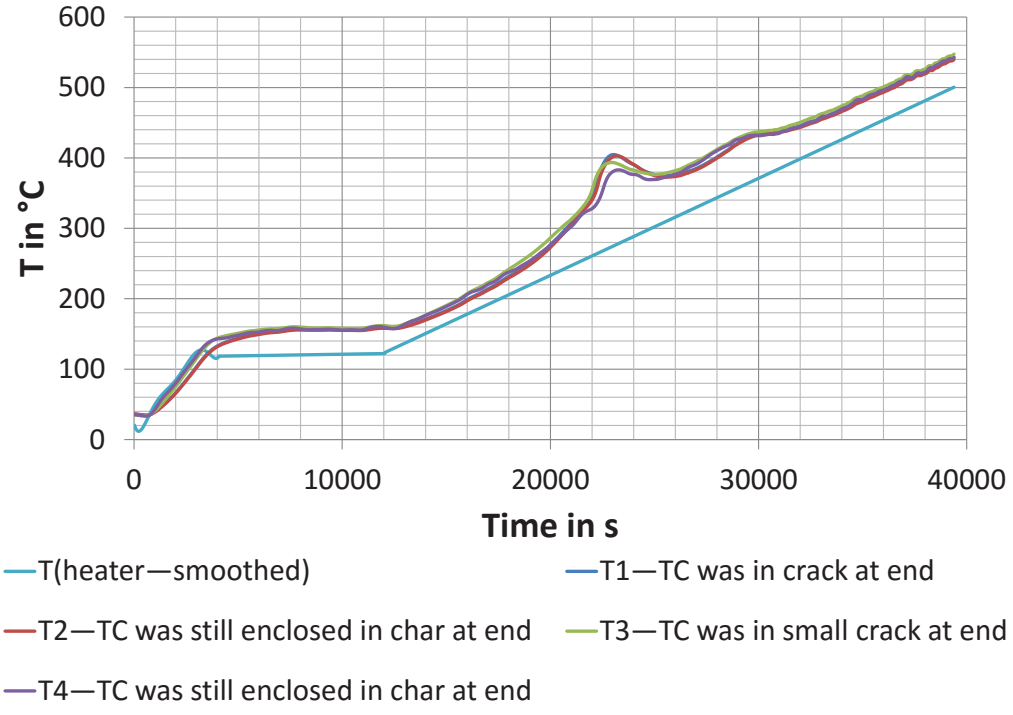

Figure D-3. Corresponding temperature profile to Figure D-1 as a function of time. T1 to T4 refer to the thermocouple positions in Figure 5-1. The sample shrunk onto the thermocouples providing exact temperature readings except in the case of TC1 and TC3 where a crack was present at the end of the run. T = Temperature in °C; TC = thermocouple; t = time in s.

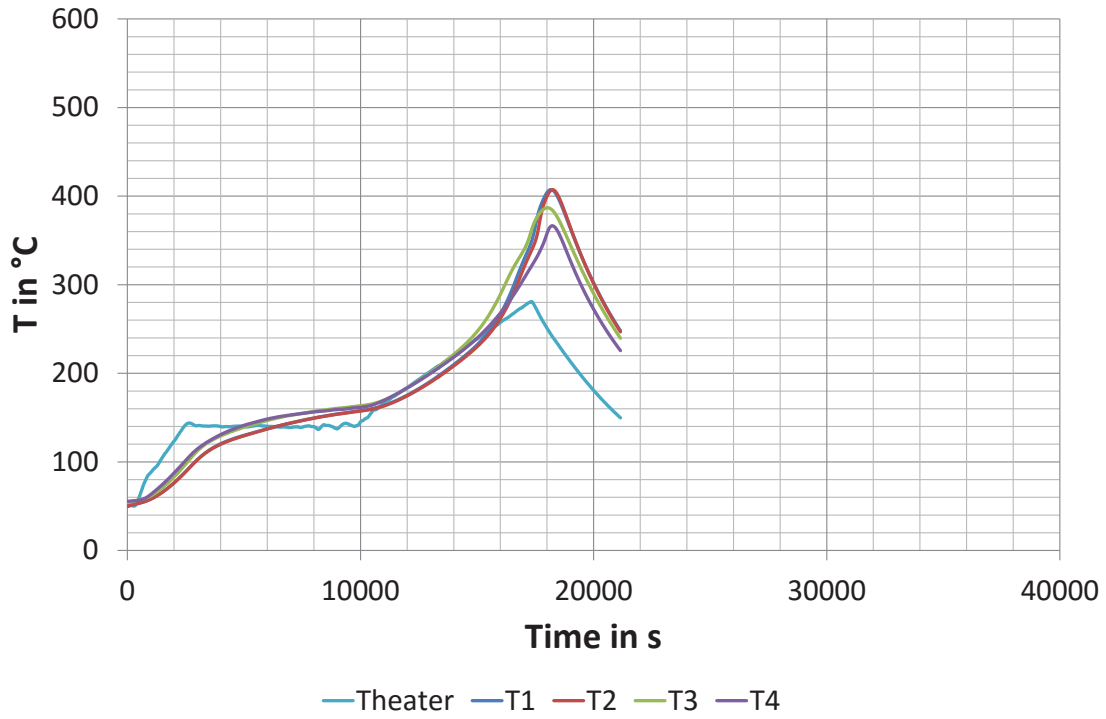

Figure D-4. Temperature profile as a function of time of a large pine cylinder (d = 120 mm, h = 60 mm) undergoing pyrolysis. The cylinder was pyrolysed from room temperature to 140 °C at 2 °C/min, where the temperature was held for 120 min before pyrolysis continued at 1.12 °C/min till it stopped at 280 °C. T1 to T4 refer to the thermocouple positions in Figure 5-1. d = diameter in mm; h = height in mm; T = Temperature in °C; t = time in s.

D.2 Heat Flow Analysis of TGA Experiments

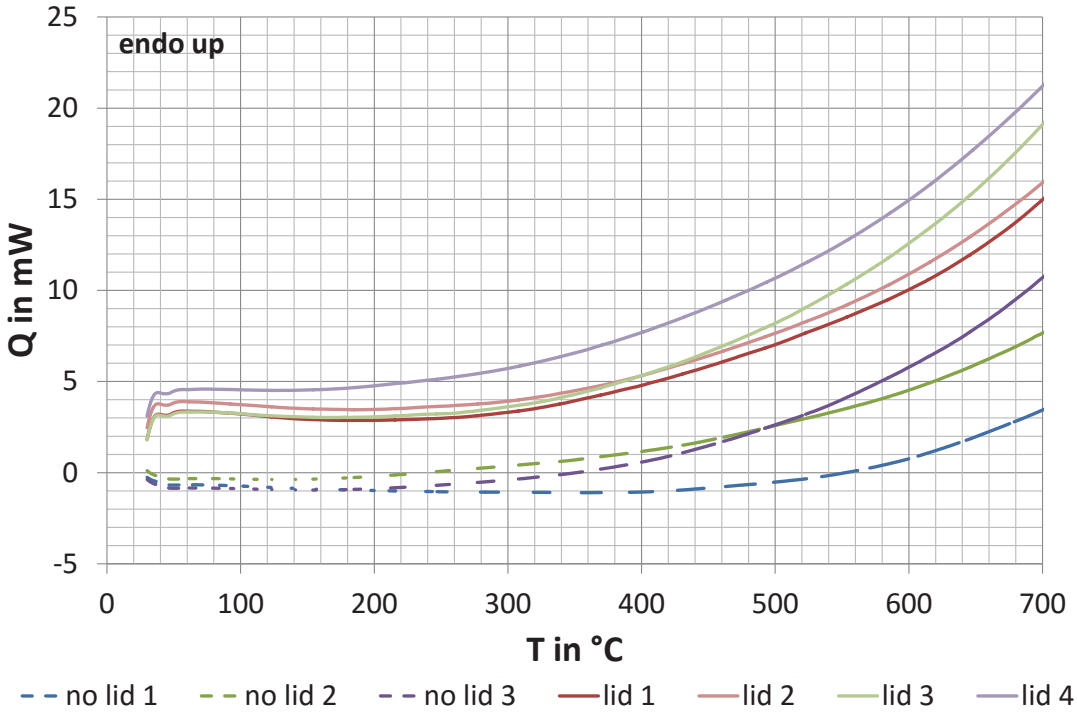

Figure D-5. Recorded heat flows of blank runs employing crucibles with and without a lid. It is important to note that the blank runs were performed before subsequent pine sawdust pyrolysis experiments. Q = heat flow in mW; T = Temperature in °C.

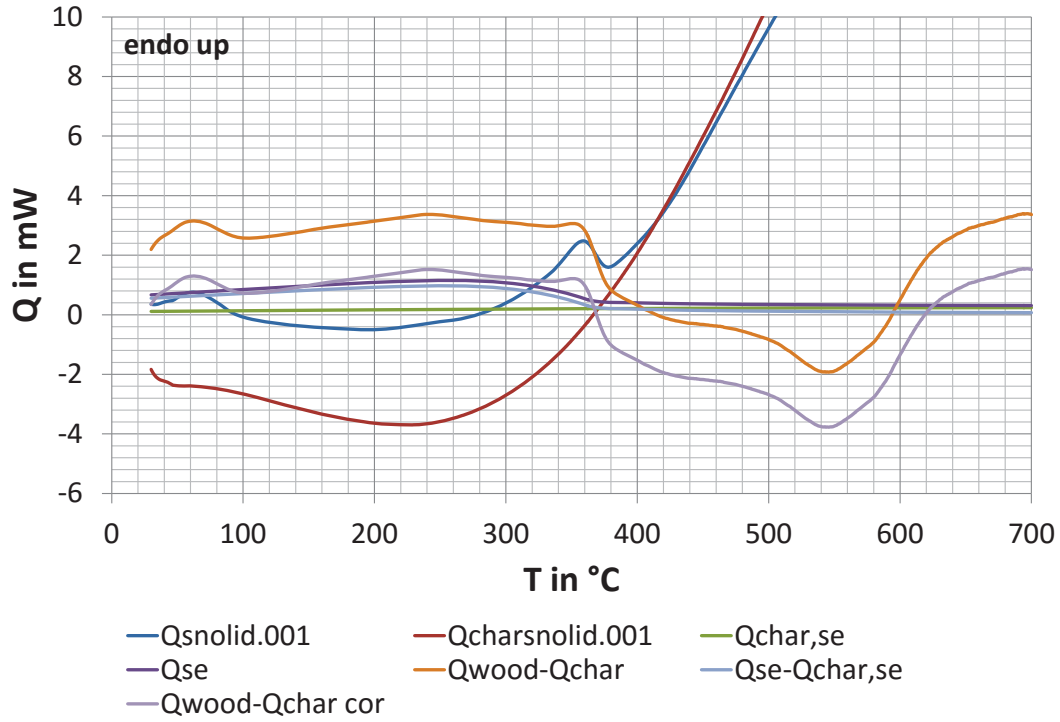

Figure D-6. Heat flows used for determining the offset for the heat of pyrolysis in Figure 5-10. "Qsnolid.001" and "Qcharsnolid.001" are the heat flow measured during pyrolysis of the pine sawdust and the resulting char respectively. "Qse" and "Qchar,se" are the calculated sensible heat flows required to heat the solid in "Qsnolid.001" and "Qcharsnolid.001" correspondingly. "Qwood-Qchar cor" is the offset corrected difference curve. Q = heat flow in mW; T = temperature in °C.

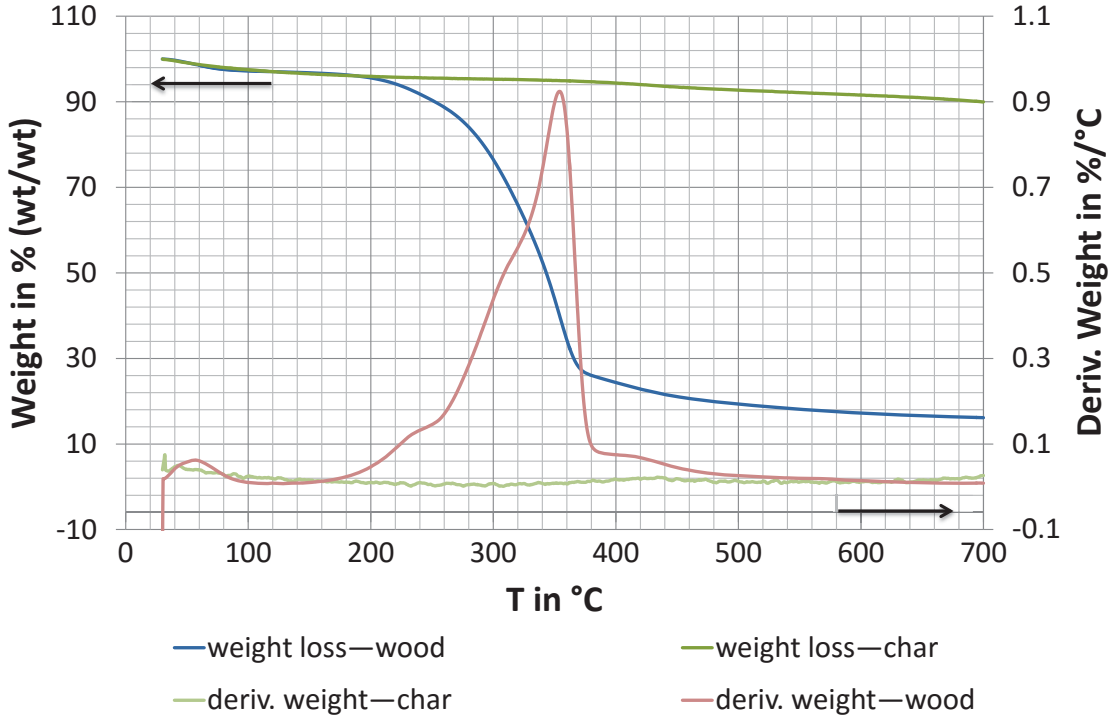

Figure D-7. Weight-loss and derivative weight-loss of feedstock and subsequent char pyrolysis in crucibles without a lid. The here depicted experiments belong to run "snolid.001" in Figure 5-11. deriv. = derivative; T = temperature in °C.

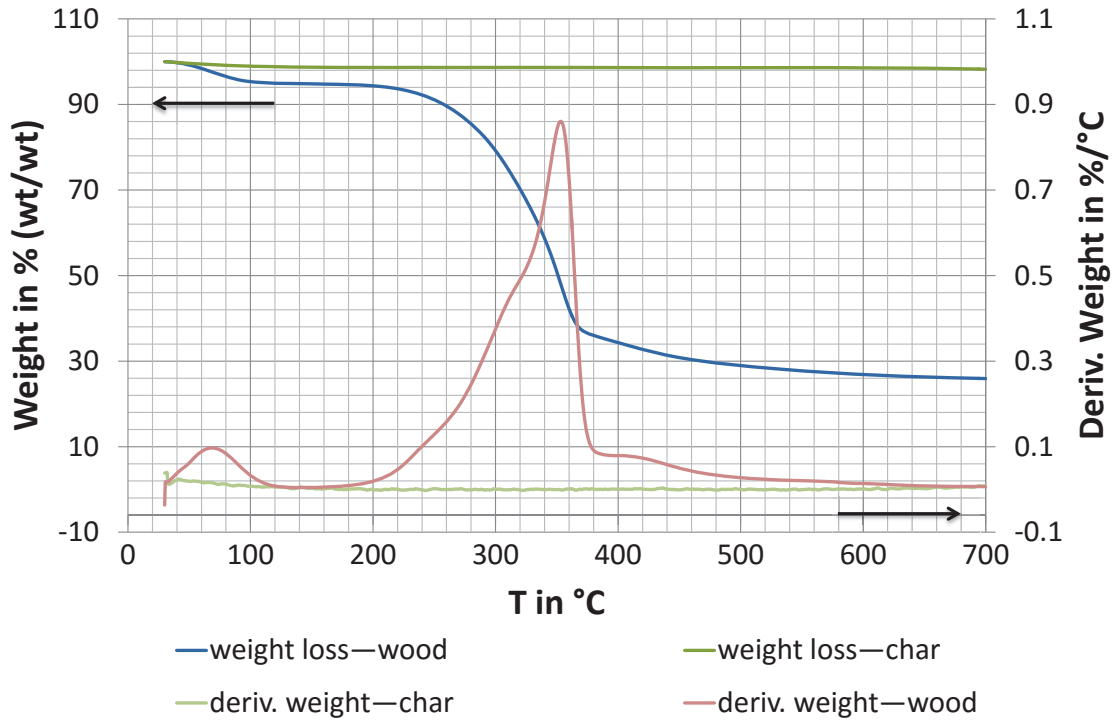

Figure D-8. Weight-loss and derivative weight-loss of feedstock and subsequent char pyrolysis in crucibles with a lid. The here depicted experiments belong to run "slid.001" in Figure 5-12. deriv. = derivative; T = temperature in °C.

Table D-1. Char weight-loss during pyrolysis in crucibles without a lid from 30 to 700 °C.

Sample	**Weight-loss**
	% (wt/wt)
snolid.001	10.01
snolid.002	4.70
snolid.003	4.68
snolid.004	3.27
μ in % (wt/wt)	5.664
σ in pp	2.974
CV	0.525

Note. The char pyrolysis has been performed under the same conditions as the feedstock pyrolysis immediately after it had been completed and the sample had cooled back down to room temperature.

Table D-2. Char weight-loss during pyrolysis in crucibles with a lid from 30 to 700 °C.

Sample	**Weight-loss**
	% (wt/wt)
slid.001	1.75
slid.002	2.49
slid.003	1.29
slid.004	1.26
μ in % (wt/wt)	1.696
σ in pp	0.576
CV	0.339

Note. The char pyrolysis has been performed under the same conditions as the feedstock pyrolysis immediately after it had been completed and the sample had cooled back down to room temperature.

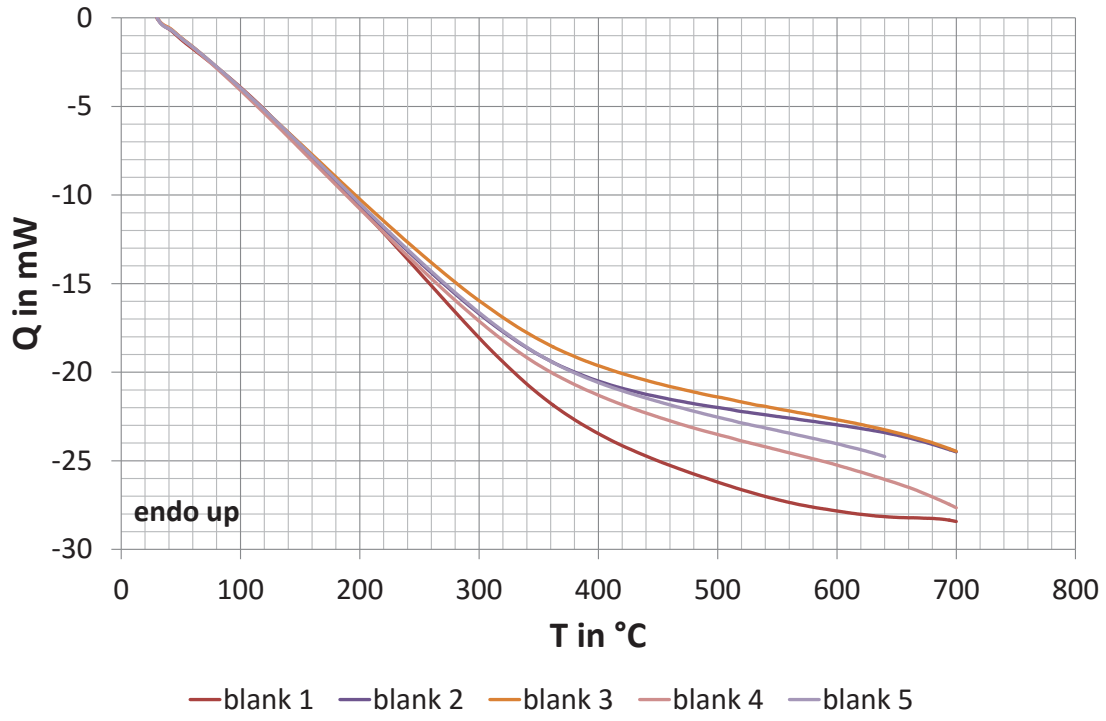

Figure D-9. Recorded heat flows of blank runs without a lid. The blank runs were performed subsequently without opening the furnace to eliminate possible effects caused by interfering with the sample crucible. It is important to note that the heat flows were adjusted to have a common starting point at 30 °C, and are different to Figure D-5 as they were done after equipment maintenance/ repair work and re-calibration. Q = heat flow in mW; T = Temperature in °C.

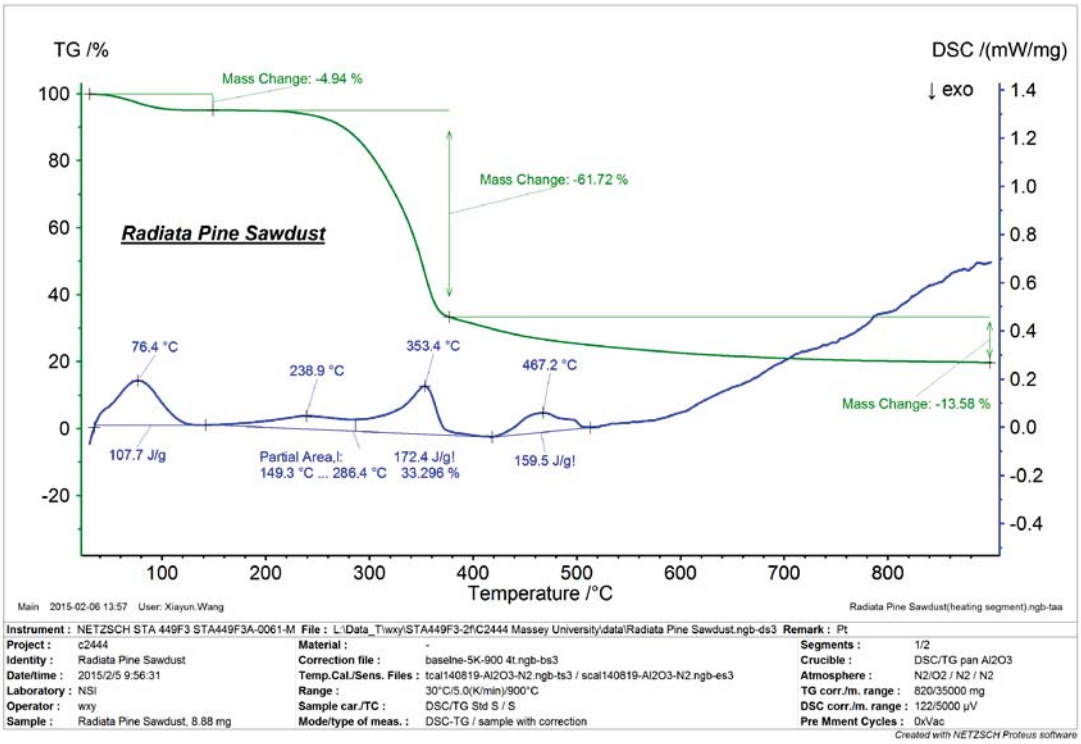

Figure D-10. TG/DSC measurement of air-dried pine sawdust pyrolysed in a crucible without a lid. The analysis was carried out by NETZSCH Scientific Instruments Trading (Shanghai) Ltd (Waigaoqiao Free Trade Zone Shanghai, P.R. China) with a NETZSCH (Selb, Germany) STA449 F3 Jupiter TG/DSC equipped with a true heat flux-DSC sensor (thermally coupled). DSC = differential scanning calorimeter; TG = thermogravimetry.

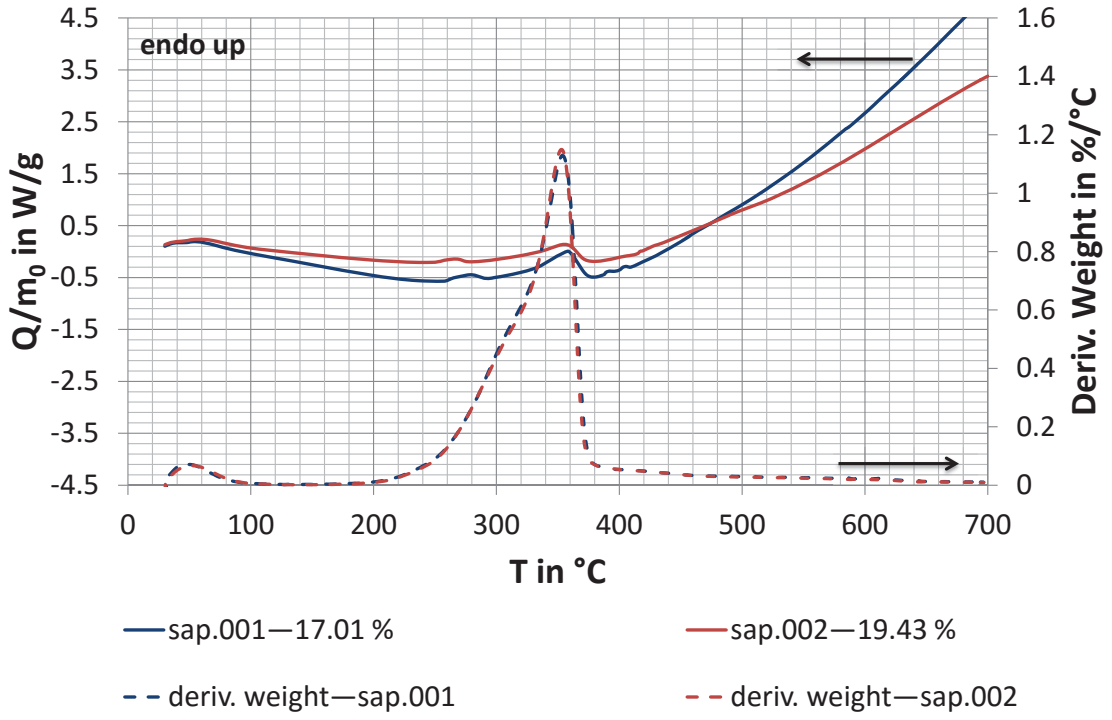

Figure D-11. Raw heat flow data of sapwood slices pyrolysed in crucibles without a lid. The secondary y-axis shows the corresponding derivative weight-loss curves. Legend: sample name—char yield at 695 °C in % (wt/wt) daf. daf = dry ash free; deriv. = derivative; m_0 = initial dry ash free weight in mg; Q = heat flow in mW; T = temperature in °C.

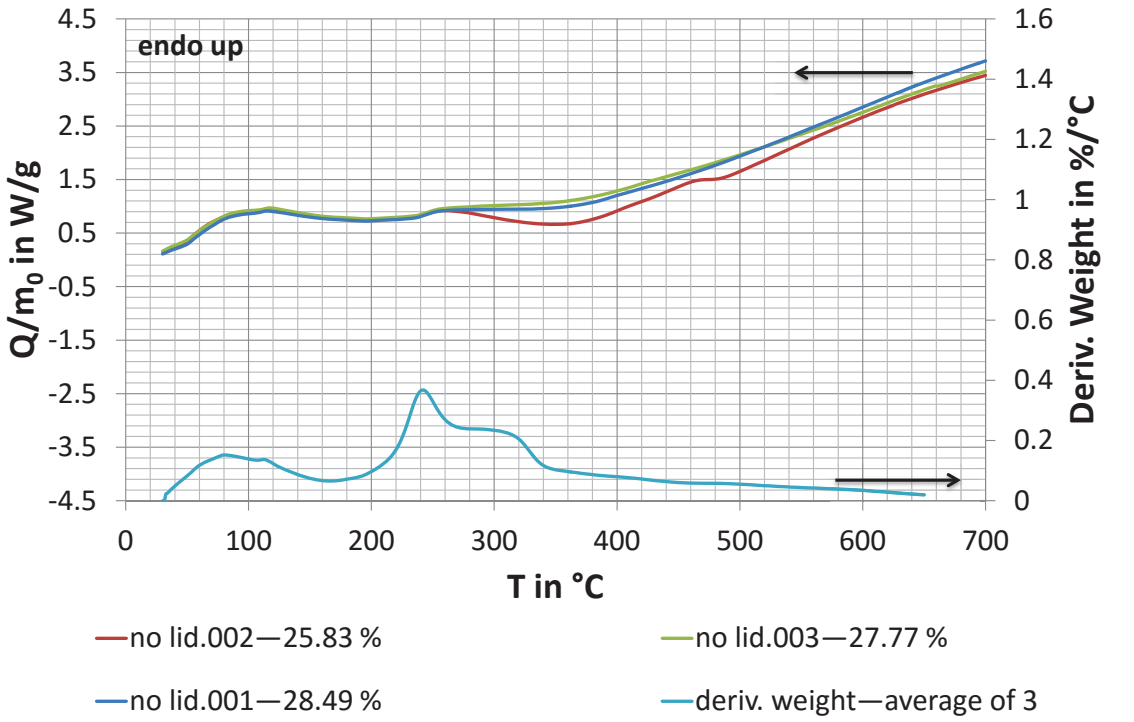

Figure D-12. Raw heat flow data of pine sawdust impregnated with 5 % (wt/wt) Mg pyrolysed in crucibles without a lid. The secondary y-axis shows the corresponding average derivative weight-loss curve. Legend: sample name—char yield at 695 °C in % (wt/wt) daf. daf = dry ash free; deriv. = derivative; m_0 = initial dry ash free weight in mg; Q = heat flow in mW; T = temperature in °C.

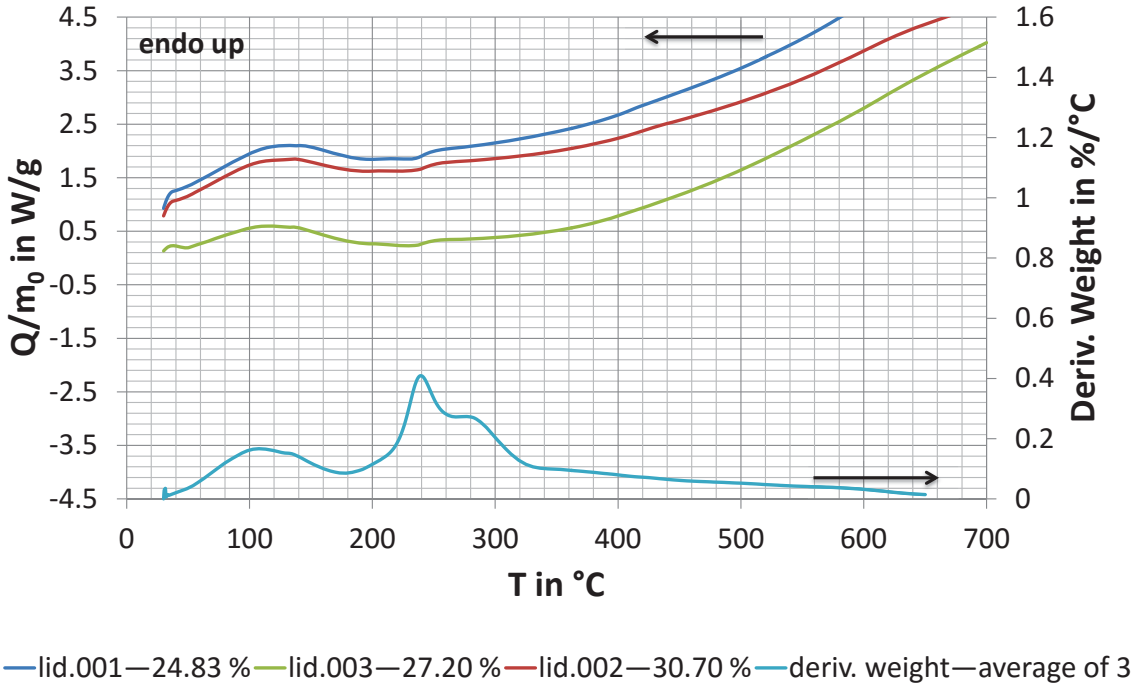

Figure D-13. Raw heat flow data of pine sawdust impregnated with 5 % (wt/wt) Mg pyrolysed in crucibles with a lid. The secondary y-axis shows the corresponding average derivative weight-loss curve. Legend: sample name—char yield at 695 °C in % (wt/wt) daf. daf = dry ash free; deriv. = derivative; m_0 = initial dry ash free weight in mg; Q = heat flow in mW; T = temperature in °C.

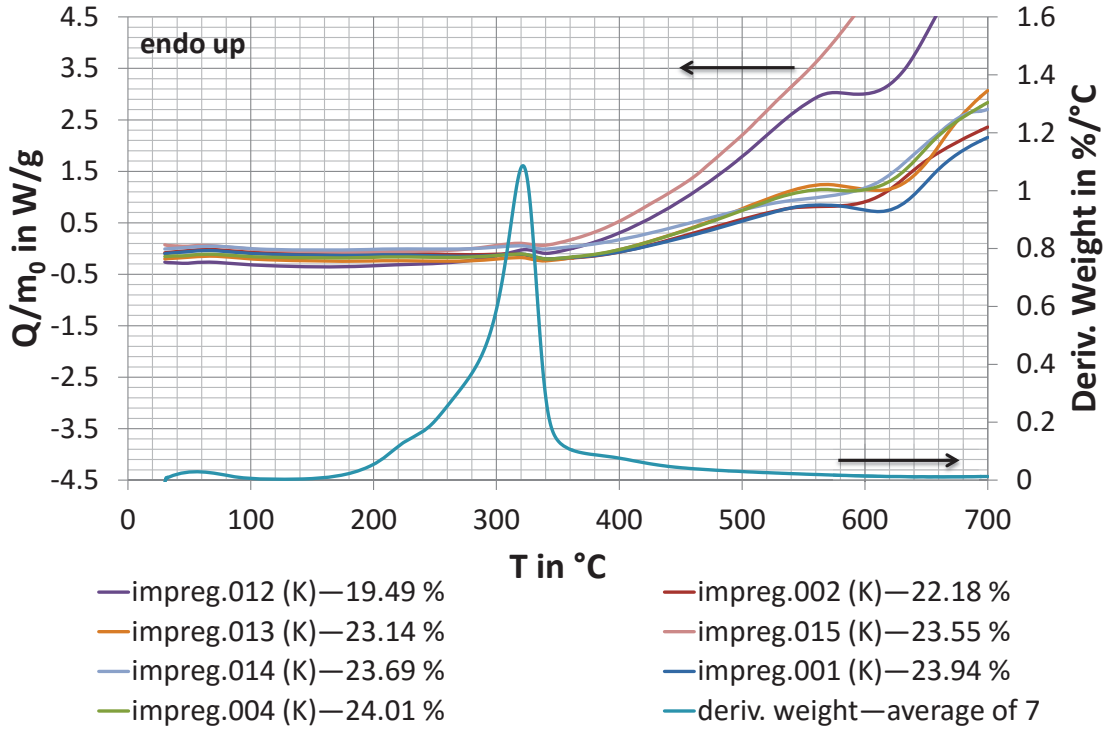

Figure D-14. Raw heat flow data of pine sawdust impregnated with 2 % (wt/wt) K pyrolysed in crucibles without a lid. The secondary y-axis shows the corresponding average derivative weight-loss curve. Legend: sample name—char yield at 695 °C in % (wt/wt) daf. daf = dry ash free; deriv. = derivative; m_0 = initial dry ash free weight in mg; Q = heat flow in mW; T = temperature in °C.

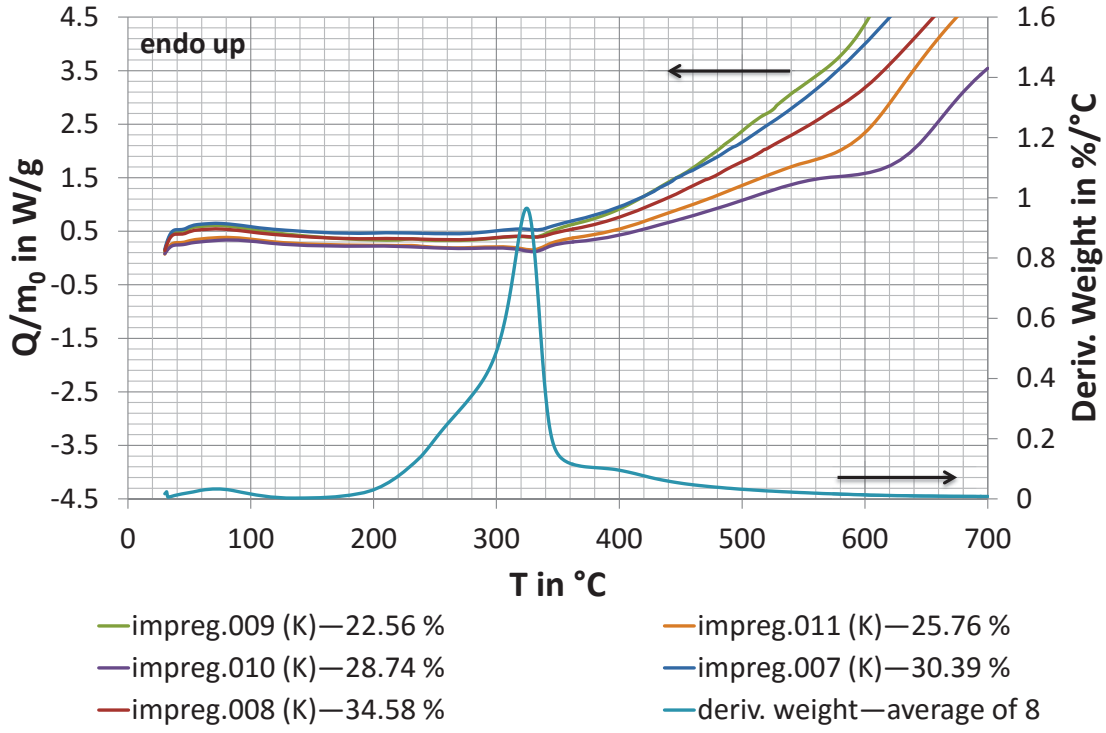

Figure D-15. Raw heat flow data of pine sawdust impregnated with 2 % (wt/wt) K pyrolysed in crucibles with a lid. The secondary y-axis shows the corresponding average derivative weight-loss curve. Legend: sample name—char yield at 695 °C in % (wt/wt) daf. daf = dry ash free; deriv. = derivative; m_0 = initial dry ash free weight in mg; Q = heat flow in mW; T = temperature in °C.

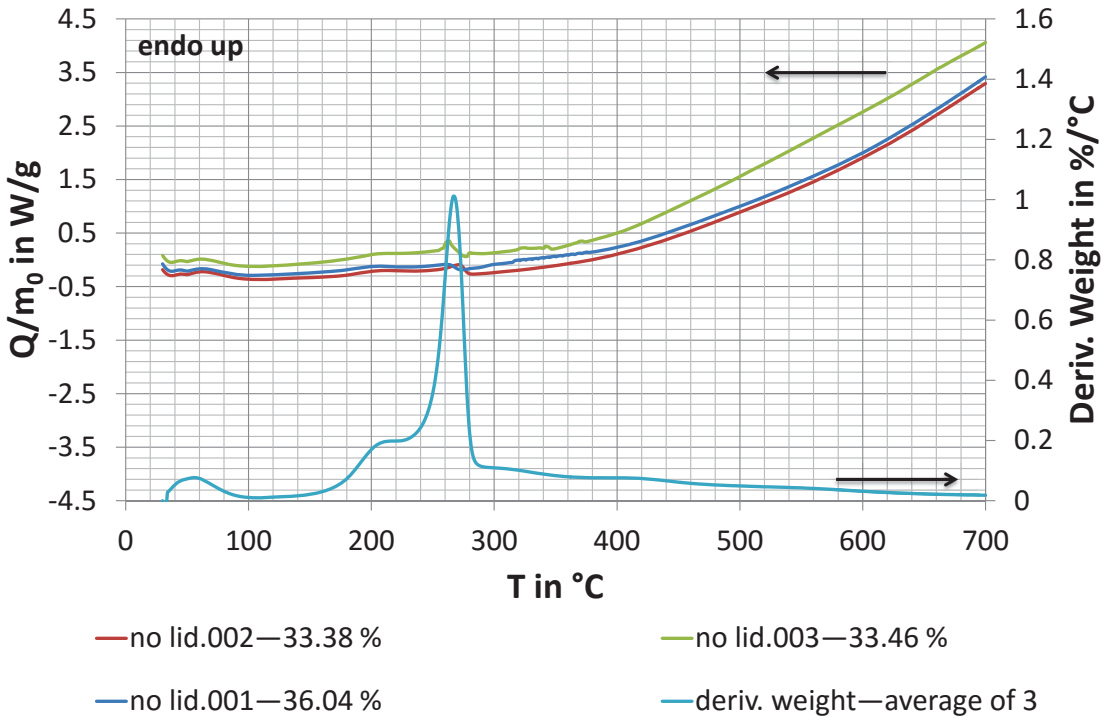

Figure D-16. Raw heat flow data of pine sawdust impregnated with 1.75 % (wt/wt) P pyrolysed in crucibles without a lid. The secondary y-axis shows the corresponding average derivative weight-loss curve. Legend: sample name—char yield at 695 °C in % (wt/wt) daf. daf = dry ash free; deriv. = derivative; m_0 = initial dry ash free weight in mg; Q = heat flow in mW; T = temperature in °C.

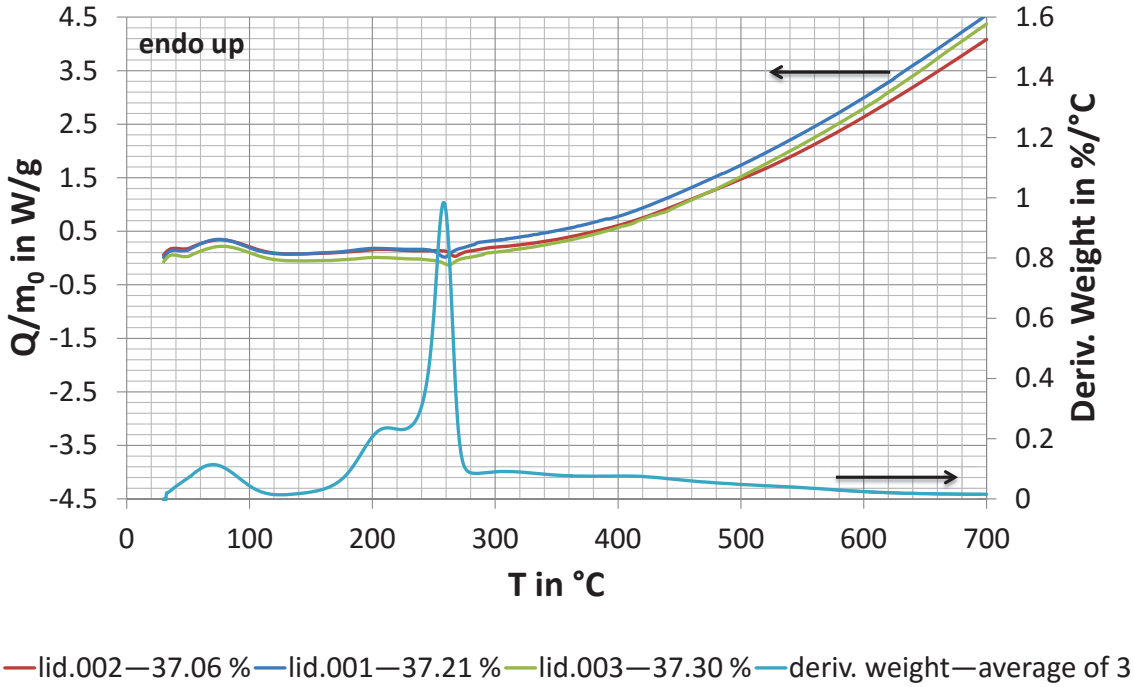

Figure D-17. Raw heat flow data of pine sawdust impregnated with 1.75 % (wt/wt) P pyrolysed in crucibles with a lid. The secondary y-axis shows the corresponding average derivative weight-loss curve. Legend: sample name—char yield at 695 °C in % (wt/wt) daf. daf = dry ash free; deriv. = derivative; m_0 = initial dry ash free weight in mg; Q = heat flow in mW; T = temperature in °C.

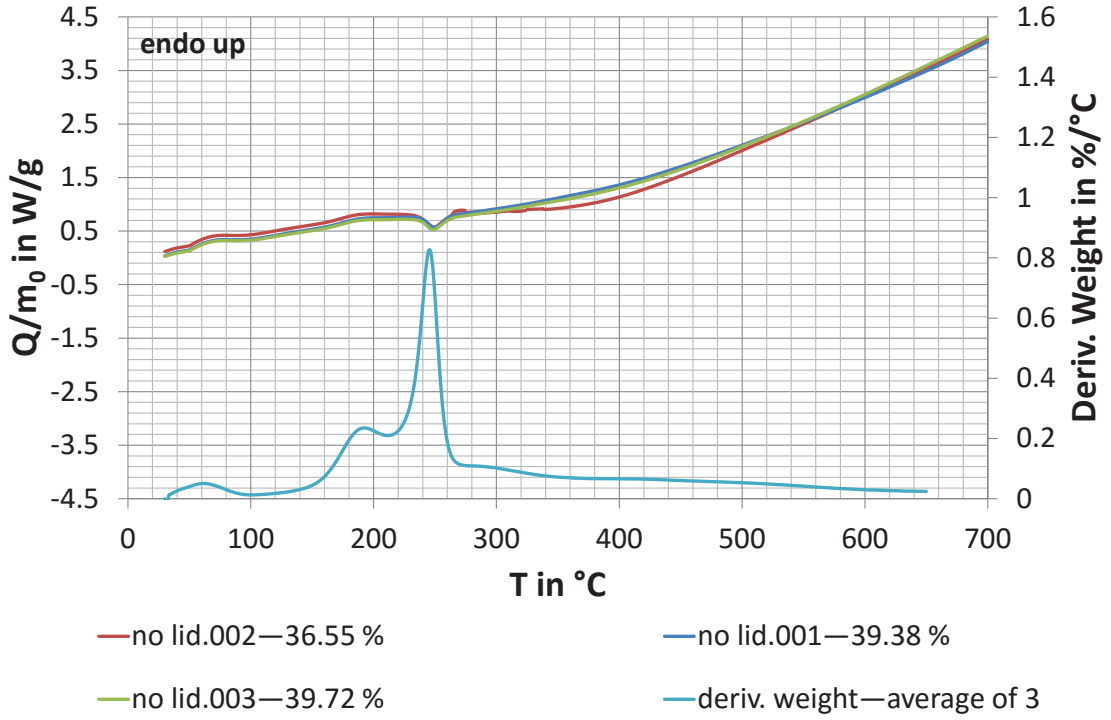

Figure D-18. Raw heat flow data of pine sawdust impregnated with 4.25 % (wt/wt) P pyrolysed in crucibles without a lid. The secondary y-axis shows the corresponding average derivative weight-loss curve. Legend: sample name—char yield at 695 °C in % (wt/wt) daf. daf = dry ash free; deriv. = derivative; m_0 = initial dry ash free weight in mg; Q = heat flow in mW; T = temperature in °C.

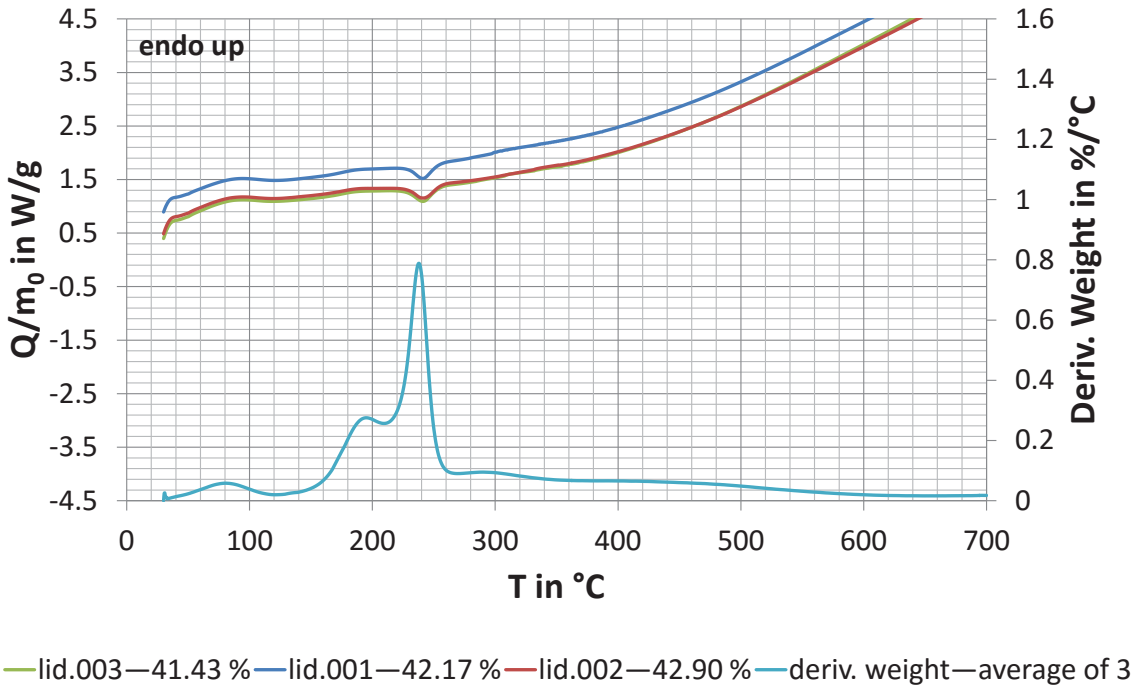

Figure D-19. Raw heat flow data of pine sawdust impregnated with 4.25 % (wt/wt) P pyrolysed in crucibles with a lid. The secondary y-axis shows the corresponding average derivative weight-loss curve. Legend: sample name—char yield at 695 °C in % (wt/wt) daf. daf = dry ash free; deriv. = derivative; m_0 = initial dry ash free weight in mg; Q = heat flow in mW; T = temperature in °C.

Appendix E Effect of Autogenous Pressure on Volatile Pyrolysis Products

E.1 Pyrograms of Open Crucible Experiments

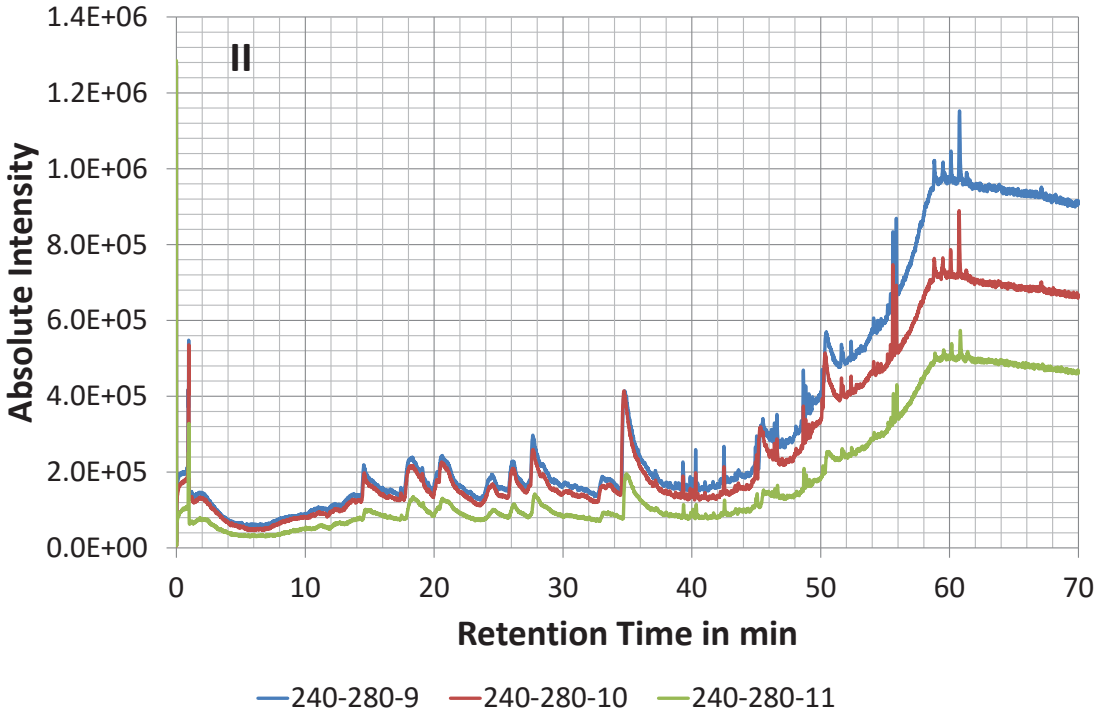

Figure E-1. Pyrograms of pine sawdust volatile fraction released between 240 to 280 °C. A compound list is given in the provided Excel file in E.3 in the sheet "pine240-280-10". The Roman numeral in the top left corner refers to the pyrolysis zone defined in Figure 3-45 in 3.3.7. Legend: start temperature in °C-highest treatment temperature in °C-run number.

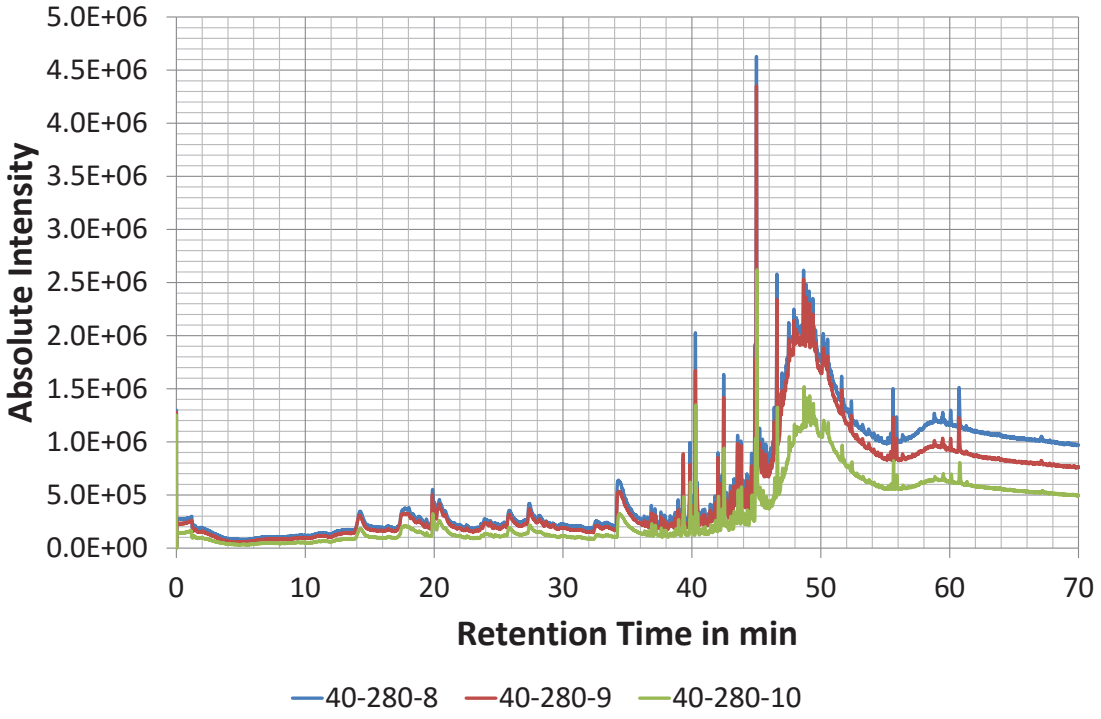

Figure E-2. Pyrograms of pine sawdust heated in open crucibles from 40 to 280 °C. Legend: start temperature in °C-highest treatment temperature in °C-run number.

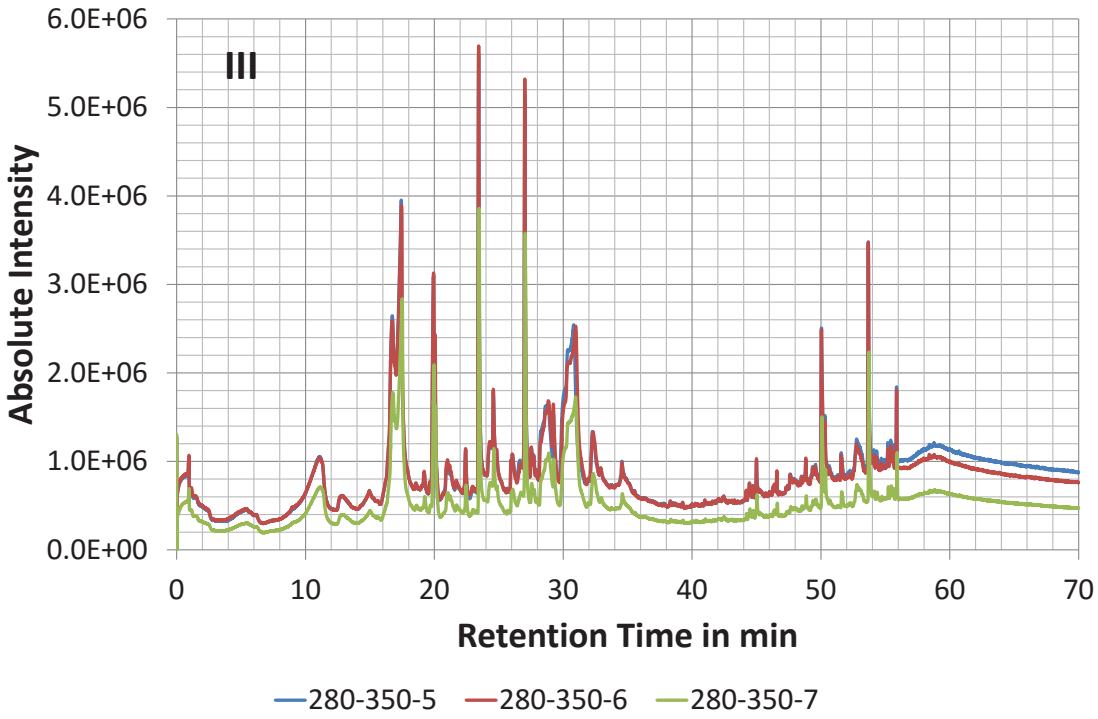

Figure E-3. Pyrograms of pine sawdust volatile fraction released between 280 to 350 °C. A compound list is given in the provided Excel file in E.3 in the sheet "pine280-350-5". The Roman numeral in the top left corner refers to the pyrolysis zone defined in Figure 3-45 in 3.3.7. Legend: start temperature in °C-highest treatment temperature in °C-run number.

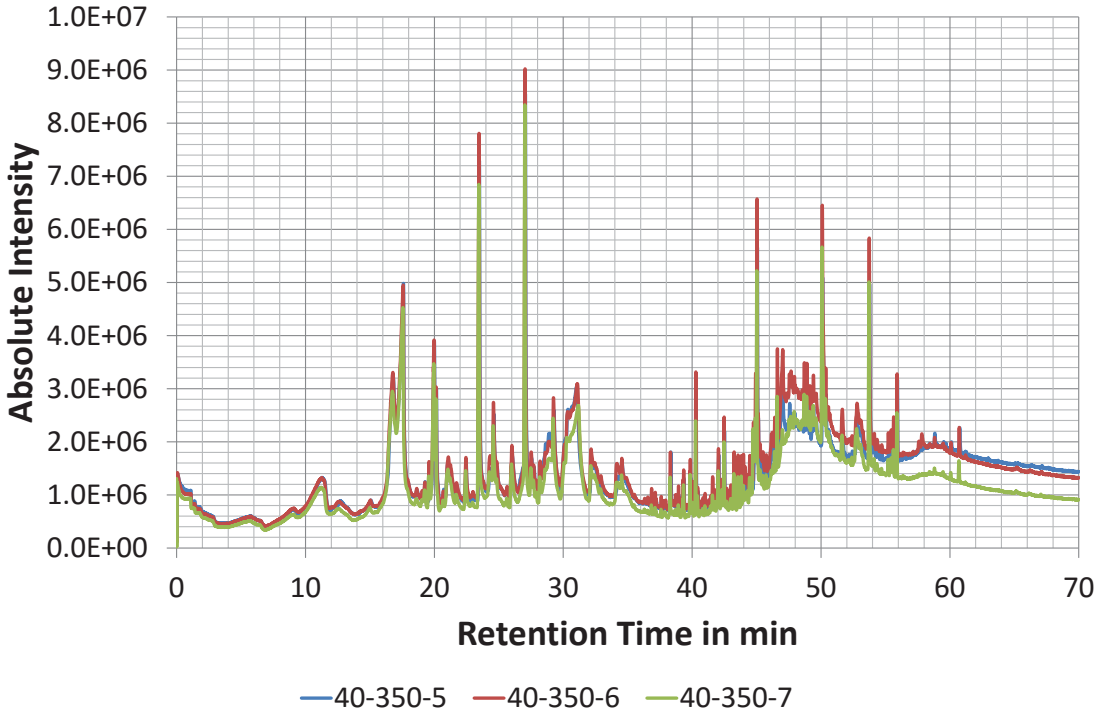

Figure E-4. Pyrograms of pine sawdust heated in open crucibles from 40 to 350 °C. A compound list is given in the provided Excel file in E.3 in the sheet "pine350-5". Legend: start temperature in °C-highest treatment temperature in °C-run number.

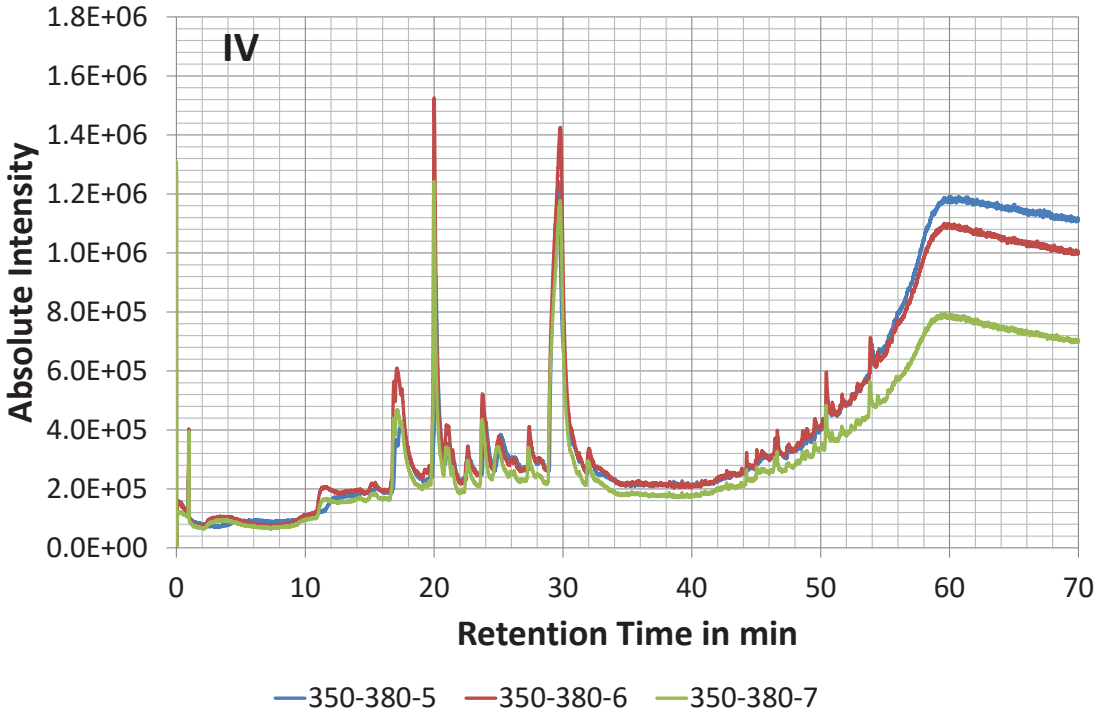

Figure E-5. Pyrograms of pine sawdust volatile fraction released between 350 to 380 °C. A compound list is given in the provided Excel file in E.3 in the sheet "pine350-380-6". The Roman numeral in the top left corner refers to the pyrolysis zone defined in Figure 3-45 in 3.3.7. Legend: start temperature in °C-highest treatment temperature in °C-run number.

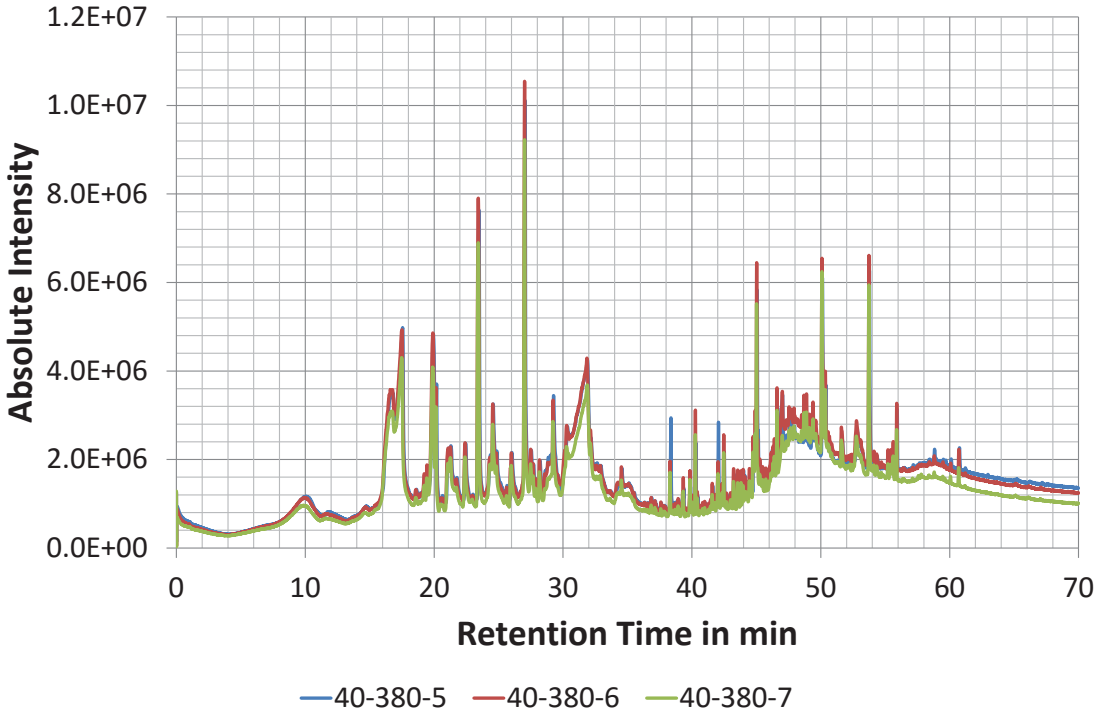

Figure E-6. Pyrograms of pine sawdust heated in open crucibles from 40 to 380 °C. A compound list is given in the provided Excel file in E.3 in the sheet "pine380-5". Legend: start temperature in °C-highest treatment temperature in °C-run number.

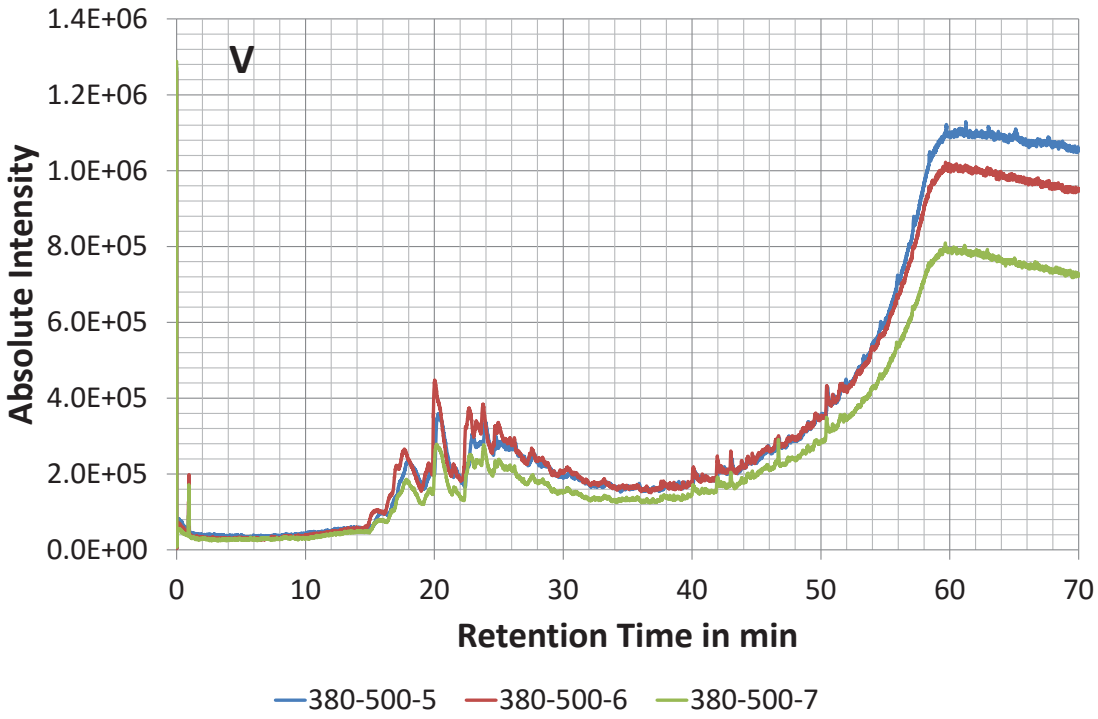

Figure E-7. Pyrograms of pine sawdust volatile fraction released between 380 to 500 °C. A compound list is given in the provided Excel file in E.3 in the sheet "pine380-500-5". The Roman numeral in the top left corner refers to the pyrolysis zone defined in Figure 3-45 in 3.3.7. Legend: start temperature in °C-highest treatment temperature in °C-run number.

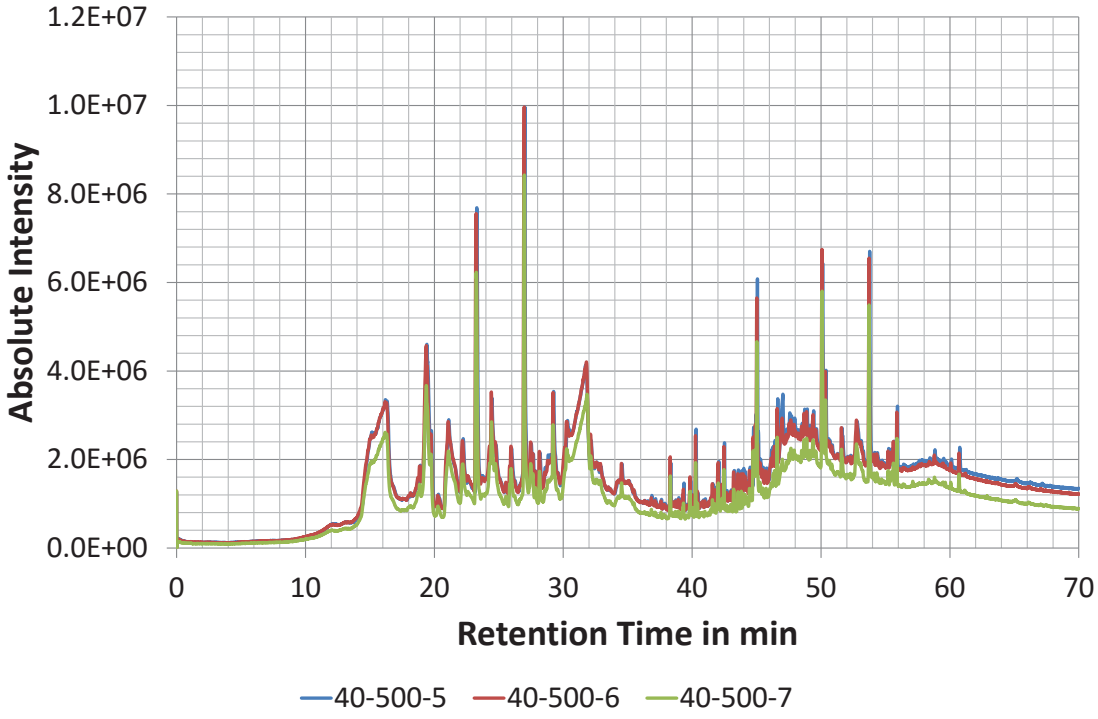

Figure E-8. Pyrograms of pine sawdust heated in open crucibles from 40 to 500 °C. A compound list is given in the provided Excel file in E.3 in the sheet "pine500-5". Legend: start temperature in °C-highest treatment temperature in °C-run number.

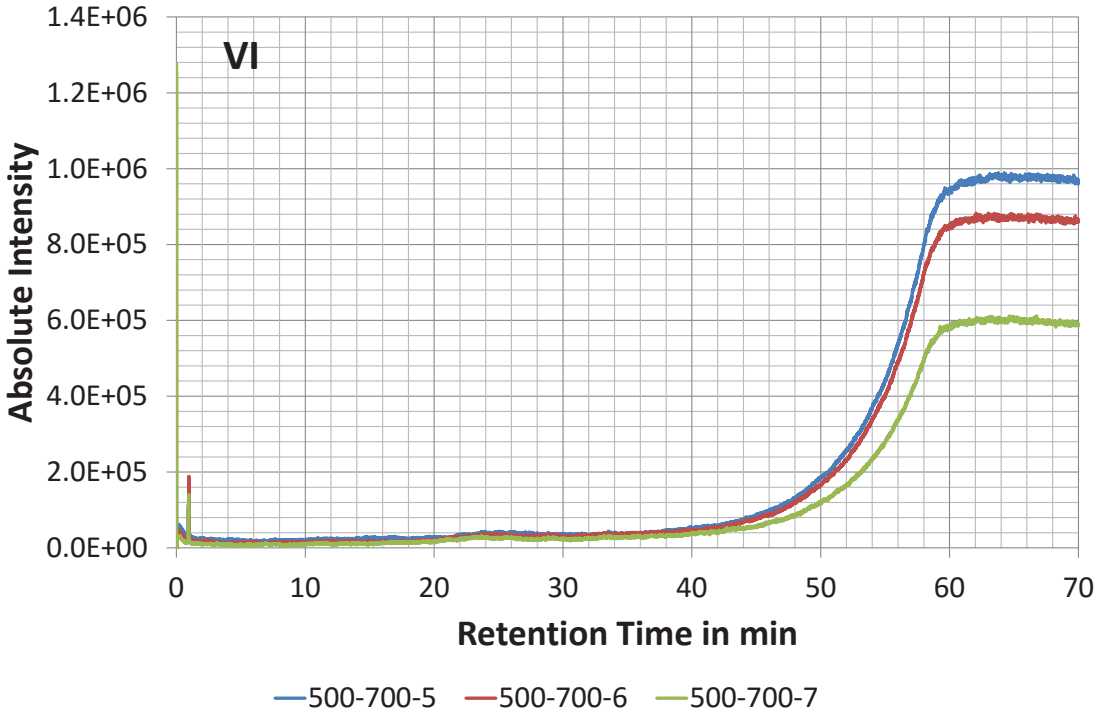

Figure E-9. Pyrograms of pine sawdust volatile fraction released between 500 to 700 °C. A compound list is given in the provided Excel file in E.3 in the sheet "pine500-700-5". The Roman numeral in the top left corner refers to the pyrolysis zone defined in Figure 3-45 in 3.3.7. Legend: start temperature in °C-highest treatment temperature in °C-run number.

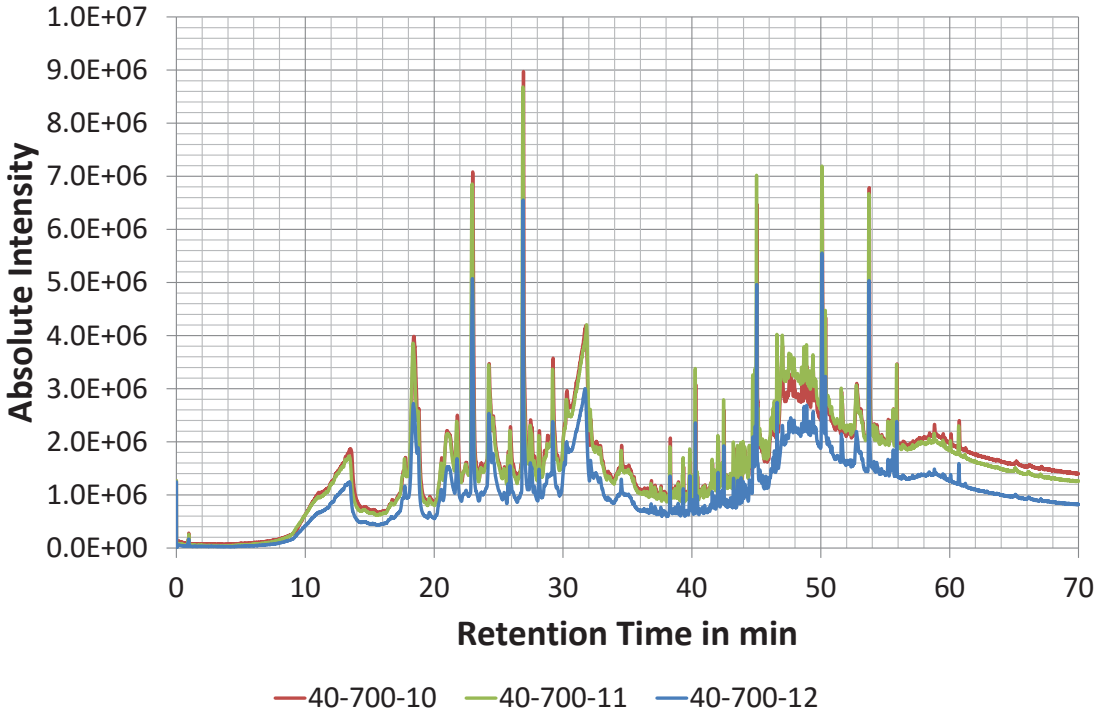

Figure E-10. Pyrograms of pine sawdust heated in open crucible from 40 to 700 °C. A compound list is given in the provided Excel file in E.3 in the sheet "pine700-10". Legend: start temperature in °C-highest treatment temperature in °C-run number.

E.2 Pyrograms of Sealed Glass Capsule Experiments

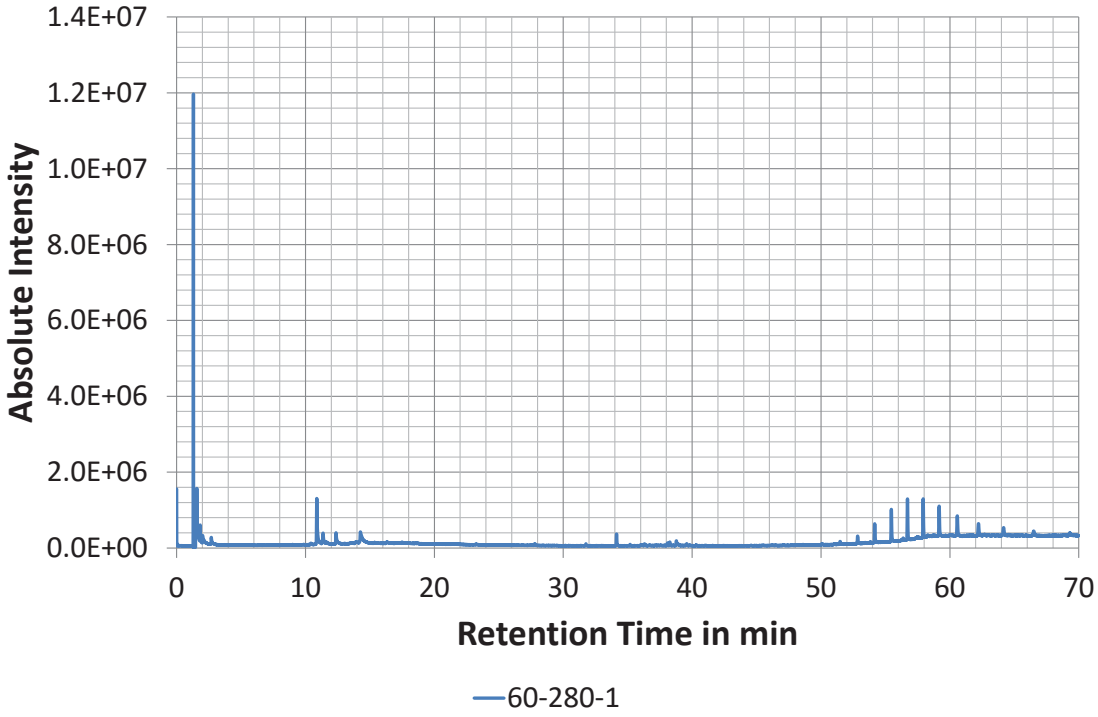

Figure E-11. Pyrogram of pine sawdust heated in a sealed glass capsule from 60 to 280 °C. A compound list is given in the provided Excel file in E.3 in the sheet "A (60-280-1)". Legend: start temperature in °C-highest treatment temperature in °C-run number.

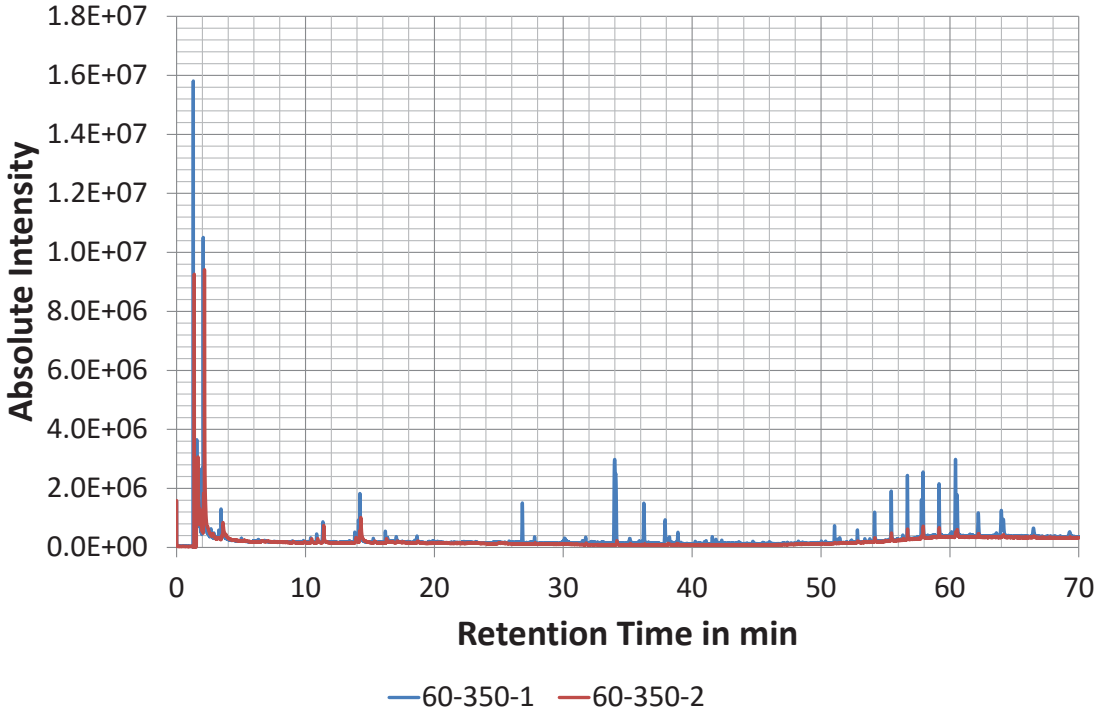

Figure E-12. Pyrograms of pine sawdust heated in a sealed glass capsule from 60 to 350 °C. A compound list is given in the provided Excel file in E.3 in the sheet "A (60-350-1)" and "A (60-350-2)" for run "60-350-1" and "60-350-2" respectively. Legend: start temperature in °C-highest treatment temperature in °C-run number.

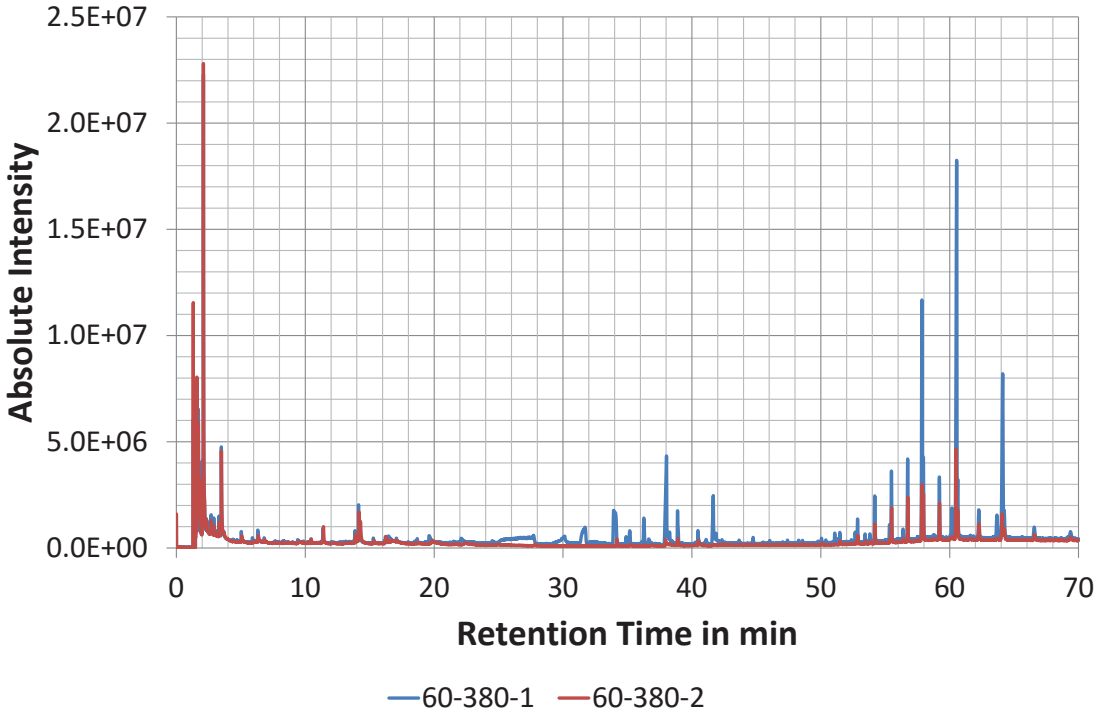

Figure E-13. Pyrograms of pine sawdust heated in a sealed glass capsule from 60 to 380 °C. A compound list is given in the provided Excel file in E.3 in the sheet "A (60-380-1)" and "A (60-380-2)" for run "60-380-1" and "60-380-2" respectively. Legend: start temperature in °C-highest treatment temperature in °C-run number.

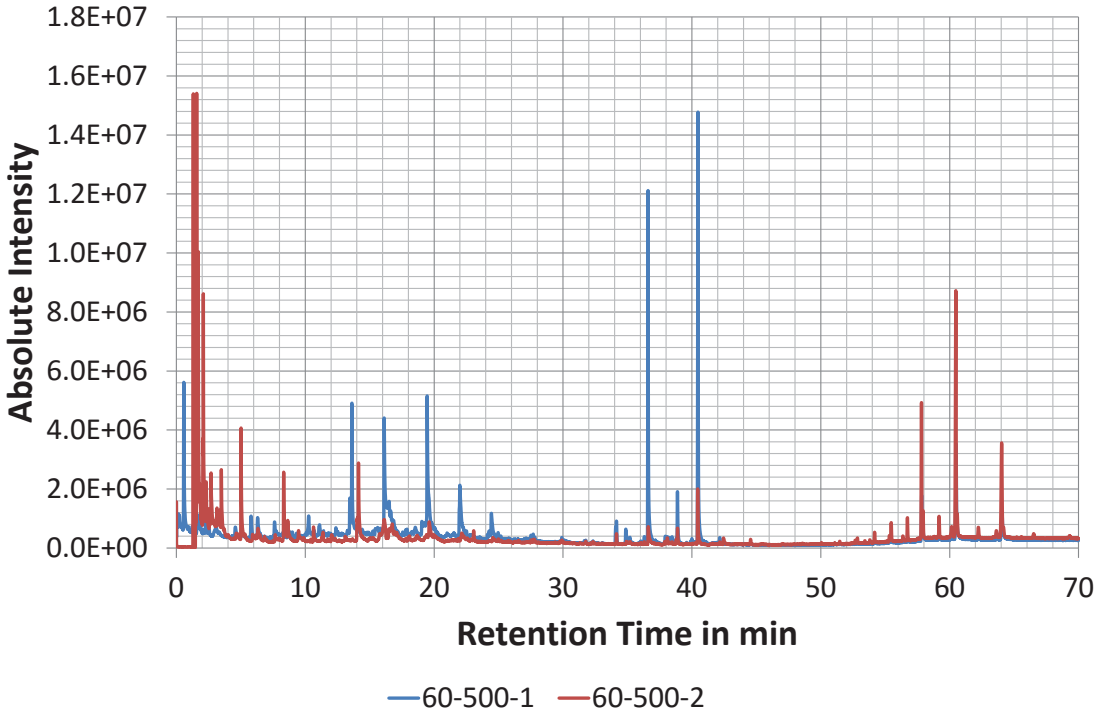

Figure E-14. Pyrograms of pine sawdust heated in a sealed glass capsule from 60 to 500 °C. A compound list is given in the provided Excel file in E.3 in the sheet "A (60-500-1)" and "A (60-500-2)" for run "60-500-1" and "60-500-2" respectively. Legend: start temperature in °C-highest treatment temperature in °C-run number.

E.3 Compound Identification of Pyrograms

The identified compounds are listed in the Excel file “Compound Identification.xlsx” that can be found on the provided CD in the location chapter 6/data/Py-GCMS.

The pyrograms, as recorded by the equipment, can be found on the provided CD in the location chapter 6/data/Py-GCMS/Pyrograms.

E.4 Record Numbers

The respective record numbers can be found on the provided CD in the location chapter 6/data/endnote in the endnotefile “Biochar Pyrolysis Engineering.enl”.

Appendix F Tar-char/ Coke *versus* Wood-char/ Charcoal

F.1 SEM Micrographs

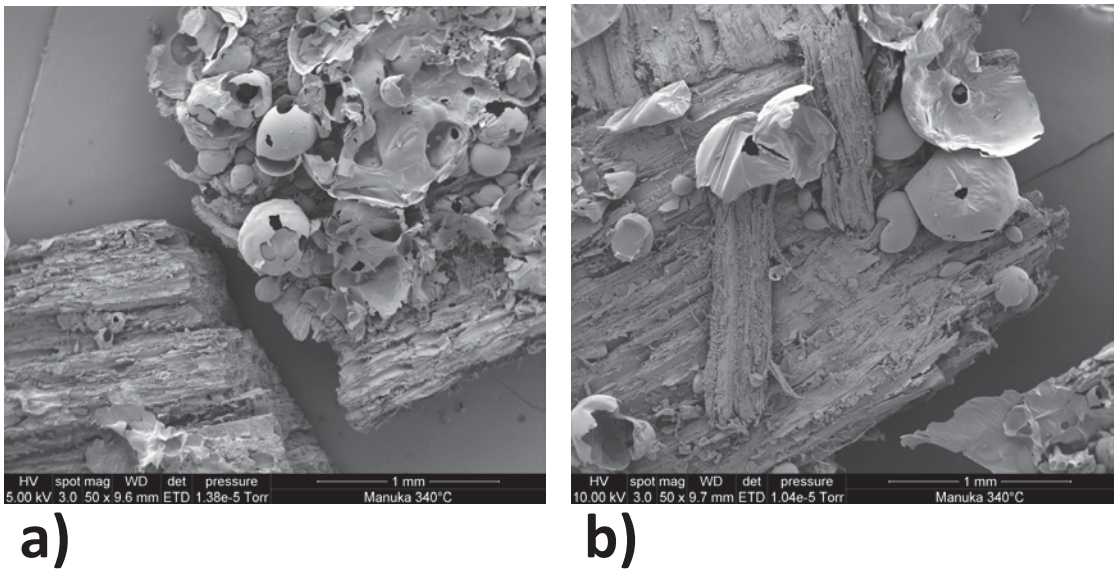

Figure F-1. SEM micrographs of coke bubbles on Manuka bisquettes pyrolysed on a modified Bradley food smoker at 340 °C. The pyrolysed bisquettes were obtained from Haris (2012). The bubbles were partly broken by energy dispersive X-ray analysis because of their thin walls. SEM = Scanning electron microscope.

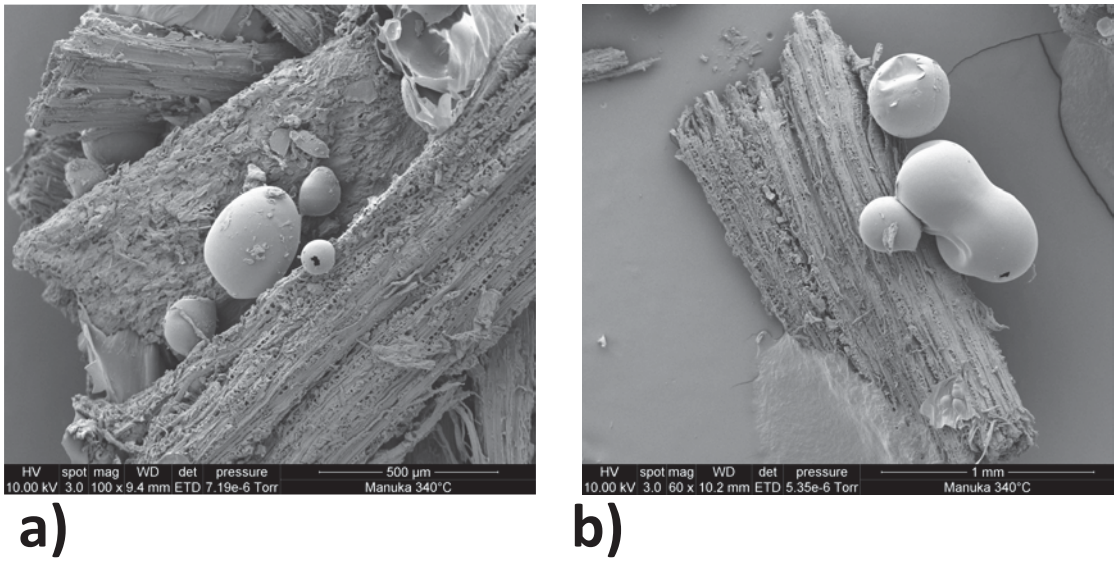

Figure F-2. SEM micrographs of coke bubbles on Manuka bisquettes pyrolysed on a modified Bradley food smoker at 340 °C. The pyrolysed bisquettes were obtained from Haris (2012). SEM = Scanning electron microscope.

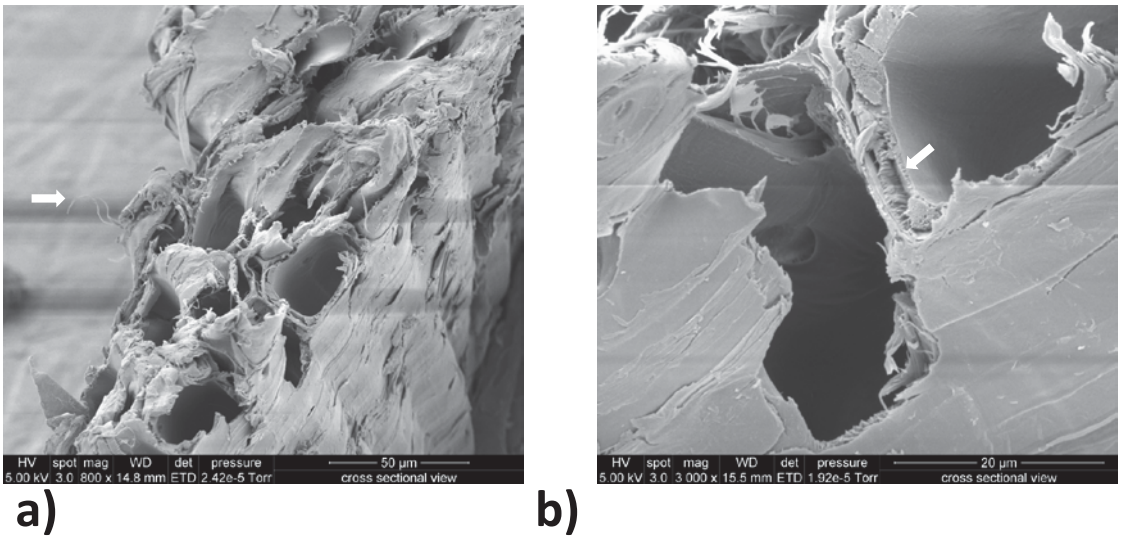

Figure F-3. SEM micrographs of radiata pine wood. a) Cross sectional view of tracheid cell. The white arrow points to a cell wall fibre. b) Magnification of cell wall section. The white arrow points out the fibrous structure of the cell wall. SEM = Scanning electron microscope. Adapted from Caco (2014).

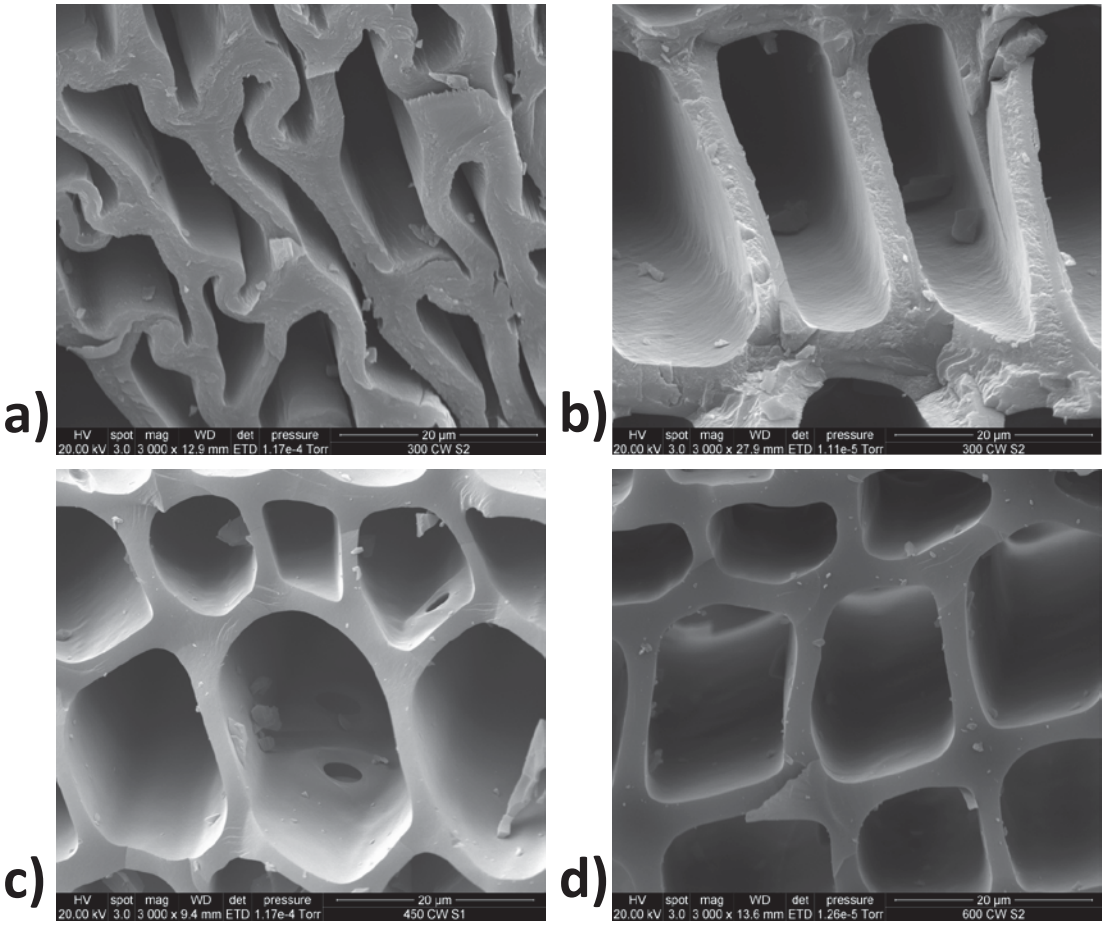

Figure F-4. SEM micrographs of pine-char produced at various HTT. a) and b) Char pyrolysed at 300 °C. c) Char pyrolysed at 450 °C with visible pits. d) Char pyrolysed at 600 °C. HTT = highest treatment temperature; SEM = Scanning electron microscope. Adapted from Caco (2014).

F.2 Yield

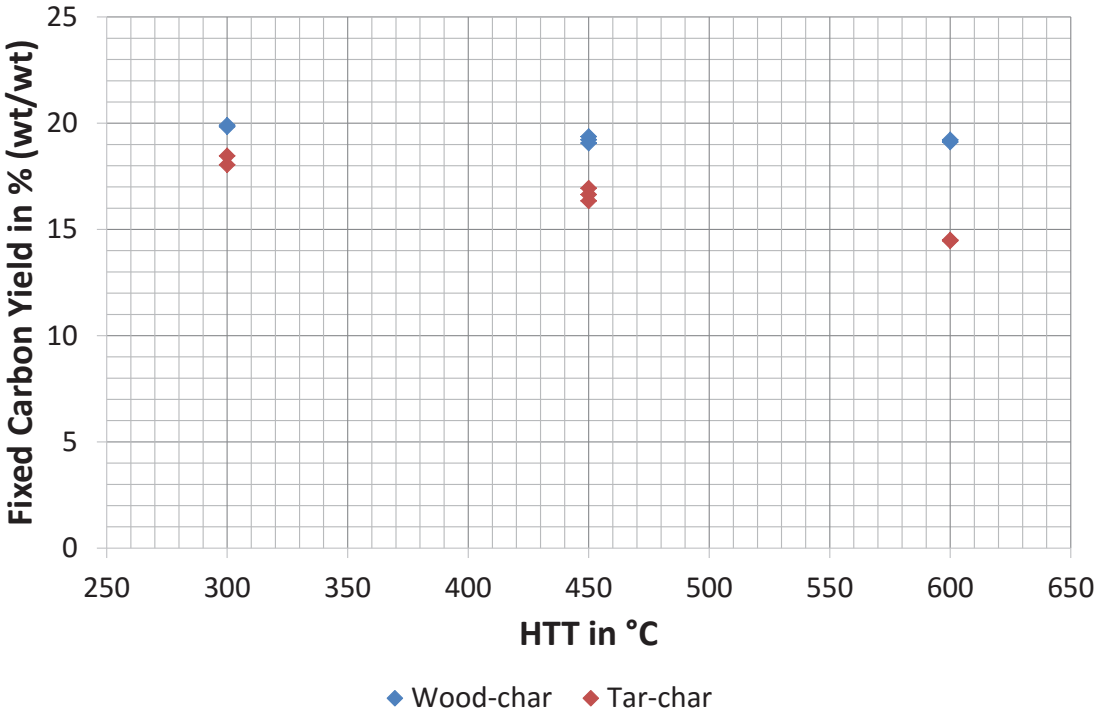

Figure F-5. Comparison of wood-char and tar-char fixed carbon yields. The tar used for producing coke was collected from pine pyrolysis with a HTT of 500 °C. It is important to note that the yield of wood-char and tar-char is calculated based on the initial weight of the wood and tar respectively, and that for calculating the ash content of the feed it was assumed that no inorganics are lost during pyrolysis as the ash content was only measured for the char/ coke. For each experiment one repetition was done except for the run at 450 °C where two repetitions were performed. Adapted from Caco (2014). HTT = highest treatment temperature; wt = weight.

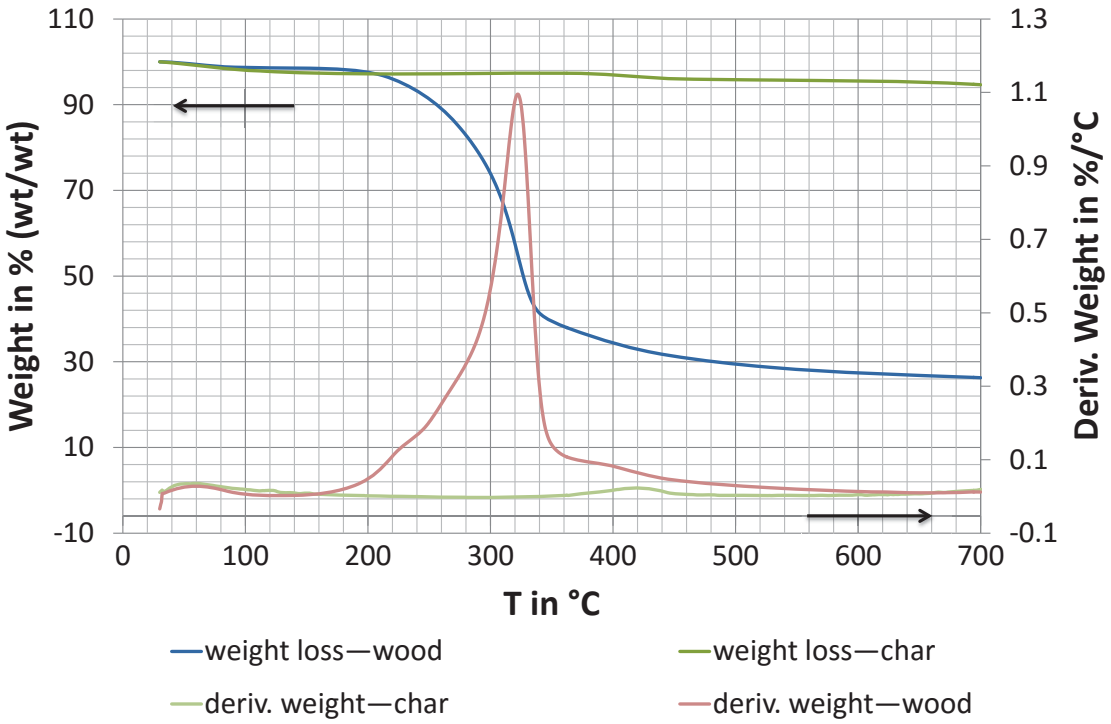

Figure F-6. Weight-loss and derivative weight-loss of pine wood impregnated with 2 % (wt/wt) K and its char pyrolysed in crucibles without a lid. The here depicted experiment is run "impreg.014" in Figure C-1 in Appendix C.1.3 and is representative for the samples pyrolysed under this condition. deriv. = derivative; T = temperature in °C.

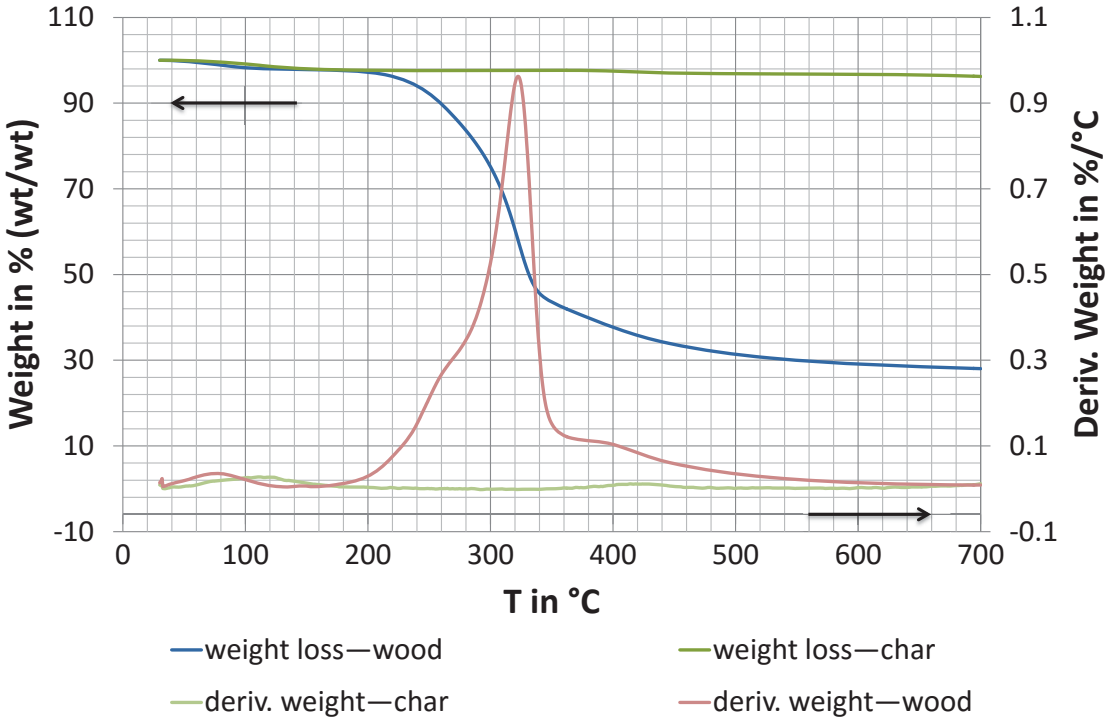

Figure F-7. Weight-loss and derivative weight-loss of pine wood impregnated with 2 % (wt/wt) K and its char pyrolysed in crucibles with a lid. The here depicted experiment is run "impreg.011" in Figure C-2 in Appendix C.1.3 and is representative for the samples pyrolysed under this condition. deriv. = derivative; T = temperature in °C.

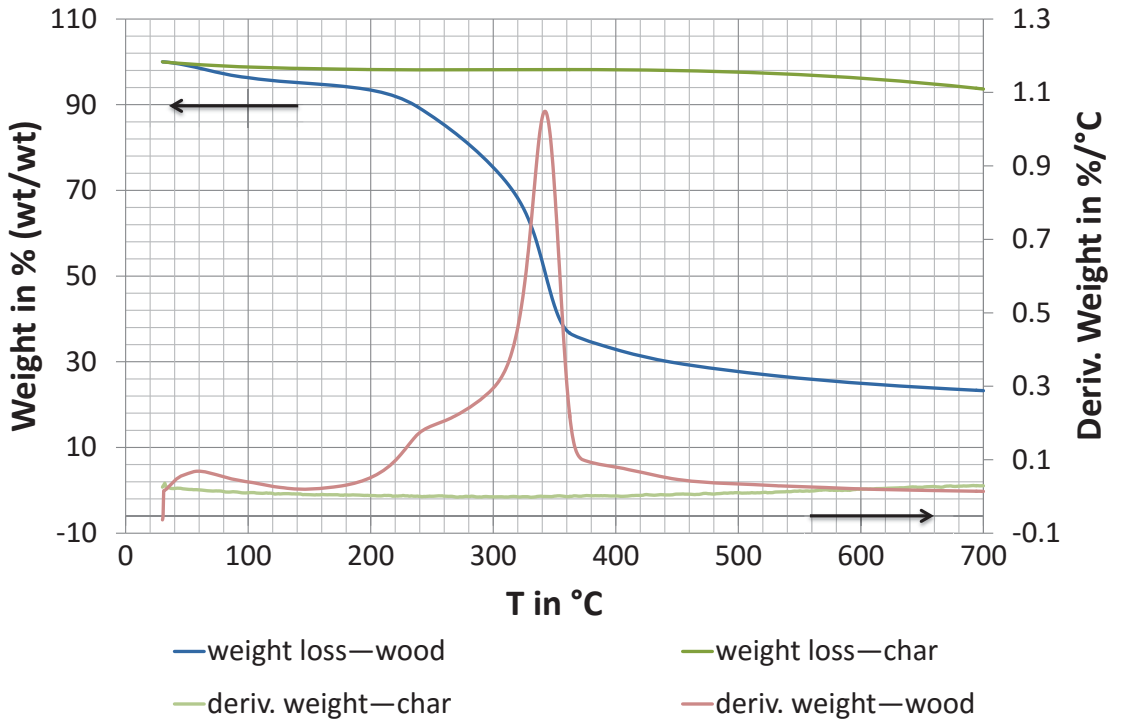

Figure F-8. Weight-loss and derivative weight-loss of pine wood impregnated with 2 % (wt/wt) Mg and its char pyrolysed in crucibles without a lid. The here depicted experiment is run "no lid.002" in Figure C-3 in Appendix C.1.5 and is representative for the samples pyrolysed under this condition. deriv. = derivative; T = temperature in °C.

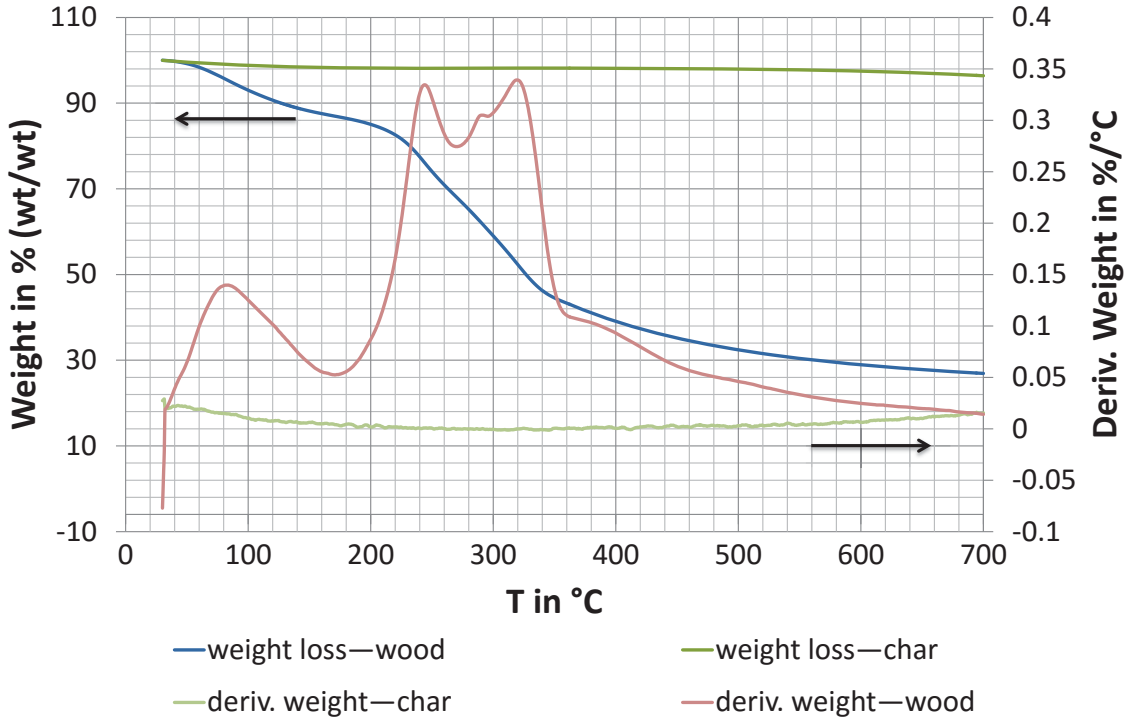

Figure F-9. Weight-loss and derivative weight-loss of pine wood impregnated with 2 % (wt/wt) Mg and its char pyrolysed in crucibles with a lid. The here depicted experiment is run "lid.001" in Figure C-4 in Appendix C.1.5 and is representative for the samples pyrolysed under this condition. deriv. = derivative; T = temperature in °C.

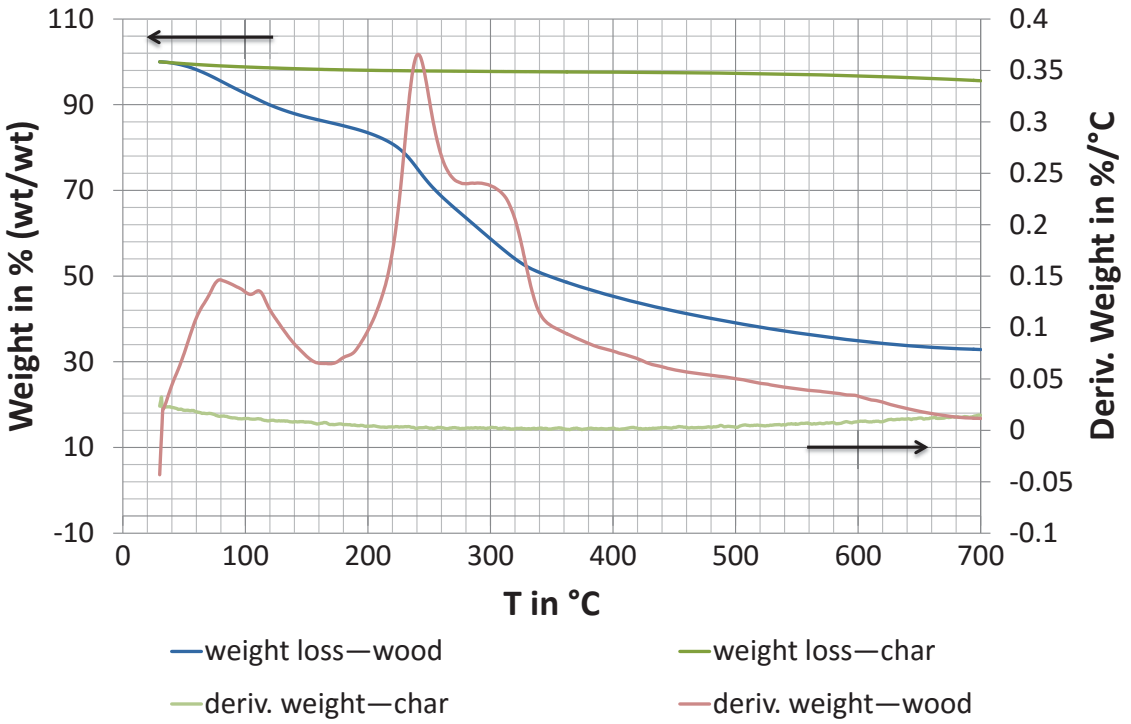

Figure F-10. Weight-loss and derivative weight-loss of pine wood impregnated with 5 % (wt/wt) Mg and its char pyrolysed in crucibles without a lid. The here depicted experiment is run "no lid.001" in Figure C-5 in Appendix C.1.5 and is representative for the samples pyrolysed under this condition. deriv. = derivative; T = temperature in °C.

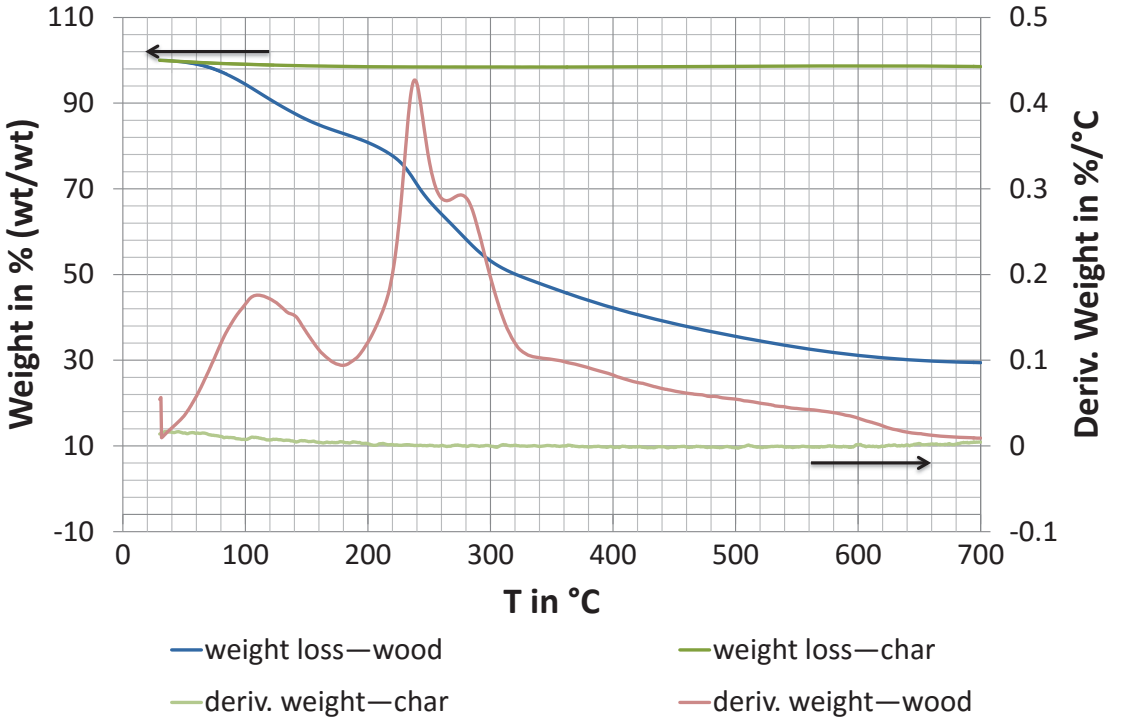

Figure F-11. Weight-loss and derivative weight-loss of pine wood impregnated with 5 % (wt/wt) Mg and its char pyrolysed in crucibles with a lid. The here depicted experiment is run "lid.001" in Figure C-6 in Appendix C.1.5 and is representative for the samples pyrolysed under this condition. deriv. = derivative; T = temperature in °C.

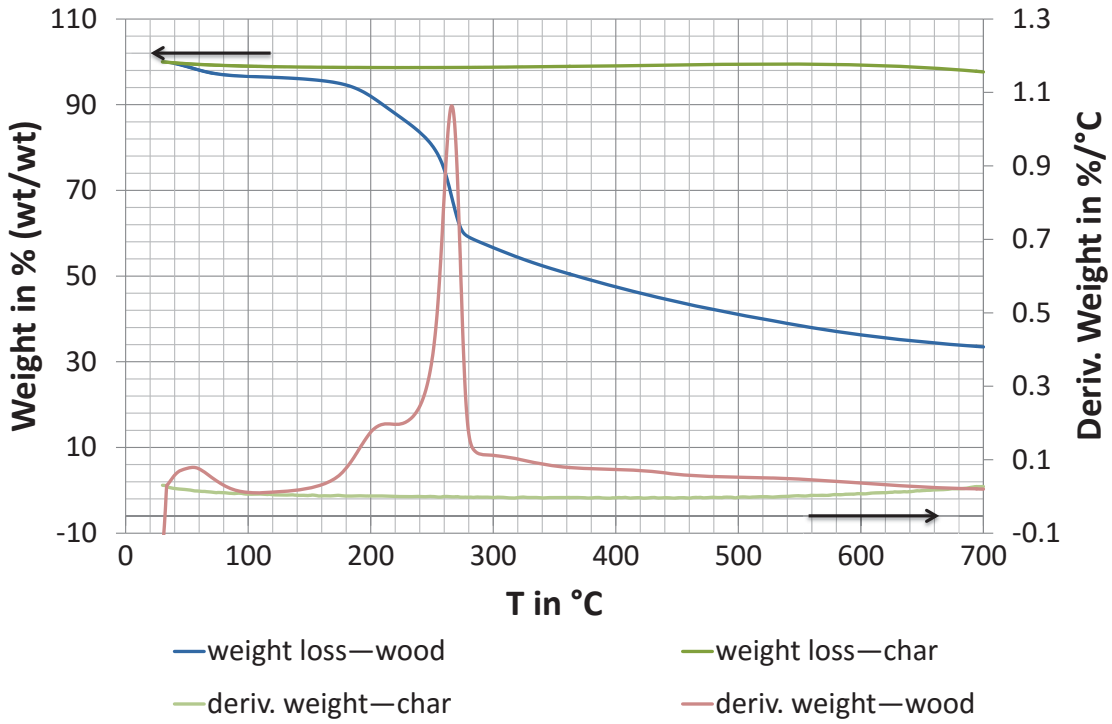

Figure F-12. Weight-loss and derivative weight-loss of pine wood impregnated with 1.75 % (wt/wt) P and its char pyrolysed in crucibles without a lid. The here depicted experiment is run "no lid.003" in Figure C-11 in Appendix C.2.1 and is representative for the samples pyrolysed under this condition. deriv. = derivative; T = temperature in °C.

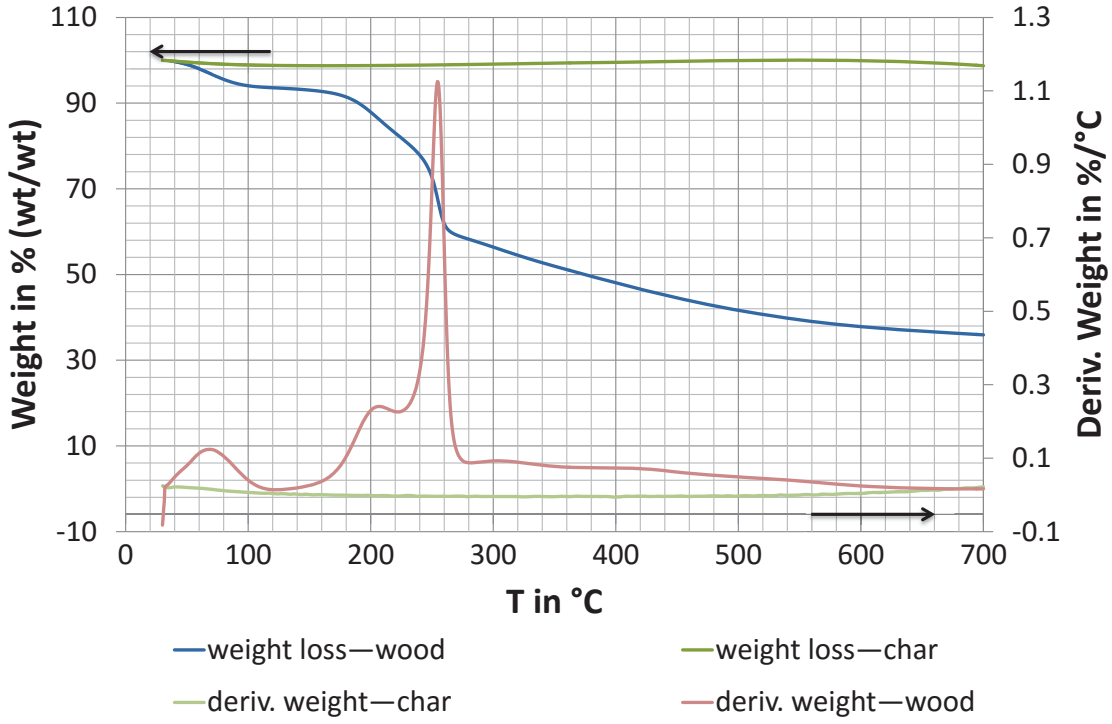

Figure F-13. Weight-loss and derivative weight-loss of pine wood impregnated with 1.75 % (wt/wt) P and its char pyrolysed in crucibles with a lid. The here depicted experiment is run "lid.001" in Figure C-12 in Appendix C.2.1 and is representative for the samples pyrolysed under this condition. deriv. = derivative; T = temperature in °C.

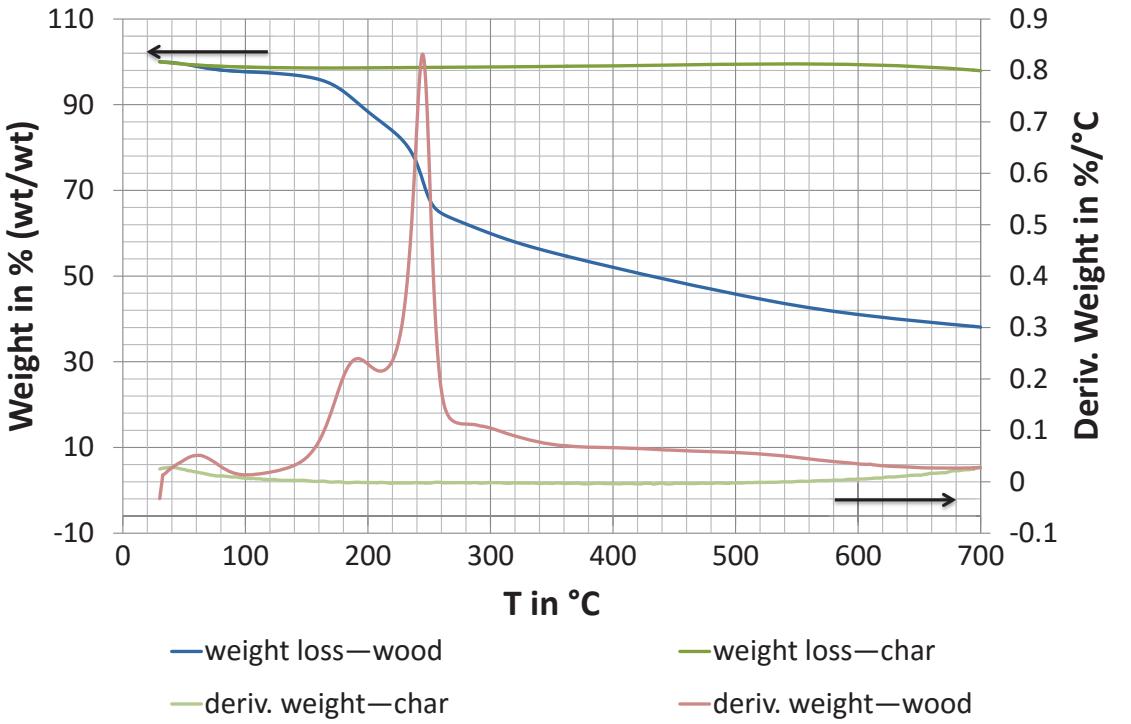

Figure F-14. Weight-loss and derivative weight-loss of pine wood impregnated with 4.25 % (wt/wt) P and its char pyrolysed in crucibles without a lid. The here depicted experiment is run "no lid.002" in Figure C-13 in Appendix C.2.1 and is representative for the samples pyrolysed under this condition. deriv. = derivative; T = temperature in °C.

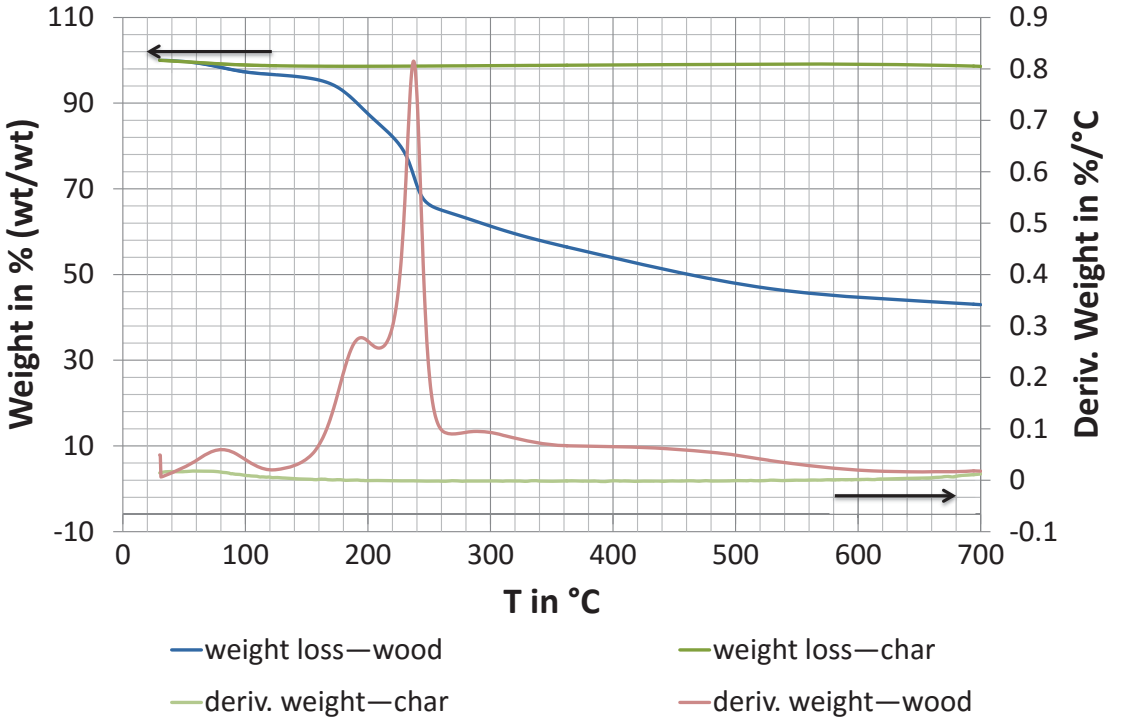

Figure F-15. Weight-loss and derivative weight-loss of pine wood impregnated with 4.25 % (wt/wt) P and its char pyrolysed in crucibles with a lid. The here depicted experiment is run "lid.001" in Figure C-14 in Appendix C.2.1 and is representative for the samples pyrolysed under this condition. deriv. = derivative; T = temperature in °C.

F.3 Temperature Profile

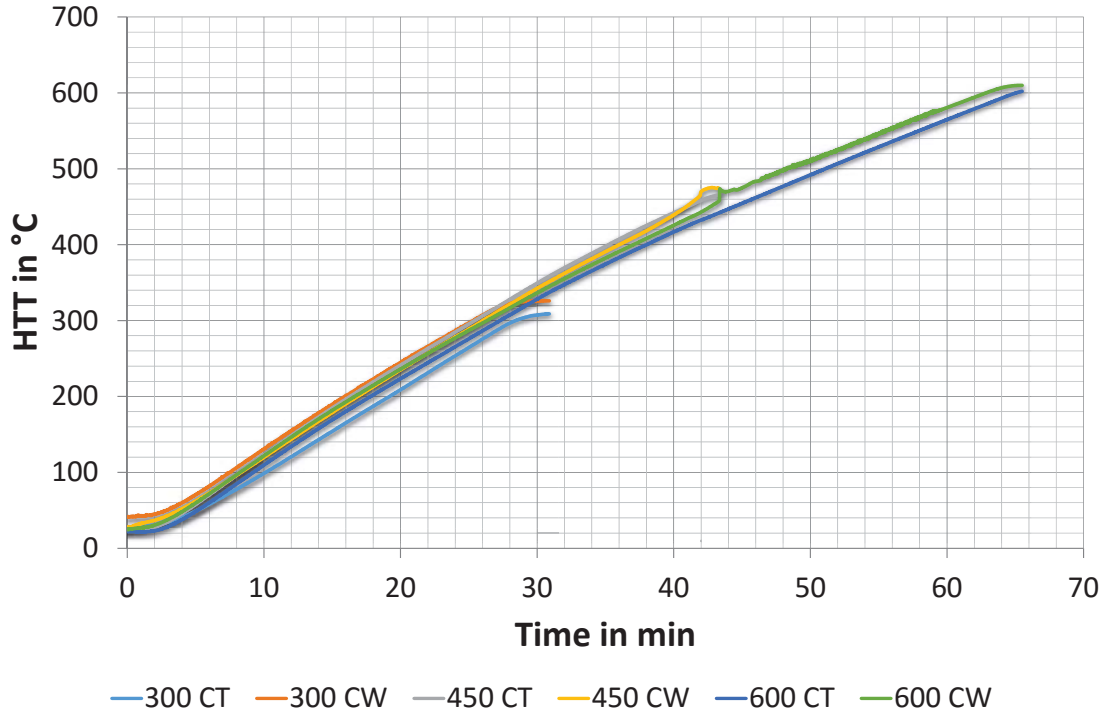

Figure F-16. Recorded furnace temperature profiles from Caco (2014).

F.4 Ultimate Analysis

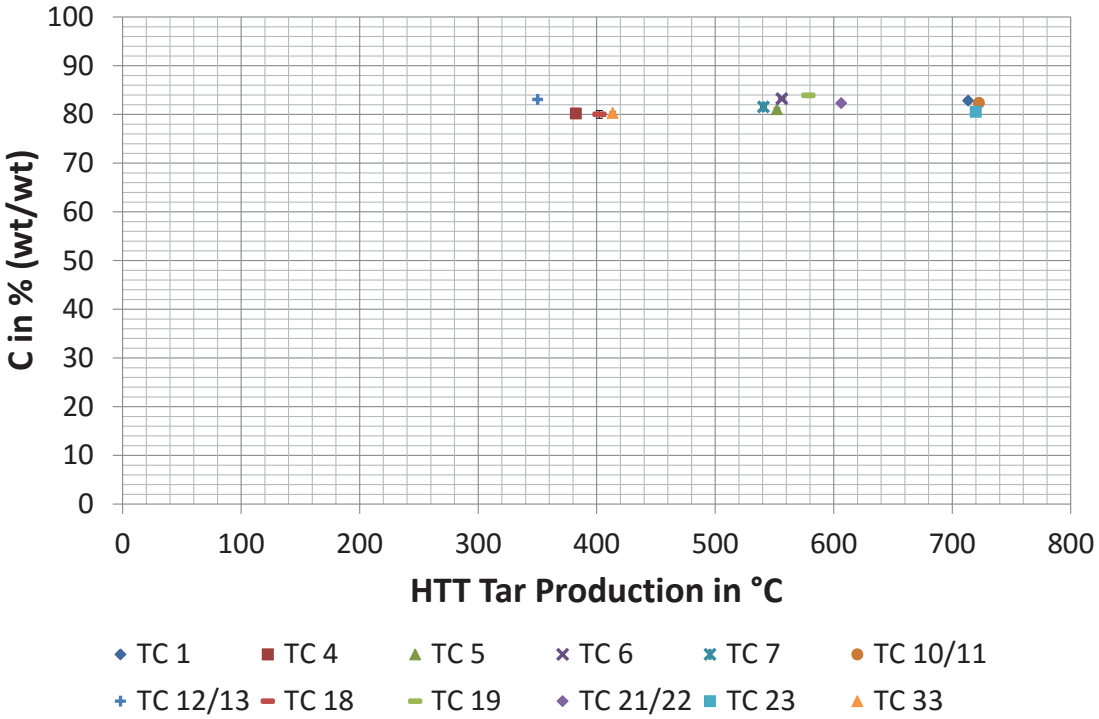

Figure F-17. Carbon content of tar-char produced at 300 °C as a function of the HTT of the tar collection process. The error bars represent the standard deviation. Two repetitions per analysis were done except in a few cases where only enough sample was present for one repeat analysis. C = carbon; HTT = highest treatment temperature; TC = tar-char; wt = weight.

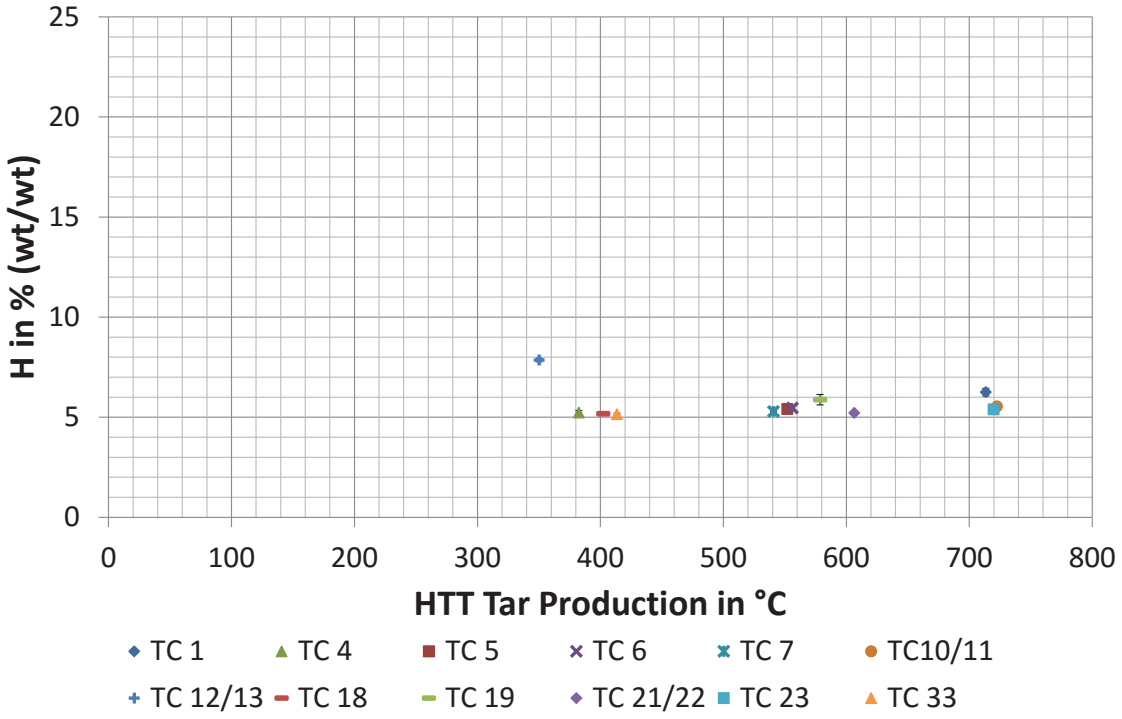

Figure F-18. Hydrogen content of tar-char produced at 300 °C as a function of the HTT of the tar collection process. The error bars represent the standard deviation. Two repetitions per analysis were done except in a few cases where only enough sample was present for one repeat analysis. H = hydrogen; HTT = highest treatment temperature; TC = tar-char; wt = weight.

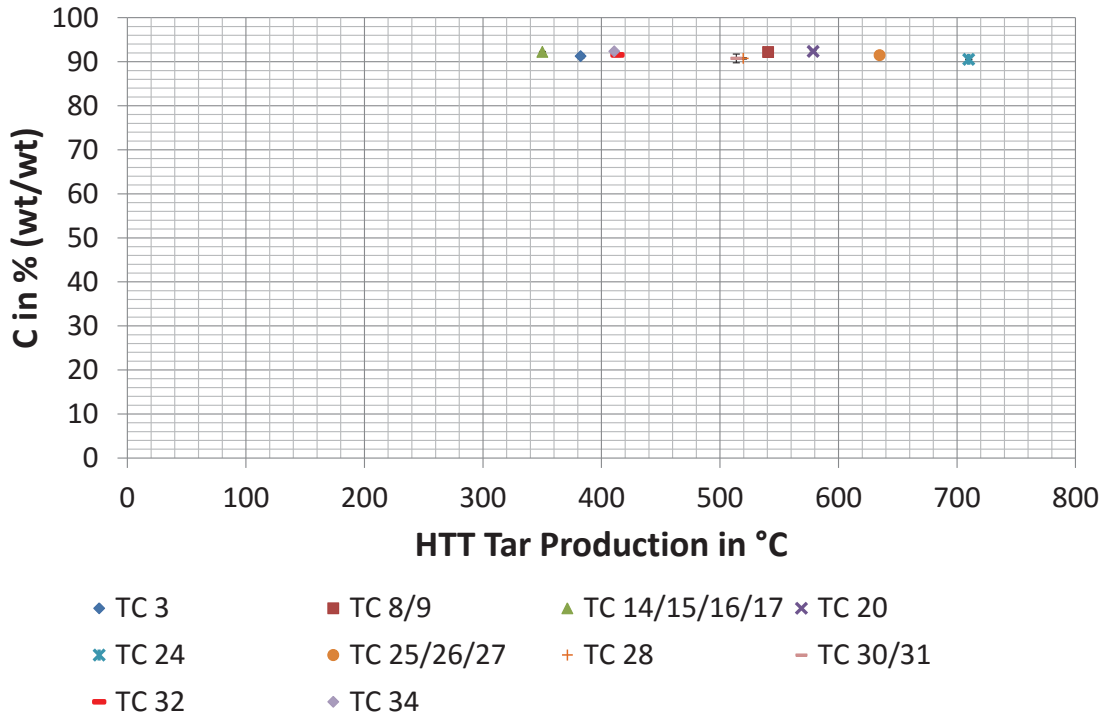

Figure F-19. Carbon content of tar-char produced at 600 °C as a function of the HTT of the tar collection process. The error bars represent the standard deviation. Two repetitions per analysis were done except in a few cases where only enough sample was present for one repeat analysis. C = carbon; HTT = highest treatment temperature; TC = tar-char; wt = weight.

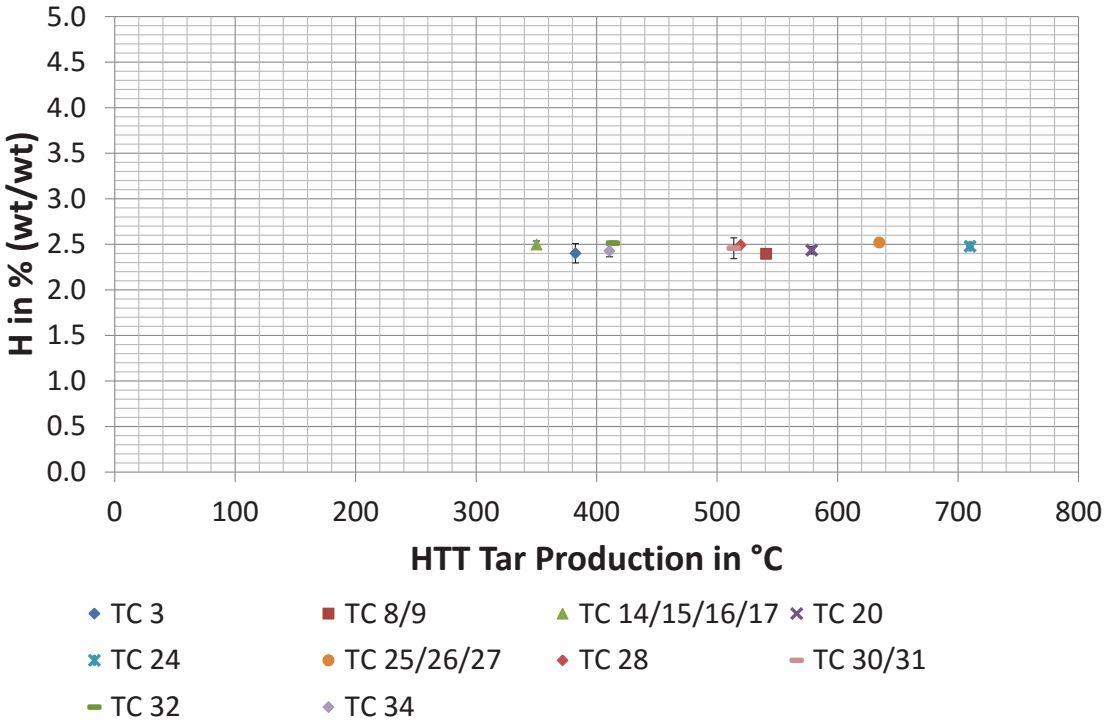

Figure F-20. Hydrogen content of tar-char produced at 600 °C as a function of the HTT of the tar collection process. The error bars represent the standard deviation. Two repetitions per analysis were done except in a few cases where only enough sample was present for one repeat analysis. H = hydrogen; HTT = highest treatment temperature; TC = tar-char; wt = weight.

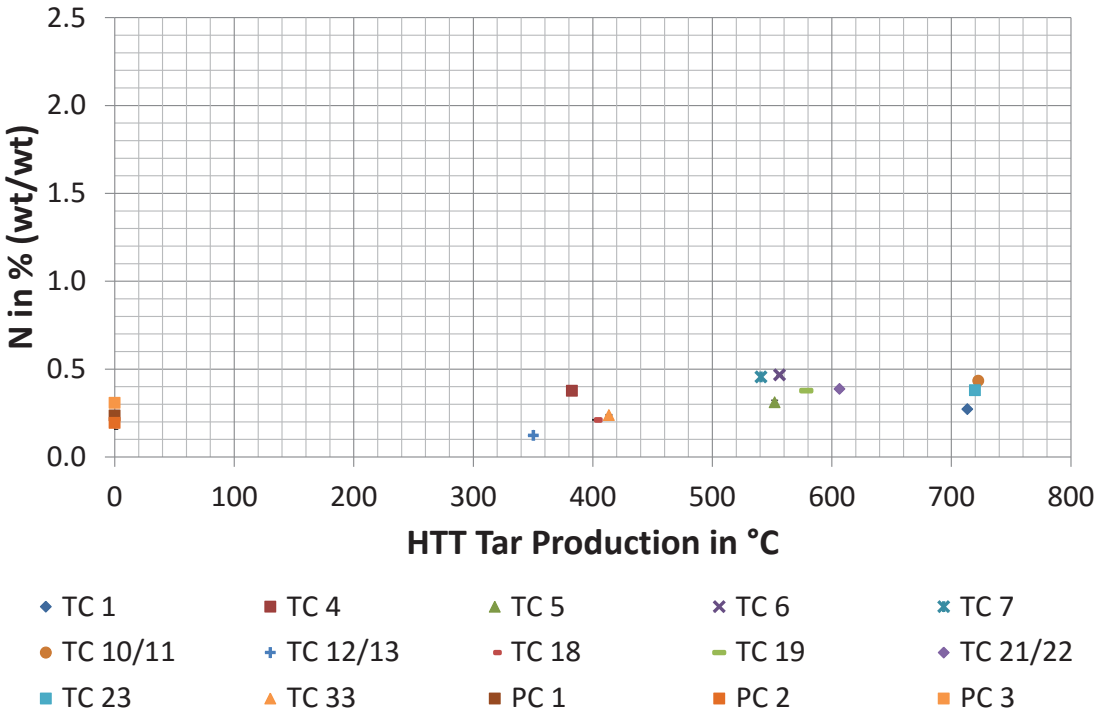

Figure F-21. Nitrogen content of tar-char produced at 300 °C as a function of the HTT of the tar collection process. Pine-char samples at a tar HTT of 0 °C were included for comparison. The error bars represent the standard deviation. Two repetitions per analysis were done except in a few cases of tar-char samples where only enough sample was present for one repeat analysis. HTT = highest treatment temperature; N = nitrogen; PC = pine-char; TC = tar-char; wt = weight.

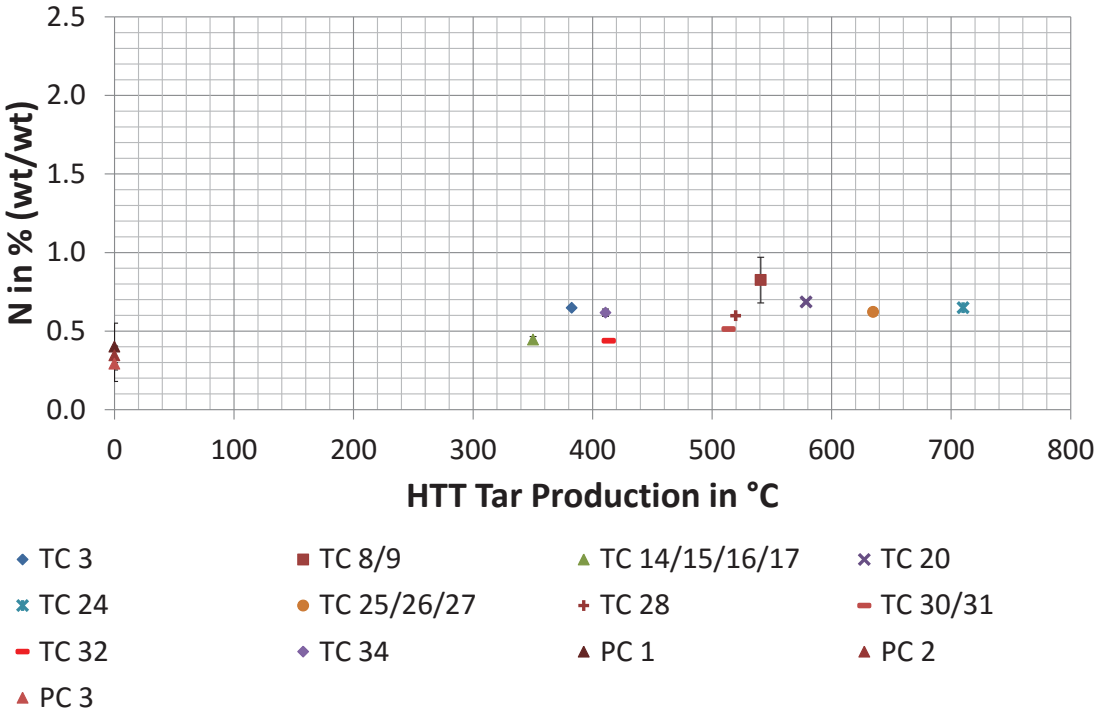

Figure F-22. Nitrogen content of tar-char produced at 600 °C as a function of the HTT of the tar collection process. Pine-char samples at a HTT of 0 °C were included for comparison. The error bars represent the standard deviation. Two repetitions per analysis were done except in a few cases of tar-char samples where only enough sample was present for one repeat analysis. HTT = highest treatment temperature; N = nitrogen; PC = pine-char; TC = tar-char; wt = weight.

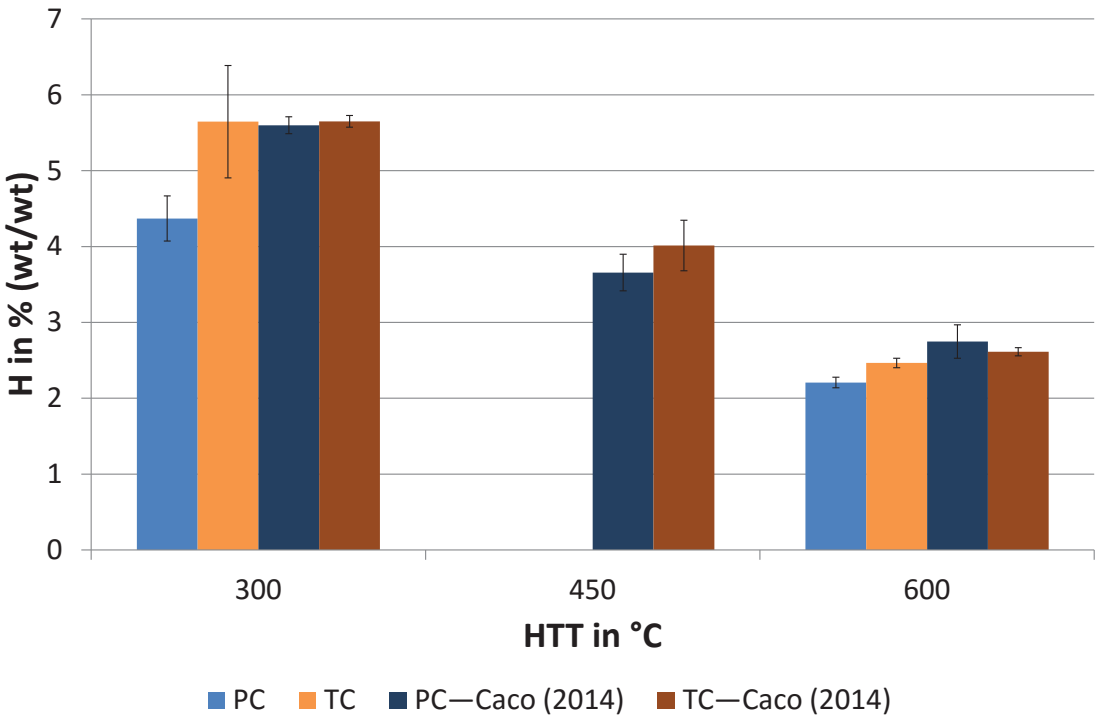

Figure F-23. Comparison of hydrogen content of pine-char and tar-char as a function of the HTT of the pyrolysis process. The error bars represent the standard deviation. In the case of pine-char three samples at 300 and 600 °C were analysed with two repetitions per sample. For the tar-char twelve and ten samples were analysed at 300 and 600 °C respectively with at least one repeat ultimate analysis per sample. The results of Caco (2014) represent the average of two samples for pine-char and tar-char at 300 and 600 °C respectively with two repetitions for each analysis. In the case of 450 °C three samples were analysed with at least one repetition per sample. H = hydrogen; HTT = highest treatment temperature; PC = pine-char; TC = tar-char; wt = weight.

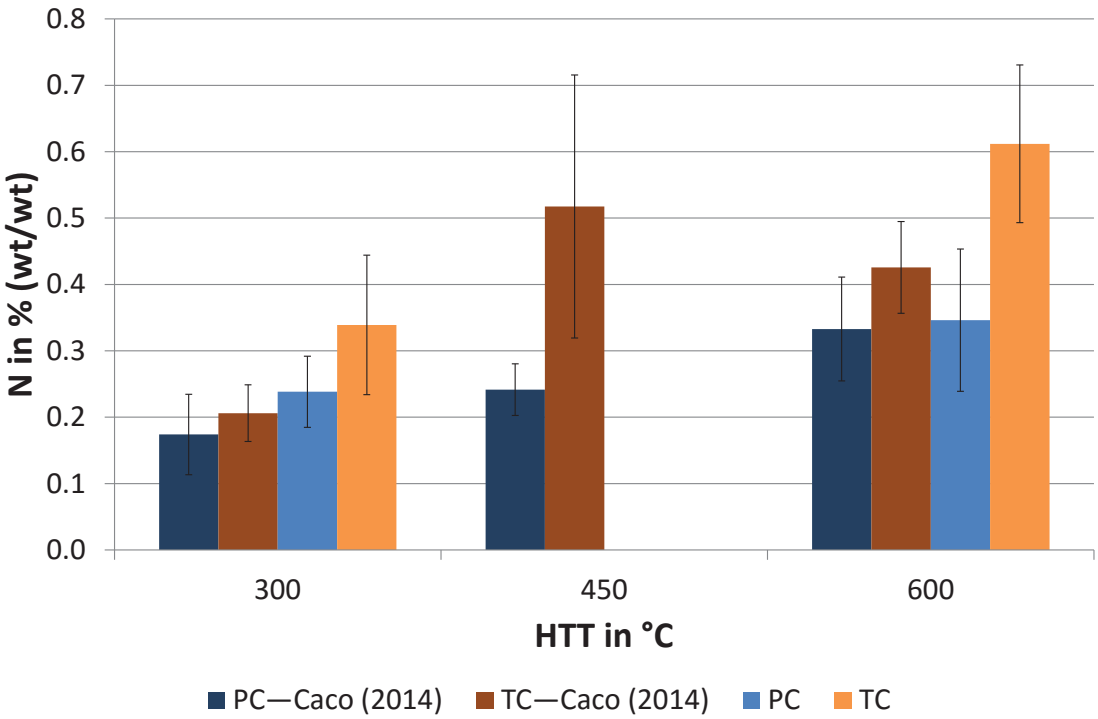

Figure F-24. Comparison of nitrogen content of pine-char and tar-char as a function of the HTT of the pyrolysis process. The error bars represent the standard deviation. In the case of pine-char three samples at 300 and 600 °C were analysed with two repetitions per sample. For the tar-char twelve and ten samples were analysed at 300 and 600 °C respectively with at least one repeat ultimate analysis per sample. The results of Caco (2014) represent the average of two samples for pine-char and tar-char at 300 and 600 °C respectively with two repetitions for each analysis. In the case of 450 °C three samples were analysed with at least one repetition per sample. HTT = highest treatment temperature; N = nitrogen; PC = pine-char; TC = tar-char; wt = weight.

F.5 Proximate Analysis

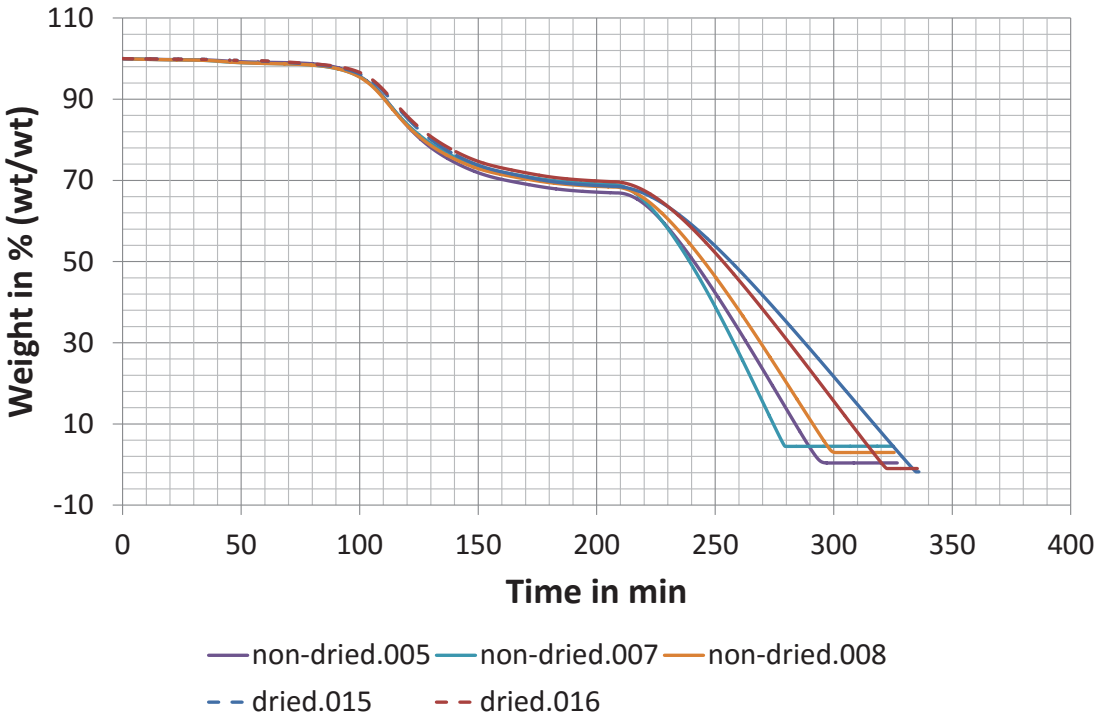

Figure F-25. Weight-loss recorded during proximate analysis of ground, dried and ground, non-dried coke in Figure 7-19. Ground means the sample size was reduced by grinding in a mortar and pestle. wt = weight.

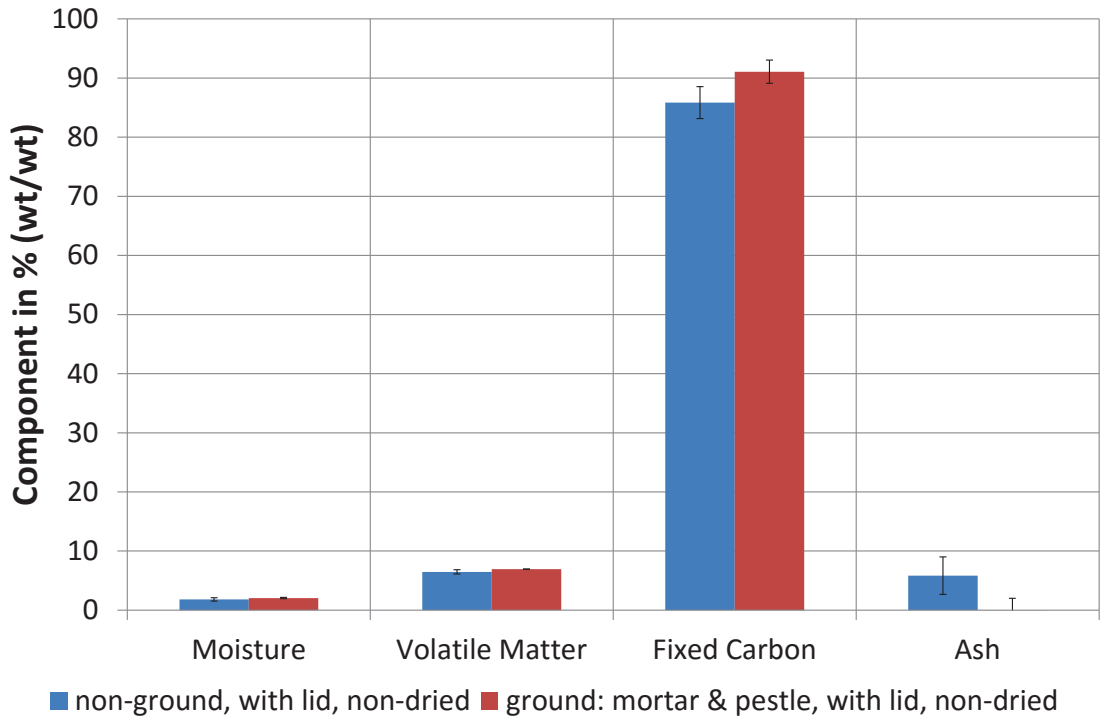

Figure F-26. Proximate analysis results of ground and non-ground coke produced from tar pyrolysis with a HTT of 600 °C. The tar for coke production was collected from pine pyrolysis with a HTT of 350 °C. Non-ground means the coke was crushed with tweezers to fit the TGA crucible. Non-dried means the sample was not oven-dried before proximate analysis. The error bars represent the standard deviation. Two repetitions for each analysis run were done. HTT = highest treatment temperature; wt = weight.

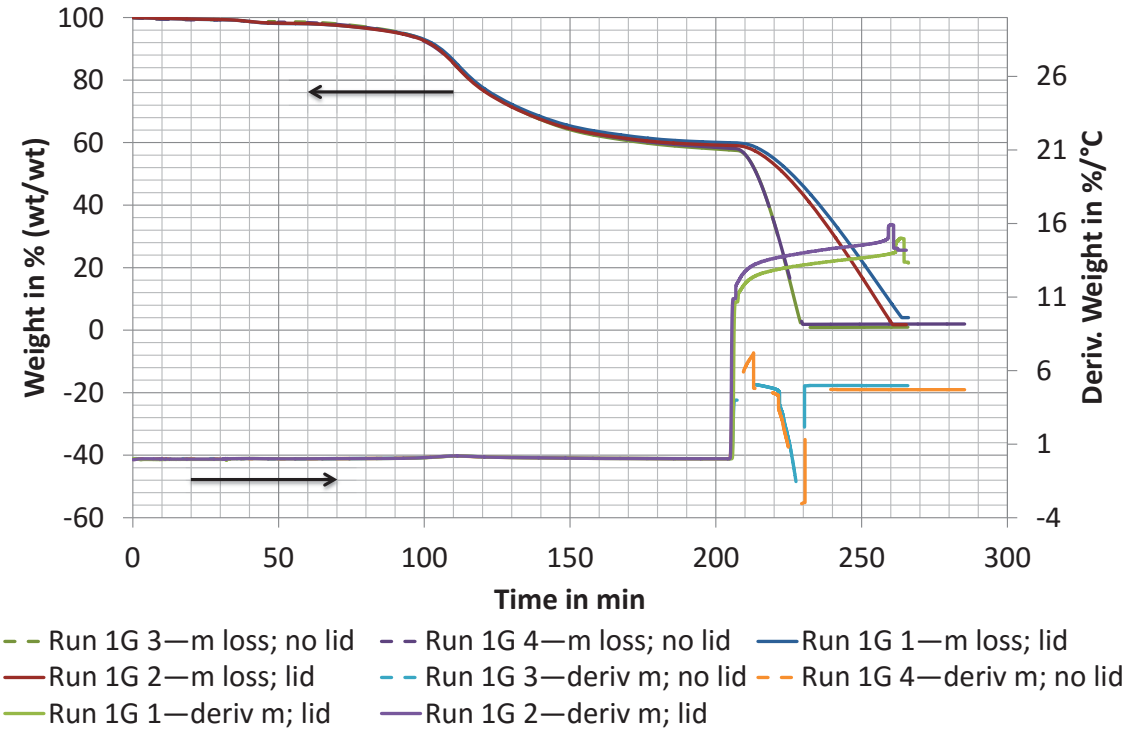

Figure F-27. Weight-loss and derivative weight-loss curves of pine-char proximate analysis performed with and without a lid. The char was obtained from Bashir (2012) and was produced by pine pyrolysis in a drum pyrolyser to a HTT of 356 °C. The proximate analysis was done by Bridges (2013). Legend: sample name—parameter displayed; lid or no lid. deriv m = derivative weight-loss; HTT = highest treatment temperature; m loss = weight-loss; wt = weight.

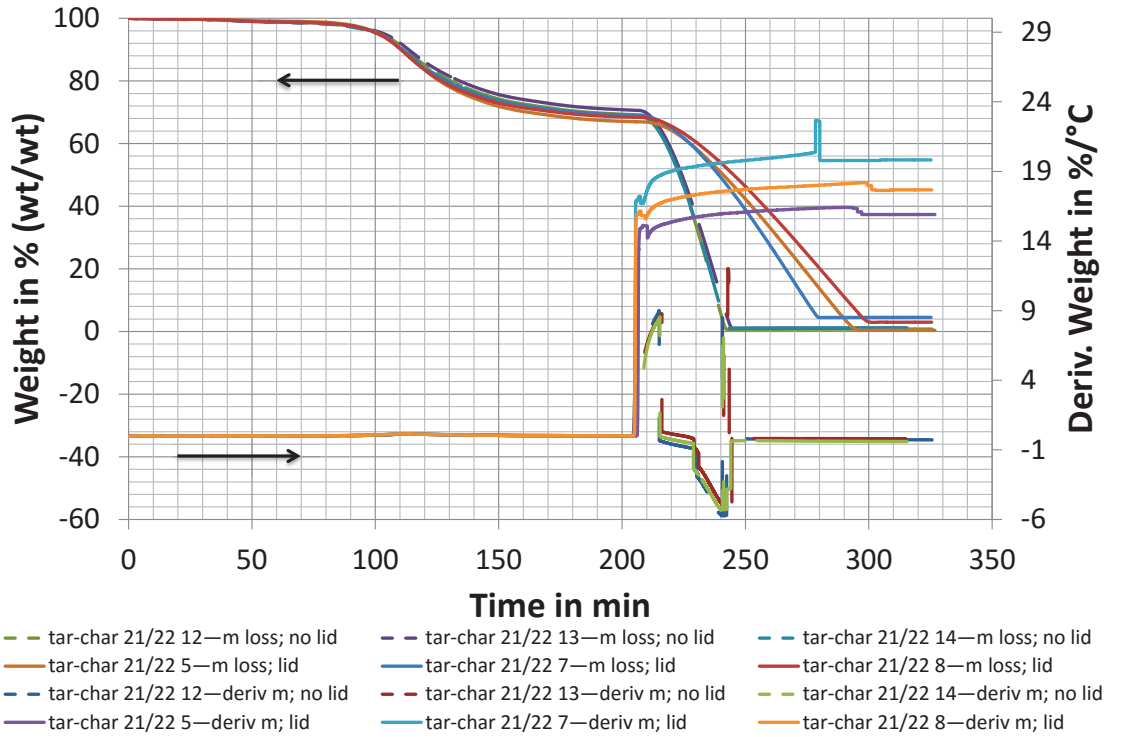

Figure F-28. Weight-loss and derivative weight-loss curves of tar-char proximate analysis performed with and without a lid. The coke was produced from tar pyrolysis with a HTT of 300 °C. The tar for coke production was collected from pine pyrolysis with a HTT of 606 °C. Legend: sample name—parameter displayed; lid or no lid. deriv m = derivative weight-loss; HTT = highest treatment temperature; m loss = weight-loss; wt = weight.

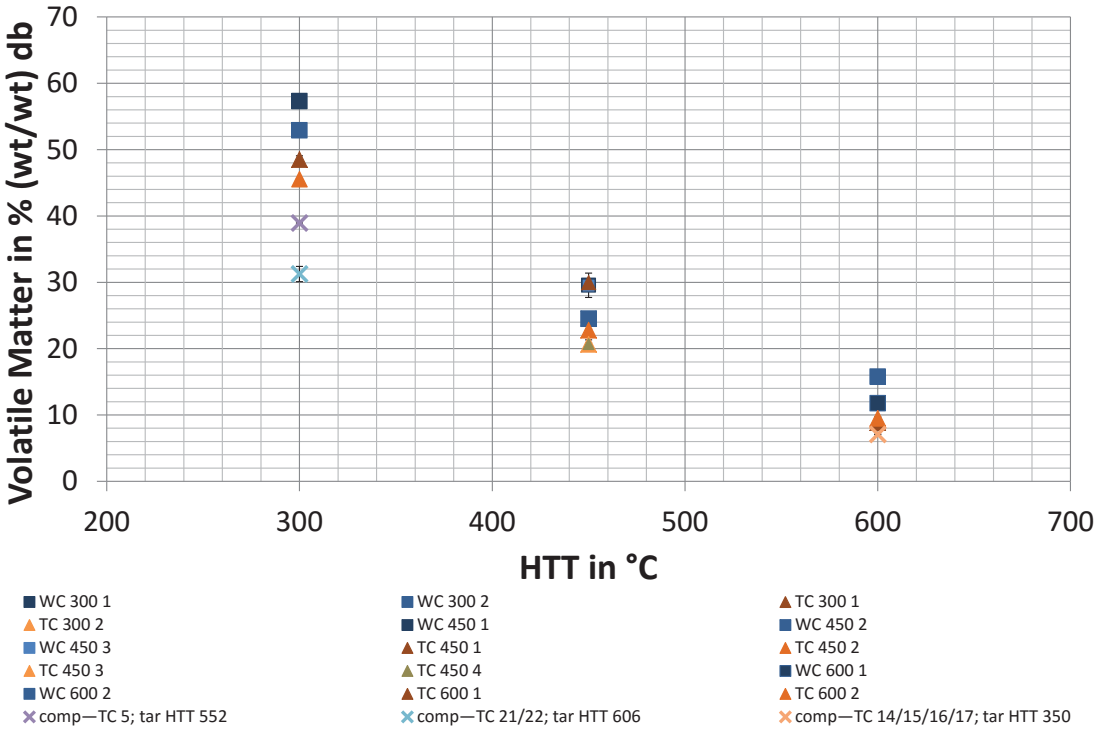

Figure F-29. Volatile matter content of pine-char and tar-char produced at various HTT's. The error bars represent the standard deviation. Two repetitions for each analysis run were carried out except for the sample "TC 5" was only one repeat run done. The analysis was adapted from Caco (2014) except the samples labelled by "comp", which were done separately in crucibles with a lid. Also they were produced in a different furnace than the one used by Caco (2014). Legend: Samples from Caco (2014): Char type_pyrolysis HTT in °C_sample number; remaining tar-char samples: comparison—sample name; HTT of tar collection in °C. comp = comparison; db = dry basis; HTT = highest treatment temperature; TC = tar-char; WC = wood char; wt = weight.

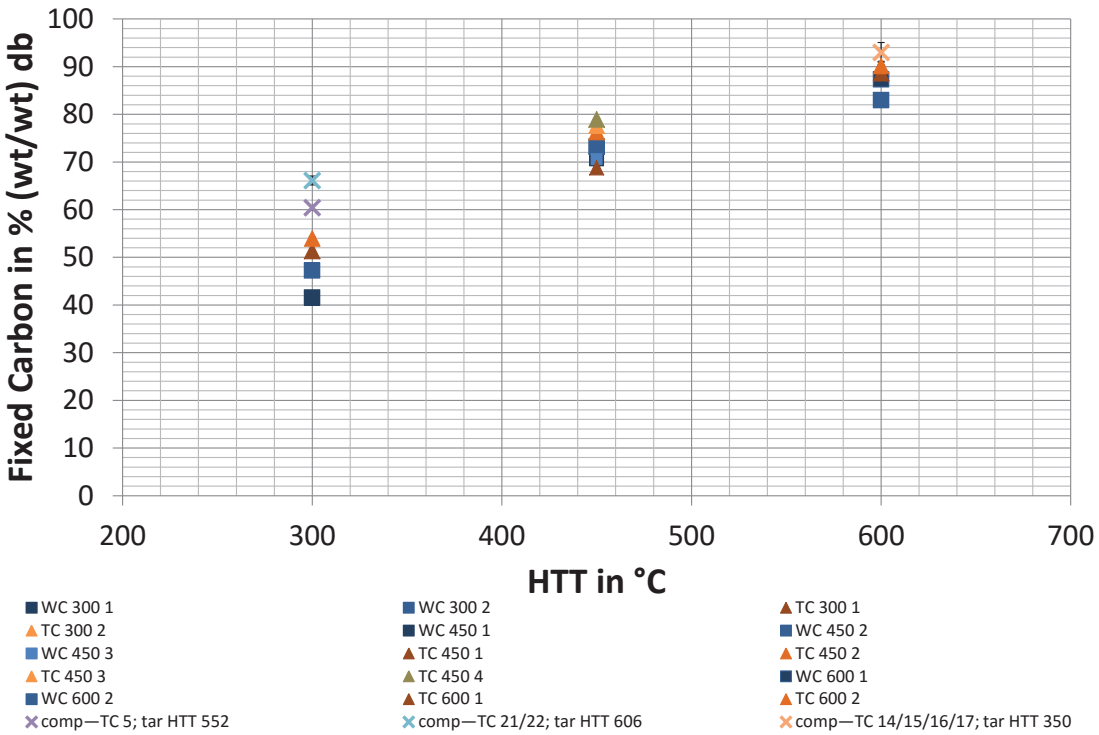

Figure F-30. Fixed carbon content of pine-char and tar-char produced at various HTT's. The error bars represent the standard deviation. Two repetitions for each analysis run were carried out except for the sample "TC 5" was only one repeat run done. The analysis was adapted from Caco (2014) except the samples labelled by "comp", which were done separately in crucibles with a lid. Also they were produced in a different furnace than the one used by Caco (2014). Legend: Samples from Caco (2014): Char type_pyrolysis HTT in °C_sample number; remaining tar-char samples: comparison—sample name; HTT of tar collection in °C. comp = comparison; db = dry basis; HTT = highest treatment temperature; TC = tar-char; WC = wood char; wt = weight.

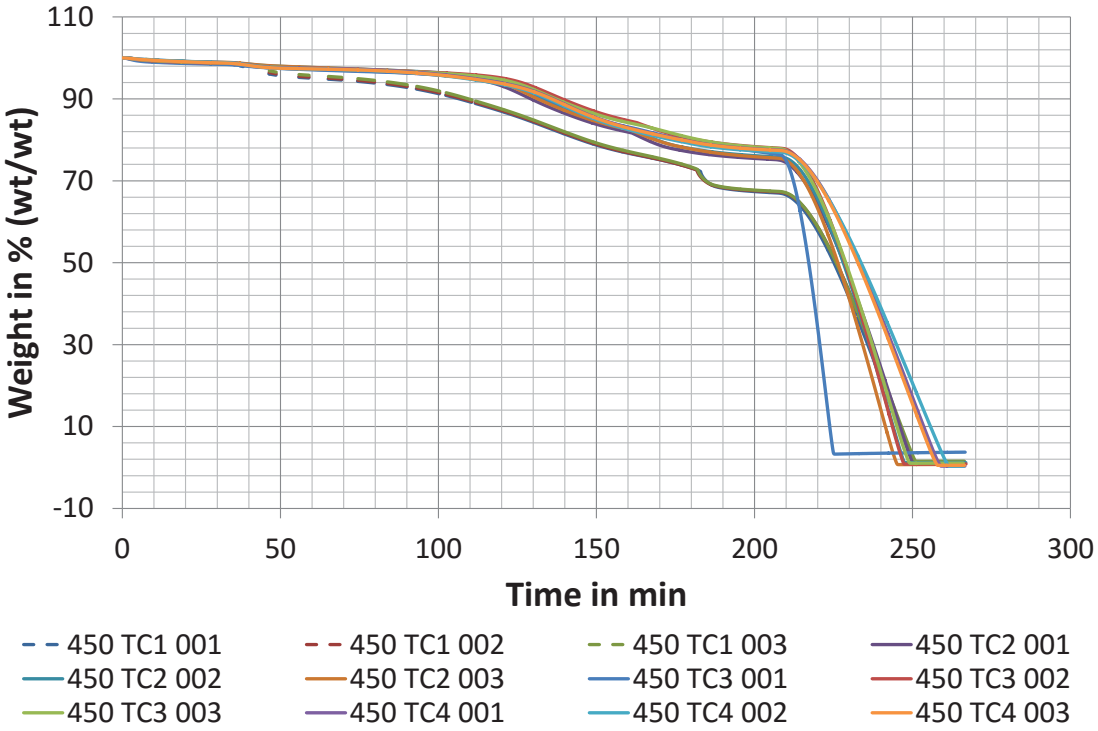

Figure F-31. Weight-loss curves of proximate analysis of tar-char samples produced at a HTT of 450 °C. Legend: HTT in °C_sample number_analysis number. HTT = highest treatment temperature; TC = tar-char; wt = weight.

F.6 Surface Area

The surface area analysis results can be found on the provided CD in the location chapter 7/data.

F.7 References

Bashir, F. (2012). *Fracturing of wood during pyrolysis* (Unpublished final year project report). Massey University, Palmerston North, New Zealand. The report can be accessed by contacting J.R.Jones@massey.ac.nz

Bridges, R. (2013). *Design and characterisation of an 'open source' pyrolyser for biochar production* (Master's thesis, Massey University, Palmerston North, New Zealand). Retrieved from http://mro.massey.ac.nz/handle/10179/5864

Caco, N. (2014). *Understanding the differences between char and tar-char* (Unpublished final year project report). Massey University, Palmerston North, New Zealand. The report can be accessed by contacting J.R.Jones@massey.ac.nz

Haris, N. A. (2012). *Smoke generator for food smoking* (Unpublished final year project report). Massey University, Palmerston North, New Zealand. The report can be accessed by contacting J.R.Jones@massey.ac.nz

Appendix G High Temperature High Pressure Reactor

G.1 Initially Proposed Reactor Designs

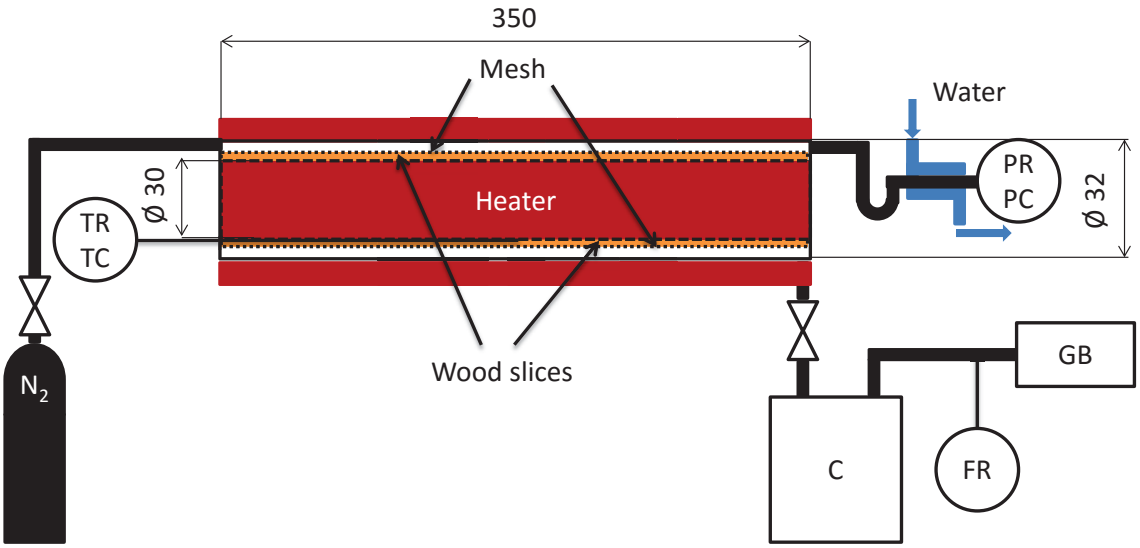

Figure G-1. Schematic of initially proposed apparatus for studying pyrolysis of pine shavings. The core part of the equipment is an inner pipe and an outer pipe that are electrically heated. Around the inner pipe are planed wood slices, approximately 90 µm thick, placed. The gap between the two pipes is very small, about 1 mm, to achieve high autogenous pressures for studying secondary char forming reactions in which the reactor is sealed. For studying primary reactions, a nitrogen purge gas flow or vacuum can be applied. Measurements are in mm. C = Condenser; FR = flow recorder; GB = gas bag; PC = pressure controller; PR = pressure recorder; TC = temperature controller; TR = temperature recorder.

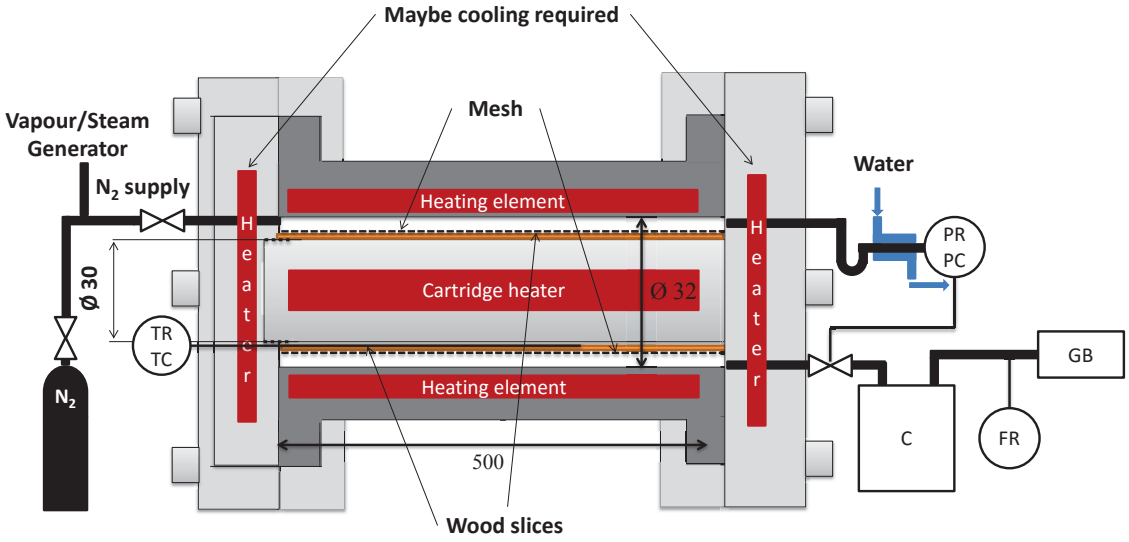

Figure G-2. Schematic of initially proposed apparatus for studying pyrolysis of pine shavings and cylindrical wood rods in one reactor. In this configuration the reactor allows the pyrolysis of pine shavings. The core part of the equipment is an inner pipe and an outer pipe that are electrically heated. Around the inner pipe are planed wood slices, approximately 90 µm thick, placed. The gap between the two pipes is very small, about 1 mm, to achieve high autogenous pressures for studying secondary char forming reactions in which the reactor is sealed. For studying primary reactions, a nitrogen purge gas flow or vacuum can be applied. Measurements are in mm. C = Condenser; FR = flow recorder; GB = gas bag; PC = pressure controller; PR = pressure recorder; TC = temperature controller; TR = temperature recorder.

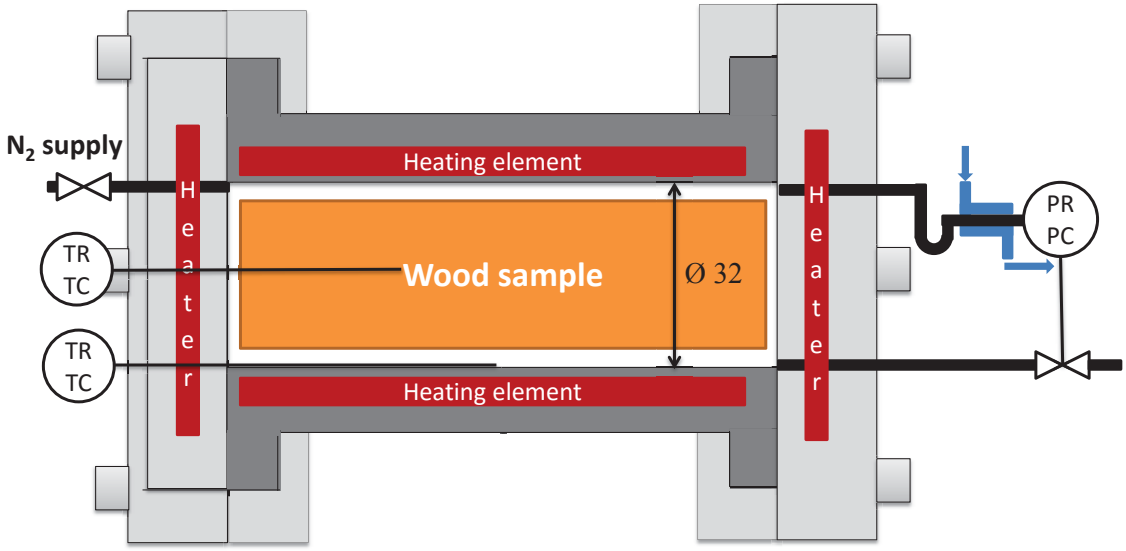

Figure G-3. Schematic of initially proposed apparatus for studying pyrolysis of pine shavings and cylindrical wood rods in one reactor. In this configuration the reactor allows the pyrolysis of cylindrical pine rods (this can be attained by exchanging the left flange in Figure G-2). Measurements are in mm. PC = pressure controller; PR = pressure recorder; TC = temperature controller; TR = temperature recorder.

G.2 Tender Documents

The tender documents were prepared by Worley Parsons and can be found on the CD provided.

G.2.1 Process Requirements and Description

The respective document can be found on the CD provided in the location chapter 8/data/tender documents/170271-RPT-X0001-R2 (Process Requirements and Description Document).pdf.

G.2.2 General Specifications

The respective document can be found on the CD provided in the location chapter 8/data/tender documents/170271-SPC-M0001-R0 (General Specification).pdf.

G.2.3 Specification for Pressure Vessels

The respective document can be found on the CD provided in the location chapter 8/data/tender documents/170271-SPC-M1801-R0 (Pressure Vessel) (2).pdf.

G.2.4 Datasheets

The respective document can be found on the CD provided in the location chapter 8/data/tender documents/170271-Datasheets.pdf.

G.2.5 Supplier Data Instructions Form

The respective document can be found on the CD provided in the location chapter 8/data/tender documents/170271-SDRL-M1801-R0.pdf.

G.3 Final Reactor Design

The detailed engineering of the final reactor design was completed by Fitzroy Engineering Group Limited. The equipment drawings can be found on the CD provided in the location chapter 8/data/final reactor design/Pyrolysis report drawings-20150204.pdf, and the respective equipment data in the location chapter 8/data/final reactor design/Pyrolysis report-20150204 (2).pdf.

G.4 Process Description

The following process description is an updated version of the one in the base package developed with Worley Parsons (see G.2.1).

G.4.1 Preparation Sequence

Table G-1 details the preparation steps that must be taken to prepare the pyrolysis process for operation. At the end of this sequence the process will be purged, pressure tested, and is ready for any mode of operation. This sequence **has to be** completed before any mode of operation.

Table G-1. Preparation sequence.

Step No.	Action/ Description
1	**Sample Preparation** • Prepare sample and introduce to V-101 chamber, close and secure V-101 door by putting ram assembly in operating position (HC-101), engage hydraulic pump (P-103).
2	**Equipment Inspection** • Inspect all vessels, instruments and piping connections. Check connections are secure and in good condition. Ensure process valves, controllers and equipment are in the correct position: • Closed: *HV-109*, PCV-101, XV-101, XV-102, XV-106, *HV-106, HV-110, HV-111*, XV-107, XV-105, *HV-114 (before closing HV-114 make sure condenser is drained).* • Open: XV-103, XV-108, XV-104, PCV-104. • Off: all pumps except P-103, system controllers and heaters. Check Condenser (V-105) water supply. • *Open HV-106* check FIT-104 reads > 1 m^3/hr and TIT-107 & 108 show temperatures within 2 °C of each other. • If either of the conditions above is not met halt the experiment.
3	**Operation Set Point** • *Select mode of operation. Either: Autogenous, Augmented, Vacuum or Water Vapour/Steam Injection.* • *Enter operation details: controller set points, controller ramp profiles, operation time, etc.*

(continued)

Step No.	Action/ Description
4	**Nitrogen Purge** • Open *HV-109*. • Activate PIC-101 to fill V-103 to operation set pressure. Operation set pressure must have a minimum pressure of 500 kPa(g) otherwise in case of vacuum operation or a set point pressure below 500 kPa(g) the leak test below cannot be carried out. • When V-103 is at set pressure, activate PIC-103 and set to control pressure to 100 kPa(g) (control via PCV-101 & PCV-104; XV-108 remains open). • Open XV-101. • If after 5 minutes pressure is not increasing at PIT-103 and/or PIT-104 deactivate: PIC-101, PIC-103 and close: XV-101, *HV-109*. Repeat steps 1-3. • When PIT-103 and PIT-104 reach 90 kPa(g), deactivate PIC-103, close: XV-101 & XV-104. XV-108 & PCV-104 are open.
5	**Vacuum Clean** • *Turn on vacuum system.* • Check PIT-105 reads -60 kPa(g). • Open XV-106. • Run vacuum until PIT-103 & PIT-104 reach -60 kPa(g), then close XV-106. • *Turn off vacuum system.* Steps 4 and 5 can be repeated if further amounts of contaminant are present in the reactor.
6	**Pressure/Leak Test** • Open XV-101 & XV-104, activate PIC-103 and set to 500 kPa(g) (control via PCV-101 & PCV-104; XV-108 remains open). • When PIT-103 and PIT-104 read 500 kPa(g), close XV-101 and deactivate PIC-103, XV-108 is open, and PCV-104 is closed. • Hold pressure for five minutes. • Check pressure readings from PIT-103 and 104. If within 5 kPa(g) of 500 kPa(g), leak test is successful, proceed to step 8. If unsuccessful proceed to step 7.

(continued)

Step No.	Action/ Description
7	**Pressure Test Unsuccessful** • Close XV-108. • Open PCV-104 to bring upstream section to atmospheric pressure. • When PIT-104 reads 0 kPa(g) pressure test reactor. • Open XV-101 and activate PIC-103, set to 500 kPa(g) (control via PCV-101, PCV-104 remains open). • When PIT-103 reads 500 kPa(g), close XV-101 and deactivate PIC-103 (XV-108 remains closed). • Hold pressure for five minutes. • Check PIT-103 pressure. If within 5 kPa(g) of 500 kPa(g), pressure leak is downstream of XV-108. If not within 5 kPa(g) of 500 kPa(g) pressure leak is upstream of XV-108. • Open XV-108 to bring upstream section to atmospheric pressure. • When PIT-103 and 104 read 0 kPa(g) end sequence. Repeat steps 1 to 6.
8	**Pressure Test Successful** • Open PCV-104 to bring upstream section to atmospheric pressure. • When PIT-103 & 104 read 0 kPa(g) system is purged and leak tested, ready for the experiment to begin.
9	**Utilities** • Turn on pipe line heaters (they are controlled in accordance to reactor temperature TIT-104). Note: the water injection line heater is only required for water vapour/steam injection mode. • Turn on heater for valve XV-108. • Activate/reset FIT-101 totaliser.
10	**Proceed to selected mode of operation**

Note. Steps in italics indicate a manual action (not PLC controlled). The here described steps refer to the P&ID in 8.3.2.

No. = number; PLC = programmable logic controller.

G.4.2 Mode 1: Autogenous Operation

In autogenous mode the pyrolysis reactor (V-101) is isolated and heated without or minimal removal of pyrolysis products. When the operation time limit is reached all products are removed and collected for analysis. The process steps are outlined in Table G-2. Before commencement of this mode the preparation sequence in Table G-1 has to be completed!

Table G-2. Autogenous operation.

Step No.	Action/ Description
	Autogenous Operation • Close XV-103, XV-108 & PCV-104. • Open XV-101 & XV-107. • Activate PIC-103 and set to control pressure to set point specified during Preparation Sequence. • Activate TIC-104, set controller to ramp V-101 temperature to set point specified during Preparation Sequence. Note: pipeline heater follow ramp profile of TIT-104.
1-11	• Pressure in V-105 is controlled by PIC-103 by monitoring PIT-103 & PIT-104. If PIT-103 > PIT-104, then PCV-101 opens until PIT-103 – PIT-104 < x (x is the desired differential e.g. 0.01 bar). If PIT-103 ≥ set point pressure (e.g. 200 bar), then PCV-101 closes, XV-108 & PCV-104 open and PIT-103 and PIT-104 is controlled by PIC-103 via PCV-104 to set point pressure. The overpressure is most likely short lived. Meaning that PCV-104 will close (heat loss if no further generation of vapour will cause a reduction in pressure). The cool condenser will be a mass flow away from the reactor. Therefore, when PIT-103 ≤ y (y is allowable threshold) XV-108 is closed. Pressure in V-105 is controlled again by PIC-103 by monitoring PIT-103 & PIT-104. This process is repeated as many times as required. When TIC-104 reaches set point hold temperature until reaction time limit is reached. Then proceed to step 1-12.
	Note: by the push of a button XV-104 can be closed and XV-105 opened so that gas can be collected either in a gas bag or analysed by a gas analyser. Again by a push of the button XV-105 closes and XV-104 opens so that the gases are vented.
	Reaction Time Limit Reached
1-12	• Close XV-107, open XV-108. • Set PIC-103 to ramp down pressure to 0 kPa(g) via PCV-104. • TIC-104 to continue to control temperature to set point. • When PIT-103 and PIT-104 reads 0 kPa(g), proceed to step 1-13.

(continued)

Step No.	Action/ Description
1-13	**Nitrogen Purge System** • Open XV-103, set PIC-103 to 100 kPa(g). • Deactivate PIC-101, *close HV-109*. • Run purge until FIT-101 records no flow. • Deactivate TIC-104 and PIC-103 but XV-108 & PCV-104 remain open, close XV-101. • When PIT-103 and PIT-104 read 0 kPa(g) and TIT-103 & 104 reach 25 ºC, turn off pipe line heater, heater for valve XV-108 and *close HV-106*.
1-14	**Product Removal** • Disengage hydraulic closing system. • *Hinge ram assembly out of way.* • *Open V-101 and remove any remaining char.* • *Remove liquids from V-106 by opening HV-114.* • *Clean filter F-101.*
Operation is completed!	

Note. This table is a continuation of Table G-1. Steps in italics indicate a manual action (not PLC controlled). The here described steps refer to the P&ID in 8.3.2.

No. = number; PLC = programmable logic controller.

G.4.3 Mode 2: Augmented Operation

In this mode of operation the reactor is brought to pyrolysis pressure. Then Nitrogen is continuously passed through the reactor, which undergoes a set heating profile, until the reaction time limit is reached. During this time the set pressure is maintained. Char and condensable liquids are collected as pyrolysis products; non-condensable pyrolysis gases are continuously vented but can be sampled if required. The process steps are detailed in Table G-3. Before commencement of this mode the preparation sequence in Table G-1 has to be completed!

Table G-3. Augmented operation.

Step No.	Action/ Description
2-11	**Augmented Operation** • Open XV-101. • Activate PIC-103 and control reactor pressure (PIT-103 & 104) and flow rate to settings specified during Preparation Sequence via PCV-101 & PCV-104. XV-108 remains open. • Activate TIC-101 & control pipe line temperature to follow TIT-104. • When set point pressure and flow is attained activate TIC-104 to ramp reactor temperature to set point specified during Preparation Sequence. • When TIC-104 reaches set point hold temperature until experiment time limit is reached. Note: by the push of a button XV-104 can be closed and XV-105 opened so that gas can be collected either in a gas bag or analysed by a gas analyser. Again by a push of the button XV-105 closes and XV-104 opens so that the gases are vented.
2-12	**Reaction Time Limit Reached** • Close XV-101. • Set PIC-103 to ramp down pressure to 0 kPa(g) via PCV-104. XV-108 remains open. • TIC-104 to continue to control temperature to set point. • When PIT-103 and PIT-104 read 0 kPa(g), proceed to step 2-13.
2-13	**Nitrogen Purge System** • Open: XV-101. • Set PIC-103 to 100 kPa(g). • Deactivate PIC-101, *close HV-109*. • Run purge until FIT-101 records no flow. • Deactivate TIC-101, TIC-104 and PIC-103 but XV-108 & PCV-104 remain open, close: XV-101. • When PIT-103 and PIT-104 read 0 kPa(g) and TIT-103 & 104 reach 25 ºC, turn off pipeline heaters, heater for valve XV-108, and *close HV-106.*
2-14	**Product Removal** • Disengage hydraulic closing system. • *Hinge ram assembly out of way.* • *Open V-101 and remove any remaining char.* • *Remove liquids from V-106 by opening HV-114.* • *Clean filter F-101.*
Operation is completed!	

Note. This table is a continuation of Table G-1. Steps in italics indicate a manual action (not PLC controlled). The here described steps refer to the P&ID in 8.3.2.

No. = number; PLC = programmable logic controller.

G.4.4 Mode 3: Vacuum Operation

In this mode pyrolysis products are continuously evacuated by the vacuum system. Char and condensable liquids are collected as products, non-condensable pyrolysis gases are collected in the vacuum system. The process steps are outlined in Table G-4. Before commencement of this mode the preparation sequence in Table G-1 has to be completed!

Table G-4. Vacuum operation.

Step No.	Action/ Description
3-11	**Vacuum Operation** • Close XV-104 & XV-103, PIC-103 to remain off. • *Turn on Vacuum System*. • Check PIT-105 reads -60 kPa(g), then open XV-106. • When PIT-103 & PIT-104 reads -60 kPa(g) activate TIC-104 and ramp to set point. Note pipeline heater follow ramp profile of TIT-104. • When TIC-104 reaches set point hold temperature until experiment time limit is reached.
3-12	**Reaction Time Limit Reached** • Close XV-106 and open XV-104. • *Turn off vacuum system.*
3-13	**Nitrogen Purge System** • Open: XV-101, XV-103. • Activate and set PIC-103 to 100 kPa(g). • Deactivate PIC-101, *close HV-109*. • Run purge until FIT-101 records no flow. • Deactivate TIC-104 and PIC-103 but XV-108 and PCV-104 remain open, close: XV-101. When PIT-103 and PIT-104 read 0 kPa(g) and TIT-103 & 104 reach 25 ºC, turn off pipe line heater, heater for valve XV-108, and close *HV-106.*
3-14	**Product Removal** • Disengage hydraulic closing system. • *Hinge ram assembly out of way.* • *Open V-101 and remove any remaining char.* • *Remove liquids from V-106 by opening HV-114.* • *Clean filter F-101.*
Operation is completed!	

Note. This table is a continuation of Table G-1. Steps in italics indicate a manual action (not PLC controlled). The here described steps refer to the P&ID in 8.3.2.

No. = number; PLC = programmable logic controller.

G.4.5 Mode 4: Steam/ Water Vapour Injection

In this mode water vapour/steam is introduced to the pyrolysis reactor. Char and condensable liquids are collected as pyrolysis products, non-condensable pyrolysis gases are vented but can be sampled if required. Before commencement of this mode the preparation sequence in Table G-1 has to be completed! The operator can choose between two different operating procedures, which can be selected in step 3 of the preparation sequence:

1. the reactor is pressurised to a set point using an inert gas, upon attainment of the set pressure the reactor is heated at a controlled rate to a set target temperature during which the pressure is maintained at the set point value (see G.4.3 augmented operation), at the target temperature water is injected at a specified flow rate for a specified time (it is important to note that water will only be injected if the target temperature is above the saturation temperature at the respective set point pressure);
2. in this mode the sample undergoes a heating profile in a steam atmosphere when the reactor temperature is above the saturation temperature at the respective set point pressure, that is, this mode is similar to 1 but instead of an inert gas steam is used (however water is only introduced when the reactor temperature reaches the saturation temperature of water vapour for the set point pressure, below this temperature the pressure is maintained with nitrogen).

The process steps are detailed in Table G-5.

Table G-5. Steam/ water vapour injection.

Step No.	Action/ Description
4-11	**Steam/ Water Vapour Operation** • Open XV-101. • Activate PIC-103 and control reactor pressure (PIT-103 & 104) and flow rate to settings specified during Preparation Sequence via PCV-101 & PCV-104. XV-108 remains open. • Activate TIC-101 & control pipe line temperature to follow TIT-104. • When set point pressure and flow is attained activate TIC-104 to ramp reactor temperature to set point specified during Preparation Sequence. **Procedure (a):** • When TIC-104 reaches set point (target temperature) start water injection (step 4-12) & hold temperature until reaction time limit is reached (step 4-13). **Procedure (b):** • When TIC-104 reaches minimum water injection temperature at respective pressure start water injection (step 4-12) & continue with heating profile until reaction time limit is reached (step 4-13).

(continued)

Step No.	Action/ Description
4-12	**Water Injection** • Open XV-102. • Activate TIC-102 (temperature set point is always at 200 °C). • Turn on P-102 to control flow of water into reactor to parameters specified during Preparation sequence. • When steam activation time limit is attained close XV-102, turn off: P-102 and deactivate TIC-102. • Maintain V-101 pressure and temperature settings until reaction time limit is reached.
4-13	**Reaction Time Limit Reached** • Close XV-101. • Set PIC-103 to ramp down pressure to 0 kPa(g) via PCV-104. XV-108 remains open. • TIC-104 to continue to control temperature to set point. • When PIT-103 and PIT-104 read 0 kPa(g) proceed to step 4-14.
4-14	**Nitrogen Purge System** • Open: XV-101. • Set PIC-103 to 100 kPa(g). • Deactivate PIC-101, close *HV-109*. • Run purge until FIT-101 records no flow. • Deactivate TIC-104, TIC-101 and PIC-103 but XV-108 & PCV-104 remain open, close: XV-101. • When PIT-103 and PIT-104 read 0 kPa(g) and TIT-103 & 104 reach 25 ºC, turn off pipeline heaters, heater for valve XV-108, and *close HV-106.* Depressurise water injection line: • Open XV-109. • *Slightly open HV-108* and manipulate to achieve desired flow rate through V-107. • When *HV-106* is fully closed and no flow is seen through V-107, close XV-109 and *HV-108.*
4-15	**Product Removal** • Disengage hydraulic closing system. • *Hinge ram assembly out of way.* • *Open V-101 and remove any remaining char.* • *Remove liquids from V-106 by opening HV-114.* • *Clean filter F-101.*
Operation is completed!	

Note. This table is a continuation of Table G-1. Steps in italics indicate a manual action (not PLC controlled). The here described steps refer to the P&ID in 8.3.2.

No. = number; PLC = programmable logic controller.

G.4.6 Steam Cleaning Procedure

The cleaning sequence outlined in Table G-6 will be run after any mode of Operation! Before commencement of this procedure the preparation sequence in Table G-1 has to be completed but without the introduction of a sample!

Table G-6. Steam cleaning procedure.

Step No.	Action/ Description
	Reactor Cleaning Step
	• Close: XV-103 and XV-108.
	• Activate TIC-104 to ramp reactor temperature to cleaning temperature (T ≥ 200 °C).
	• When TIC-104 reaches set point water can be injected.
	• Open XV-102, activate TIC-102 (temperature set point is always at 200 °C).
5-11	• Activate PIC-103 and set maximum pressure to a value slightly below the saturation pressure of steam at the set reactor temperature to prevent the presence of liquid water.
	• Turn on P-102 to control flow of water into reactor until set pressure is obtained at PIT-103.
	• When set point pressure is obtained close XV-102, turn off P-102, and deactivate TIC-102.
	• Maintain V-101 at temperature set point until reactor cleaning step time limit is reached.
	Reactor Cleaning Step Time Limit Reached
5-12	• When reactor cleaning step time limit is reached open XV-108 to depressurise upstream section to atmospheric pressure.
	• When PIT-103 and PIT-104 read 0 kPa(g) proceed to step 5-13.
	Steps 5-11 and 5-12 can be repeated if required.
	Nitrogen Purge System
	• Open: XV-101.
	• Set PIC-103 to 100 kPa(g).
	• Deactivate PIC-101, close *HV-109*.
	• Run purge until FIT-101 records no flow.
	• Deactivate TIC-104 and PIC-103 but XV-108 & PCV-104 remain open, close: XV-101.
5-13	• When PIT-103 and PIT-104 read 0 kPa(g) and TIT-103 & 104 reach 25 ºC, turn off pipeline heaters, heater for valve XV-108, and *close HV-106*.
	Depressurise water injection line:
	• Open XV-109.
	• *Slightly open HV-108* and manipulate to achieve desired flow rate through V-107.
	• When *HV-106* is fully closed and no flow is seen through V-107, close XV-109 and *HV-108*.
Operation is completed!	

Note. This table is a continuation of Table G-1. Steps in italics indicate a manual action (not PLC controlled). The here described steps refer to the P&ID in 8.3.2.

No. = number; PLC = programmable logic controller.